frontiers | Research Topics

Climate change and associated impacts

Edited by
Dabang Jiang, Xiaoguang Yang, Huopo Chen, Qiang Zhang and Claudio Fabian Szlafsztein

Published in
Frontiers in Earth Science
Frontiers in Environmental Science

ISSN 1664-8714
ISBN 978-2-83251-997-4
DOI 10.3389/978-2-83251-997-4

About Frontiers

Frontiers is more than just an open access publisher of scholarly articles: it is a pioneering approach to the world of academia, radically improving the way scholarly research is managed. The grand vision of Frontiers is a world where all people have an equal opportunity to seek, share and generate knowledge. Frontiers provides immediate and permanent online open access to all its publications, but this alone is not enough to realize our grand goals.

Frontiers journal series

The Frontiers journal series is a multi-tier and interdisciplinary set of open-access, online journals, promising a paradigm shift from the current review, selection and dissemination processes in academic publishing. All Frontiers journals are driven by researchers for researchers; therefore, they constitute a service to the scholarly community. At the same time, the *Frontiers journal series* operates on a revolutionary invention, the tiered publishing system, initially addressing specific communities of scholars, and gradually climbing up to broader public understanding, thus serving the interests of the lay society, too.

Dedication to quality

Each Frontiers article is a landmark of the highest quality, thanks to genuinely collaborative interactions between authors and review editors, who include some of the world's best academicians. Research must be certified by peers before entering a stream of knowledge that may eventually reach the public - and shape society; therefore, Frontiers only applies the most rigorous and unbiased reviews. Frontiers revolutionizes research publishing by freely delivering the most outstanding research, evaluated with no bias from both the academic and social point of view. By applying the most advanced information technologies, Frontiers is catapulting scholarly publishing into a new generation.

What are Frontiers Research Topics?

Frontiers Research Topics are very popular trademarks of the *Frontiers journals series*: they are collections of at least ten articles, all centered on a particular subject. With their unique mix of varied contributions from Original Research to Review Articles, Frontiers Research Topics unify the most influential researchers, the latest key findings and historical advances in a hot research area.

Find out more on how to host your own Frontiers Research Topic or contribute to one as an author by contacting the Frontiers editorial office: frontiersin.org/about/contact

Climate change and associated impacts

Topic editors

Dabang Jiang — Institute of Atmospheric Physics, Chinese Academy of Sciences (CAS), China

Xiaoguang Yang — China Agricultural University, China

Huopo Chen — Institute of Atmospheric Physics, Chinese Academy of Sciences (CAS), China

Qiang Zhang — Beijing Normal University, China

Claudio Fabian Szlafsztein — Federal University of Pará, Brazil

Citation

Jiang, D., Yang, X., Chen, H., Zhang, Q., Szlafsztein, C. F., eds. (2023). *Climate change and associated impacts*. Lausanne: Frontiers Media SA.

doi: 10.3389/978-2-83251-997-4

Table of contents

frontiers | Frontiers in Earth Science

ORIGINAL RESEARCH
published: 20 May 2022
doi: 10.3389/feart.2022.904851

Summer Temperature Reconstruction for the Source Area of the Northern Asian Great River Basins, Northern Mongolian Plateau Since 1190 CE and its Linkage With Inner Asian Historical Societal Changes

Feng Chen[1,2]*, *Youping Chen*[1], *Nicole Davi*[3,4] *and Heli Zhang*[2]

[1]Yunnan Key Laboratory of International Rivers and Transboundary Eco-Security, Institute of International Rivers and Eco-Security, Yunnan University, Kunming, China, [2]Institute of Desert Meteorology, China Meteorological Administration/Key Laboratory of Tree-ring Physical and Chemical Research of China Meteorological Administration, Urumqi, China, [3]Department of Environmental Science, William Paterson University, Wayne, NJ, United States, [4]Tree-Ring Laboratory, Lamont-Doherty Earth Observatory, Palisades, NY, United States

OPEN ACCESS

Edited by:
Claudio Fabian Szlafsztein,
Federal University of Pará, Brazil

Reviewed by:
Eduardo Zorita,
Helmholtz Centre for Materials and Coastal Research (HZG), Germany
Olga Solomina,
Institute of Geography (RAS), Russia

***Correspondence:**
Feng Chen
feng653@163.com

Specialty section:
This article was submitted to Geoscience and Society, a section of the journal Frontiers in Earth Science

Received: 28 March 2022
Accepted: 09 May 2022
Published: 20 May 2022

Citation:
Chen F, Chen Y, Davi N and Zhang H (2022) Summer Temperature Reconstruction for the Source Area of the Northern Asian Great River Basins, Northern Mongolian Plateau Since 1190 CE and its Linkage With Inner Asian Historical Societal Changes. Front. Earth Sci. 10:904851. doi: 10.3389/feart.2022.904851

Mid-to-high latitudes of Asia and its adjacent Arctic area are some of the most sensitive regions to climate warming in Eurasia, but spatio-temporal temperature variation over this region is still limited by a lack of long-term temperature records. Here, June-July temperature reconstructions are developed from a *Larix sibirica* composite chronology that presents a stable positive linkage with large-scale recorded temperatures and spans 1190–2019 CE for the source area of the Northern Asian great river Basins, northern Mongolian Plateau, Inner Asia. The warmest reconstructed period and low summer sea ice extent in the Arctic Ocean over the past 830 years was estimated to occur in the late twentieth century (1990s–present), with a mean temperature (15.2°C) higher than the long-term mean (13.9°C) of 1190–2019 CE, which is linked with the rapid increase in global temperature. A relationship also exists between the reconstructed temperature and the AMO index, suggesting that the atmospheric patterns over the Arctic and North Atlantic Oceans influence the temperature variations of northern Mongolian Plateau. In addition, we also propose that the warm climate promoted high vegetation productivity and favored the formation of power of the nomadic tribes in the Mongolian Plateau, such as the warm periods 1210s–1250s and 1400s–1430s. Our temperature reconstruction provides us with an opportunity to understand the regional effects of climate warming from multiple perspectives.

Keywords: dendrochronology, Northern Mongolian Plateau, temperature reconstruction, streamflow variation, Atlantic Multidecadal Oscillation

INTRODUCTION

As the homeland of the nomadic people in Inner Asia, climate change on the Mongolian Plateau has some vital influences on the historical progress in Eurasia and has become an important research topic (Pederson et al., 2014; Büntgen et al., 2016; Hessl et al., 2018). Modern instrumental climate records show that the Mongolian Plateau is undergoing significant climatic shifts (Jiang et al., 2016; Wang et al., 2016; Zhang et al., 2020). Based on tree-ring records, climatic shifts include unprecedented climate warming synchronized with similar temperature increases in Eurasia (D'Arrigo et al., 2001; Davi et al., 2015; Büntgen et al., 2016; Zhang et al., 2020), and wetting-warming trends have been particularly pronounced in the Altai Mountains (Chen et al., 2014; Chen et al., 2016); in contrast, the warm-dry trends are more pronounced in central-southern Mongolian Plateau (Li et al., 2009; Liu et al., 2019; Zhang et al., 2020). How regional climate change will affect large-scale water and energy transports in the future is difficult to forecast, as climate forcings in the Mongolian Plateau are highly complex (Jiang et al., 2016; Hessl et al., 2018). As the Mongolian Plateau is a source area for the great northern Asian rivers, such as the Yenisei, Lena, and Ob rivers, climate change in this area is affected by a variety of climate systems, including the Asian monsoon, Siberian High and mid-latitude westerlies (Iwao and Takahashi, 2006; Wang and Feng, 2013; Luo and Wang, 2019). There is only limited understanding of how climate change in this area will affect the exchange of water and energy in mid- and high-latitude Asia. This lack of understanding is in part due to poor temporal coverage of instrumental data.

Over the past 20 years, the Mongolian Plateau has become a hot spot for tree-ring studies in Asia. A large number of climate and streamflow reconstructions have been established based on tree rings (D'Arrigo et al., 2001; Davi et al., 2010; Myglan et al., 2012; Pederson et al., 2013; Davi et al., 2013; Chen et al., 2014; Davi et al., 2015; Chen et al., 2016) and have provided some valuable information for revealing regional climate change and its influences (Pederson et al., 2014; Büntgen et al., 2016; Hessl et al., 2018). As a wide-spread species in northern and Central Asia, Siberian larch (*Larix sibirica*) has played an important role in these studies (Hantemirov and Shiyatov, 2002; Briffa et al., 2013; Davi et al., 2015; Büntgen et al., 2016), revealing the relationships between temperature and volcanic and solar activities over the past 1000–2000 years. The upper tree line of this area is covered by widespread larch forests, which have high sensitivity to summer temperature (Chen et al., 2012; Davi et al., 2015). Although the region is an important source region for the major rivers in northern Asia, as mentioned above, there is still a need to better understand the role of regional climate on the hydrothermal interactions in mid- and high-latitude Asia. Meanwhile, tree-ring evidences revealed that extreme climate events in Mongolian Plateau have had some important impacts on the historical process of Eurasia (Pederson et al., 2014; Büntgen et al., 2016; Di Cosmo et al., 2017; Hessl et al., 2018). However, our understanding about the impacts of climate change on the rise and fall of Mongolian Plateau's nomadic empire is still limited.

Here, we use tree-ring width data from Siberian larch from four sites (**Table 1**) to create a mean June–July temperature reconstruction for the northern Mongolian Plateau since 1190 CE. Our aim is to develop a composite chronology and subsequent temperature reconstruction that minimizes uncertainty to evaluate large-scale temperature variations in the northern Mongolian Plateau, examine linkages between large-scale atmospheric circulation and reconstructed temperature, and temperature influences on hydrological systems in northern Asia. In particular, we focus on possible impacts of past temperature variation on Inner Asian historical societal changes.

MATERIALS AND METHODS

Tree-Ring Data and Climate Data

The Kelan River (KLR) Siberian larch (*Larix sibirica*) tree-ring width data are composed of 116 radii from 58 living trees growing at the sparsely populated rubble pile on either side of the ridge line of the Altay Mountains, China, and span 1170–2019 CE (850 years). This site represents the highest larch treeline in China's Altay Mountains (**Figure 1**). Standard dendrochronology techniques were used to develop the cross-dated and tree-ring width chronology (Cook and Kairiukstis, 1990). After air drying, mounting and progressively polishing to >600 grit with abrasive papers, the ring widths of the tree-ring samples from the KLR site were measured to an accuracy of 0.001 mm using a LINTAB measuring system and the cross-dating quality was controlled using the TSAP software package (Rinn 2003). Previous studies have shown that larch tree-ring records from the KOK, SUK, and OZN sites (**Table 1**) contribute knowledge related to the temperature variations in the northern Mongolian Plateau (**Figure 1**), including the Altay Mountains (Myglan et al., 2012; Davi et al., 2015). First, each individual tree-ring width series was detrended using the negative exponential curve, and the detrended sequences were combined into two regional chronologies for the Altay Mountains (KLR, KOK, and SUK) and the northern Mongolian Plateau (OZN). All sequences of the four sites (KLR, KOK, SUK, and OZN) were then combined into a new composite chronology (standard version) for regional temperature reconstruction of the northern Mongolian Plateau using the "signal-free" approach (Melvin and Briffa, 2008). By using a signal-free data-adaptive curve-fitting method where the detrending functions subsequently are forced to the same average as the local mean (Björklund et al., 2013), the composite chronology retained the long-term, centennial scale signals in excess of the segment lengths of the individual series as possible while removed non-climate signals.

The chronology reliability over time was assessed based on the running average correlation between the tree-ring width series (Rbar) and the expressed population signal (EPS) (computed over 50 years lagged by 25 years). The tree-ring width chronologies that started with fewer than 3 trees were truncated to ensure the stability of climate signals. In general,

TABLE 1 | Information about the sampling sites, meteorological and gauge stations in the northern Mongolian Plateau.

Name	Code	Time span	Longitude (E)	Latitude (N)	Elevation (m)	Trees/cores
Kelan river	KLR	1170–2019	88°20′	48°08′	2400	58/116
Sukor	SUK	1153–2012	88°10′	50°04′	2100	26/27
Kokcy	KOK	1273–2011	86°34′	49°22′	2200	23/23
Ondor Zuun Nuruu	OZN	715–2005	99°05′	51°09′	2400	104/209
Kusur	Lena	1950–2011	127°39′	70°42′		
Salekhard	Ob	1950–2011	66°36′	66°32′		
Igarka	Yenisey	1950–2011	86°30′	41°29′		

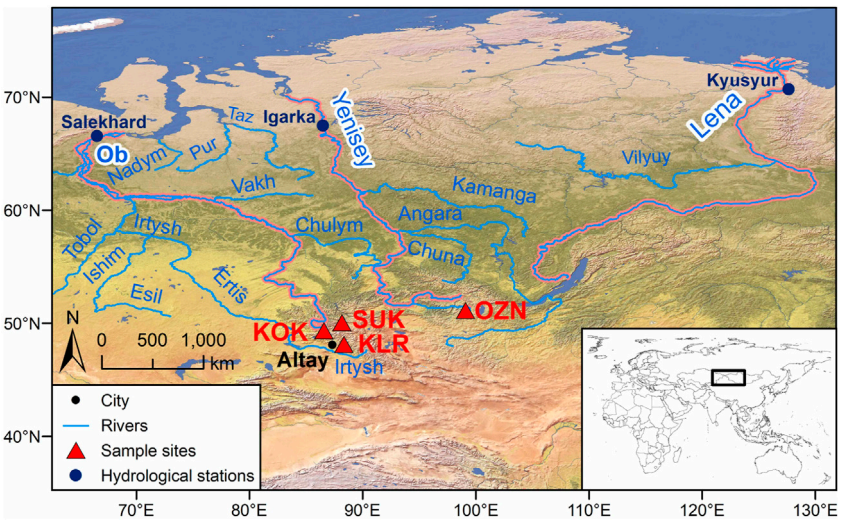

FIGURE 1 | Map of study area showing the locations of the main rivers (Yenisei, Lena and Ob) in norther Asia and the locations of the four tree-ring sampling sites (KLR, KOK, SUK, and OZN). See text for additional details.

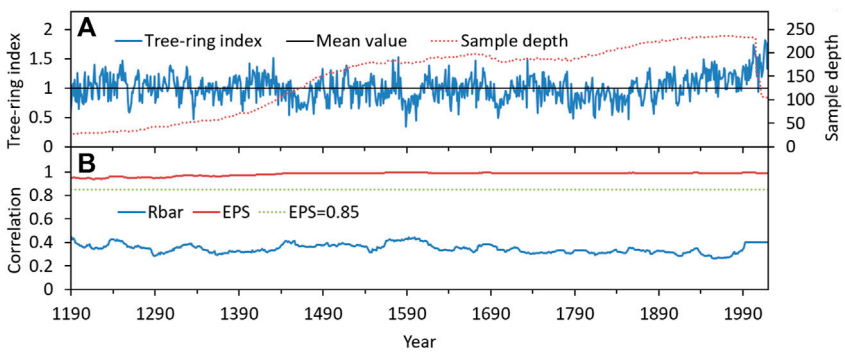

FIGURE 2 | Plots of **(A)** the composite chronology (bule line) and sample depth (red dotted line), and **(B)** running expressed population signal (EPS, blue line) and Rbar (mean correlation between ring-width series, red line) statistics.

an EPS value greater than or equal to 0.85 is a widely accepted threshold value for an adequate sample depth in reliable tree-ring chronologies, and thus, our composite chronology used in the temperature reconstructions below was truncated at 1190 CE (**Figure 2**). The common period for the two regional chronologies of the Altay Mountains and the northern Mongolian Plateau (Tree number >4) is 1190–2005 CE. To guarantee the length of the calibration period, the temperature reconstruction sequence is still extended from 2012 to 2019 by using the KLD tree-ring data.

To verify that our composite chronology has large-scale temperature signals, we also used gridded temperature data for

the same period in analysis. The monthly temperature data from the Climatic Research Unit (0.5 ° × 0.5 °; Harris et al., 2014) were obtained from the KNMI Climate Explorer (http://climexp.knmi.nl/) for the northern Mongolian Plateau (averaged over 45–55°N, 85–105°E) for the period from 1901 to 2018. At the same time, station temperature records from the Altay city (47°26′ N, 88°03′ E, 735.3 m a.s.l.) were compared herein to the composite chronology (**Figure 1**). The Altay station data cover the years 1955–2019. Thus, we performed analyses over a 64-year calibration period.

We assessed the strength of the resulting linear regression models based on adjusted r^2, *F*-values and the PRESS statistic (Weisberg, 1985). The temperature reconstruction for the northern Mongolian Plateau was created using the most appropriate model (Cook and Kairiukstis, 1990) from 1955 to 2018. We used a split calibration-verification scheme (Cook and Kairiukstis, 1990) to assess the reliability of the temperature reconstruction, that is, calibration (1955–1986) and verification (1987–2018), as well as calibration (1987–2018) and verification (1955–1986). The test statistics [the coefficient of efficiency (CE), the reduction of error (RE) and the sign test] for the temperature reconstruction are presented in **Table 2**. Meanwhile, to verify the reliability of the temperature reconstruction, we also correlated the temperature reconstruction with the station data (1955–2019) and CRU data (1901–1954).

To assess the stability of the temperature-tree-growth relationship in terms of the long-term climate, moving correlation calculations were calculated. To further explore the links between our temperature reconstructions and large-scale atmospheric circulations, we also correlated the temperature reconstruction with sea surface temperature (SST) data (1854–2019, Smith and Reynolds, 2005) and their related atmospheric-oceanic circulation patterns, such as the El Niño-Southern Oscillation (ENSO, NINO3.4, 1870–2019, Rayner et al., 2003), Atlantic Multidecadal Oscillation (AMO, 1900–2019, Enfield et al., 2001), sea ice cover (1870–2019, Rayner et al., 2003) and the AMO reconstruction (2017). We used instrumental streamflow data from the Salekhard, Igarka, and Kyusyur stations at the three large river catchments with at least 62 (1950–2011, **Supplementary Figure S1**), the streamflow data is provided by Global Runoff Data Centre (GRDC, https://www.bafg.de) years of streamflow measurements to reveal the effects of temperature changes in river source areas on the streamflow processes in northern Asia.

RESULTS

Climate Signals in Larch and Temperature Reconstruction

Although the distance between the sampling sites is over 800 km (**Figure 1**; **Table 1**), the two regional chronologies from the Altay Mountains and northern Mongolian Plateau are significantly positive correlated (r = 0.42, p< 0.01) over the common period 1190–2005 CE, and this result reflected the similar growth patternsat the upper tree line in this area. Consequently, we combined the detrended series of all cores from the four sites into a composite chronology. **Figure 3** shows the response of the radial growth of larch trees in the northern Mongolian Plateau to the mean temperature (CRU) from January to December in terms of Pearson correlation coefficients. Some significant positive correlations with temperatures from June to September were observed, with the strongest correlation appearing in June, which is the warmest season in the region (**Figure 3**). Similar responses of ring width to June-July temperature of the current growth year were found in larch trees from the northern Mongolian Plateau (Chen et al., 2012; Davi et al., 2015; Büntgen et al., 2016), indicating that warm season temperatures primarily control the radial growth of larch in the northern Mongolian Plateau.

After screened the composite chronology in correlation analysis with several seasonal mean temperature subsets from January to December of the current growth year, the highest correlation (r = 0.722, p < 0.01) was found between the composite chronology and mean June–July temperature (CRU) for the gridcells from 45 to 55° N to 85–105° E during the period 1955–2018. The model between the composite chronology and mean June–July temperature for the 1955–2018 calibration period was significant (F = 67.46, p < 0.001, adjusted r^2 = 0.513, PRESS = 28.32, Durbin-Watson = 1.463).

The model obtained was:

$$Y = 3.237X + 10.726 \quad (1)$$

where Y is mean June–July temperature and X is the composite chronology.

During the period (1955–2018) of the temperature data and tree-ring widths, the temperature reconstruction accounted for 52.1% of the actual temperature variance. As shown in **Figure 4**, the temperature reconstruction fits very well with the actual temperature series, and the first differences in the tree-ring series can also explain 23.4% of the actual temperature variances. Although the meteorological stations were relatively sparse before 1955, the correlation between the temperature reconstruction and CRU

TABLE 2 | Calibration and verification statistics for the June-July temperature reconstruction.

	Calibration (1987–2018)	Verification (1955–1986)	Calibration (1955–1986)	Verification (1987–2018)
RE	0.27	0.32	0.32	0.27
CE	0.14	0.20	0.20	0.14
Sign test		19+/13-		24+/8-[b]
First-order sign test		23+/8-[b]		23+/8-[b]

[a]*Significant at* p < *0.01*
[b]*significant at* p < *0.05*

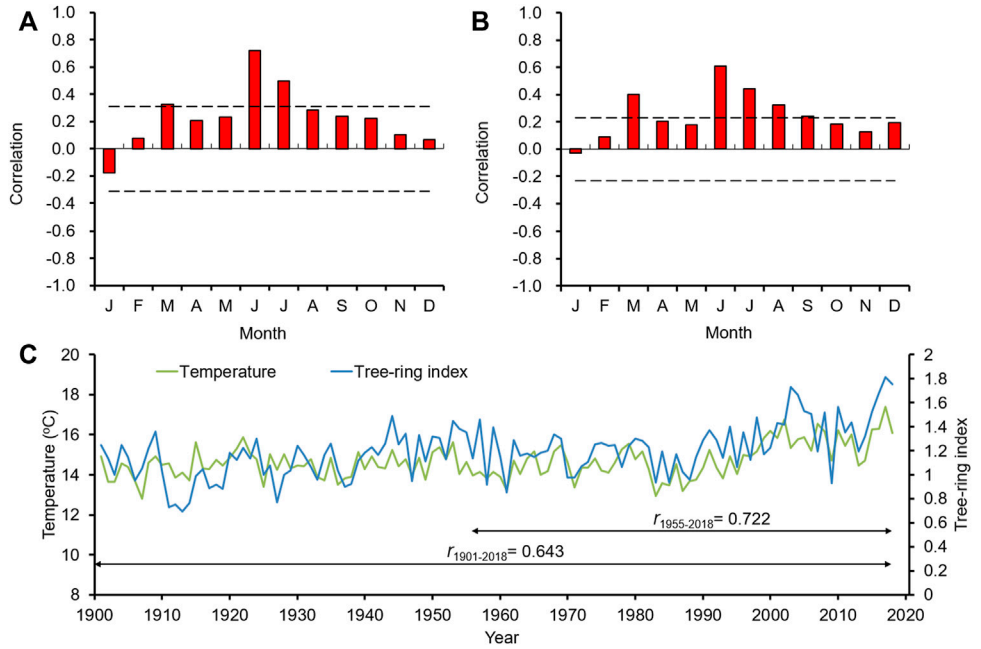

FIGURE 3 | Simple correlations of the composite chronology with the monthly CRU mean temperature **(A)** (1955–2018; **(B)** (1901–2018) from January to current December. The dash lines indicate significant variables ($p < 0.01$). **(C)** CRU mean June–July temperature and the composite chronology during their common period 1901–2018.

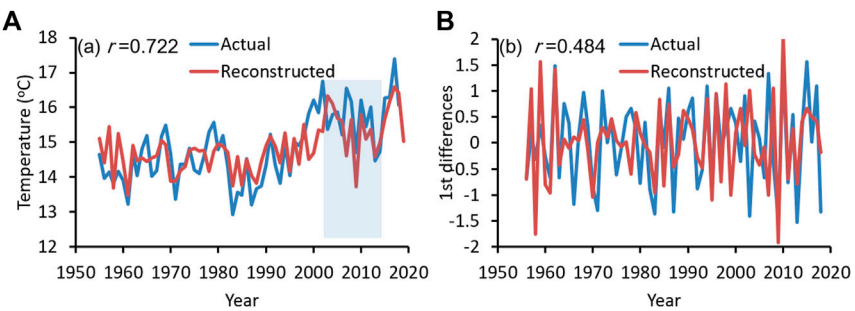

FIGURE 4 | (A) Comparison between the acutal and reconstructed mean June–July temperature for the period 1955–2018. **(B)** Comparison between the first differences of acutal and reconstructed mean June–July temperature for the period 1955–2018. The blue shadow indicates the recent warming hiatus.

temperature decreased from 1901–1954, the tree-ring series still explained 41.3% of the actual temperature variances from 1901–2018, and at the same time, the correlation between the temperature reconstruction and station temperature records from the Altay city reached 0.54 ($p < 0.01$) during the period from 1955–2019. Both RE and CE were positive, and the results of the sign tests were significant ($p < 0.05$), except for the sign test of the original values during the 1955–1986 period (**Table 2**), and these results demonstrate the validity of the temperature reconstruction model.

Temperature History

Figure 5 shows the reconstructed temperature of the northern Mongolian Plateau for the 1190–2019 period, with its average being 13.9°C cooler than that measured for the 1901–2018 period (14.7°C). The coldest summers are in 1589 (11.8°C) and 1601 (12.2°C), and the warmest summers are in 2017 (16.6°C), 2018 (16.4°C), and 2003 (16.3°C). Evidence of a pronounced Medieval Warm Period (MWP, 1190s–1430s), Little Ice Age (LIA, 1440s–1850s), and modern warm period (1850s–2010s) is revealed by our temperature reconstruction (Mann et al., 2009; Davi et al., 2015). For the MWP, high temperatures in the 1210s–1250s, 1270s–1320s, 1380s, and 1400s–1430s and low temperatures in the 1190s–1200s, 1260s, 1330s–1370s, and 1390s are recorded, with some fluctuations within a narrow range. During the LIA, the temperature reconstruction shows strong downward fluctuations (1440s–1510s, 1580s–1600s, 1680s–1720s, and 1760s–1850s) through a generally cold

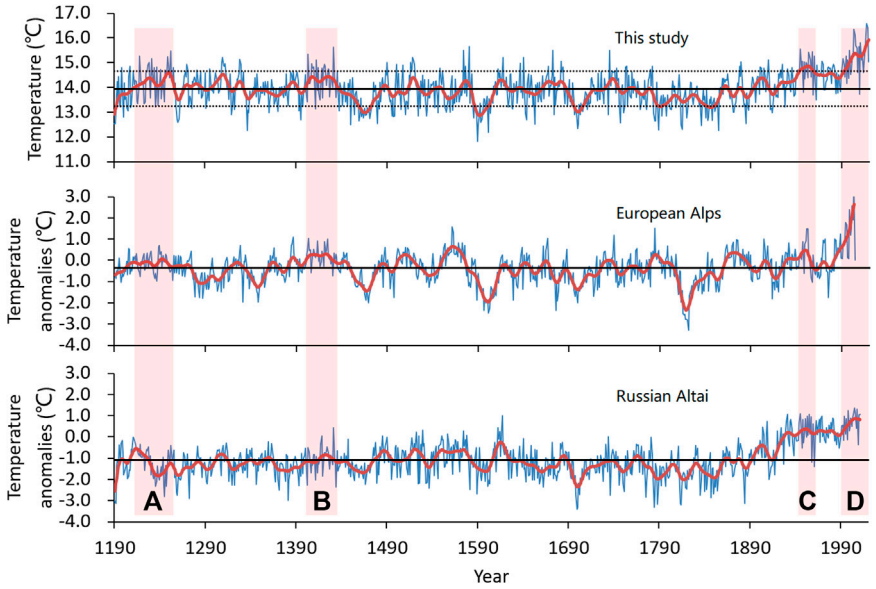

FIGURE 5 | Original (Thick) and 20-year low-pass filtered (thin) temperature reconstruction for northern Mongolian Plateau, the European Alps, and Russian Altai. The long-term average of the temperature reconstruction of northern Mongolian Plateau during 1190–2019 CE (13.9°C). The boxes mark important Asian historical landmarks: **(A)** Mongol conquests (1210s–1250s), **(B)** The rise of Oirat Mongols (1400s–1430s), **(C)** the warm period 1940s–1950s and **(D)** the warm period 1990s–present.

period from the 1440s–1850s. The temperatures showed a ladder-like, upward trend and discontinuously increased since the 1860s with notable depressions in the 1870s–1890s, 1910s–1920s, and 1960s–1980s. Meanwhile, correlations of this study with Russian Altai and European Alps (Büntgen et al., 2016), computed over the common periods are 0.32 and 0.72, and two remarkably warming episodes (1940s–1950s and 1990s–present) were found in the northern Mongolian Plateau, which resembles other findings in the European Alps and suggests the influence of similar large-scale forcings on the Eurasian climate. Undoubtedly, the last 30 years (1990s–present, 15.2°C) was the warmest period over the past 830 years in the northern Mongolian Plateau, and our temperature reconstruction also captures large-scale temperature signals for Central and northern Asia (**Figure 6A**).

Spatial correlations of the temperature reconstruction with June-July SSTs (1854–2019) show that positive correlations are located in the North Atlantic and equatorial Indian and Pacific Oceans (**Figure 6B**), and the trend exhibit good synchronization with the global annual average SSTs during 1870–2000 (Rayner et al., 2003). Significant negative correlations are found with the Hadley Centre sea ice cover (Rayner et al., 2003) in the Arctic Ocean, with the highest correlations occurring on the Arctic coast of northern Asia, especially in the Ob estuary (**Figure 6C**), and this may means that the recent temperature variability in the study area may have strong associations with unprecedented low summer sea ice extent in the Arctic Ocean (Kinnard et al., 2011).

To reveal the influences of large-scale temperature variations on vegetation productivity change and the water cycle in Central and northern Asia, we analyzed multiple correlations of our temperature reconstruction with various lags of monthly and seasonal combinations of the normalized difference vegetation index (NDVI, Tucker et al., 2005) and streamflow data (Yenisei, Lena and Ob) for the common period. Due to the flat topography and relatively uniform climate in Siberia, our temperature reconstructions are closely related (r = 0.68) to a NDVI field north of approximately 45–70° latitude with a large east-west expansion during the 1981–2019 period (**Figure 6D**). Meanwhile, the temperature reconstruction is negatively correlated (r = -0.40, p < 0.01) with the July-August streamflow data from the Salekhard, Igarka, and Kyusyur stations during the 1950–2011 period and is positively correlated (r = 0.40, p < 0.01) with streamflow from January-May of the previous year (**Figures 7A,B**). The temperature reconstruction is positively correlated with the average April-July NINO3.4 (5°N-5°S 170°W-120°W) SST index (r = 0.20, p < 0.05) over the 1870–2019 period, and a significant correlation (r = 0.40, p < 0.01) was found between the temperature reconstruction and previous September-July AMO over the 1900–2019 period (**Figures 7C,D**). Meanwhile, a strong correlation (r = 0.43, p < 0.01) was also found between the temperature reconstruction and August-April AMO over the 1900–2019 period. Interestingly, most of the cycles fall within the range of AMO variability based on the results of the multi-taper method (MTM) spectral analysis (**Figure 8A**), and correlation between this study and the AMO reconstruction (Wang et al., 2017), computed over the 1190–2010 common period is 0.30, and increase to 0.58 after 20-yr smoothing, and

suggesting strong teleconnections between AMO and the temperature variability in the source area of the Northern Asian great river Basins.

Testing for Tree-Ring Divergence in the Northern Mongolian Plateau

The earth's climate is always changing, and the reliability of tree-ring records, especially their ability to record low-frequency signals, has been questioned (Büntgen et al., 2008). Since the 1960s, due to the influence of global warming and its associated regional environmental/climate changes, the temporal stability of the relationship between tree rings and temperature has weakened in some parts of the world (D'Arrigo et al., 2008). Meanwhile, global warming has not shown a linear upward trend, and the recent global warming slowdown, which started after 1997/1998 and has lasted for nearly 15 years related to equatorial Pacific surface cooling (Kosaka and Xie, 2013; Medhaug et al., 2017). Both global warming and warming hiatuses are likely to have had some significant impacts on larch tree growth; however, whether they will have an impact on the stability of the reconstruction is worth further discussion. To investigate the stability of the temperature-growth relationship, a 31-year correlation was observed between the temperature reconstruction and CRU June–July temperatures during the 1901–2018 period (**Figure 9A**). The correlations throughout the whole period were greater than 0.34 ($p < 0.05$), and there were relatively high correlations ($p < 0.01$) with the CRU June–July temperatures in the warm periods 1940s–1950s and 1980s–2010s over the past 80 years (**Figure 9A**). Meanwhile, no significant correlations between tree-ring series and precipitation were revealed (not shown). The results revealed that old larch trees could effectively record the temperature changes without precipitation restrictions at the upper tree line in the northern Mongolian Plateau. The temperature-sensitive tree-ring width series of larch trees did not continue to increase, and the growth rate slowed during the 2000–2015 period (**Figure 4A** and **Figure 9B**), and suggesting a possible connection between regional temperature and the recent global warming hiatus. These results indicate that summer temperature variations over the past 100 years have had some stable positive impacts on the radial growth of larch trees in the northern Mongolian Plateau. Despite this slowdown in growth, the upward trend has not changed and regional temperatures remain significantly warmer.

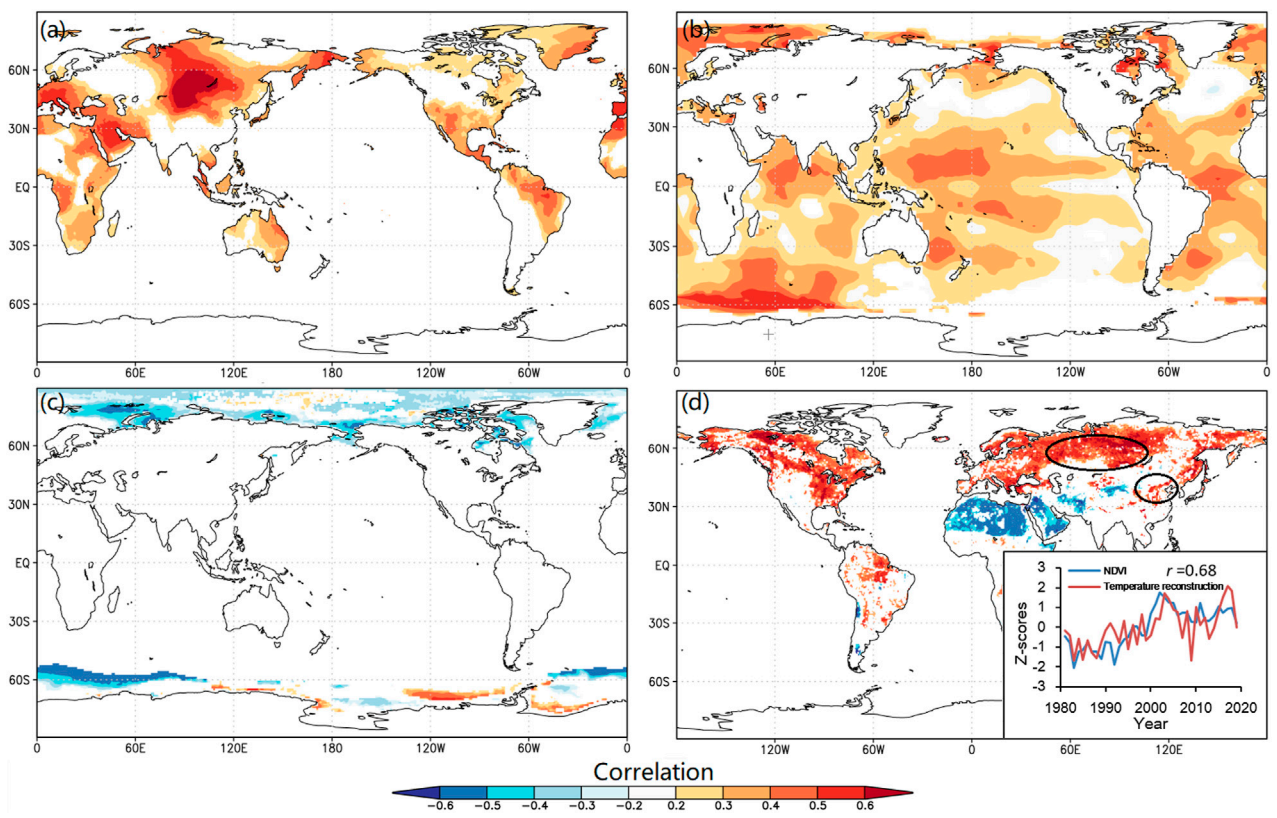

FIGURE 6 | Spatial correlation patterns of temperature reconstruction with CRU temperature **(A)**, (1955–2018), SSTs **(B)**, (1854–2019), sea ice **(C)**, 1870–2019) and NDVI **(D)**, 1981–2019) for the common periods. Note that only correlations ($p < 0.05$) are shown in this figure. Comparison between the Normalized (z-score) NDVI series and the temperature reconstruction is shown in the inside panel of **(D)**.

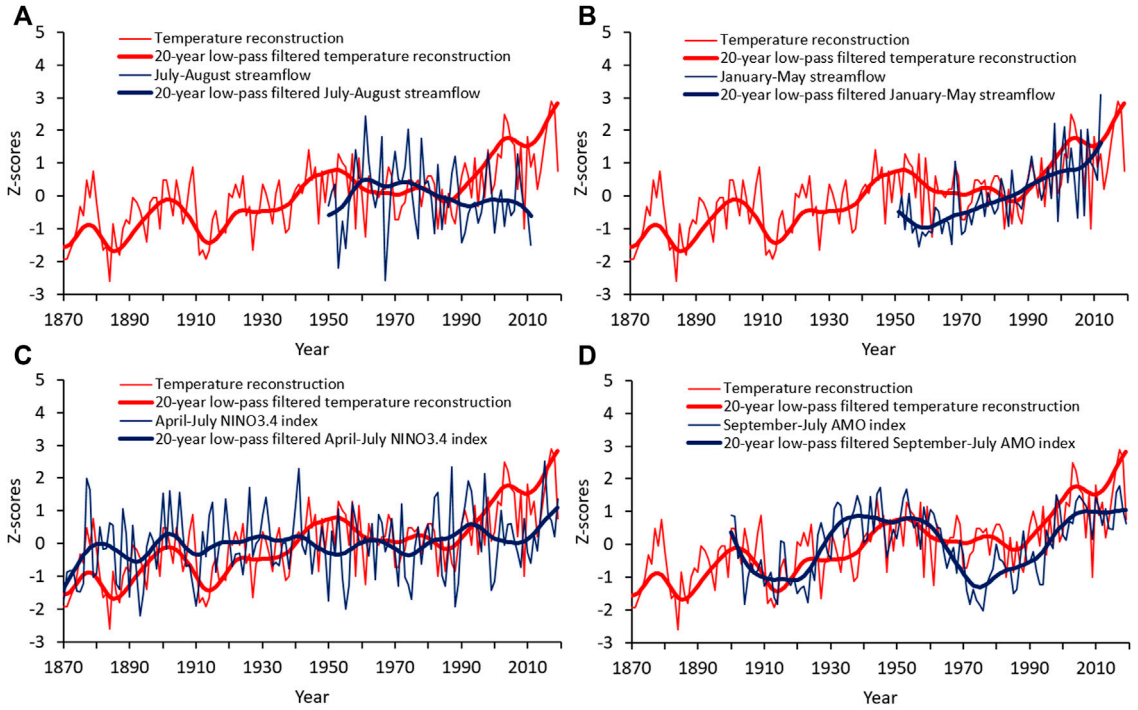

FIGURE 7 | Comparison of the temperature reconstruction (thin lines) and its 20-year low-pass filtered values (thick lines) with **(A)** July-August streamflow, **(B)** January-May streamflow, **(C)** April-July NINO3.4 SST index and **(D)** August-April AMO index.

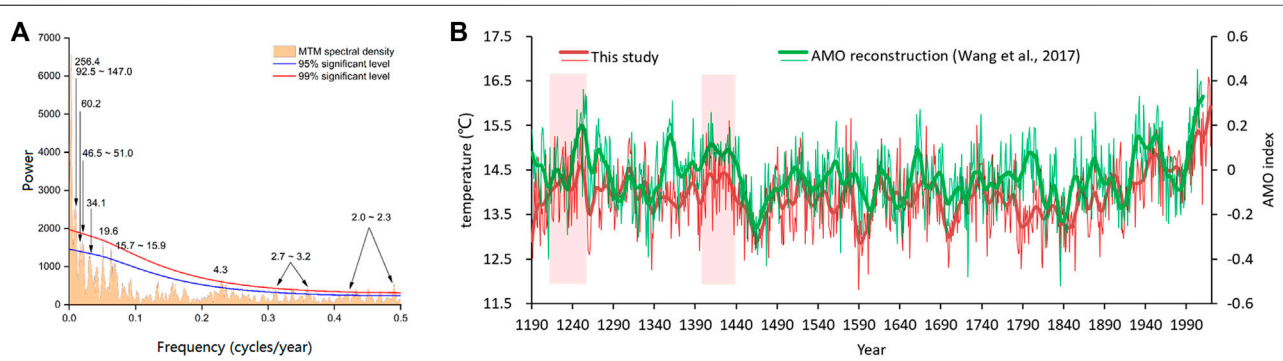

FIGURE 8 | (A) Power spectrum of June–July temperature (1190–2019). **(B)** Comparison between the reconstructed mean June–July temperature and reconstructed AMO (Wang et al., 2017) for the period 1190–2010. The thick lines are the 20-year low-pass filtered values. The boxes mark important Asian historical landmarks: Mongol conquests and the rise of Oirat Mongols.

DISCUSSION

Linkages With Water and Atmospheric-Oceanic Circulations

Considering the distance from the ocean and the possibility of being affected by other climatic forcings, the low correlation between the temperature reconstruction and ENSO is not surprising. The eastern equatorial Pacific has some of the warmest SSTs and plays an important role in global temperature change (Kosaka and Xie, 2013; Chen and Jin, 2018; Koutavas, 2018). Although SSTs in this area do not directly affect the temperature of the study area, recent SST fluctuations through global ocean–atmosphere–land processes has shown impacts in this study, and as a result, the temperature reconstruction is synchronized with global warming and the recent warming slowdown. More importantly, climate anomalies in the adjacent Arctic and North Atlantic Oceans will more than likely lead to the unusually high summer temperatures in Eurasia (Serreze and Barry, 2011; Cohen et al., 2014). Although the season of our reconstruction is relatively short, our results indicate that the SSTs in the adjacent Arctic and North Atlantic Oceans have a significant positive effect on summer temperature variations in Eurasia (**Figure 6B**), and showed that high SSTs that cause high

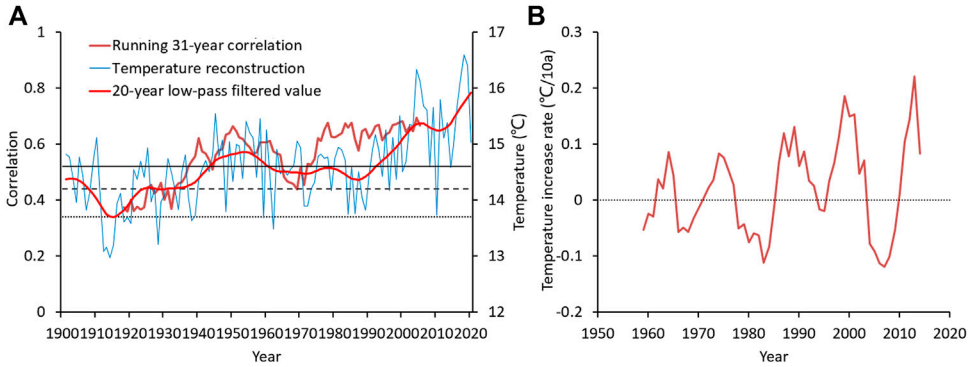

FIGURE 9 | (A) Comparison of temperature reconstruction with running 31-year correlation between the composite chronology and CRU June–July temperatures. The dash and dotted lines indicate the 95 and 99% significance level, respectively. **(B)** The moving ten-years increase rate of temperature reconstruction.

temperature in one year also tend to carry over their effect on the climate of the subsequent cold season. The Atlantic Multidecadal Oscillation (AMO) is defined as the fluctuation pattern of North Atlantic SSTs, and has a 60–80 years cycle (Enfield et al., 2001; Wang et al., 2017; Zhang et al., 2019), and the linkages to the North Atlantic SSTs suggest the connection of regional temperature variations to the large-scale circulations (**Figure 7D**). Meanwhile, as the AMO has some important influences on the winter and summer monsoon intensity in East Asia, the temperature variations in the northern Mongolian Plateau affect the climate of the whole Eurasian continent through the interaction of water and energy over Asia (Lu et al., 2006; Wang et al., 2017; Nagaraju et al., 2018; Huang et al., 2019; Fang et al., 2019; Monerie et al., 2019). The linkages may suggest a framework for the relationship of the temperature and NDVI anomaly in the northern Mongolian Plateau with the SST anomalies in surrounding oceans and the atmospheric circulation anomalies (**Figure 7**). During the positive phase of the AMO, the Asian winter monsoon is weakening and warmer over most of the Mongolian Plateau (Wang et al., 2009; Chylek et al., 2014), which reduces the risk of freeze injury and promotes vegetation growth in our study area (Liu et al., 2015; Peng et al., 2020), and while the southern Mongolian Plateau can be affected by the enhanced Asian summer monsoon and lead to the NDVI increase at the northern fringe of the East Asian summer monsoon in China (Wang et al., 2009; Wang et al., 2011), the climate condition has improved, and during the cold phase of the AMO, the opposite pattern occurs.

Eurasia is an important heat source for the Arctic in summer, and the temperature in Eurasia may also have some feedback effects on the Arctic climate change (Matsumura et al., 2014). Studies have shown that rivers flowing into the Arctic Ocean provide warm water that accelerates the rate of sea ice melt (Ekwurzel et al., 2001; Adam and Lettenmaier, 2008; Shu et al., 2017; Lesack et al., 2014). However, unlike glacier-fed rivers, the streamflow of the headwaters area mostly depends on precipitation variation in the study area, including the Yenisei, Lena and Ob rivers (Davi et al., 2013; Chen et al., 2016). In the three great river basins, all of which originate from the northern Mongolian Plateau, the correlation coefficients are greater than 0.73 (**Supplementary Figure S1**), indicating that there are strong common signals between them. Although the Siberian forests provide a stable supply of water for rivers, streamflow variation is still likely related to precipitation or drought changes (Troy et al., 2012). Therefore, the increase in regional evaporation and the decrease in regional water supply under relatively high temperature conditions (IPCC AR5, 2013; Huang et al., 2016; Zhang et al., 2020) will lead to a decrease in streamflow from the source area of the Northern Asian great river Basins and increase in warm water temperature from Eurasia to the Arctic Ocean (Liu et al., 2005; Georgiadi et al., 2017), and causing the changes in Arctic sea ice melt onset, freezeup, and melt season length (Markus et al., 2009; Nummelin et al., 2016; Lambert et al., 2019). In addition, due to the advance of snowmelt season results from climate warming, the high-level warm water transport from the Eurasian continent during the cold season (January–May) of previous year, which also should provide relatively abundant warm water that will affect the water and energy balance in the Arctic and cause Arctic sea ice anomalies and summer temperatures for the next year (Park et al., 2017; Durocher et al., 2019; Lambert et al., 2019; Park et al., 2020). Seen together, these results suggest significant relationships between the temperature change and the water circulation of Northern Asian great river basins. However, the mechanism how these circulations interact and how they influence on the climate change in the Arctic needs to be further studied, especially for the Arctic sea ice.

Possible Impacts on Regional Environment and Human Activity

In the context of the modern climate, the unprecedented warming may have led to abrupt shift to hotter and drier climate occurred at Mongolian Plateau and a continued increase in evaporation, causing water stress for the vegetation growth during the growing season, and has some serious impacts for Mongolian Plateau's ecosystems (Hessl et al., 2018; Zhang et al., 2020). Based on observational data and climate reconstructions, the recent 30 years may have been one of the worst drought periods in the Mongolian Plateau in the last century (Li et al., 2009; Davi et al., 2010; Fang et al., 2010; Pederson et al., 2014; Tong et al., 2018; Zhang et al., 2020). According to the climate prediction results, drought in the Mongolian region will intensify under continued warming (Intergovernmental Panel on Climate Change Fifth Assessment Report (IPCC AR5), 2013; Hessl et al., 2018). However, our research showed that the impacts of climate

warming on different parts of Mongolian Plateau vary greatly due to complex geographical environment and spatial differences in local temperature and vegetation growth. The climate is relatively humid in the upper treeline of the study area and its northern area, and at high elevation, summer temperature is the dominant growth factor. Under warm climate conditions, tree growth and its related vegetation productivity rapidly increase for the source area of the Northern Asian great river Basins, northern Mongolian Plateau (**Figure 6D**). In the modern period, Siberia (Russia) and Xinjiang (China) will benefit from increased vegetation production (Yao et al., 2018; Iegorova et al., 2019), whereas Mongolia will be threatened by drought (IPCC AR5; Rao et al., 2015; Hessl et al., 2018). Some studies have indicated that climate change drove the migration of Mongolian Plateau nomads and that the Mongol Empire's expansion (1219–1260 CE) was based on ample material resources in the longer historical context (Pederson et al., 2014; Büntgen et al., 2016; Ganiev and Kukarskih, 2018). Based on the climate patterns, distribution of the correlations with vegetation productivity and the transfer function between temperature reconstruction and NDVI (**Figure 6D**), it is possible that one of the targets of the Mongol conquests during the warm period 1210s–1250s (with positive AMO) was to obtain better grassland in northern and eastern Asia, and the increased NDVI (+2.3%) also provided a better material basis for the conquests (Pederson et al., 2014). Similarly, during the warm period 1400s–1430s, with high NDVI (+2.7%) and wet condition (Pederson et al., 2014; Hessl et al., 2018), the Oirat Mongols (leader: Toghon Taishi) completed the unification of the Mongolian Plateau in 1438 CE, and the Oirat Mongols (leader: Esen Taishi) attacked the northern part of the Ming Empire and captured the Zhengtong Emperor during the Tumu crisis (1449 CE) (Mote, 1998; Harris, 2015) (**Figure 8**). With the onset of the Little Ice Age, Mongolian Plateau was once again divided, and no strong unified regime has ever been established in the region.

The AMO-dominated framework shown earlier probably played an important role in these historical processes. However, our study reveals a positive contribution of climate warming to the vegetation productivity in northern Mongolian Plateau, we also should recognize that the impact of this unprecedented warming on the ecosystem is highly uncertain (Hessl et al., 2018; Zhang et al., 2020), and this unprecedented temperature and high evaporation in the study area and its northern area also may lead to reduced tree growth and transboundary river runoff significantly when climate warm beyond a physiological threshold, causing irreversible damage to the ecosystem. More importantly, as the melting of Arctic sea ice accelerates under unprecedented warming conditions, it could make Arctic shipping lanes possible and lengthen the sailing time, making it easier to transport material and energy across northern Asia (Khon et al., 2010; Stroeve et al., 2012; Aksenov et al., 2017). As can be seen above, the effects of climate change are not limited by national boundaries, we must therefore strengthen international collaboration to address climate change.

CONCLUSION

We have shown the June-July temperature variations for the northern Mongolian Plateau since 1190 CE based on tree-ring width data of larch trees. The final reconstruction indicates relatively warm summers in the 13–14th and twentieth centuries divided by prolonged cooling from the 1440s–1850s. The warmest period occurred during the late 20th century and early 21st century. Temperature reconstruction is negatively correlated with streamflow and Arctic sea ice, meaning that during warmer summers, low streamflow tends to occur over northern Asia. Some links between AMO and northern Asian temperature are also revealed. More studies are needed to better understand the feedback of temperature in the hinterland of Eurasia to large-scale oceanic and atmospheric circulations and the impacts of climate change on water systems. Grasslands with higher vegetation productivity under the consistently warm and wet conditions attracted nomads and strengthened the power of Inner Asian steppe empires.

Given the rapid warming of Northern Eurasia over the past 40 years, a more comprehensive picture of past and potential climate change impacts is essential for developing appropriate risk management strategies. At present, there is great uncertainty in the prediction of temperature changes in Northeast Asia. According to the results of the climate observations (Intergovernmental Panel on Climate Change Fifth Assessment Report (IPCC AR5), 2013), the temperature in the Arctic region is rising. Understanding of the climate dynamics of Northern and Central Asia has been limited, in part because of the lack of instrumental records and the complexity of the climatic change in the region and because it is difficult to describe the effects and feedbacks of many possible forcing effects. The temperature reconstruction described here, combined with existing instrumental climate and hydrographic data, provides an important tool for a better understanding of climate-driven mechanisms in the region.

DATA AVAILABILITY STATEMENT

The original contributions presented in the study are included in the article/**Supplementary Material**, further inquiries can be directed to the corresponding author.

AUTHOR CONTRIBUTIONS

FC contributed to conception and design of the study. FC, HZ, and YC organized the database. FC performed the statistical analysis. FC wrote the first draft of the manuscript. FC, HZ, YC, and ND wrote sections of the manuscript. All authors contributed to manuscript revision, read, and approved the submitted version.

FUNDING

This research was supported by NSFC (U1803341) and the National Key R&D Program of China (2018YFA0606401).

SUPPLEMENTARY MATERIAL

The Supplementary Material for this article can be found online at: https://www.frontiersin.org/articles/10.3389/feart.2022.904851/full#supplementary-material

REFERENCES

Adam, J. C., and Lettenmaier, D. P. (2008). Application of New Precipitation and Reconstructed Streamflow Products to Streamflow Trend Attribution in Northern Eurasia. *J. Clim.* 21 (8), 1807–1828. doi:10.1175/2007jcli1535.1

Aksenov, Y., Popova, E. E., Yool, A., Nurser, A. J. G., Williams, T. D., Bertino, L., et al. (2017). On the Future Navigability of Arctic Sea Routes: High-Resolution Projections of the Arctic Ocean and Sea Ice. *Mar. Policy* 75, 300–317. doi:10.1016/j.marpol.2015.12.027

Björklund, J. A., Gunnarson, B. E., Krusic, P. J., Grudd, H., Josefsson, T., Östlund, L., et al. (2013). Advances towards Improved Low-Frequency Tree-Ring Reconstructions, Using an Updated Pinus Sylvestris L. MXD Network from the Scandinavian Mountains. *Theor. Appl. Climatol.* 113, 697–710. doi:10.1007/s00704-012-0787-7

Briffa, K. R., Melvin, T. M., Osborn, T. J., Hantemirov, R. M., Kirdyanov, A. V., Mazepa, V. S., et al. (2013). Reassessing the Evidence for Tree-Growth and Inferred Temperature Change during the Common Era in Yamalia, Northwest Siberia. *Quat. Sci. Rev.* 72, 83–107. doi:10.1016/j.quascirev.2013.04.008

Büntgen, U. L. F., Frank, D., Wilson, R. O. B., Carrer, M., Urbinati, C., and Esper, J. A. N. (2008). Testing for Tree-Ring Divergence in the European Alps. *Glob. Change Biol.* 14 (10), 2443–2453. doi:10.1111/j.1365-2486.2008.01640.x

Büntgen, U., Myglan, V. S., Ljungqvist, F. C., McCormick, M., Di Cosmo, N., Sigl, M., et al. (2016). Cooling and Societal Change during the Late Antique Little Ice Age from 536 to Around 660 AD. *Nat. Geosci.* 9 (3), 231–236. doi:10.1038/ngeo2652

Chen, F., Yuan, Y.-j., Wei, W.-s., Fan, Z.-a., Zhang, T.-w., Shang, H.-m., et al. (2012). Climatic Response of Ring Width and Maximum Latewood Density of *Larix Sibirica* in the Altay Mountains, Reveals Recent Warming Trends. *Ann. For. Sci.* 69 (6), 723–733. doi:10.1007/s13595-012-0187-2

Chen, F., Yuan, Y.-j., Wei, W.-s., Zhang, T.-w., Shang, H.-m., and Zhang, R. (2014). Precipitation Reconstruction for the Southern Altay Mountains (China) from Tree Rings of Siberian Spruce, Reveals Recent Wetting Trend. *Dendrochronologia* 32 (3), 266–272. doi:10.1016/j.dendro.2014.06.003

Chen, F., Yuan, Y., Davi, N., and Zhang, T. (2016). Upper Irtysh River Flow since AD 1500 as Reconstructed by Tree Rings, Reveals the Hydroclimatic Signal of Inner Asia. *Clim. Change* 139 (3-4), 651–665. doi:10.1007/s10584-016-1814-y

Chen, Y. Y., and Jin, F. F. (2018). Dynamical Diagnostics of the SST Annual Cycle in the Eastern Equatorial Pacific: Part I a Linear Coupled Framework. *Clim. Dyn.* 50 (5-6), 1841–1862. doi:10.1007/s00382-017-3725-7

Chylek, P., Klett, J. D., Lesins, G., Dubey, M. K., and Hengartner, N. (2014). The Atlantic Multidecadal Oscillation as a Dominant Factor of Oceanic Influence on Climate. *Geophys. Res. Lett.* 41 (5), 1689–1697. doi:10.1002/2014gl059274

Cohen, J., Screen, J. A., Furtado, J. C., Barlow, M., Whittleston, D., Coumou, D., et al. (2014). Recent Arctic Amplification and Extreme Mid-latitude Weather. *Nat. Geosci.* 7 (9), 627–637. doi:10.1038/ngeo2234

D'Arrigo, R., Jacoby, G., Frank, D., Pederson, N., Cook, E., Buckley, B., et al. (2001). 1738 Years of Mongolian Temperature Variability Inferred from a Tree-Ring Width Chronology of Siberian Pine. *Geophys. Res. Lett.* 28 (3), 543–546. doi:10.1029/2000gl011845

D'Arrigo, R., Wilson, R., Liepert, B., and Cherubini, P. (2008). On the 'Divergence Problem'in Northern Forests: a Review of the Tree-Ring Evidence and Possible Causes. *Global and planetary change* 60, 289–305.

Davi, N., Jacoby, G., Fang, K., Li, J., D'Arrigo, R., Baatarbileg, N., et al. (2010). Reconstructing Drought Variability for Mongolia Based on a Large-Scale Tree Ring Network: 1520–1993. *J. Geophys. Res. Atmos.* 115 (D22), 1520–1993. doi:10.1029/2010jd013907

Davi, N. K., D'Arrigo, R., Jacoby, G. C., Cook, E. R., Anchukaitis, K. J., Nachin, B., et al. (2015). A Long-Term Context (931-2005 C.E.) for Rapid Warming over Central Asia. *Quat. Sci. Rev.* 121, 89–97. doi:10.1016/j.quascirev.2015.05.020

Davi, N. K., Pederson, N., Leland, C., Nachin, B., Suran, B., and Jacoby, G. C. (2013). Is Eastern Mongolia Drying? A Long-Term Perspective of a Multidecadal Trend. *Water Resour. Res.* 49 (1), 151–158. doi:10.1029/2012wr011834

Di Cosmo, N., Oppenheimer, C., and Büntgen, U. (2017). Interplay of Environmental and Socio-Political Factors in the Downfall of the Eastern Türk Empire in 630 CE. *Clim. change* 145 (3-4), 383–395. doi:10.1007/s10584-017-2111-0

Durocher, M., Requena, A. I., Burn, D. H., and Pellerin, J. (2019). Analysis of Trends in Annual Streamflow to the Arctic Ocean. *Hydrol. Process.* 33 (7), 1143–1151. doi:10.1002/hyp.13392

Ekwurzel, B., Schlosser, P., Mortlock, R. A., Fairbanks, R. G., and Swift, J. H. (2001). River Runoff, Sea Ice Meltwater, and Pacific Water Distribution and Mean Residence Times in the Arctic Ocean. *J. Geophys. Res.* 106 (C5), 9075–9092. doi:10.1029/1999jc000024

Enfield, D. B., Mestas-Nuñez, A. M., and Trimble, P. J. (2001). The Atlantic Multidecadal Oscillation and its Relation to Rainfall and River Flows in the Continental US. *Geophys. Res. Lett.* 28 (10), 2077–2080. doi:10.1029/2000gl012745

E. R. Cook and L. Kairiukstis (Editors) (1990). *Methods of Dendrochronology: Applications in the Environmental Sciences* (Netherland: Kluwer), 408.

Fang, K., Davi, N., Gou, X., Chen, F., Cook, E., Li, J., et al. (2010). Spatial Drought Reconstructions for Central High Asia Based on Tree Rings. *Clim. Dyn.* 35 (6), 941–951. doi:10.1007/s00382-009-0739-9

Fang, K., Guo, Z., Chen, D., Wang, L., Dong, Z., Zhou, F., et al. (2019). Interdecadal Modulation of the Atlantic Multi-Decadal Oscillation (AMO) on Southwest China's Temperature over the Past 250 Years. *Clim. Dyn.* 52 (3-4), 2055–2065. doi:10.1007/s00382-018-4244-x

Ganiev, R., and Kukarskih, V. (2018). Climate Extremes and the Eastern Turkic Empire in Central Asia. *Clim. change* 149 (3-4), 385–397. doi:10.1007/s10584-018-2236-9

Georgiadi, A. G., Kashutina, E. A., and Milyukova, I. P. (2017). Long-term Changes of Water Flow, Water Temperature and Heat Flux of the Largest Siberian Rivers. *Polarforschung* 87 (2), 167–176. doi:10.2312/polarforschung.87.2.167

Hantemirov, R. M., and Shiyatov, S. G. (2002). A Continuous Multimillennial Ring-Width Chronology in Yamal, Northwestern Siberia. *The Holocene* 12 (6), 717–726. doi:10.1191/0959683602hl585rp

Harris, I., Jones, P. D., Osborn, T. J., and Lister, D. H. (2014). Updated High-Resolution Grids of Monthly Climatic Observations - the CRU TS3.10 Dataset. *Int. J. Climatol.* 34 (3), 623–642. doi:10.1002/joc.3711

Harris, L. J. (2015). Into the Frontiers: the Relay System and Ming Empire in the Borderlands, 1368-1449. *Ming Stud.* 2015 (72), 3–23. doi:10.1179/0147037x15z.00000000044

Hessl, A. E., Anchukaitis, K. J., Jelsema, C., Cook, B., Byambasuren, O., Leland, C., et al. (2018). Past and Future Drought in Mongolia. *Sci. Adv.* 4 (3), e1701832. doi:10.1126/sciadv.1701832

Huang, D., Dai, A., Yang, B., Yan, P., Zhu, J., and Zhang, Y. (2019). Contributions of Different Combinations of the IPO and AMO to Recent Changes in Winter East Asian Jets. *J. Clim.* 32 (5), 1607–1626. doi:10.1175/jcli-d-18-0218.1

Huang, J., Yu, H., Guan, X., Wang, G., and Guo, R. (2016). Accelerated Dryland Expansion under Climate Change. *Nat. Clim. Change* 6 (2), 166–171. doi:10.1038/nclimate2837

Iegorova, L. V., Gibbs, J. P., Mountrakis, G., Bastille-Rousseau, G., Paltsyn, M. Y., Ayatkhan, A., et al. (2019). Rangeland Vegetation Dynamics in the Altai Mountain Region of Mongolia, Russia, Kazakhstan and China: Effects of Climate, Topography, and Socio-Political Context for Livestock Herding Practices. *Environ. Res. Lett.* 14 (10), 104017. doi:10.1088/1748-9326/ab1560

Intergovernmental Panel on Climate Change Fifth Assessment Report (IPCC AR5) (2013). Summary for Policymakers: The Physical Science Basis. Contribution of Working Group I to the IPCC Fifth Assessment Report Climate Change. Available at: http://en.wikipedia.org/wiki/IPCC_Fifth_Assessment_Report (Accessed May 15, 2022).

Iwao, K., and Takahashi, M. (2006). Interannual Change in Summertime Precipitation over Northeast Asia. *Geophys. Res. Lett.* 33 (16), L16703. doi:10.1029/2006gl027119

Jiang, L., Yao, Z., and Huang, H. (2016). Climate Variability and Change on the Mongolian Plateau: Historical Variation and Future Predictions. *Clim. Res.* 67 (1), 1–14. doi:10.3354/cr01347

Khon, V. C., Mokhov, I. I., Latif, M., Semenov, V. A., and Park, W. (2010). Perspectives of Northern Sea Route and Northwest Passage in the Twenty-First Century. *Clim. change* 100 (3-4), 757–768. doi:10.1007/s10584-009-9683-2

Kinnard, C., Zdanowicz, C. M., Fisher, D. A., Isaksson, E., de Vernal, A., and Thompson, L. G. (2011). Reconstructed Changes in Arctic Sea Ice over the Past 1,450 Years. *Nature* 479 (7374), 509–512. doi:10.1038/nature10581

Kosaka, Y., and Xie, S.-P. (2013). Recent Global-Warming Hiatus Tied to Equatorial Pacific Surface Cooling. *Nature* 501 (7467), 403–407. doi:10.1038/nature12534

Koutavas, A. (2018). Temperature Correlations between the Eastern Equatorial Pacific and Antarctica over the Past 230,000 Years. *Earth Planet. Sci. Lett.* 485, 43–54. doi:10.1016/j.epsl.2017.12.041

Lambert, E., Nummelin, A., Pemberton, P., and Ilıcak, M. (2019). Tracing the Imprint of River Runoff Variability on Arctic Water Mass Transformation. *J. Geophys. Res. Oceans* 124 (1), 302–319. doi:10.1029/2017jc013704

Lesack, L. F. W., Marsh, P., Hicks, F. E., and Forbes, D. L. (2014). Local Spring Warming Drives Earlier River-Ice Breakup in a Large Arctic Delta. *Geophys. Res. Lett.* 41 (5), 1560–1567. doi:10.1002/2013gl058761

Li, J., Cook, E. R., D'arrigo, R., Chen, F., and Gou, X. (2009). Moisture Variability across China and Mongolia: 1951–2005. *Clim. Dyn.* 32 (7-8), 1173–1186. doi:10.1007/s00382-008-0436-0

Liu, B., Yang, D., Ye, B., and Berezovskaya, S. (2005). Long-term Open-Water Season Stream Temperature Variations and Changes over Lena River Basin in Siberia. *Glob. Planet. Change* 48, 96–111. doi:10.1016/j.gloplacha.2004.12.007

Liu, Y., Cai, W., Sun, C., Song, H., Cobb, K. M., Li, J., et al. (2019). Anthropogenic Aerosols Cause Recent Pronounced Weakening of Asian Summer Monsoon Relative to Last Four Centuries. *Geophys. Res. Lett.* 46, 5469–5479. doi:10.1029/2019gl082497

Liu, Y., Li, Y., Li, S., and Motesharrei, S. (2015). Spatial and Temporal Patterns of Global NDVI Trends: Correlations with Climate and Human Factors. *Remote Sens.* 7 (10), 13233–13250. doi:10.3390/rs71013233

Lu, R., Dong, B., and Ding, H. (2006). Impact of the Atlantic Multidecadal Oscillation on the Asian Summer Monsoon. *Geophys. Res. Lett.* 33 (24), L24701. doi:10.1029/2006gl027655

Luo, X., and Wang, B. (2019). How Autumn Eurasian Snow Anomalies Affect East Asian Winter Monsoon: a Numerical Study. *Clim. Dyn.* 52 (1-2), 69–82. doi:10.1007/s00382-018-4138-y

Mann, M. E., Zhang, Z., Rutherford, S., Bradley, R. S., Hughes, M. K., Shindell, D., et al. (2009). Global Signatures and Dynamical Origins of the Little Ice Age and Medieval Climate Anomaly. *Science* 326 (5957), 1256–1260. doi:10.1126/science.1177303

Markus, T., Stroeve, J. C., and Miller, J. (2009). Recent Changes in Arctic Sea Ice Melt Onset, Freeze up, and Melt Season Length. *J. Geophys. Res. Oceans* 114 (C12), C12024. doi:10.1029/2009jc005436

Matsumura, S., Zhang, X., and Yamazaki, K. (2014). Summer Arctic Atmospheric Circulation Response to Spring Eurasian Snow Cover and its Possible Linkage to Accelerated Sea Ice Decrease. *J. Clim.* 27 (17), 6551–6558. doi:10.1175/jcli-d-13-00549.1

Medhaug, I., Stolpe, M. B., Fischer, E. M., and Knutti, R. (2017). Reconciling Controversies about the 'global Warming Hiatus'. *Nature* 545 (7652), 41–47. doi:10.1038/nature22315

Melvin, T. M., and Briffa, K. R. (2008). A "Signal-free" Approach to Dendroclimatic Standardisation. *Dendrochronologia* 26 (2), 71–86. doi:10.1016/j.dendro.2007.12.001

Monerie, P. A., Robson, J., Dong, B., Hodson, D. L. R., and Klingaman, N. P. (2019). Effect of the Atlantic Multidecadal Variability on the Global Monsoon. *Geophys. Res. Lett.* 46 (3), 1765–1775. doi:10.1029/2018gl080903

Mote, F. W. (1998). *The Cambridge History of China: The Ming Dynasty*, 2. Cambridge, UK:: Cambridge University Press.

Myglan, V. S., Oidupaa, O. C., and Vaganov, E. A. (2012). A 2367-Year Tree-Ring Chronology for the Altai-Sayan Region (Mongun-Taiga Mountain Massif). *Archaeol. Ethnology Anthropol. Eurasia* 40 (3), 76–83. doi:10.1016/j.aeae.2012.11.009

Nagaraju, C., Ashok, K., Balakrishnan Nair, T. M., Guan, Z., and Cai, W. (2018). Potential Influence of the Atlantic Multi-Decadal Oscillation in Modulating the Biennial Relationship between Indian and Australian Summer Monsoons. *Int. J. Climatol.* 38 (14), 5220–5230. doi:10.1002/joc.5722

Nummelin, A., Ilicak, M., Li, C., and Smedsrud, L. H. (2016). Consequences of Future Increased Arctic Runoff on Arctic Ocean Stratification, Circulation, and Sea Ice Cover. *J. Geophys. Res. Oceans* 121 (1), 617–637. doi:10.1002/2015jc011156

Park, H., Watanabe, E., Kim, Y., Polyakov, I., Oshima, K., Zhang, X., et al. (2020). Increasing Riverine Heat Influx Triggers Arctic Sea Ice Decline and Oceanic and Atmospheric Warming. *Sci. Adv.* 6 (45), eabc4699. doi:10.1126/sciadv.abc4699

Park, H., Yoshikawa, Y., Yang, D., and Oshima, K. (2017). Warming Water in Arctic Terrestrial Rivers under Climate Change. *J. Hydrometeorol.* 18 (7), 1983–1995. doi:10.1175/jhm-d-16-0260.1

Pederson, N., Hessl, A. E., Baatarbileg, N., Anchukaitis, K. J., and Di Cosmo, N. (2014). Pluvials, Droughts, the Mongol Empire, and Modern Mongolia. *Proc. Natl. Acad. Sci. U.S.A.* 111 (12), 4375–4379. doi:10.1073/pnas.1318677111

Pederson, N., Leland, C., Nachin, B., Hessl, A. E., Bell, A. R., Martin-Benito, D., et al. (2013). Three Centuries of Shifting Hydroclimatic Regimes across the Mongolian Breadbasket. *Agric. For. meteorology* 178-179, 10–20. doi:10.1016/j.agrformet.2012.07.003

Peng, X., Zhang, T., Frauenfeld, O. W., Wang, S., Qiao, L., Du, R., et al. (2020). Northern Hemisphere Greening in Association with Warming Permafrost. *J. Geophys. Res. Biogeosciences* 125 (1), e2019JG005086. doi:10.1029/2019jg005086

Rao, M. P., Davi, N. K., D'Arrigo, R. D., Skees, J., Nachin, B., Leland, C., et al. (2015). Dzuds, Droughts, and Livestock Mortality in Mongolia. *Environ. Res. Lett.* 10 (7), 074012. doi:10.1088/1748-9326/10/7/074012

Rayner, N. A. A., Parker, D. E., Horton, E. B., Folland, C. K., Alexander, L. V., Rowell, D. P., et al. (2003). Global Analyses of Sea Surface Temperature, Sea Ice, and Night Marine Air Temperature since the Late Nineteenth Century. *J. Geophys. Res. Atmos.* 108 (D14), 4407. doi:10.1029/2002jd002670

Rinn, F. (2003). *TSAPWin: Time Series Analysis and Presentation for Dendrochronology and Related Applications, Version 0.55 User Reference.* Heidelberg: Rinntech, 76.

Serreze, M. C., and Barry, R. G. (2011). Processes and Impacts of Arctic Amplification: A Research Synthesis. *Glob. Planet. change* 77 (1-2), 85–96. doi:10.1016/j.gloplacha.2011.03.004

Shu, Q., Qiao, F., Song, Z., and Xiao, B. (2017). Effect of Increasing Arctic River Runoff on the Atlantic Meridional Overturning Circulation: a Model Study. *Acta Oceanol. Sin.* 36 (8), 59–65. doi:10.1007/s13131-017-1009-z

Smith, T. M., and Reynolds, R. W. (2005). A Global Merged Land-Air-Sea Surface Temperature Reconstruction Based on Historical Observations (1880-1997). *J. Clim.* 18 (12), 2021–2036. doi:10.1175/jcli3362.1

Stroeve, J. C., Kattsov, V., Barrett, A., Serreze, M., Pavlova, T., Holland, M., et al. (2012). Trends in Arctic Sea Ice Extent from CMIP5, CMIP3 and Observations. *Geophys. Res. Lett.* 39 (16), L16502. doi:10.1029/2012gl052676

Tong, S., Lai, Q., Zhang, J., Bao, Y., Lusi, A., Ma, Q., et al. (2018). Spatiotemporal Drought Variability on the Mongolian Plateau from 1980-2014 Based on the SPEI-PM, Intensity Analysis and Hurst Exponent. *Sci. of the Total Environ.* 615, 1557–1565. doi:10.1016/j.scitotenv.2017.09.121

Troy, T. J., Sheffield, J., and Wood, E. F. (2012). The Role of Winter Precipitation and Temperature on Northern Eurasian Streamflow Trends. *J. Geophys. Res. Atmos.* 117 (D5), DO5131. doi:10.1029/2011jd016208

Tucker, C. J., Pinzon, J. E., Brown, M. E., Slayback, D. A., Pak, E. W., Mahoney, R., et al. (2005). An Extended AVHRR 8-km NDVI Dataset Compatible with MODIS and SPOT Vegetation NDVI Data. *Int. J. Remote Sens.* 26 (20), 4485–4498. doi:10.1080/01431160500168686

Wang, J., Yang, B., Ljungqvist, F. C., Luterbacher, J., Osborn, T. J., Briffa, K. R., et al. (2017). Internal and External Forcing of Multidecadal Atlantic Climate Variability over the Past 1,200 Years. *Nat. Geosci.* 10 (7), 512–517. doi:10.1038/ngeo2962

Wang, L., Yao, Z.-J., Jiang, L.-G., Wang, R., Wu, S.-S., and Liu, Z.-F. (2016). Changes in Climate Extremes and Catastrophic Events in the Mongolian Plateau from 1951 to 2012. *J. Appl. Meteorology Climatol.* 55 (5), 1169–1182. doi:10.1175/jamc-d-14-0282.1

Wang, W., and Feng, Z. (2013). Holocene Moisture Evolution across the Mongolian Plateau and its Surrounding Areas: A Synthesis of Climatic Records. *Earth-Science Rev.* 122, 38–57. doi:10.1016/j.earscirev.2013.03.005

Wang, X., Brown, P. M., Zhang, Y., and Song, L. (2011). Imprint of the Atlantic Multidecadal Oscillation on Tree-Ring Widths in Northeastern Asia since 1568. *PloS one* 6 (7), e22740. doi:10.1371/journal.pone.0022740

Wang, Y., Li, S., and Luo, D. (2009). Seasonal Response of Asian Monsoonal Climate to the Atlantic Multidecadal Oscillation. *J. Geophys. Res. Atmos.* 114 (D2), DO2112. doi:10.1029/2008jd010929

Weisberg, S. (1985). *Applied Linear Regression*. 2nd ed. New York:: JohnWiley, 283.

Yao, J., Chen, Y., Zhao, Y., Mao, W., Xu, X., Liu, Y., et al. (2018). Response of Vegetation NDVI to Climatic Extremes in the Arid Region of Central Asia: a

Case Study in Xinjiang, China. *Theor. Appl. Climatol.* 131 (3-4), 1503–1515. doi:10.1007/s00704-017-2058-0

Zhang, P., Jeong, J.-H., Yoon, J.-H., Kim, H., Wang, S.-Y. S., Linderholm, H. W., et al. (2020). Abrupt Shift to Hotter and Drier Climate over Inner East Asia beyond the Tipping Point. *Science* 370 (6520), 1095–1099. doi:10.1126/science.abb3368

Zhang, R., Sutton, R., Danabasoglu, G., Kwon, Y. O., Marsh, R., Yeager, S. G., et al. (2019). A Review of the Role of the Atlantic Meridional Overturning Circulation in Atlantic Multidecadal Variability and Associated Climate Impacts. *Rev. Geophys.* 57 (2), 316–375. doi:10.1029/2019rg000644

Conflict of Interest: The authors declare that the research was conducted in the absence of any commercial or financial relationships that could be construed as a potential conflict of interest.

Publisher's Note: All claims expressed in this article are solely those of the authors and do not necessarily represent those of their affiliated organizations, or those of the publisher, the editors and the reviewers. Any product that may be evaluated in this article, or claim that may be made by its manufacturer, is not guaranteed or endorsed by the publisher.

frontiers | Frontiers in Earth Science

ORIGINAL RESEARCH
published: 20 May 2022
doi: 10.3389/feart.2022.900866

Amplifying Flood Risk Across the Lower Yellow River Basin, China, Under Shared Socioeconomic Pathways

Jinbo Song[1,2], *Qiang Zhang*[1,2]*, *Wenhuan Wu*[1,2], *Vijay P. Singh*[3,4,5], *Zexi Shen*[1,2], *Gang Wang*[1,2] and *Chong-Yu Xu*[6]

[1]State Key Laboratory of Earth Surface Processes and Resource Ecology, Beijing Normal University, Beijing, China, [2]Faculty of Geographical Science, Beijing Normal University, Beijing, China, [3]Department of Biological and Agricultural Engineering, Texas A&M University, College Station, TX, United States, [4]Zachry Department of Civil and Environmental Engineering, Texas A&M University, College Station, TX, United States, [5]National Water and Energy Center, UAE University, Al Ain, United Arab Emirates, [6]Department of Geosciences and Hydrology, University of Oslo, Oslo, Norway

The ecological conservation and high-quality development of the Yellow River basin (YRB) has been adopted as a major national strategy of China. However, the YRB is still afflicted by floods. Here, we proposed a flood risk indicator using direct economic loss degree and improved the SNRD (station-based nonlinear regression downscaling model) and simulated extreme precipitation processes. The correlation coefficient of downscaled average extreme precipitation of CMORPH and CMIP6 data reached 0.817. Moreover, we evaluated flood risk and flood hazard across the YRB based on the sixth phase Coupled Model Intercomparison Project (CMIP6) data under different SSPs. Under SSP126, SSP245, and SSP585 scenarios, the areas with increasing flood hazards during 2015–2045 accounted for 65.2, 69.0, and 64.5% of the entire YRB. In the spatial pattern, flood hazards decreased from southeastern to northwestern parts of the YRB. When compared with the spatial pattern of flood risks in 2015, regions with high flood risks expanded slightly and regions with low flood risks shrunk slightly. Higher flood risks can be observed in the middle and lower YRB and particularly in the lower YRB. These findings are critical for the mitigation of flood risk across the YRB under warming climate.

Keywords: flood risk, risk evaluation, CMIP6, shared socioeconomic pathways, Yellow River basin

OPEN ACCESS

Edited by:
Xing Yuan,
Nanjing University of Information Science and Technology, China

Reviewed by:
Fei Yuan,
Hohai University, China
Weili Duan,
Xinjiang Institute of Ecology and Geography (CAS), China

***Correspondence:**
Qiang Zhang
zhangq68@bnu.edu.cn

Specialty section:
This article was submitted to Interdisciplinary Climate Studies, a section of the journal Frontiers in Earth Science

Received: *21 March 2022*
Accepted: *19 April 2022*
Published: *20 May 2022*

Citation:
Song J, Zhang Q, Wu W, Singh VP, Shen Z, Wang G and Xu C-Y (2022) Amplifying Flood Risk Across the Lower Yellow River Basin, China, Under Shared Socioeconomic Pathways. Front. Earth Sci. 10:900866. doi: 10.3389/feart.2022.900866

INTRODUCTION

Floods have devastating casualties and property losses (Lai et al., 2016; Hu et al., 2018; Li et al., 2021; Zhang et al., 2022). According to the "Yearbook of Meteorological Disasters in China", from 2003 to 2018, the annual average disaster-affected population of China reached 107.127 million due to rainstorms and floods, accounting for 32.3% of the total population affected by all meteorological disasters. The average annual direct economic loss due to floods reached to 134.95 billion RMB, accounting for 44.5% of the total direct economic loss by all meteorological disasters (CMA, 2020). In the backdrop of global warming and rapid urbanization, the threats of floods to agricultural production, human life, and socioeconomic development will be further exacerbated. The Intergovernmental Panel on Climate Change (IPCC) Sixth Assessment Report (AR6) shows that intensifying global warming will lead to increased frequency and intensity of future extreme

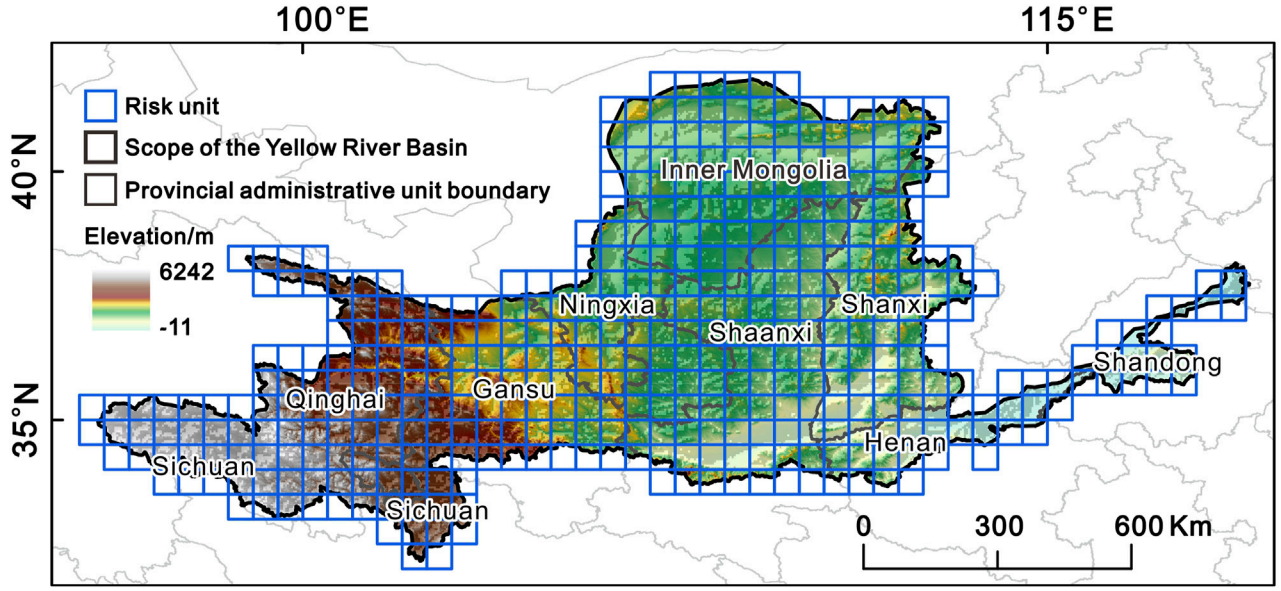

FIGURE 1 | Yellow River basin and the division of flood risk units. Considering the resolution of CMORPH data (0.25° × 0.25°) and the size of the study area, the entire YRB was subdivided into 419 risk units with a grid size of 0.5°*0.5°.

precipitation changes (IPCC, 2021). In China, precipitation extremes will be more frequent and more severe in the future (Duan et al., 2019), and climate change and land use change would increase the probability of heavy rains and flooding; moreover, rapid urbanization caused by increasing population and economic development will also increase flood risk (Duan et al., 2016). It has been well evidenced that increasing temperature tends to trigger the intensification of precipitation. The temperature changes can influence precipitation changes by altering the thermodynamic properties of air masses and, hence, the moisture transportation (Zhang et al., 2013). Meanwhile, with respect to population exposure to extreme precipitation, more people and the land in China will be exposed to extreme precipitation events (Wang et al., 2020; Ridolfi et al., 2021). In addition to the increase in extreme precipitation, the booming development of the socio-economy will also lead to a significant increase in flood risk (Hallegatte et al., 2013; Yu et al., 2019).

The AR6 report attached considerable importance to extreme weather and climate events at regional scales (IPCC, 2021), and signified risk evaluation of rainstorms and floods in different regions. The YRB is an important grain-producing area in China, holding an unshakable position in socioeconomic development, and ecological conservation in China. Nowadays, ecological protection and high-quality development of the YRB are accepted as major national strategies, while frequent floods and resultant frequent levee breaches and channel avulsions pose great challenges to the regional sustainability of the socio-economy (Chen et al., 2012; Zhang and Fang, 2017). Floods severely constrain regional, social, and economic development, posing a huge threat to the population and cities in the basin, especially in the lower YRB. The lower YRB has a low-lying terrain with a dense population and a highly-developed socio-economy. In addition, there has been built an 800-km long confined and super-elevated channel belt perching around 10 m above the surrounding ground; hence, economic losses and fatalities would be massive if the river banks were breached. The documentary records show that the lower Yellow River changed its course on 26 occasions from 602 BCE to 1949 CE (YRCC, 2001). Therefore, a thorough investigation of flood risk and relevant driving factors and predicting future spatiotemporal evolution of flood risk in the YRB under different SSPs are of great significance for flood control, flood mitigation, and high-quality development of the YRB.

A number of publications have been reported to address the evaluation of flood risk. Many techniques have been used for flood risk evaluation, such as risk evaluation based on historical flood data and mathematical-statistical methods (Benito et al., 2004; Rodda, 2005; Coeur and Lang, 2008), flood risk evaluation based on remote sensing and GIS techniques (Sanyal and Lu, 2005; Mason et al., 2010; Waghwala and Agnihotri, 2019), and index system-based flood risk evaluation (Okazawa et al., 2011; Kandilioti and Makropoulos, 2012). In addition, flood risk evaluation has also been done, based on the modeling of flood scenarios (Abdulrazzak et al., 2019). Using the flood data from 1989 to 2015, Luu et al. (2019) used the multiple linear regression TOPSIS method for the evaluation of flood risk across Vietnam. Rahman and Thakur (2018) extracted flood-induced submerged areas using Synthetic Aperture Radar (SAR) data and analyzed the flood-induced submerged area, flood inundation process, and spatiotemporal evolution of floods. Zischg et al. (2018) validated a 2D flood model and quantified flood risk across Sweden.

It is of paramount importance to evaluate flood risk in a warming climate based on multisource datasets at the river basin

scale since mitigation of flood is done at the river basin scale (Beylich et al., 2021). Therefore, a lot of work has been done on the evaluation of flood risk at river basin scales in China. Zhang et al. (2018) evaluated the flood risk in the Pearl River Basin of China, based on the peak flow data of 78 stations from 1951 to 2014 and historical flood records of the past 1,000 years. Wu et al. (2015) developed a model for the evaluation of flood risk based on GIS and disaster risk theory and evaluated flood risk across the Huai River basin. Liu et al. (2019) did an integrated risk assessment for agricultural drought and flood based on entropy information diffusion theory in the middle and lower Yangtze River basin, China. However, relatively few reports are available, addressing flood risk evaluation over the YRB. Ji et al. (2021), based on the cellular automata-Markov model and SWAT model, predicted the future runoff and flood risk over the YRB in the context of land use and climate changes. Liu et al. (2018) analyzed the impacts of climate change on flood risk across the YRB for the next 30 years. Qiu et al. (2010) used a distributed hydrological model to analyze the impact of land-use changes on flood risk over the YRB. However, a lot of studies at present are subjective in the selection of indicators for flood risk evaluation, while the weights should be optimally determined.

In order to study the driving factors of flood risk of YRB and temporal and spatial evolution of flood risk under different SSPs in the future, we conducted the following tasks: 1) we proposed a flood risk indicator to reflect the degree of harmful effects caused by floods, especially the degree of direct economic loss, and the flood hazard indicator to reflect the frequency and intensity of rainstorms and floods; 2) we analyzed the driving factors behind the flood risk of YRB by using the geodetector method (Wang and Hu, 2012) and correlation analysis, screened-out indicators having significant impacts on the flood risk indicator and took the power of determinant value obtained by the geodetector as the indicator weight; 3) based on CMIP6 data, we used the FLUS model and improved the SNRD downscaling model to explore future land use changes and precipitation patterns across the YRB, which would affect the flood risk indicator and flood hazard indicator of YRB in the future; and 4) we calculated the flood risk indicator and the flood hazard indicator and evaluated the temporal and spatial evolution of flood risk covering a period of 2015–2045 under different SSPs. This study helped in highlighting flood risk changes in both space and time, bridging the knowledge gap in regional sustainability in the backdrop of a warming climate, and enhancing mitigation of floods over the YRB. These points constitute the major objectives and motivation of this study.

DATA AND METHODS

Study Regions, Analysis Procedure, and Data Sources

The Yellow River flows through nine provinces of China, that is, Qinghai, Sichuan, Gansu, Ningxia, Inner Mongolia, Shaanxi, Shanxi, Henan, and Shandong, with a basin area of 795,000 km^2 (YRCC, 2020). Considering the resolution of CMORPH data (0.25° × 0.25°) and the size of the study area, we divided the entire YRB into 419 risk units with a grid size of 0.5°*0.5° (**Figure 1**). The analysis procedure of this current study is shown in **Figure 2**. The multisource data included precipitation, land use, social, and economy, and so on (**Supplementary Table S1**).

The precipitation data we used included CMORPH data (Janowiak et al., 2005) and Coupled Model Intercomparison Project Phase 6 (CMIP6) data (https://esgf-index1.ceda.ac.uk/search/cmip6-ceda/). The CMORPH data (0.25° × 0.25°, 3 h, https://ftp.cpc.ncep.noaa.gov/precip/CMORPH_V1.0/) from 1998 to 2014 was used for daily precipitation calculation of each risk unit, construction, and precision evaluation of CMIP6 data downscaling model, and precipitation indicators calculation of provinces in the Yellow River basin from 2004 to 2018. Based on the historical CMIP6 data from 1998–2010 and 2011–2014 (combined with CMORPH data), the downscaling model was constructed and tested. Based on the CMIP6 data of SSP126, SSP245, SSP370, and SSP585 from 2015 to 2045, daily precipitation at each risk unit under different SSPs was calculated, which was used to predict the future flood hazard indicator and risk indicator.

In this study, we also used the ESA land use data (http://maps.elie.ucl.ac.be/CCI/viewer/) from 2004 to 2018. The land use types in the Yellow River basin were divided into cropland, green land (including forest and grassland), water area, built-up land, and unused land. This data was used to simulate the land usage pattern in the study area from 2015 to 2045, and calculate the land use indicators of each province in the YBR from 2004 to 2018. Combining the land use data, land use driving factor data, and the FLUS model, we predicted the future land use pattern of the YRB. The driving factors behind land use included natural factors, accessibility factors, and social and economic factors: 1) The natural factors included elevation, slope and aspect, elevation data sourced from Geospatial Data Cloud Platform (http://www.gscloud.cn), and slope and aspect data were calculated based on the elevation data; 2) The accessibility factors included distance to rivers, roads, railways, coastlines, and administrative centers, they were calculated based on vector data in the 1:100 million national basic geographic database and were sourced from the national geographic information resource directory service system (www.webmap.cn); 3) The social and economic factors (http://www.resdc.cn/DOI) included the spatial distribution of population density (Xu, 2017b) and GDP data (Xu, 2017a) in 2015.

We also used social and economic data, terrain data, and disaster data. The data of population quantity, population density, GDP, average GDP per person, and GDP per unit area of each province from 2004 to 2018 were sourced from Statistical Yearbooks of provinces across the YRB and were used as various social and economic indicators of the provinces within the YRB from 2004 to 2018. Shared socioeconomic path (SSPs) population and economic estimation data (Huang et al., 2019; Jing et al., 2019) was used to calculate the population and GDP indicators under different SSPs in the study area from 2015 to 2045. Terrain data, including elevation, slope, and aspect was used to calculate the terrain indicator of each risk unit in the study area and each province within the YRB. The disaster data referred

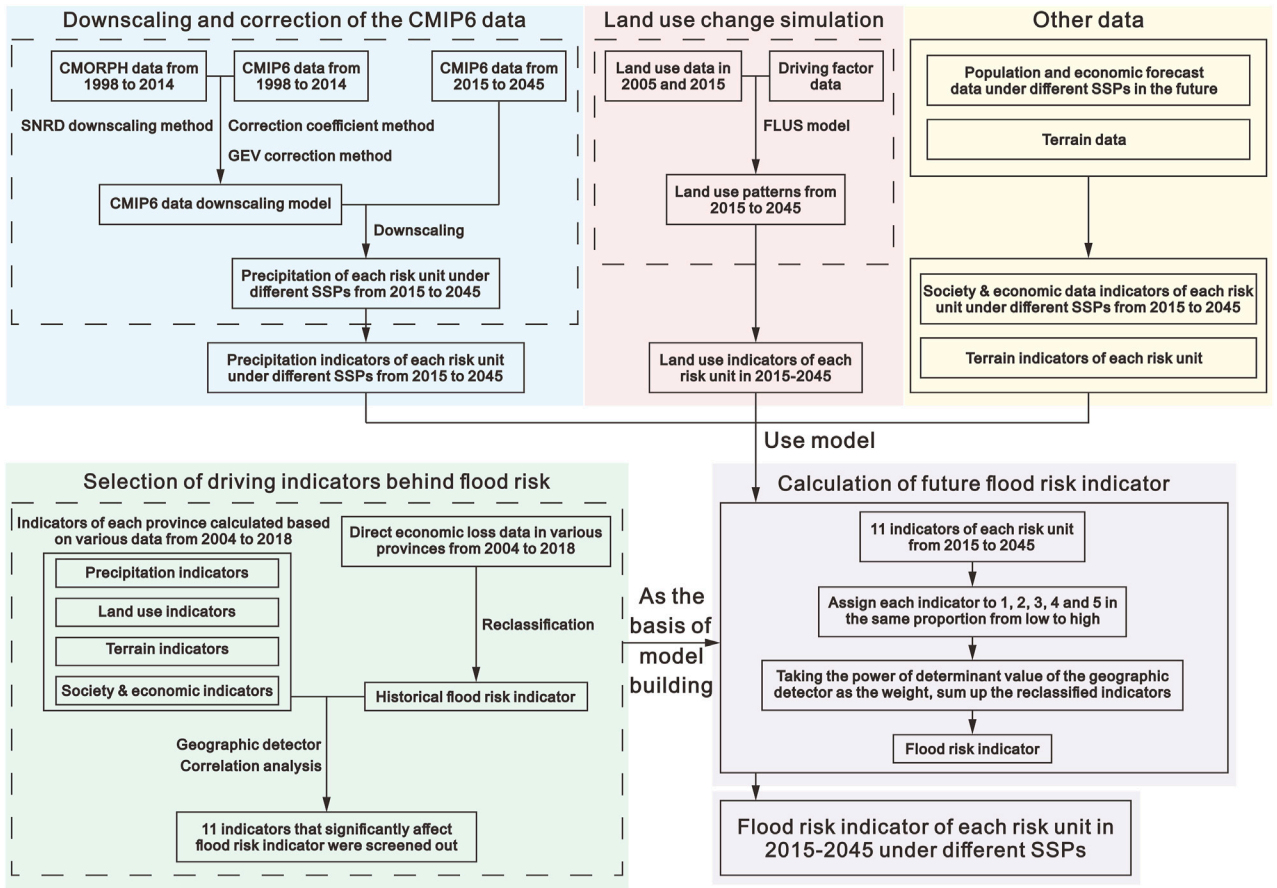

FIGURE 2 | Analysis procedure of this current study.

to flood-induced direct economic loss data by provinces from 2004 to 2018, which were extracted from the Yearbook of Meteorological Disasters in China (CMA, 2020) and were used to screen the influencing factors of flood risk.

Downscaling and Correction of the CMIP6 Dataset

We used the precipitation datasets from 20 CMIP6 models with high temporal resolution (day) under historical, SSP126, SSP245, SSP370, and SSP585 scenarios of future emissions (**Supplementary Table S2**). Meanwhile, we improved a precipitation downscaling model based on precipitation data during the period from 1998 to 2010 to downscale the CMIP6 dataset. In addition, we used the precipitation data covering a period from 2011 to 2014 to evaluate the downscaling performance of the improved precipitation downscaling model. Then we had done the precipitation downscaling practice for the CMIP6 data from 2015 to 2045. The improvement and evaluation of the downscaling model can be elaborated as follows: 1) Adoption of the basic precipitation downscaling model. Based on the historical precipitation data of CMIP6 and the CMORPH data from 1998 to 2010 (the CMORPH precipitation data were used to reflect the actual observed precipitation data and hereafter), a nonlinear regression downscaling model (station-based nonlinear regression downscaling model, SNRD) (Shen et al., 2021) was used to downscale the CMIP6 precipitation data. Based on the SNRD model, 20 CMIP6 models can be ensembled to produce one new precipitation downscaling dataset which has the same spatial resolution ($0.5^{\circ} \times 0.5^{\circ}$) as the risk unit. 2) Improvement of the abovementioned precipitation downscaling models. The first step was to correct the precipitation data using the correction coefficient method with the aim to overcome the underestimation of summer precipitation and the overestimation of winter precipitation. Correction of daily precipitation at each risk unit can be elaborated as follows:

$$a_i = \frac{\left(\sum_{j=1998}^{2010} b_{ij} - \sum_{j=1998}^{2010} c_{ij}\right)}{\sum_{j=1998}^{2010} d_{ij}}, \quad (1)$$

$$T_{ij} = P_{ij} + a_i\left(j = 2011, 2012, \ldots, 2045\right), \quad (2)$$

where i denotes the month, j denotes the year, a_i denotes the correction coefficient for the ith month, b_{ij} denotes the monthly CMORPH precipitation for the ith month of the jth year, c_{ij} denotes the monthly CMIP6 precipitation of the ith month of the

TABLE 1 | Indicators that significantly affect the flood risk indicator.

Indicator category	Indicator name	Correlation coefficient between this indicator and flood risk indicator	Power of determinant value
Precipitation indicator A_1	Rainstorm days* B_1	0.604	0.425
	Days of heavy rain* B_2	0.573	0.367
	Rainstorm days+ B_3	0.686	0.472
	Five-day maximum precipitation+ B_4	0.628	0.397
Land use indicator A_2	Quantity of cropland B_5	0.459	0.366
	Quantity of built-up land B_6	0.475	0.359
Terrain indicator A_3	Height variation coefficient B_7	0.499	0.393
	Number of pixels at medium and lower elevations B_8	0.526	0.388
	Number of pixels at slightly high and lower elevations B_9	0.526	0.441
Socioeconomic indicators A_4	Population quantity B_{10}	0.532	0.437
	GDP B_{11}	0.597	0.413

*j*th year, and the d_{ij} denotes the number of days of the *i*th month in the *j*th year. P_{ij} denotes the downscaled CMIP6 daily precipitation of the *i*th month in the *j*th year, and T_{ij} denotes the corrected downscaled daily precipitation.

The second step was to fit extreme precipitation using the generalized extreme value (GEV) distribution (Kharin and Zwiers, 2005), enhancing the modeling performance of the precipitation downscaling model. In this study, we defined the time period with daily precipitation of the top 5% for a certain period as extreme precipitation days, and then we obtained the fitting parameters at each risk unit by fitting the extreme daily precipitation data from 1998 to 2010, and these parameters were used to obtain extreme precipitation during the period of 2011–2045 at each risk unit. The final step was to deal with the outliers and negative precipitation values of the aforementioned downscaled precipitation. The downscaled extreme precipitation at risk units exceeding the maximum precipitation relative to the historical precipitation (1998–2010) was corrected to the maximum precipitation during the historical period, and the negative precipitation value in the downscaling results was corrected to 0. Then, we verified the abovementioned precipitation downscaling model by comparison between precipitation indicators, such as rainstorm days, days of heavy rain, and five-day maximum precipitation for each risk unit during 2011–2014, and the precipitation indicators based on CMORPH precipitation data during 2011–2014. In this study, we downscaled the CMIP6 data from 2015 to 2045 under different SSPs to explore changes in precipitation across the YRB.

FLUS Model-Based Simulation of Future Land Use Changes

The land use and land cover changes over the YRB would significantly affect the future evolution of flood risk (Qiu et al., 2010; Ji et al., 2021). Here, we simulated the spatial patterns of land use and land cover changes over the YRB using the FLUS model during a period from 2015 to 2045. The FLUS model is based on the historical land use pattern of a certain area and simulates the future land use changes in the area under the impacts of various driving factors. This model contains two computing modules, i.e., cellular automata and optimal probability computation based on the artificial neural network. The FLUS model can be called by GeoSOS-FLUS software for land use simulation (Liu et al., 2017). Based on land use driving factor data of the Yellow River basin and land use data from 2005 to 2015, we simulated and predicted the spatial pattern of land use changes using the FLUS model in 2025, 2035, and 2045. Furthermore, we set the same model parameters in GeoSOS-FLUS and simulated land use pattern in 2015 based on the spatial patterns of land use changes in 2005. We compared the simulated spatial pattern of land use in 2015 with the real-world spatial pattern of land use in 2015, evaluating modeling performance of FLUS in simulating land use changes based on the Kappa coefficient and the overall modelling accuracy.

Selection of Driving Indicators Behind Flood Risk

Here, we listed flood-induced direct economic loss recorded in the Yearbook of Meteorological Disasters in China (CMA, 2020) in the provinces passed by the Yellow River from 2004 to 2018 and categorized flood-induced direct economic loss into low, slightly low, middle, slightly high, and high level in equal proportions (each accounted for 20% of the records). We assigned 1, 2, 3, 4, and 5 to different levels of flood-induced direct economic loss as the historical flood risk indicator over the years. It was generally accepted that flood risk was jointly determined by the precipitation factor, land use factor, terrain factor, and social and economic factor. Extreme precipitation can induce serious floods, and precipitation is one of the most important indicators affecting flood hazards and flood risks (Okazawa et al., 2011). Land use changes will affect flood risk in the river basin, for example, the increase of built-up land and cropland with high property value will increase the potential damage when floods occur (Schmitt et al., 2004). At the same time, urbanization and the increase of impervious surfaces will affect infiltration and flood runoff (Ogden et al., 2011). The terrain factors, such as elevation and slope, will affect the drainage capacity and the possibility of flooding in the area, and social and economic factors, such as population density, will affect the potential danger of flood to human life and health (Kandilioti and Makropoulos, 2012). Therefore, we calculated 77

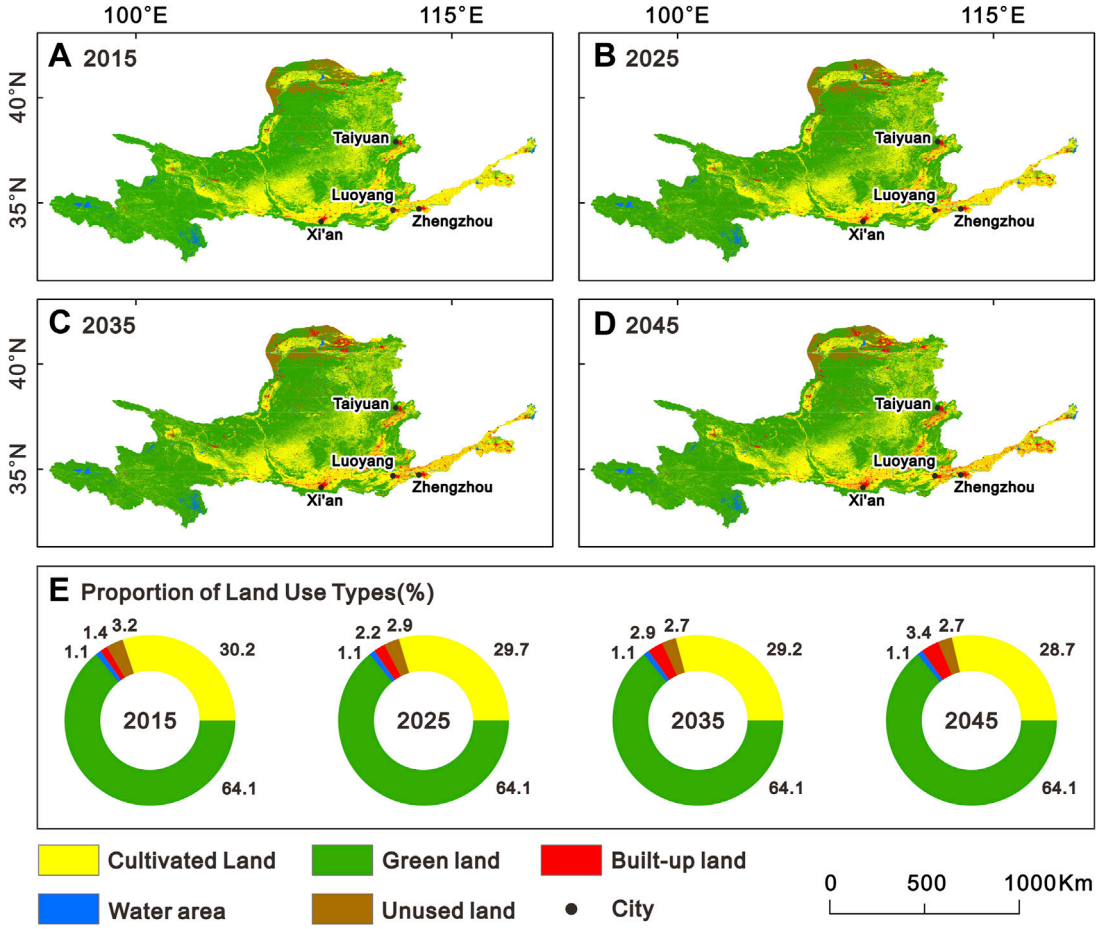

FIGURE 3 | Spatial pattern and area proportion of land use types in the Yellow River basin from 2015 to 2045. **(A–D)** Respectively refer to the spatial pattern of land use in 2015, 2025, 2035, and 2045. **(E)** Refers to the proportion of various land use types over the years.

indicators that may influence flood risk (**Supplementary Table S3**), including 26 precipitation indicators (Nos. 1–26), 10 land use indicators (Nos. 27–37), and 36 terrain indicators (Nos. 38–74), five social and economic indicators (Nos. 74–79).

Then, we screened out the indicators that were significantly correlated with the historical flood risk indicator (the correlation coefficient was significant at 0.001 significance level). Then, we performed attribution analysis using the geodetector method to screen out the indicators with a power of the determinant value of >0.35. In so doing, the screened-out indicators were convincing and the number of indicators screened out was moderate. Finally, a total of 11 indicators that significantly affected flood risk indicators were screened out (**Table 1**). We calculated the future flood risk indicator based on the screened-out indicators listed in **Table 1**.

Calculation of Future Flood Risk Indicator

Based on the screened-out indicators (**Table 1**), we calculated future flood risk indicators for each risk unit following the analysis procedure as shown in **Figure 2**. First, we computed indicators in **Table 1** for each risk unit from 2015 to 2045 under different SSPs. Here, precipitation and society and economic data were changing over the years and SSPs, land use was also changing over the years, and terrain data were kept the same in different years under SSPs. Then, we listed the values of each indicator at each SSP, each year, and each risk unit, and reassigned 1, 2, 3, 4, and 5 to each indicator in the order from low to high in equal proportion to eliminate the influence of different dimensions and magnitudes on each indicator. Finally, we took the power of determinant value obtained by the geodetector method as the indicator weight and did the weighted sum of each indicator at each risk unit to calculate the future flood risk for all risk units under SSPs.

Therefore, the calculation method of flood risk indicator was as follows:

$$\begin{aligned} I_{risk} = {} & 0.425B_1 + 0.367B_2 + 0.472B_3 + 0.397B_4 + 0.366B_5 \\ & + 0.359B_6 + 0.393B_7 + 0.388B_8 + 0.441B_9 + 0.437B_{10} \\ & + 0.413B_{11}, \end{aligned} \tag{3}$$

where I_{risk} denotes the flood risk indicator; $B_1, B_2, B_3, \ldots, B_{11}$ are the indicators assigned 1, 2, 3, 4, and 5; B_1 denotes the indicator "Rainstorm days*"; B_2 denotes the indicator "Days of heavy

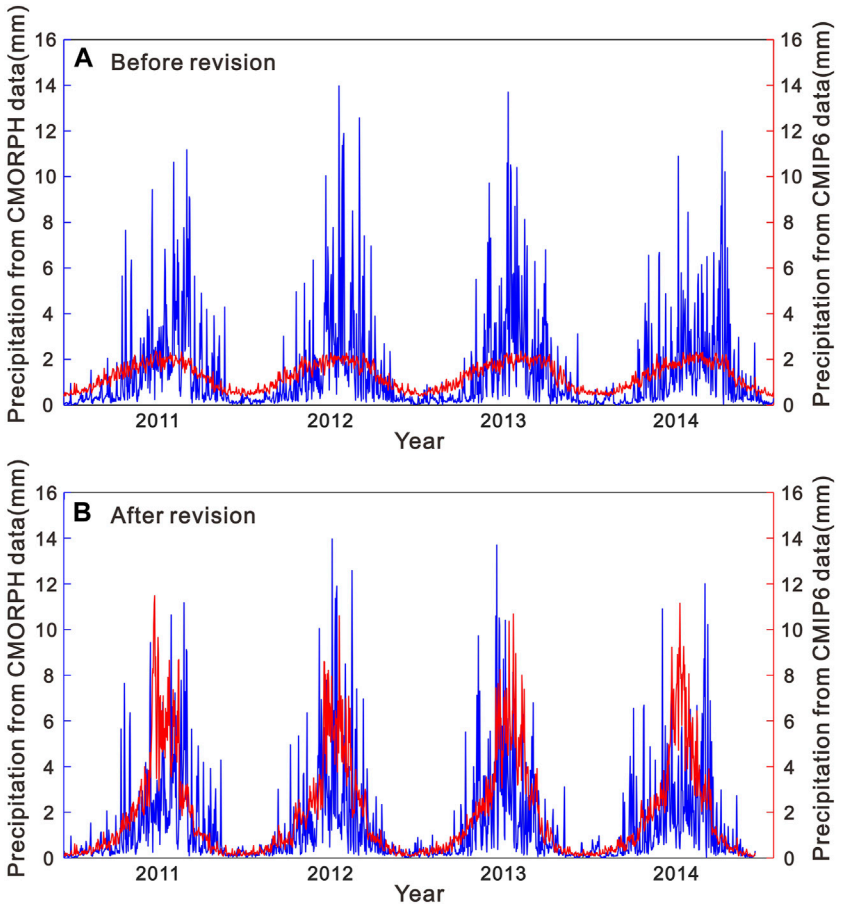

FIGURE 4 | Comparison of the average daily precipitation in the Yellow River basin obtained from CMORPH and CMIP6 downscaling data from 2011 to 2014 before **(A)** and after correction **(B)**.

rain*"; B_3 denotes the indicator "Rainstorm days$^+$"; B_4 denotes the indicator "Five-day maximum precipitation$^+$"; B_5 denotes the indicator "Quantity of cropland"; B_6 denotes the indicator "Quantity of built-up land"; B_7 denotes the indicator "Height variation coefficient"; B_8 denotes the indicator "Number of pixels at medium and lower elevations"; B_9 denotes the indicator "Number of pixels at slightly high and lower elevations; B_{10} denotes the indicator "population quantity"; and B_{11} denotes the indicator "GDP."

We evaluated the reliability of the results by a comparison between the calculated flood risk indicator using the aforementioned methods and the real flood risk indicator obtained by actual flood-induced direct economic loss, and the correlations were significant at the 0.001 significance level. The power of the determinant obtained by the geodetector reached 0.484. These verification results well-evidenced the modeling accuracy and can be accepted for further calculation of the future flood risk indicator. In this case, we adopted the abovementioned techniques to calculate the flood risk indicator across the YRB covering the period from 2015 to 2045 under different SSPs. It is worth noting that the indicators "Rainstorm days*" and "Rainstorm days$^+$" at each risk unit had the same values, which were equal to the number of rainstorm days for the risk unit in a certain year and SSPs. Moreover, the indicators "Days of heavy rain*" and "Five-day maximum precipitation$^+$" were the number of heavy rain days and the five-day largest precipitation amount for the risk unit in a certain year and SSP.

Different from the flood risk indicator, the flood hazard indicator is only determined by the precipitation indicator in **Table 1**. The calculation procedure was as follows: calculate the "Rainstorm days*", "Rainstorm days$^+$", "Days of heavy rain*", and "Five-day maximum precipitation $^+$", rank indicators from low to high values, and assign 1, 2, 3, 4, and 5 to each ranked indicators in equal proportion. Then, we took the power of determinant value by geodetector as the index weight and did weighted summation of each index to calculate the flood hazard indicator.

Therefore, the calculation method for flood hazard indicator was as follows:

$$I_{hazard} = 0.425B_1 + 0.367B_2 + 0.472B_3 + 0.397B_4, \quad (4)$$

where I_{hazard} denotes the flood hazard indicator; B_1, B_2, B_3, and B_4 are the indicators assigned 1, 2, 3, 4, and 5; B_1 denotes the indicator "Rainstorm days*"; B_2 denotes the indicator "Days of

TABLE 2 | Correlation coefficient between downscaled CMIP6 data and CMORPH data.

Precipitation indicator	Correlation coefficient
Rainstorm days	0.691
Days of heavy rain	0.825
Five-day maximum precipitation	0.733

heavy rain*"; B_3 denotes the indicator "Rainstorm days$^+$"; and B_4 denotes the indicator "Five-day maximum precipitation$^+$".

The advantages of the flood risk indicator calculation method proposed in this study are as follows: 1) the flood risk indicator was rigorously defined and used to reflect flood-induced direct economic loss; 2) rigorous selection of risk-related indicators that were directly related to flooding risk; 3) when calculating the flood risk indicator, precipitation, land use, terrain, social and economic, and other indicators were thoroughly considered, showing holistic impacts of driving factors on the flood.

After the calculation of the flood risk indicator and flood hazard indicator at all risk units in 2015–2045 under different SSPs, the following methods were adopted for further processing:

1) When displaying and analyzing the spatial distribution pattern of flood risk indicator (and flood hazard indicator), we divided the flood risk indicator (and flood hazard indicator) of each year, each SSP, and each risk unit into low, slightly low, medium, slightly high, and high grades (all accounting for 20%) according to the proportional method, and used the Kriging interpolation method to process the data of each risk unit, and drew a map based on the interpolation results.
2) Using Mann–Kendall (MK) trend test (Guo et al., 2018) with a significance level of 0.05 to explore the changing trend of flood hazard indicators under different SSPs.
3) Because the frequency and intensity of extreme precipitation events fluctuate over time, the flood hazard indicator and flood risk indicator tend to fluctuate over time. Therefore, in order to reflect the overall change trend of flood risk indicator and eliminate the influence of interannual fluctuation, we calculated linear regression between the flood hazard indicator of each risk unit under each SSPs and the year, and then calculated the fitting values of flood risk indicators of each risk unit under SSPs from 2015 to 2045 according to the regression equation, and used them to replace the measured values. Based on this value, the flood risk indicator of each risk unit under each SSP was calculated.

RESULTS AND DISCUSSION

Land Use and Land Cover Changes

The comparison between simulated and real-world land use patterns in 2015 showed a Kappa coefficient of 0.958 and the overall modeling accuracy was 0.979, indicating that the prediction accuracy was acceptable. The simulated land use pattern over the YRB from 2015 to 2045 is shown in **Figure 3**,

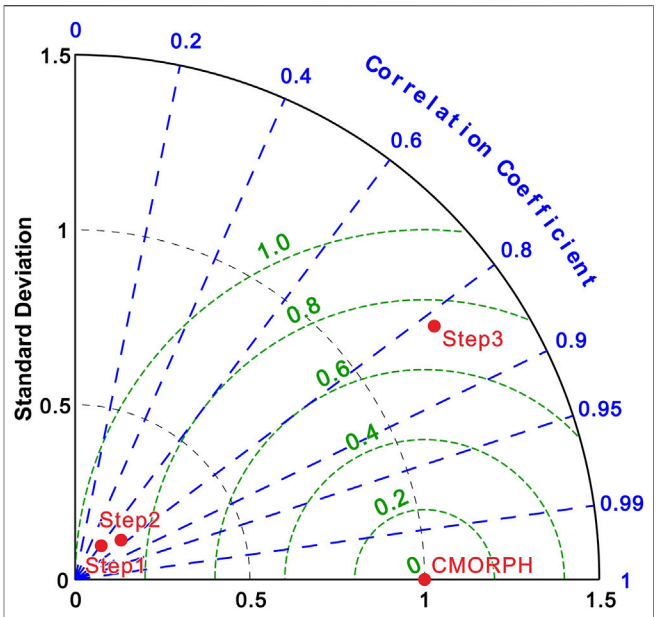

FIGURE 5 | Standardized Taylor diagram of spatial distribution sequence of average precipitation in extreme precipitation period of each risk unit obtained from CMORPH data and CMIP6 downscaling data in different stages of correction (Step 1: before correction; Step 2: only correction by correction coefficient method; Step 3: complete all corrections).

which reveals the expanding built-up land area from 1.4 to 3.4% during 2015–2045 based on the FLUS model, and expanding built-up land was found mainly in Xi'an, Zhengzhou, Luoyang, and Taiyuan, while the cultivated land and unused land decreased slightly and the proportion of cultivated land (unused land) decreased from 30.2 (3.2%) to 28.7% (2.7%) in the future 30 years. Green land and cultivated lands were the main land use and land cover types across the YRB, accounting for 64.1 and 29.5% of the average annual land area of the YRB, respectively. The cultivated land was mainly distributed in the southeastern parts of the YRB, and the green land was mainly distributed in the western and northwestern parts of the YRB.

Precipitation Downscaling Performance of Downscaling Models

Comparison of areal average daily precipitation of the downscaled CMIP6 and CMORPH data across the YRB from 2011 to 2014 indicated underestimation (overestimation) of summer (winter) precipitation by SNRD (**Figure 4A**). In addition, downscaled precipitation by SNRD poorly described the extreme precipitation processes. **Figure 4B** shows that the improved SNRD model well overcame the underestimation (overestimation) of summer (winter) precipitation. The improved or modified SNRD enhanced the downscaling performance of the SNRD model.

Based on the CMIP6 data and the CMORPH data, we computed the long-term average of rainstorm days, days of heavy rain, and five-day maximum precipitation for all risk

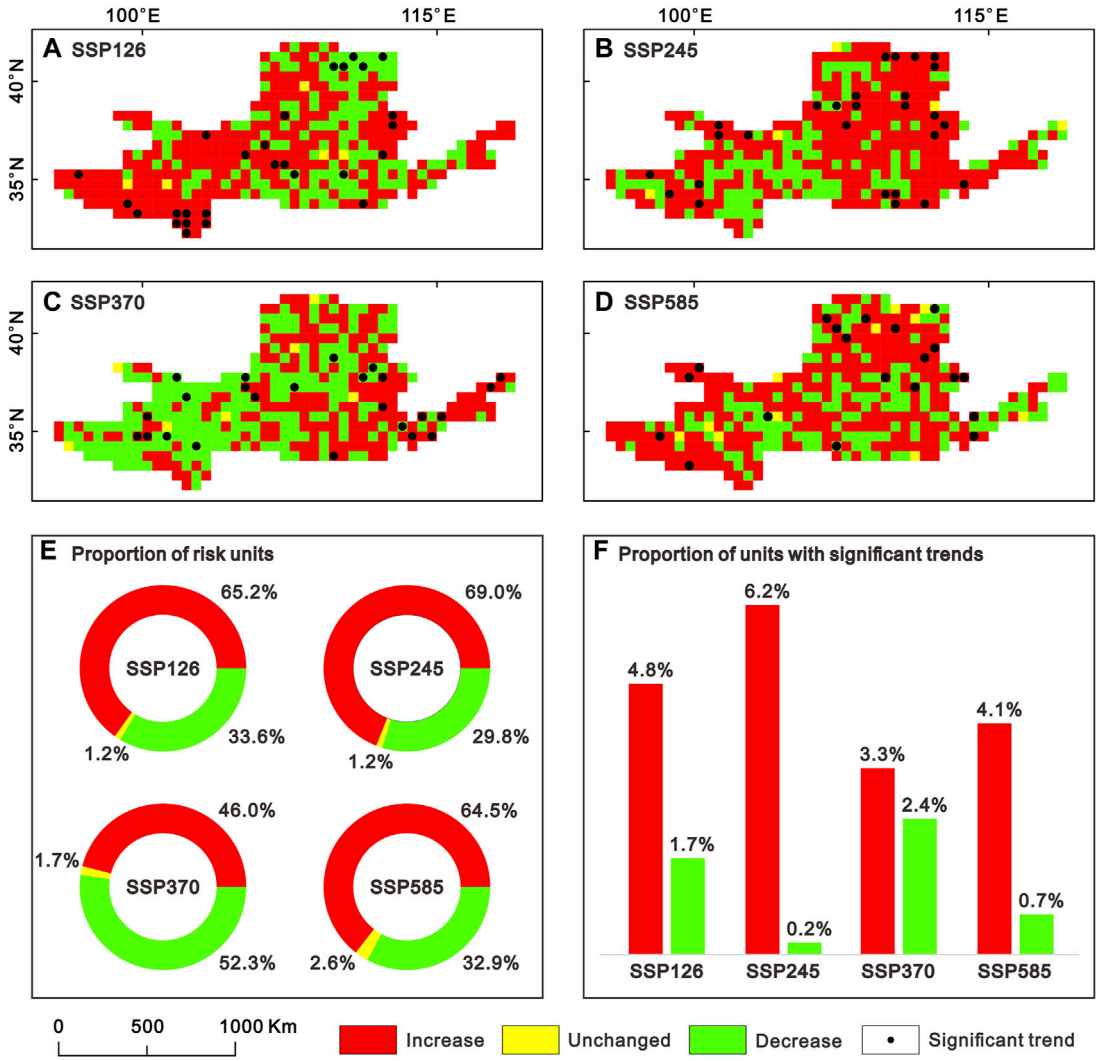

FIGURE 6 | Trends in flood hazard indicators in the Yellow River basin from 2015 to 2045 under SSP126, SSP245, SSP370, and SSP585 based on the Mann-Kendall (MK) trend test with a significance level of 0.05 **(A–D)**; the proportion of risk units with various trends under SSP126, SSP245, SSP370, and SSP585 **(E)** and proportion of risk units with a significant increase or decrease under SSP126, SSP245, SSP370, and SSP585 **(F)**.

units. Then, we did a correlation analysis of the downscaled CMIP6 data and CMORPH data (**Table 2**). We found that correlations between downscaled CMIP6 data and CMORPH data were statistically significant at 0.001 significance level. Based on the downscaled CMIP6 data using the original SNRD (Step 1), corrected downscaled precipitation using the correction coefficient (Step 2), and holistically corrected downscaled precipitation (Step 3) from 2011 to 2014, we calculated the average precipitation during the time interval with precipitation amount larger than 5% percentile for 2011–2014. We standardized the Taylor plot (**Figure 5**), reflecting differences in average precipitation by the downscaled CMIP6 after different corrections and CMORPH data. **Figure 5** shows a closer relation of corrected downscaled CMIP6 by the correction coefficient to CMORPH data with increased correlation coefficients from 0.611 to 0.758 and was significant at 0.001 significance level. The standard deviation and central RMSE were closer to the CMORPH data. After all, corrections were done to the SNRD-based downscaling practice, the downscaled CMIP6 data was closer to the CMORPH data with a correlation coefficient increased to 0.817. These findings evidenced that the corrected downscaled CMIP6 data can better depict precipitation changes after correction by the GEV distribution function.

Flood Hazard Indicator

It can be seen from **Figure 6** that under SSP126, SSP245, and SSP585, the risk units with an increasing (significantly increasing) flood hazard indicator from 2015 to 2045 reached 65.2, 69.0, and 64.5% (4.8, 6.2, and 4.1% respectively), being significantly more than the risk units with decreasing flood hazard indicator (33.6, 29.8, and 32.9%, respectively) and significantly decreasing flood hazard indicator (1.7, 0.2, and 0.7% respectively). Under SSP370,

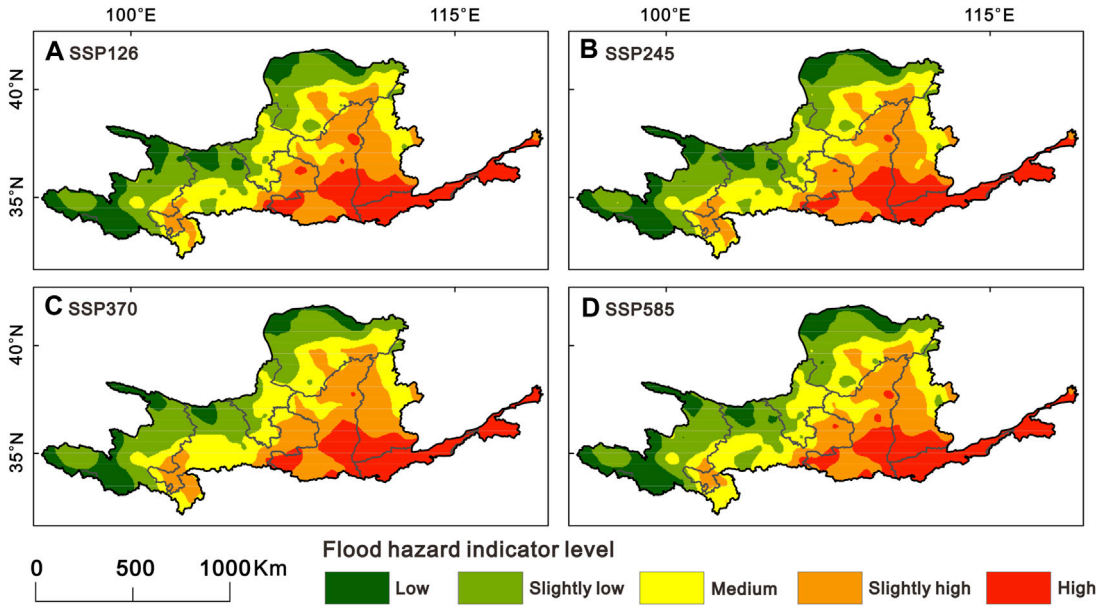

FIGURE 7 | Spatial distribution of flood hazard indicator (multiyear average from 2015 to 2045) in the Yellow River basin under SSP126 **(A)**, SSP245 **(B)**, SSP370 **(C)**, and SSP585 **(D)**.

the proportion of risk units with an upward trend in the flood hazard indicator was 46.0%, being slightly less than the risk units with a downward trend (52.3%) in the flood hazard indicator, while risks units with a significant upward trend (3.3%) in flood hazard indicator were more than risk units with a significant downward trend (2.4%) in flood hazard indicator. All these findings indicated that the overall flood hazard indicator across the YRB was amplified from 2015 to 2045, which was manifested by the increase in the frequency and intensity of rainstorms and flood events.

The spatial pattern of long-term (from 2015 to 2045) average flood hazard indicators under different SSPs is shown in **Figure 7**. It can be seen from **Figure 7** that no remarkable difference can be identified in the flood hazard indicator over the YRB under different SSPs, while the flood hazard indicator was subjected to obvious spatial differentiation, and this spatial differentiation tended to be weak in the southeastern parts to the northwestern parts of the YRB. Meanwhile, high and slightly high flood hazard indicator area was identified mainly concentrated in the southeastern parts of the YRB. This was because the extreme precipitation amounts decreased from southeastern to northwestern parts of the YRB, and higher extreme precipitation amount can be observed in eastern and southeastern parts of the YRB (Li et al., 2017) with higher frequency and intensity of rainstorms and flood events.

Flood Risk Indicator

Figure 8 demonstrates the flood risk indicator over the YRB covering a period from 2015 to 2045 under different SSPs. We found no distinct differences in flood risk indicator values under different SSPs. The period from 2015 to 2045 witnessed a slight increase in the flood risk indicator over the YRB. When compared to the spatial distribution of flood risk indicators in 2015, in 2045, areas with high flood risk indicators would expand slightly, but areas with low flood risk indicators would shrink slightly. Just as presented in the aforementioned section, the flood hazard indicator over the YRB would increase as a whole from 2015 to 2045. Also, the rainstorm and flood events would become more frequent and intensified. Meanwhile, the built-up land would increase from 1.4 to 3.4% in 2045 (**Figure 3**), according to the estimated population and the economic data of the shared socioeconomic pathways (SSPs), under SSP126, SSP245, SSP370, and SSP585, the total GDP of the YRB in 2045 would be 3.93, 3.75, 3.00, and 4.29 times higher than that of 2015, respectively. Therefore, given the occurrence of floods, the YRB would suffer higher economic losses. Furthermore, the flood risk indicator would be subject to more obvious spatial differentiation. High and slightly high flood risk indicator area is mainly distributed in the southeastern parts of the YRB, including the lower and middle YRB, the southern part of the YRB, and the northern part of the Ningxia (**Figure 9A**).

The lower YRB is low-lying in terrain with high risks of extreme precipitation and is vulnerable to flooding inundation (**Figures 9A,C**). In addition, the lower YRB is dominated by cultivated land and built-up land (**Figure 3**) with a highly-developed economy and dense population (**Figures 9D,E**), such as, according to China City Statistical Yearbook 2020 (Urban Social and Economic Investigation Division of National Bureau of Statistics, 2020), Zhengzhou (in 2019, the city's annual average population reached 8.73 million, and the regional GDP reached 1.159 trillion RMB), and Jinan (with an

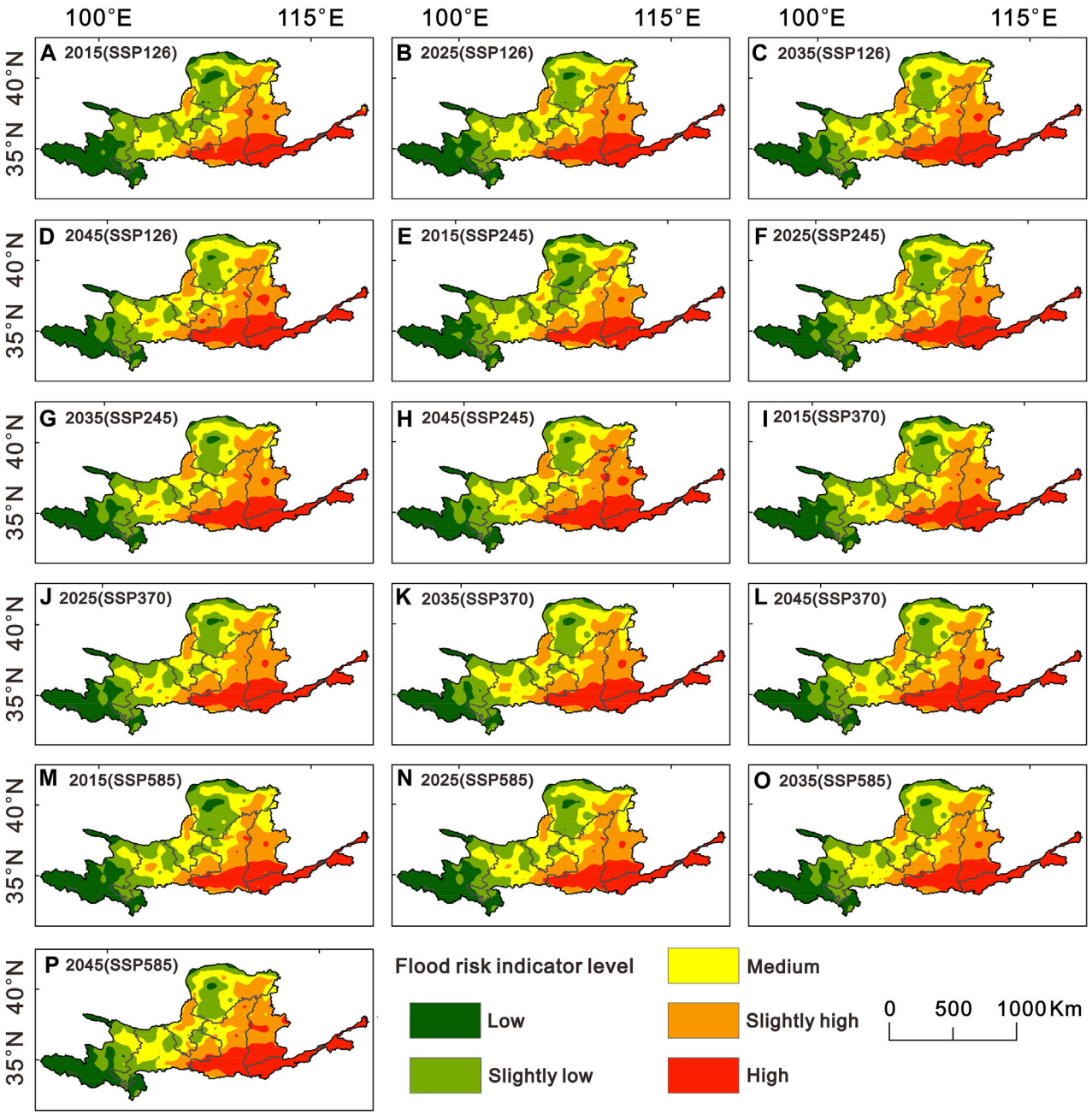

FIGURE 8 | Flood risk indicator in the Yellow River basin under SSP126 **(A–D)**, SSP245 **(E–H)**, SSP370 **(I–L)**, and SSP585 **(M–P)** from 2015 to 2045.

average annual population of 7.91 million in 2019 and a GDP of 944.3 billion RMB) (**Figure 9A**). Massive economic losses can be expected given the occurrence of flood events. For example, on July 17–22, 2021, Henan Province suffered torrential rain, with an hourly rainfall of 201.9 mm from 16:00 to 17:00 on July 20, breaking the record of the maximum hourly rainfall on the Chinese mainland. The accumulated rainfall in 3 h was 333 mm and that in 24 h was 627.4 mm (Zhong et al., 2021), which caused extremely serious casualties and property losses. Therefore, the lower YRB is at high flood risk. According to the "Yellow River Yearbook", in the 20 years from 1919 to 1938, floods occurred in 14 out of 20 years in the lower YRB. The river banks along the lower YRB are higher than the surrounding ground. There stands an 800-km long confined and super-elevated channel belt perching around 10 m above the surrounding ground (Chen et al., 2012). If the river bank breaches, flood bursts, and massive economic losses and fatalities would occur. In addition, more evidence

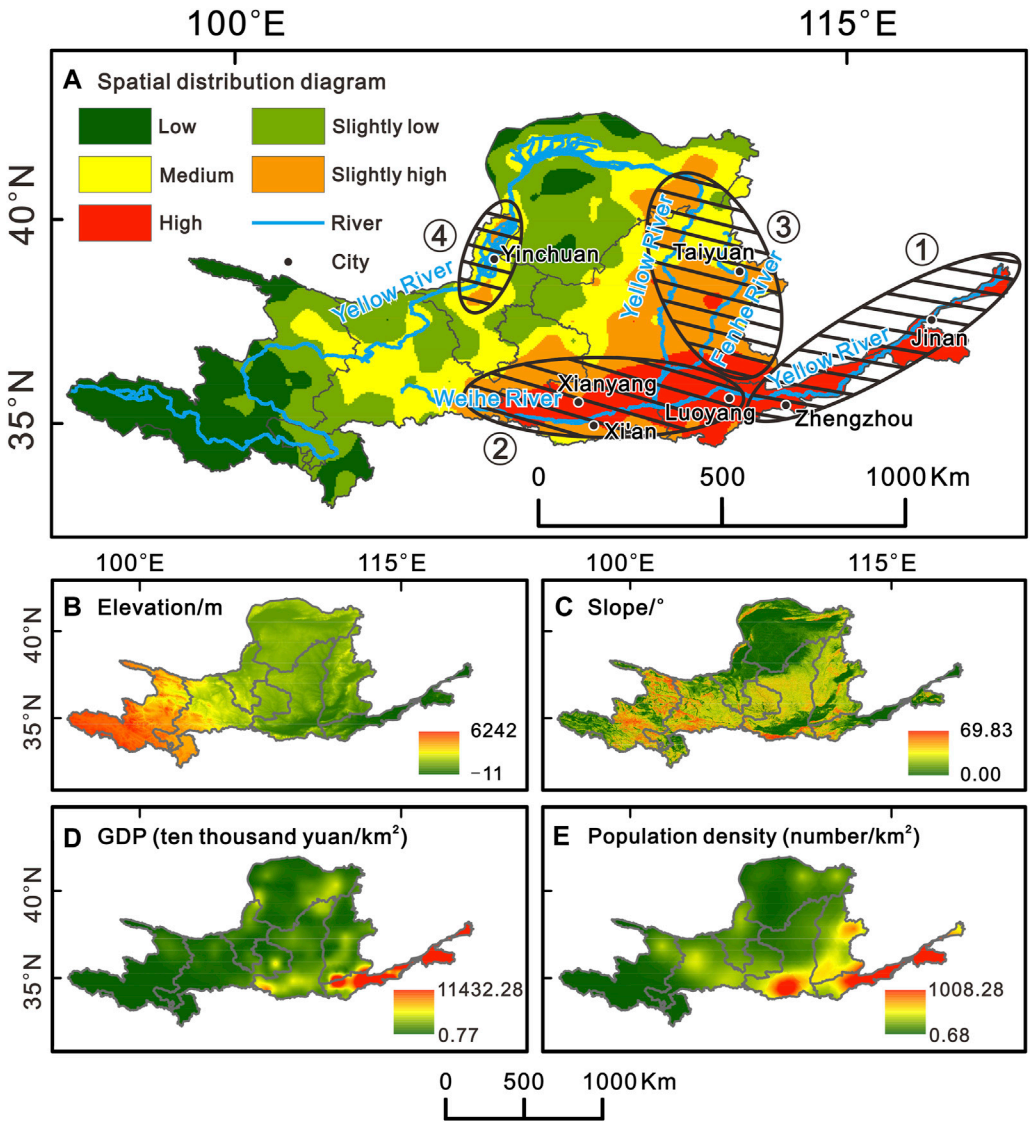

FIGURE 9 | Spatial pattern of regions with slightly high and high flood risks in the Yellow River Basin **(A)** and distribution map of some influencing factors **(B–E)**. Note: In **Figure 9A**, ① the lower reaches of the Yellow River, ② the southern part of the Yellow River basin, ③ the middle Yellow River basin, and ④ the northern part of Ningxia. **Figure 9A** shows the spatial pattern of flood risks in the Yellow River basin in 2025 under SSP245. **Figures 9D–E** shows the spatial pattern of distribution of population and GDP under shared socioeconomic pathways (SSPs) in 2025 under SSP245.

indicated that the length of the elevated channel and riverbank in the lower YRB increased to 550 km, and the main trough is 1.16 m higher than the floodplain on average, posing a serious threat to the downstream cities and residents (Zhang and Fang, 2017).

The distribution of high flood risk indicators in the southern part of the YRB can be attributed to the high frequency of extreme precipitation events. Vast low-lying plains combined with hills and highlands accelerate flow confluence when heavy precipitation events occur (**Figures 9B,C**). At the same time, the Wei River flows through this region (**Figure 9A**), and the Wei River has high sediment content and muddy water. The sand deposition is serious, and the river bed will also rise. Floods with high sediment content have posed serious threats to this region (Li and Xia, 2020). In addition, built-up land and arable land in this area are widely distributed (**Figure 3**) with a densely populated and highly-developed economy (**Figures 9D,E**). For example, according to China City Statistical Yearbook 2020 (Urban Social and Economic Investigation Division of National Bureau of Statistics, 2020), Luoyang (the city's annual average population reached 7.43 million in 2019 and a regional GDP reached 503.5 billion RMB), Xi'an (with an average annual population of 9.4 million in 2019 and a GDP of 932.1 billion RMB), Xianyang (with an average population of 4.59 million in

2019 and a GDP of 2,195 million RMB) (**Figure 9A**), are all under high flood risk.

The middle YRB is dominated by the Fenhe Plain, the spatial combination of hills and plains accelerates the speed of flow in plain areas (**Figures 9B,C**). High frequent extreme precipitation renders the middle YRB susceptible to floods (YRCC, 2020). Meanwhile, built-up land and arable land in this area are widely distributed (**Figure 3**). A relatively dense population and developed socio-economy render this region susceptible to flood-induced losses (**Figures 9D,E**). The middle YRB is not only seriously threatened by torrential rains and floods, but is also the main source of floods for the lower YRB, posing a threat to the lower YRB (YRCC, 2020). The mainstream of the Yellow River flows through the northern part of Ningxia (**Figure 9A**), which is located in the Ningxia Plain with low-lying terrain (**Figures 9B,C**). There are major cities, such as Yinchuan with an average annual population of 1.97 million and a regional GDP of 189.7 billion RMB in 2019 (Urban Social and Economic Investigation Division of National Bureau of Statistics, 2020) (**Figure 9**), being highly susceptible to floods. From the Qing Dynasty to 1949, there occurred 24 recorded serious floods in Ningxia, about one serious flood even per 13 years (YRCC, 2020).

CONCLUSION

There are still critical scientific issues in flood risk evaluation, such as subjectivity in the selection of evaluation indicators and obscure definitions of flood risk. Here, we classified flood-induced direct economic losses, quantifying flood risk indicators. Meanwhile, correlation analysis and geodetector were adopted to evaluate the weights of indicators, such as precipitation, land use, terrain, social, and economy that have profound impacts on flood risk over the YRB. Furthermore, we did a holistic evaluation of flood risk indicators and flood hazard indicators using the FLUS model and the improved SNRD downscaling model across the YRB from 2015 to 2045 under different SSPs. We obtained the following important findings and conclusions.

1) From the simulated land use pattern over the YRB from 2015 to 2045, we detected expanding built-up land area from 1.4 to 3.4% from 2015 to 2045 and a slight decrease in cultivated land and unused land from 30.2 (3.2%) to 28.7% (2.7%) in the future 30 years. The cultivated land is mainly distributed in the southeastern parts of the YRB, and the green land is mainly distributed in the western and northwestern parts of the YRB. These changes in land use and land cover change have enhanced susceptibility to flooding. In addition, we improved the SNRD precipitation downscaling model using correction coefficient and GEV model, greatly improving the accuracy of downscaled extreme precipitation.
2) In most areas of the Yellow River basin, the flood hazard is increasing from 2015 to 2045 under SSP126, SSP245, and SSP585, which is manifested by the increase in the frequency and intensity of rainstorm and flood events. Therefore, we can conclude that flood hazards would be amplified in the backdrop of climate change during 2015–2045. With respect to the spatial pattern of flood hazard indicators, we identified high and slightly high flood hazard indicators mainly concentrated in the southeastern parts of the YRB of the basin. Specifically, flood hazard indicators decreases from southeastern to northwestern parts of the YRB as a whole, and high and slightly high flood hazard indicator was identified mainly in the middle and lower YRB.
3) We detected no distinct difference in flood risk indicators across the YRB under different SSPs. From 2015 to 2045, we depicted a slight increase in the flood risk indicator over the YRB. Meanwhile, when compared to the spatial distribution of flood risk indicators in 2015, we found slightly expanded areas with high flood risk indicators and slightly shrunk regions with low flood risk indicators. Specifically, we found regions with high and slightly high flood risk indicators mainly in the southeastern parts of the YRB, including the lower and middle YRB, the southern YRB, and the northern parts of Ningxia.
4) For evaluating uncertainties, we first calculated the daily precipitation of each risk unit in 2015–2045 under different SSPs based on CMIP6 data but we must admit that the simulation of future precipitation by each CMIP6 model itself was uncertain and the spatial resolution of CMIP6 data was coarse, although we used the SNRD method to downscale CMIP6 data and corrected the downscaling result, the uncertainty of future precipitation prediction still existed. Second, we used the FLUS model to predict the future land use change in the Yellow River basin based on the land use pattern in 2005 and 2015, which was based on the assumption that land use change in 2005–2015 in the Yellow River basin would remain unchanged in 2015–2045. Once the new land use policy is adopted in the Yellow River basin, the future land use simulation based on the FLUS model would be modified, which would introduce uncertainty. At the same time, shared socioeconomic path (SSPs) population and economic estimation data used in this study also involve uncertainties because the data of the future period is obtained by estimation. Finally, there are uncertainties in flood risk assessment methods, although this study screened the driving indicators behind flood risk and verified the accuracy of the research method many times. However, the model constructed in this study was still relatively simple, with inadequate consideration given to some indicators that are difficult to quantify, such as disaster prevention policies and disaster mitigation capabilities but the mechanism of flood disaster is very complicated. Therefore, the calculation method of future flood risk indicator was also one of the sources of uncertainty.

In this study, we inadequately considered the disaster mitigation capability of each risk unit in the Yellow River basin, including fortification level, drainage pipeline construction level, reliability of disaster prevention system, emergency rescue management capability, etc. Because these factors were difficult to express quantitatively, it was also difficult to predict their changing trends with time under different SSPs. Therefore, the flood risk indicator calculated in this study has not included these factors; our findings here

reflected the relative degree of potential losses that each risk unit would suffer under the influence of a flood disaster. The results can better reflect which areas need to improve their disaster mitigation capabilities to deal with high potential flood risks.

DATA AVAILABILITY STATEMENT

The original contributions presented in the study are included in the article/**Supplementary Material**, further inquiries can be directed to the corresponding author.

AUTHOR CONTRIBUTIONS

JS contributed to the computation and original version of the manuscript. QZ contributed to the funding support, the idea behind this study, revision of the original version, and guidance. WW, ZS, GW, and C-YX contributed to the revision of this manuscript. VS contributed to the editing of the manuscript, critical improvement of the analysis, interpretation of this results and overall improvement of the quality of this manuscript.

FUNDING

This research was financially supported by the National Natural Science Foundation of China, Grant No. 42041006, the China National Key R&D Program, Grant No. 2019YFA0606900, and the Research Council of Norway (FRINATEK Project No. 274310).

SUPPLEMENTARY MATERIAL

The Supplementary Material for this article can be found online at: https://www.frontiersin.org/articles/10.3389/feart.2022.900866/full#supplementary-material

REFERENCES

Abdulrazzak, M., Elfeki, A., Kamis, A., Kassab, M., Alamri, N., Chaabani, A., et al. (2019). Flash Flood Risk Assessment in Urban Arid Environment: Case Study of Taibah and Islamic Universities' Campuses, Medina, Kingdom of Saudi Arabia. *Geomatics, Nat. Hazards Risk* 10, 780–796. doi:10.1080/19475705.2018.1545705

Benito, G., Lang, M., Barriendos, M., Llasat, M. C., Frances, F., Ouarda, T., et al. (2004). Use of Systematic, Palaeoflood and Historical Data for the Improvement of Flood Risk Estimation. Review of Scientific Methods. *Nat. Hazards* 31, 623–643.

Beylich, M., Haberlandt, U., and Reinstorf, F. (2021). Daily vs. Hourly Simulation for Estimating Future Flood Peaks in Mesoscale Catchments. *Hydrology Res.* 52, 821–833. doi:10.2166/nh.2021.152

Cœur, D., and Lang, M. (2008). Use of Documentary Sources on Past Flood Events for Flood Risk Management and Land Planning. *COMPTES RENDUS Geosci.* 340, 644–650. doi:10.1016/j.crte.2008.03.001

Chen, Y., Syvitski, J. P. M., Gao, S., Overeem, I., and Kettner, A. J. (2012). Socio-Economic Impacts on Flooding: A 4000-Year History of the Yellow River, China. *AMBIO* 41, 682–698. doi:10.1007/s13280-012-0290-5

China Meteorological Administration (CMA) (2020). *Yearbook of Meteorological Disasters in China 2019*. Beijing: Meteorological Press, 183–185. (in Chinese).

Duan, W., Hanasaki, N., Shiogama, H., Chen, Y., Zou, S., Nover, D., et al. (2019). Evaluation and Future Projection of Chinese Precipitation Extremes Using Large Ensemble High-Resolution Climate Simulations. *J. Clim.* 32, 2169–2183. doi:10.1175/JCLI-D-18-0465.1

Duan, W., He, B., Nover, D., Fan, J., Yang, G., Chen, W., et al. (2016). Floods and Associated Socioeconomic Damages in China over the Last Century. *Nat. Hazards* 82, 401–413. doi:10.1007/s11069-016-2207-2

Guo, M., Li, J., He, H., Xu, J., and Jin, Y. (2018). Detecting Global Vegetation Changes Using Mann-Kendal (MK) Trend Test for 1982-2015 Time Period. *Chin. Geogr. Sci.* 28, 907–919. doi:10.1007/s11769-018-1002-2

Hallegatte, S., Green, C., Nicholls, R. J., and Corfee-Morlot, J. (2013). Future Flood Losses in Major Coastal Cities. *Nat. Clim. Change* 3, 802–806. doi:10.1038/NCLIMATE1979

Hu, P., Zhang, Q., Shi, P., Chen, B., and Fang, J. (2018). Flood-induced Mortality across the Globe: Spatiotemporal Pattern and Influencing Factors. *Sci. Total Environ.* 643, 171–182. doi:10.1016/j.scitotenv.2018.06.197

Huang, J., Qin, D., Jiang, T., Wang, Y., Feng, Z., Zhai, J., et al. (2019). Effect of Fertility Policy Changes on the Population Structure and Economy of China: From the Perspective of the Shared Socioeconomic Pathways. *Earth's Future* 7, 250–265. doi:10.1029/2018EF000964

IPCC (2021). *Climate Change 2021: The Physical Science Basis*. Cambridge University Press. In Press.

Janowiak, J. E., Kousky, V. E., and Joyce, R. J. (2005). Diurnal Cycle of Precipitation Determined from the CMORPH High Spatial and Temporal Resolution Global Precipitation Analyses. *J. Geophys. Res.* 110. doi:10.1029/2005JD006156

Ji, G., Lai, Z., Xia, H., Liu, H., and Wang, Z. (2021). Future Runoff Variation and Flood Disaster Prediction of the Yellow River Basin Based on CA-Markov and SWAT. *Land* 10, 421. Land. 10. doi:10.3390/land10040421

Jing, C., Tao, H., Jiang, T., Wang, Y., Zhai, J., Cao, L., et al. (2020). Population, Urbanization and Economic Scenarios over the Belt and Road Region under the Shared Socioeconomic Pathways. *J. Geogr. Sci.* 30, 68–84. doi:10.1007/s11442-020-1715-x

Kandilioti, G., and Makropoulos, C. (2012). Preliminary Flood Risk Assessment: the Case of Athens. *Nat. Hazards* 61, 441–468. doi:10.1007/s11069-011-9930-5

Kharin, V. V., and Zwiers, F. W. (2005). Estimating Extremes in Transient Climate Change Simulations. *J. Clim.* 18, 1156–1173. doi:10.1175/JCLI3320.1

Lai, C., Shao, Q., Chen, X., Wang, Z., Zhou, X., Yang, B., et al. (2016). Flood Risk Zoning Using a Rule Mining Based on Ant Colony Algorithm. *J. Hydrology* 542, 268–280. doi:10.1016/j.jhydrol.2016.09.003

Li, B. Q., Hou, B. D., Dong, X. Y., and Wang, H. J. (2017). A Multifactor Analysis of the Spatial Distribution of Annual Mean Extreme Precipitation-Taking the Yellow River Basin as an Example. *IOP Conf. Ser. Earth Environ. Sci.* 82, 012025. doi:10.1088/1755-1315/82/1/012025

Li, J., and Xia, J. (2020). Modelling of Hyperconcentrated Flood Routing and Channel Evolution in the Lower Weihe River. *Arab. J. Geosci.* 13. doi:10.1007/s12517-020-06028-9

Li, X., Hu, Q., Wang, R., Zhang, D., and Zhang, Q. (2021). Influences of the Timing of Extreme Precipitation on Floods in Poyang Lake, China. *Hydrology Res.* 52, 26–42. doi:10.2166/nh.2021.078

Liu, L., Jiang, T., Xu, H., and Wang, Y. (2018). Potential Threats from Variations of Hydrological Parameters to the Yellow River and Pearl River Basins in China over the Next 30 Years. *Water* 10, 883. doi:10.3390/w10070883

Liu, X., Liang, X., Li, X., Xu, X., Ou, J., Chen, Y., et al. (2017). A Future Land Use Simulation Model (FLUS) for Simulating Multiple Land Use Scenarios by Coupling Human and Natural Effects. *Landsc. Urban Plan.* 168, 94–116. doi:10.1016/j.landurbplan.2017.09.019

Liu, Y., You, M., Zhu, J., Wang, F., and Ran, R. (2019). Integrated Risk Assessment for Agricultural Drought and Flood Disasters Based on Entropy Information Diffusion Theory in the Middle and Lower Reaches of the Yangtze River, China. *Int. J. Disaster Risk Reduct.* 38, 101194. doi:10.1016/j.ijdrr.2019.101194

Luu, C., von Meding, J., and Mojtahedi, M. (2019). Analyzing Vietnam's National Disaster Loss Database for Flood Risk Assessment Using Multiple Linear

Regression-TOPSIS. *Int. J. Disaster Risk Reduct.* 40, 101153. doi:10.1016/j.ijdrr.2019.101153

Mason, D. C., Speck, R., Devereux, B., Schumann, G. J.-P., Neal, J. C., and Bates, P. D. (2010). Flood Detection in Urban Areas Using TerraSAR-X. *IEEE Trans. Geosci. Remote Sens.* 48, 882–894. doi:10.1109/TGRS.2009.2029236

Ogden, F. L., Raj Pradhan, N., Downer, C. W., and Zahner, J. A. (2011). Relative Importance of Impervious Area, Drainage Density, Width Function, and Subsurface Storm Drainage on Flood Runoff from an Urbanized Catchment. *Water Resour. Res.* 47. doi:10.1029/2011WR010550

Okazawa, Y., Yeh, P. J.-F., Kanae, S., and Oki, T. (2011). Development of a Global Flood Risk Index Based on Natural and Socio-Economic Factors. *Hydrological Sci. J.* 56, 789–804. doi:10.1080/02626667.2011.583249

Qiu, Y., Jia, Y., Zhao, J., Wang, X., Bennett, J., and Zhou, Z. (2010). Valuation of Flood Reductions in the Yellow River Basin under Land Use Change. *J. Water Resour. Plann. Manage.* 136, 106–115. doi:10.1061/(ASCE)0733-9496

Rahman, M. R., and Thakur, P. K. (2018). Detecting, Mapping and Analysing of Flood Water Propagation Using Synthetic Aperture Radar (SAR) Satellite Data and GIS: A Case Study from the Kendrapara District of Orissa State of India. *Egypt. J. Remote Sens. Space Sci.* 21, S37–S41. doi:10.1016/j.ejrs.2017.10.002

Ridolfi, E., Mondino, E., and Di Baldassarre, G. (2021). Hydrological Risk: Modeling Flood Memory and Human Proximity to Rivers. *Hydrology Res.* 52, 241–252. doi:10.2166/nh.2020.195

Rodda, H. J. E. (2005). The Development and Application of a Flood Risk Model for the Czech Republic. *Nat. Hazards* 36, 207–220. doi:10.1007/s11069-004-4549-4

Sanyal, J., and Lu, X. X. (2005). Remote Sensing and GIS-Based Flood Vulnerability Assessment of Human Settlements: a Case Study of Gangetic West Bengal, India. *Hydrol. Process.* 19, 3699–3716. doi:10.1002/hyp.5852

Schmitt, T., Thomas, M., and Ettrich, N. (2004). Analysis and Modeling of Flooding in Urban Drainage Systems. *J. Hydrology* 299, 300–311. doi:10.1016/j.jhydrol.2004.08.012

Shen, Z., Zhang, Q., Singh, V. P., Sun, P., He, C., and Cheng, C. (2021). Station-based Non-linear Regression Downscaling Approach: A New Monthly Precipitation Downscaling Technique. *Int. J. Climatol.* 41, 5879–5898. doi:10.1002/joc.7158

Shui-xin, Z., Yan, Z., Sheng, H., Zi-tong, C., Wei-yu, D., Ye-rong, F., et al. (2021). Verification and Assessment of Real-Time Forecasts of Two Extreme Heavy Rain Events in Zhengzhou by Operational NWP Models. *J. Trop. Meteorology* 27, 406–417. doi:10.46267/j.1006-8775.2021.035

Urban Social and Economic Investigation Division(USEID) of National Bureau of Statistics (2020). *CHINA CITY STATISTICAL YEARBOOK 2020*, 13-19. Beijing: China Statistics, 69–75. (in Chinese).

Waghwala, R. K., and Agnihotri, P. G. (2019). Flood Risk Assessment and Resilience Strategies for Flood Risk Management: A Case Study of Surat City. *Int. J. Disaster Risk Reduct.* 40, 101155. doi:10.1016/j.ijdrr.2019.101155

Wang, G., Zhang, Q., Yu, H., Shen, Z., and Sun, P. (2020). Double Increase in Precipitation Extremes across China in a 1.5 ˚C/2.0 ˚C Warmer Climate. *Sci. Total Environ.* 746, 140807. doi:10.1016/j.scitotenv.2020.140807

Wang, J.-F., and Hu, Y. (2012). Environmental Health Risk Detection with GeogDetector. *Environ. Model. Softw.* 33, 114–115. doi:10.1016/j.envsoft.2012.01.015

Wu, Y., Zhong, P.-a., Zhang, Y., Xu, B., Ma, B., and Yan, K. (2015). Integrated Flood Risk Assessment and Zonation Method: a Case Study in Huaihe River Basin, China. *Nat. Hazards* 78, 635–651. doi:10.1007/s11069-015-1737-3

Xu, X. L. (2017a). *Data from: China's GDP Spatial Distribution Kilometer Grid Data Set. Data Registration and Publishing System of Chinese Academy of Sciences Resources and Environment Science Data Center*. Available at: http://www.resdc.cn/DOI.

Xu, X. L. *Data from: China's Population Spatial Distribution Kilometer Grid Data Set. Data Registration and Publishing System of Chinese Academy of Sciences Resources and Environment Science Data Center*. (2017b). Available at: http://www.resdc.cn/

Yellow River Conservancy Commission (YRCC) (2001). *The Chronicle of Events of the Yellow River*. Yellow River Water Conservancy Publishing House, 715. (in Chinese).

Yellow River Conservancy Commission (YRCC) (2020). *Yellow River Yearbook 2020*. Yellow River Yearbook Press, 86–92. (in Chinese).

Yu, H., Zhang, Q., Xu, C.-Y., Du, J., Sun, P., and Hu, P. (2019). Modified Palmer Drought Severity Index: Model Improvement and Application. *Environ. Int.* 130, 104951. doi:10.1016/j.envint.2019.104951

Zhang, H., Luo, J., Wu, J., and Yu, M. (2022). Spatial-temporal Characteristics and Driving Factors of Flash Floods in Shaanxi Province Considering Regional Differentiation. *Hydrology Res.* 53, 156–174. doi:10.2166/nh.2021.103

Zhang, Q., Gu, X., Singh, V. P., Shi, P., and Sun, P. (2018). More Frequent Flooding? Changes in Flood Frequency in the Pearl River Basin, China, since 1951 and over the Past 1000 Years. *Hydrol. Earth Syst. Sci.* 22, 2637–2653. doi:10.5194/hess-22-2637-2018

Zhang, Q., Li, J., Singh, V. P., and Xiao, M. (2013). Spatio-temporal Relations between Temperature and Precipitation Regimes: Implications for Temperature-Induced Changes in the Hydrological Cycle. *Glob. Planet. Change* 111, 57–76. doi:10.1016/j.gloplacha.2013.08.012

Zhang, X., and Fang, X. (2017). Temporal and Spatial Variation of Catastrophic River Floodings in the Lower Yellow River from AD 960 to 1938. *Holocene* 27, 1359–1369. doi:10.1177/0959683617690590

Zischg, A. P., Mosimann, M., Bernet, D. B., and Röthlisberger, V. (2018). Validation of 2D Flood Models with Insurance Claims. *J. Hydrology* 557, 350–361. doi:10.1016/j.jhydrol.2017.12.042

Conflict of Interest: The authors declare that the research was conducted in the absence of any commercial or financial relationships that could be construed as a potential conflict of interest.

frontiers | Frontiers in Earth Science

ORIGINAL RESEARCH
published: 26 May 2022
doi: 10.3389/feart.2022.917660

Upper-Tropospheric Temperature Pattern Over the Asian-Pacific Region in CMIP6 Simulations: Climatology and Interannual Variability

Qiwei Fan[1,2] *and Botao Zhou*[1,2]*

[1]*Collaborative Innovation Center on Forecast and Evaluation of Meteorological Disasters/Key Laboratory of Meteorological Disaster, Ministry of Education/Joint International Research Laboratory of Climate and Environment Change, Nanjing University of Information Science and Technology, Nanjing, China,* [2]*School of Atmospheric Sciences, Nanjing University of Information Science and Technology, Nanjing, China*

Temperature is a most important indicator for climate change. However, compared to surface air temperature, relatively less attention has been shown to the upper-tropospheric temperature (UTT). Given that the Asian-Pacific UTT plays a remarkable role in the climate system, its future change deserves great attention. In this study, based on the Coupled Model Intercomparison Project phase 6 (CMIP6) simulations, the fidelity of 30 CMIP6 models on the Asian-Pacific UTT patterns was evaluated and their future changes under the scenarios of the Shared Socioeconomic Pathway (SSP) 2–4.5 and 5–8.5 were projected. The evaluation indicates that the CMIP6 models have a good capacity to reproduce the climatology and interannual variability of seasonal UTT during 1965–2014, with the multi-model ensemble mean (MME) outperforming individual models. The observed seesaw oscillation between the Asian UTT and the North Pacific UTT during four seasons, named Asian-Pacific Oscillation (APO), is also well performed. The MME projects a similar spatial change under both scenarios in the second half of the 21st century, with lager changes in magnitude under SSP5-8.5 than under SSP2-4.5. Compared to 1965–2014, during 2050–2099, spring, summer and autumn UTTs are projected to cool (warm) in a widespread area of Asia (the North Pacific). The projected winter UTT decreases in East Asia and most of the North Pacific. In addition, an increased interannual variability of seasonal UTT is anticipated particularly in the mid-low latitudes of the Asian-Pacific sector. The APO phenomenon is expected to still be dominant in the future climate, but its intensity (interannual variability) tends to weaken (enlarge) in each season as compared to the current.

Keywords: CMIP6, evaluation and projection, upper-tropospheric temperature, climatology, interannual variability

OPEN ACCESS

Edited by:
Dabang Jiang,
Institute of Atmospheric Physics (CAS), China

Reviewed by:
Zhiping Tian,
Institute of Atmospheric Physics (CAS), China
Dong Chen,
Institute of Atmospheric Physics (CAS), China

****Correspondence:***
Botao Zhou
zhoubt@nuist.edu.cn

Specialty section:
This article was submitted to Geoscience and Society, a section of the journal Frontiers in Earth Science

Received: *11 April 2022*
Accepted: *29 April 2022*
Published: *26 May 2022*

Citation:
Fan Q and Zhou B (2022) Upper-Tropospheric Temperature Pattern Over the Asian-Pacific Region in CMIP6 Simulations: Climatology and Interannual Variability. Front. Earth Sci. 10:917660. doi: 10.3389/feart.2022.917660

INTRODUCTION

Upper-tropospheric temperature (UTT) change in Asia and surrounding oceans has been documented to exert pronounced impacts on climate variations. For instance, the East Asian UTT cooling in spring may cause a decrease of precipitation in South China (Xin et al., 2006; Xin et al., 2008). During the summer time, the UTT cooling trend from 1950 to 2000 in East Asia contributes to the "southern flood and northern drought" pattern *via* weakening the East Asian

TABLE 1 | Information about the CMIP6 models used in this study.

ID	Model name	Country	Atmospheric resolution (lon × lat: number of grids, L: vertical levels)
1	ACCESS-CM2	Australia	192 × 144, L85
2	ACCESS-ESM1-5	Australia	192 × 145, L38
3	AWI-CM-1-1-MR	Germany	384 × 192, L95
4	BCC-CSM2-MR	China	320 × 160, L46
5	CAMS-CSM1-0	China	320 × 160, L31
6	CAS-ESM2-0	China	256 × 128, L30
7	CESM2-WACCM	United States	288 × 192, L70
8	CIESM	China	288 × 192, L30
9	CMCC-CM2-SR5	Italy	288 × 192, L30
10	CMCC-ESM2	Italy	288 × 192, L30
11	CanESM5	Canada	128 × 64, L49
12	EC-Earth3	European	512 × 256, L91
13	EC-Earth3-CC	European	512 × 256, L91
14	EC-Earth3-Veg	European	512 × 256, L91
15	EC-Earth3-Veg-LR	European	320 × 160, L62
16	FGOALS-f3-L	China	360 × 180, L32
17	FGOALS-g3	China	180 × 80, L26
18	FIO-ESM-2-0	China	192 × 288, L26
19	GFDL-ESM4	United States	360 × 180, L49
20	IITM-ESM	India	192 × 94, L64
21	IPSL-CM6A-LR	France	144 × 143, L79
22	KACE-1-0-G	Korea	192 × 144, L85
23	MIROC6	Japan	256 × 128, L81
24	MPI-ESM1-2-HR	Germany	384 × 192, L95
25	MPI-ESM1-2-LR	Germany	192 × 96, L47
26	MRI-ESM2-0	Germany	320 × 160, L80
27	NESM3	China	192 × 96, L47
28	NorESM2-LM	Norway	144 × 96, L32
29	NorESM2-MM	Norway	288 × 192, L32
30	TaiESM1	China	288 × 192, L30

summer monsoon (EASM) (Yu et al., 2004), and its recent reversal favors the intensification of the EASM (Zhao et al., 2015). The winter mode characterized by the positive (negative) UTT centered in southern China (Mongolia) tends to decrease precipitation in southern China and increase surface air temperature in the southeastern Tibet Plateau (Jiang et al., 2013). The East Asian UTT also significantly affects changes of the tropical Pacific sea surface temperature (SST) (Nan et al., 2009; Zhang and Zhou, 2012, 2015). The UTT variability in Asia has been identified to change harmoniously with that in the North Pacific, which exhibits a seesaw oscillation and is referred to as the Asian-Pacific Oscillation (APO, Zhao et al., 2007). Abnormal variation of this oscillation pattern can result in significant anomalies in atmospheric circulations and climate, such as the precipitation in East Asia (Zhao et al., 2007; Zhao et al., 2008; Zhou and Zhao, 2010; Zhao et al., 2012; Fang et al., 2014; Hua et al., 2019; Si et al., 2019; Lin et al., 2021), the frequency of tropical cyclone in the western North Pacific (Zhou et al., 2008), and the SST in the North Pacific (Zhao et al., 2010; Zhou et al., 2010; Wang and Chen, 2017).

Considering significant roles of the Asian-Pacific UTT in the climate system, its potential change in a future warmer world deserves great attention. Climate models and emission scenarios, coordinated by the Coupled Model Intercomparison Project (CMIP), are essential for the projection of future climate. Some CMIP3 and CMIP5 studies indicated that the potential behavior of future changes of the Asian-Pacific UTT differs from that in surface temperature (Sun and Ding, 2011; Dai et al., 2013; Ma and Yu, 2014; Zhou, 2016; Zhou and Xu, 2017; Zhou et al., 2018). Contrary to the warming of surface temperatures (IPCC, 2013), the summer upper-tropospheric thermal contrast between Asia and the Pacific is projected to weaken under warmer scenarios (Sun and Ding, 2011; Zhou, 2016; Zhou et al., 2018).

However, those CMIP3 and CMIP5 studies only focused on the summer situation. In addition, compared with the CMIP3 and CMIP5, the current CMIP6 models behave more complicated physical processes and higher spatial resolutions (Eyring et al., 2016; Simpkins, 2017; Stouffer et al., 2017; Tebaldi et al., 2021), and show some improvements in the simulation of historical climate (e.g., Chen et al., 2020; Ha et al., 2020; Jiang et al., 2020; Yang et al., 2021). Meanwhile, a set of new scenarios named Shared Socioeconomic Pathways (SSPs) is developed for climate projection under the CMP6 framework (O'Neill et al., 2016; Gidden et al., 2019). Two questions arise naturally: 1) How well do the state-of-the-art CMIP6 models capture the observed Asian-Pacific UTT pattern? 2) How will the Asian-Pacific UTT pattern change under the SSP scenarios? This study, following the previous studies and extending summer season to four seasons, is aimed to address these issues.

DATA AND METHODS

Monthly air temperature outputs from 30 CMIP6 models (**Table 1**) for the historical simulation (1965–2014) and the SSP2-4.5 and SSP5-8.5 scenarios (2050–2099) are employed in this study. SSP5-8.5 (SSP2-4.5) is featured with a peak of radiation forcing at 8.5 (4.5) W m^{-2} by 2100, following the pathway of a high (a moderate) socioeconomic development (O'Neill et al., 2016; Gidden et al., 2019). More details can be referred to the website https://www.wcrp-climate.org/wgcm-cmip. The NCEP/NCAR reanalysis data (Kalnay et al., 1996) are applied as observation (OBS) for the evaluation of model performance. Because the horizontal resolutions vary among different models, we use the bilinear interpolation to remap all the data to a $1^{\circ} \times 1^{\circ}$ grid.

This study mainly focuses on the climatology and interannual variability of seasonal UTT. The UTT is defined as the temperature averaged in the upper troposphere (300–200 hPa), in which the zonal mean is removed. We use standard deviation (SD) to represent interannual variability. December-January-February (DJF), March-April-May (MAM), June-July-August (JJA) and September-October-November (SON) are, in turn, defined as winter, spring, summer and autumn. The arithmetic average of 30 models is defined as the multi-model ensemble mean (MME), and the Student's t-test is adopted for the statistical significance.

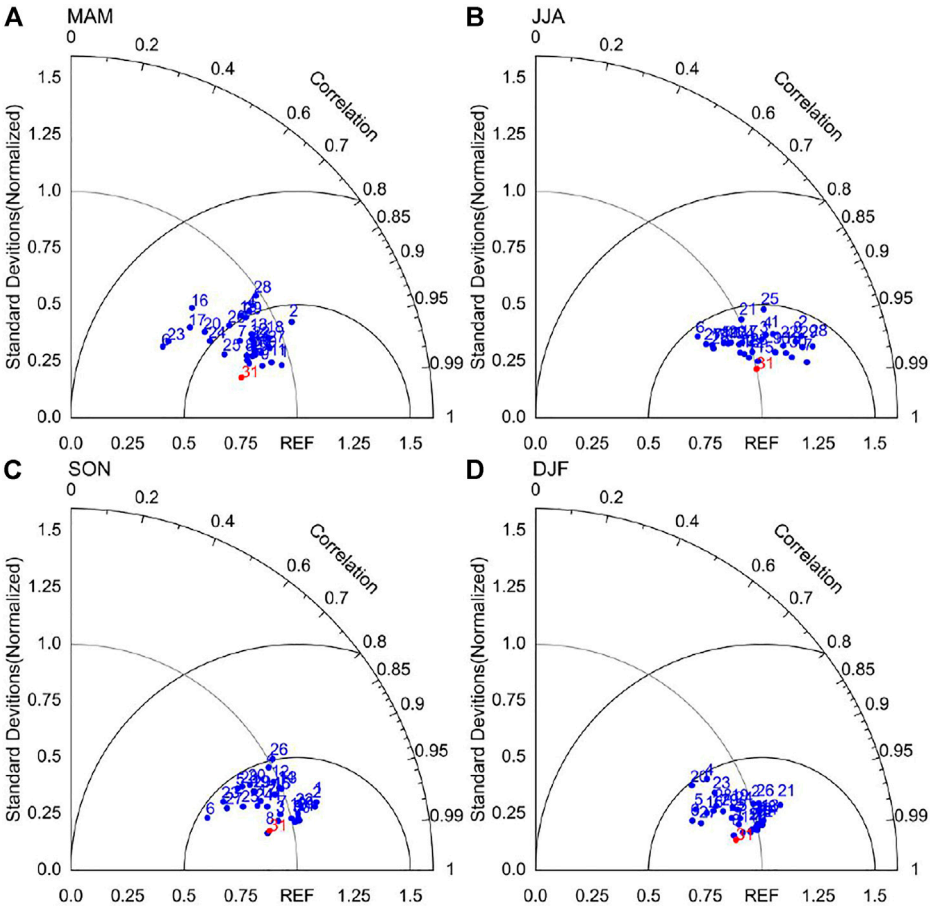

FIGURE 1 | Taylor diagram of **(A)** spring, **(B)** summer, **(C)** autumn and **(D)** winter UTT over the Asian-Pacific sector during 1965–2014. Numbers 1–30 represent the individual models (see **Table 1** for which model each number indicates). Number 31 represents MME. REF indicates the NCEP/NCAR reanalysis and acts as the reference point.

EVALUATION OF MODEL PERFORMANCE

Climatology

Figure 1 shows the Taylor diagrams for the climatology of seasonal UTT during 1965–2014 over the Asian-Pacific region (0°-60°N, 30°E-90°W; 61 × 241 grids) to quantify each model's performance. With reference to the observation in each season, all the root mean square errors (RMSEs) of individual models are lower than 0.75; all the SCCs are larger than 0.75 and higher above 0.90 for most models; the standard deviation ratios vary from 0.5 to 1.25 for spring UTT and from 0.75 to 1.25 for the UTT of the other three seasons. These results suggest that the CMIP6 models have a good capacity in capturing the climatologic pattern of seasonal UTT. Compared to individual models, the MME simulation is noted to have a higher SCC and a lower RMSE, implying better performance of the MME than individual models. Specifically, the SCCs between the MME simulation and the observation are 0.97, 0.98, 0.98 and 0.99 (significant at the 99.9% level) for spring, summer, autumn and winter UTT, respectively. Their respective RMSEs in the MME simulation are 0.31, 0.22, 0.21 and 0.18.

The climatological distributions of seasonal UTT from the observation and the MME simulation are further plotted (**Figure 2**). A general resemblance can be clearly seen. In spring (**Figures 2A, E**), positive values cover the southwest-northeast oriented region from the mid-low latitudes of Asia to the high latitudes of the North Pacific, with negative values residing on the either flank. The positive and negative centers are located in East Asia and the eastern Pacific, respectively. In summer (**Figures 2B, F**), the positives in the Eurasian continent and the negatives in the central-eastern Pacific are most dominant. The climatological distribution of autumn UTT (**Figures 2C, G**) is similar to that in spring. In winter (**Figures 2D, H**), compared to the autumn season, the negatives in northeastern Asia expand southward and the positive center moves eastward to the western Pacific. Also, the negatives in the Pacific shift eastward slightly.

Through the empirical orthogonal function (EOF) analysis, Zhao et al. (2007); Zhao et al. (2008) highlighted a seesaw

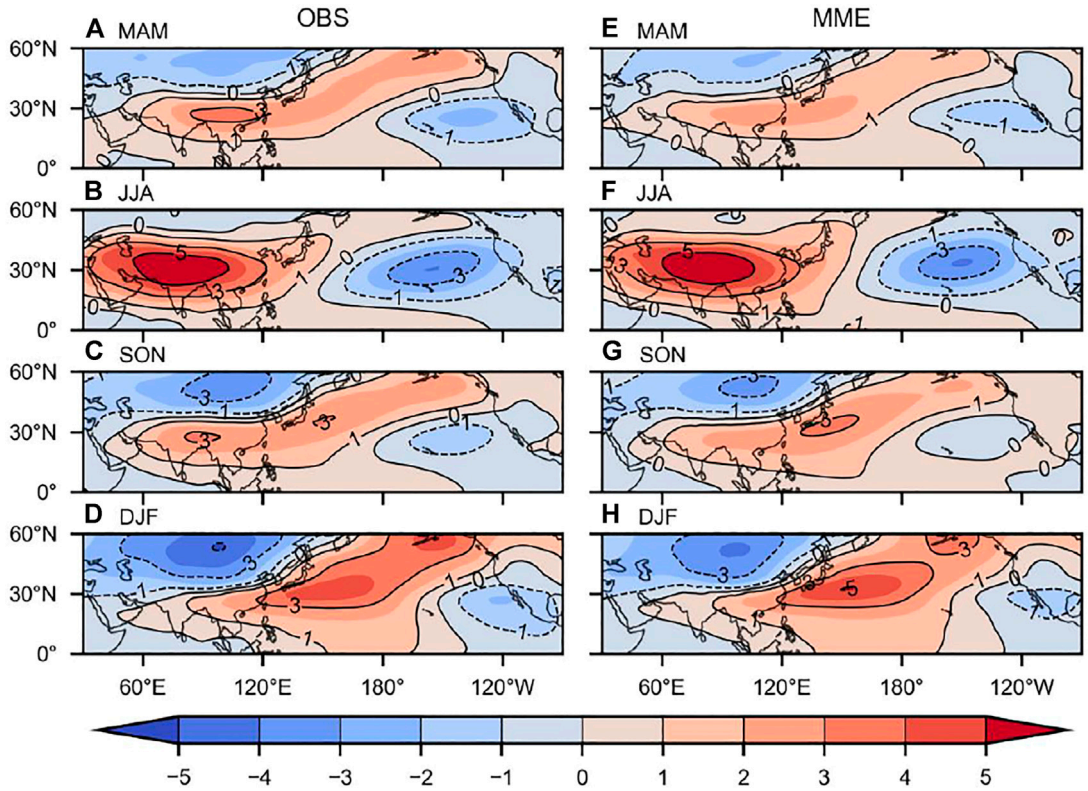

FIGURE 2 | Climatological distribution of **(A,E)** spring, **(B,F)** summer, **(C,G)** autumn and **(D,H)** winter UTT (unit: °C) during 1965–2014 from **(A–D)** NCEP/NCAR reanalysis and **(E–H)** MME simulation.

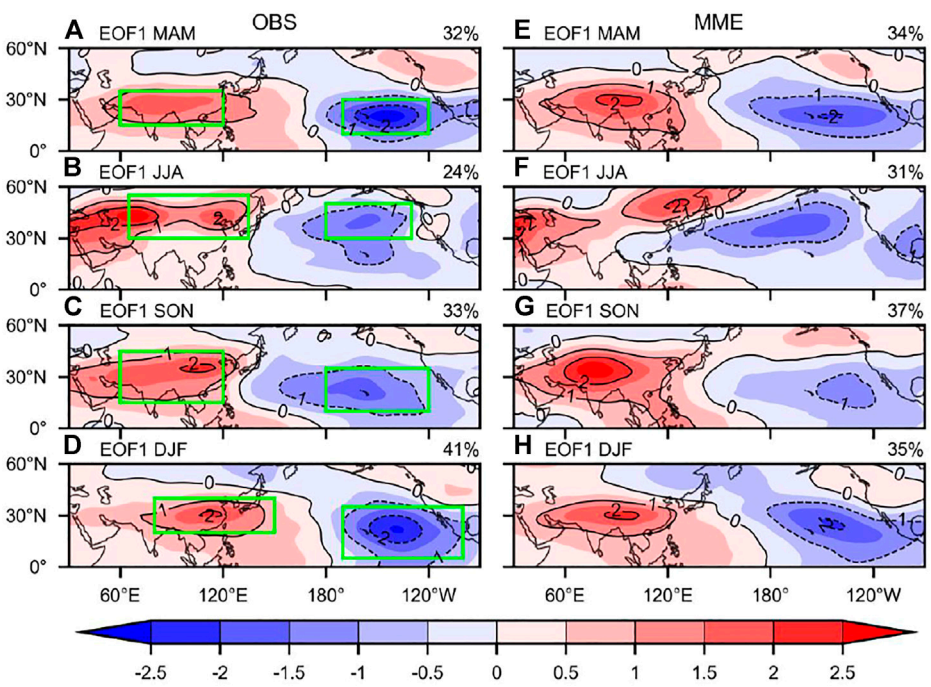

FIGURE 3 | EOF1 (×0.01) mode of **(A,E)** spring, **(B,F)** summer, **(C,G)** autumn and **(D,H)** winter UTT during 1965–2014 from **(A–D)** NCEP/NCAR reanalysis and **(E–H)** MME simulation. Green boxes in **(A–D)** are used to define APO index.

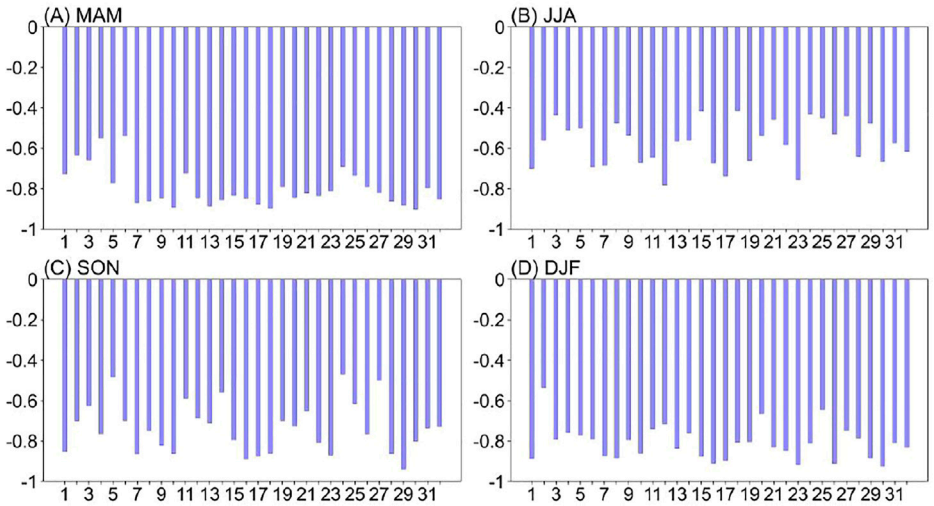

FIGURE 4 | AI-PI correlations in **(A)** spring, **(B)** summer, **(C)** autumn and **(D)** winter during 1965–2014. Numbers 1–30 represent the individual models (see **Table 1** for which model each number indicates). Number 31 and 32 represent MME and observation, respectively.

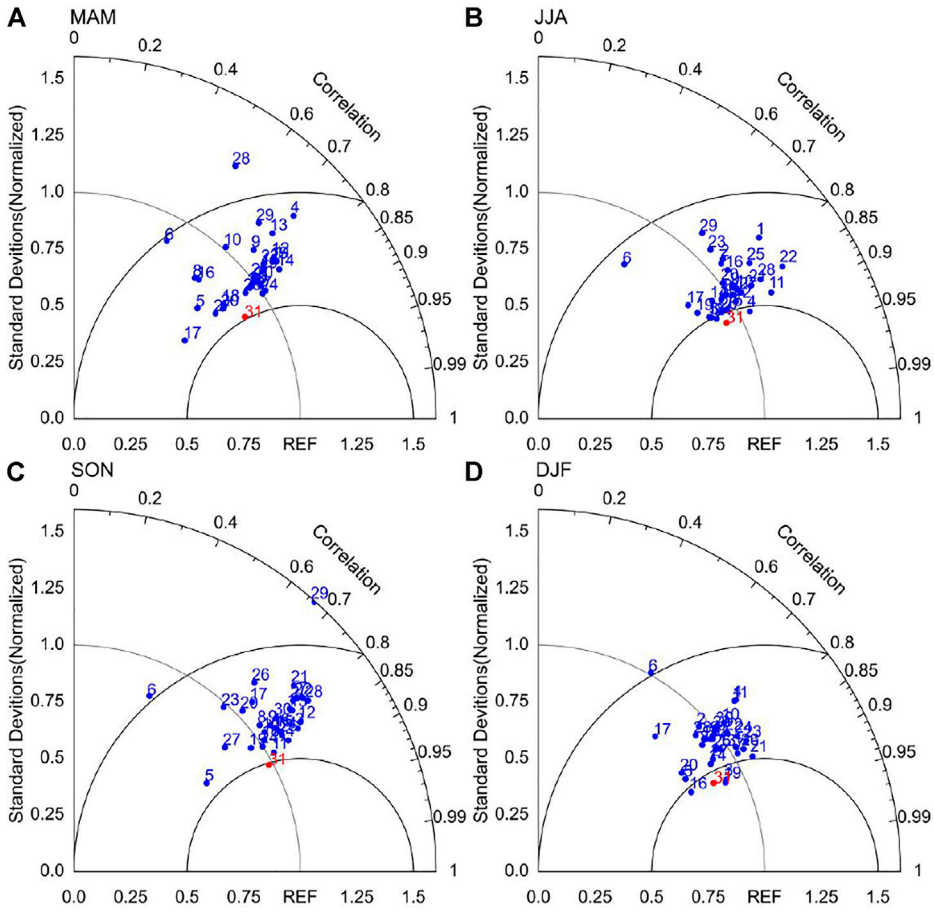

FIGURE 5 | Same as in **Figure 1**, but for **(A)** spring, **(B)** summer, **(C)** autumn and **(D)** winter UTT standard deviation during 1965–2014.

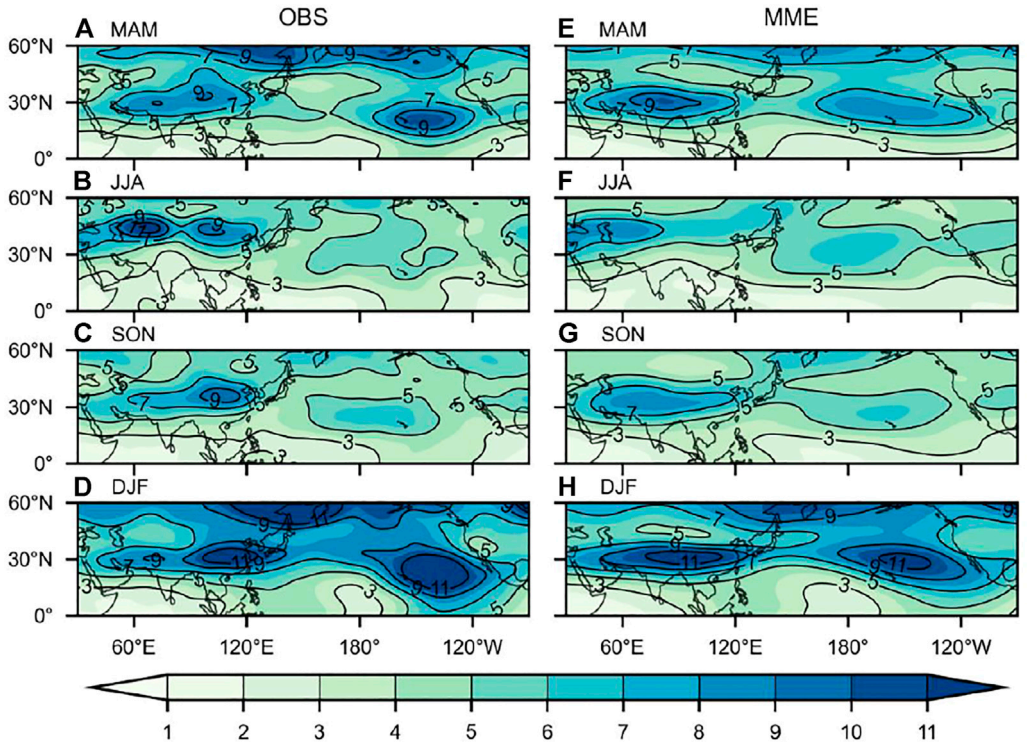

FIGURE 6 | Spatial distribution of standard deviation (unit: 10^{-1}°C) of **(A,E)** spring, **(B,F)** summer, **(C,G)** autumn and **(D,H)** winter UTT during 1965–2014 from **(A–D)** NCEP/NCAR reanalysis and **(E–H)** MME simulation.

oscillation in the UTT variability over the Asian-Pacific sector (i.e., APO), which features a warming of the Asian UTT accompanied with a cooling of the North Pacific UTT and vice versa. Accordingly, the EOF analysis for seasonal UTT in the observation and the MME simulation was conducted. Shown in **Figures 3A–D**, the first leading pattern (EOF1) of spring, summer, autumn and winter UTT in the observation, explaining 32, 24, 33 and 41% of their respective total variance, clearly displays a seesaw structure in the Asian-Pacific region. These oscillation features can be reasonably reproduced by the MME simulation (**Figures 3E–H**). The MME simulated EOF1 pattern from spring to winter accounts for 34, 31, 37 and 35% of the total variance, respectively. Their corresponding spatial correlations with the observed EOF1 patterns are 0.92, 0.84, 0.92, and 0.91, all higher than the 99.9% significance level.

Following Zhao et al. (2007), we refer to the location of positive (negative) center shown in **Figure 3** and then define the regional mean UTT as AI (PI) index to measure the variation of the Asian (the North Pacific) UTT. The APO index is calculated as the AI minus the PI. The definition for four seasons is shown as follows:

$$I_{APO\text{-}MAM} = UTT_{(15^{\circ}\text{-}35^{\circ}N,60^{\circ}\text{-}120^{\circ}E)} - UTT_{(10^{\circ}\text{-}30^{\circ}N,170^{\circ}\text{-}120^{\circ}W)}$$
$$I_{APO\text{-}JJA} = UTT_{(30^{\circ}\text{-}55^{\circ}N,65^{\circ}\text{-}135^{\circ}E)} - UTT_{(30^{\circ}\text{-}50^{\circ}N,180^{\circ}\text{-}130^{\circ}W)}$$
$$I_{APO\text{-}SON} = UTT_{(15^{\circ}\text{-}45^{\circ}N,60^{\circ}\text{-}120^{\circ}E)} - UTT_{(10^{\circ}\text{-}35^{\circ}N,180^{\circ}\text{-}120^{\circ}W)}$$
$$I_{APO\text{-}DJF} = UTT_{(20^{\circ}\text{-}40^{\circ}N,80^{\circ}\text{-}150^{\circ}E)} - UTT_{(5^{\circ}\text{-}35^{\circ}N,170^{\circ}\text{-}100^{\circ}W)}$$

where the left-hand side of each equation represents the APO index for each season and the first (second) term on the right-hand side indicates the corresponding AI (PI) index.

Figure 4 shows the observed and simulated AI-PI correlations for the period of 1965–2014. The observed correlations (represented by the number 32) are −0.85 in spring, −0.62 in summer, −0.73 in autumn and −0.83 in winter. All the correlations are above the 99.9% significance level, again demonstrating the inverse linkage of the Asian UTT to the North Pacific UTT. Such an inverse relationship in four seasons can be well simulated by the CMIP6 models. For the MME simulation (represented by the number 31), the seasonal AI-PI correlations from spring to winter are, in turn, −0.80, −0.57, −0.74 and −0.81, also higher than the 99.9% significance level and close to the observation.

Interannual Variability

Figure 5 displays the Taylor diagrams for the simulated seasonal interannual variability of UTT over the Asian-Pacific region. Most models show a SCC value of above 0.75 in four seasons, with the RMSE less than 0.75. Seasonally, the best performance is shown for winter SD. Also, the MME simulation generally outperforms its ensemble members for all seasons. For the MME simulation, the SCCs in spring, summer, autumn and winter are 0.86, 0.89, 0.88 and 0.90 (significant at the 99.9% level), and the RMSEs are 0.51, 0.46, 0.49 and 0.45, respectively. The MME simulated SD

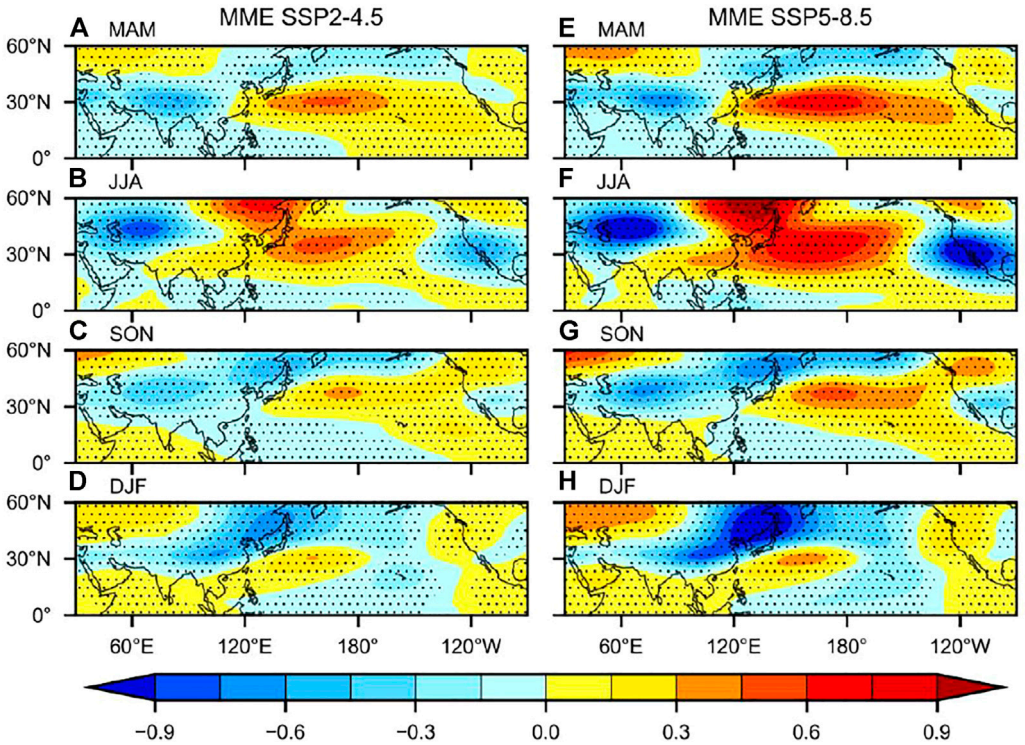

FIGURE 7 | MME projected changes of **(A,E)** spring, **(B,F)** summer, **(C,G)** autumn and **(D,H)** winter UTT (unit: °C) during 2050–2099 relative to 1965–2014 under **(A–D)** SSP2-4.5 and **(E–H)** SSP5-8.5. Regions above the 95% significance level are dotted.

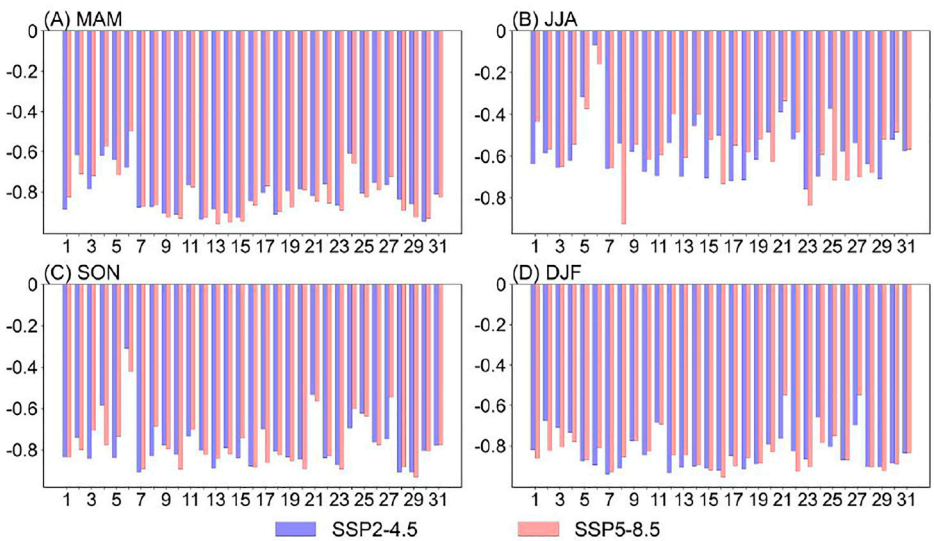

FIGURE 8 | AI-PI correlations in **(A)** spring, **(B)** summer, **(C)** autumn and **(D)** winter during 2050–2099 under SSP2-4.5 and SSP5-8.5. Numbers 1–30 represent individual models (see **Table 1** for which model each number indicates). Number 31 represents MME.

distributions in four seasons, which are similar to the observation, exhibit large interanual variability (SD exceeding 0.6) in Asia and the central-eastern Pacific (**Figure 6**). These results illustrates that the MME performs well in capturing the interannual variability of the Asian-Pacific UTT.

In brief, the MME shows a good capacity to reproduce the climatology and interannual variability of seasonal UTT in the

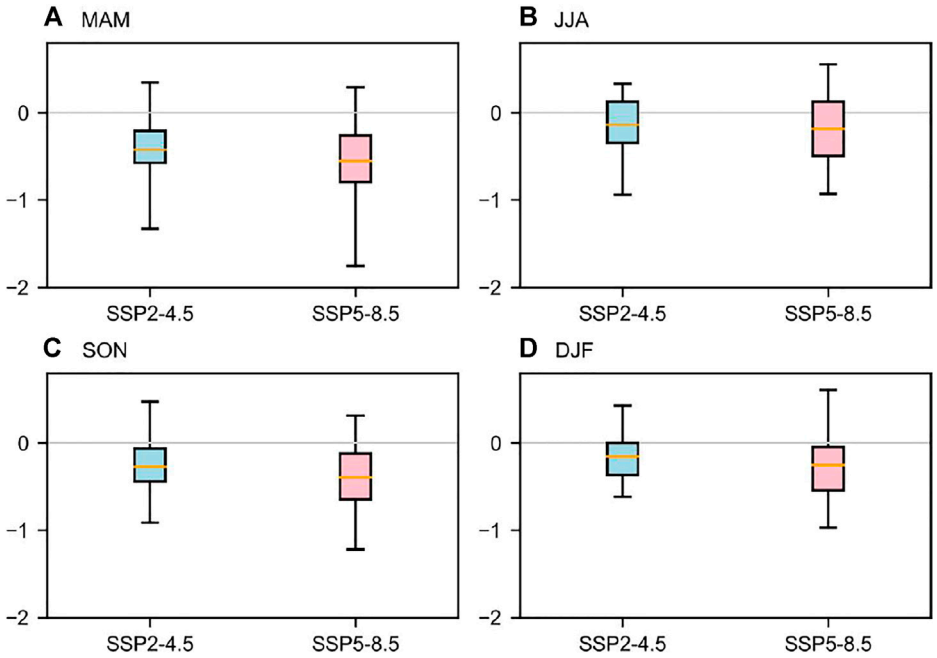

FIGURE 9 | Projected changes of **(A)** spring, **(B)** summer, **(C)** autumn and **(D)** winter APO during 2050–2099 relative to 1965–2014 under SSP2-4.5 (blue) and SSP5-8.5 (pink). Boxes indicate the interquartile model spread (25th and 75th quantiles) with the horizontal line indicating the MME and the whiskers showing the ensemble range.

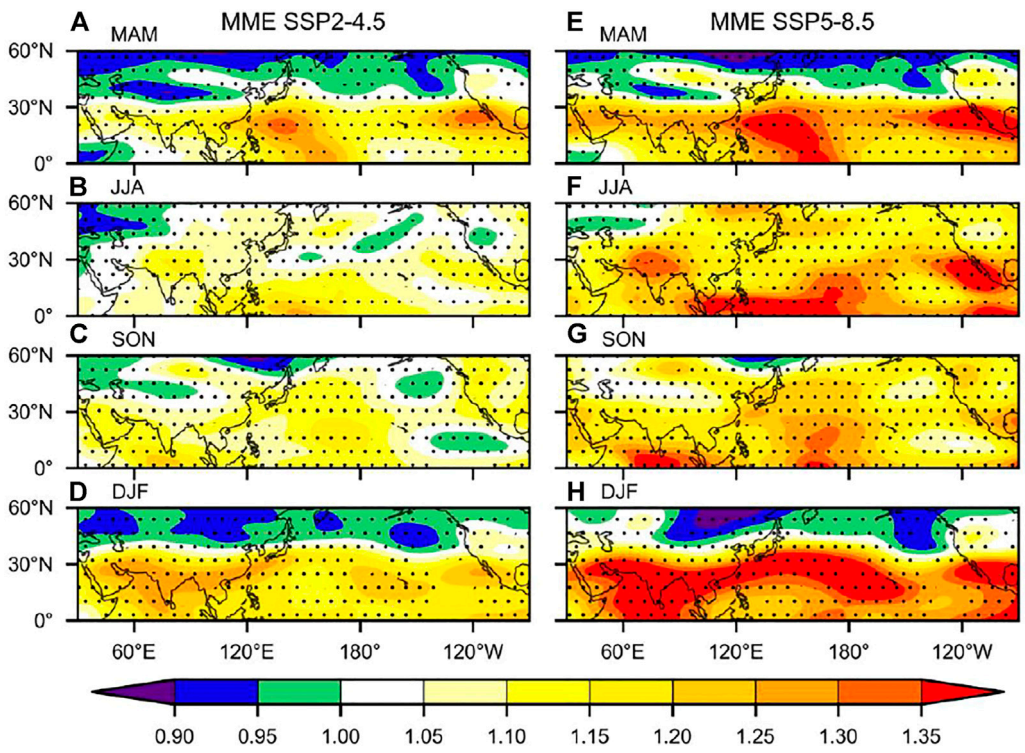

FIGURE 10 | Ratio of MME projected UTT standard deviation during 2050–2099 under **(A–D)** SSP2-4.5 and **(E–H)** SSP5-8.5 to that during 1965–2014 in **(A,E)** spring, **(B,F)** summer, **(C,G)** autumn and **(D,H)** winter. Regions above the 95% significance level are dotted.

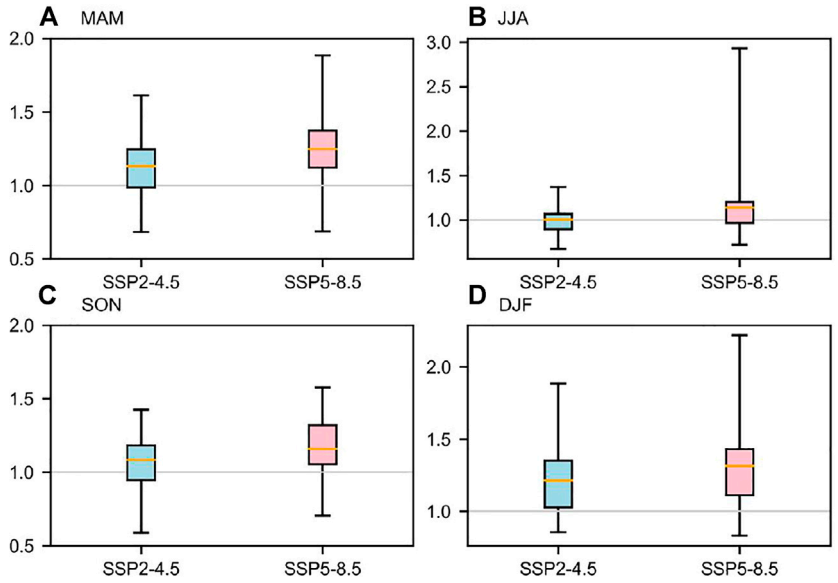

FIGURE 11 | Same as **Figure 9**, but for the projected ratio of APO standard deviation in **(A)** spring, **(B)** summer, **(C)** autumn and **(D)** winter.

Asian-Pacific sector. The APO pattern in each season can also be well captured. All of these provide a basis for using the MME to project their future changes.

PROJECTED CHANGES

Climatology

Figure 7 presents the MME projected seasonal UTT anomalies during 2050–2099 (relative to 1965–2014) under the scenarios of SSP2-4.5 and SSP5-8.5. The anomalous patterns for the two scenarios are similar in each season. However, the changes in magnitude are larger under SSP5-8.5 than that under SSP2-4.5, due to stronger external forcing imposed on the models. In spring (**Figures 7A, E**), significant negative anomalies are dominant in a widespread region of Asia and significant positive anomalies are pronounced in large areas of the North Pacific. Such an anomalous pattern generally opposites to the current climatological UTT distribution (**Figure 2E**), indicating a weakening of the upper-tropospheric thermal difference between the Asian continent and the North Pacific in a warmer scenario. Decreases in UTT over most Eurasia are projected in summer (**Figures 7B, F**). In comparison, the projected UTT increases in the North Pacific with an exception that a decrease of UTT occurs over the eastern Pacific. In combination with **Figure 2F**, the projected change in summer UTT hints that the UTT centers at current climate will shift eastward in the future climate, in addition to a weakening of the upper-tropospheric thermal difference between Asia and the North Pacific. This finding conforms to the CMIP5 result (Zhou, 2016). The case for the projected change of autumn UTT (**Figures 7C, G**) approximates that for spring UTT. In winter (**Figures 7D, H**), decreases in UTT are projected to occur in East Asia and the North Pacific except some parts of the western and eastern Pacific where an increase of UTT is projected.

We further calculated the AI-PI correlations in both scenarios. **Figure 8** illustrates that the AI and PI projected from all the CMIP6 models are negatively correlated in each season. The MME projected spring, summer, autumn and winter AI-PI correlations under SSP2-4.5 (SSP5-8.5) are −0.81 (−0.82), −0.57 (−0.57), −0.77 (−0.77) and −0.84 (−0.83), respectively, all of which exceed the 99.9% significance level. It suggests that current out-of-phase relationship in the Asian-Pacific UTT (i.e., APO pattern) will still exist in a warmer world.

Changes of the APO intensity for SSP2-4.5 and SSP5–8.5 during the second half of the 21st century are displayed in **Figure 9**. During 2050–2099 relative to 1965–2014, the change of APO intensity projected by individual models from spring to winter under SSP2-4.5 (SSP5-8.5) is in the range of −1.33–0.34°C (−1.75–0.29°C), −0.94–0.33°C (−0.93–0.55°C), −0.91–0.47°C (−1.22–0.31°C) and −0.61–0.43°C (−0.97–0.61°C), respectively. The MME projected spring, summer, autumn and winter APO intensity decreases by 0.42°C, 0.13°C, 0.27°C and 0.15°C under SSP2-4.5, and further to 0.55°C, 0.19°C, 0.39°C and 0.25°C under SSP5-8.5, respectively. In other words, with reference to current climate, the APO intensity tends to weaken by 19.9% (26.1%) in spring, 2.5% (3.7%) in summer, 31.8% (45.9%) in autumn and 11.4% (18.9%) in winter over the course of the second half of the 21st century under SSP2-4.5 (SSP5-8.5).

Interannual Variability

To examine future changes of the UTT interannual variability, we plotted the MME simulated SD ratio between 2050–2099 and 1965–2014 (**Figure 10**). The distribution of SD ratio under SSP2-4.5 and SSP5-8.5 resembles each other in each season, showing an increase of interannual variability over most of the Asian-Pacific

sector, particularly over the mid-low latitudes in the future. Due to stronger external forcing, the projected changes in SD under SSP5-8.5 are greater than that under SSP2-4.5. Seasonally, the projected greatest increase of SD occurs in winter.

Accordingly, the MME projected interannual variability of APO is enhanced in four seasons, with larger enhancement under SSP5-8.5 than under SSP2-4.5 (**Figure 11**). During 2050–2099 under SSP5-8.5 (SSP2-4.5), the MME projects a percentage increase of 25% (13%), 13% (1%), 16% (8%) and 31% (21%), respectively, for the SD of spring, summer, autumn and winter APO. Large inter-model spreads are also noted in the projection of APO interannual variability. Moreover, the model spread becomes wider under SSP5-8.5 as compared to that under SSP2-4.5. For SSP5-8.5, the largest model spread is found for the SD of summer APO, which ranges from a decrease of 28% to an increase of 193%, followed by the SD of winter APO, ranging from a decrease of 17% to an increase of 122%. The largest model spread for the SD of summer APO mainly results from the CIESM projection which shows considerably greater change as compared to other models. The model spreads for the SD of spring and autumn APO are in the range of −31%–88% and −30%–58%, respectively. For SSP2-4.5, the projected percentage changes in the SD of spring, summer, autumn and winter APO are −32%–61%, −33%–37%, −41%–42% and −15%–89%, respectively.

CONCLUSION

The performance of 30 CMIP6 models in the simulation of the Asian-Pacific seasonal UTT, including the climatology, the interannual variability and the APO pattern during 1965–2014, was evaluated in this study. Based on the evaluation, their changes under SSP2-4.5 and SSP5-8.5 over the course of the second half of the 21st century were further projected. The main findings are summarized below:

1) The evaluation results show that the CMIP6 models perform well in reproducing the observed climatology and interannual variability of seasonal UTT pattern in the Asian-Pacific sector. The MME outperforms individual models with a higher SCC and lower RMSE. The MME simulated climatological distribution of seasonal UTT, including the position of warm and cold centers and the north-south migration from spring to winter, well resembles the observation. The simulated SD pattern with large interanual variability over Asia and the central-eastern Pacific is broadly comparable to the observation. The observed APO pattern in four seasons can also be captured.
2) The MME projects that future changes in the UTT climatology and interannual variability are spatially similar for the two scenarios, however, the magnitudes of changes under SSP5-8.5 are larger than that under SSP2-4.5. During 2050–2099 relative to 1965–2014, spring, summer and autumn UTTs are projected to fall in larger areas of Asia and rise in most of the North Pacific, signifying a weakening of the upper-tropospheric thermal contrast between the two regions. The winter UTT is projected to decrease in East Asia and the North Pacific except that an increase of UTT occurs over some parts of the western and the eastern Pacific. The projected UTT interannual variability increases in four seasons particularly over the mid-low latitudes of the Asian-Pacific sector.
3) The MME projects that current APO phenomenon still exists in the future climate. However, a weakening of APO intensity and an enlargement of its interannual variability are anticipated. The changes in magnitude under SSP5-8.5 are greater than that under SSP2-4.5. For SSP5-8.5, the projected weakening of APO intensity is the highest in autumn, and that during the summer time is the lowest. The largest increase of APO interannual variability is projected in winter, and the projected smallest increase occurs in summer.

DATA AVAILABILITY STATEMENT

The original contributions presented in the study are included in the article, further inquiries can be directed to the corresponding author.

AUTHOR CONTRIBUTIONS

BZ designed and supervised the research; QF performed data analysis. QF and BZ prepared the manuscript.

FUNDING

This research was supported by the National Natural Science Foundation of China (42025502).

ACKNOWLEDGMENTS

We acknowledge the World Climate Research Program's Working Group on Coupled Modeling and thank the climate modeling groups for producing and sharing their model outputs.

REFERENCES

Chen, H., Sun, J., Lin, W., and Xu, H. (2020). Comparison of CMIP6 and CMIP5 Models in Simulating Climate Extremes. *Sci. Bull.* 65, 1415–1418. doi:10.1016/j.scib.2020.05.015

Dai, A., Li, H., Sun, Y., Hong, L. C., LinHo, L., Chou, C., et al. (2013). The Relative Roles of Upper and Lower Tropospheric Thermal Contrasts and Tropical Influences in Driving Asian Summer Monsoons. *J. Geophys. Res. Atmos.* 118, 7024–7045. doi:10.1002/jgrd.50565

Eyring, V., Bony, S., Meehl, G. A., Senior, C. A., Stevens, B., Stouffer, R. J., et al. (2016). Overview of the Coupled Model Intercomparison Project Phase 6

(CMIP6) Experimental Design and Organization. *Geosci. Model Dev.* 9, 1937–1958. doi:10.5194/gmd-9-1937-2016

Fang, K., Davi, N., and D'Arrigo, R. (2014). A Reconstruction of the Asia-Pacific Oscillation Index for the Past 1500 Years and its Association with the Asian Summer Monsoon. *Int. J. Climatol.* 34, 2505–2514. doi:10.1002/joc.3856

Gidden, M. J., Riahi, K., Smith, S. J., Fujimori, S., Luderer, G., Kriegler, E., et al. (2019). Global Emissions Pathways under Different Socioeconomic Scenarios for Use in CMIP6: A Dataset of Harmonized Emissions Trajectories through the End of the Century. *Geosci. Model Dev.* 12, 1443–1475. doi:10.5194/gmd-12-1443-2019

Ha, K. J., Moon, S., Timmermann, A., and Kim, D. (2020). Future Changes of Summer Monsoon Characteristics and Evaporative Demand over Asia in CMIP6 Simulations. *Geophys. Res. Lett.* 47, e2020GL087492. doi:10.1029/2020GL087492

Hua, W., Lin, Z., Wang, X., and Fan, G. (2019). Weakening Relationship between East Asian Summer Monsoon and Asian-Pacific Oscillation after 1990s. *Adv. Meteorology* 2019, 1–9. doi:10.1155/2019/6012301

IPCC (2013). *Climate Change 2013: The Physical Science Basis. Contribution of Working Group I to the Fifth Assessment Report of the Intergovernmental Panel on Climate Change*. Cambridge, UK and New York: Cambridge University Press.

Jiang, X., Yang, S., Li, Y., Ke, Z., Li, J., and Hu, H. (2013). Dominant Modes of Wintertime Upper-Tropospheric Temperature Variations over Asia and Links to Surface Climate. *J. Clim.* 26, 9043–9060. doi:10.1175/JCLI-D-12-00774.1

Jiang, D., Hu, D., Tian, Z., and Lang, X. (2020). Differences between CMIP6 and CMIP5 Models in Simulating Climate over China and the East Asian Monsoon. *Adv. Atmos. Sci.* 37, 1102–1118. doi:10.1007/s00376-020-2034-y

Kalnay, E., Kanamitsu, M., Kistler, R., Collins, W., Deaven, D., Gandin, L., et al. (1996). The NCEP/NCAR 40-year Reanalysis Project. *Bull. Amer. Meteor. Soc.* 77, 437–471. doi:10.1175/1520-0477(1996)077<0437:tnyrp>2.0.co;2

Lin, Z., Zhu, J., Hua, W., and Fan, G. (2021). Impact of the August Asian-Pacific Oscillation on Autumn Precipitation in Central Eastern China. *Asia-Pacific J. Atmos. Sci.* 57, 181–190. doi:10.1007/s13143-020-00187-1

Ma, J., and Yu, J.-Y. (2014). Paradox in South Asian Summer Monsoon Circulation Change: Lower Tropospheric Strengthening and Upper Tropospheric Weakening. *Geophys. Res. Lett.* 41, 2934–2940. doi:10.1002/2014GL059891

Nan, S., Zhao, P., Yang, S., and Chen, J. (2009). Springtime Tropospheric Temperature over the Tibetan Plateau and Evolutions of the Tropical Pacific SST. *J. Geophys. Res.* 114, D10104. doi:10.1029/2008JD011559

O'Neill, B. C., Tebaldi, C., Van Vuuren, D. P., Eyring, V., Friedlingstein, P., Hurtt, G., et al. (2016). The Scenario Model Intercomparison Project (ScenarioMIP) for CMIP6. *Geosci. Model Dev.* 9, 3461–3482. doi:10.5194/gmd-9-3461-2016

Si, D., Zhao, P., and Wang, M. (2019). Inter-decadal Change of the Middle-upper Tropospheric Land-Sea Thermal Contrast in the Late 1990s and the Associated Northern Hemisphere Hydroclimate. *Int. J. Climatol.* 39, 3271–3281. doi:10.1002/joc.6017

Simpkins, G. (2017). Progress in Climate Modelling. *Nat. Clim. Change* 7, 684–685. doi:10.1038/nclimate3398

Stouffer, R. J., Eyring, V., Meehl, G. A., Bony, S., Senior, C., Stevens, B., et al. (2017). CMIP5 Scientific Gaps and Recommendations for CMIP6. *Bull. Am. Meteorol. Soc.* 98, 95–105. doi:10.1175/BAMS-D-15-00013.1

Sun, Y., and Ding, Y. (2011). Responses of South and East Asian Summer Monsoons to Different Land-Sea Temperature Increases under a Warming Scenario. *Chin. Sci. Bull.* 56, 2718–2726. doi:10.1007/s11434-011-4602-0

Tebaldi, C., Debeire, K., Eyring, V., Fischer, E., Fyfe, J., Friedlingstein, P., et al. (2021). Climate Model Projections from the Scenario Model Intercomparison Project (ScenarioMIP) of CMIP6. *Earth Syst. Dynam.* 12, 253–293. doi:10.5194/esd-12-253-2021

Wang, L., and Chen, L. (2017). Interannual Variation of the Asian-Pacific Oscillation. *Dyn. Atmos. Oceans* 77, 17–25. doi:10.1016/j.dynatmoce.2016.10.009

Xin, X., Yu, R., Zhou, T., and Wang, B. (2006). Drought in Late Spring of South China in Recent Decades. *J. Clim.* 19, 3197–3206. doi:10.1175/JCLI3794.1

Xin, X., Li, Z., Yu, R., and Zhou, T. (2008). Impacts of Upper Tropospheric Cooling upon the Late Spring Drought in East Asia Simulated by a Regional Climate Model. *Adv. Atmos. Sci.* 25, 555–562. doi:10.1007/s00376-008-0555-x

Yang, X., Zhou, B., Xu, Y., and Han, Z. (2021). CMIP6 Evaluation and Projection of Temperature and Precipitation over China. *Adv. Atmos. Sci.* 38, 817–830. doi:10.1007/s00376-021-0351-4

Yu, R., Wang, B., and Zhou, T. (2004). Tropospheric Cooling and Summer Monsoon Weakening Trend over East Asia. *Geophys. Res. Lett.* 31, L22212. doi:10.1029/2004GL021270

Zhang, L., and Zhou, T. (2012). The Interannual Variability of Summer Upper-Tropospheric Temperature over East Asia. *J. Clim.* 25, 6539–6553. doi:10.1175/JCLI-D-11-00583.1

Zhang, L., and Zhou, T. (2015). Decadal Change of East Asian Summer Tropospheric Temperature Meridional Gradient Around the Early 1990s. *Sci. China Earth Sci.* 58, 1609–1622. doi:10.1007/s11430-015-5117-3

Zhao, P., Zhu, Y., and Zhang, R. (2007). An Asian-Pacific Teleconnection in Summer Tropospheric Temperature and Associated Asian Climate Variability. *Clim. Dyn.* 29, 293–303. doi:10.1007/s00382-007-0236-y

Zhao, P., Chen, J., Xiao, D., Nan, S., Zou, Y., and Zhou, B. (2008). Summer Asian-Pacific Oscillation and its Relationship with Atmospheric Circulation and Monsoon Rainfall. *Acta Meteorol. Sin.* 22, 455–471.

Zhao, P., Cao, Z., and Chen, J. (2010). A Summer Teleconnection Pattern over the Extratropical Northern Hemisphere and Associated Mechanisms. *Clim. Dyn.* 35, 523–534. doi:10.1007/s00382-009-0699-0

Zhao, P., Wang, B., and Zhou, X. (2012). Boreal Summer Continental Monsoon Rainfall and Hydroclimate Anomalies Associated with the Asian-Pacific Oscillation. *Clim. Dyn.* 39, 1197–1207. doi:10.1007/s00382-012-1348-6

Zhao, S., Li, J., Yu, R., and Chen, H. (2015). Recent Reversal of the Upper-Tropospheric Temperature Trend and its Role in Intensifying the East Asian Summer Monsoon. *Sci. Rep.* 5, 11847. doi:10.1038/srep11847

Zhou, B.-T., and Xu, Y. (2017). CMIP5 Analysis of the Interannual Variability of the Pacific SST and its Association with the Asian-Pacific Oscillation. *Atmos. Ocean. Sci. Lett.* 10, 138–145. doi:10.1080/16742834.2017.1260427

Zhou, B. (2016). The Asian-Pacific Oscillation Pattern in CMIP5 Simulations of Historical and Future Climate. *Int. J. Climatol.* 36, 4778–4789. doi:10.1002/joc.4668

Zhou, B., Cui, X., and Zhao, P. (2008). Relationship between the Asian-Pacific Oscillation and the Tropical Cyclone Frequency in the Western North Pacific. *Sci. China Ser. D-Earth Sci.* 51, 380–385. doi:10.1007/s11430-008-0014-7

Zhou, B., Zhao, P., and Cui, X. (2010). Linkage between the Asian-Pacific Oscillation and the Sea Surface Temperature in the North Pacific. *Chin. Sci. Bull.* 55, 1193–1198. doi:10.1007/s11434-009-0386-x

Zhou, B., Xu, Y., and Shi, Y. (2018). Present and Future Connection of Asian-Pacific Oscillation to Large-Scale Atmospheric Circulations and East Asian Rainfall: Results of CMIP5. *Clim. Dyn.* 50, 17–29. doi:10.1007/s00382-017-3579-z

Zhou, B., and Zhao, P. (2010). Influence of the Asian-Pacific Oscillation on Spring Precipitation over Central Eastern China. *Adv. Atmos. Sci.* 27, 575–582. doi:10.1007/s00376-009-9058-7

Conflict of Interest: The authors declare that the research was conducted in the absence of any commercial or financial relationships that could be construed as a potential conflict of interest.

frontiers | Frontiers in Earth Science

ORIGINAL RESEARCH
published: 30 June 2022
doi: 10.3389/feart.2022.914232

Amplifying Meteorological Droughts Across Middle- and Low-Latitude Northern Hemisphere

Danzhou Wang[1,2,3], *Qiang Zhang*[1,2,3]*, *Vijay P. Singh*[4,5], *Zexi Shen*[1,2,3], *Gang Wang*[1,2,3], *Wenhuan Wu*[1,2,3] *and Ruyue Yuan*[1,2,3]

[1]Key Laboratory of Environmental Change and Natural Disaster, Ministry of Education, Beijing Normal University, Beijing, China, [2]State Key Laboratory of Earth Surface Processes and Resource Ecology, Beijing Normal University, Beijing, China, [3]Faculty of Geographical Science, Beijing Normal University, Beijing, China, [4]Department of Biological and Agricultural Engineering and Zachry Department of Civil and Environmental Engineering, Texas A&M University, Killeen, TX, United States, [5]National Water and Energy Center, UAE University, Al Ain, United Arab Emirates

Drought changes and the underlying causes have, in the backdrop of warming climate, aroused widespread concern. However, exact changes in patterns of meteorological droughts in both space and time are still open for debate. The Northern Hemisphere is home to 90% of the world's population and has been afflicted by droughts over time. Here we present the evolution of spatiotemporal patterns of meteorological droughts, quantified by standardized precipitation evapotranspiration index across the Northern Hemisphere and related causes during a period of 1961–2018. We found amplifying droughts characterized by higher frequency, longer duration, and stronger severity across middle- and low-latitudes of the Northern Hemisphere, specifically, Mongolia, China and Central Asia expanding along central Eurasia, Circum-Mediterranean region, and southwestern North America (NA). Russia, Central Asia, China and the Indian Peninsula are regions with frequent droughts. Period of 1961–2018 witnessed spatial evolution of droughts in counterclockwise direction over North America. In general, the spatial evolution of meteorological droughts in Northern Hemisphere also followed counterclockwise direction due to the atmospheric pressure belt, wind belt, atmospheric circulation, and sea-land breeze. SPEI-based droughts were in close relation with El Niño-Southern Oscillation (ENSO) and Atlantic Multidecadal Oscillation (AMO). In particular, La Niña phenomenon could dry out southern NA and central and western Russia; and Atlantic Multidecadal Oscillation might affect the spatiotemporal variation of the drought in mid-high latitudes. These findings help understand meteorological droughts in the context of global warming.

Keywords: meteorological droughts, standardized precipitation evapotranspiration index, spatiotemporal evolution, attribution analysis, northern hemisphere

OPEN ACCESS

Edited by:
Tomas Halenka,
Charles University, Czechia

Reviewed by:
Bo Sun,
Nanjing University of Information Science and Technology, China
Keyan Fang,
Fujian Normal University, China

***Correspondence:**
Qiang Zhang
zhangq68@bnu.edu.cn

Specialty section:
This article was submitted to Interdisciplinary Climate Studies, a section of the journal Frontiers in Earth Science

Received: *06 April 2022*
Accepted: *10 June 2022*
Published: *30 June 2022*

Citation:
Wang D, Zhang Q, Singh VP, Shen Z, Wang G, Wu W and Yuan R (2022) Amplifying Meteorological Droughts Across Middle- and Low-Latitude Northern Hemisphere. Front. Earth Sci. 10:914232. doi: 10.3389/feart.2022.914232

1 INTRODUCTION

Drought is of stochastic nature afflicting society and eco-environment and is often considered as one of the costliest natural hazards (Mishra & Singh, 2010; Hayes et al., 2011; Svoboda and Fuchs, 2016; Yu et al., 2019). Drought-induced global economic losses have been estimated to be as high as six to eight billion US dollars each year (Wilhite, 2000; Yu et al., 2019). Recent decades witnessed growing

population and expansion of agricultural, energy, and industrial sectors which pushed up the demand for water resources and water scarcity risk over the globe (Vörösmarty et al., 2000; Mishra & Singh, 2010; Sternberg, 2011; Yu et al., 2019). Meanwhile, anthropogenic global warming is accelerating the global hydrological cycle (e.g., Allen and Ingram, 2002) and hence is altering the spatiotemporal patterns of precipitation resulting in increased hydrometeorological extremes, such as floods and droughts (Easterling et al., 2000; Dore, 2005; Zhang et al., 2013), while there are remarkable discrepancies in terms of drought variations under changing climate. Dai et al. (1998) and Dai (2011) indicated the amplification of droughts and showed continuously enhancing drought risk in a warming climate, while Sheffield and Wood (2008) and Sheffield et al. (2012) argued that little change was observed in global droughts over the past 60 years. The Northern Hemisphere is home to ~90% of the world's population, and accounts for about 66.6% of the world's land area (Miller et al., 2010). Drought events were usually recognized as four categories: i.e. meteorological drought caused by insufficient precipitation, agricultural drought caused by insufficient soil moisture, hydrological drought caused by insufficient river flow and water storage, and socioeconomic drought caused by insufficient demand and supply of economic commodities brought about by drought (Mishra & Singh, 2010). While, meteorological drought is usually the starting point for other three droughts and therefore thorough investigation of meteorological droughts and relevant causes are of paramount importance in the sustainability of reginal water resources and socio-economy over Northern Hemisphere.

A multitude of studies have addressed spatiotemporal patterns of droughts at regional and even global scales (Zhang et al., 2015; Herrera-Estrada et al., 2017). Shiau and Lin (2016) analyzed meteorological drought variations in both space and time over Taiwan, China, using quantile regression and cluster analysis techniques. Spinoni et al. (2019) detected a remarkable increase in the frequency and severity of meteorological droughts during the periods of 1951–1980 and 1981–2016 across the Mediterranean region, the Sahel, the Congo River basin, northeastern China, and central Asia. Zhang et al. (2021) quantified relationships between drought and 23 drought factors using remote sensing data during the period of 2002–2016 across China and found that precipitation and soil moisture made relatively large contributions to droughts. Recent studies started to focus on the spatiotemporal evolution of hydrometeorological variables, such as air temperature (e.g., Ji et al., 2014) and droughts (Xu et al., 2015; Yu et al., 2019). Wang et al. (2015) analyzed drought evolution trajectories and found that drought evolution can be attributed to the East Asian summer monsoon. Zhou et al. (2019) analyzed spatiotemporal variations of meteorological drought within Poyang Lake Basin, China, in terms of drought clusters, migration trajectory and migration direction. In this study, we attempt to depict meteorological drought evolution as well as migration trajectories over the Northern Hemisphere.

Highlighting causes behind meteorological droughts can help understand meteorological droughts and drought hazards. Previous studies have linked spatiotemporal evolutions of droughts with sea surface temperature (SST) and large-scale climate indices reflecting the occurrence of the climate events (Wu & Kinter, 2009). Erfanian et al. (2017) found that warmer-than-usual SSTs in the Tropical Pacific (also El Niño events) and Atlantic were the main driving factors behind extreme droughts in South America. However, SST anomalies also results from atmospheric circulation anomalies (Andreas & Hazeleger, 2005; Zhe et al., 2016; Turner et al., 2022). Madden Julian Oscillation (MJO; Zhang 2005) often affects the evolution of SST anomalies; SST anomalies in the tropics can also feedback extratropical circulation anomalies (Lau, 1997). Besides, relations between MJO and precipitation extremes also indirectly corroborate the impact of SST on droughts (e.g. Zheng et al., 2020). Hence, we attempted to quantify the relationship between SST and spatiotemporal evolution of meteorological droughts across Northern Hemisphere, and investigate causes behind meteorological droughts from the perspective of SST changes.

El Niño Southern Oscillation (ENSO) and other large-scale climate events such as Pacific Decadal Oscillation (PDO) have substantial impacts on the occurrence and development of regional and global droughts (Özger et al., 2009; Wang & Arun, 2015; Wang et al., 2019; Gore et al., 2020; Nguyen et al., 2021; Pieper et al., 2021). Sun and Yang (2012) found that the interactions between La Nina, North Atlantic Oscillation (NAO), and thermal conditions of the Qinghai-Tibet Plateau triggered severe droughts in southern China in spring. Feng et al. (2020) evidenced the important role of large-scale climate drivers such as ENSO in drought forecasting, showing critical relations between drought and large-scale climate drivers.

Temporal features of droughts involve frequency, intensity, duration and trend, and spatial features include drought-affected area, drought centroid, drought cluster and severity (Mishra et al., 2010; Mishra & Singh, 2010; Zhou et al., 2019). Yevjevich (1967) proposed a one-dimensional method to extract duration, severity and intensity of droughts from drought index sequence. Andreadis et al. (2005) and Lloyd-Hughes (2012) proposed the three-dimensional clustering method (e.g., Xu et al., 2015). Perez et al. (2011) developed the methodologies for characterizing droughts can be classified into non-contiguous and contiguous drought area analyses (i.e., NCDA and CDA). The one-dimensional method does not take into account the spatial distribution of drought events and is suitable for research based on site data. The three-dimensional clustering method can use spatial heterogeneity to correct spatial discontinuity caused by abnormal drought indices and is more suitable for grid data-based research. Considering that the data in the present study is a grid dataset, we use a three-dimensional clustering method (Andreadis et al., 2005) to identify meteorological droughts and characterize meteorological droughts in terms of duration, severity, intensity, spatial range, drought centroid and migration trajectory to delineate the spatiotemporal pattern and evolution of meteorological droughts.

Here we attempt to analyze the evolution of meteorological droughts in both space and time and anatomize causes behind their spatiotemporal evolutions in Northern Hemisphere. This study can help understand changes of meteorological droughts, relevant causes and mitigation to meteorological droughts over Northern Hemisphere.

2 DATA AND METHODS

2.1 Data

We used SPEI to meteorological drought (Vicenteserrano et al., 2010) during a period of 1961–2018. The gridded SPEI data were sourced from Consejo Superior de Investigaciones Científicas (CSIC, https://spei.csic.es) with a spatial resolution of 0.5°×0.5°. Drought grade classification is shown in **Supplementary Table S1** (Yu et al., 2019). Since droughts make no sense in arid regions, such as desert as well as extremely cold areas, so we excluded these areas from the study regions considered in here by mask processing (Spinoni et al., 2019). Here we analyzed seasonal and interannual drought variations (Liu et al., 2020) using the following concepts. We calculated annual SPEI from the 12-months SPEI (SPEI 12) and seasonal droughts (SPEI 03) during spring (March to May), summer (June to August), autumn (September to November), and winter (December to February of the subsequent year). Droughts at decadal scales were computed by averaging annual SPEI for every 10 years.

Relative humidity (RH), latitudinal wind velocity (V/U) of 850 h Pa, and the SST were sourced from the ERA5 reanalysis data with a spatial resolution of 0.25°×0.25° (https://cds.climate.copernicus.eu/#!/search?text=ERA5&type=dataset). Global mean temperature anomaly data (TA) from HadCRUT5 with a spatial resolution of 5°×5° was also analyzed (https://crudata.uea.ac.uk/cru/data/temperature/). The duration of the abovementioned data was 1961–2018 (**Supplementary Table S2**).

Large-scale climate indices (**Supplementary Table S3**) considered in this study included the Southern Oscillation Index (SOI) (Ropelewski & Jones, 1987), the Atlantic Multidecadal Oscillation (AMO) (Kerr, 2000), and the East Pacific-North Pacific (EP-NP) (Linkin & Nigam, 2007). SOI and EP-NP data were sourced from the Climate Prediction Center (CPC) of the National Oceanic and Atmospheric Administration (NOAA). AMO was calculated by the Physical Sciences Laboratory (PSL) of NOAA using the HardiSST v1.1 SST dataset (https://www.cpc.ncep.noaa.gov/and https://psl.noaa.gov/gcos_wgsp/Timeseries/).

2.2 Methods

2.2.1 Modified Mann–Kendall Trend Test and Sen's Slope

The MMK trend test (Hamed & Rao, 1998) was used to quantify the significance of SPEI trends (at 5% significance level). The magnitude of the SPEI trend was estimated by Sen's slope (Sen, 1968) as:

$$\beta = \text{Median}\frac{a_j - a_i}{j - a} \quad \forall i < j \tag{1}$$

where a_i, a_j denote two series. Positive (negative) values of β indicate an upward (downward) trend.

2.2.2 Identification of Long-Term Drought Events

Drought events were defined as SPEI < -0.5, while a long-term drought event was defined by the drought with a duration of at least

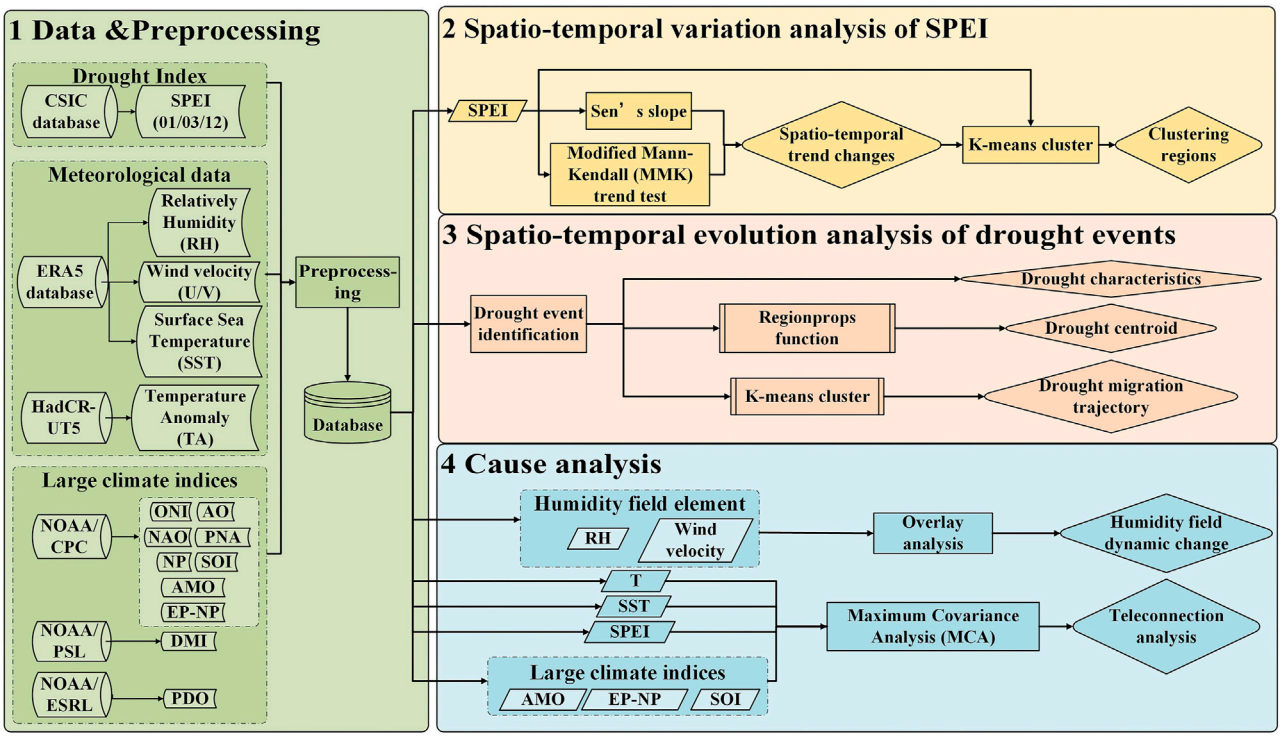

FIGURE 1 | Analysis procedure of this current study.

3 months. Here we considered three aspects of drought features, i.e., frequency refers to the number of drought occurrences during a given period (Spinoni et al., 2019); duration refers to consecutive time intervals dominated by drought events (Haile et al., 2020); and severity is represented by cumulative SPEI values throughout the drought period. Smaller cumulative SPEI value shows severer drought and vice versa (Yu et al., 2019); Centroid refers to the geometric center of the drought-affected region, depicting a 3-dimensional space-time space defined by longitude, latitude, and time (Xu et al., 2015). Here we use the MatLab image processing function regionprops (The MathWorks, 2014) identify the centroids of drought events.

2.2.3 K-Means Clustering Method

The K-means method was used to classify a given data set into *K* clusters (*K* is a hyperparameter), giving the center point corresponding to each sample data (Mcrae, 1971). Here we identified regions with homogeneous dry and/or wet conditions based on temporal mean SPEI value, coordinate position, and trends of SPEI (MMK value and Sen's slope). We also used the K-means method to delineate the spatiotemporal pattern of propagation trajectory of drought events.

2.2.4 Maximum Covariance Analysis

MCA is a singular value decomposition (SVD) analysis that has been widely used for extracting coupled modes of variability between time series of two fields (Bretherton et al., 1992; Mo, 2003). Here we used MCA to quantify teleconnection relationship between SPEI and SST. The SPEI and SST anomalies (SSTA) were smoothed with a 5-years bandwidth Butterworth low-pass filter implemented by the bwfilter function in the mFilter library of the R package to filter out high-frequency signals within 5 years, highlighting the interdecadal trend. Then we quantify the time coefficients obtained by MCA with those of other large-scale climate indices, and evaluate the significance of time coefficients to anatomize the atmospheric circulation background of the spatiotemporal evolution of drought in the Northern Hemisphere. The analysis procedure of this current study is illustrated in **Figure 1**.

3 RESULTS AND DISCUSSION

3.1 Spatiotemporal Evolution of SPEI-Based Drought

3.1.1 Spatiotemporal Evolution of SPEI-Based Dry-Wet Changes

North America (NA) was dominated by wetting conditions while drought-affected regions were observed in southeastern parts of NA from 1961 to 1970 (**Figure 2A**); The drought-affected areas in NA shifted roughly counterclockwise along an east-central-northern-west-south trajectory and drought intensity increased over time from 1971 to 2018 (**Figures 2B–G**); Severe drought occurred in southwestern parts of NA (**Figure 2F**). In Eurasia, the drought-affected areas had evolved from scattered distribution to continuous distribution in patches with amplified droughts (**Figure 2**): From 1961 to 1970, scattered drought-affected areas were found in Russia and the Qinghai-Tibet Plateau (**Figure 2A**); Besides, the drought-affected regions were mainly concentrated in the area between 30°N and 60°N in Eurasia, and distributed along an east-west strip from 1971 to 2018 (**Figures 2B–F**). During 1981–2000, the entire Eurasian continent was dominated by mild drought, and drought-affected regions were located mainly in central Eurasia with expanding drought-affected areas (**Figures 2C,D**). Drought intensity increased over Eurasia, and moderate drought-affected regions were concentrated in Mongolia, northern and western China, and the northern Indian peninsula during a period from 2001 to 2010. Meanwhile, moderate drought started to occur in Central Asia (**Figure 2E**). The period from 2011 to 2018 witnessed intensifying droughts in Eurasia and the drought-affected regions were concentrated between 50°N and 60°N, such as southern Europe, southern Kazakhstan, Mongolia, and Russia (**Figure 2F**). Moreover, Northern Hemisphere was dominated mainly by mild droughts and all drought types continued to increase with time and it was particularly the case during 2010–2018, that is, 23.1% (mild drought: 18.1%, moderate drought: 4.5%, severe drought: 0.5%) (**Supplementary Figure S1A**). In addition, droughts mainly occurred during spring and summer (**Supplementary Figure S1B**) and particularly in June and July (**Supplementary Figure S3M**). In Eurasia, the arid areas were concentrated along the east-west strip between 30°N and 50°N with similar spatiotemporal patterns of droughts during spring and at the yearly scale (**Supplementary Figures S2A,C**).

3.1.2 Spatiotemporal Evolution of Trends in SPEI-Based Dry-Wet Conditions

Here we used MMK and Sen's slope methods to quantify SPEI trends with significance level of 0.05. Sen's slope of SPEI in Northern Hemisphere ranged between -0.499 and 0.677. Scattered regions with significant drying conditions (significant decrease in SPEI) and/or with significant wetting conditions (significant increase in SPEI) were found across Northern Hemisphere (**Figure 3**). The period of 1961–2018 witnessed the propagation of drying conditions across NA along the northwest-southeast diagonal direction (**Figure 3**): the period from 1961 to 1970 was dominated by significant drying trends in northwestern NA (**Figure 3A**); regions with significant drying conditions began to spread to central NA from 1971 to 1990 and concentrated in southwestern parts of NA from 1981 to 1991 (**Figures 3B,C**); regions with significant drying tendency shrunk and propagated from southeastern to northwestern parts of NA during 1991–2018 (**Figures 3D–F**). However, no depictable spatial pattern could be identified for drying and/or wetting tendency over the Eurasian continent (**Figure 3**). We could still identify specific time intervals dominated by significant drying tendency over NA such as periods of 1971–1990 across NA and 1961–1970 and 1991–2010 across Eurasia (**Figure 3**). Furthermore, areas dominated by decreasing and increasing droughts reached the trough values during 2010–2018 (significant drying: 1.3%; significant wetting: 1.4%) (**Supplementary Figures S1B**).

At annual and seasonal scales, regions dominated by SPEI-based significant drying tendency during 1961–2018 were concentrated mostly in mid-latitudes of Eurasia and western parts of NA (**Supplementary Figures S4A,C–F**). Nevertheless, spring and summer were characterized by a significant drying

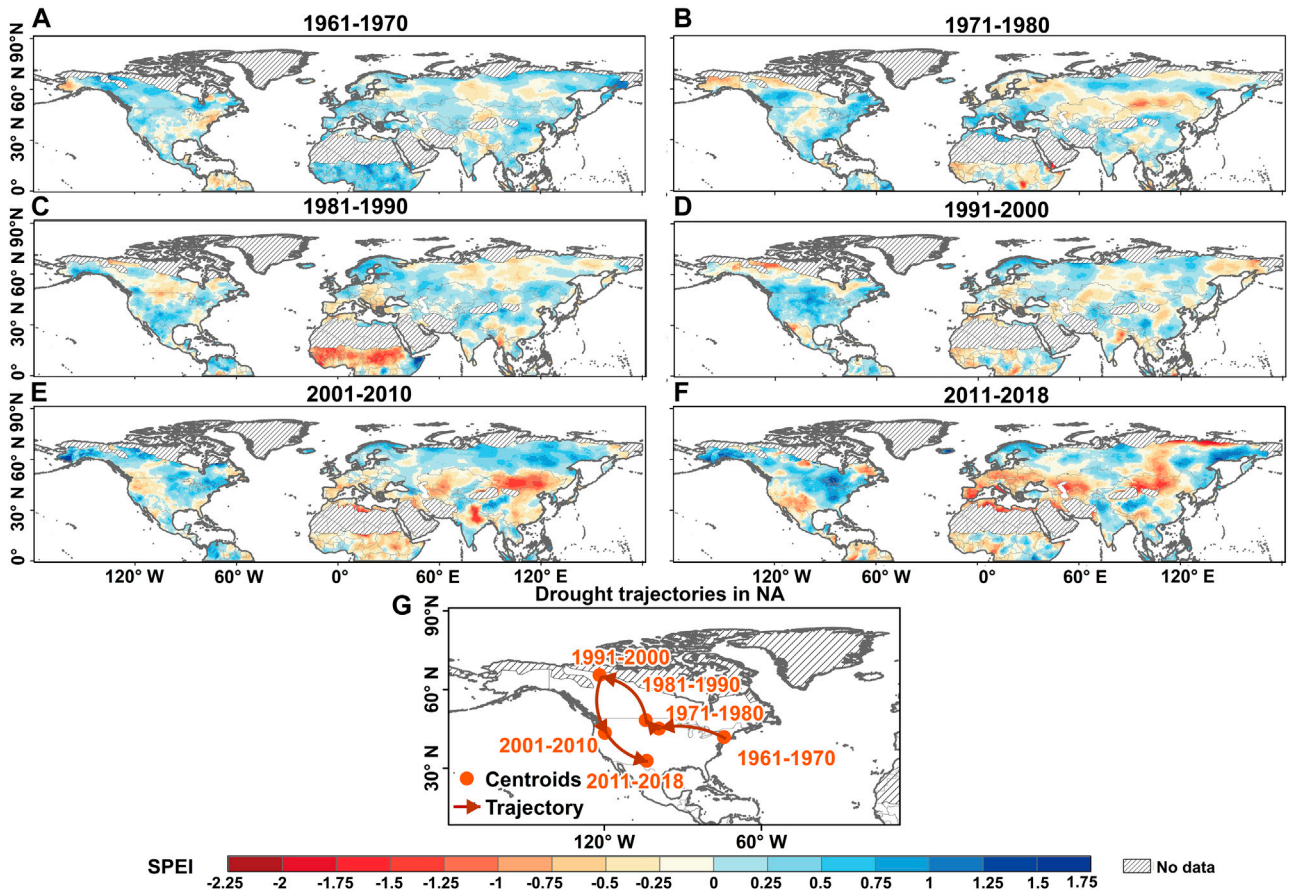

FIGURE 2 | Spatiotemporal evolution of SPEI during the period from 1961 to 2018. **(A)** 1961–1970; **(B)** 1971–1980; **(C)** 1981–1990; **(D)** 1991–2000; **(E)** 2001–2010; **(F)** 2011–2018; **(G)** Drought trajectories in North America (NA). The slashed area was excluded from analysis by mask processing.

tendency and autumn a significant wetting tendency (**Supplementary Figures S4C–E**) and areas dominated by the significant drying tendency accounted for as high as 18.8% in spring and 17.6% in autumn (**Supplementary Figures S4B**).

3.1.3 Regionalization of Wetting/Drying Tendency

The Northern Hemisphere can be subdivided into seven subregions with different wetting/drying tendencies, i.e. R1-R7 (**Figure 4G**; **Table 1**). At seasonal scales, all subregions are subject to a wetting tendency (**Figure 4A**). However, we found no evident changes in drying/wetting conditions (**Figure 4C**). At decadal scales, R2, R6, and R7 were in a drying tendency over time and R4 and R5 in a wetting tendency (**Figures 4B,D**). In probability sense, wetting/drying changes within all subregions followed a normal distribution (**Figures 4E,F**). Therefore, we could find that R7 was the driest region out of seven subregions and would be in a persistently drying tendency, while R5 was the wettest region out of seven subregions and would be in a persistently wetting tendency (**Table 1**).

3.2 Drought Identification

3.2.1 Identification and Features of Droughts

We analyzed drought features, such as drought frequency, drought duration, and drought severity. A spatial pattern of drought events is illustrated in **Figure 5**. The 30 drought events with the largest drought intensity considered in this study are displayed in **Supplementary Table S4**. Drought events with higher frequency, longer duration and stronger severity occurred mainly along the middle and low latitudes, especially in Mongolia, China, Central Asia in central Eurasia, the Circum-Mediterranean regions and the southwestern NA (**Figures 5A–C**), and this phenomenon can be attributed to warming climate and amplifying Arctic warming (e.g., Cohen et al., 2014).

The top 100 long-term droughts occurred mainly in southern NA, Caribbean Rim, North Africa, East Africa, East and South India, Mediterranean region, Mongolia and Russia (**Figure 5D**). Meanwhile, the top 10 long-term droughts occurred mainly during 1992–2018 with drought duration ranging between 33 and 42 months, and most of these droughts occurred in R1 (4 drought events) and R7 (4 drought events) regions (**Supplementary Table S4**, **Figure 5D**), pointing to amplifying droughts along middle and low latitudes of the Northern Hemisphere. For example, the drought event that began in 1998 in the eastern Mediterranean Levant region, which comprises Cyprus, Israel, Jordan, Lebanon, Palestine, Syria, and Turkey, was recognized as the worst drought of the past nine centuries (NASA, 2016). In eastern Africa, we found a severe drought event that was ranked as the second most severe drought

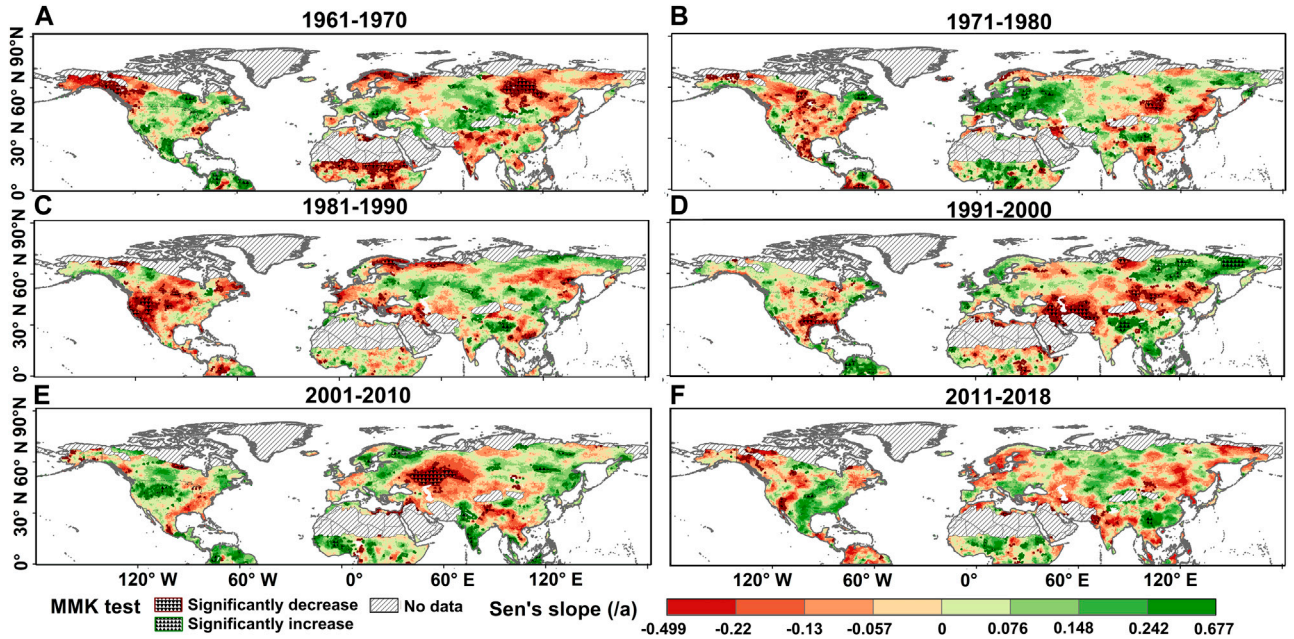

FIGURE 3 | Spatiotemporal evolution of trends in SPEI at interdecadal scales based on MMK trend and Sen's slope method from 1961 to 2018. **(A)** 1961–1970; **(B)** 1971–1980; **(C)** 1981–1990; **(D)** 1991–2000; **(E)** 2001–2010; **(F)** 2011–2018.

(**Supplementary Table S4**), lasting 39 months from June 2008 to September 2011 (**Figure 5D**). In addition, one drought occurred during 2010–2011 in Eastern Africa was one of the most recent extreme drought events that affected over 20 million people and caused widespread crop failure (AghaKouchak, 2015). Another severe drought occurred in South India that can be ranked as the fourth most severe drought (**Supplementary Table S4**), lasting 31 months from September 2015 to May 2018, and the drought reached its peak value in November 2017 (**Figure 5D**) (Mishra et al., 2021).

For further understanding of the statistical relations amongst drought features considered in this study, we performed linear fitting analysis between drought severity and duration (**Supplementary Figure S5**). The color shaded range of the linear fitting started to expand from the drought duration of 20 months and the data points also tended to be more scattered, implying increasing violation of linear relations between drought duration and severity with drought duration of longer than 20 months, and that droughts with duration of >20 months were scarce (**Supplementary Figure S5**). Thus, we took drought duration of 20 months as the threshold value for the identification of a large-scale long-term drought.

3.2.2 Identification of Centroid and Migration Trajectory of Drought

Identification of drought centroid and migration trajectory are important for mitigation to drought hazards. **Figure 6A** shows drought trajectories across NA, Europe (EU), Central Asia and Tibet (CT), North Asia, East and Southeast Asia (NES), and South Asia (SAS). We depicted and analyzed drought trajectories for each region considered in this study (**Figure 6**). We attempted to delineate the evolution of droughts over five subregions. We observed the clear spatial pattern of drought evolution over NA (**Supplementary Table S4**), and analyzed the spatial pattern of drought evolution during a period from March 2013 to March 2016 across NA. We did similar analyses for other four regions considered in the study, i.e. EU, CT, NES, SAS. Drought migration trajectories in NA at 6 months followed a counterclockwise direction (**Figures 6B–G**). Meanwhile, extremely low cumulative SPEI values mainly appeared in the northeastern NA (**Figures 6B–E**). For drought evolution over other four regions (**Supplementary Figures S6, S8, S10, S12**), the propagation of droughts also followed a counterclockwise direction (**Supplementary Figures S6A–C, S8A,B, S10A–C, S12C**). We also found some drought evolution trajectories in clockwise direction (**Supplementary Figures S8D, S12B**). Therefore, we concluded that migration of drought trajectories in the Northern Hemisphere mainly followed a counterclockwise direction.

3.3 Mechanistic Analyses for Drought Evolution

3.3.1 Changes of RH and V/U Behind Drought Evolution

We analyzed RH and V/U to investigate potential causes behind drought evolution in the Northern Hemisphere. RH in the Pacific Ocean near western NA decreased from March to April in 2013 (**Figure 7A**), which could be attributed to a clockwise wind with an increasing velocity within the Pacific Ocean and the cold and dry air mass from high to low latitudes along the western coast of NA. The aforementioned driving factors together with the joint

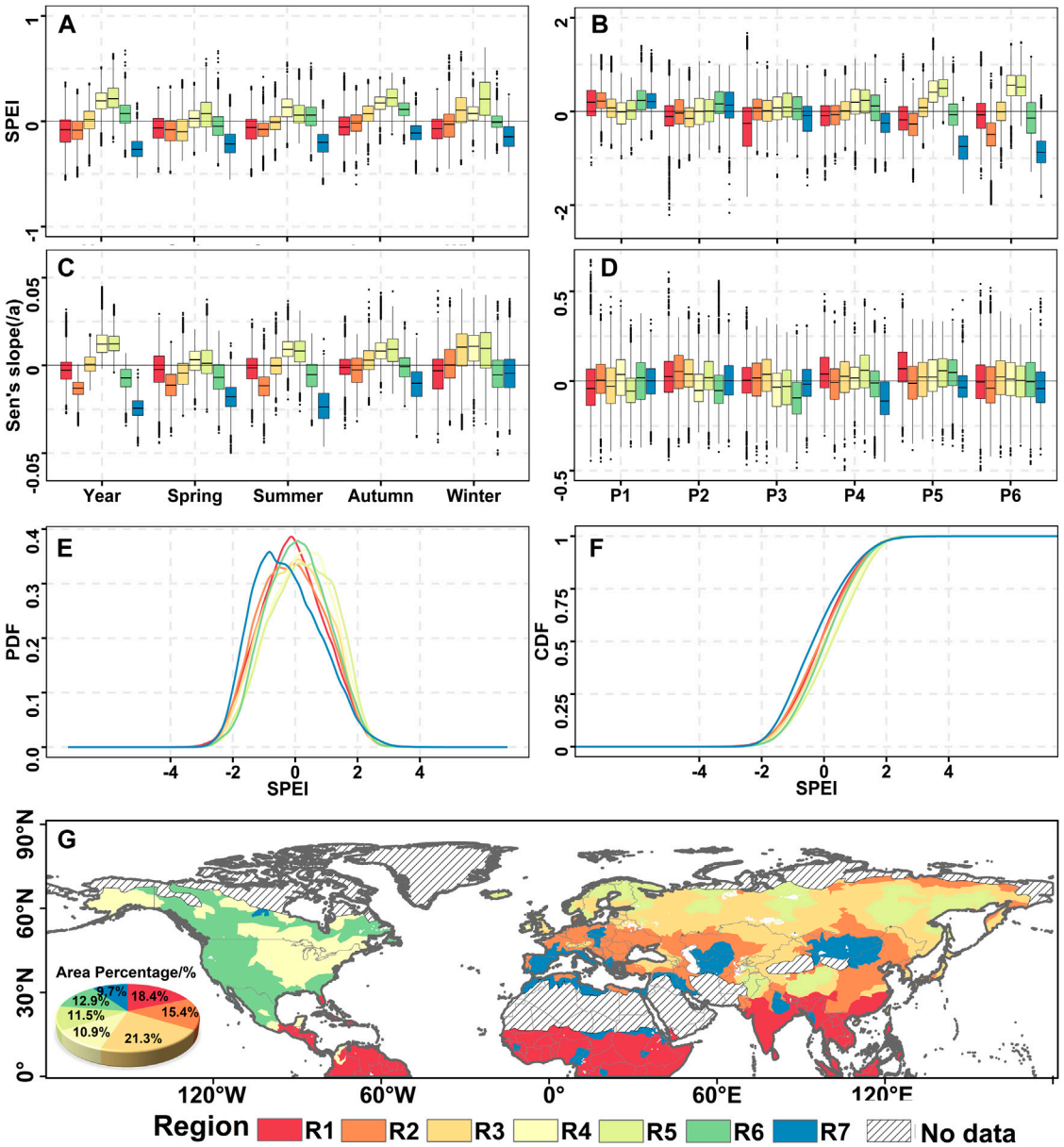

FIGURE 4 | Statistical analysis results for SPEI within subregions by clustering analysis. **(A,C)**: box plots and Sen's slope of SPEI at annual and seasonal scales; **(B,D)**: box plots and Sen's slope of SPEI at decadal scale; **(E)** Probability distributions of SPEI; **(F)** Cumulative probability distributions of SPEI; **(G)** Subregions subdivided by K-means method.

TABLE 1 | Characteristics of dry and wet changes in the cluster regions from 1961 to 2018.

Region	Distribution location	The status of dry and wet	Changing trend
R1	0°N-30°N middle and low latitudes	Normal	Not significantly
R2	0°N-60°N middle latitudes and northern Russia	Normal to mild drought	Wetting to drying
R3	Eurasia between 30°N and 70°N	Normal	Not significantly
R4	NA, a small part in northern South America	Normal to mild wet	Drying to wetting
R5	Eurasia between 50°N and 70°N, a small part in the Qinghai-Tibet Plateau and northern Pakistan around 30°N	Normal to mild wet	Wetting
R6	NA (concentrated in the western region)	Normal	Drying to wetting
R7	Scattered distribution, concentrated in Mongolia, Central Asia and around the Mediterranean	Normal to moderate drought	Wetting

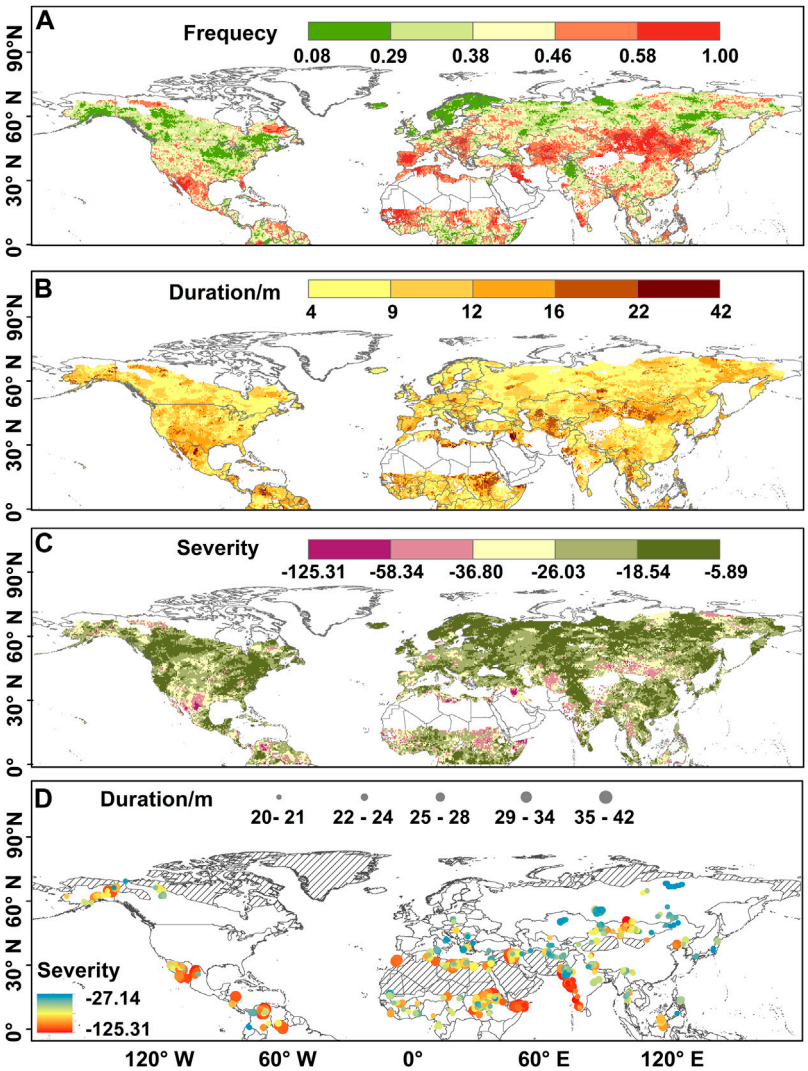

FIGURE 5 | Spatial pattern of top 100 long-term droughts in terms of **(A)** drought frequency is the number of drought occurrences, whose range is 0–1; **(B)** drought duration is consecutive time intervals dominated by drought events, whose unit is month; **(C)** drought severity is cumulative SPEI values; and **(D)** drought centroid is the geometric center of the drought-affected region.

influence of subtropical high pressure, cold current and south wind, the drought centroid in NA began to appear in the southwestern region and moved southward (**Figure 6B**). Southeasterly winds prevailed in central NA from April to May (**Figure 7B**), and warm and humid air masses from March to April affected drought occurrences over eastern NA (**Figure 7A**). The wind direction and warm and humid air masses pushed the dry air masses in the central and southern regions northwards, so the drought centroid began to move northwestward (**Figure 6B**). From May to June, the warm air masses from low latitudes were likely to be forced to be lifted up in the subpolar low-pressure belt in the northern NA, which was prone to rainfall changes (**Figure 7C**). During summer in the Northern Hemisphere, the drought centroid moved northward and then returned to the warmer and drier western NA (**Figure 6B**). Cold current appeared again along the western coast of NA from June to July causing warm and dry conditions (**Figure 7D**) and then the westward propagation of drought centroid (**Figure 6B**). Then cold current began to appear along the eastern coast of NA causing trying tendency within NA (**Figure 7E**), triggering southeastward propagation of the drought centroid (**Figure 6B**); From August to September, the northeasterly wind began in the southern parts of NA (**Figure 7F**), causing northeastward propagation of the drought centroid (**Figure 6B**). From September to October, the wind velocity on the western coast of NA increased, the wind direction brought cold current along the coastline again, causing cold but humid conditions due to the influence of the subpolar low-pressure belt (**Figure 7G**), which in turn caused the westward propagation of the drought centroid (**Figure 6C**). From

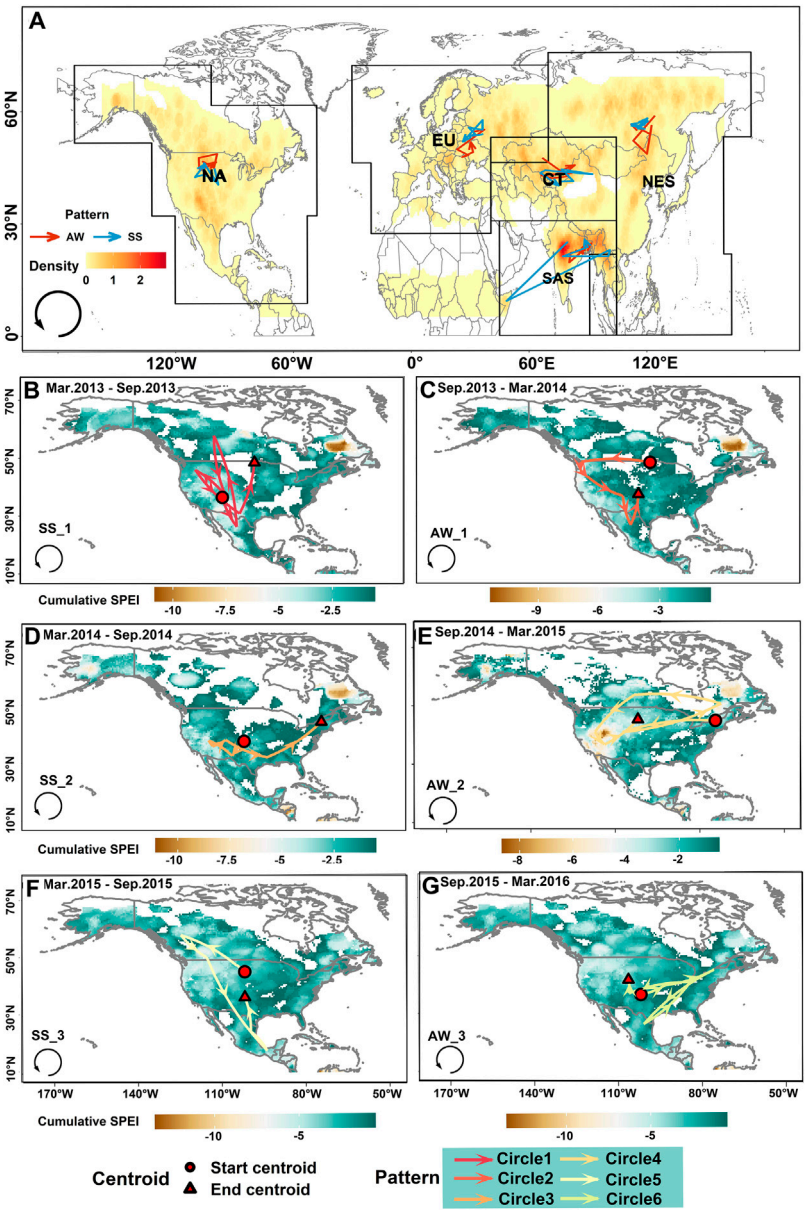

FIGURE 6 | Spatial pattern of droughts in terms of centroids, migration trajectories. **(A)** Drought centroids and migration trajectories in Northern Hemisphere. **(B–G)** Drought centroids and migration trajectories in NA from March 2013 to March 2016. **(B)** March 2013–September 2013. **(C)** September 2013–March 2014. **(D)** March 2014–September 2014. **(E)** September 2014–March 2015. **(F)** March 2015–September 2015. **(G)** September 2015–March 2016. AW: autumn and winter; SS: spring and summer. Density: the point density of drought centroids.

November to January of the next year 2014, southwesterly and northwesterly winds began to prevail in NA (**Figures 7I,J**), causing southeastward propagation of the drought centroid (**Figure 6C**). From January to February in 2014, the strong land breeze in southern NA caused a decrease of water vapor (**Figure 7K**), triggering southward movement of the drought centroid (**Figure 6C**). From February to March, the strong sea breeze from southern North America blew toward the central region (**Figure 7L**) causing the northward shift of droughts (**Figure 6C**). Therefore, drought migration trajectory is heavily reliant on season, the atmospheric pressure belt, wind belt, the circulation, and the sea and land breeze. However, these driving factors have varying impacts on drought propagation.

We also found close relations between drought migration trajectories and the water vapor changes in other regions considered in this study (**Supplementary Figures S6–13**). Most of the drought centroids concentrated in mid-latitudes of the Northern Hemisphere were heavily affected by prevailing westerly winds, subtropical high-pressure belt, and subpolar low-pressure belt, so the migration of drought centroids in large areas followed a counterclockwise pattern. For example, in **Supplementary Figures S8, 9**, severe drought conditions over

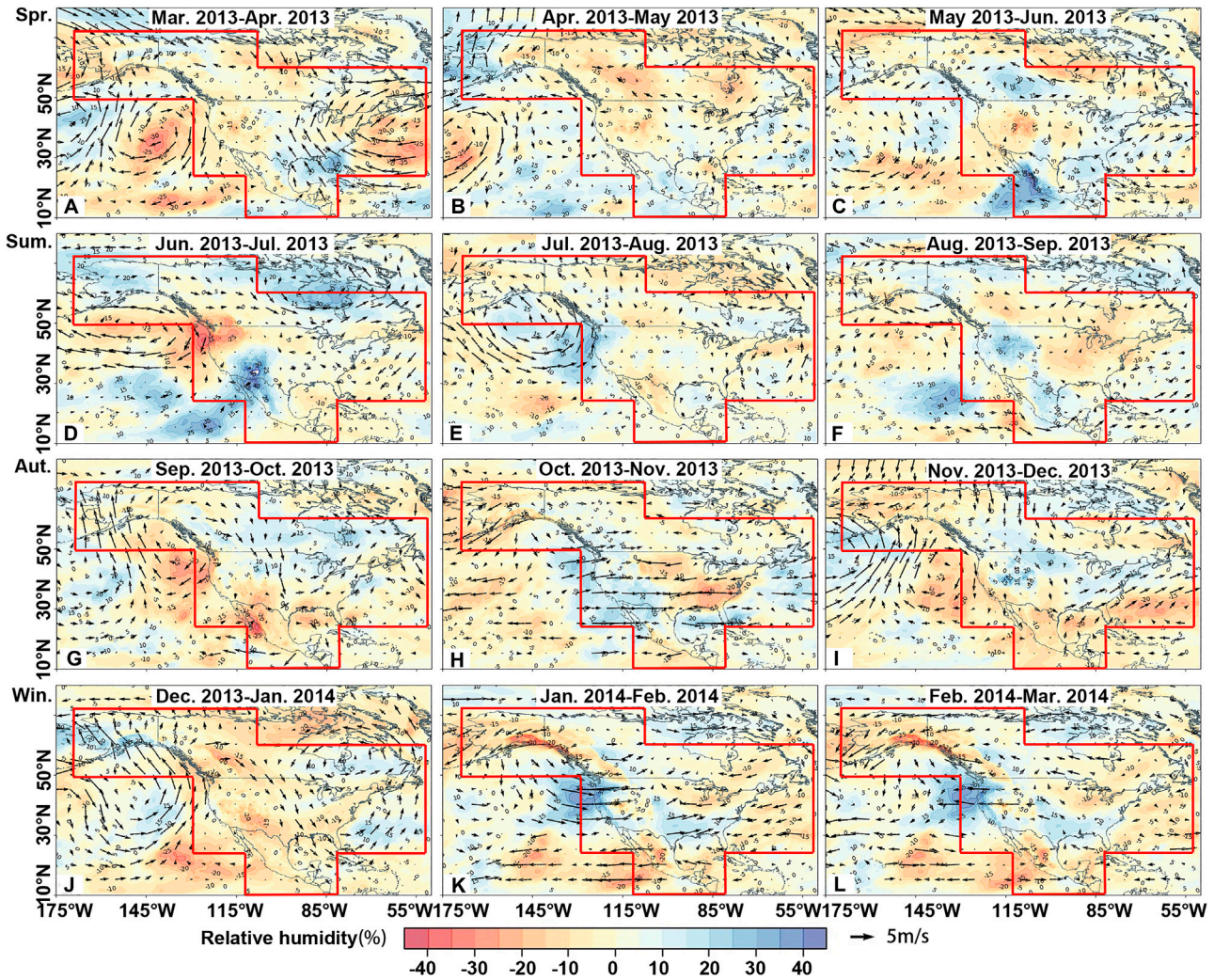

FIGURE 7 | Spatial pattern of water vapor changes in NA from March 2013 to March 2014. **(A)** March 2013–April 2013. **(B)** April 2013–May 2013. **(C)** May 2013–June 2013. **(D)** June 2013–July 2013. **(E)** July 2013–August 2013. **(F)** August 2013–September 2013. **(G)** September 2013–October 2013. **(H)** October 2013–November 2013. **(I)** November 2013–December 2013. **(J)** December 2013–January 2014. **(K)** January 2014–February 2014. **(L)** February 2014–March 2014. The red box refers to the boundary of the study region.

much of southern India from October to December were reliant on seasonal winter rainfall associated with the northeastern monsoon (NEM) (Mishra et al., 2021).

3.3.2 Spatial Coupling Relationship Between SPEI and SST

We attempted to quantify the teleconnection relationship between SPEI and SST through the MCA method. The top four coupled modes of the MCA method explained 17.9, 6.5, 5.7 and 4.8% of the variance, respectively. The correlation coefficients of the time coefficients between SSTA and SPEI in modes one and 4 (M1, 4) were all greater than 0.95 (p<0.001), indicating significant response relationship between SSTA and SPEI (**Figures 8A,J**). However, the correlation coefficients of time coefficients between SSTA and SPEI in modes two and 3 (M2, 3) were 0.074 and 0.15 respectively (p<0.001), indicating that SSTA was not related to SPEI (**Figures 8D,G**).

The SSTA time coefficient in M1 generally showed a significant upward trend, while the SPEI time coefficient showed a slow upward trend, where the SSTA time coefficient had risen sharply since 1975 and the SPEI time coefficient had indeed risen slowly around zero. In M1, the correlation coefficient between SSTA time coefficient and TA was 0.96 (p < 0.001), while that between SPEI time coefficient and TA was 0.89 (p < 0.001), indicating that SPEI was greatly possible to be affected by global warming (**Figure 8A**). SSTA in M1 showed a different intensity of SST warming (**Figure 8B**) but was in line with global warming (**Figure 8A**). Besides, the SPEI values were relatively low between 60°N and 75°N in northern Russia, Mediterranean region and northern Africa (**Figure 8C**), and were high in other regions, especially in most parts of NA, Central Asia, eastern Russia, and

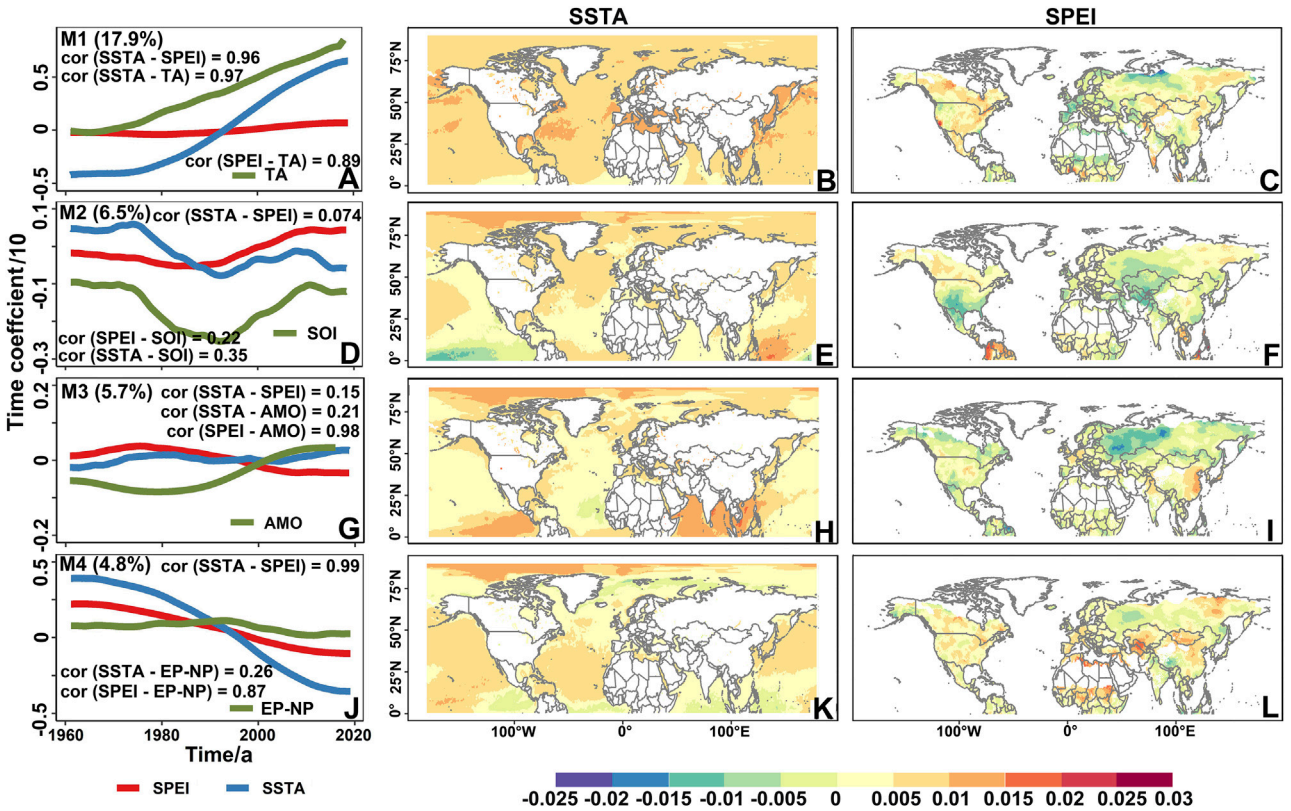

FIGURE 8 | Spatial coupling of SPEI and SSTA based on MCA. Left column **(A,D,G,J)**: SPEI (red), SST anomaly (blue) time coefficient and correlation index series (green) (percentage represents the variance contribution rate of each modal interpretation, and the correlation coefficient between each index is marked in the figure); Middle column **(B,E,H.K)**: spatial distribution of SSTA; Right column **(C,F,I,L)**: spatial distribution of SPEI.

eastern China. These observations evidenced the impact of SST changes on meteorological drought changes.

In M2, the SSTA time coefficients were in downward trend, while the SPEI time coefficients in upward trend. The correlation coefficient between SSTA time coefficient and SOI was 0.35 ($p < 0.001$), while that between SPEI time coefficient and SOI was 0.22 ($p < 0.001$), indicating that the SPEI may be affected by SOI and ENSO events (**Figure 8D**). SSTA in M2 mainly manifested as a cooling phenomenon in the west-central Pacific region, which may be related to the La Niña phenomenon (**Figure 8E**). Correspondingly, the SPEI value of the SPEI field distribution was relatively low in southern NA, Central Asia, and central and western Russia, and the SPEI changes were consistent with the linear trend of SOI (**Figure 8F**). Thus, it could be seen that the meteorological drought during 1961–2018 could be related to ENSO events, especially the La Niña phenomenon. Our findings were consistent with those of other scholars. For example, Stevens and Ruscher (2014) examined the relationship between surface climatological variables and climatic oscillations in the Apalachicola-Vhattahoochee-Flint River basin in southern NA. They showed that the meteorological drought at 24-months time scale in the southern part of the basin was largely influenced by SOI. And Sun et al. (2022) demonstrated impacts of ENSO, and speccifically La Niña-like condition on the East Asian climate anomalies during autumn–winter 2020/2021.

In M3, SSTA and SPEI time coefficients were in steady trends in general with moderate fluctuations. The correlation coefficient between SSTA time coefficient and AMO was 0.21 ($p < 0.001$), while that between SPEI time coefficient and AMO was 0.98 ($p < 0.001$), indicating potential impacts of AMO on SPEI changes (**Figure 8G**). Besides, SSTA in M3 was in decreasing tendency along the east coast of the Atlantic Ocean near Africa, but was in increasing in the Arctic Circle and low latitudes near the equator (**Figure 8H**). In the corresponding SPEI field, the SPEI values of most regions were relatively low, especially in western Russia, while that were relatively high in eastern China and northern Indian peninsula (**Figure 8I**). So, changes in the AMO might affect the spatiotemporal changes in mid- and high-latitude drought-affected regions.

In M4, the SSTA and SPEI time coefficients were in decreasing tendency with correlation coefficient of 0.26 ($p < 0.001$) between SSTA time coefficient and EP-NP, and that of 0.87 ($p < 0.001$) between SPEI time coefficient and EP-NP, indicating that SPEI might be affected by EP-NP (**Figure 8J**). Moreover, SSTA near the equator and high latitudes of the North Hemisphere was in decreasing tendency and was rising in Arctic Circle and mid-

latitudes of the North Hemisphere (**Figure 8K**). The SPEI values in western Russia were relatively low, while the SPEI values over other regions except western Russia were relatively high (**Figure 8L**). Hence, the EP-NP changes potentially affected the spatiotemporal changes of droughts in mid-high North Hemisphere.

In addition to climate indices, many scholars are beginning to find that Arctic sea ice is increasingly affecting drought. Chen et al. (2021) found that the influence of the early spring Arctic sea ice on the subsequent summer drought takes place mainly through the Eurasian snow from spring to summer. which ultimately affects the subsequent drought through soil moisture–precipitation feedback and soil moisture–temperature feedback. Sun et al. (2022) attributed drought in South China during autumn 2020 to water vapor divergence anomalies induced by an anomalous anticyclone over eastern China, which are caused by an anomalous Eurasian atmospheric wave-train triggered by the negative sea ice anomalies in the Barents Sea-Kara Sea region.

4 CONCLUSION

The present study analyzed the evolution of the spatiotemporal pattern of drought in the Northern Hemisphere during the past about 60 years from 1961 to 2018 and its causes from the basic idea of "phenomenon-law-essence". The following conclusions can be drawn from this study:

1) In the context of global warming, terrestrial meteorological drought in the Northern Hemisphere from 1961 to 2018 was amplifying, and often spring and summer were concentrated seasons for its occurrence. For different regions, the drought-affected region in NA shifted counterclockwise, and its significant drying region showed a wandering evolution characteristic in the northwest-southeast diagonal direction. In Eurasia, the drought-affected areas had evolved from scattered distribution to continuous distribution, while, the specific time intervals were dominated by significant drying tendency over NA such as periods of 1971–1990 across NA and 1961–1970 and 1991–2010 across Eurasia. Among the seven subregions, R7 scattered but concentrated in Mongolia, Central Asia, and around the Mediterranean region was the driest region and in persistently drying tendency, while R5 was mainly distributed in Eurasia between 50°N and 70°N, in a small part of the Tibetan Plateau and in northern Pakistan at about 30°N was the wettest region and in persistently drying tendency.
2) Amplifying droughts were characterized by higher frequency, longer duration and stronger severity across middle- and low-latitudes of the Northern Hemisphere, specifically, Mongolia, China and Central Asia expanding along the central Eurasia, Circum-Mediterranean region and southwestern NA. In terms of the characteristics of drought events, the absolute value of drought severity in each region of northern Hemisphere showed a good linear increase relationship with drought duration, where the duration was less than 20 months. Surprisingly, the drought migration trajectories in five regions, i.e., NA, EU, CT, NES, and SAS, followed a counterclockwise direction.
3) The drought evolution had a strong relationship with season, atmospheric pressure belt, wind belt, the atmospheric circulation, and the sea-land breeze. Most of the drought centroids in the Northern Hemisphere were concentrated in mid latitudes, so they were easily affected by the prevailing westerly winds, subtropical high-pressure belt and subpolar low-pressure belt. About the coupling relationship between SPEI and SST, SPEI was mainly affected by global warming, and was related to SOI and AMO; In particular, La Niña phenomenon could dry out southern NA and central and western Russia; AMO might affect the spatiotemporal variation of SPEI in mid-high latitudes.

In short, this study used a variety of methods to analyze the spatiotemporal pattern of meteorological droughts, the identification of drought events, the evolution of characteristics, and the cause mechanisms in the Northern Hemisphere based on the SPEI index. However, the cause of drought can be further analyzed from the perspective of physical mechanisms in combination with a more stable mathematical model.

DATA AVAILABILITY STATEMENT

The original contributions presented in the study are included in the article/**Supplementary Material**, further inquiries can be directed to the corresponding author.

AUTHOR CONTRIBUTIONS

DW and QZ designed the research and wrote the manuscript. DW performed the analysis. VS, ZS, GW, WW, and RY discussed and modified the manuscript. All authors contributed to the interpretation of results.

FUNDING

This research was supported by the China National Key R&D Program (Grant No. 2019YFA0606900) and the National Natural Science Foundation of China (Grant No. 42041006).

ACKNOWLEDGMENTS

Here we also thank the editor, Tomas Halenka, and reviewers for their pertinent and professional comments and suggestions which are greatly helpful for quality improvement of this manuscript.

SUPPLEMENTARY MATERIAL

The Supplementary Material for this article can be found online at: https://www.frontiersin.org/articles/10.3389/feart.2022.914232/full#supplementary-material

REFERENCES

AghaKouchak, A. (2015). A Multivariate Approach for Persistence-Based Drought Prediction: Application to the 2010-2011 East Africa Drought. *J. Hydrol.* 526, 127–135. doi:10.1016/j.jhydrol.2014.09.063

Allen, M. R., and Ingram, W. J. (2002). Constraints on Future Changes in Climate and the Hydrologic Cycle. *Nature* 419, 228–232. doi:10.1038/nature01092

Andreadis, K. M., Clark, E. A., Wood, A. W., Hamlet, A. F., and Lettenmaier, D. P. (2005). Twentieth-century Drought in the Conterminous United States. *J. Hydrometeorol.* 6 (6), 985–1001. doi:10.1175/jhm450.1

Andreas, S., and Hazeleger, W. (2005). The Relative Roles of Tropical and Extratropical Forcing on Atmospheric Variability. *Geophys. Res. Lett.* 32, 18. doi:10.1029/2005GL023757

Bretherton, C. S., Smith, C., and Wallace, J. M. (1992). An Intercomparison of Methods for Finding Coupled Patterns in Climate Data. *J. Clim.* 5 (6), 541–560. doi:10.1175/1520-0442(1992)005<0541:aiomff>2.0.co;2

Chen, D., Gao, Y., Zhang, Y., and Wang, T. (2022). Effects of Spring Arctic Sea Ice on Summer Drought in the Middle and High Latitudes of Asia. *Atmos. Ocean. Sci. Lett.* 15, 100138. doi:10.1016/j.aosl.2021.100138

Cohen, J., Screen, J. A., Furtado, J. C., Barlow, M., Whittleston, D., Coumou, D., et al. (2014). Recent Arctic Amplification and Extreme Mid-latitude Weather. *Nat. Geosci.* 7, 627–637. doi:10.1038/ngeo2234

Corzo Perez, G. A., van Huijgevoort, M. H. J., Voss, F., and van Lanen, H. A. J. (2011). On the Spatio-Temporal Analysis of Hydrological Droughts from Global Hydrological Models. *Hydrol. Earth Syst. Sci.* 15 (9), 2963–2978. doi:10.5194/hess-15-2963-2011

Dai, A. (2011). Drought under Global Warming: a Review. *WIREs Clim. Change* 2 (1), 45–65. doi:10.1002/wcc.81

Dai, A., Trenberth, K. E., and Karl, T. R. (1998). Global Variations in Droughts and Wet Spells: 1900-1995. *Geophys. Res. Lett.* 25 (17), 3367–3370. doi:10.1029/98gl52511

Dore, M. H. I. (2005). Climate Change and Changes in Global Precipitation Patterns: What Do We Know? *Environ. Int.* 31, 1167–1181. doi:10.1016/j.envint.2005.03.004

Easterling, D. R., Meehl, G. A., Parmesan, C., Changnon, S. A., Karl, T. R., and Mearns, L. O. (2000). Climate Extremes: Observations, Modeling, and Impacts. *Science* 289, 2068–2074. doi:10.1126/science.289.5487.2068

Erfanian, A., Wang, G., and Fomenko, L. (2017). Unprecedented Drought over Tropical South America in 2016: Significantly Under-predicted by Tropical SST. *Sci. Rep.* 7, 5811. doi:10.1038/s41598-017-05373-2

Feng, P., Wang, B., Luo, J.-J., Liu, D. L., Waters, C., Ji, F., et al. (2020). Using Large-Scale Climate Drivers to Forecast Meteorological Drought Condition in Growing Season across the Australian Wheatbelt. *Sci. Total Environ.* 724, 138162. doi:10.1016/j.scitotenv.2020.138162

Gore, M., Abiodun, B. J., and Kucharski, F. (2020). Understanding the Influence of ENSO Patterns on Drought over Southern Africa Using SPEEDY. *Clim. Dyn.* 54, 307–327. doi:10.1007/s00382-019-05002-w

Haile, G. G., Tang, Q., Leng, G., Jia, G., Wang, J., Cai, D., Sun, S., Baniya, B., and Zhang, Q. (2020). Long-term spatiotemporal variation of drought patterns over the Greater Horn of Africa, *Sci. Total Environ.* 704, 135299. doi:10.1016/j.scitotenv.2019.135299

Hamed, K. H., and Ramachandra Rao, A. (1998). A Modified Mann-Kendall Trend Test for Autocorrelated Data. *J. Hydrol.* 204, 182–196. doi:10.1016/s0022-1694(97)00125-x

Zhe, H, Luo, F., and Wan, J. (2016). The Observational Influence of the North Atlantic SST Tripole on the Early Spring Atmospheric Circulation. *Geophys. Res. Lett.* 43 (6), 2998–3003. doi:10.1002/2016GL068099

Hayes, M., Svoboda, M., Wall, N., and Widhalm, M. (2011). The Lincoln Declaration on Drought Indices: Universal Meteorological Drought Index Recommended. *Bull. Am. Meteorol. Soc.* 92 (4), 485–488. doi:10.1175/2010bams3103.1

Herrera-Estrada, J. E., Satoh, Y., and Sheffield, J. (2017). Spatiotemporal Dynamics of Global Drought. *Geophys. Res. Lett.* 44, 2254–2263. doi:10.1002/2016gl071768

Ji, F., Wu, Z., Huang, J., and Chassignet, E. P. (2014). Evolution of Land Surface Air Temperature Trend. *Nat. Clim. Change* 4, 462–466. doi:10.1038/nclimate2223

Kerr, R. A. (2000). A North Atlantic Climate Pacemaker for the Centuries. *Science* 288 (5473), 1984–1985. doi:10.1126/science.288.5473.1984

Lau, N.-C. (1997). Interactions between Global SST Anomalies and the Midlatitude Atmospheric Circulation. *Bull. Amer. Meteor. Soc.* 78, 21–33. doi:10.1175/1520-0477(1997)078<0021:ibgsaa>2.0.co;2

Linkin, M., and Nigam, S. (2007). The North Pacific Oscillation–West Pacific Teleconnection Pattern: Mature-Phase Structure and Winter Impacts. *J. Clim.* 21 (9), 1979–1997.

Liu, W., Zhu, S., Huang, Y., Wan, Y., Wu, B., and Liu, L. (2020). Spatiotemporal Variations of Drought and Their Teleconnections with Large-Scale Climate Indices over the Poyang Lake Basin, China. *Sustainability* 12 (9), 3526. doi:10.3390/su12093526

Lloyd-Hughes, B. (2012). A Spatio-Temporal Structure-Based Approach to Drought Characterisation. *Int. J. Climatol.* 32 (3), 406–418. doi:10.1002/joc.2280

McRae, D. J. (1971). MIKCA: a FORTRAN IV Iterative K-Means Cluster Analysis Program. *Behav. Sci.* 16, 423–424. doi:10.1177/003693307101600113

Miller, F. P., Vandome, A. F., and Mcbrewster, J. (2010). *Northern Hemisphere*. Mishawaka, IN, United States: Alphascript Publishing.

Mishra, A. K., and Singh, V. P. (2010). A Review of Drought Concepts. *J. Hydrol.* 391 (1-2), 202–216. doi:10.1016/j.jhydrol.2010.07.012

Mishra, P. T., Chandra, R., Saxena, S. K., Verma, S., and Bhuyan, A. (2010). High Sensitivity C-Reactive Protein (hsCRP) Level in Cerebrovascular Accident (Stroke). *J. Indian Acad. Clin. Med.* 11 (3), 204–207.

Mishra, V., Thirumalai, K., Jain, S., and Aadhar, S. (2021). Unprecedented Drought in South India and Recent Water Scarcity. *Environ. Res. Lett.* 16, 054007. doi:10.1088/1748-9326/abf289

Mo, R. (2003). Efficient Algorithms for Maximum Covariance Analysis of Datasets with Many Variables and Fewer Realizations: a Revisit. *J. Atmos. Ocean. Technol.* 20, 1804–1809. doi:10.1175/1520-0426(2003)020<1804:eafmca>2.0.co;2

NASA (2016). NASA Finds Drought in Eastern Mediterranean Worst of Past 900 Years. Available at: https://www.nasa.gov/feature/goddard/2016/nasa-finds-drought-in-eastern-mediterranean-worst-of-past-900-years.

Nguyen, P., Min, S., and Kim, Y. (2021). Combined Impacts of the El Niño-Southern Oscillation and Pacific Decadal Oscillation on Global Droughts Assessed Using the Standardized Precipitation Evapotranspiration Index. *Int. J. Climatol.* 41 (S1), E1645–E1662. doi:10.1002/joc.6796

Özger, M., Mishra, A. K., and Singh, V. P. (2009). Low Frequency Variability in Drought Events Associated with Climate Indices. *J. Hydrol.* 364, 152–162.

Pieper, P., André, D., and Johanna, B. (2021). Improving Seasonal Predictions of Meteorological Drought by Conditioning on ENSO States. *Environ. Res. Lett. ERL* 16, 9. doi:10.1088/1748-9326/ac1cbb

Ropelewski, C. F., and Jones, P. D. (1987). An Extension of the Tahiti-Darwin Southern Oscillation Index. *Mon. Wea. Rev.* 115, 2161–2165. doi:10.1175/1520-0493(1987)115<2161:aeotts>2.0.co;2

Sen, P. K. (1968). Estimates of the Regression Coefficient Based on Kendall's Tau. *J. Am. Stat. Assoc.* 63, 1379–1389. doi:10.1080/01621459.1968.10480934

Sheffield, J., and Wood, E. F. (2008). Projected Changes in Drought Occurrence under Future Global Warming from Multi-Model, Multi-Scenario, IPCC AR4 Simulations. *Clim. Dyn.* 31 (1), 79–105. doi:10.1007/s00382-007-0340-z

Sheffield, J., Wood, E. F., and Roderick, M. L. (2012). Little Change in Global Drought over the Past 60 Years. *Nature* 491 (7424), 435–438. doi:10.1038/nature11575

Shiau, J.-T., and Lin, J.-W. (2016). Clustering Quantile Regression-Based Drought Trends in Taiwan. *Water Resour. Manage* 30, 1053–1069. doi:10.1007/s11269-015-1210-9

Spinoni, J., Barbosa, P., De Jager, A., McCormick, N., Naumann, G., Vogt, J. V., et al. (2019). A New Global Database of Meteorological Drought Events from 1951 to 2016. *J. Hydrol. Reg. Stud.* 22, 100593. doi:10.1016/j.ejrh.2019.100593

Sternberg, T. (2011). Regional Drought Has a Global Impact. *Nature* 472 (7342), 169. doi:10.1038/472169d

Stevens, K. A., and Ruscher, P. H. (2014). Large Scale Climate Oscillations and Mesoscale Surface Meteorological Variability in the Apalachicola-Chattahoochee-Flint River Basin. *J. Hydrol.* 517, 700–714. doi:10.1016/j.jhydrol.2014.06.002

Sun, B., Wang, H., Li, H., Zhou, B., Duan, M., and Li, H. (2022). A Long-Lasting Precipitation Deficit in South China During Autumn-Winter 2020/2021:

Combined Effect of ENSO and Arctic Sea Ice. *JGR Atmos.* 127, e2021JD035584. doi:10.1029/2021JD035584

Sun, C. H., and Yang, S. (2012). Persistent Severe Drought in Southern China during Winter-Spring 2011: Large-Scale Circulation Patterns and Possible Impacting Factors. *J. Geophys. Res.* 117 (D10), D10112. doi:10.1029/2012jd017500

Svoboda, M., and Fuchs, B. A. (2016). "Handbook of Drought Indicators and Indices," in *Integrated Drought Management Program (IDMP), Integrated Drought Management Tools and Guidelines Series 2* (Geneva: World Meteorological Organization). Available at: https://digitalcommons.unl.edu/droughtfacpub/117/.

The Math Works (2014). *Image Processing ToolboxTM User's Guide, Version R2014*. Massachusetts, United States: The MathWorks.

Turner, K. J., Burls, N. J., von Brandis, A., Lübbecke, J., and Claus, K. (2022). *Seasonality in the Relationship between Equatorial-Mean Heat Content and Interannual Eastern Equatorial Atlantic Sea Surface Temperature Variability*. Clim Dyn. doi:10.1007/s00382-021-06116-w

Vicente-Serrano, S. M., Beguería, S., and López-Moreno, J. I. (2010). A Multiscalar Drought Index Sensitive to Global Warming: The Standardized Precipitation Evapotranspiration Index. *J. Clim.* 23, 1696–1718. doi:10.1175/2009jcli2909.1

Vörösmarty, C. J., Green, P., Salisbury, J., and Lammers, R. B. (2000). Global Water Resources: Vulnerability from Climate Change and Population Growth. *Science* 289 (5477), 284–288. doi:10.1126/science.289.5477.284

Wang, H., and Kumar, A. (2015). Assessing the Impact of ENSO on Drought in the U.S. Southwest with NCEP Climate Model Simulations. *J. Hydrol.* 526, 30–41. doi:10.1016/j.jhydrol.2014.12.012

Wang, M., Gu, Q., Jia, X., and Ge, J. (2019). An Assessment of the Impact of Pacific Decadal Oscillation on Autumn Droughts in North China Based on the Palmer Drought Severity Index. *Int. J. Climatol.* 39 (14), 5338–5350. doi:10.1002/joc.6158

Wang, S., Li, W., Zhou, Y., Yan, F., Wang, F., and Liu, W. (2015). Space-time Evolution of Historical Drought Hazards in Eastern China. *Nat. Hazards* 77, 2027–2047. doi:10.1007/s11069-015-1685-y

Wilhite, D. A. (2000). *Drought as a Natural Hazard: Concepts and Definitions*. Lincoln, United States: University of Nebraska - Lincoln.

Wu, R., and Kinter, J. L. (2009). Analysis of the Relationship of U.S. Droughts with SST and Soil Moisture: Distinguishing the Time Scale of Droughts. *J. Clim.* 22, 4520–4538. doi:10.1175/2009jcli2841.1

Xu, K., Yang, D., Yang, H., Li, Z., Qin, Y., and Shen, Y. (2015). Spatio-temporal Variation of Drought in China during 1961-2012: A Climatic Perspective. *J. Hydrol.* 526, 253–264. doi:10.1016/j.jhydrol.2014.09.047

Yevjevich, V. (1967). *An Objective Approach to Definitions and Investigations of Continental Hydrologic Droughts*. Fort Collins, United States: Colorado State University. Available at: http://hdl.handle.net/10217/61303.

Yu, H., Zhang, Q., Xu, C.-Y., Du, J., Sun, P., and Hu, P. (2019). Modified Palmer Drought Severity Index: Model Improvement and Application. *Environ. Int.* 130, 104951. doi:10.1016/j.envint.2019.104951

Zhang, C. (2005). Madden–Julian Oscillation. *Rev. Geophys.* 43, RG 2003. doi:10.1029/2004rg000158

Zhang, Q., Li, J., Singh, V. P., and Xiao, M. (2013). Spatio-temporal Relations between Temperature and Precipitation Regimes: Implications for Temperature-Induced Changes in the Hydrological Cycle. *Glob. Planet. Change* 111, 57–76. doi:10.1016/j.gloplacha.2013.08.012

Zhang, Q., Shi, R., Singh, V. P., Xu, C., Yu, H., Fan, K., et al. (2021). Droughts across China: Drought Factors, Prediction and Impacts. *Sci. Total Environ.* 803, 150018. doi:10.1016/j.scitotenv.2021.150018

Zhang, Q., Sun, P., Li, J., Singh, V. P., and Liu, J. (2015). Spatiotemporal Properties of Droughts and Related Impacts on Agriculture in Xinjiang, China. *Int. J. Climatol.* 35 (7), 1254–1266. doi:10.1002/joc.4052

Zheng, Y., Zhang, Q., Luo, M., Sun, P., and Singh, V. P. (2020). Wintertime Precipitation in Eastern China and Relation to the Madden-Julian Oscillation: Spatiotemporal Properties, Impacts and Causes. *J. Hydrol.* 582, 124477. doi:10.1016/j.jhydrol.2019.124477

Zhou, H., Liu, Y., and Liu, Y. (2019). An Approach to Tracking Meteorological Drought Migration. *Water Resour. Res.* 55, 3266–3284. doi:10.1029/2018wr023311

Conflict of Interest: The authors declare that the research was conducted in the absence of any commercial or financial relationships that could be construed as a potential conflict of interest.

Publisher's Note: All claims expressed in this article are solely those of the authors and do not necessarily represent those of their affiliated organizations, or those of the publisher, the editors and the reviewers. Any product that may be evaluated in this article, or claim that may be made by its manufacturer, is not guaranteed or endorsed by the publisher.

frontiers | Frontiers in Earth Science

ORIGINAL RESEARCH
published: 08 July 2022
doi: 10.3389/feart.2022.922013

Identification of Degradation Areas of Ecological Environment and Degradation Intensity Assessment in the Yellow River Basin

Tiantian Li[1,2†], *Qiang Zhang*[1,2*†], *Vijay P. Singh*[3], *Jiaqi Zhao*[1,2], *Jinbo Song*[1,2], *Shuai Sun*[1,2,4], *Gang Wang*[1,2], *Zexi Shen*[1,2] *and Wenhuan Wu*[1,2,5]

[1]State Key Laboratory of Earth Surface Processes and Resource Ecology, Beijing Normal University, Beijing, China, [2]Faculty of Geographical Science, Beijing Normal University, Beijing, China, [3]Department of Biological and Agricultural Engineering and Zachry Department of Civil and Environmental Engineering, Texas A&M University, College Station, TX, United States, [4]National Meteorological Information Center, China Meteorological Administration, Beijing, China, [5]National Key Laboratory of Remote Sensing Information and Imagery Analyzing Technology, Beijing Research Institute of Uranium Geology, Beijing, China

OPEN ACCESS

Edited by:
Xingcai Liu,
Institute of Geographic Sciences and Natural Resources Research (CAS), China

Reviewed by:
Kun Shi,
Nanjing Institute of Geography and Limnology (CAS), China
Ying Zhu,
Xi'an University of Architecture and Technology, China

***Correspondence:**
Qiang Zhang
zhangq68@bnu.edu.cn

[†]*These authors have contributed equally to this work*

Specialty section:
This article was submitted to Interdisciplinary Climate Studies, a section of the journal Frontiers in Earth Science

Received: *17 April 2022*
Accepted: *20 June 2022*
Published: *08 July 2022*

Citation:
Li T, Zhang Q, Singh VP, Zhao J, Song J, Sun S, Wang G, Shen Z and Wu W (2022) Identification of Degradation Areas of Ecological Environment and Degradation Intensity Assessment in the Yellow River Basin. Front. Earth Sci. 10:922013. doi: 10.3389/feart.2022.922013

Ecological conservation and high-quality development of the YRB (Yellow River Basin) has been adopted as a national strategy. However, the ecological environment of the YRB is fragile and it has degraded in recent years. Here we proposed an ecological degradation index system based on the Pressure-State-Response (PSR) model and evaluated trends in ecological degradation of the YRB using the Mann-Kendall trend test. We found an upward-downward-upward trend in the ecological degradation index (EDI) during the period of 2000–2019. We also observed an intensifying degradation of eco-environment from the upper to the lower YRB. Meanwhile, 69.9% of the YRB is under degraded eco-environment, while 29.5% of the YRB is dominated by improved eco-environment. Specifically, the ecological degradation intensity of Henan and Shandong Province with dense population and rapid economic development is the highest. Due to active and effective improvement measures taken by the government, the degradation intensity has been having a decreasing tendency. However, higher degradation intensity of eco-environment of the YRB should arouse human concerns. As to the driving factors, human activities can be regarded as the major driving factors for degraded eco-environment, and water stress and economic development exert increasing impacts on the eco-environment of the YRB. Our finding can provide a decision-making basis for the ecological management and high-quality development of the YRB.

Keywords: intensity of ecological degradation, landscape ecological risk index, PSR model, land use change, the yellow river basin

INTRODUCTION

The Yellow River is the second largest river in China and is an important ecological safety barrier. It plays a crucial role in Chinese economic development and food security. It directly supports 12% of the national population, feeds 15% of the irrigation area, and contributes to 9% of China's GDP (Miao et al., 2010; Chen et al., 2012). At the same time, there are rich mineral resources, where coal and petroleum mining volume account for 50% and 25% of the total production in China (Wen et al., 2008). The Central Chinese government issued the "Ecological Protection and High-Quality

Development Plan for the Yellow River Basin" on 8 October 2021. Therefore, the ecological protection and high-quality development of the YRB have become major national strategies and it is the great revival and sustainable development target of China.

In recent years, rapid population growth, booming urbanization and industrialization, and warming climate combine to afflict the ecosystem of the YRB (Li et al., 2017; Zhang et al., 2017). The continuous degradation of watershed ecological environment may eventually inflict damaging effects on the ecosystem structure, loss of ecosystem service functions (Heinrichs et al., 2016). Ecological fragility is a challenging issue for the YRB with low vegetation coverage, severe wind and sand, serious soil erosion (Huang et al., 2012), excessive development of agriculture (Liu et al., 2019), as well as the long-term overuse of land resources by increased urbanization and population boom (Zhang et al., 2022), which have resulted in expanding ecologically vulnerable areas in the YRB. The ecological degradation and ecological sustainable development have aroused widespread human concerns. Therefore, for the ecological protection and sustainable development of the YRB, it is of great significance to comprehensively understand the evolution of landscape or ecosystem and identify the ecologically-degraded areas and relevant driving factors.

Nowadays, ecological environment issues have aroused widespread concerns. A large body of studies addressed the factors affecting ecological environment, including human activities (Song et al., 2014), soil erosion (Zhao et al., 2013), biological integrity (Niu et al., 2021), etc. Song et al. (2014) believed that human activities usually exert remarkable impacts on fluvial ecosystems. Previous studies have shown that human activities have changed one-third to half of the Earth terrestrial surface. If the impact of human activities is ignored, the structure and function of ecosystem cannot be properly grasped (Vitousek et al., 2008). Zhao et al. (2013) investigated the evolution of the ecological environment by analyzing changes in soil erosion in the YRB. Patil et al. (2018) analyzed flow and sediment deposition to anatomize mechanisms behind changes of the fluvial ecosystem and ecological degradation. Niu et al. (2021) quantitatively evaluated the ecological health at the headwater region of the YRB by analyzing the biological integrity of bacterial communities, and found that grazing pressure was the leading factor in ecological degradation. In addition, the rising demand of energy leads to an increase in hydropower production, which will also cause more pressure on the fluvial ecosystem (Gorla & Perona, 2013). Wohlfart et al. (2016) argued that the adverse consequences of unreasonable continuous development of watershed resources not only offset the benefits of economic development, but also threatened social stability. Due to the complexity of ecosystem structure and driving factors of ecological degradation of the YRB, a multitude of studies attempted to address the ecological degradation at different spatial scales. Zhang et al. (2018) found that the ecological risk was lower in the upper YRB and was higher in the lower YRB by analyzing the hydrological changes over the YRB. Moreover, researchers used various methods to analyze ecosystem quality and ecosystem evolution. Pettorelli et al. (2005) reasoned that using NDVI (Normalized Difference Vegetation Index) to monitor vegetation distribution and dynamic changes can better reflect the impact of environmental changes on ecological degradation and fragmentation. Das et al. (2020) and Wang et al. (2021) used the Pressure-State-Response (PSR) model to assess the quality of ecosystems. Zhang et al. (2017) proposed a Pressure-Support-State-Response (PSSR) model and used a single-factor evaluation method to reflect the dynamic changes in the vulnerability of the YRB Delta wetland ecosystem. However, most studies are based on single influencing factors to explore the driving factors behind the ecosystem degradation, but these studies usually did not compare degradation evolution characteristics in respect of spatial distribution under the same standard. Therefore, here we integrated the impacts of climate change, underlying surface changes, human activities, economic development and government response measures on the ecological degradation. We analyzed the temporal and spatial characteristics and identified the influencing factors of ecological degradation in the YRB.

The YRB (95°53′-119°05′E, 32°10′-41°50′N) (**Figure 1**) is sourced from the Bayan Har Mountains of the Qinghai-Tibet Plateau and flows into the Bohai Sea. It is of 795,000 km^2 in drainage area with a river length of 5,464 km (YRCC, 2020). The terrain is high in the west and low in the east and runs through arid and semi-humid climate regions. The precipitation decreases from southeast to northwest and monthly precipitation is extremely spatially uneven. In addition, the flood and drought disasters occur frequently. In the past 20 years, the temperature of the YRB has increased under 1°C. The area accounts for 8.3% of the country's land area, and the per capita water consumption of the YRB is 23% of the national per capita water consumption (YRCC, 2020).

Therefore, we integrated aforementioned factors and developed a comprehensive indicator system of ecological degradation based on the PSR model. We formulated the following objectives: 1) to develop a comprehensive ecological degradation indicator system in the YRB; 2) to incorporate the landscape ecological risk index into the assessment of ecological degradation intensity, divide ecological units with the same scale, and consider the impact of the landscape scale on ecological degradation; 3) to identify key driving factors affecting the ecological degradation of the YRB; and 4) to analyze the ecological degradation trend of the YRB during 2000–2019 and identify the degradation area within the YRB.

DATA AND METHODS

Data

The precipitation data was sourced from the China Meteorological Administration Land Data Assimilation System (CLDAS) and is a grid data at daily scale with spatial resolution of 0.0625°×0.0625° during January 2000 to December 2019. The dataset was sourced from http://data.cma.cn/. We used the precipitation data to calculate the annual rainstorm days, annual heavy rain days, annual dry days, and precipitation intensity in the YRB.

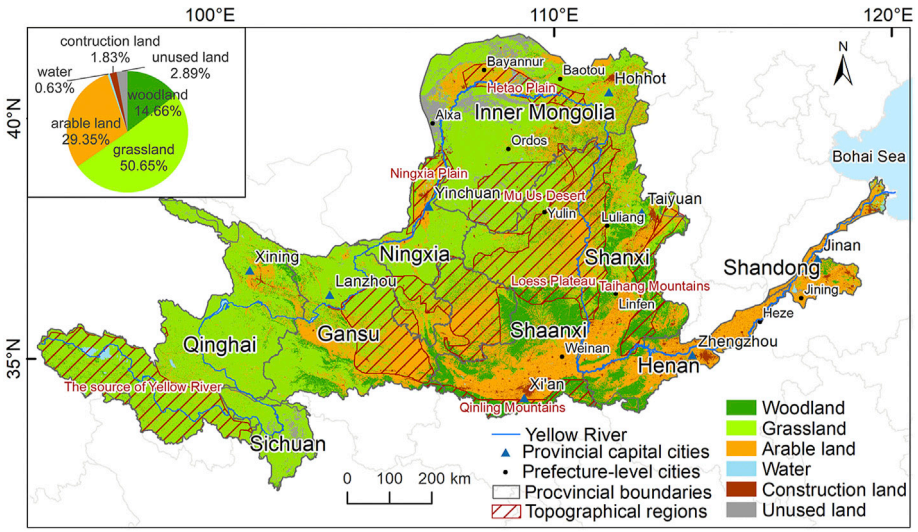

FIGURE 1 | Spatial distribution map of land use in the Yellow River Basin in 2019.

The land use data was issued by ESA (European Space Agency) with spatial resolution of 300 m×300 m from 2000 to 2019 which was sourced from http://maps.elie.ucl.ac.be/CCI/viewer/. In this study, land use types were classified into six categories: woodland, grassland, arable land, water, construction land, and unused land, which were used to calculate the proportion of different land use types.

The population density, urbanization rate, GDP per capita, number of reservoirs, total reservoir capacity, area of soil erosion control and proportion of environmental protection expenditure were obtained from the 2000–2019 statistical yearbooks of provinces within the YRB.

Ecological Degradation Index System

The Pressure-State-Response model (PSR) was proposed by the Organization for Economic Cooperation and Development (OECD) and the United Nations Environment Programme (UN-EP) which has been widely used for environmental quality evaluation (Xu et al., 2017; Clab et al., 2018). In this study, the PSR model (Wang et al., 2018; Qiu et al., 2022) was applied to establish the indicator system of ecological degradation in the YRB. It can strengthen the correlation between the indicators (Wolfslehner & Vacik, 2008), so that the index system has a strong theoretical basis.

Pressure increases the vulnerability of ecological environment. The pressure layer included seven indicators: the annual rainstorm, annual heavy rain days, annual dry days, precipitation intensity, urbanization rate, population density, and per capita GDP. Due to the large latitude and longitude span of the YRB, precipitation has spatial and temporal heterogeneity. In order to reflect the impact of climatic variations on the ecological environment of the YRB, we chose the annual dry days and precipitation intensity to reflect the dry and wet conditions and rainfall intensity in different areas of the YRB. The climate in the upper YRB is dry, the middle YRB is affected by rainfall and the terrain of the Loess Plateau, and the soil erosion is serious. The lower YRB is prone to floods due to the low terrain. So the annual rainstorm and the annual heavy rain days are selected to reflect the impact of different intensities of rainfall on the ecological environment. Among them, the rainstorm refers to the consecutive 24-h rainfall of more than 50 mm, heavy rain refers to the consecutive 24-h rainfall of more than 20 mm, and drought refers to the consecutive 24-h rainfall of less than 1 mm (i.e., no rain). The precipitation intensity is the ratio of total daily precipitation to 24 h. The population density of the YRB is 143 persons per km^2, which is higher than the national average of 134 persons per km^2 (YRCC, 2020). Considering the widespread impact of population growth (Sun et al., 2018), We chose the population density index to reflect the population pressure carried by the ecological environment of the YRB. After 2000, the average annual growth rate of GDP in the YRB was as high as 14.1%, which was also higher than the national average (YRCC, 2020). The rapid economic development, accompanied by the continuous expansion of cities, has brought about tremendous changes in the landscape and ecosystem structure of the YRB. Therefore, the per capita GDP indicator and the urbanization rate indicator are also included in the pressure indicator.

State represented the structure of the ecological environment. The land use is both the cause and the result of environmental change (Turner et al., 2007), and it is an important source of information for understanding the interaction between human activities and the ecological environment (El-Hamid et al., 2020). The landscape pattern based on land use determines the distribution form of the environment and it has a significant impact on the stability of the ecological environment (Paukert et al., 2011; Liu et al., 2012). Landscape ecological risk is the adverse consequence of the interaction between landscape patterns and ecological processes under the influence of natural or human factors

TABLE 1 | Selection of indicators for ecological degradation assessment in the Yellow River Basin.

Target	Layers	Secondary indicator	Tendency
Ecological degradation Index (EDI)	Pressure	Number of rainstorm days	positive
		Number of heavy rainy days	positive
		Number of dry days	positive
		Precipitation intensity (%)	positive
		Urbanization rate (%)	positive
		Population density (person/km^2)	positive
		GDP per capita (×10^{6}RMB)	positive
	State	Landscape ecological risk index	positive
		Proportion of woodland area	negative
		Proportion of grassland area	negative
		Proportion of arable land	positive
		Proportion of water body area	negative
		Proportion of construction land area	positive
		Proportion of unused land area	negative
	Response	Number of reservoirs	negative
		Total reservoir capacity (×10^{8}m^3)	negative
		Area of Soil erosion control (ha)	negative
		Proportion of environmental protection expenditure (%)	negative

(Xu et al., 2021). Landscape ecological risk index is often used to assess and predict the impact of human activities and natural disasters on the structure and function of regional landscapes (Peng et al., 2015). Therefore, we selected the landscape ecological risk index and the proportion of woodland, grassland, cultivated land, water, construction land, and unused land to represent the actual ecological environment state of the YRB.

Response refers to the environmental protection and some improvement measures taken by the government to solve the problem of ecological degradation (Sun et al., 2016). The construction of reservoirs not only brings huge social and economic benefits to the YRB in terms of water storage, power generation, flood control and irrigation, but also can change the fluvial morphology and the spatial-temporal distribution of water resources. This directly or indirectly affects the ecological environment (Qiu et al., 2019). Reservoir dispatch management has important practical significance for further improving the ecological health of the YRB (Bai et al., 2020). In this paper, we chose the number of reservoirs and the total capacity of reservoirs to represent the government's response to the protection of ecological environment quality in the YRB. Since soil erosion is the most important ecological problem in the YRB, we chose the area of soil erosion control to represent the positive feedback from the government. In addition, we use the proportion of environmental protection expenditure to directly reflect the government's investment in ecological protection of YRB. The above four indicators construct the response layer index. The ecological degradation index system of the YRB based on the PSR model included three layers and 18 secondary indicators (**Table 1**).

According to the impact of indicators on ecological degradation, it can be divided into positive indicators and negative indicators. The higher the positive index value, the greater the impact on ecological degradation, and vice versa. Because the pressure indicators accelerate the degradation of ecological environment in the YRB, they are all positive indicators. In the state layer, since woodland, grassland, and water bodies contribute to the conservation of soil and water in the ecological environment, they are negative indicators. Unused land does not change the structure of the ecosystem, and its state is relatively stable, so the area of unused land is also a negative indicator. However, cultivated land and construction land have a high degree of land reclamation, which seriously damages the original structure of the ecosystem and promotes ecological degradation. Therefore, cultivated land and construction land are positive indicators. Similarly, landscape ecological risk describes the fragmentation of landscape structure, which is also a positive indicator. Here we attached remarkable importance to the role of reservoir in the ecological environment. On the one hand, the reservoir can divert water and have positive effects on flood control and drought mitigation. On the other hand, the water quality of the water storage area deteriorates and submerges the surrounding land, which has a negative effect on the ecological environment. However, in our study area, the reservoir is mainly for irrigation, regulation of water and sediment, generation of electricity and flood control (Zhang et al., 2021), the positive effects outweigh the negative effects. Therefore, we defined the number of reservoirs and the total reservoir capacity as negative indicators. Then, the secondary indicators were dimensionless processed by extreme standardization method. The indices with positive ecological impacts were standardized using **Eq. 1**, the indices with negative ecological impacts were standardized using **Eq. 2**:

$$X'_{ij} = \frac{X_{ij} - \min(X_{ij})}{\max(X_{ij}) - \min(X_{ij})} \quad (1)$$

$$X'_{ij} = \frac{\max(X_{ij}) - X_{ij}}{\max(X_{ij}) - \min(X_{ij})} \quad (2)$$

TABLE 2 | Cumulative variance contribution rate (%) of principal components obtained by principal component analysis from 2000 to 2019.

Years	Cumulative variance contribution rate (%)	years	Cumulative variance contribution rate (%)	Years	Cumulative variance contribution rate (%)
2000	88.169	2007	85.681	2014	85.224
2001	87.616	2008	85.976	2015	85.227
2002	87.722	2009	85.241	2016	84.381
2003	87.031	2010	88.110	2017	84.132
2004	87.776	2011	84.594	2018	84.765
2005	87.120	2012	84.340	2019	88.284
2006	85.494	2013	84.875		

where X_{ij} refers to the raw data; $\max(X_{ij})$ refers to the maximum value in the *i*th indicator; $\min(X_{ij})$ refers to the minimum value in the *i*th indicator; and X'_{ij} refers to the non-dimensionalized data.

Determination of Indicator Weights and Calculation of the EDI

In this paper, the weight of each index was obtained, based on the principal component analysis (PCA) method, which can eliminate the influence of commonality between variables, and automatically and objectively assign the weight according to the contribution of each factor to the principal component (Hu and Xu, 2018). The subjectivity of human decision can be greatly reduced. If the cumulative variance contribution rate of the principal component factors is greater than 70%, it means that the principal component has a good explanatory ability to the total difference with convincing reliability of the data. The cumulative variance contribution rate calculation equation is as follows:

$$A_k = \frac{\sum_{k=1}^{i}\lambda_k}{\sum_{k=1}^{p}\lambda_k}\ (k = 1, 2\cdots p) \tag{3}$$

Where A_k is the cumulative variance contribution rate of the principal component, λ_k is the eigenvalue of the index correlation coefficient matrix, and $k = 1, 2\cdots p$ is the corresponding *i*th principal component.

In this paper, the cumulative contribution rate of the principal components calculated by SPSS software (https://www.ibm.com/analytics/spss-statistics-software) is above 84% (As shown in **Table 2**), implying the reliability of analysis of this current study. Therefore, we used SPSS software to calculate the weights of indicators. The method of calculating the index weight using the principal component analysis method is as follows:

a. Calculate the coefficient of the corresponding indicator in each principal component. The specific calculation equation is as follows:

$$\sigma_k = \frac{\beta_k}{\sqrt{\alpha_k}} \tag{4}$$

Where σ_k is the coefficient of the index corresponding to the *k*th principal component obtained from SPSS software, α_k is the eigenvalue corresponding to the principal component index, and β_k is the eigenvector corresponding to the principal component index.

b. Use the cumulative variance contribution rate of the principal components to determine the comprehensive score coefficient. The specific calculation equation is as follows:

$$\gamma_i = \frac{\sum_{k=1}^{p} A_k\sigma_k}{\sum_{k=1}^{p} k} \tag{5}$$

Where γ_i is the comprehensive coefficient of each index, A_k is the cumulative contribution rate of the principal component index, and σ_k is the coefficient of each principal component index.

c. Calculate indicator weights. The specific calculation equation is as follows:

$$W_i = \frac{\gamma_i}{\sum_{i=1}^{n}\gamma_i} \tag{6}$$

Where W_i is the weight of the *i*th index, and W_i is the comprehensive coefficient of each index.

Then, the normalized value of each indicator was multiplied by the corresponding weight to calculate the final Ecological Degradation Index (EDI). The specific calculation equation is as follows:

$$EDI = \sum_{i=1}^{n} X'_{ij} \times W_i \tag{7}$$

Where *EDI* is the intensity of ecological degradation in the YRB, X'_{ij} is the standardized value of the *ith* indicator, and W_i is the weight of the *ith* indicator.

The greater the value of EDI, the higher the degree of ecological degradation, indicating the worse quality of the ecological environment. The EDI is divided into five grades to compare the ecological degradation intensity in different parts of the YRB.

Landscape Ecological Risk Index

The landscape ecological risk assessment focuses on spatiotemporal heterogeneity and its scale effect, and risk zoning is an important step to improve the accuracy of ecological risk indicators and the spatial visualization of ecological risk (Fan et al., 2016). Landscape metrics vary with scale (or size) (Gal et al., 2007). In this paper, we considered the

resolution of CLDAS data (0.0625°×0.0625°) and the size of the study area, and it was found that 0.125°×0.125° could better reflect the spatial differences of the ecological degradation areas in the YRB and facilitate the unified calculation of indicators. Therefore, we performed equidistant sampling based on ArcGIS, and divided the study area into 5,671 units with a scale of 0.125° × 0.125°. In data processing, grids were used as small research units for spatial sampling, and the landscape ecological risk index value for each ecological unit was calculated from the landscape pattern index. The Fragstats software (https://fragstats.software.informer.com/) was used to calculate the landscape pattern: Edge Density (ED), Area-weighted Mean Shape Index (SHAPE_AM), Patch Cohesion Index (COHESION), Aggregation Index (AI), Interspersion Juxtaposition Index (IJI) Largest Patch Index (LPI). They can reflect ecological changes between different regions.

The landscape fragmentation index (Fi), landscape disturbance index (Di), and landscape dominant index (Doi) were constructed, based on the landscape pattern indices selected above. The landscape vulnerability index (Vi) was superimposed to calculate the final Landscape Ecological Risk Index (ERI) (Peng et al., 2010). The landscape fragmentation index (Fi) represents the process of landscape type transformation from a single continuous entirety to a complex discontinuous patch (Llausas and Nogue, 2012). The larger the value, the lower the stability of the corresponding landscape ecosystem. The landscape pattern index obtained based on Fragstats software represents the influence of different land object types and their structure, distribution and other characteristics on the landscape, and is multiplied by the corresponding weight to calculate the Di (Peng et al., 2010), where Di represents the degree of separation between different patches in the landscape type, and the larger the value, the more complex the corresponding spatial distribution of the landscape. The landscape dominance index (Doi) indicates that a region takes a single or multiple landscape types as the overall landscape, which directly reflects the impact of this landscape type on the landscape pattern (Liu et al., 2020). The landscape vulnerability index (Vi) reflects the vulnerability of different ecosystems, and the vulnerability level can reflect the sensitivity and resilience of the landscape to external risk disturbances. The greater the vulnerability of the landscape, the greater the ecological risk. The landscape ecological risk index is as follows:

$$\mathrm{ERI}_k = \sum_{i=1}^{N} \frac{A_{ki}}{A_k} \sqrt{D_i \times V_i} \tag{8}$$

where $\mathrm{ERI_k}$ is the landscape ecological risk index of a unit k and the larger the value, the higher the ecological risk of the ecological unit; N is the number of landscape types; $\mathrm{A_{ki}}$ is the area of landscape type i in unit k; and $\mathrm{A_k}$ is the total area of the ecological unit k. The calculation of the landscape disturbance index (Di) is as follows:

$$\mathrm{Di} = \mathrm{a}(\mathrm{ED}) + \mathrm{b}(\mathrm{SHAPE\_AM}) + \mathrm{c}(\mathrm{COHESION}) + \mathrm{d}(\mathrm{AI}) + \mathrm{e}(\mathrm{IJI}) + \mathrm{f}(\mathrm{LPI}) \tag{9}$$

where a, b, c, d, e, and f are the weights of the corresponding landscape indices, which are calculated by the CRITIC objective weighting method. The formula for calculating the weight of the CRITIC method is as follows:

a. Calculate the standard deviation of the jth indicator. In the CRITIC method, the standard deviation is used to represent the difference and fluctuation of the internal values of each indicator. The larger the standard deviation, the greater the numerical difference of the indicator, the more information it can reflect and the more weight should be assigned to the indicator. The specific calculation is as follows:

$$S_j = \sqrt{\frac{\sum_{i=1}^{n}\left(X'_{ij} - \overline{X_j}\right)^2}{n-1}} \tag{10}$$

Where S_j is the standard deviation of the jth indicator, X'_{ij} is the standardized indicator value calculated in **formula (1)** and **formula (2)**, $\overline{X_j}$ represents the average of the normalized values of the jth indicator, and n is the total number of indicator values.

b. Carry out the conflict test of the indicators, the conflict between the indicators is represented by the correlation coefficient. The stronger the correlation with other indicators, the less conflict between the indicator and other indicators and the more evaluation content can be reflected. The repetition will weaken the evaluation strength of the indicator to a certain extent, and the weight assigned to the indicator should be reduced. The specific calculation is as follows:

$$R_j = \sum_{i=1}^{p}\left(1 - r_{ij}\right) \tag{11}$$

Where R_j represents the conflict between indicators, r_{ij} represents the correlation coefficient between indicators i and j, p represents the total number of indicators.

c. Calculate the information flux of the indicator. The larger the value of information flux, the greater the role it plays in the entire indicator system, and more weights should be assigned to it. The specific calculation formula is as follows:

$$C_j = S_j \times R_j \tag{12}$$

Where C_j represents the information flux of the jth indicator, S_j is the standard deviation of the jth indicator, and R_j is the conflict value of the jth indicator.

d. Weight calculation. The specific calculation formula is as follows:

$$W_j = \frac{C_j}{\sum_{j=1}^{p} C_j} \tag{13}$$

Where W_j is the objective weight of the jth indicator, and C_j is the information flux of the jth indicator.

TABLE 3 | Landscape index weights and their ecological significance.

Calculated indicators	Landscape index	Weight	Ecological significance
Landscape fragmentation index (Fi)	Edge density (ED)	0.13	Reflection the landscape fragmentation, reveal the degree to which landscape types are divided by boundaries, and the higher the boundary density, the higher the landscape fragmentation
	Area-weighted mean shape index (SHAPE_AM)	0.12	Measuring the complexity of the spatial pattern of the landscape has an edge effect on the shape analysis of the natural landscape
Landscape disturbance index (Di)	Patch cohesion index (COHESION)	0.12	It reflects the aggregation and dispersion state of patches in the landscape. The value is between -1 and 1. When the index result is -1, the patch is in a completely dispersed state, when the result is 0, it is randomly distributed, and when the result is 1, it is aggregated distribution
	Aggregation Index (AI)	0.17	It is derived from the calculation of the proximity matrix at the patch type level and reflects the degree of landscape aggregation and separation
	Interspersion Juxtaposition Index (IJI)	0.31	Characterizing the overall distribution and juxtaposition of each type of block, it reflects the distribution characteristics of ecosystems that are severely restricted by certain natural conditions. Smaller values indicate that the patch type is only adjacent to a few other types
Landscape dominant index (Doi)	Largest patch index (LPI)	0.15	Characterizing the proportion of the largest patch of a certain type to the entire landscape area is helpful to determine the dominant type of landscape, and changes in its value can change the intensity and frequency of disturbances, reflecting the direction and strength of human activities
landscape vulnerability index (Vi)	Obtained by expert Scoring		Indicates the sensitivity of different landscape types to external disturbances, the larger the value, the greater the ecological risk

The weight and ecological significance of the landscape ecological risk index we selected are shown in **Table 3**.

Landscape vulnerability index (Vi) refers to the vulnerability of the landscape ecosystem when encountering different factors. Generally, the lower the ecosystem level, the higher the internal vulnerability of the system. It was generally obtained through expert scoring. Generally speaking, the vulnerability of unused land, water, cultivated land, grassland, woodland, and constructed land was 6, 5, 4, 3, 2 and 1. Then normalization was performed to obtain the respective vulnerability indices Vi (Qiao et al., 2021).

Finally, after analysis of the landscape ecological risk index value of 5,671 ecological units, mapping of the landscape ecological risk index was done by the Kriging interpolation method in ArcGIS (https://www.esri.com/). The landscape ecological risk index value was classified using the natural breakpoint method: the lowest ecological risk (7.0–7.8), the lower ecological risk (7.8–8.2), the medium ecological risk (8.2–8.5), the higher ecological risk (8.5–8.8), and the highest ecological risk (8.8–9.2).

Mann-Kendall Trend Test

In this study, the Mann-Kendall trend test method (Jiang et al., 2015) was used to decide the ecological degradation index and the trend of the six land use types. Trends were divided into three grades: increasing trend ($Zs>0$), decreasing trend ($Zs<0$), and no trend ($Zs=0$). Significance was quantified at the 0.05 significance level.

RESULTS

Pressure Layer Index

From 2000 to 2019, the pressure index of the YRB continued to rise, indicating increasing pressure, and the spatial pattern of pressure index showed decreasing pressure from upper to lower YRB. The pressure intensity was the greatest in Henan and Shandong provinces with the highest population density and high level of economic development (**Figure 2A**). For the secondary indicators of the pressure layer, the number of heavy rain days and the precipitation intensity showed the same spatial distribution as the pressure index, and gradually increased from northwest to southeast of the YRB (**Figures 2B,C**), while the number of dry days gradually decreased from north to south of the YRB. Inner Mongolia and northern Ningxia province had the highest average number of dry days (**Figure 2D**), while Sichuan province had the least number of dry days. The urbanization level across the YRB was higher in the middle and lower YRB and lower urbanization in the upper YRB. Inner Mongolia had the highest urbanization rate, and Qinghai Province had the slowest urbanization rate (**Figure 2E**). The spatial pattern of urbanization rate was in line with that of per capita GDP (**Figure 2G**). Therefore, we found that the higher the urbanization rate and per capita GDP, the higher the pressure index value, such as in Shandong Province in the lower YRB, while the upper YRB was dominated by lower urbanization rate and per capita GDP, and hence lower pressure index, implying that urbanization was conducive to economic development, but it would also bring greater pressure on the ecological environment. Meanwhile, the population density of Shandong Province was much higher than that of other provinces (districts) over the YRB, and the spatial distribution of population density was similar to that of the pressure index (**Figure 2F**), indicating that population density had remarkable impacts on pressure.

The pressure in the Yellow River Basin showed an increasing trend during 2000–2019 (**Figure 2H**). The largest magnitude of trends of pressure can be found in Inner Mongolia, Shaanxi, Shanxi, Henan, and Shandong Province and even 99.93% of the YRB was dominated by increasing pressure, indicating that the ecological environment of the YRB was under enormous

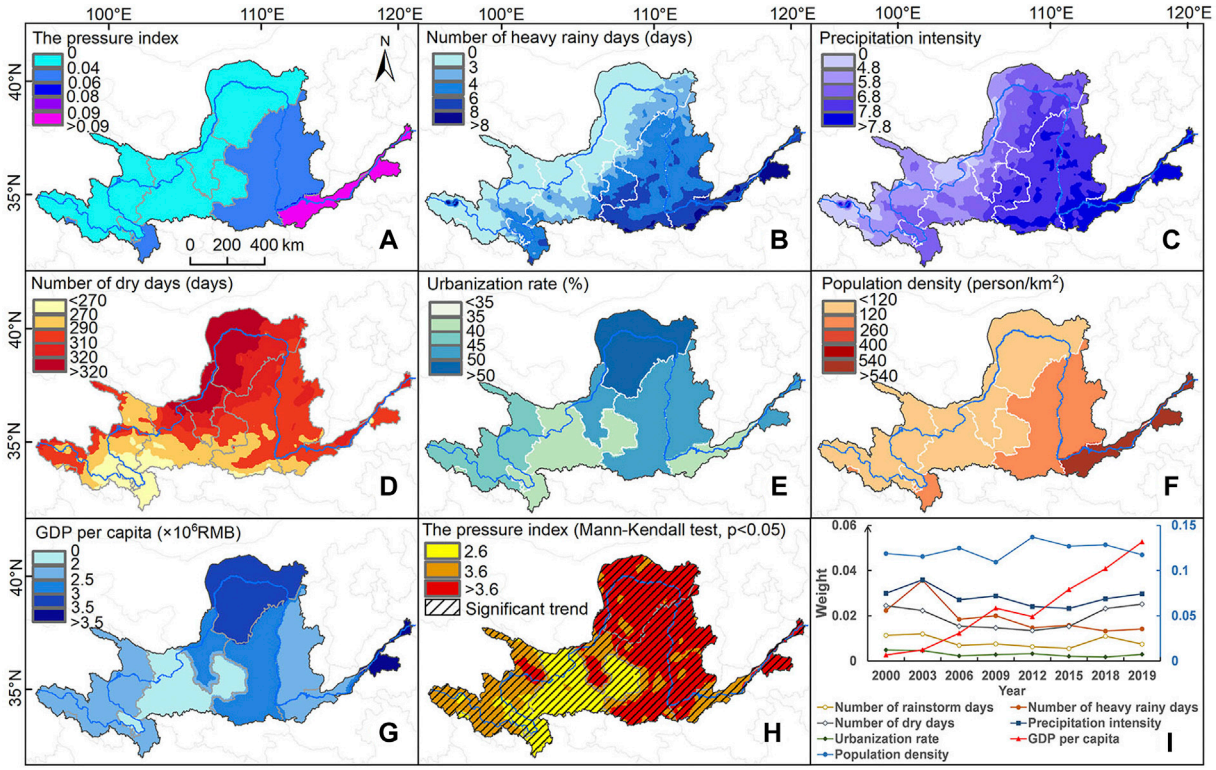

FIGURE 2 | Spatial distribution of pressure index **(A)**, spatial distribution of pressure layer indicators **(B–G)**, Mann-Kendall test results of pressure index at the 0.05 significance level **(H)**, the trend of pressure layer indicator weight over time **(I)**.

pressure. Therefore, it is critical to take reasonable and effective measures to alleviate the pressure on the ecological environment of the YRB. It can be seen from **Figure 2I** that the weight of population density indicator is the highest, indicating the greatest impact of population density on the pressure. Among climatic factors, before 2013, precipitation had a greater impact than drought on pressure, meanwhile the impact of drought on pressure was enhancing. After 2013, the weight of the drought indicator exceeded the weight of precipitation intensity and the number of heavy rain days, indicating that the drought had an amplifying impact on the ecological pressure (Gampe et al., 2021). Therefore, negative impacts of dry weather on the ecological environment of the YRB should arouse considerable concern.

State Layer Index

In the past 20 years, the spatial distribution of the state index increased from east to west of the YRB, and the difference between the north and the south of the YRB was obvious (**Figure 3A**). Grassland is the dominant land use type in the YRB, which is mainly distributed in the upper YRB and specifically the Mu Us Sandy Land, accounting for 49.96% of the total area of the YRB. Cultivated land and woodland accounted for 30.25 and 15.03% of the YRB. The cultivated land is mainly distributed in the Hetao Plain in the upper YRB, the Fenhe-Weihe Basin in the middle YRB, as well as the plains and valley basins in the lower YRB with good water and heat conditions in Shaanxi Province and southern Shanxi Province.

The land use of the watershed changed significantly in its spatial distribution and area during the study period. Based on the results of the Mann-Kendall trend test, the increased woodland area accounted for 25.37% of the total watershed area., while the decreased woodland area reached 59.71%, of which 39.9% passed the 0.05 significance level. Among them, Alxa, northwestern Ordos City, southern Shaanxi Province, Luliang City, Linfen City, Heze City, and Jining City showed an increasing trend of woodland (**Figure 3D**). Changes in the woodland area followed a "decreasing-increasing-decreasing" temporal pattern during the past 20 years, and the overall area of the woodland had decreased by 0.8%. The decrease of woodland was started by early agricultural reclamation activities, and vegetation restoration due to environmental protection policies, such as the project of Grain for Green which triggered the increase of woodlands, which was followed by decrease of woodland due to increased demand for land for agricultural development, urban construction, etc.

We found increasing grassland area over 50.29% of the YRB, located in upper YRB, specifically the Mu Us sandy land (**Figure 3E**). Under the influence of natural factors and various ecological protection projects, the vegetation of the Mu Us Sandy Land has basically been restored (Xiu et al., 2018). The area with

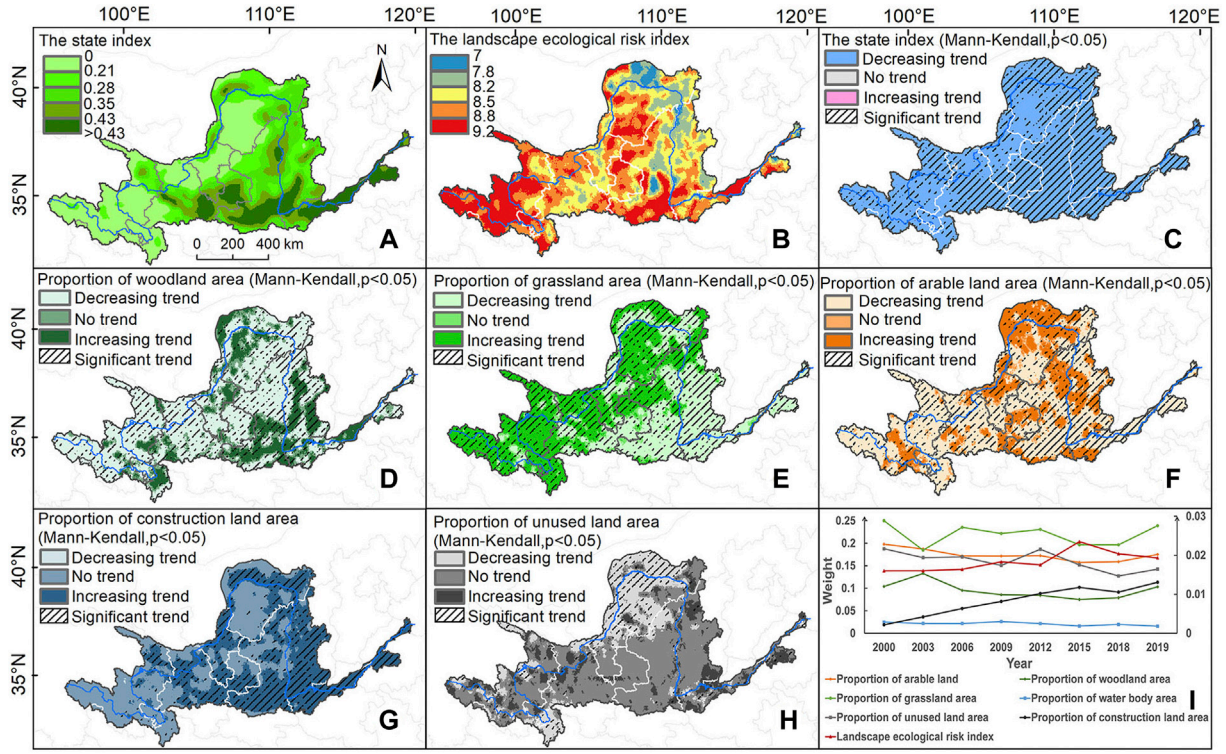

FIGURE 3 | Spatial distribution of state index **(A)**, spatial distribution of landscape ecological risk index **(B)**, Mann-Kendall test results of state layer indicators at the 0.05 significance level **(C–H)**, the trend of weights of each indicator over time **(I)**. Note: The weight values of grassland, arable land and woodland correspond to the left axis of **Figure 3I**, and the weight values of construction land, water body and unused land correspond to the right axis of **Figure 3I**.

decreasing grassland accounted for 39.18% of the YRB, mainly concentrated in the lower YRB. In order to promote rapid economic development, grassland and cultivated land were continuously converted into construction land. As a result, the construction land area in the lower YRB increased dramatically (**Figure 3G**). Meanwhile, 56.2% of the regional construction land in the entire YRB had an increasing tendency, no evident changes in 43.7% of the regional construction land and a decreasing tendency in only 0.1% of the regional construction land.

We also found decreasing arable land which accounted for 65.97% of the YRB. In the upper YRB and the Loess Plateau, the conversion of land types from arable land to woodland and grassland is remarkable due to ecological protection projects initiated by Chinese government, while the arable land in the lower YRB was mainly converted to the construction land. The area of the increased cultivated land accounted for 22.68% of the YRB (**Figure 3F**). Specifically, the Hetao Plain is of flat terrain and good soil quality with an irrigation area of 11 million acres (HIAAB/BWCB, 2007). It is one of the three largest irrigation areas in China and an important commercial grain base in Ningxia and Inner Mongolia (Kerschbaumer et al., 2015), where the area of arable land increased significantly. In addition, the area of cultivated land is increasing in Yulin City, Shaanxi Province, which is located in the agricultural and animal husbandry interlaced belt in North China. This is mainly due to the implementation of land engineering (Wu et al., 2019) in Yulin City, where agriculture is the main industry for the growing demand of food. In addition, 11.36% of the regional cultivated land area is relatively stable and no changes can be detected.

We found little changes in 55.95% of the unused land area within the YRB, while an increasing tendency was detected in 19.59% of the unused land area. Another 24.46% of the unused land showed a decreasing trend (**Figure 3H**). The decreased unused land areas were mainly distributed in the Hetao Plain and the Ningxia Plain, and most of them were converted into woodland and arable land.

The landscape Ecological Risk Index (ERI) witnessed a persistent decrease from 2000 to 2016, and shifted to increase from 2016 to 2019. The increase of ERI was mainly due to the conversion of landscape types. The expansion of construction land and traffic roads encroached large areas of woodland and arable land, and the shape of the landscape pattern became irregular and diversified, resulting in a decrease in the anti-interference ability. In terms of the spatial distribution, areas with the lowest ecological risk accounted for 4.43%, the lower ecological risk areas accounted for 11.16%, medium ecological risk areas accounted for 21.02%, higher ecological risk areas accounted for 29.48%, and highest ecological risk areas accounted for 33.91% of the YRB, respectively (**Figure 3B**). Among them, the source of Yellow River, Ordos city' Xi'an city, Weinan city, and the Henan province had the highest landscape ecology risk.

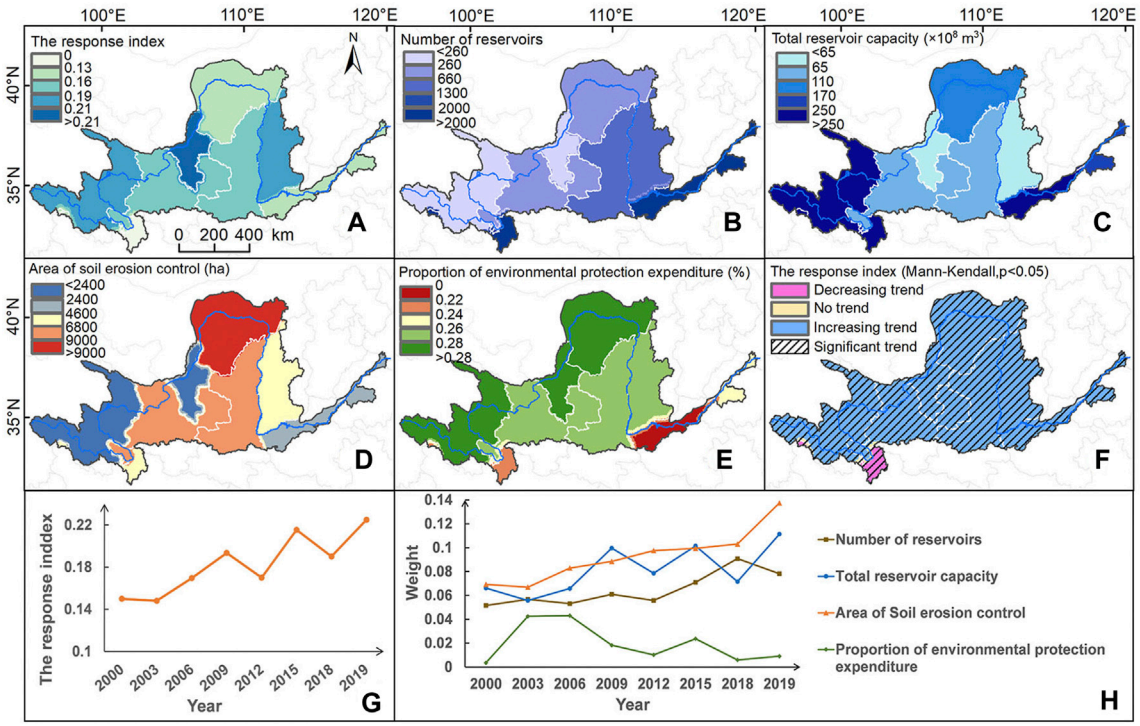

FIGURE 4 | Spatial distribution of response index **(A)**, spatial distribution of response layer indicators **(B–E)**, Mann-Kendall test results of response index at the 0.05 significance level **(H)**, time change of stress index **(G)**, and change of each indicator weight over time trend **(H)**.

The larger the value of the state index, the more complex the structure of the ecological landscape. Based on **Figure 3I**, we found that grassland, cultivated land, and woodland were assigned a larger weight, indicating large contributions of these land types to the state index, while water bodies, construction land, and unused land had minor contribution to the state index. It is due to the fact that the landscape structure of the YRB is mainly grassland, cultivated land, and woodland, and these land types account for 94.65% of the YRB with high vulnerability to external driving factors. Land use and land cover conversion amongst these three land types have remarkable impacts on the state index. From 1999 to 2012, the total woodland area of Ningxia, Shaanxi, and Shanxi provinces accounted for 11.20% of the total area of these three provinces (Xiao, 2015). The vegetation coverage of the Loess Plateau almost doubled. Large-scale afforestation and ecological protection projects tended to green the YRB (Fu et al., 2016).

Response Layer Index

The response index had an increasing tendency during a period from 2000 to 2019 (**Figure 4G**), indicating that the government have been responding positively to the ecological degradation of the YRB. **Figures 4B,C** show that the Aba Prefecture and Shandong Province had the largest number of reservoirs, Qinghai Province, Henan, and Shandong Province had the largest total reservoir capacity, indicating that reservoirs played a great role in water governance in the upper and lower reaches in the YRB. The upper reaches of the YRB is mainly used for water conservation and the lower reaches of the YRB for water and sediment regulation. The area of soil erosion control in the middle and lower YRB is significantly higher than in the upper YRB (**Figure 4D**), indicating that the ecological protection measures in the middle and lower YRB are mainly for soil erosion control. The proportion of environmental protection expenditures in the upper and middle YRB is significantly higher than in the lower YRB (**Figure 4E**), indicating that the environmental protection in the downstream YRB is not enough, the investment in environmental protection should be increased and the restoration of ecological environmental should be strengthened. Among all the response indicators, the area of soil erosion control was assigned to the largest weight (**Figure 4H**), indicating that the control of soil erosion is the most critical measure for the ecological protection of the YRB. The second is the influence of reservoirs in significantly changing the hydraulic conditions of the natural rivers (Xu et al., 2018). In order to store and use water efficiently, the government has carried out large-scale reservoir construction activities and achieved relatively high benefits. However, because of severe soil erosion and excessive sediment production in the YRB, the long-term safe storage capacity of reservoirs is at risk of being reduced (Liu et al., 2018).

EDI

We divided the ecological degradation indices into 5 grades to evaluate the magnitude of degradation intensity: grade I

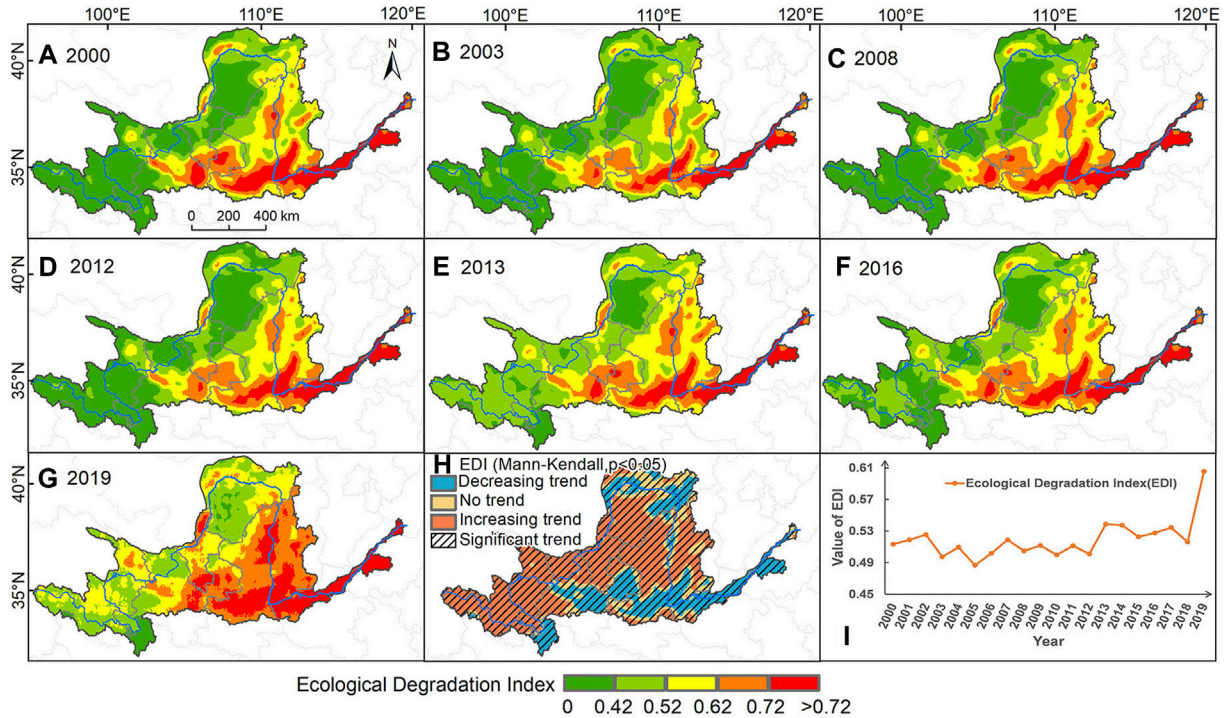

FIGURE 5 | Spatial distribution of ecological degradation index EDI in 2000, 2003, 2008, 2012, 2013, 2016 and 2019 **(A–G)**, Mann-Kendall test results at the 0.05 significance level of EDI **(H)**, and the trend of ecological degradation index over time **(I)**.

(0–0.42), grade II (0.42–0.52), grade III (0.52–0.62), grade IV (0.62–0.72) and V grade (>0.72) (**Figure 5**). From the perspective of time scale, the EDI of the watershed increased from 2000 to 2002 (**Figure 5I**), and the ecology continued to degrade. From 2003 to 2005, the ecological degradation was alleviated and it showed a downward trend. The main reason is that in 2002, the government fully launched the ecological protection project of returning farmland to forests. At the same time, policies and measures, such as pollution control and soil erosion control, were conducted, which jointly promoted the improvement of the ecological environment quality of the YRB. However, as the poverty elimination goal stimulated economic development and exacerbated man-land relations, the area of woodland and grassland showed a decreasing trend in 2005 with increased built-up areas. In addition, due to the imperfect compensation mechanism for returning farmland to forest and grassland, some farmers had converted woodland for agricultural purposes (Bennett, 2008; Song et al., 2014). Affected by the climate, there occurred rainstorms in 2005, where the precipitation intensity was high. Multiple factors led to the increasing trend of EDI in 2005 and the decline of the ecological environment quality of the YRB. We detected moderate changes in EDI during a period from 2005 to 2012. The increase of EDI occurred since 2013, reaching its peak value in 2019. On the one hand, it is due to pressure of human activities and the economic development. On the other hand, the compensation forest species in Grain-to-Green project ended in 2011 for more agricultural production and economic development and crop planting was resumed. These lands may undergo repeated logging and land type replacement, making the ecosystem structure of the YRB more fragile (Guo & Gong, 2016).

Although the government started the second phase of the Grain-to-Green project in 2014, the grassland has continued to increase. Recent years witnessed increasing impacts of human activities, alongside the rapid economic growth, on degradation of ecological environment quality. In terms of spatial distribution, the EDI intensity is the highest in the lower YRB because of the massive pressure on population and economic development. The upper reaches of the YRB are least affected by human activities and have the lowest EDI intensity.

Approximately 69.9% of the regional ecological environment further degraded from 2000 to 2019, while 29.5% of the regional ecological environment improved (**Figure 5H**). The intensity of ecological degradation in different times and spaces was affected by the comprehensive effects of climate change, human activities, socio-economic development, and land use and land cover conversion. Although Hebei and Shandong provinces had the highest intensity of ecological degradation, they also had a higher degree of response to ecological degradation, so the intensity of ecological environment degradation gradually decreased. The EDI of Gansu Province, Shaanxi Province, southern parts of Shanxi Province, eastern parts of Bayannur City, Inner Mongolia, and Baotou City had a decreasing tendency, and the ecological environment gradually

improved, while in most areas of Qinghai Province, Lanzhou, Ningxia, Ordos City, and Yulin City, Taiyuan City and Yangquan City, the intensity of ecological degradation continued to increase.

DISCUSSION

In this paper we found that population density was proportional to the pressure index. The rapid population growth was the main factor driving the increase in pressure, and the contribution rate of population density to the pressure index is 54.5%. The contribution of precipitation to the pressure index was second, with a contribution rate of 21.2%. The impact of drought on the pressure index continued to increase, which can be attributed to drought-induced water shortage, enhancing vegetation degradation and land desertification, modifying the structure and stability of the ecological environment, rendering the YRB more prone to degradation. The implementation of ecological protection projects, such as Grain-to-Green project, has greatly increased the vegetation coverage, which has played a key role in controlling soil erosion. However, Chen, 2015 believed that continued expansion of vegetation would potentially exert negative impacts on eco-environment because of the introduction of exotic plant species and high-density planting. Therefore, in order to ensure the sustainable and high-quality development of the YRB, attention should be paid to the balance between food supply and vegetation coverage suitable for climatic conditions, water supply and soil erosion, so as to maintain a good historical landscape in the YRB.

CONCLUSION

In this current study, we used 18 indicators to develop a comprehensive evaluation index system for ecological degradation assessment and grade zoning. By mapping of the EDI in the YRB, the intensity of ecological degradation in different regions can be visually presented. Moreover, the Mann-Kendall trend test was used to determine the areas where the degree of ecological degradation was enhanced or improved. The main conclusions of this paper are as follows:

(1) From 2000 to 2019, the pressure on the ecological environment of the Yellow River Basin has continued to increase, and the rapid population growth is the main driving factor. The stimulus of economic development and the increase of drought days under the background of climate warming have an increasing impact on the ecological pressure of the YRB. The government should strengthen the allocation of resources in various cities, especially in the densely populated lower reaches of the YRB in Henan Province and Shandong Province, and carry out rational control between population and resources. For green spaces and forests that have not yet been developed or have been slightly damaged by humans, natural restoration is the main focus, and human intervention is minimized. Optimize the development pattern of land resources, and limit economic activities to the range that the resources and environment can bear. Strengthen the construction of flood control facilities in the lower reaches of the YRB, and strengthen the conservation and utilization of water resources in the upper reaches of the YRB, such as Ningxia Province and Inner Mongolia, and optimize the water use structure.

(2) During 2000 to 2019, the area of grassland and construction land increased in an accelerating way, while the arable land decreased, and the area of woodland also decreased slowly. These four land use types are dominant over the fluvial landscape of the YRB, accounting for 96.5% of the total area of the YRB. In addition, due to no coordination amongst food demand, ecological protection demand, and ecological compensation, there occurred frequent conversions between land use types. With the enhancement of human activities, the landscape diversity gradually decreased and the landscape fragmentation increased, and the intensity of ecological degradation in the YRB was increasing. It is necessary to strengthen the modernization of agriculture according to local conditions. For example, we should strengthen centralized grain production in areas with suitable climate and sufficient water resources, such as the Hetao Irrigation Area, the Fenwei Basin, and the Ningxia Plain, and develop these areas into key grain bases. Convert other areas with scattered arable land and normal crop planting conditions into forest land or nature reserves. Especially Gansu and Shaanxi provinces should continue to expand the construction of forest land and grassland.

(3) In the process of ecological degradation governance, soil erosion control is the most critical ecological improvement measure, and downstream areas of the YRB need to increase investment and construction for ecological environmental protection. Strengthen the utilization efficiency of reservoirs, develop new functions of reservoirs and promote major projects such as embankment construction, river regulation, floodplain management, and ecological restoration as a whole.

(4) The overall ecological environment of the YRB presents an obvious trend of degradation, and the EDI in the lower YRB is the highest. The ecological environment of Qinghai Province, Lanzhou City, Ningxia, Ordos City, and Yulin City, Taiyuan City and Yangquan City are further degraded. The protection is far from enough, and more and more reasonable protection measures must be taken to curb the ecological degradation as soon as possible. For example, the construction of artificial afforestation and nature reserves has been increased in Ningxia and Gansu provinces, and comprehensive environmental management has been strengthened in Henan and Shandong provinces in the lower reaches of the YRB.

DATA AVAILABILITY STATEMENT

Publicly available datasets were analyzed in this study. This data can be found here: The precipitation data The China

Meteorological Administration Land Data Assimilation System (CLDAS), http://data.cma.cn/. The land use data: ESA (European Space Agency), http://maps.elie.ucl.ac.be/CCI/viewer/Statistical yearbooks of provinces within the Yellow River Basin.

AUTHOR CONTRIBUTIONS

TL is responsible for the conceptualization, methodology, data analysis, and writing- Original draft preparation. QZ: gave the necessary guidance and the original revision of the paper (TL and QZ have the equal contribution to this paper.) VS: proposed amendments and review for this paper. JZ and JS: provided help to the data management and analysis of this paper. SS: supported the Meteorological data of this paper. GW, ZS, WW: Reviewing and Editing.

FUNDING

This research has been supported by The Major Science and Technology Projects of Inner Mongolia Autonomous Region (2020ZD0009) and Collaborative Innovation Center for Integrated Management of Water Resources and Water Environment in the Inner Mongolia Reaches of the Yellow River, Hohhot, China.

REFERENCES

Abd El-Hamid, H. T., Caiyong, W., Hafiz, M. A., and Mustafa, E. K. (2020). Effects of Land Use/land Cover and Climatic Change on the Ecosystem of North Ningxia, China. *Arab. J. Geosci.* 13, 1–13. doi:10.1007/s12517-020-06047-6

Bai, T., Liu, X., Ha, Y.-p., Chang, J.-x., Wu, L.-z., Wei, J., et al. (2020). Study on the Single-Multi-Objective Optimal Dispatch in the Middle and Lower Reaches of Yellow River for River Ecological Health. *Water* 12 (3), 915. doi:10.3390/w12030915

Bennett, M. T. (2008). China's Sloping Land Conversion Program: Institutional Innovation or Business as Usual? *Ecol. Econ.* 65, 699–711. doi:10.1016/j.ecolecon.2007.09.017

Chen, Y., Syvitski, J. P. M., Gao, S., Overeem, I., and Kettner, A. J. (2012). Socio-economic Impacts on Flooding: a 4000-year History of the Yellow River, China. *Ambio* 41, 682–698. doi:10.1007/s13280-012-0290-5

Chen, Y., Wang, K., Lin, Y., Shi, W., Song, Y., and He, X. (2015). Balancing Green and Grain Trade. *Nat. Geosci.* 8, 739–741. doi:10.1038/ngeo2544

Chiyuan Miao, C., Jinren Ni, J., and Borthwick, A. G. L. (2010). Recent Changes of Water Discharge and Sediment Load in the Yellow River Basin, China. *Prog. Phys. Geogr. Earth Environ.* 34, 541–561. doi:10.1177/0309133310369434

Das, S., Pradhan, B., Shit, P. K., and Alamri, A. M. (2020). Assessment of Wetland Ecosystem Health Using the Pressure-State-Response (PSR) Model: A Case Study of Mursidabad District of West Bengal (India). *Sustainability* 12, 5932. doi:10.3390/su12155932

Dongguang, W., Fawang, Z., Eryong, Z., Cunrong, G., and Han, Z. (2008). Outline of the Yellow River Basin, China. *Bull. Geol. Surv. Jpn.* 60, 9–18. doi:10.9795/bullgsj.60.9

Fan, J., Wang, Y., Zhou, Z., You, N., and Meng, J. (2016). Dynamic Ecological Risk Assessment and Management of Land Use in the Middle Reaches of the Heihe River Based on Landscape Patterns and Spatial Statistics. *Sustainability* 8, 536. doi:10.3390/su8060536

Fu, B., Wang, S., Liu, Y., Liu, J., Liang, W., and Miao, C. (2017). Hydrogeomorphic Ecosystem Responses to Natural and Anthropogenic Changes in the Loess Plateau of China. *Annu. Rev. Earth Planet. Sci.* 45, 223–243. doi:10.1146/annurev-earth-063016-020552

Gampe, D., Zscheischler, J., Reichstein, M., O'Sullivan, M., Smith, W. K., Sitch, S., et al. (2021). Increasing Impact of Warm Droughts on Northern Ecosystem Productivity over Recent Decades. *Nat. Clim. Chang.* 11, 772–779. doi:10.1038/s41558-021-01112-8

Gorla, L., and Perona, P. (2013). On Quantifying Ecologically Sustainable Flow Releases in a Diverted River Reach. *J. Hydrology* 489, 98–107. doi:10.1016/j.jhydrol.2013.02.043

Guo, J., and Gong, P. (2016). Forest Cover Dynamics from Landsat Time-Series Data over Yan'an City on the Loess Plateau during the Grain for Green Project. *Int. J. Remote Sens.* 37, 4101–4118. doi:10.1080/01431161.2016.1207264

Heinrichs, J. A., Bender, D. J., and Schumaker, N. H. (2016). Habitat Degradation and Loss as Key Drivers of Regional Population Extinction. *Ecol. Model.* 335, 64–73. doi:10.1016/j.ecolmodel.2016.05.009

HIAAB/BWCB (2007). Introduction to Inner Mongolia Hetao Irrigation. Hetao Water Resources. In *Inner Mongolia Hetao Irrigation Administration Bureau/Inner Mongolia Bayannur Bureau of Water Resources*. Available from: http://www.zghtgq.com/plus/list.php?tid=43 ((in Chinese).

Hu, X., and Xu, H. (2018). A New Remote Sensing Index for Assessing the Spatial Heterogeneity in Urban Ecological Quality: a Case from Fuzhou City, China. *Ecol. Indic.* 89, 11–21. doi:10.1016/j.ecolind.2018.02.006

Huang, J., Guan, X., and Ji, F. (2012). Enhanced Cold-Season Warming in Semi-arid Regions. *Atmos. Chem. Phys.* 12 (2), 5391–5398. doi:10.5194/acp-12-5391-2012

Jiang, W., Yuan, L., Wang, W., Cao, R., Zhang, Y., and Shen, W. (2015). Spatio-temporal Analysis of Vegetation Variation in the Yellow River Basin. *Ecol. Indic.* 51, 117–126. doi:10.1016/j.ecolind.2014.07.031

Kerschbaumer, L., Köbbing, J. F., Ott, K., Zerbe, S., and Thevs, N. (2015). Development Scenarios on Hetao Irrigation Area (China): a Qualitative Analysis from Social, Economic and Ecological Perspectives. *Environ. Earth Sci.* 73, 815–834. doi:10.1007/s12665-014-3061-8

Li, H., Zhang, Q., Singh, V. P., Shi, P., and Sun, P. (2017). Hydrological Effects of Cropland and Climatic Changes in Arid and Semi-arid River Basins: a Case Study from the Yellow River Basin, China. *J. Hydrology* 549, 547–557. doi:10.1016/j.jhydrol.2017.04.024

Liao, C., Yue, Y., Wang, K., Fensholt, R., Tong, X., and Brandt, M. (2018). Ecological Restoration Enhances Ecosystem Health in the Karst Regions of Southwest China. *Ecol. Indic.* 90, 416–425. doi:10.1016/j.ecolind.2018.03.036

Liu, D., Chen, H., Zhang, H., Geng, T., and Shi, Q. (2020). Spatiotemporal Evolution of Landscape Ecological Risk Based on Geomorphological Regionalization during 1980-2017: A Case Study of Shaanxi Province, China. *Sustainability* 12, 941. doi:10.3390/su12030941

Liu, D., Chen, J., and Ouyang, Z. (2020). Responses of Landscape Structure to the Ecological Restoration Programs in the Farming-Pastoral Ecotone of Northern China. *Sci. Total Environ.* 710, 136311. doi:10.1016/j.scitotenv.2019.136311

Liu, D. D., Qu, R. J., Zhao, C. H., Liu, A. P., and Deng, X. Z. (2012). Landscape Ecological Risk Assessment in Yellow River Delta. *J. Food Agric. Environ.* 10, 970–972. doi:10.1016/j.foodres.2011.12.018

Liu, Y., Liu, Y., Li, J., Lu, W., Wei, X., and Sun, C. (2018). Evolution of Landscape Ecological Risk at the Optimal Scale: a Case Study of the Open Coastal Wetlands in Jiangsu, China. *Ijerph* 15, 1691. doi:10.3390/ijerph15081691

Llausàs, A., and Nogué, J. (2012). Indicators of Landscape Fragmentation: the Case for Combining Ecological Indices and the Perceptive Approach. *Ecol. Indic.* 15, 85–91. doi:10.1016/j.ecolind.2011.08.016

Niu, L., Guo, Y., Li, Y., Wang, C., Hu, Q., Fan, L., et al. (2021). Degradation of River Ecological Quality in Tibet Plateau with Overgrazing: a Quantitative Assessment Using Biotic Integrity Index Improved by Random Forest. *Ecol. Indic.* 120, 106948. doi:10.1016/j.ecolind.2020.106948

Patil, R., Wei, Y., Pullar, D., and Shulmeister, J. (2018). Understanding Hydro-Ecological Surprises for Riverine Ecosystem Management. *Curr. Opin. Environ. Sustain.* 33, 142–150. doi:10.1016/j.cosust.2018.05.021

Paukert, C. P., Pitts, K. L., Whittier, J. B., and Olden, J. D. (2011). Development and Assessment of a Landscape-Scale Ecological Threat Index for the Lower Colorado River Basin. *Ecol. Indic.* 11, 304–310. doi:10.1016/j.ecolind.2010.05.008

Peng, J., Dang, W. X., Liu, Y. X., Zong, M. L., and Hu, X. X. (2015). Review on Landscape Ecological Risk Assessment. *Acta Geogr. Sin.*, 70:664–677. doi:10.11821/dlxb201504013

Peng, J., Wang, Y., ZhangZhang, Y., Wu, J., Li, W., and Li, Y. (2010). Evaluating the Effectiveness of Landscape Metrics in Quantifying Spatial Patterns. *Ecol. Indic.* 10, 217–223. doi:10.1016/j.ecolind.2009.04.017

Pettorelli, N., Vik, J. O., Mysterud, A., Gaillard, J.-M., Tucker, C. J., and Stenseth, N. C. (2005). Using the Satellite-Derived NDVI to Assess Ecological Responses to Environmental Change. *Trends Ecol. Evol.* 20, 503–510. doi:10.1016/j.tree.2005.05.011

Qiao, F., Bai, Y., Xie, L., Yang, X., and Sun, S. (2021). Spatio-Temporal Characteristics of Landscape Ecological Risks in the Ecological Functional Zone of the Upper Yellow River, China. *Ijerph* 18, 12943. doi:10.3390/ijerph182412943

Qiu, J., Li, T.-J., and Li, F.-F. (2019). Evaluation of Environmental and Ecological Impacts of the Leading Large-Scale Reservoir on the Upper Reaches of the Yellow River. *Sustainability* 11 (14), 3818. doi:10.3390/su11143818

Qiu, M., Zuo, Q., Wu, Q., Yang, Z., and Zhang, J. (2022). Water Ecological Security Assessment and Spatial Autocorrelation Analysis of Prefectural Regions Involved in the Yellow River Basin. *Sci. Rep.* 12, 5105. doi:10.1038/s41598-022-07656-9

Song, C., Zhang, Y., Mei, Y., Liu, H., Zhang, Z., Zhang, Q., et al. (2014). Sustainability of Forests Created by China's Sloping Land Conversion Program: a Comparison Among Three Sites in Anhui, Hubei and Shanxi. *For. Policy Econ.* 38, 161–167. doi:10.1016/j.forpol.2013.08.012

Sun, J., Li, Y. P., Gao, P. P., and Xia, B. C. (2018). A Mamdani Fuzzy Inference Approach for Assessing Ecological Security in the Pearl River Delta Urban Agglomeration, China. *Ecol. Indic.* 94, 386–396. doi:10.1016/j.ecolind.2018.07.011

Sun, T., Lin, W., Chen, G., Guo, P., and Zeng, Y. (2016). Wetland Ecosystem Health Assessment through Integrating Remote Sensing and Inventory Data with an Assessment Model for the Hangzhou Bay, China. *Sci. Total Environ.* 566-567, 627–640. doi:10.1016/j.scitotenv.2016.05.028

Turner, B. L., Lambin, E. F., and Reenberg, A. (2007). The Emergence of Land Change Science for Global Environmental Change and Sustainability. *Proc. Natl. Acad. Sci. U.S.A.* 104, 20666–20671. doi:10.1073/pnas.0704119104

Vitousek, P. M., Mooney, H. A., Lubchenco, J., and Melillo, J. M. (2008). Human Domination of Earth's Ecosystems. *Springer U. S.* 277, 3–13. doi:10.1007/978-0-387-73412-5_1

Wang, F., Lu, Y., Li, J., and Ni, J. (2021). Evaluating Environmentally Sustainable Development Based on the PSR Framework and Variable Weigh Analytic Hierarchy Process. *Ijerph* 18, 2836. doi:10.3390/ijerph18062836

Wang, Z., Tang, L., Qiu, Q., Chen, H., Wu, T., and Shao, G. (2018). Assessment of Regional Ecosystem Health-A Case Study of the Golden Triangle of Southern Fujian Province, China. *Ijerph* 15, 802. doi:10.3390/ijerph15040802

Wohlfart, C., Kuenzer, C., Chen, C., and Liu, G. (2016). Social-ecological Challenges in the Yellow River Basin (China): a Review. *Environ. Earth Sci.* 75, 1066. doi:10.1007/s12665-016-5864-2

Wolfslehner, B., and Vacik, H. (2008). Evaluating Sustainable Forest Management Strategies with the Analytic Network Process in a Pressure-State-Response Framework. *J. Environ. Manag.* 88, 1–10. doi:10.1016/j.jenvman.2007.01.027

Wu, W., Chen, Z., Li, Y., Wang, Y., Yan, J., and Song, C. (2019). Land Engineering and its Role for Sustainable Agriculture in the Agro-Pastoral Ecotone: a Case Study of Yulin, Shaanxi Province, China. *J. Geogr. Sci.* 29, 818–830. doi:10.1007/s11442-019-1630-1

Xiao, J. (2014). Satellite Evidence for Significant Biophysical Consequences of the "Grain for Green" Program on the Loess Plateau in China. *J. Geophys. Res. Biogeosci.* 119, 2261–2275. doi:10.1002/2014JG002820

Xiu, L., Yan, C., Li, X., Qian, D., and Feng, K. (2018). Monitoring the Response of Vegetation Dynamics to Ecological Engineering in the Mu Us Sandy Land of China from 1982 to 2014. *Environ. Monit. Assess.* 190, 543. doi:10.1007/s10661-018-6931-9

Xu, B., Yang, D., Yao, P., Burnett, W. C., Ran, X., Charette, M., et al. (2018). A New Perspective for Assessing Water Transport and Associated Retention Effects in a Large Reservoir. *Geophys. Res. Lett.* 45, 9642–9650. doi:10.1029/2018GL079687

Xu, W., Wang, J., Zhang, M., and Li, S. (2021). Construction of Landscape Ecological Network Based on Landscape Ecological Risk Assessment in a Large-Scale Opencast Coal Mine Area. *J. Clean. Prod.* 286, 125523. doi:10.1016/j.jclepro.2020.125523

Xu, Y., Cai, Y., Sun, T., and Tan, Q. (2017). A Multi-Scale Integrated Modeling Framework to Measure Comprehensive Impact of Coastal Reclamation Activities in Yellow River Estuary, China. *Mar. Pollut. Bull.* 122, 27–37. doi:10.1016/j.marpolbul10.1016/j.marpolbul.2017.05.065

Yaacobi, G., Ziv, Y., and Rosenzweig, M. L. (2007). Effects of Interactive Scale-dependent Variables on Beetle Diversity Patterns in a Semi-arid Agricultural Landscape. *Landsc. Ecol.* 22, 687–703. doi:10.1007/s10980-006-9061-7

Yellow River Conservancy Commission (YRCC) (2020). *Yellow River Yearbook*. China: Yellow River Yearbook Press, 85–93. (in Chinese).

Zhang, Q., Zhang, Z., Shi, P., Singh, V. P., and Gu, X. (2018). Evaluation of Ecological Instream Flow Considering Hydrological Alterations in the Yellow River Basin, China. *Glob. Planet. Change* 160, 61–74. doi:10.1016/j.gloplacha.2017.11.012

Zhang, X., Liu, K., Wang, S., Wu, T., Li, X., Wang, J., et al. (2022). Spatiotemporal Evolution of Ecological Vulnerability in the Yellow River Basin under Ecological Restoration Initiatives. *Ecol. Indic.* 135, 108586. doi:10.1016/j.ecolind.2022.108586

Zhang, X., Wang, L., Fu, X., Li, H., and Xu, C. (2017). Ecological Vulnerability Assessment Based on PSSR in Yellow River Delta. *J. Clean. Prod.* 167, 1106–1111. doi:10.1016/j.jclepro.2017.04.106

Zhang, Y., Cao, Z., Wang, W., and Jin., X. (2021). Using Systems Thinking to Study the Coordination of the Water-Sediment-Electricity Coupling System: a Case Study on the Yellow River. *Sci. Rep.* 11, 21974. doi:10.1038/s41598-021-01578-8

Zhao, G., Mu, X., Wen, Z., Wang, F., and Gao, P. (2013). Soil Erosion, Conservation, and Eco-Environment Changes in the Loess Plateau of China. *Land Degrad. Dev.* 24, 499–510. doi:10.1002/ldr.2246

Conflict of Interest: The authors declare that the research was conducted in the absence of any commercial or financial relationships that could be construed as a potential conflict of interest.

Publisher's Note: All claims expressed in this article are solely those of the authors and do not necessarily represent those of their affiliated organizations, or those of the publisher, the editors and the reviewers. Any product that may be evaluated in this article, or claim that may be made by its manufacturer, is not guaranteed or endorsed by the publisher.

frontiers | Frontiers in Environmental Science

REVIEW
published: 13 July 2022
doi: 10.3389/fenvs.2022.905428

Visualizing a Field of Research With Scientometrics: Climate Change Associated With Major Aquatic Species Production in the World

Mohamad N. Azra[1,2*†], *Mohd Iqbal Mohd Noor*[3,4†], *Yeong Yik Sung*[2] *and Mazlan Abd Ghaffar*[2,5,6*]

[1]Institute of Marine Biotechnology (IMB), Universiti Malaysia Terengganu (UMT), Kuala Terengganu, Malaysia, [2]Climate Change Adaptation Laboratory, Institute of Marine Biotechnology (IMB), Universiti Malaysia Terengganu (UMT), Kuala Terengganu, Malaysia, [3]Faculty of Business Management, Universiti Teknologi MARA (UiTM), Pahang, Malaysia, [4]Institute for Biodiversity and Sustainable Development, Universiti Teknologi MARA (UiTM), Shah Alam, Malaysia, [5]Faculty of Science and Marine Environment, Universiti Malaysia Terengganu, Kuala Terengganu, Malaysia, [6]Higher Institution Centre of Excellence (HICoE), Institute of Tropical Aquaculture and Fisheries (AKUATROP), Universiti Malaysia Terengganu, Kuala Terengganu, Malaysia

OPEN ACCESS

Edited by:
Huopo Chen,
Institute of Atmospheric Physics (CAS), China

Reviewed by:
Luigi Aldieri,
University of Salerno, Italy
Guo Donglin,
Institute of Atmospheric Physics (CAS), China

***Correspondence:**
Mohamad N. Azra
azramn@umt.edu.my
Mazlan Abd Ghaffar
mag@umt.edu.my

[†]These authors share first authorship

Specialty section:
This article was submitted to Interdisciplinary Climate Studies, a section of the journal Frontiers in Environmental Science

Received: 27 March 2022
Accepted: 25 May 2022
Published: 13 July 2022

Citation:
Azra MN, Mohd Noor MI, Sung YY and Abd Ghaffar M (2022) Visualizing a Field of Research With Scientometrics: Climate Change Associated With Major Aquatic Species Production in the World. Front. Environ. Sci. 10:905428. doi: 10.3389/fenvs.2022.905428

Climate change research on major aquatic species assists various stakeholders (e.g. policymakers, farmers, funders) in better managing its aquaculture activities and productivity for future food sustainability. However, there has been little research on the impact of climate change on aquatic production, particularly in terms of scientometric analyses. Thus, using the bibliometric and scientometric analysis methods, this study was carried out to determine what research exists on the impact of climate change on aquatic production groups. We focused on finfish, crustaceans, and molluscs. Data retrieved from Web of Science was mapped with CiteSpace and used to assess the trends and current status of research topics on climate change associated with worldwide aquatic production. We identified ocean acidification as an important research topic for managing the future production of aquatic species. We also provided a comprehensive perspective and delineated the need for: i) more international collaboration for research activity focusing on climate change and aquatic production in order to achieve the United Nations Sustainable Development Goal by 2030; ii) the incorporation of work from molecular biology, economics, and sustainability.

Keywords: aquaculture production, climate action, crustaceans, environment, finfish, molluscs, sustainable development goals (SDG), state of world fisheries and aquaculture

1 INTRODUCTION

The process of climate change is being accelerated due to human activities negatively impacting the environment (e.g., burning fossil fuels, land clearing, and agricultural activities releasing greenhouse gases to the atmosphere), and is currently leading to an overall increase in global temperature. As the ocean absorbs the majority of excess heat (e.g., Sun energy/solar radiation) from this warming, it acts as a buffer for terrestrial life. Consequently, this leads to serious impacts on ocean ecology. This issue has been highlighted in the United Nations Sustainable Development Goals (SDG), where goal 13 states we must "*take urgent action to combat climate change and its impacts*" (UN SDG, 2021). One aspect that requires urgent action is combating the effects of climate change on oceanic productivity

(Steeves et al., 2018; Thakur et al., 2018; Sainz et al., 2019; Heasman et al., 2020; Maulu et al., 2021). This includes many marine fisheries, as decreases in productivity of marine capture, particularly in tropical regions such as Africa and Asia (Cheung et al., 2010; Pauly and Cheung, 2018; Oremus et al., 2020), are increasingly common.

Since 2010, the Food and Agriculture Organization has collected data on the main species produced in global aquaculture, specifically three different groups of finfish, crustaceans, and molluscs (FAO). Previously, the world's major species production were divided into six different groups including: freshwater fishes, diadromous fishes, marine fishes, crustaceans, molluscs, and other aquatic animals not elsewhere included (FAO, 2011). Aquatic algae were excluded from the list of aquatic species produced because they were regarded as a non-animal item. These lists are managed by The State of World Fisheries and Aquaculture (SOFIA) (FAO, 2021), which aims to provide comprehensive, objective, and global views on fisheries and aquaculture related data to policy-makers, civil society, and those whose livelihoods depend on aquatic resources. The top two major species produced in the world for finfish, crustaceans and molluscs are, respectively: i) grass carp, *Ctenopharyngodon idellus* and ii) silver carp, *Hypophthalmichthys molitrix;* i) Whiteleg shrimp, *Penaeus vannamei* and ii) red swamp crawfish, *Procambarus clarkii;* and i) cupped oysters nei, *Crassostrea* spp. and ii) Japanese carpet shell, *Ruditapes philippinarum* (FAO, 2020). These six species have seen important increases in annual production since 2010, where their total production accounted for almost half of the global production of all 466 managed species in 2018 (47.8%). The importance of managing aquatic production responsibly is thus widely prioritized and recognized. As climate change influences the aquatic environment, understanding these impacts on major species production is truly needed.

Various authors have conducted studies on the impact of climate change on aquaculture activities, mostly in review-based studies (Callaway et al., 2012; Rosa et al., 2012; Froehlich et al., 2018). However, research on the impact of climate change on aquaculture production specifically is limited, especially in terms of scientometric-based analysis. As a result, there is an urgent need to assess the current literature surrounding the impacts of climate change on major aquatic production to improve management and risk assessment of aquaculture activities and its future productivity.

In this study, bibliometric and scientometric analyses were combined to analyze global trends of climate change research regarding the top globally produced finfish, crustacean, and mollusc species. Scientometric study usually refers to the analysis of analyzing and measuring currents patterns of available scientific literature (Azra et al., 2021). Nalimov and Mulcjenko (1971) were first to define scientometrics as "the quantitative methods of research on the development of science as an informational process". Scientometrics is also known for its ability to synthesis quantitative literatures systematically and comprehensively. Recently, it has also become an essential tool for assessing a researcher's research and development, collaboration, and academic quality. Various tools can be used to determine relevant subject areas such as VOSviewer, CiteSpace, etc. (Zhou and Song, 2021). To our knowledge, the present article is the first report detailing scientometric analysis on climate change impacts on major aquaculture species produced worldwide. We are specifically interested in the following questions:

RQ1. What are the overall publication trends in terms of publication output?

RQ2. Where is this research area situated on the map of Web of Sciences database?

RQ3. Who are the dominant knowledge carriers in these areas?

RQ4. What are the dominant topics/clusters, and what is their temporal evolution?

RQ5. What are the impactful publications and keywords for these areas?

Answering these research questions will help inform the current body of research and identify important research gaps regarding the impacts of climate change on aquatically produced species.

2 METHODS

Scientometric analysis is a date and information visualization analysis tool that can explore important changes along with the development trends of a research domain (Chen and Song, 2019). This analysis has been regarded as an important tool to summarize historical research achievements and reveal what direction future research trends should take. The details for the research framework used in this study is shown in **Figure 1**.

2.1 Data Source

We used Web of Science (WOS) databases to conduct a literature search for the scientometric analysis. We chose to focus on WOS instead of other databases such as PubMed, Google Scholar, or Scopus, due to the efficiency with which WOS can extract bibliographic data from search results (Azra et al., 2022). According to Meho and Rogers (2008), WOS indexed publications have the highest data quality of literature and the most authenticated information when compared to other database platforms. Furthermore, the result for visual analysis coding using the WOS database is more compatible with the CiteSpace software used for data analysis in this study (Chen 2004). The WOS searches were based on the "topic" (TS) field, which includes article titles, abstracts, keywords, and "KeyWords Plus" (automatically generated terms pulled from the titles of cited articles).

2.2 Article Search

A robust set of search keywords are key for quality literature syntheses (Azzeri et al., 2020). A good search keyword can retrieve the most relevant influential studies. Search keyword formulation begins by applying the PECo method for formulating research objectives/questions, where "P" stands for Population, "E" stands for Exposure and "Co." for context.

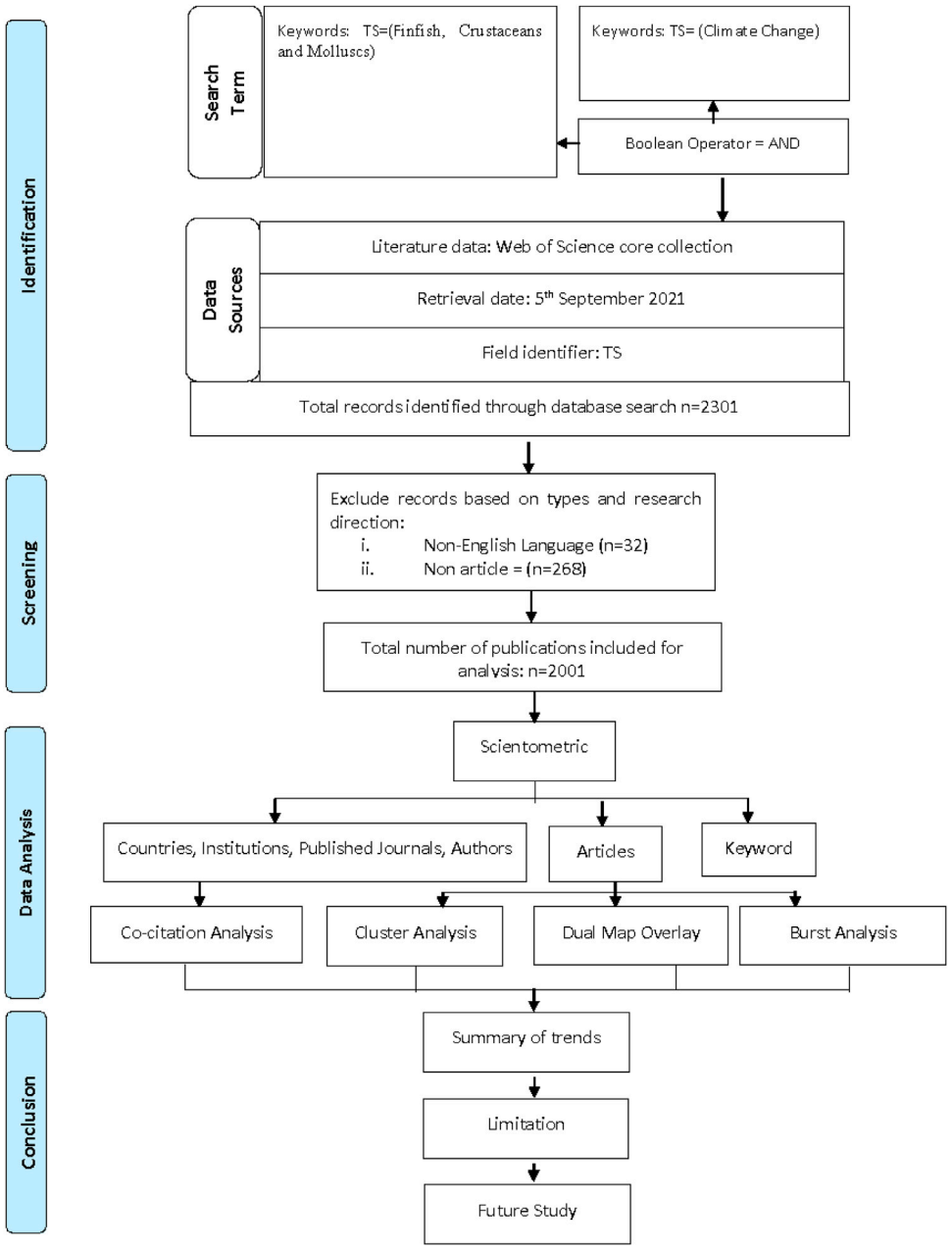

FIGURE 1 | Methodological framework for the current study.

The primary goal of our scientometric analysis was to examine recent trends in research regarding the effects of climate change on the top aquatic production groups, namely finfish, crustaceans, and molluscs. Our "Population" keywords focused on Aquatic Species Production, specifically for animals; keywords on Climate Change were our "Exposure" terms. No "Context" component was included as this criterion is discussed in the result analysis. The search was conducted on 5 September 2021. The search strings are presented below.

2.2.1 Population Keywords—Selection of Species

Species' common names were based on the FAO catalogue published in their respective website or referred to on their "Cultured Aquatic Species Information Programme" (**Supplementary Appendix S1A**). For molluscs, we chose species based on the available fact sheet provided by the FAO, particularly the Cupped oysters nei, *Crassostrea spp*. According to FAO terminology, the "nei" is defined as "not elsewhere included," which is when the species cannot be identified, and more than one species is included in the same group. However,

TABLE 1 | Overview of techniques and tools used to answer our research questions.

Id	Research question focus	Software	Summary of techniques/tools
RQ1	Publication output trends	Excel	Descriptive analysis for number of Publications, published journals, authors, universities/institutes, and country/region
RQ2	Research Area in WOS database	CiteSpace	Dual Map Overlay that shows inter-domain specialty, and specialty trends linking research areas
RQ3	Dominant knowledge carriers	CiteSpace	Co-citation Analysis for (Author, Journal, Country, Institutions, and Articles) to determine development status and scientific structure for each variable
RQ4	Dominant topic/cluster	CiteSpace	Document Cluster Analysis to identify the tip cluster of research in focus areas
RQ5	Impactful publications and keyword	CiteSpace	Burstness metric used to determine influential publications and top keywords

we chose the species based on the FAO Cultured Aquatic Species Information Programme or Introduced Species Fact Sheets in which the species was listed as a cultured species for the genus *Crassostrea*. For each of the three groups (finfish, crustaceans, molluscs), we list the top two major species produced globally and their associated references in **Supplementary Appendix S1A**. To identify articles based on these six species, the following key terms were used:

TS= ((“grass carp”) OR (“white amur”) OR (“*Ctenopharyngodon idellus*”) OR (“silver carp”) OR (“*Hypophthalmichthys molitrix*”) OR (“whiteleg shrimp”) OR (“white shrimp”) OR (“penaeus vannamei”) OR (“litopenaeus vannamei”) OR (“red swamp crawfish”) OR (“*Procambarus clarkii*”) OR (“pacific cupped oyster”) OR (“*Crassostrea gigas*”) OR (“american cupped oyster”) OR (“*Crassostrea virginica*”) OR (“mangrove cupped oyster”) OR (“crassostrea rhizophorae”) OR (“japanese carpet shell”) OR (“ruditapes philippinarum”))

2.2.2 Exposure Keywords

Keywords associated with our topic “Climate Change” included:

TS=[(climat*) OR (“global warm*”) OR (“seasonal* variat*”) OR (“extrem* event*”) OR (“environment* variab*”) OR (“anthropogenic effect*”) OR (“multiple stres*”) OR (“greenhouse effect*”) OR (“sea level ris*”) OR (erosio*) OR (“agricult* runoff”) OR (“weather* variab*”) OR (“weather* extrem*”) OR (“extreme* climat*”) OR (“environment* impact*”) OR (“environment* chang*”) OR (“anthropogenic stres*”) OR (“temperature ris*”) OR (“temperature effect*”) OR (“warm* ocean”) OR (“sea surface* temperat*”) OR (heatwav*) OR (acidific*) OR (hurrican*) OR (el-nino) OR (“el nino”) OR (“la nina”) OR (la-nina) OR (drought*) OR (flood*) OR (“high precipit*”) OR (“heavy rainfall*”) OR (“CO2 concentrat*”) OR (“melt* of the glacier*”) OR (“melt* ice*”)]

2.3 Eligibility Criteria

2.3.1 Inclusion Criteria

Articles retrieved from WOS searches were included in our subsequent analyses only if they were published in peer-reviewed journals and were written in English.

2.3.2 Exclusion Criteria

We excluded a study if it was not considered original research, if it was published in a journal that did not conduct peer-review, or if it was not written in English. Such studies may have included proceedings papers, reviews, book reviews, abstracts, editorial materials, letters, or news.

2.4 Data Analysis

To address our first research question, we used Excel to visualize descriptive analyses for the number of publications, published journals, authors, universities/institutes, and countries/regions where the authors were affiliated with at time of publication. Then, to answer research questions two through five, we used four visualization analyses in CiteSpace Software. **Section 2.4.1** describes CiteSpace techniques and tools in detail. **Table 1** summarizes the techniques and tools used to answer the research questions.

2.4.1 Scientometric Analysis

CiteSpace V version 5.2. R 2.3.26.2018 for 64-bit windows was used for visualization and knowledge graph analysis because it allows for the creation of multiple bibliometric networks and the application of multiple methods of analysis (Chen, 2004; Chen and Leydesdorff, 2014). The threshold setting was set at “*Top 50 N″* per slice, which allowed the selection of most cited items from each slice to form a network based on the choice of input value and multiple node types. Consequently, the top 50 most cited articles were displayed and ranked accordingly by CiteSpace. The “Time Slicing” was set to 1981–2021 and “Years per slice” at 1 year. To prune the generated network, the “Pruning” parameter was chosen. All term sources in Web of Science, including title, abstract, author keywords, and keywords plus, were chosen for text processing.

2.4.1.1 Dual Map Overlay

We used dual-map overlay to investigate the inter-domain specialty to specialty trends that connect research areas. The citation link trajectory reveals multi-disciplinary relationships. A change in trajectory from one to another indicates that a paper from one discipline was influenced by other articles from another discipline. Ovals represent the number of authors who have published in the field and the number of relevant papers that have been published. The width of the oval represents the author-to-author ratio, while the height of the oval represents the number of papers published. The retrieved literature was divided into two categories: 1) cited journals and 2) citing journals (i.e., the latter cited references from the former) (Chen and Leydesdorff, 2014).

2.4.1.2 Co-Citation Analysis

Co-citation analysis is used to determine the status of scientific development and changes in scientific structure. The co-citation analysis generates a science map with nodes, connections, and density values to show the main structure of selected variables (for this study: i) Author, ii) Journal, iii) Countries, iv) Institutions, and v) Articles) to obtain the cluster of co-citing variables, where a co-citation instance occurs when two sources are cited together in one paper (Chen 2004; Chen and Leydesdorff 2014; Aryadoust and Ang 2019).

A variable's quality was assessed using degree, centrality, and sigma (Chen et al., 2009; Chen et al., 2010). The degree value represents the number of citations a variable receives from another variable of the same type (e.g., the number of citations one author receives from another author), with a higher degree indicating more citations. Centrality is a measure of influence that shows the degree to which the same variables are close to each other, where variables with high centrality have a greater influence on the network because they connect more variables and thus more information and paths pass through them. Sigma is the sum of the centrality and burstness scores (described below), ranging from 0 to 1 where the highest value is associated with high value research articles (e.g. available raw data, scientifically analyzed data, etc.) (Chen et al. 2009; Chen et al., 2010).

2.4.1.3 Document Cluster Analysis

Based on the documents retrieved, multidimensional clustering was used to identify research clusters in focus areas. Because log-likelihood ratio (LLR) could provide the best results in terms of uniqueness and coverage, it was used to automatically extract the cluster label. "Timeline view" and "cluster view" were in the Document Cluster Analysis was used to visualize the network's shape and form. The "timeline view" displayed a vertical range of chronological time periods from left to right, whereas the "cluster view" displayed a spatial network of colour-coded and automatically labeled representations in a landscape format (Chen 2004; Chen and Leydesdorff 2014; Aryadoust and Ang 2019).

The modularity Q index, average silhouette metric, and centrality metric were used to assess the quality and homogeneity of the document cluster analysis, as well as the detected clusters (Chen et al., 2009; Chen et al., 2010). The modularity Q index ranges between 0 and 1, with larger index indicating higher reliability. The average silhouette metric has a value between −1 and 1, where values greater than 0 indicate greater homogeneity. Centrality is a measure of influence that shows the degree to which publications or journals stand between each other, where publications with high centrality have higher influence on the network as they connect more publications or journals and therefore more information and paths pass through them.

2.4.1.4 Burstness Analysis

Citation burstness and sigma, both temporal metrics, were used to identify influential publications and top keywords. Burst detection is defined as a sudden increase in the number of citations for a specific article, or "an abrupt elevation of the frequencies [of citations] over a specific time interval," as indicated by a red ring around the node (Chen et al., 2009; Chen et al., 2010). Sigma is the sum of the centrality and burstness scores, ranging from 0 to 1, with the highest sigma value associated with high-value research articles (Chen et al., 2009; Chen et al., 2010).

2.4.1.5 Knowledge Map Identification

The parameters for knowledge map identification methods include node, degree, burstiness, and centrality. The node is a parameter used to determine the frequency with which a variable has been cited, where a large node indicates a high number of citations, and the line is the connection between the nodes, indicating that these nodes appear in the same articles. Degree refers to the number of connections between variables in the knowledge map, with a higher Degree value indicating more communication and cooperation between the same variables (e.g. institutions, countries). The burstiness of a node is indicated by red rings surrounding it. It shows where the articles begin to "burst" and how strong the "burst" strength is. Purple rings indicate a node's centrality; a node with a high centrality indicates a strategic position and the ability to bridge different nodes in the chosen networks.

3 RESULTS

3.1 Descriptive Statistics

3.1.1 Evolution of Publications

Between January 1982 and June 2021, 2001 articles were published that contained research about the impact of climate change on aquatic production of one of the six species of interest. The number of publications increased from 1 in 1982 to 205 by 2020 (**Figure 2**). The number of published articles increased annually, with a 10-years average of 134 publications per year.

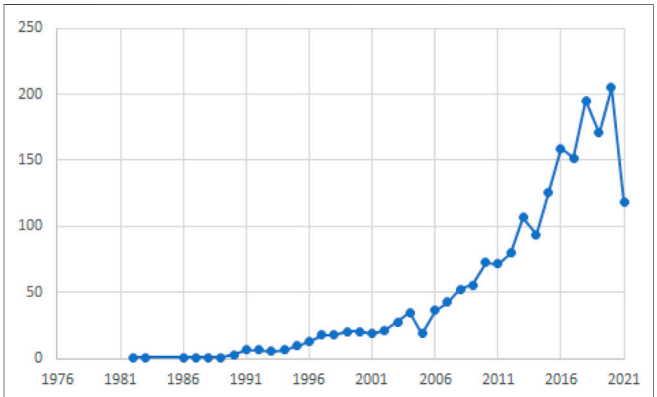

FIGURE 2 | Number of research articles regarding climate change impacts on aquatic production of the top six aquaculture species published annually since 1980.

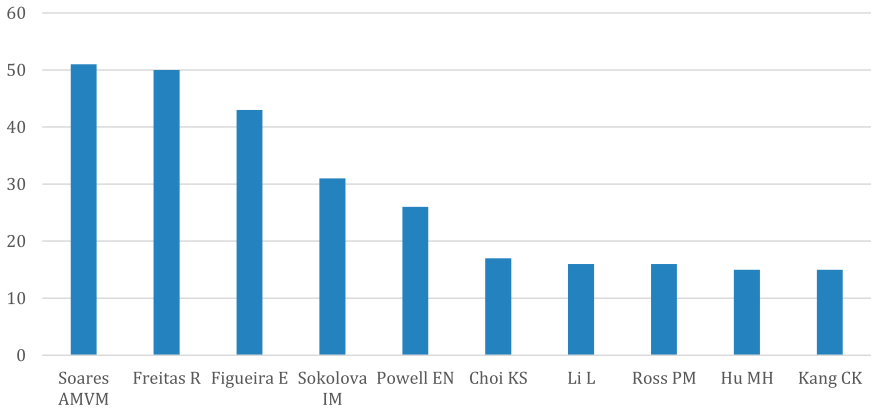

FIGURE 3 | Top ten most productive authors for the time period 1980 to 2021, regarding research on climate change impacts on aquatic production of six aquaculture species.

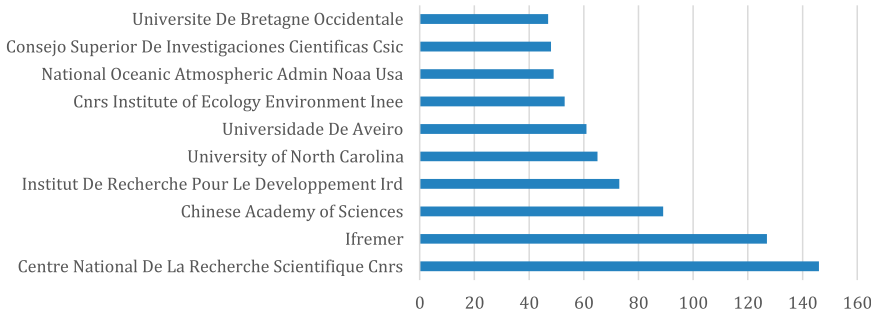

FIGURE 4 | Number of publications from the top ten (of 1806) institutions that have researched impacts of climate change on the top six aquaculture species.

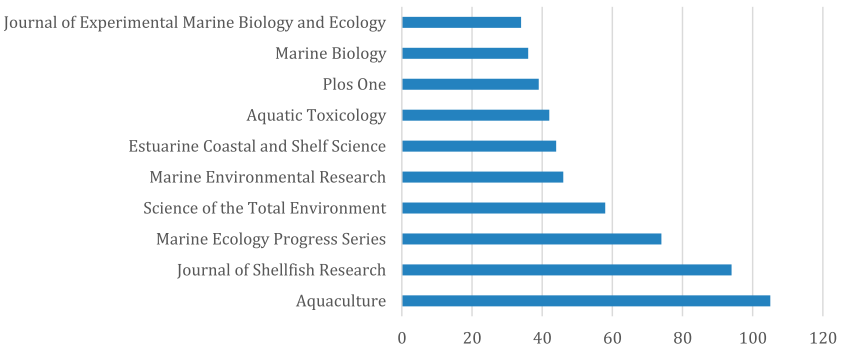

FIGURE 5 | Number of publications from the top ten journals containing research about climate change impacts on aquatic production of the top six aquaculture species published between 1980 and 2021.

3.1.2 Productive Authors

Since 1980, only five authors produced more than 20 publications related to the effect of climate change on the production of the world's top six cultured species (**Figure 3**). Out of a total of 6,762 authors, only 1,507 authors (22.29%) contributed more than one article. Soares AMVM published the most publications with 51, followed by Freitas R (50 publications) and Figueira E (43 publications).

3.1.3 Top Institutions

Figure 4 shows the top ten institutions in terms of total publications. With 146 publications, the Centre National De

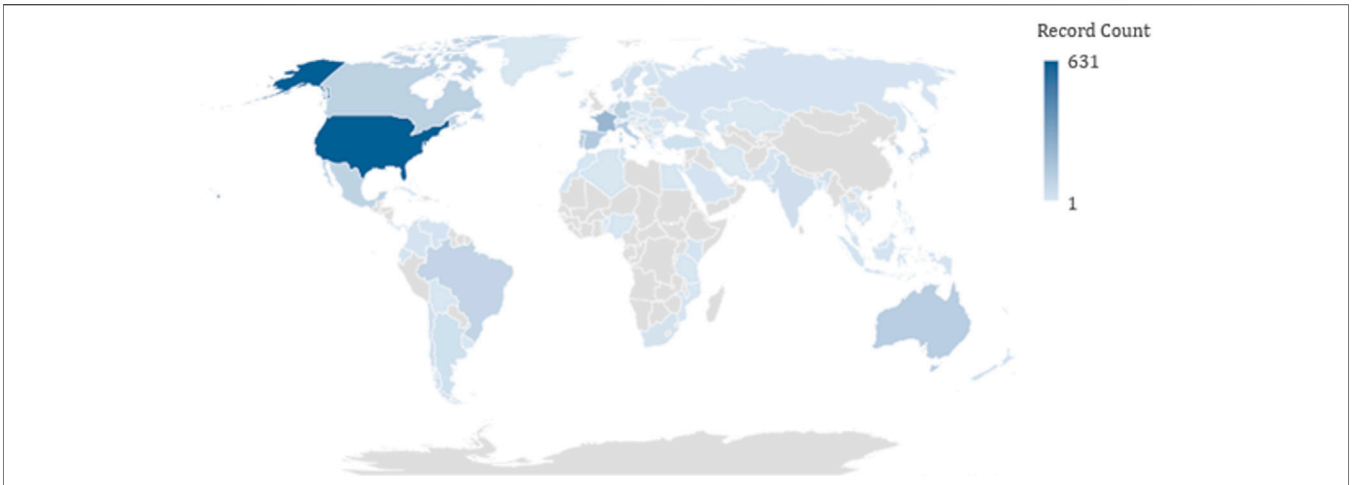

FIGURE 6 | Number of publications produced from countries around the world. Dark blue represents the highest total number of publications, whereas lighter shades represent fewer publications.

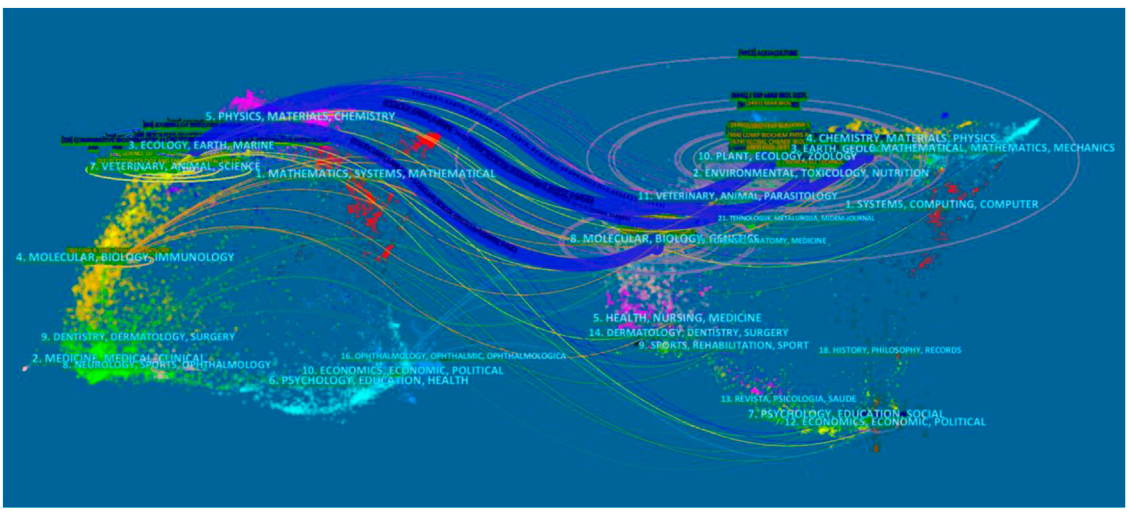

FIGURE 7 | Dual map overlay on impact of climate change on major aquatic species production in the world. Points represent literature, ellipses represent groups of subject matter, and directional lines represent connection between subjects. Each unique discipline is represented by a different colour.

La Recherche Scientifique Cnrs, France was the leading institution, followed by Ifremer (France) (127 publications) and the Chinese Academy of Sciences (China) (89 publications). Institutions produced 1.1 articles on average.

3.1.4 Productive Journals

Figure 5 illustrates the top ten journals by number of publications. In total, we identified eligible articles from 466 journals. Of these, Aquaculture had the most publications (105), followed by Journal of Shellfish Research (94 publications), and Marine Ecology Progress Series (74 publications). On average, most journals produced 4.23 articles within the 38 years of publication (1982–2021).

3.1.5 Regional Distribution

Figure 6 shows the ranking of countries that have published research related to climate change and aquatic species production. The number of publications is scaled from one to 631 on a gradient from white to dark blue. There were 85 countries with relevant publications, where the top five countries accounted for 69.51% of total publications. The United States of America had the most publications (631), followed by China (291 publications), and France (224

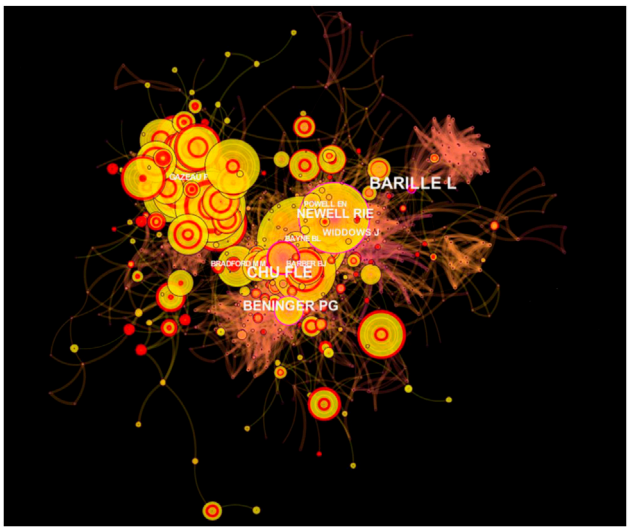

FIGURE 8 | Network of authors co-citation, where coloured circles represent author node and the lines connecting them represent connections.

publications). The remaining countries had a mean of 10.5 publications.

3.2 Scientometric Analysis

3.2.1 Dual-Map Overlay

Figure 7 illustrates a dual-map overlay for research on the global impact of climate change on major aquatic species production. Dual-map overlay identifies the most productive disciplines using the photovoice method and the intellectual foundation of this domain. Based on the thickness of the blue line in the map, "Ecology, Earth, and Marine" is the most productive discipline. The majority of the publications in "Ecology, Earth, Marine" were cited from four sub-disciplines: i)" Earth, Geology, Geophysics"; ii)" Environmental, Toxicology, Nutrition"; (iii) "Plant, Ecology, Zoology" and iv) "Molecular, Biology. Genetics".

3.2.2 Co-Citation Analysis

Co-citation analysis generates a science map that includes nodes, connections, and density values to show the main structure of a selected variable's development status and changes over time. The results of co-citation analysis for author, journal, country/region, institution, and article document are shown below.

3.2.2.1 Author Co-Citation Analysis

There were 736 nodes and 3,085 connections in the author co-citation network. The co-citation network density value was 0.0114, indicating that there is very little coordination and cooperation between authors. Density values represent the percentage of actual links between authors divided by the probability link. Higher density means higher connectedness between authors in these domain areas. The degree value represents the number of citations an author receives from another author for the same articles, where higher degrees indicate higher citations. Centrality is a measure of influence that shows the degree to which an author has on another's, where an author with high centrality in the network is also one that has a great influence on the domain area's behavior (e.g. Author A is cited by author B and author C, thus Author A is the center of information and paths for Author B and Author C must pass through). Sigma value is associated with high value research articles where any paper with sigma value more than 1 has high degree and centrality.

Figure 8 depicts authors that have a centrality score greater than 0.1, where font size increases as centrality score increases. Fu-Lin E. Chu was the most interconnected author, with a centrality score of 0.18, degree of 69, and a sigma of 26.62; in total Chu had 75 network connections (1.16 percent from overall connections). Laurent Barillé was the second most influential author, with a sigma score of 3.77, a centrality score of 0.19, and a degree score of 58. Frédéric Gazeau was the third most influential author (Degree: 32; Centrality: 0.19, Sigma: 3.28). **Table 2** shows the details for the top ten authors with the most influence in these fields.

TABLE 2 | The co-citation score for the top ten authors regarding research on climate change impacts on aquatic production of the top six aquaculture species.

Author	Degree	Centrality	Sigma
Fu-lin E. Chu	69	0.18	26.62
Laurent Barillé	58	0.19	3.77
Frédéric Gazeau	32	0.1	3.28
Peter A Gabbot	54	0.08	2.78
Eric N. Powell	40	0.1	2.22
Lars Tomanek	21	0.05	2.11
Carlos Ruiz Miguel	37	0.05	1.85
Widdows	35	0.11	1.75
Hans-Otto Pörtner	20	0.05	1.65
Velez C	20	0.03	1.60

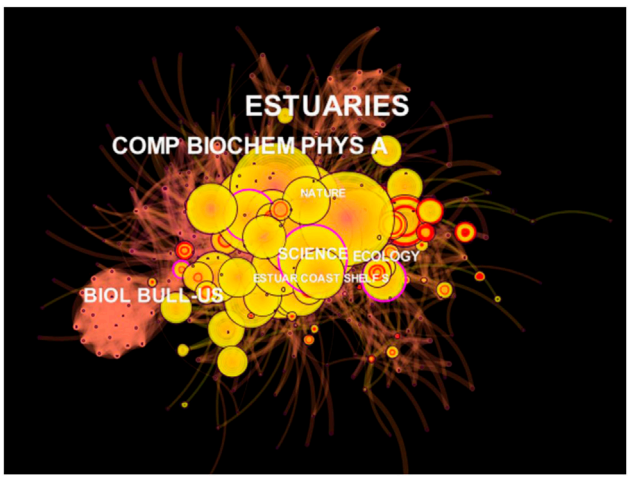

FIGURE 9 | Network of journal co-citation. Journal name sizes scales with centrality score (**Table 2**).

TABLE 3 | The co-citation score for the top ten journals publishing articles about climate change impacts on aquatic production of the top six aquaculture species.

Journal	Impact factor (Quartile WOS)	Degree	Centrality	Sigma
Journal of shellfish research	1.396 (Q3)	39	0.07	36.34
Estuaries	2.133 (Q1)	62	0.23	31.38
Biology Bulletin US	0.392 (Q4)	50	0.16	8.00
Biology Bulletin	0.392 (Q4)	35	0.07	4.98
Oceanologica Acta	1.823 (Q2)	21	0.06	2.53
Ecological Monographs	10.315 (Q1)	26	0.04	2.25
Veliger	0.125 (Q4)	37	0.08	1.96
Analytical Biochemistry	3.365 (Q2)	20	0.04	1.94
Geochimica et Cosmochimica Acta	5.01 (Q1)	22	0.04	1.92
Aquatic Living Resources	1.885 (Q1)	24	0.04	1.88

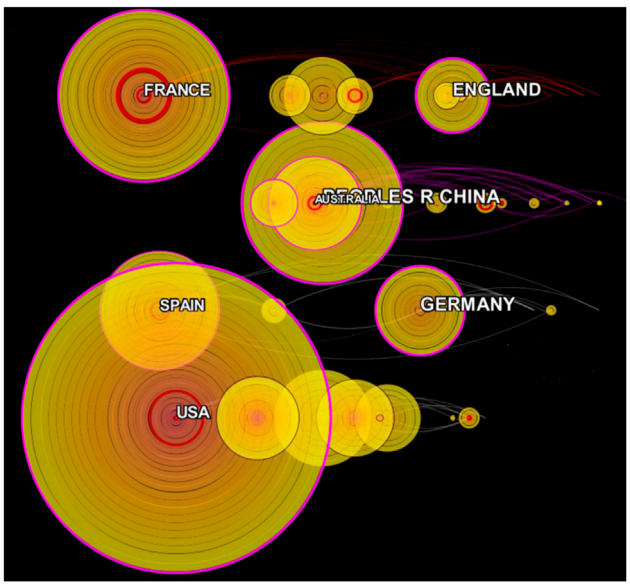

FIGURE 10 | Network of country/region co-citation analysis where each node represents a country, and lines represent each country's cooperation with another. Node size reflects centrality score (**Table 4**); only countries with centrality scores >0.1 are shown here.

3.2.2.2 Journal Co-Citation Analysis

Figure 9 illustrates the knowledge map for the journal co-citation analysis, including only journals with centrality scores greater than 0.1. The journal co-citation network had 336 nodes, 1731 connections, and a density of 0.0308. With a sigma score of 36.34, Journal of Shellfish Research (IF:1.396; Q3) was the most influential journal. The second and third most influential journals were Estuaries (IF: 2.133; Q1) and Biology Bulletin US (IF: 0.392; Q4), which had sigma scores of 31.38 and 8.00, respectively. **Table 3** shows the details for the top ten journals with the highest influence.

3.2.2.3 Countries/Region Co-Citation Analysis

Figure 10 demonstrates a network of co-citations based on the countries/regions of lead authors to obtain a more comprehensive analysis of country distribution and cooperation in field areas.

TABLE 4 | The co-citation score of the top ten countries involved in publishing research about the impacts of climate change on the top six aquaculture species.

Country/Region	Degree	Centrality	Sigma
United States of America	19	0.21	72.14
France	21	0.21	18.00
Spain	19	0.19	3.81
Australia	15	0.14	1.72
Japan	7	0.05	1.21
Sweden	11	0.02	1.09
Scotland	9	0.02	1.06
Argentina	8	0.01	1.03
China	17	0.23	1.00
Germany	20	0.23	1.00

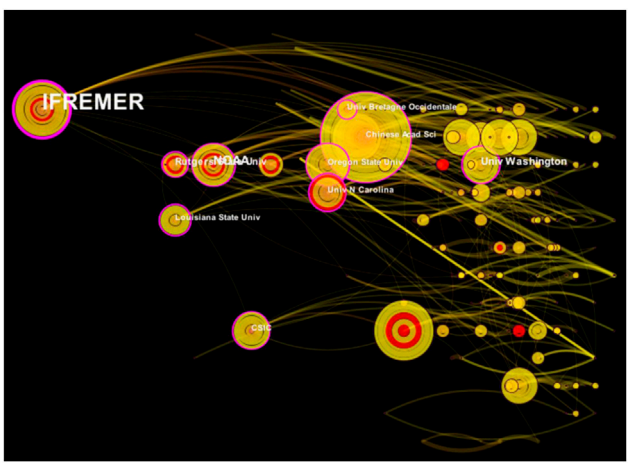

FIGURE 11 | Network of institutions co-citation analysis where each node represents an institution and yellow lines represent cooperation. Only institutions with a centrality score greater than 0.1 are shown.

Each node represents a country, and the lines represent each country's cooperation with another. The size of the nodes reflects the country's centrality score, and only countries with a centrality score greater than 0.1 are shown in **Figure 10**. The co-citation network of countries/regions has 52 nodes, 189 connections, and a density of 0.1425.

TABLE 5 | Co-citation scores from the top ten institutions involved in research on climate change impacts on aquatic production of six aquaculture species.

Institutions	Country	Degree	Centrality	Sigma
Ifremer	France	21	0.3	22.53
University of North Carolina at Chapel Hill	United States of America	11	0.11	3.05
Rutgers University	United States of America	10	0.14	2.53
National Oceanic and Atmospheric Administration	United States of America	13	0.17	2.50
Université de Bretagne Occidentale	France	10	0.11	1.53
The University of Maryland	United States of America	9	0.08	1.43
University of Aveiro	Portugal	9	0.07	1.31
Old Dominion University	United States of America	3	0.01	1.05
Sydney Institute of Marine Science	Australia	3	0.01	1.04
The University of Southern Mississippi	United States of America	3	0	1.01

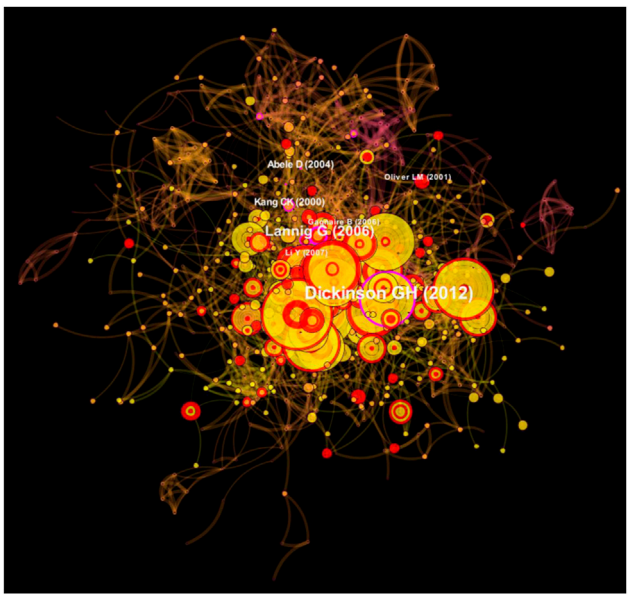

FIGURE 12 | Network of document co-citation analysis where only articles with centrality scores greater than 0.1 are shown.

Table 4 lists the top ten countries by co-citation score. The United States of America has the greatest influence among countries focusing on climate change and aquatic production research. This is based on a sigma score of 72.14, while France ranked second with a sigma score of 18.00, and Spain ranked third with a sigma score of 3.81. To improve the sigma score and gain more citations, a country/region should improve paper quality and strengthen collaboration with others.

3.2.2.4 Institution Analysis

Figure 11 shows the analysis of cooperation among institutions, where each node represents an institution and the yellow lines between them represents cooperation. For ease of display, we only show institutions with a centrality score greater than 0.1. The network has 283 nodes, 371 connections, and a density of 0.0093. Ifremer from France had the highest sigma score (22.53), followed by The University of North Carolina at Chapel Hill (3.05), and Rutgers University (2.53). Interestingly, although our focus was on global research, the most influential universities were primarily located in France and the United States of America. This suggests the need for increased collaboration from institutions around the world. **Table 5** shows the co-citation scores from the top ten institutions.

3.2.2.5 Document Citation Analysis

Figure 12 illustrates document co-citation analysis for research areas; the network had 899 nodes and 2,289 connections, with a density of 0.0057. Only articles with a centrality score greater than 0.1 were listed, alphabetically. A "central" article plays a mediating role in our field of interest.

Table 6 displays the top ten most influential scientific publications according to the sigma score. Dickinson et al. (2012) had the most influential article with a sigma score of 4.99, and was titled "Interactive effects of salinity and elevated CO_2 levels on juvenile eastern oysters, *Crassostrea virginica*". Lannig et al. (2006) had the second highest sigma value. Their study was titled "Temperature-dependent stress response in *Crassostrea virginica*: Pollution reduces temperature tolerance in oysters" and was published in Aquatic Toxicology. Doney et al. (2009), published in Annual Review of Marine Science, had the third most influential article with a sigma score of 2.08. Their article was titled "Ocean Acidification: The Other CO2 Problem."

3.2.3 Document Cluster Analysis

The modularity Q index and the average silhouette metric for the Document Cluster Analysis was 0.8337 and 0.9201, respectively. This suggests a high level of reliability and homogeneity for the network. Our analysis yielded a total of 19 co-citation clusters, of which seven are summarized in **Figure 13**. Each cluster was labeled and then numbered and ranked according to size, where #0 was the largest cluster. The solid yellow line within each cluster represents the cluster's lifetime. Text mining and a keyword analysis algorithm in CiteSpace software were used to generate cluster labels, then the loglikelihood ratio (LLR) was used to name these clusters.

Table 7 summarizes the seven major clusters identified by Document Cluster analysis, where each cluster represents a different research topic and its size is equal to the number of publications it has. Each of the seven clusters has more than 30 publications, with Cluster #0 having the most (118 publications).

TABLE 6 | Co-citation scores for the top ten articles related to research on climate change impacts on the production of the top six aquaculture species.

Article title	References	Degree	Centrality	Sigma
Interactive effects of salinity and elevated CO_2 levels on juvenile eastern oysters, *Crassostrea virginica*	Dickinson et al. (2012)	17	0.27	4.99
Temperature-dependent stress response in oysters, *Crassostrea virginica*: Pollution reduces temperature tolerance in oysters	Lannig et al. (2006)	18	0.22	4.11
Ocean Acidification: The Other CO_2 Problem	Doney et al. (2009)	32	0.07	2.08
Storage metabolism in the Pacific oyster (*Crassostrea gigas*) in relation to summer mortalities and reproductive cycle (West Coast of France)	Berthelin et al. (2000)	14	0.09	2.04
Oyster Reefs at Risk and Recommendations for Conservation, Restoration, and Management	Beck et al. (2011)	14	0.06	2.03
Proteomic response to elevated P_{CO2} level in eastern oysters, *Crassostrea virginica*: evidence for oxidative stress	Tomanek et al. (2011)	16	0.06	1.93
Elevated level of carbon dioxide affects metabolism and shell formation in oysters *Crassostrea virginica*	Beniash et al. (2010)	19	0.06	1.91
Impacts of ocean acidification on marine shelled molluscs	Gazeau et al. (2013)	21	0.04	1.81
Effects of temperature and salinity on haemocyte activities of the Pacific oyster, *Crassostrea gigas* (Thunberg)	Gagnaire et al. (2006)	26	0.12	1.62
Synergistic impacts of heat shock and spawning on the physiology and immune health of *Crassostrea gigas*: an explanation for summer mortality in Pacific oysters	Li et al. (2007)	6	0.13	1.6

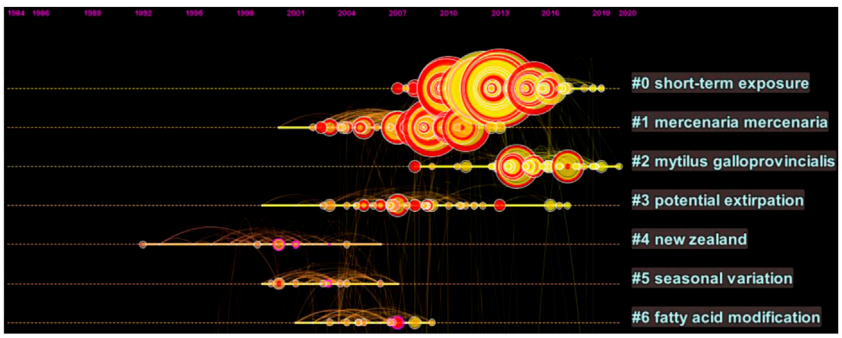

FIGURE 13 | Summary of seven of the 19 identified document cluster lifetimes (solid lines). Cluster labels were generated from CiteSpace. Circle size corresponds to cluster size (i.e. number of publications).

TABLE 7 | The seven major clusters that emerged from Document Co-citation Analysis. Size represents the number of publications in a cluster, and silhouette score indicates levels of homogeneity. Labels were derived from log likelihood ratios (LLR).

ClusterID	Size	Silhouette	Label (LLR)	Year average
0	118	0.82	Short-term exposure	2012
1	62	0.947	*Mercenaria mercenaria*	2007
2	59	0.84	*Mytilus galloprovincialis*	2015
3	58	0.946	potential extirpation	2007
4	45	0.867	new zealand	1998
5	42	0.898	seasonal variation	2002
6	38	0.907	fatty acid modification	2005

Cluster silhouette score ranged from 0.814 to 0.968, indicating a high degree of homogeneity among publications in each cluster (silhouette score ranges from -1 to 1, where scores higher than 0 are considered homogenous).

3.2.4 Burst Analysis

To identify the most influential or landmark publications as well as keywords, we used a burst analysis; trends among studies and keywords are described below.

3.2.4.1 Document Burst

Table 8 shows the top ten publications with the most powerful citation bursts, where the duration of each burst is shown in the rightmost columns. A burst reflects the emergence of a keyword in a publication during a specific time period. The blue line represents the timeline (from 1982 to 2021), while the red line represents the burst period. The publication with the most recent and strongest burst was Gazeau et al. (2013), which is the current hotspot publication (strength = 15.82, 2016–2021).

3.2.4.2 Keyword Burst

Table 9 displays the keywords with the highest citation burst. Keyword analysis has been used to detect emerging trends and research area hotspots over time. The burst reflects the emergence of a keyword in a particular subject area during a specific time period. As above, the blue line represents the timeline (from 1982 to 2021), while the red line represents the burst period. Beginning in 1992 and ending in 2005, the word "seasonal variation" had the highest burst strength (16.17). The next top two keywords were "perkinsus marinus" (Strength = 11.48, 1994–2012) and "seawater acidification" (Strength = 10.32, 2016–2021). Although one of the shorter bursts (5 years), "seawater acidification" had the most recent burst time period,

TABLE 8 | Top ten publications with the strongest citation bursts between 1982 and 2021. Red sections in the timeline represent the burst period.

Title	References	Strength	Begin	End	1982–2021
Impacts of ocean acidification on marine shelled molluscs	Gazeau et al. (2013)	15.82	2016	2021	—
Impact of Ocean Acidification on Energy Metabolism of Oyster, *Crassostrea gigas*-Changes in Metabolic Pathways and Thermal Response	Lannig et al. (2010)	13.84	2013	2018	—
The oyster genome reveals stress adaptation and complexity of shell formation	Wang et al. (2012)	12.02	2015	2021	—
Elevated level of carbon dioxide affects metabolism and shell formation in oysters *Crassostrea virginica*	Beniash et al. (2010)	11.49	2013	2018	—
Proteomic response to elevated P_{CO2} level in eastern oysters, *Crassostrea virginica*: evidence for oxidative stress	Tomanek et al. (2011)	11.28	2015	2019	—
Impact of elevated CO_2 on shellfish calcification	Gazeau et al. (2007)	10.73	2009	2014	—
Ocean Acidification: The Other CO_2 Problem	Doney et al. (2009)	10.35	2012	2017	—
Impacts of ocean acidification on marine organisms: quantifying sensitivities and interaction with warming	Kroeker et al. (2013)	10.1	2015	2021	—
Ecosystem effects of ocean acidification in times of ocean warming: a physiologist's view	Pörtner, (2008)	9.71	2012	2016	—
Seasonal variation in weight and biochemical composition of the Pacific oyster, *Crassostrea gigas* in relation to the gametogenic cycle and environmental conditions of the Bizert lagoon, Tunisia	Dridi et al. (2007)	9.63	2009	2015	—

TABLE 9 | Top ten keywords with strongest citation burst for the time period 1982 to 2021. Red section on timelines represents the period of the burst.

Keywords	Strength	Begin	End	1982–2021
Seasonal variation	16.17	1992	2005	—
Perkinsus marinus	11.48	1994	2012	—
seawater acidification	10.32	2016	2021	—
Gametogenesis	8.38	1992	2010	—
Ostrea eduli	7.92	1996	2008	—
Crassostrea virginica	7.63	1995	2000	—
biochemical composition	7.21	1993	2007	—
Mortality	6.9	2007	2012	—
Cadmium	6.43	2003	2015	—

continuing into 2021, indicating a more recent emerging interest for this topic.

4 DISCUSSION

Our study aimed to present a scientometric analysis for research on the effects of climate change on the top major aquatic production. We discuss our results in detail below.

4.1 Research Question Discussion

4.1.1 RQ1: What Are the Overall Publication Trends in Terms of Publication Output?

To answer our first research question, we performed a descriptive analysis on the number of publications, published journals, authors, universities/institutes, and the countries/regions of affiliation. The number of articles published increased annually, with a 10-years average of 134 publications per year. The United States of America had the greatest number of papers published in the field, while France had the second highest number of publications. With 13.64 total publications, Centre National De La Recherche Scientifique Cnrs and Ifremer from France together had the highest publication rate for institutions. This demonstrates that developed countries such as the United States of America and France are leading in this field. While other countries may have a relatively large number of publications, such as China, they have yet to emerge as prominent research institutions and/or scholars. This result may be due to France and the United States having more resources to conduct scientific analyses. As such, we strongly suggest that more international scientific research exchanges and collaboration be conducted in the future.

4.1.2 RQ2: Where is This Research Area Situated on the Map of Web of Sciences Database?

Publications were largely situated within the discipline "Ecology, Earth, and Marine" and there were few publications in other disciplines. While this result may not be surprising given the nature of the research, we suggest that multidisciplinary studies would be beneficial to fully understand the impact of climate change on aquatic production. For example, research joining ecology and economics would give deeper insights on the economic effects of climate change.

4.1.3 RQ3: Who Are the Dominant Knowledge Carriers in These Areas?

To answer our third research question, a co-citation analysis of the author, journal, country, institutions, and articles was performed. We found that Fu-Lin E. Chu was the most influential author, with a focus on nutrition and host/parasite interactions in shellfish and fish. Laurent Barillé was the second most influential author, with a background in multi- and hyperspectral remote sensing of intertidal areas. Frédéric Gazeau, the third most influential author, studied coastal metabolism, the effects of ocean acidification and warming on various marine organisms, and the use of techniques to study the effects of ocean acidification on marine communities. The work from these top three researchers demonstrates the multi-disciplinarity of climate change and aquatic production research. It is critical for the experts in these fields to engage with others in different focus areas to build connections between sub-disciplines. For example, work on host/parasite interactions would greatly benefit from research on ocean acidification–does increasing acidification change host/parasite interactions? Increased inter-disciplinary cooperation would help address

such questions and give a better picture of climate change impacts on aquacultured species.

Our analysis on scientific journals revealed that ecology and biology research dominated the research areas. Some of the most prestigious journals in biology science have published articles in this area. For example, the Journal of Shellfish Research, Estuaries, and Biology Bulletin US were among the most influential journals. For influential institutions, Ifremer from France, the University of North Carolina, and Rutgers University from the United States of America were the most influential. As a result, it is not surprising that France and the United States ranked first and second in the co-citation analysis results discussed above. However, this again demonstrates that research affiliations are unbalanced, with most research conducted by France and the United States. Because research on climate change impacts affects the entire world, it is clear that collaboration within this research domain would be beneficial.

Of the top ten most influential scientific publications, Matoo's (2013) article was the most influential. Matoo (2013) investigated the interactions of salinity and partial pressure of CO2 (PCO2) on biomineralization and energy homeostasis in juvenile *Crassostrea virginica*, a common estuarine bivalve. According to the study, the combined effects of elevated PCO2 and fluctuating salinity may endanger the survival of eastern oysters by weakening their shells and increasing energy consumption. Their results suggest that the production of these bivalves may be at risk as climate change may affect both PCO2 and salinity. Lannig et al. (2006) had the article with the second highest co-citation score. Their research assessed how temperature and a toxic metal, cadmium (Cd), affects energy metabolism. They found that oysters exposed to elevated temperature, but not Cd, showed no significant change in condition, survival rate, or lipid peroxidation. However, those exposed to both Cd and temperature stress died quickly. Doney, Fabry, Feely, and Kleypas (2009) had the third highest co-citation score. Their work discussed the impact of decreased calcium carbonate saturation on shell-forming marine organisms ranging from plankton to benthic molluscs, echinoderms, and corals. Together, these three works demonstrate the impacts of continued ocean warming and ocean acidification on aquatic organisms, especially for shell-forming species. It is clear there are interactive effects of ocean temperature, acidification, and environmental metals that warrant further investigation. Regardless, their results support the increasing need to decrease effects of climate change to maintain current production of shelled organisms.

4.1.4 RQ4: What Are the Dominant Topics/Clusters, and What is Their Temporal Evolution?

To answer our fourth question, we used a document cluster analysis which yielded a total of 19 co-citation clusters. Publications were assigned to each cluster because they were cited by a similar group of publications, indicating a co-citation relationship. According to our results, the dominant research topics and directions were "short-term exposure"; "*Mercenaria* mercenaria"; "*Mytilus galloprovincialis*"; "potential extirpation"; "New Zealand"; "seasonal variation"; and "fatty acid modification." This indicates that the majority of research focuses on two species, particularly from New Zealand, and on the effects of relatively short time periods of exposure. While it is important to study the short-term exposure to stressors in marine organisms, climate change is likely to have longer term impacts, and as such there is a need to understand how long-term stress will impact species.

4.1.5 RQ5: What Are the impactful Publications and Keywords for These Areas?

The document burst analysis showed a pattern of new research topics emerging, with previous burst publications gradually being replaced by more recent publications. Gazeau et al. (2007) investigated the calcification rates of edible mussels (*Mytilus edulis*) and the Pacific oyster (*Crassostrea gigas*), which decreased linearly as pCO2 increased. Gazeau et al. (2013) had the most recent burst citation, and studied pteropods, which have a negative relationship with the level of ocean acidification. The blood of shelled molluscs may have lower pH, which can affect several physiological processes (e.g., respiration, excretion, etc.) and, in some cases, increase their mortality over time. The shift in focus from the previous study, which focused on impact, to the current study, which focused on resilience, demonstrates an increased understanding of the issues in the research areas. It also indicates that the current body of research is focusing on understanding acidification effects. This is important to understand for future management of important shelled species that are cultured. Again, the most important papers identify effects of ocean acidification as being significant and important to mitigate.

5 CONCLUSION

In general, ocean acidification was identified as a reoccurring important climate change impact to understand, particularly with respect to the production of aquatic species. With the world still struggling to find effective solutions to combat climate change, research on climate action and aquatic production is increasingly important to mitigate or minimize environmental effects on the aquaculture industry. Here, we have compiled a cluster of related research from different disciplines and noted important research gaps and future directions. Most of the research focused on ocean acidification effects, but next we need to understand how to mitigate such effects. There is a significant gap that requires further investigation and international collaboration.

Our study only obtained papers from Web of Science (WOS) databases, which may have resulted in publication bias. However, WOS is regarded as having higher publication standards because its database is geared towards science and social sciences, and because it has larger databases with a broader scope than other available datasets (Bar-Ilan, 2008; Adriaanse and Rensleigh, 2013). Future research could compare other databases with WOS to map these research areas and perhaps identify missing links. Additionally, we used CiteSpace software rather than collecting data manually, thus some irrelevant subjects may have been included in the analysis. Still, CiteSpace allows our analysis to be reproducible, and striking a balance between

stringent criteria and over-excluding specific studies is difficult. Future research with a high precision goal should consider using more stringent keyword searches or reviewing exported data manually to reduce the likelihood of irrelevant studies.

In our co-citation analyses, only the names of the primary (first) authors were used. Although citing publications did not have such a restriction, databases of cited publications downloaded from WoS did not include the names of other contributing authors. If these databases made more author names available, the co-citation analysis could produce different results, possibly identifying more collaboration than we detected. Regardless, our study offers a comprehensive view on the current body of research studying the effects of climate change on the production of top aquatic species. We clearly demonstrate the need for more international collaboration. Addressing climate change impacts is important to the sustainable research agenda in conjunction with achieving the SDGs goal by 2030. We also suggest that studies in disciplines other than "Ecology, Earth, and Marine" should be encouraged in the future, as they may offer important insights that would otherwise be overlooked (e.g. economic perspectives).

AUTHOR CONTRIBUTIONS

All authors conceptualized this study. MNA and MM formulated the research objectives, whereas MNA pointed out the inclusion and exclusion criteria under the supervision of other two authors MAG and YS The expert in the subject is MNA and MAG Then, MM performed the searches. YS proof-read the article and reviewed the overall manuscript scientifically. All authors have read and agreed to the published version of the manuscript.

FUNDING

The Department of Higher Education, Ministry of Higher Education Malaysia, provided funding through the Long Term Research Grant Scheme (LRGS) program (LRGS/1/2020/UMT/01/1; LRGS UMT Vot No. 56040) titled 'Ocean climate change: potential risk, impact, and adaptation towards marine and coastal ecosystem services in Malaysia.'

ACKNOWLEDGMENTS

The first author wishes to express his gratitude to the Sustainable Ocean Alliance (SOA) and the Environmental Defense Fund (EDF) in the United States of America (United States) for his inaugural fellowship on Leadership for Climate Resilient Fisheries (LCRF).

SUPPLEMENTARY MATERIAL

The Supplementary Material for this article can be found online at: https://www.frontiersin.org/articles/10.3389/fenvs.2022.905428/full#supplementary-material

REFERENCES

Aryadoust, V., and Ang, B. H. (2019). Exploring the Frontiers of Eye Tracking Research in Language Studies: A Novel Co-Citation Scientometric Review. *Comput. Assist. Lang. Learn.* 34, 898–933. doi:10.1080/09588221.2019.1647251

Azra, M. N., Noor, M. I. M., Ikhwanuddin, M., and Ahmed, N. (2021). "Global Trends on Covid-19 and Food Security Research: A Scientometric Study," in *Advances in Food Security and Sustainability*. Editor M. Cohen. 6th Edition, 1–33. Cambridge, Massachusetts, Academic Press. Available at: (https://www.ncbi.nlm.nih.gov/pmc/articles/PMC8426152/pdf/main.pdf). doi:10.1016/bs.af2s.2021.07.005

Azra, M. N., Noor, M. I. M., Sung, Y. Y., Dawood, M. A. O., and Ghaffar, M. A. (2022). Trends and Developments in Thermal Tolerance: A Scientometric Research Study. *J. Ther. Biol.* 106, 103234. doi:10.1016/j.jtherbio.2022.103234

Azzeri, A., Ching, G. H., Jaafar, H., Mohd Noor, M. I., Razi, N. A., Then, A. Y.-H., et al. (2020). A Review of Published Literature Regarding Health Issues of Coastal Communities in Sabah, Malaysia. *Ijerph* 17, 1533. doi:10.3390/ijerph17051533

Bar-Ilan, J. (2008). Which H-Index? - A Comparison of WoS, Scopus and Google Scholar. *Scientometrics* 74, 257–271. doi:10.1007/s11192-008-0216-y

Beck, M. W., Brumbaugh, R. D., Airoldi, L., Carranza, A., Coen, L. D., Crawford, C., et al. (2011). Oyster Reefs at Risk and Recommendations for Conservation, Restoration, and Management. *BioScience* 61, 107–116. doi:10.1525/bio.2011.61.2.5

Beniash, E., Ivanina, A., Lieb, N., Kurochkin, I., and Sokolova, I. (2010). Elevated Level of Carbon Dioxide Affects Metabolism and Shell Formation in Oysters Crassostrea Virginica (Gmelin). *Mar. Ecol. Prog. Ser.* 419, 95–108. doi:10.3354/meps08841

Berthelin, C., Kellner, K., and Mathieu, M. (2000). Storage Metabolism in the Pacific Oyster (*Crassostrea gigas*) in Relation to Summer Mortalities and Reproductive Cycle (West Coast of France). *Comp. Biochem. Physiology Part B Biochem. Mol. Biol.* 125, 359–369. doi:10.1016/S0305-0491(99)00187-X

Callaway, R., Shinn, A. P., Grenfell, S. E., Bron, J. E., Burnell, G., Cook, E. J., et al. (2012). Review of Climate Change Impacts on Marine Aquaculture in the UK and Ireland. *Aquat. Conserv. Mar. Freshw. Ecosyst.* 22, 389–421. doi:10.1002/aqc.2247

Chen, C., Chen, Y., Horowitz, M., Hou, H., Liu, Z., and Pellegrino, D. (2009). Towards an Explanatory and Computational Theory of Scientific Discovery. *J. Inf.* 3, 191–209. doi:10.1016/j.joi.2009.03.004

Chen, C., Ibekwe-SanJuan, F., and Hou, J. (2010). The Structure and Dynamics of Cocitation Clusters: A Multiple-Perspective Cocitation Analysis. *J. Am. Soc. Inf. Sci.* 61, 1386–1409. doi:10.1002/asi.21309

Chen, C., and Leydesdorff, L. (2014). Patterns of Connections and Movements in Dual-Map Overlays: A New Method of Publication Portfolio Analysis. *J. Assn Inf. Sci. Tec.* 65, 334–351. doi:10.1002/asi.22968

Chen, C. (2004). Searching for Intellectual Turning Points: Progressive Knowledge Domain Visualization. *Proc. Natl. Acad. Sci. U.S.A.* 101, 5303–5310. doi:10.1073/pnas.0307513100

Chen, C., and Song, M. (2019). Visualizing a Field of Research: A Methodology of Systematic Scientometric Reviews. *Plos One* 14, e0223994. doi:10.1371/journal.pone.0223994

Cheung, W. W. L., Lam, V. W. Y., Sarmiento, J. L., Kearney, K., Watson, R., Zeller, D., et al. (2010). Large-Scale Redistribution of Maximum Fisheries Catch Potential in the Global Ocean Under Climate Change. *Glob. Change Biol.* 16, 24–35. doi:10.1111/j.1365-2486.2009.01995.x

Dickinson, G. H., Ivanina, A. V., Matoo, O. B., Pörtner, H. O., Lannig, G., Bock, C., et al. (2012). Interactive Effects of Salinity and Elevated CO_2 Levels on Juvenile Eastern Oysters, Crassostrea Virginica. *J. Exp. Biol.* 215, 29–43. doi:10.1242/jeb.061481

Doney, S. C., Fabry, V. J., Feely, R. A., and Kleypas, J. A. (2009). Ocean Acidification: The Other CO_2 Problem. *Annu. Rev. Mar. Sci.* 1, 169–192. doi:10.1146/annurev.marine.010908.163834

Dridi, S., Romdhane, M. S., and Elcafsi, M. h. (2007). Seasonal Variation in Weight and Biochemical Composition of the Pacific Oyster, *Crassostrea gigas* in Relation to the Gametogenic Cycle and Environmental Conditions of the Bizert Lagoon, Tunisia. *Aquaculture* 263, 238–248. doi:10.1016/j.aquaculture.2006.10.028

FAO (2020). *Food and Agriculture Organization of the United Nation (FAO), 2020 Edition of the State of World Fisheries and Aquaculture: Sustainability in Action*. Rome, Italy: The Publishing Group (OCCP). 244. doi:10.4060/ca9229en

FAO (2021). Publications: The Collection of the State of World Fisheries and Aquaculture (SOFIA). Available at: http://www.fao.org/fishery/publications/sofia/en (Assessed at 1st September, 2021).

FAO (2011) *World Aquaculture 2010. FAO Fisheries and Aquaculture Technical Paper: 500/1. Aquaculture Service: Fisheries and Aquaculture Resources Use and Conservation Division*. Rome: FAO Fisheries and Aquaculture Department, Food And Agriculture Organization Of The United Nations. Available at: http://www.fao.org/3/ba0132e/ba0132e.pdf.

Froehlich, H. E., Gentry, R. R., and Halpern, B. S. (2018). Global Change in Marine Aquaculture Production Potential Under Climate Change. *Nat. Ecol. Evol.* 2, 1745–1750. doi:10.1038/s41559-018-0669-1

Gagnaire, B., Frouin, H., Moreau, K., Thomas-Guyon, H., and Renault, T. (2006). Effects of Temperature and Salinity on Haemocyte Activities of the Pacific Oyster, *Crassostrea gigas* (Thunberg). *Fish Shellfish Immunol.* 20, 536–547. doi:10.1016/j.fsi.2005.07.003

Gazeau, F., Parker, L. M., Comeau, S., Gattuso, J.-P., O'Connor, W. A., Martin, S., et al. (2013). Impacts of Ocean Acidification on Marine Shelled Molluscs. *Mar. Biol.* 160, 2207–2245. doi:10.1007/s00227-013-2219-3

Gazeau, F., Quiblier, C., Jansen, J. M., Gattuso, J.-P., Middelburg, J. J., and Heip, C. H. R. (2007). Impact of Elevated CO_2 on Shellfish Calcification. *Geophys. Res. Lett.* 34, L07603. doi:10.1029/2006GL028554

Heasman, K. G., Scott, N., Ericson, J. A., Taylor, D. I., and Buck, B. H. (2020). Extending New Zealand's Marine Shellfish Aquaculture into Exposed Environments - Adapting to Modern Anthropogenic Challenges. *Front. Mar. Sci.* 7, 565686. doi:10.3389/fmars.2020.565686

Kroeker, K. J., Kordas, R. L., Crim, R., Hendriks, I. E., Ramajo, L., Singh, G. S., et al. (2013). Impacts of Ocean Acidification on Marine Organisms: Quantifying Sensitivities and Interaction with Warming. *Glob. Change Biol.* 19, 1884–1896. doi:10.1111/gcb.12179

Lannig, G., Eilers, S., Portner, H. O., Sokolova, I. M., and Bock, C. (2010). Impact of Ocean Acidification on Energy Metabolism of Oyster, *Crassostrea gigas*—Changes in Metabolic Pathways and Thermal Response. *Marine Drugs* 8, 2318–2339. doi:10.3390/md8082318

Lannig, G., Flores, J. F., and Sokolova, I. M. (2006). Temperature-Dependent Stress Response in Oysters, *Crassostrea Virginica*: Pollution Reduces Temperature Tolerance in Oysters. *Aquat. Toxicol.* 79, 278–287. doi:10.1016/j.aquatox.2006.06.017

Li, Y., Qin, J. G., Abbott, C. A., Li, X., and Benkendorff, K. (2007). Synergistic Impacts of Heat Shock and Spawning on the Physiology and Immune Health of Crassostrea Gigas: An Explanation for Summer Mortality in Pacific Oysters. *Am. J. Physiology-Regulatory, Integr. Comp. Physiology* 293, R2353–R2362. doi:10.1152/ajpregu.00463.2007

Matoo, O. B. (2013). Interactive Effects of Ocean Acidification and Multiple Stressors on Physiology of Marine Bivalves. *Diss. Abstr. Int.* 75 (Suppl. B), 248. Available at: https://ninercommons.uncc.edu/islandora/object/etd%3A1255/datastream/PDF/download/citation.pdf.

Maulu, S., Hasimuna, O. J., Haambiya, L. H., Monde, C., Musuka, C. G., Makorwa, T. H., et al. (2021). Climate Change Effects on Aquaculture Production: Sustainability Implications, Mitigation, and Adaptations. *Front. Sustain. Food Syst.* 5, 609097. doi:10.3389/fsufs.2021.609097

Meho, L. I., and Rogers, Y. (2008). Citation Counting, Citation Ranking, and h -Index of Human-Computer Interaction Researchers: A Comparison of Scopus and Web of Science. *J. Am. Soc. Inf. Sci. Technol.* 59, 1711–1726. doi:10.1002/asi.20874

Nalimov, V., and Mulcjenko, B. (1971). *Measurement of Science: Study of the Development of Science as an Information Process*. Washington DC: Foreign Technology Division, 1–210. Available at: https://eric.ed.gov/?id=ED065286.

Oremus, K. L., Bone, J., Costello, C., García Molinos, J., Lee, A., Mangin, T., et al. (2020). Governance Challenges for Tropical Nations Losing Fish Species Due to Climate Change. *Nat. Sustain* 3, 277–280. doi:10.1038/s41893-020-0476-y

Pauly, D., and Cheung, W. W. L. (2018). Sound Physiological Knowledge and Principles in Modeling Shrinking of Fishes Under Climate Change. *Glob. Change Biol.* 24, e15–e26. doi:10.1111/gcb.13831

Pörtner, H. (2008). Ecosystem Effects of Ocean Acidification in Times of Ocean Warming: A Physiologist's View. *Mar. Ecol. Prog. Ser.* 373, 203–217. doi:10.3354/meps07768

Rosa, R., Marques, A., and Nunes, M. L. (2012). Impact of Climate Change in Mediterranean Aquaculture. *Rev. Aquac.* 4, 163–177. doi:10.1111/j.1753-5131.2012.01071.x

S. Adriaanse, L., and Rensleigh, C. (2013). Web of Science, Scopus and Google Scholar a Content Comprehensiveness Comparison. *Electron. Libr.* 31, 727–744. doi:10.1108/EL-12-2011-0174

Sainz, J. F., Di Lorenzo, E., Bell, T. W., Gaines, S., Lenihan, H., and Miller, R. J. (2019). Spatial Planning of Marine Aquaculture Under Climate Decadal Variability: A Case Study for Mussel Farms in Southern California. *Front. Mar. Sci.* 6, 253. doi:10.3389/fmars.2019.00253

Steeves, L. E., Filgueira, R., Guyondet, T., Chassé, J., and Comeau, L. (2018). Past, Present, and Future: Performance of Two Bivalve Species Under Changing Environmental Conditions. *Front. Mar. Sci.* 5, 184. doi:10.3389/fmars.2018.00184

Thakur, K. K., Vanderstichel, R., Barrell, J., Stryhn, H., Patanasatienkul, T., and Revie, C. W. (2018). Comparison of Remotely-Sensed Sea Surface Temperature and Salinity Products with *In Situ* Measurements from British Columbia, Canada. *Front. Mar. Sci.* 5, 121. doi:10.3389/fmars.2018.00121

Tomanek, L., Zuzow, M. J., Ivanina, A. V., Beniash, E., and Sokolova, I. M. (2011). Proteomic Response to Elevated PCO2 Level in Eastern Oysters, *Crassostrea Virginica*: Evidence for Oxidative Stress. *J. Exp. Biol.* 214, 1836–1844. doi:10.1242/jeb.055475

UN SDG (2021). United Nation Sustainable Development Goals, Goal 13: Take Urgent Action to Combat Climate Change and its Impacts (Updates as COVID-19 Response). Available at: https://www.un.org/sustainabledevelopment/climate-change/ (Assessed at 4th September, 2021).

Zhang, G., Fang, X., Guo, X., Li, L., Luo, R., Xu, F., et al. (2012). The Oyster Genome Reveals Stress Adaptation and Complexity of Shell Formation. *Nature* 490, 49–54. doi:10.1038/nature11413

Zhou, C., and Song, W. (2021). Digitalization as a Way Forward: A Bibliometric Analysis of 20 Years of Servitization Research. *J. Clean. Prod.* 300, 126943. doi:10.1016/j.jclepro.2021.126943

Conflict of Interest: The authors declare that the research was conducted in the absence of any commercial or financial relationships that could be construed as a potential conflict of interest.

Publisher's Note: All claims expressed in this article are solely those of the authors and do not necessarily represent those of their affiliated organizations, or those of the publisher, the editors and the reviewers. Any product that may be evaluated in this article, or claim that may be made by its manufacturer, is not guaranteed or endorsed by the publisher.

frontiers | Frontiers in Earth Science

ORIGINAL RESEARCH
published: 22 July 2022
doi: 10.3389/feart.2022.925358

Performance of CMIP6 HighResMIP Simulations on West African Drought

Felix Olabamiji Ajibola[1,2,3], *Botao Zhou*[1,2]*, *Shamsuddin Shahid*[4] *and Md. Arfan Ali*[5]

[1]Collaborative Innovation Center on Forecast and Evaluation of Meteorological Disasters/Key Laboratory of Meteorological Disaster, Ministry of Education/Joint International Research Laboratory of Climate and Environment Change, Nanjing University of Information Science and Technology, Nanjing, China, [2]School of Atmospheric Sciences, Nanjing University of Information Science and Technology, Nanjing, China, [3]National Weather Forecasting Research and Climate Research Centre, Nigerian Meteorological Agency, Abuja, Nigeria, [4]Department of Water & Environmental Engineering, School of Civil Engineering, Faculty of Engineering, Universiti Teknologi Malaysia (UTM), Johor Bahru, Malaysia, [5]School of Marine Science, Nanjing University of Information Science and Technology, Nanjing, China

This study evaluated the performance of seven CMIP6 HighResMIP models in the simulations of drought over two sub-regions of West Africa: the Guinea coast and the Sahel during the historical period of 1985–2014, in terms of the potential evapotranspiration index (PET), climatic water availability (CWA), and standardized precipitation evapotranspiration index (SPEI) at three time scales (i.e., 1, 3, and 12 months). The Climate Research Unit (CRU) TS v4.03 datasets were used as the observation reference. The observation shows that the PET and CWA during August (i.e., the rainfall annual peak) were less than 30 and 200 mm/month over the Guinea coast, respectively. The corresponding values over the Sahel were 100 and -50 mm/month, respectively. A significant decreasing trend was observed in drought over the Guinea coast (except Nigeria) and the Sahel. The frequencies of extreme and severe droughts were observed over Nigeria, Liberia, and Sierra Leone during the historical period. The seven HighResMIP models show different behaviors in simulating all of the abovementioned observation features. Among all the simulations, the ENSEMBLE, ECMWF, and IPSL generally perform better in almost all the statistical indices used, although there are still biases that need to be resolved in the models.

Keywords: highresmip, model evaluation, drought, West Africa, SPEI

OPEN ACCESS

Edited by:
Dabang Jiang,
Institute of Atmospheric Physics (CAS), China

Reviewed by:
Cheng Sun,
Beijing Normal University, China
Guo Donglin,
Institute of Atmospheric Physics (CAS), China

***Correspondence:**
Botao Zhou
zhoubt@nuist.edu.cn

Specialty section:
This article was submitted to Geoscience and Society, a section of the journal Frontiers in Earth Science

Received: *21 April 2022*
Accepted: *15 June 2022*
Published: *22 July 2022*

Citation:
Ajibola FO, Zhou B, Shahid S and Ali MA (2022) Performance of CMIP6 HighResMIP Simulations on West African Drought. Front. Earth Sci. 10:925358. doi: 10.3389/feart.2022.925358

1 INTRODUCTION

Drought, one of the devastating precipitation extremes, has attracted the attention of meteorologists, geologists, ecologists, and environmentalists. Droughts affect any zone, and the largest aspect that is mostly affected is agriculture. It is responsible for agriculture losses globally four times that of floods, and when it is compared to hydrological disasters, the consequences are higher (Dai et al., 2011; Ahmed et al., 2016; Ebi and Bowen 2016; Damania et al., 2017; Mohsenipour et al., 2018; Qutbudin et al., 2019).

Drought has affected a lot of regions in West Africa, starting from the 1970s onward. Kasei et al. (2010) assessed drought intensity, areal extent, and recurrence frequency, using the standardized precipitation index (SPI) over 52 meteorological stations in West Africa within 1961, 1970, 1983, 1992, and 2001. The assessment indicated that nearly 75% of West Africa was under extreme drought during the period. Sante et al. (2019) examined the characteristics of drought over Cote d'Ivoire using the Markov chains 1 and 2. They discovered that most of the

TABLE 1 | Description of the CMIP6 HighResMIP models used.

Model Institute(s)	Short name	Resolution Lat x lon
EC-Earth Consortium, Rossby Center, Swedish Meteorological and Hydrological Institute/SMHI Sweden	EC-Earth3P	0.70 ×0.70
European Centre for Medium-Range Weather Forecasts	ECMWF-IFS-LR (ECMWF)	1× 1
Chinese Academy of Sciences, Beijing, China	FGOALS-f3-H(FGOAL)	0.25 × 0.25°
Institute for Numerical Mathematics, Russian Academy of Science, Moscow, Russian	INM-CM5-H (INM)	0.5 × 0.67°
Institute Pierre Simon Laplace, France	IPSL-CM6A-ATM-HR (IPSL)	0.7 ×0.5
Max Planck Institute for Meteorology, Germany	MPI-M-MIP-ESM1.2-XR (MPI)	0.47 ×0.47
Meteorological Research Institute, Japan	MRI-AGCM3-2-H (MRI)	**0.56 ×0.56**

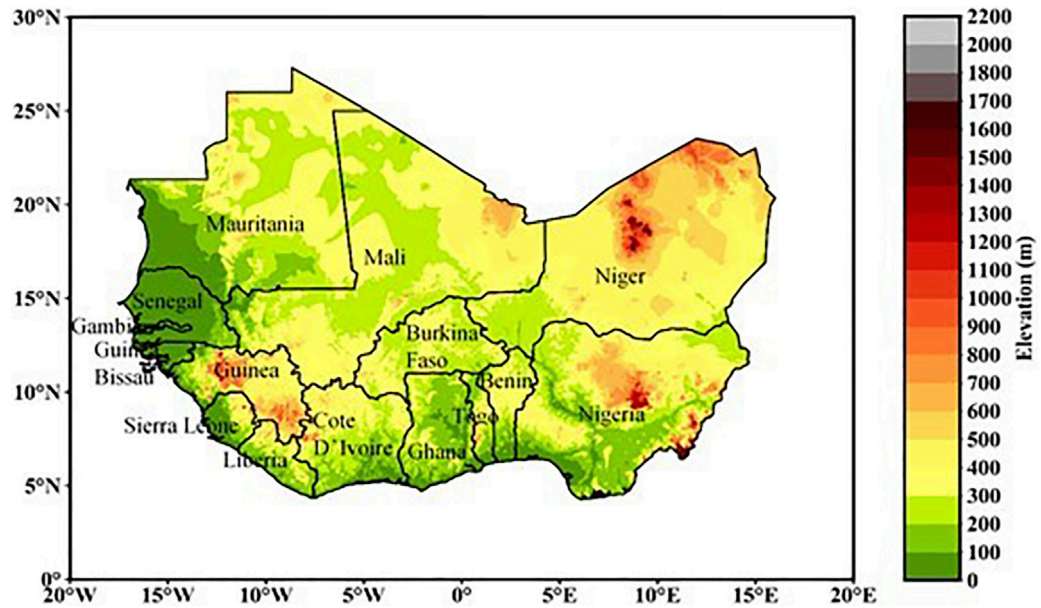

FIGURE 1 | Map of the study area showing the elevation of the study domain. The division is between the Guinea Coast and Sahel. Gnitou et al., 2019.

remarkable droughts in terms of intensity and duration transpired during the 1970s. Hassanein et al. (2013) investigated the change of drought during 1961–2008 using the standardized precipitation evapotranspiration index (SPEI) at time scale 12, and a gradual increase in drought during the decades was concluded.

Due to sparse gauge data sets, several studies involving drought are limited to a small area in West Africa. To improve the understanding and knowledge of past and future changes in drought, global climate models (GCMs) under the supervision of the Couple Model Intercomparison Project (CMIP) have been widely used. For example, based on the CMIP5 simulations, Rodríguez-Fonseca et al. (2015) concluded that the Sahel experienced the most dramatic drought starting from 1970; Shiru et al. (2020) projected that increases in temperature will result in a decrease in SPEI, which indicates an increase in drought frequency over Nigeria. At present, the CMIP has evolved to the sixth phase (CMIP6), in which some improvements have been made in physics processes and model resolutions (Eyring et al., 2016). Some recent studies have started to use the CMIP6 simulations for the evaluation and projection of drought (e.g., Cook et al., 2020; Papalexiou et al., 2021; Wang et al., 2021; Yang et al., 2021). Wang et al. (2021) revealed that the CMIP6 has high simulation accuracy at mid-latitudes for drought analysis. However, Papalexiou et al. (2021) showed that no single model can perform better over a large region. Therefore, the challenge of coarse resolutions has discouraged some researchers from using GCMs. The establishment of the High-Resolution Model Intercomparison Project (HighResMIP) at 25–50 km is timely as the main aim is to increase the horizontal resolution of models (Haarsma et al., 2016). A question arises as to whether the HighResMIP models show a better performance in the simulation of drought over West Africa. Thus, this study is motivated to assess the performance of seven CMIP6 HighResMIP models in simulating drought over West Africa.

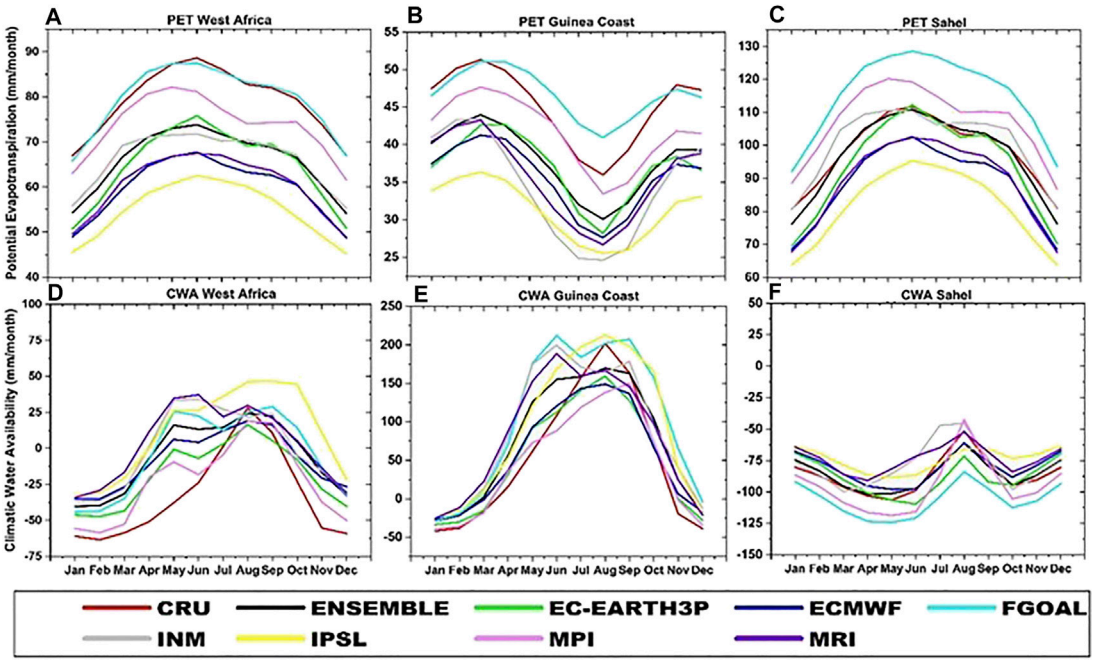

FIGURE 2 | Annual cycle of potential evapotranspiration (PET) and climatic water availability (CWA) over West Africa, Guinea Coast, and the Sahel during the historical period 1985–2014 with respect to CRU. **A–C** and **C–F** represents PET and CWA respectively, over West Africa, Guinea Coast and Sahel.

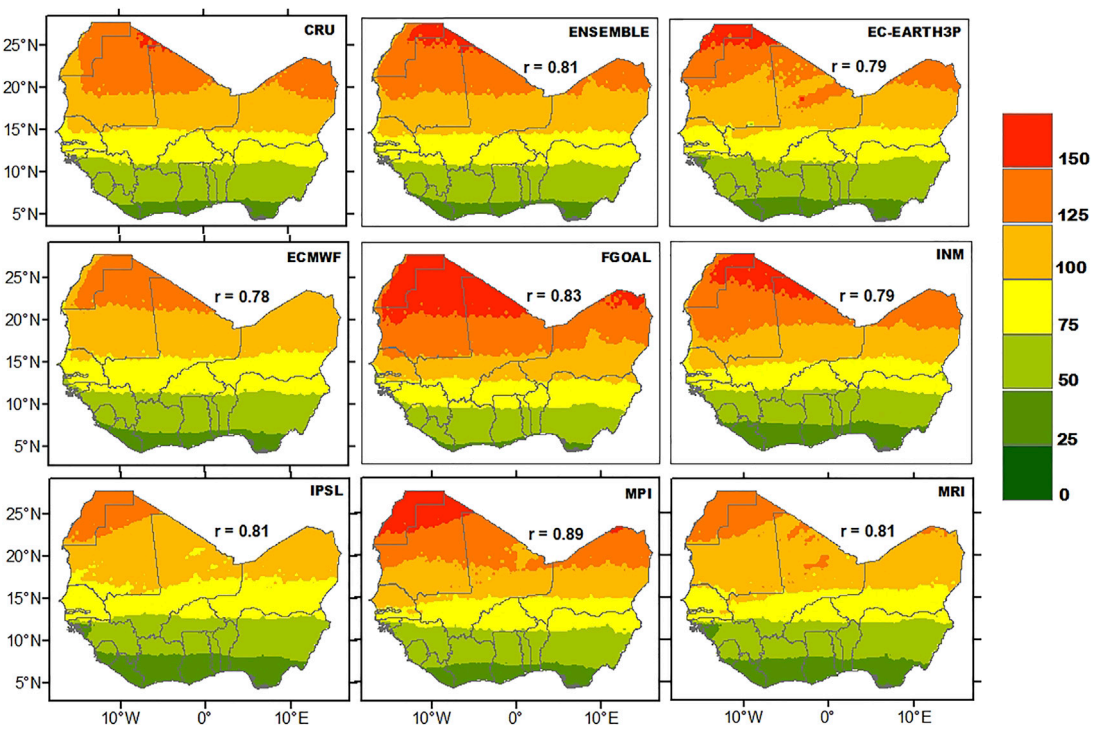

FIGURE 3 | Observed and simulated climatological distribution of potential evapotranspiration (PET) over West Africa during 1985–2014. r is the Pearson pattern correlation between CRU and each HighResMIP simulation.

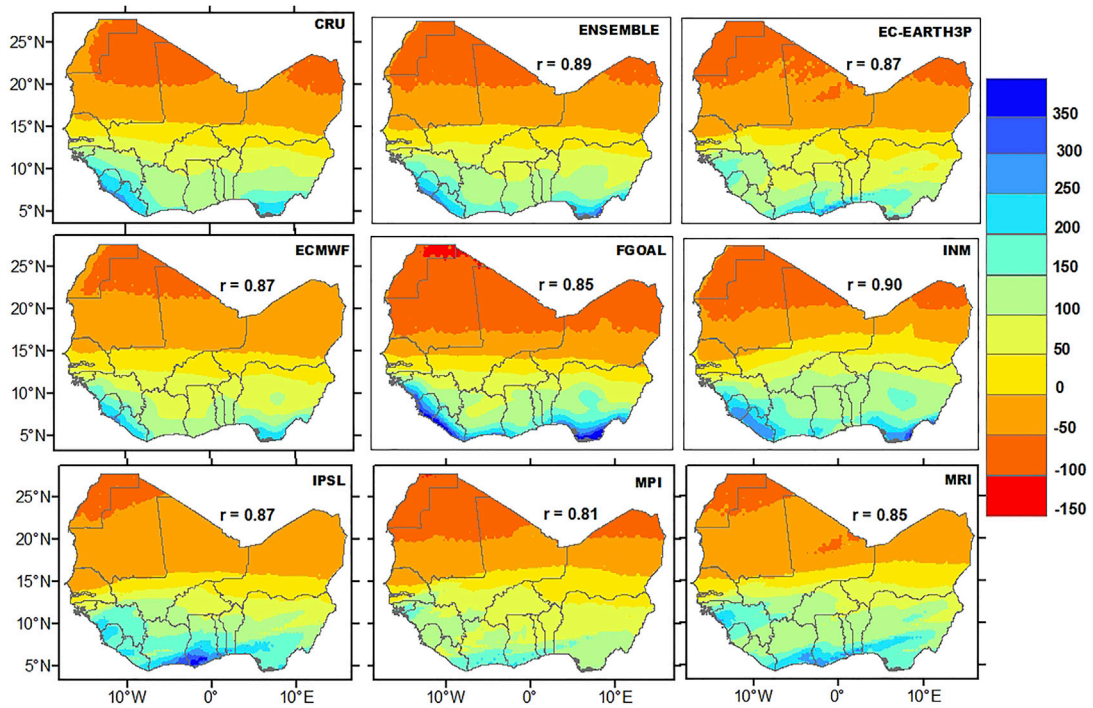

FIGURE 4 | Observed and simulated climatological distribution of climatic water availability (CWA) over West Africa during 1985–2014. r indicates the Pearson pattern correlation between CRU and each HighResMIP simulation.

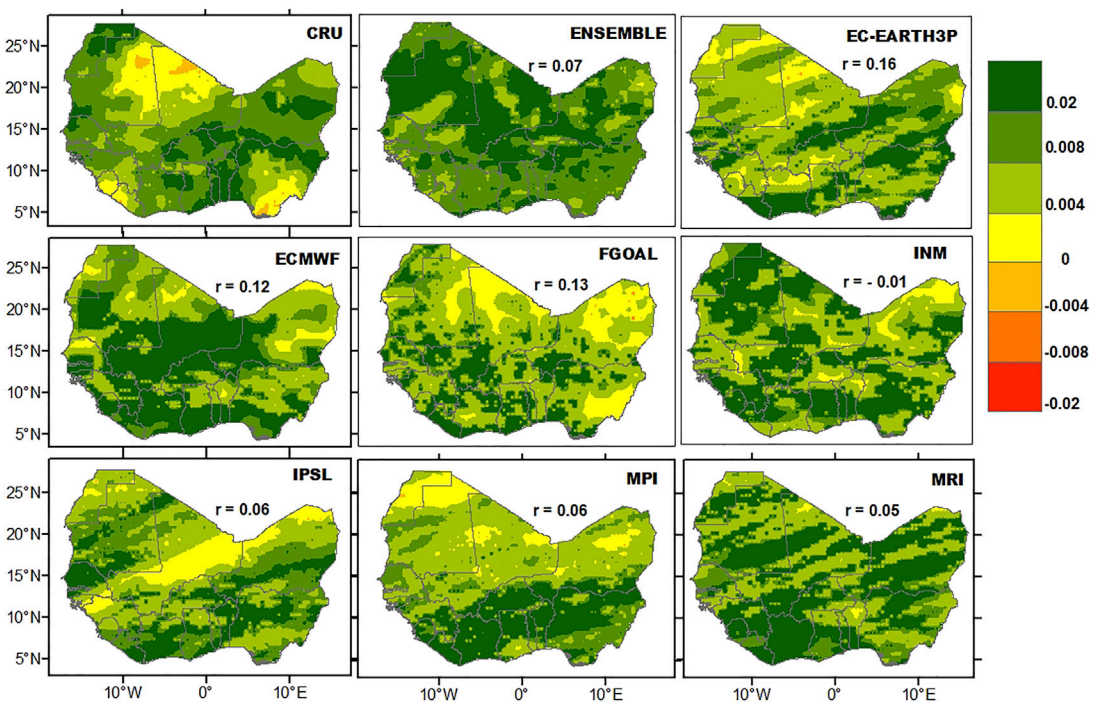

FIGURE 5 | Observed and simulated climatological distribution of standardized evapotranspiration index 1 (SPEI-1) over West Africa during 1985–2014. r indicates the Pearson pattern correlation between the observation and each HighResMIP simulation.

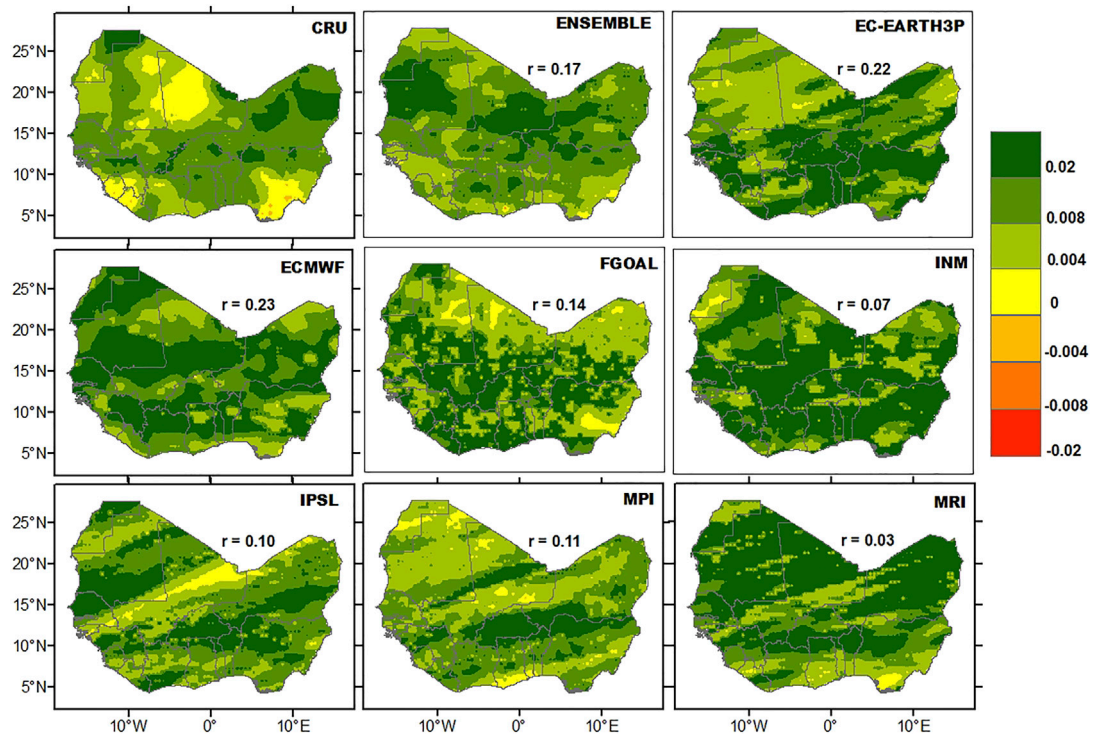

FIGURE 6 | Same as **Figure 5** but for SPEI-3.

2 MATERIAL AND METHODS

2.1 Observation and CMIP6 Datasets

The study used monthly precipitation and maximum and minimum temperatures from the Climate Research Unit (CRU TS v4.03), which was produced at 0.5 km resolution (https://crudata.uea.ac.uk/cru/data/hrg/). For the model dataset, the monthly precipitation, maximum and minimum temperatures of the historical simulations for the period 1985–2014 from seven HighResMIP models (see **Table 1**) were used. These data were archived by the Earth System Grid Federation (ESGF) under the CMIP6 (https://esgf-node.ipsl.upmc.fr/search/cmip6). West Africa is located in the domain of latitude 0°-30°N and longitude 20°W-20°E (see **Figure 1**). For the purpose of this study, we refer to it as two climatic zones: Guinea coast (south of 15°N) and the Sahel (north of 15°N).

2.2 Methods

2.2.1 Standardized Precipitation Evapotranspiration Index

The difference between precipitation (PRE) and potential evapotranspiration (PET) index, called climatic water availability (CWA), was used to calculate the SPEI (Vicente-Serrano et al., 2012). The SPEI is different from SPI because maximum and minimum temperatures are usually used to calculate PET, which is crucial in deriving the SPEI. There are several methods used in the calculation of PET, such as those by Hargreaves, Thornthwaite, and Penman-Monteith (Thornthwaite, 1948; Monteith, 1965; Hargreaves and Samani, 1985). Donohue et al. (2010) proposed that the Hargreaves method is better because it does not overestimate PET. In this study, the Hargreaves method was used to estimate PET.

The probability density function of a log-logistic distribution is given as

$$f(x) = \frac{\beta}{\alpha}\left(\frac{x-\gamma}{\alpha}\right)\left[1+\left(\frac{x-\gamma}{\alpha}\right)\right]^{-2}, \quad (1)$$

where α, β, and γ are, respectively, scale, shape, and origin parameters. The probability distribution function for the CWA series is then given as

$$f(x) = \left[1+\left(\frac{\alpha}{x}-\gamma\right)\beta\right]^{-1}. \quad (2)$$

The SPEI is retrieved as the standardized values of $f(x)$; this is in harmony with the method used by Abramowitz and Stegun (1964).

$$\mathrm{SPEI} = -2\ln(P) - \frac{C_0 + C_1 W + C_2 W^2}{1 + d_1 W + d_2 W^2 + d_3 W^3}. \quad (3)$$

For $P \le 0.5$, p is the probability of exceeding a determined CWA value, $P = 1 - f(x)$

If $P > 0.5$, p is replaced by $1 - P$, and the sign of the resultant SPEI is reversed. The constants are C_0=2.515,517, C_1=0.802,853, C_2=0.001308, $d1$=1.432,788, $d2$=0.189,269, and $d3$=0.001308.

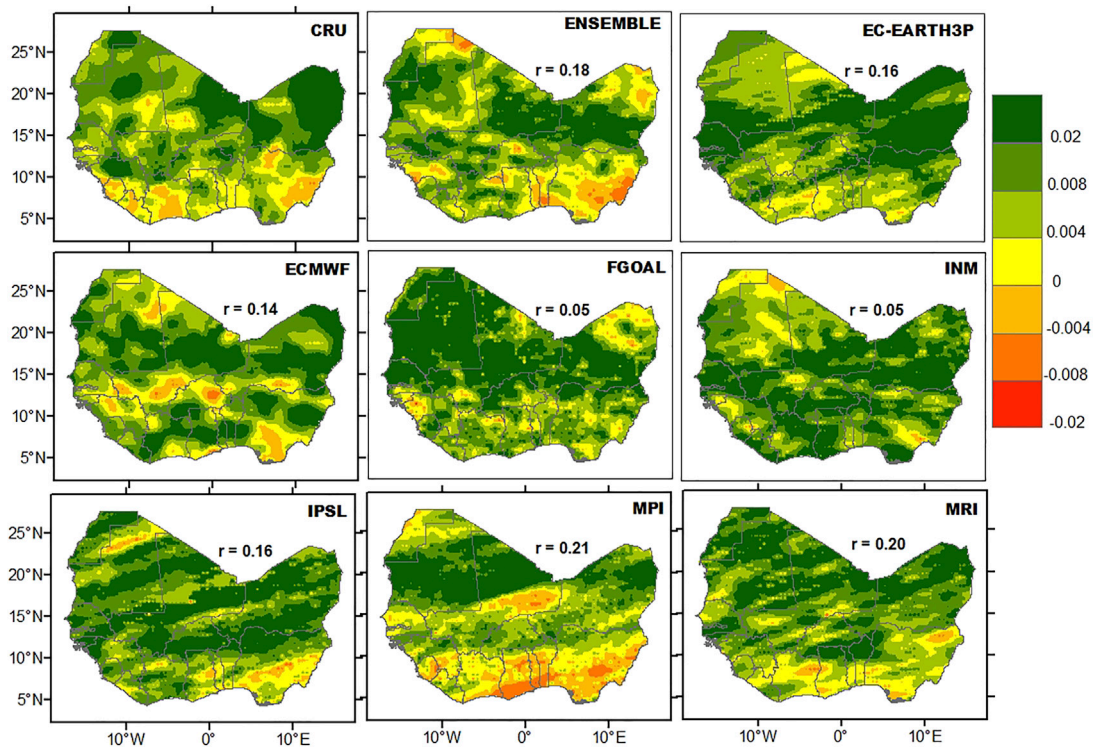

FIGURE 7 | Same as **Figure 5** but for SPEI-12.

2.3.3 Trend Analysis

The Z statistics (Morid et al., 2006; Patel et al., 2007; Akhtari et al., 2009; Dogan et al., 2012) is usually used to detect trends in climate data. This was used for trend analysis in this study. The positive (negative) value of Z statistics indicates an increasing (decreasing) trend. The significance of trends in data series was determined by the Mann–Kendall test (Mann 1945; Kendall 1975; Wang et al., 2005). The Mann–Kendall test is a nonparametric test with non-homogenous time series, which makes it have low sensitivity to short break (Tabari et al., 2011). The data required need not be normally distributed before the test is carried out.

3 RESULTS

3.1 Annual Cycle of PET and CWA

Figure 2 presents the annual cycle of PET and CWA over West Africa and the two sub-regions: Guinea Coast and Sahel. In general, the observed annual cycle of PET and CWA are reproduced by the HighResMIP individual models and the ENSEMBLE. Over the Guinea Coast (**Figure 2B**), the observed PET reached its highest value (greater than 50 mm/month) during the driest period (from November to March) and dropped to its lowest value (less than 40 mm/month) during the rainy period (from April to October). This pattern is adequately captured by the HighResMIP models, but with variations in the magnitude of the simulated amount. Most of the simulations underestimate the PET magnitude, except the FGOAL model, which exhibits slight overestimation. Over the Sahel (**Figure 2C**), the FGOAL and MPI models consistently overestimate the PET magnitude, while the MRI, ECMWF, and IPSL models show an underestimation. In comparison, the INM and ENSEMBLE perform better in reproducing the PET pattern. Due to low PET and high PRE during the rainy period over the Guinea coast, the CWA is high as the annual peak during August (200 mm/month) in the observation (**Figure 2E**). The CWA pattern is adequately reproduced by the HighResMIP simulations, although there are variations in the simulated values. Over the Sahel sub-region (**Figure 2F**), the observed CWA was negative throughout the year. The negative pattern of CWA is well-captured but with overestimation or underestimation by the HighResMIP models.

3.2 Spatial Distribution of PET and CWA

Figure 3 shows the climatological distribution of PET over West Africa. The observation displayed a low PET over the coastal areas, which increased from the south to the north. Over the coastal areas and the Sahel, the PET was observed in the range of 0–100 mm/month and 100–150 mm/month, respectively. Such a PET pattern is adequately simulated by the HighResMIP models and the ENSEMBLE with a strong positive pattern correlation ($r>0.75$). However, the FGOAL model overestimates the magnitude over the northern region.

The observed CWA showed low climatic water over the Sahel, which ranges from 0 to -100 mm/month and the high value ranging from 50 to 250 mm/month over the coastal area of West

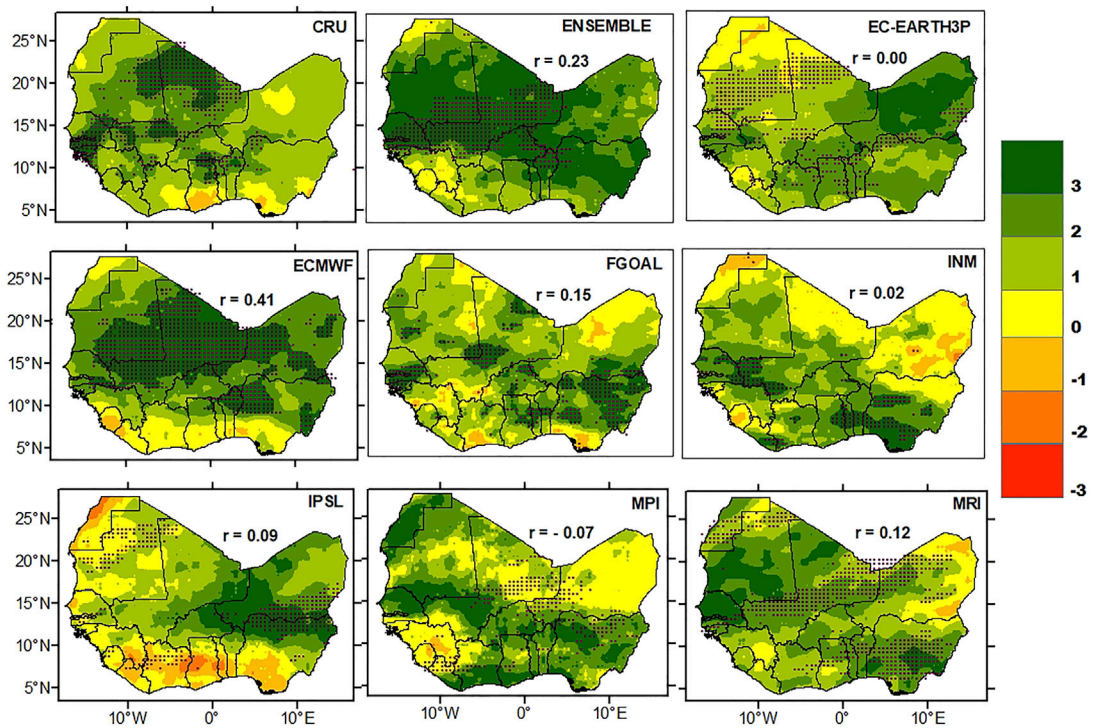

FIGURE 8 | Observed and simulated distribution of Z-statistics for SPEI-1 over West Africa during 1985–2014. The positive and negative values indicate the grid with increasing and decreasing trends, respectively. The grids with significant trends at the 0.05 confidence level are hatched. r indicates the Pearson pattern correlation between CRU and each HighResMIP simulation.

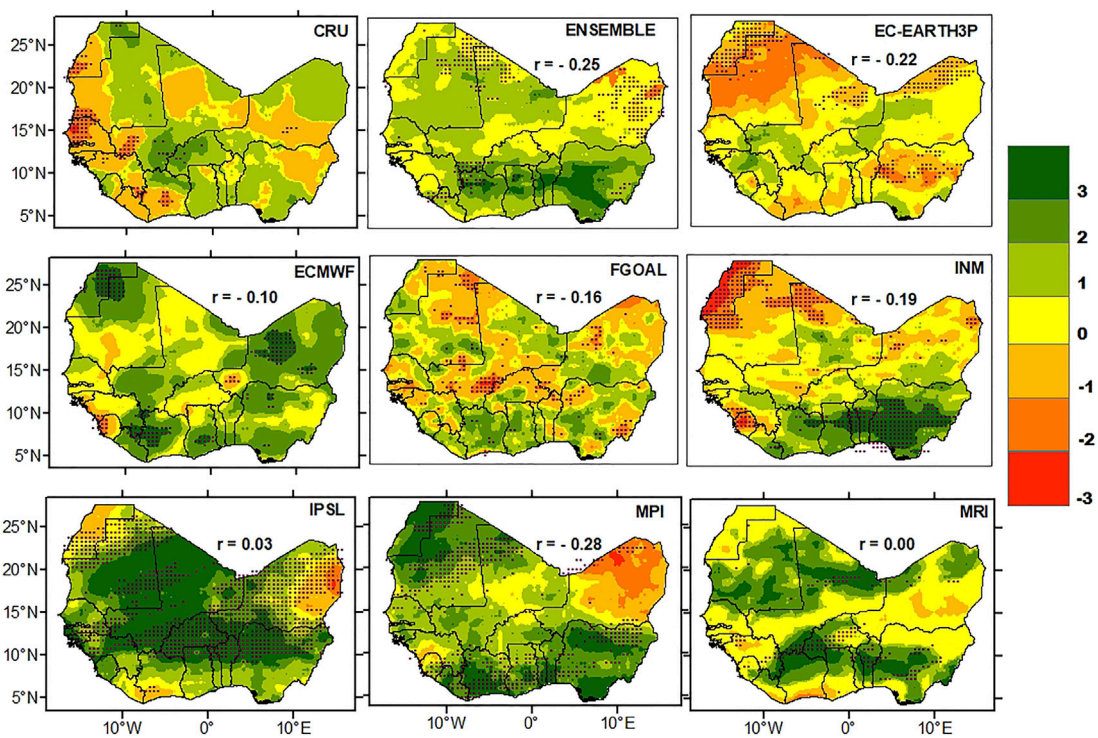

FIGURE 9 | Same as **Figure 8** but for SPEI-3.

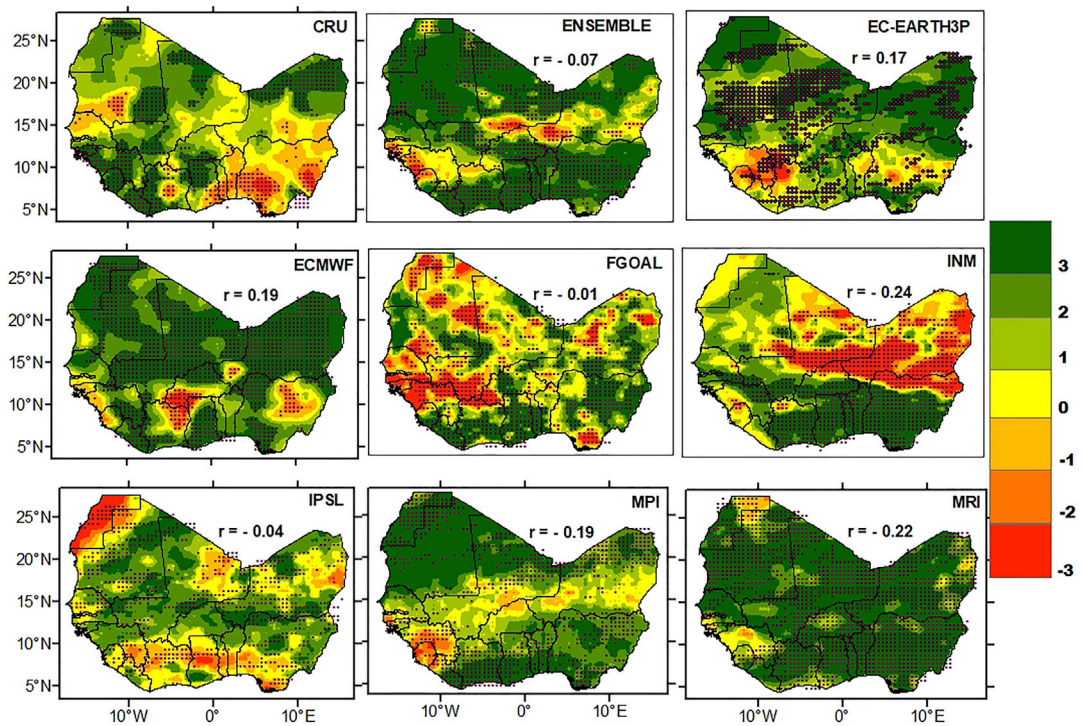

FIGURE 10 | Same as **Figure 8** but for SPEI-12.

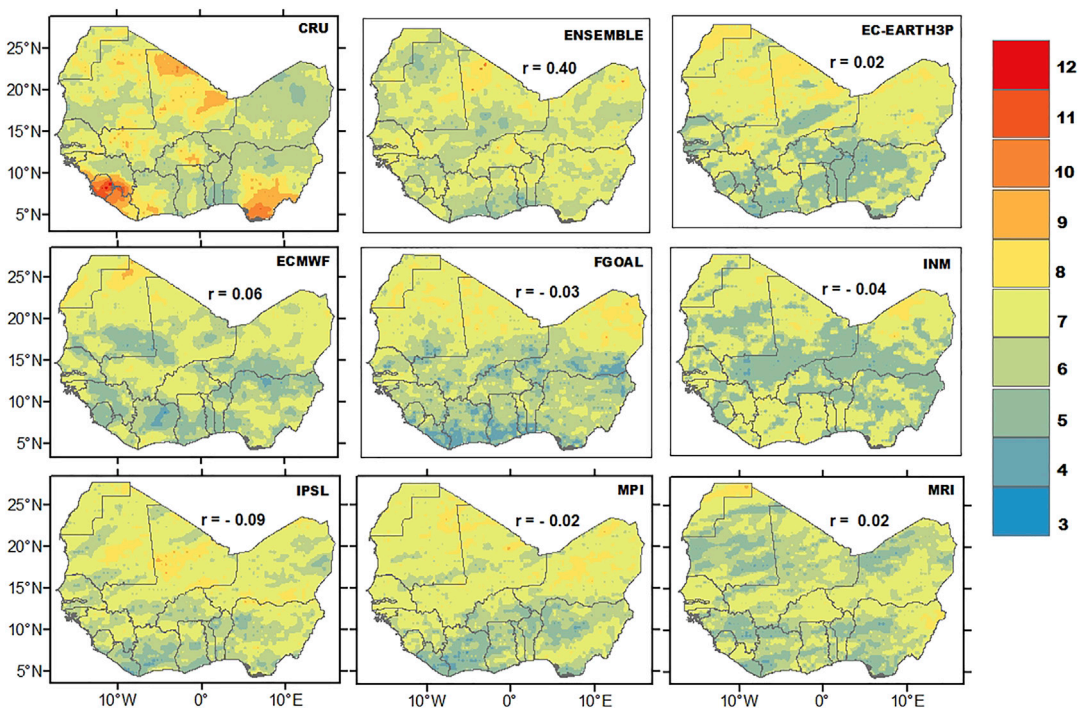

FIGURE 11 | Observed and simulated distribution of frequencies of severe meteorological drought (SPEI-1) over West Africa during1985–2014. r indicates the Pearson pattern correlation between the CRU and each HighResMIP simulation.

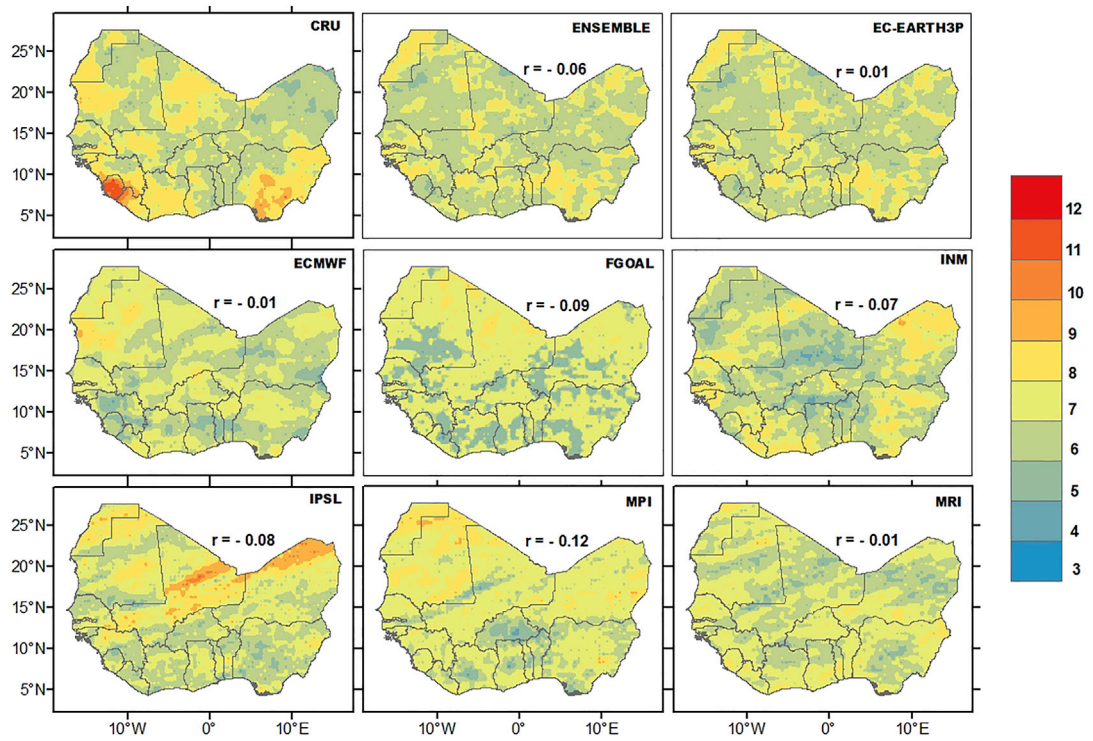

FIGURE 12 | Same as **Figure 11** but for the frequency of agricultural drought (SPEI-3).

Africa (**Figure 4**). This result agrees with the findings of previous studies (Nicholson et al., 2003; Afiesimama et al., 2006; Gbobaniyi et al., 2014; Akinsanola et al., 2017, 2018; Ajibola et al., 2020). The HighResMIP simulations perform well in reproducing the spatial pattern of CWA (r>0.80). However, the FGOAL and INM models overestimate the CWA magnitude over southern Nigeria, Liberia, and Sierra Leone, while the EC-EARTH3P and MPI models consistently underestimate the CWA over the high rainy region of the study area. In comparison, the ECMWF model and the ENSEMBLE perform adequately in reproducing the two climatic variables spatially.

3.3 Spatial Distribution of the SPEI

Figures 5–7 present the climatological distribution of the SPEI during the historical period considered. The SPEI-1 represents the meteorological drought, the SPEI-3 depicts the agricultural drought, and the SPEI-12 shows a glimpse of hydrological drought. In the observation, positive SPEI-1 (**Figure 5**) and SPEI-3 (**Figure 6**) indicate wet conditions appearing over West Africa, except Nigeria, Sierra Leone, and Mali, where the SPEI-1 and SPEI-3 is around 0. This pattern is not well-reproduced by the HighResMIP models except the FGOAL, which reproduces the SPEI-1 pattern over Nigeria. As the SPEI timescale increased to 12 (**Figure 7**), negative SPEI-12 was observed over coastal cities in the southwest and Nigeria in the southeast, which signifies dry hydrological condition. The negative SPEI-12 over Nigeria can be reproduced by the ENSEMBLE, ECMWF, and MPI simulations. Overall, the Pearson pattern correlation between the observation and simulations is positive but low. It has to be noted that the SPEI in each grid could either be positive or negative, and its temporal average could result in low pattern correlation between the observation and simulations, as also suggested by Quenum et al. (2019).

3.4 Drought Trends

The spatial distribution of Z-statistics for the SPEI-1 is shown in **Figure 8**. The positive (negative) value represents a trend toward wetter (drier) condition. The observation indicated significant positive (increasing) trends over Mali, Guinea Bissau, Senegal, Ghana, Togo, and Benin. Insignificant negative (decreasing) trends were observed over few regions in the coastal area (Nigeria and Ghana). The ENSEMBLE, EC-EARTH3P, ECMWF, and FGOAL can reproduce the significant increasing trends of SPEI-1 over Ghana. The ECMWF model performs better than other simulations over the areas with significant positive changes observed and produces a strong pattern correlation (r = 0.41) with the observation.

The Z-statistics for the observed SPEI-3 showed that most of the region had negative (decreasing) trends, with 3.4% of the grids significant at the 0.05 level (**Figure 9**). Most of the simulations can reproduce the insignificant negative trends over most cities in

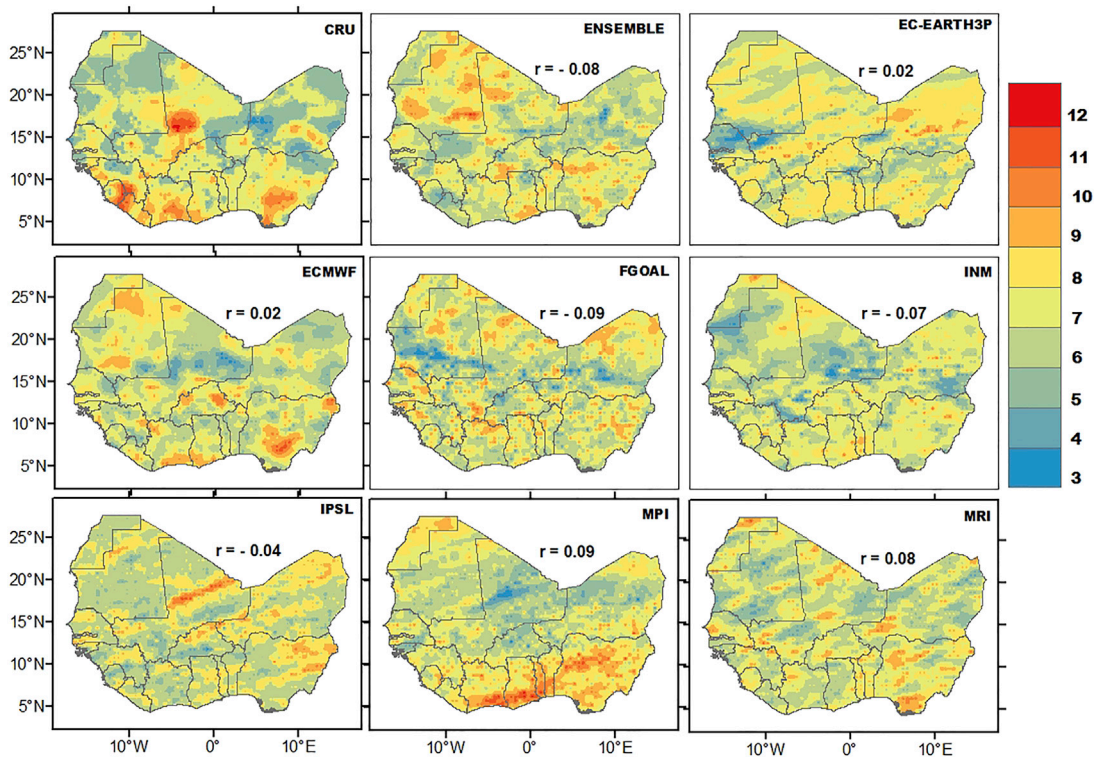

FIGURE 13 | Same as **Figure 11** but for the frequency of hydrological drought (SPEI-12).

West Africa, except the IPSL and MPI models, which simulated positive (increasing) trends. Most of the models reproduce a negative correlation with the observation except IPSL. This seemingly indicates the inability of HighResMIP models to reproduce agricultural drought trend pattern.

The trends of SPEI-12 were observed to be more significant than the aforementioned SPEIs. Except Nigeria, Benin, Togo, southeast Ghana, and south Cote D'Ivoire, where significant negative (decreasing) trends were observed, most of the study region had positive (increasing) trends, with significant increasing trends over north Ghana, Burkina Faso, Cote D'Ivoire, Liberia, Sierra Leone, Guinea, Mali, and Nigeria (**Figure 10**). Most of the simulations have a role in simulating the widespread increasing trends. The EC-EARTH3P and ECMWF can also reproduce the decreasing trend over Nigeria. Most of the simulations show a phase opposition in simulating hydrological drought patterns, except EC-EARTH3P and ECMWF, which show a positive correlation with the observation.

3.5 Frequency of Drought Events

The HighResMIP performances to reproduce the frequency of severe meteorological, agricultural, and hydrological droughts ($-1.99 \leq SPEI \leq -1.5$) are evaluated in **Figures 11–13**, respectively. The observation showed that as the scale of the SPEI increases, the spread of high frequency of severe drought events also increases. For the severe meteorological drought event (SPEI-1), the high frequency, varying from 8 to 12, is located over southern Nigeria, Cote D'Ivoire, Sierra Leone, Guinea, Liberia, Burkina Faso, and Mali. In the remaining regions, the frequencies mostly varied from 5 to 8 (**Figure 11**). Compared to the meteorological drought, there is a more widespread frequency of severe agricultural drought events (SPEI-3), with the highest frequency occurring over Nigeria, Sierra Leone, and Liberia (**Figure 12**). High frequencies of severe hydrological droughts (SPEI-12) are shown over Nigeria, Cote D'Ivoire, Sierra Leone, Liberia, Burkina Faso, and Mali (**Figure 13**).

All the simulations consistently underestimate the high frequency of severe meteorological drought. The ENSEMBLE captures the high frequency of severe agricultural drought over Nigeria, while the MRI model reproduces the high frequency over Liberia, Sierra Leone, Guinea, and Cote D'Ivoire, although underestimated. Most of the models can reproduce the high frequency of severe hydrological drought over Nigeria, with overestimation by the MPI, while the ECMWF performs slightly better with positive pattern correlation with observation. The high frequency over Cote D'Ivoire, Sierra Leone, Liberia, Burkina Faso, and Mali is underestimated by most of the models.

High frequencies of extreme dry events ($SPEI \leq -2.0$) were observed over Nigeria, Sierra Leone, Liberia, and Mali for

meteorological and agricultural droughts and over Nigeria, Mauritania, Senegal, and Mali for hydrological droughts. These were not adequately represented in the HighResMIP simulations and ENSEMBLE.

4 SUMMARY AND CONCLUSION

West Africa has limited capacity to respond to climate change, causing havoc to the economy of the region. Since climate change such as drought has great impacts on the livelihood in this region, the information of future climate change over the region is very important for adaptation and mitigation actions. The CMIP models are essential tools to project future climate change. Before the projection, the performance of the models needs to be assessed. In this study, we evaluated the performance of seven HighResMIP models in the simulation of drought over West Africa, using the metrics of PET, CWA, and SPEI. The results are summarized below:

1) The HighResMIP individual models and the ENSEMBLE can adequately reproduce the observed annual cycle of PET and CWA over the Guinea coast and Sahel. The spatial distribution of observed PET (CWA) which increased (decreased) from the south to the north can also be captured by the models. The observed PET (CWA) pattern is adequately reproduced by each model with a spatial pattern correlation of $r>0.75$ ($r>0.8$). The ENSEMBLE performs better, and the ECMWF model outperforms among the models considered.
2) The spatial distribution of the SPEI showed a slightly negative SPEI-1 and SPEI-3 over Nigeria, Sierra Leone, and Liberia. The negative SPEI, though not pronounced in SPEI-1 and SPEI-3 until in SPEI-12 over the southern cities, indicates increasing dry condition during the study period. GCMs and ENSEMBLE could not consistently reproduce the negative SPEI-1 and SPEI-3 over the region. However, EC-EARTH3P, ECMWF, and IPSL performed better in reproducing the negative SPEI-12 over Nigeria.
3) The trends in SPEI-1, SPEI-3, and SPEI-12 based on Z-statistics and MK p-value were used to determine the region with significant drought changes. The results showed a significant positive (increase) trend in SPEI-1 over Mali, Guinea-Bissau, Senegal, and Ghana; a negative (decreasing) insignificant trend in SPEI-3 in most cities over the study region; and a significant positive (increasing) trend in SPEI-12 over Sierra Leone, Liberia, north Ghana, Cote D'Ivoire, Guinea, Mali, and Nigeria with a consistent significant negative (decreasing) trend over Nigeria, Benin, Togo, southeast Ghana, and south Cote D'Ivoire. Most of the GCMs have a role in simulating the widespread increasing (decreasing) trends. ECMWF, IPSL, EC-EARTH3P, and ENSEMBLE performed better than the remaining simulations.
4) In cases of high frequency of extreme and severe droughts, most GCMs showed a moderate performance in simulating severe droughts over Nigeria, Liberia, and Sierra Leone. The extreme frequency of drought is not adequately represented in HighResMIP simulations. The inability of most GCMs to reproduce the frequency of drought appears to be the present scenario of systematic bias in the GCM (Abiodun et al., 2019).

It is worth noting that the Pearson correlation between the simulations and observation for climatological SPEI distribution, trends, and drought frequency over West Africa is low. This is possibly due to the temporal averaging of negative and positive values of the SPEI in each grid, which might allow misrepresentation of the observed pattern in the models. In general, this study showed that the improvement of model resolution is a crucial exercise. However, the performance of a model does not stop on improving the resolution alone. Individual simulations show a high capacity in reproducing West African drought features. Simulations from ECMWF and IPSL seem to outperform other models, with the ensemble mean showing a high skill than all other models. This study serves as motivation for further studies on drought using CMIP6 HighResMIP simulations, and it can be improved by analyzing the projection of drought over West Africa.

DATA AVAILABILITY STATEMENT

The original contributions presented in the study are included in the article/Supplementary Material; further inquiries can be directed to the corresponding author.

AUTHOR CONTRIBUTIONS

Conceptualization, FA and BZ; methodology, FA; software, SS and AA; validation, BZ and AA; formal analysis, FA; investigation, BZ and FA; resources, BZ; data curation, FA; writing—original draft preparation, FA; writing—review and editing, BZ and FA; visualization, AA and SS; supervision, BZ; funding acquisition, BZ.

FUNDING

This research was jointly supported by the National Key Research and Development Program of China (2017YFA0605004) and the Program for Distinguished Professor of Jiangsu.

ACKNOWLEDGMENTS

We are grateful to the World Climate Research Program (WRCP) and the HighResMIP participating institution that make their simulation results accessible to the public. We are also grateful to the Climate Research Unit (CRU) for granting access to the reference dataset in accordance with their specific

data use and the policy evolving citation. The first author acknowledges the Nanjing University of Information Science and Technology, China, World Meteorological Organization (WMO) and Nigerian Meteorological Agency for granting him the scholarship through which the completion of the present study is possible.

REFERENCES

Abiodun, B. J., Makhanya, N., Petja, B., Abatan, A. A., and Oguntunde, P. G. (2019). Future Projection of Droughts over Major River Basins in Southern Africa at Specific Global Warming Levels. *Theor. Appl. Climatol.* 137, 1785–1799. doi:10.1007/s00704-018-2693-0

Abramowitz, M., and Stegun, I. A. (1964). *Handbook Of Mathematical Functions: With Formulas, Graphs, and Mathematical Tables*, 55. New York: Dover. ninth Dove.

Afiesimama, E. A., Pal, J. S., Abiodun, B. J., Gutowski, W. J., and Adedoyin, A. (2006). Simulation of West African Monsoon Using the RegCM3. Part I: Model Validation and Interannual Variability. *Theor. Appl. Climatol.* 86, 23–37. doi:10.1007/s00704-005-0202-8

Ahmed, K., Shahid, S., Harun, S. b., and Wang, X.-j. (2016). Characterization of Seasonal Droughts in Balochistan Province, Pakistan. *Stoch. Environ. Res. Risk Assess.* 30, 747–762. doi:10.1007/s00477-015-1117-2

Ajibola, F. O., Zhou, B., Tchalim Gnitou, G., and Onyejuruwa, A. (2020). Evaluation of the Performance of CMIP6 HighResMIP on West African Precipitation. *Atmosphere* 11, 1053. doi:10.3390/atmos11101053

Akhtari, R., Morid, S., Mahdian, M. H., and Smakhtin, V. (2009). Assessment of Areal Interpolation Methods for Spatial Analysis of SPI and EDI Drought Indices. *Int. J. Climatol.* 29, 135–145. doi:10.1002/joc.1691

Akinsanola, A. A., Ajayi, V. O., Adejare, A. T., Adeyeri, O. E., Gbode, I. E., Ogunjobi, K. O., et al. (2018). Evaluation of Rainfall Simulations over West Africa in Dynamically Downscaled CMIP5 Global Circulation Models. *Theor. Appl. Climatol.* 132, 437–450. doi:10.1007/s00704-017-2087-8

Akinsanola, A. A., Ogunjobi, K. O., Ajayi, V. O., Adefisan, E. A., Omotosho, J. A., and Sanogo, S. (2017). Comparison of Five Gridded Precipitation Products at Climatological Scales over West Africa. *Meteorol. Atmos. Phys.* 129, 669–689. doi:10.1007/s00703-016-0493-6

Cook, B., Mankin, J., Marvel, K., Williams, A., Smerdon, J., and Anchukaitis, K. (2020). Twenty-First Century Drought Projections in the CMIP6 Forcing Scenarios. *Earth's Future* 8, 6. doi:10.1029/2019EF001461

Dai, A. (2011). Drought under Global Warming: A Review. *Wiley Interdiscip. Rev.Clim. Chang.* 2, 45–65. doi:10.1002/wcc.81

Damania, R., Desbureaux, S., Hyland, M., Islam, A., Moore, S., Rodella, A. S., et al. (2017). *Uncharted Waters: The New Economics of Water Scarcity and Variability*. 1st ed. Washington, DC, USA: World Bank. doi:10.1596/978-1-4648-1179-1

Dogan, S., Berktay, A., and Singh, V. P. (2012). Comparison of Multi-Monthly Rainfall-Based Drought Severity Indices, with Application to Semi-arid Konya Closed Basin, Turkey. *J. Hydrology* 470-471, 255–268. doi:10.1016/j.jhydrol.2012.09.003

Donohue, R. J., McVicar, T. R., and Roderick, M. L. (2010). Assessing the Ability of Potential Evaporation Formulations to Capture the Dynamics in Evaporative Demand within a Changing Climate. *J. Hydrology* 386, 186–197. doi:10.1016/j.jhydrol.2010.03.020

Ebi, K. L., and Bowen, K. (2016). Extreme Events as Sources of Health Vulnerability: Drought as an Example. *Weather Clim. Extrem.* 11, 95–102. doi:10.1016/j.wace.2015.10.001

Eyring, V., Bony, S., Meehl, G. A., Senior, C. A., Stevens, B., Stouffer, R. J., et al. (2016). Overview of the Coupled Model Intercomparison Project Phase 6 (CMIP6) Experimental Design and Organization. *Geosci. Model Dev.* 9, 1937–1958. doi:10.5194/gmd-9-1937-2016

Gnitou, G. T., Ma, T., Tan, G., Ayugi, B., Nooni, I. K., Alabdulkarim, A., et al. (2019). Evaluation of the Rossby Centre Regional Climate Model Rainfall Simulations over West Africa using Large-Scale Spatial and Temporal Statistical Metrics. *Atmosphere* 10, 802.

Gbobaniyi, E., Sarr, A., Sylla, M. B., Diallo, I., Lennard, C., Dosio, A., et al. (2014). Climatology, Annual Cycle and Interannual Variability of Precipitation and Temperature in CORDEX Simulations over West Africa. *Int. J. Climatol.* 34, 2241–2257. doi:10.1002/joc.3834

George H. Hargreaves, G. L., and Zohrab A. Samani, Z. A. (1985). Reference Crop Evapotranspiration from Temperature. *Appl. Eng. Agric.* 1, 96–99. doi:10.13031/2013.26773

Haarsma, R. J., Roberts, M. J., Vidale, P. L., Senior, C. A., Bellucci, A., Bao, Q., et al. (2016). High Resolution Model Intercomparison Project (HighResMIP v1.0) for CMIP6. *Geosci. Model Dev.* 9, 4185–4208. doi:10.5194/gmd-9-4185-2016

Hassanein, M. K., Khalil, A. A., and Essa, Y. H. (2013). Assessment of Drought Impact in Africa Using Standard Precipitation Evapotranspiration Index. *Nat. Sci.* 11, 75–81.

Kasei, R., Diekkrüger, B., and Leemhuis, C. (2010). Drought Frequency in the Volta Basin of West Africa. *Sustain Sci.* 5, 89–97. doi:10.1007/s11625-009-0101-5

Kendall, M. G. (1975). *Rank Correlation Methods*. 4th Edn, Charles Griffin, London. doi:10.1007/978-1-4684-6683-6_9

Mann, H. B. (1945). Nonparametric Tests against Trend. *Econometrica* 13, 245–259. doi:10.2307/1907187

Mohsenipour, M., Shahid, S., Chung, E.-s., and Wang, X.-j. (2018). Changing Pattern of Droughts during Cropping Seasons of Bangladesh. *Water Resour. manage.* 32, 1555–1568. doi:10.1007/s11269-017-1890-4

Monteith, J. L. (1965).Evaporation and Environment, *Symposia Soc. Exp. Biol.*, 19. Cambridge: Cambridge University Press, 205–234.

Morid, S., Smakhtin, V., and Moghaddasi, M. (2006). Comparison of Seven Meteorological Indices for Drought Monitoring in Iran. *Int. J. Climatol.* 26, 971–985. doi:10.1002/joc.1264

Nicholson, S. (2003). Comments on "The South Indian Convergence Zone and Interannual Rainfall Variability over Southern Africa" and the Question of ENSO's Influence on Southern Africa. *J. Clim.* 16, 555–562. doi:10.1175/1520-0442(2003)016<0555:cotsic>2.0.co;2

Papalexiou, S. M., Rajulapati, C., Andreadis, K., Foufoula-Georgiou, E., Clark, M., and Trenberth, K. (2021). Probabilistic Evaluation of Drought in CMIP6 Simulations. *Earth's Future* 9. e2021EF002150. doi:10.1029/2021EF002150

Patel, N. R., Chopra, P., and Dadhwal, V. K. (2007). Analyzing Spatial Patterns of Meteorological Drought Using Standardized Precipitation Index. *Met. Apps* 14, 329–336. doi:10.1002/met.33

Quenum, G. M. L. D., Klutse, N. A. B., Dieng, D., Laux, P., Arnault, J., Kodja, J. D., et al. (2019). Identification of Potential Drought Areas in West Africa under Climate Change and Variability. *Earth Syst. Environ.* 3, 429–444. doi:10.1007/s41748-019-00133-w

Qutbudin, I., Shiru, M. S., Sharafati, A., Ahmed, K., Al-Ansari, N., Yaseen, Z. M., et al. (2019). Seasonal Drought Pattern Changes Due to Climate Variability: Case Study in Afghanistan. *Water* 11, 1096. doi:10.3390/w11051096

Rodríguez-Fonseca, B., Mohino, E., Mechoso, C. R., Caminade, C., Biasutti, M., Gaetani, M., et al. (2015). Variability and Predictability of West African Droughts: A Review on the Role of Sea Surface Temperature Anomalies. *J. Clim.* 28, 4034–4060. doi:10.1175/JCLI-D-14-00130.1

Santé, N., N'Go, Y. A., Soro, G. E., Meledje, N. H., and Bi, B. T. A. (2019). Characterization of Meteorological Droughts Occurrences in Côte d'Ivoire: Case of the Sassandra Watershed. *Climate* 7, 60. doi:10.3390/cli7040060

Shiru, M. S., Shahid, S., Dewan, A., Chung, E.-S., Alias, N., Ahmed, K., et al. (2020). Projection of Meteorological Droughts in Nigeria during Growing Seasons under Climate Change Scenarios. *Sci. Rep.* 10, 10107. doi:10.1038/s41598-020-67146-8

Tabari, H., Marof, S., Aeini, A., Talaee, P. H., and Mohammadi, K. (2011). Trend Analysis of Reference Evapotranspiration in the Western Half of Iran. *Agric. For. Meteorol* 151, 128–136. doi:10.1016/j.agrformet.2010.09.009

Thornthwaite, C. W. (1948). An Approach toward a Rational Classification of Climate. *Geogr. Rev.* 38, 55–94. doi:10.2307/210739

Vicente-Serrano, S. M., Beguería, S., Lorenzo-Lacruz, J., Camarero, J. J., López-Moreno, J. I., Azorin-Molina, C., et al. (2012). Performance of Drought Indices for Ecological, Agricultural, and Hydrological Applications. *Earth Interact.* 16, 1–27. doi:10.1175/2012EI000434.1

Wang, W., Gelder, V., and Vrijling, J. K. (2005). "Trend and Stationarity Analysis for Streamflow Processes of Rivers in Western Europe in the 20th Century," in

Proceedings of the IWA International Conference on Water Economics, Statistics, and Finance, Rethymno, Greece, October 8–10, 2005.

Wang, T., Tu, X., Singh, V. P., Chen, X., and Lin, K. (2021). Global Data Assessment and Analysis of Drought Characteristics Based on CMIP6. *J. Hydrol.* 596, 126091. doi:10.1016/j.jhydrol.2021.126091

Xu, Y., Zhang, X., Hao, Z., Hao, F., and Li, C. (2021). Projections of Future Meteorological Droughts in China under CMIP6 from a Three-Dimensional Perspective. *Agric. Water Manag.* 252, 106849. doi:10.1016/j.agwat.2021.106849

Conflict of Interest: The authors declare that the research was conducted in the absence of any commercial or financial relationships that could be construed as a potential conflict of interest.

Publisher's Note: All claims expressed in this article are solely those of the authors and do not necessarily represent those of their affiliated organizations, or those of the publisher, the editors, and the reviewers. Any product that may be evaluated in this article, or claim that may be made by its manufacturer, is not guaranteed or endorsed by the publisher.

frontiers | Frontiers in Earth Science

TYPE Original Research
PUBLISHED 10 August 2022
DOI 10.3389/feart.2022.963042

OPEN ACCESS

EDITED BY
Marcelo Cohen,
Federal University of Pará, Brazil

REVIEWED BY
Qingxiang Li,
School of Atmospheric Sciences, Sun Yat-sen University, China
Cheng Sun,
Beijing Normal University, China

*CORRESPONDENCE
Huopo Chen,
chenhuopo@mail.iap.ac.cn

SPECIALTY SECTION
This article was submitted to Geoscience and Society, a section of the journal Frontiers in Earth Science

RECEIVED 07 June 2022
ACCEPTED 19 July 2022
PUBLISHED 10 August 2022

CITATION
Xu H, Chen H and Wang H (2022), Increased populations will be exposed to the dangerous precipitation extremes across China in the future. *Front. Earth Sci.* 10:963042. doi: 10.3389/feart.2022.963042

Increased populations will be exposed to the dangerous precipitation extremes across China in the future

Huiwen Xu[1,2], Huopo Chen[1,3]* and Huijun Wang[1,3]

[1]Nansen-Zhu International Research Centre, Institute of Atmospheric Physics, Chinese Academy of Sciences, Beijing, China, [2]University of Chinese Academy of Sciences, Beijing, China, [3]Collaborative Innovation Center on Forecast and Evaluation of Meteorological Disasters, Nanjing University for Information Science and Technology, Nanjing, China

This study investigates the future changes in dangerous precipitation extremes with multiyear return periods and the population exposure across China at the 1.5–4°C warming levels *via* the latest simulations from the Coupled Model Intercomparison Project Phase 6 (CMIP6). The results show that the simulations project more frequent dangerous precipitation extremes across China under the warmer climate regardless of the shared socioeconomic pathway (SSP), with more substantial occurrence increases at the high warming levels. Consequently, the population exposure to dangerous precipitation extremes is anticipated to increase persistently in most regions of China except for some parts of northwestern China and the Tibetan Plateau. For the events estimated to occur once every 10 years, the 1.5, 2.0, 3.0, and 4.0°C warming relative to the current state will result in approximately 29.9, 47.8, 72.9, and 84.3% increases in the aggregated population exposure over China under the SSP5-8.5 scenario, respectively. However, the exposure change is somewhat subject to the emission scenarios, with larger proportional increases under the regional-rivalry scenario of SSP3-7.0 compared to the fossil-fueled development scenario of SSP5-8.5. The increased exposure under all the scenarios is primarily attributed to the climate change factor, and the population change and their interaction component make a minor contribution. Furthermore, compared to the 2.0°C warmer climate, the 0.5°C less warming under the 1.5°C climate can trigger remarkable decreases of 16.5–20.8% for exposure to once-in-decade events over China. Additionally, the changes in the occurrence and exposure are much larger for the rarer events. Hence, our analyses indicate that limiting warming to 1.5°C is beneficial to reducing the impacts associated with precipitation extremes across China, particularly for the more extreme events.

KEYWORDS

population exposure, precipitation extremes, CMIP6 models, global warming, avoided impacts

Introduction

Global warming has been a great challenge to the international community over the past decades. The Sixth Assessment Report (AR6) of the Intergovernmental Panel on Climate Change (IPCC) documents that human activity has unequivocally warmed the atmosphere, ocean and land. With anthropogenic climate change, climate extremes including extreme heat events, heavy precipitation and agricultural droughts have significantly increased in both frequency and intensity (IPCC, 2021). Many unprecedented extreme events surprise the society, such as the 2010 heat waves in Russia (Barriopedro et al., 2011), the 2015 European drought in summer (Ionita et al., 2017), and the heavy precipitation from Hurricane Harvey in August 2017 (Risser and Wehner, 2017; Van Oldenborgh et al., 2017). China, a populous region regulated by the East Asian monsoon and with diverse terrain, is particularly vulnerable to climate extremes. For instance, in 2018, the natural disasters caused by weather and climate extremes in China contributed to direct economic losses of about 264.5 billion yuan, along with 13.5 million affected population (Wang et al., 2021). Accounting for their destructive consequences, there is always a significant societal concern that how climate extremes in China change with global warming.

To reduce the climate change impact, the Paris Agreement, successfully signed in December 2015, pledges to limit global warming to well less than 2.0°C and set an aspirational restriction of 1.5°C above preindustrial periods. Following this, the scientific community emerges a focus to explore the changes in climate extremes at the specific warming target, such as 1.5°C, 2.0°C, and higher (Huang et al., 2017; Chen and Sun, 2018; Wu et al., 2020). Some studies have indicated that compared to the 1.5°C warming level, the additional warming of 0.5°C under the 2.0°C warmer climate will induce substantial increases in extreme high-temperature events across China (Wang et al., 2015; Chen and Sun, 2018; Wang et al., 2019; Zhou et al., 2020; Xie et al., 2021; Zhang et al., 2021; Hu et al., 2022). Chen and Sun (2019) have revealed that drought occurrence is estimated to increase by 9% in response to the 0.5°C additional warming, with extreme droughts increasing by 8%. Additionally, precipitation extremes are also projected to intensify with continuous warming over China (Jiang et al., 2020; Wu et al., 2020; Zhang et al., 2020; Xu et al., 2021).

Among these hazards, precipitation extreme is one of the most frequent disasters in China, responsible for massive socio-economic losses and mortalities (Zhai et al., 2005; Michaelides, 2013; Selvey et al., 2014). There are two typical methods to represent the precipitation extremes. One is to utilize the indices defined by the Expert Team on Climate Change Detection and Indices (ETCCDI), usually depicting the frequent climate events in 1 year. The other method is to implement the Generalized Extreme Value (GEV) distribution to obtain more extreme statistics, meaning the rare precipitation extremes with return periods (Kharin et al., 2007; Kim et al., 2020). Such rare extremes will induce more adverse consequences on the environment, human health and society (Zhang et al., 2017). Moreover, evidence has shown that human-induced warming tends to trigger larger changes in frequency and intensity of such dangerous precipitation extremes in comparison to the relatively mild events occurring per year globally (Kharin et al., 2018; Li et al., 2019; Li et al., 2021). Current studies are dedicated to understanding the changes in precipitation extremes represented by ETCCDI indices (Dong and Sun, 2018; Wu et al., 2020), whereas potential changes in the dangerous precipitation extremes with different return periods over China have received less attention.

Climate change risks result from the complex interactions of hazards, exposure, and vulnerability of society to the hazards (Leonard et al., 2013; Jones et al., 2018). Hence, other than the anticipating changes in the disasters themselves, understanding the changes in exposure to disasters is also essential for effective adaptation and mitigation of climate change risks. Previous studies have confirmed that the continuing global warming will exacerbate exposure to extreme heat events (Jones et al., 2015; Matthews et al., 2017; Rohat et al., 2019; Iyakaremye et al., 2021; Xie et al., 2022). Instead of 2.0°C, limiting the global mean temperature increase to 1.5°C can reduce the exposure to these heat extremes (Harrington and Otto, 2018; Yu et al., 2020). Chen and Sun (2019) have reported that the exposure to drought in China is on the rise under a warming climate, particularly for extreme drought. For precipitation extremes, global aggregate population exposure to precipitation extremes is projected to increase by over 50% by the end of this century (Chen and Sun, 2021). However, rarer studies focus on the population changes exposed to precipitation extremes over China, especially the dangerous events with return periods mentioned above.

Hence, the main objective of this study is to deal with these issues: 1) Compared to the current climate, how do the dangerous precipitation extremes and associated population exposure over China change at the 1.5–4.0°C warming levels under different shared socioeconomic pathways (SSPs) *via* the latest simulations from Coupled Model Intercomparison Project Phase 6 (CMIP6)? 2) To what extent can the population exposure to dangerous precipitation extremes be avoided if global warming is limited to 1.5°C? 3) What are the relative roles of changes in climate and population effect in exposure?

Data and methods

Datasets

The daily precipitation and monthly temperature outputs from the CMP6 models are employed in this study, including the historical simulations for the period of 1950–2014 and future

projections under the four SSPs spanning from 2015–2100. These data can be acquired from the website (https://esgf-node.llnl.gov/search/cmip6/). The SSPs are the new future forcing pathways related to societal development, describing the alternative evolutions of demographics, technology, economics and other societal factors (Jones and O'Neill, 2016). Given the availability of models, we use future simulations from 23, 24, 21 and 24 CMIP6 models from SSP1-2.6, SSP2-4.5, SSP3-7.0 and SSP5-8.5 scenarios, respectively (Supplementary Table S1). All the models are based on the first member (r1i1p1f1). The temperature outputs are calculated on their native girds for obtaining the periods achieving the warming targets, while the bilinear interpolation method is conducted to interpolate the precipitation simulations onto 1.5° × 1.5° grids *via* Climate Data Operator software. Moreover, we analyze the two extreme precipitation indices of maximum 1-day precipitation amount (RX1day) and the maximum 5-day precipitation amount (RX5day) calculated from the CMIP6 outputs, which are associated with the potential flood risks (Sillmann et al., 2013).

For the population exposure analysis, we apply the spatially explicit population dataset under different SSPs at a native resolution of 0.125° × 0.125°developed by Jones and O'Neill (2016). The population scenarios are in accordance with the SSPs for climate change studies, bearing the same socioeconomic assumptions. We also compare this population projection with reasonable spatial distribution to the other dataset from Inter-Sectoral Impact Model Intercomparison Project (ISI-MIP) with uniform national growth rates to justify the population data (Supplementary Figure S1).

Definition of the different warming levels

The 1.5, 2.0, 3.0, and 4.0°C global warming levels are defined as the global mean temperature increases by 1.5, 2.0, 3.0, and 4.0°C above the preindustrial level of 1861–1890. To remove the impacts of uncertainty from interannual variability on determining the warming levels, we applied the 9-year running average to the time series of the global mean temperature for individual models (Supplementary Figure S2). The 1.5–4.0°C warming periods are hereafter estimated as the 9-year windows centering on the years when the global mean temperature exceeds the corresponding warming levels for the first time under different scenarios (Supplementary Table S1). The derived centered years of the warming periods are generally similar to the results from previous studies (Zhang et al., 2018; Zhu et al., 2021), and the different centered years are attributed to the different increasing magnitudes of the global mean temperature over the coming century among the individual models and emission scenarios. Future changes under the warming climate are calculated with respect to the historical period of 1995–2014 and are first computed for individual models to obtain multi-model median ensembles (MMEs). Additionally, because the temperature of most models under SSP1-2.6 (SSP2-4.5) fails to reach the 3.0 and 4.0°C (4.0°C) warming target, the corresponding changes are not calculated. We also repeated the 21-year running average to the original time series and found little difference from the above centered years of the time windows, indicating the robustness of the defining approach of warming levels.

Dangerous precipitation extremes

RX1day and RX5day on each grid for individual models for the period of 1950–2014 were first fitted by the GEV method, deriving the cumulative density function (CDF) for the GEV analysis (Kharin et al., 2007). CDF corresponding to a specific probability p is then inverted to the quantile function of GEV, as follows.

$$X_p = \begin{cases} \mu - \sigma \ln\left[-\ln(p)\right], k = 0 \\ \mu - \frac{\sigma}{k}\ln\left[1 - (-lnp)^{-k}\right], k \neq 0 \end{cases} \quad (1)$$

Here, location parameter μ, scale parameter σ, and shape parameter k are estimated using a maximum likelihood method. Then we can derive the return values from the quantile function of GEV at each grid point (Eq. 1). For instance, the 10-year (20-year) return value is calculated when $p = 0.9$ (0.95). As shown in Figure 1, the return values over China decrease from southeast to northwest and are generally larger for the extremes with the longer return periods across China. The dangerous precipitation extremes are thus defined as the events when the RX1day and RX5day exceed their historical return values. Dangerous precipitation extremes with 10-year return period (i.e., events estimated to occur once in every 10 years) are referred to as 10-year events in the following. This is also suitable for 20-year and 50-year events.

In addition, the probability rate (PR) for the occurrence of dangerous precipitation extremes is also discussed here that is calculated as the ratio of the occurrence probability under the warmer climate to the corresponding probability in the base period of 1995–2014.

Population exposure calculation

Before the exposure investigation, we quantified the population changes as the aggregate population under the warmer climate minus the aggregate population in the baseline of 2000. The relative population changes at different warming levels under different scenarios are expressed as

$$PC_t = \frac{P_t - P_{baseline}}{P_{baseline}} \quad (2)$$

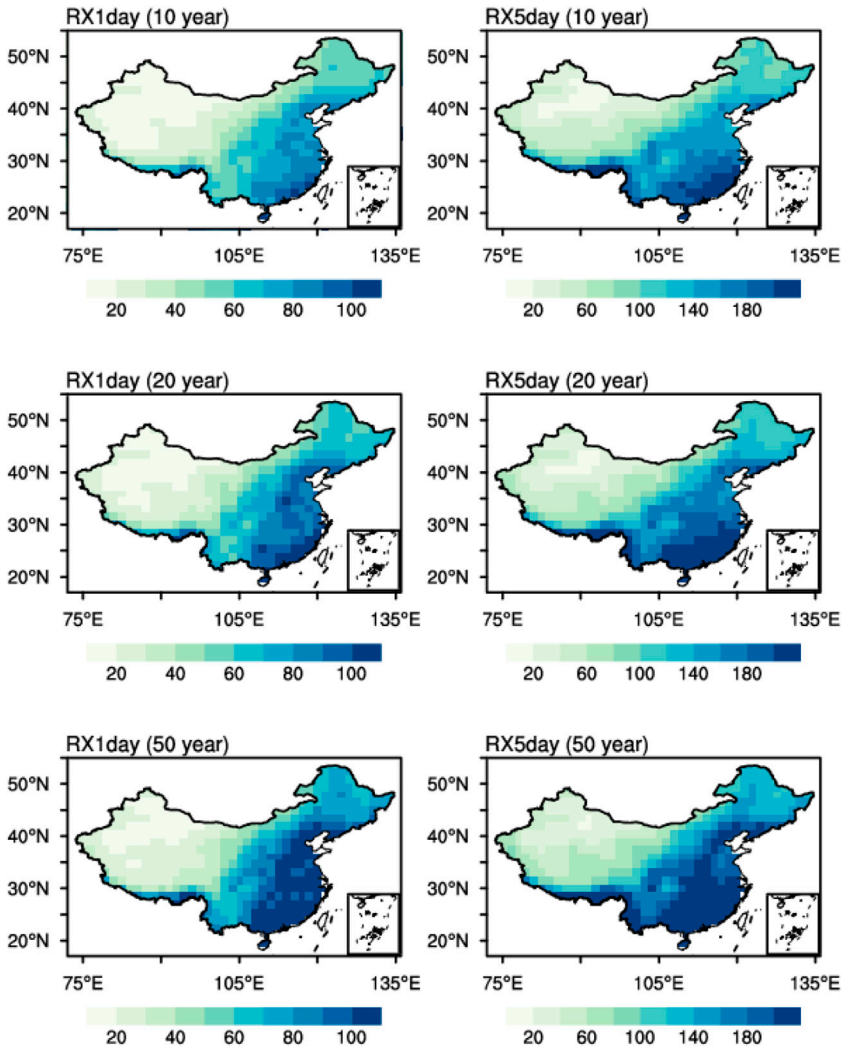

FIGURE 1
Estimated return values for the extreme events (RX1day and RX5day) that occur once in 10, 20, and 50 years fitted by the GEV analysis for the period of 1950–2014. Units: mm.

where PC_t and P_t represent the relative population changes and the population at the 1.5–4.0°C warming levels, respectively.

To calculate the population exposure to dangerous precipitation extremes, the number of people exposed to the hazard, we multiplied the frequency of dangerous precipitation extremes by the population at each grid point (Jones et al., 2015). Here, the quantified population exposure is based on the population from the baseline of 2000, and the future exposure under SSP1, SSP2, SSP3 and SSP5 is combined with the corresponding future scenarios of precipitation extreme simulations of SSP1-2.6, SSP2-4.5, SSP3-7.0 and SSP5-8.5 scenarios, respectively. The exposure changes at different warming levels relative to the baseline are estimated as follows:

$$EC_t = \frac{E_t - E_{baseline}}{E_{baseline}} \tag{3}$$

where EC_t and E_t represent the exposure change and exposure at the different warming levels of 1.5–4.0°C, respectively. The avoided impact is quantified in this study as the difference between the exposure change at 2.0°C warming levels against the 1.5°C warming level (Zhang et al., 2018).

Ultimately, we divide the changes in population exposure into three components according to Jones et al. (2015).

$$\Delta E = P_1 \times \Delta C + C_1 \times \Delta P + \Delta C \times \Delta P \tag{4}$$

In Eq. 4, $P_1 \times \Delta C$, $C_1 \times \Delta P$, $\Delta C \times \Delta P$ denote the three factors of climate change, population change and their

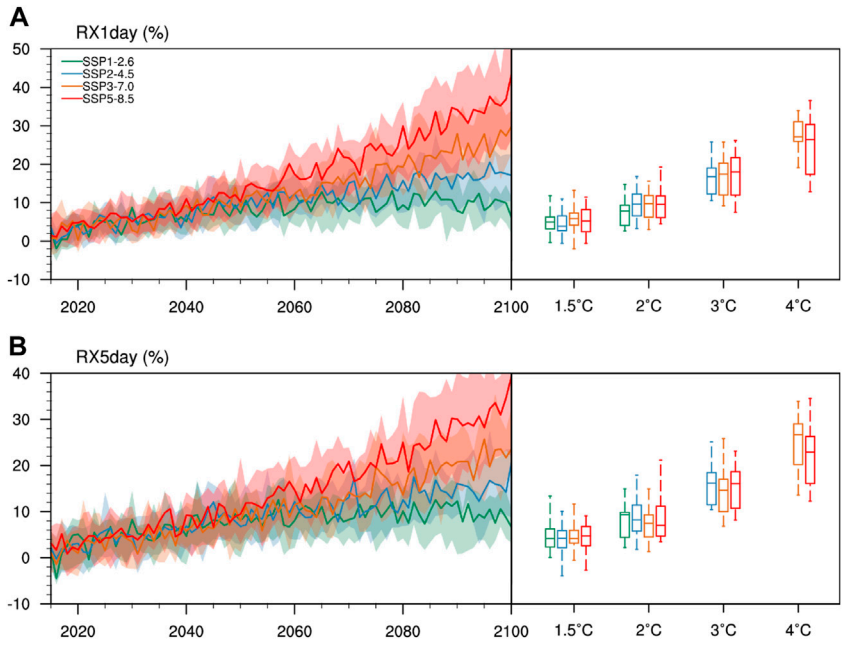

FIGURE 2
Future changes in the areal-weighted mean **(A)** RX1day and **(B)** RX5day under different emission scenarios relative to the reference period of 1995–2014. The solid lines in the left panel denote the MMEs and the shadings represent the projection uncertainty ranging from 25th to 75th quantiles. Box-and-whisker plots on the right panels depict the changes in precipitation extremes averaged over China under the 1.5, 2.0, 3.0, and 4.0°C warmer climate with respect to the present day. Herein, the solid lines in the boxes denote the MMEs, and the bounds of the boxes denote the 25th and 75th percentiles of the model simulations. The whiskers outside the boxes range represent all the inter-model ranges. Units: %.

interaction effect, respectively. Herein, ΔE, ΔC, ΔP are the changes in aggregate population exposure, dangerous precipitation extremes and population in the warmer world relative to the current climate, respectively. C_1 and P_1 mean precipitation extremes and population during the base period.

Results

Changes in precipitation extremes over China with global warming

Previous studies have shown that CMIP6 models can reasonably reproduce the basic features of precipitation extremes over China (Xu et al., 2021). Accordingly, we project the changes in precipitation extremes averaged over China during future decades based on the CMIP6 simulations (Figure 2). The MMEs of RX1day and RX5day are expected to significantly increase in the coming century relative to the current climate regardless of the scenarios, but with some differences among the four scenarios. The increase of precipitation extremes over China intensifies sequentially from low emissions of SSP1-2.6 to unconstrained emissions of SSP5-8.5, implying the vital role of societal decisions in the future increases for precipitation extremes (O'Neill et al., 2016; Riahi et al., 2017). In detail, the increase under SSP1-2.6 and SSP2-4.5 tend to be small after 2060, whereas with a clear increase under SSP3-7.0 and SSP5-8.5 scenarios. Additionally, for all scenarios, the interquartile model spreads representing the uncertainties of the future projections are also observed to be larger with time.

The regional mean changes in precipitation extremes over China at the 1.5–4.0°C warming levels with respect to the current climate are further examined (Figure 2). In line with the previous model outputs (Zhang et al., 2020), the CMIP6 simulations project more intense precipitation extremes at higher warming levels. Specifically, RX1day is reported to increase by 5.2, 9.6, 18.0, and 26.4% when the global warming reaches 1.5, 2.0, 3.0, and 4.0°C under SSP5-8.5 scenario, respectively, as well as the increases of 4.8, 7.1, 16.1, and 22.9% for RX5day. Note that the changes in RX1day and RX5day at the four warming levels from SSP5-8.5 scenario are similar to those from the other scenarios, suggesting the independence of changes to these emission scenarios. Spatially, increases for the two precipitation indices are dominant in almost all the regions of China in a warmer world, except for sporadic regions such as some parts of Southwest China and Northeast China experiencing decreases in a 1.5°C warmer world (Supplementary Figure S3).

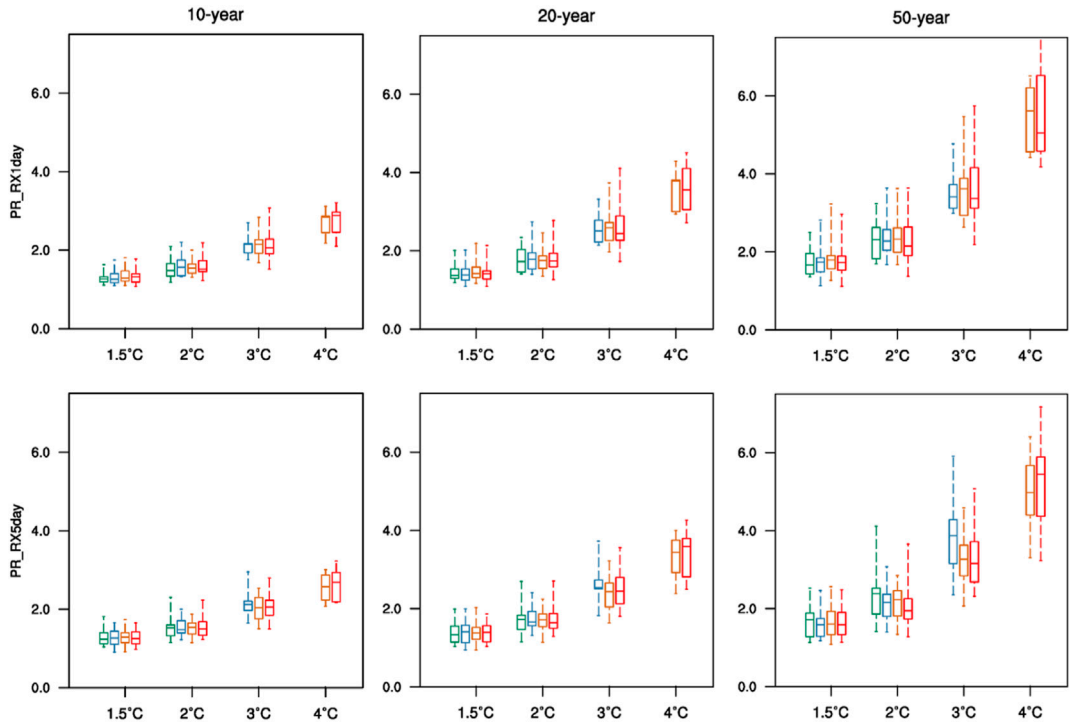

FIGURE 3
Box-and-whisker plots of the PRs of occurrence of 10-year, 20-year, and 50-year events averaged over China at the 1.5–4.0°C warming level under different scenarios. The green, blue, orange, and red boxes denote the PRs under the SSP1-2.6, SSP2-4.5, SSP3-7.0 and SSP5-8.5 scenarios, respectively.

Considering social impacts, dangerous precipitation extremes with return periods of 10–50 years are usually record-shattering and cause more irreversible damages (Zwiers et al., 2011). The changes in occurrence probability of dangerous precipitation extremes for RX1day at different warming levels are thus explored (Figure 3). The results show little difference among the emission scenarios at the same warming levels. Agreeing with the changes in precipitation extremes analyzed above, PRs of the dangerous precipitation extremes are also reported to increase with continued global warming, indicating more frequent precipitation extremes over China. For instance, the occurring probability of 20-year events under the 1.5–4.0°C warming climate increases approximately to a factor of 1.4, 1.8, 2.5, and 3.5 of that in the reference period. This indicates that the areal-mean precipitation extreme events that are expected to occur once every 20 years are expected to happen once in 14, 11, 8, and 6 years on average in the 1.5–4.0°C warmer world, respectively. Another notable feature is that PRs increase more significantly responding to the global warming with the return period extending, particularly for the high warming target. Namely, the rarer precipitation extremes show much greater increases at the given warming level. Compared to the relatively slight increases for 10-year events from the PR of 1.3 at the 1.5°C warming target to PR of 2.8 at the 4.0°C warming target, the PRs for 50-year events increase more substantially from 1.7 to 5.0 in response to global warming. Moreover, the model spreads are reported to be larger with the return periods extending. Dangerous precipitation extremes for RX5day show similar changing characteristics with RX1day.

In terms of the spatial patterns, we first consider the features of the PRs of 10-year RX1day and RX5day at the 1.5–4.0°C warming levels from SSP5-8.5 scenario. Before this, we divide China into eight subregions referring to Jiang et al., 2020 for facilitating analysis as marked in Figure 4. Almost all the regions across China experience increasing occurring probabilities (PR larger than 1) of 10-year events at the 1.5°C warming target with respect to present-day (Figure 4). The remarkable increase is mainly centered in some regions of the Tibet Plateau and southeastern China, especially for high warming scenarios. The PRs of the Tibet Plateau are even roughly larger than 3, i.e., more than twofold increases for the occurrence of 10-year events at the 4.0°C warming levels as opposed to the present day. Furthermore, the occurring probability for more intense events, such as the 20-year events, present similar change patterns, but with larger magnitudes at the same warming level (Supplementary Figure S4). Likewise, these changes are also insensitive to the warming levels from different forcing scenarios.

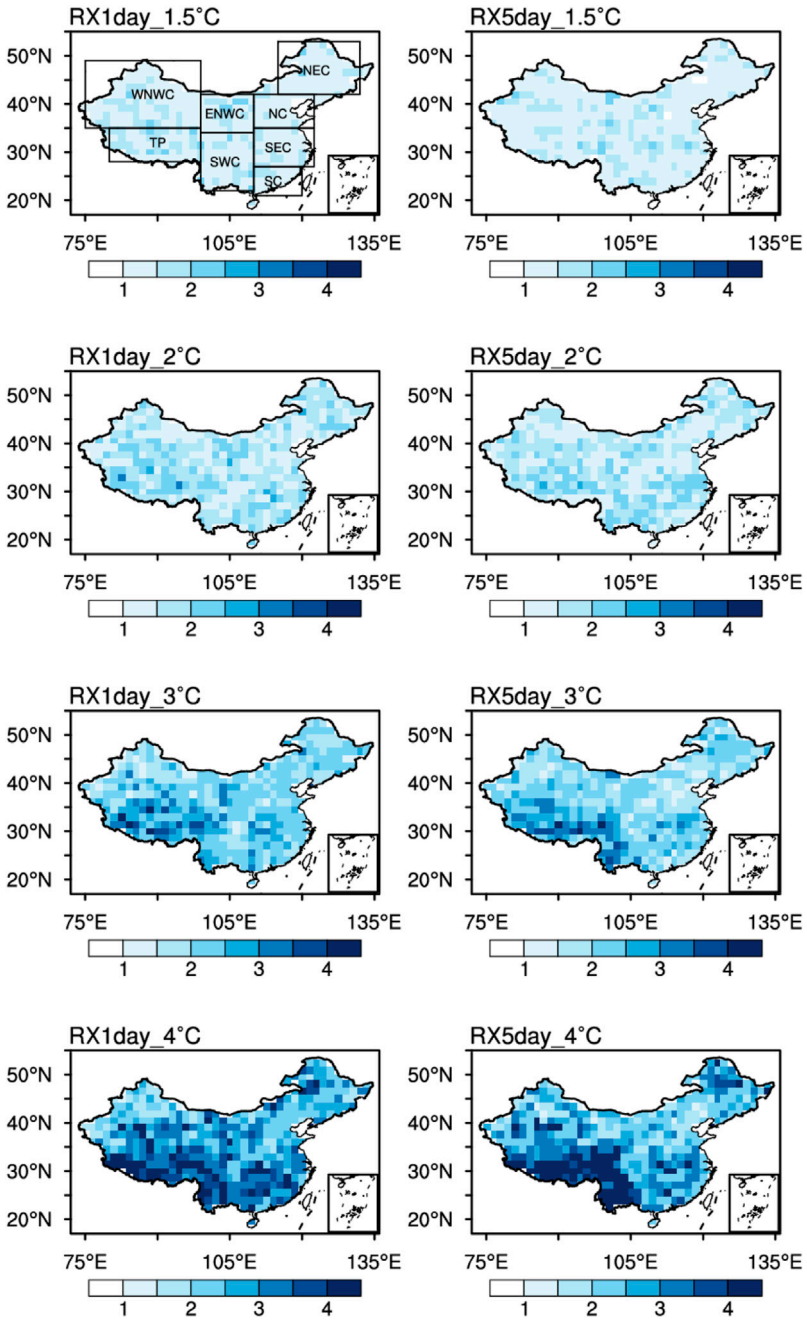

FIGURE 4
Spatial patterns for the PRs of the occurrence of 10-year RX1day and RX5day over China under the 1.5–4.0°C warmer climate under the SSP5-8.5 scenario with respect to the current climate (1995–2014). The occurrence probability of precipitation extremes is expected to increase if the PR is larger than 1.0.

Changes in population exposure over China with global warming

During the past decades, precipitation extreme events frequently hit China, posing a serious threat to human society and leaving numerous people displaced, injured, missing and even dead (Wang et al., 2012). Therefore, it is imperative to evaluate the population exposed to this natural hazard in China.

Apart from the above changing extreme events, exposure to the hazards also depends on changes in the number and spatial pattern of the human population (Jones et al., 2015). We thus project the aggregate population growth and the geographical

10.3389/feart.2022.963042

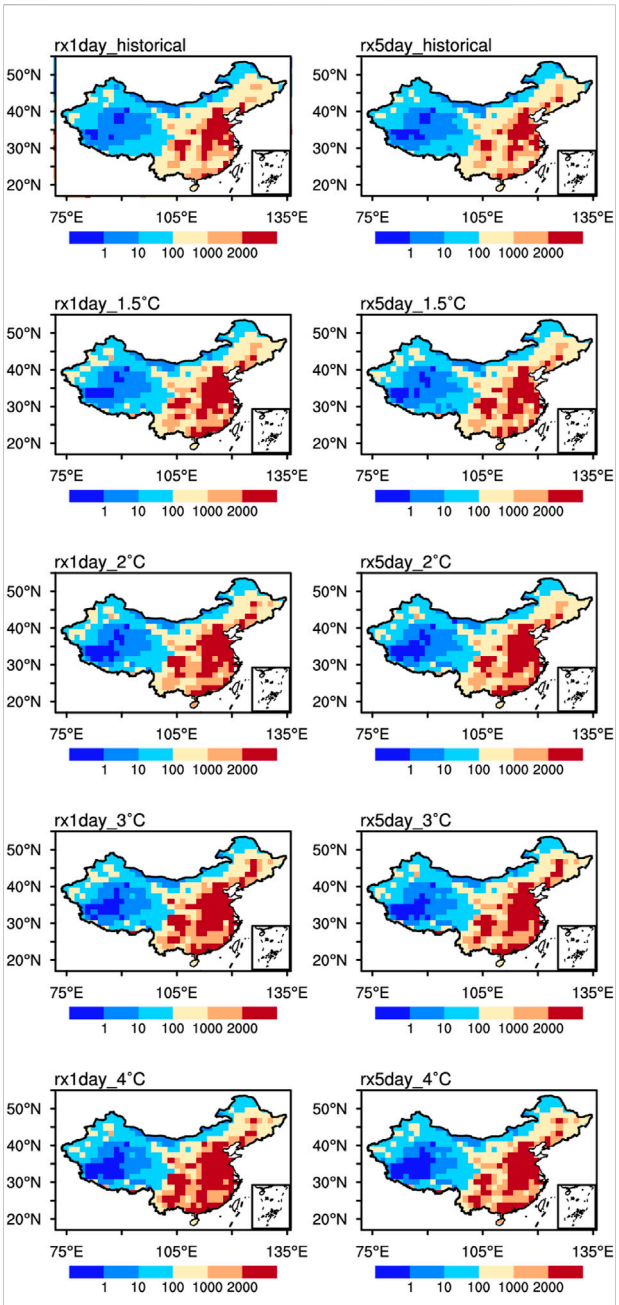

FIGURE 5
Spatial patterns of the population exposure to the 10-year events over China in the base year of 2000 (the first row) and in response to the 1.5–4.0°C warming under the SSP5-8.5 scenario (the last four rows). Units: 10^4 person-days.

distribution across China in the coming future under different scenarios (Supplementary Figures S1, S5). The total population in China is projected to peak around the year 2030 under the SSP2 and SSP3 scenarios and around the year 2020 under the scenarios of SSP1, SSP4 and SSP5, subsequently decreasing (Supplementary Figure S1). The population reduction from SSP1, SSP4 and SSP5 is more rapid with respect to that from the SSP3 scenario, along with a relatively moderate change in the population of the SSP2 scenario. By the end of the 21st century, the population is projected to decline throughout China (Supplementary Figure S5). Consistent with the demographic structure in the baseline, the dense population is still mainly concentrated in eastern China, while the regions of northwestern China and the Tibetan Plateau have a low population density by the end of the 21st century. Moreover, the population decline also varies across regions. The Tibetan Plateau is anticipated to experience the largest decrease, along with the slight proportional reduction in eastern China (Supplementary Figures S5D,E).

In the following, we further investigate the population exposure to the dangerous precipitation extremes with 10-year return periods for RX1day and RX5day over China under different warming targets from the SSP5-8.5 scenario (Figure 5). Clearly, the spatial structures of population exposure are similar to those of the population in China, with notable regional variations. In the base period of 2000, regions with a dense population including eastern China and some regions of southwestern China, such as the Sichuan Basin, have a high population exposure to dangerous precipitation extremes. Conversely, the low exposure is mainly concentrated over the Tibetan Plateau and northwestern China, also coinciding with regions sparsely populated. With the global mean temperature increasing, the future basic feature of population exposure is similar to that in the base period, but with more widespread exposure in high-exposure areas and the lower population exposed to precipitation extremes in originally low-exposure areas. This regional difference of population changes exposed to precipitation extremes may be associated with the discrepancy of future population changes in China.

Figure 6 maps the changes in population exposure to precipitation extremes for 10-year RX1day and RX5day events over China in the warmer world under SSP5-8.5 scenario against the base period. The exposure presents persistent increases in most regions of China in response to the continued global warming, but with spatial heterogeneity for the increasing magnitude. Notably, under the 4.0°C warmer climate that is estimated to occur around 2080 under SSP5-8.5 scenarios, the exposure exhibits widespread and remarkable increases over most regions of eastern and southern China with a high model agreement, increasing by over 60%. This indicates that China will experience a larger population exposed to the dangerous precipitation extremes under the future warmer climate. However, the exposure is projected to decline over some grids of northwestern China and the Tibetan Plateau as a consequence of the global mean temperature increases, and the declines over these regions are reported to strengthen and enlarge with warming. The 4.0°C global warming will result in striking decreases in population exposure of more than 60% over the Tibetan Plateau with a high model agreement. This may be attributed to the decreasing population in these areas.

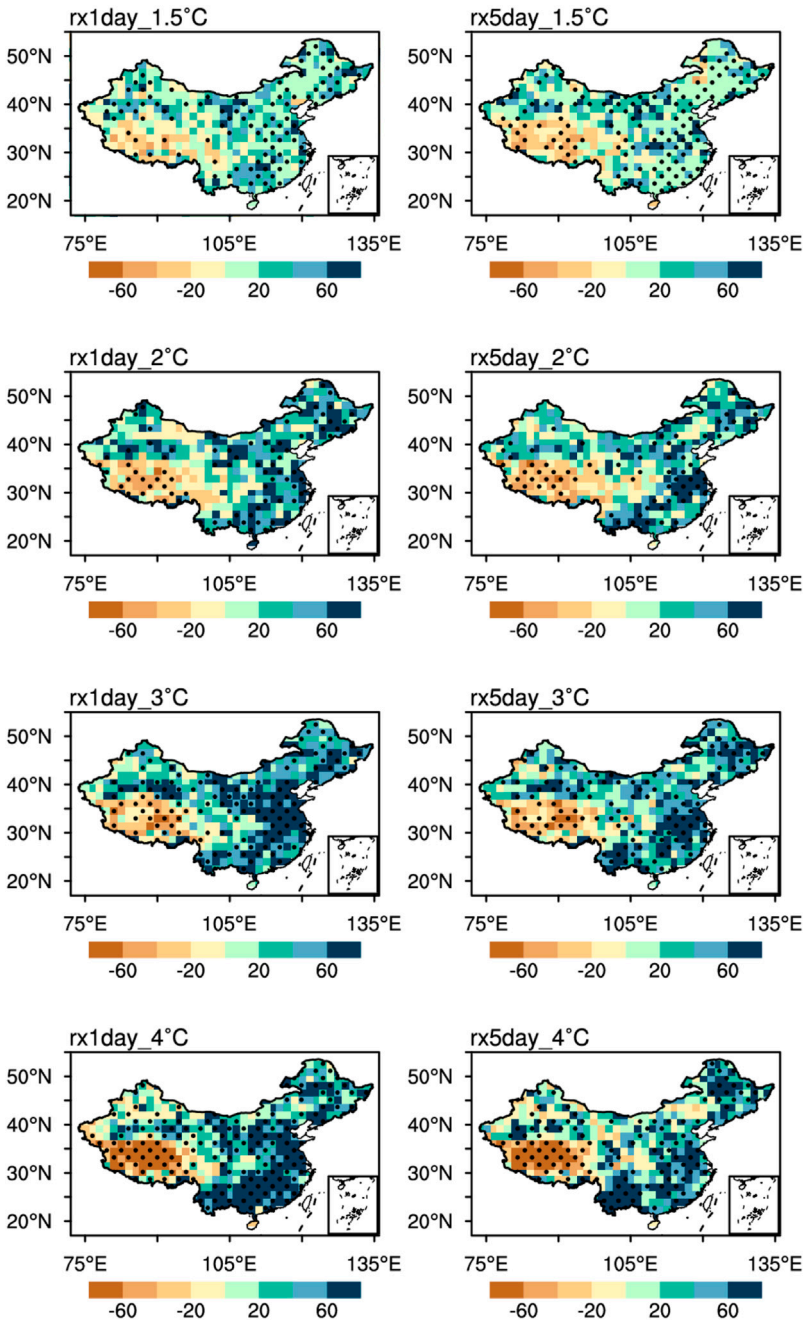

FIGURE 6
Future changes in population exposure to the 10-year events in response to the 1.5–4.0°C warming under the SSP5-8.5 scenario relative to the present day (1995–2014). The stippling is applied in regions where over 2/3 of the models are in accordance with the signs of MME changes. Units: %.

Additionally, changes in population exposure to the 20-year events bear similar geographical patterns to those for the 10-year events under a warmer climate, but with relatively large increasing magnitudes in exposure-increasing areas, particularly for the high warming levels (Supplementary Figure S6). For the other emission scenarios, the exposure distributions resemble those under SSP5-8.5, whereas there are scenario exceptions. When choosing the regional-rivalry scenario of SSP3-7.0, the increases of population exposure are expected to remarkably enlarge and enhance across China with the higher model agreement compared to the fossil-fueled development scenario of SSP5-8.5 (Supplementary Figure S7). Also

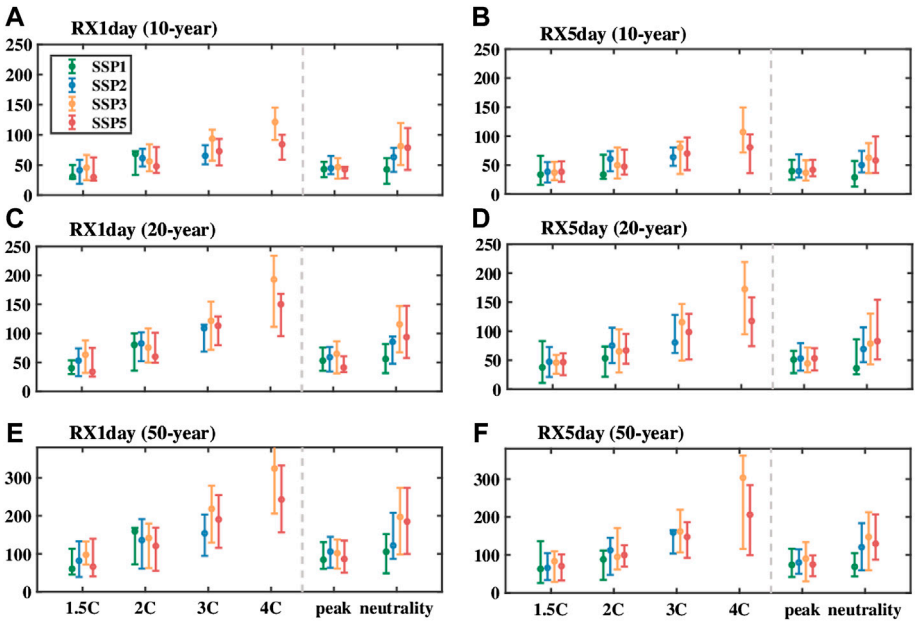

FIGURE 7
Projected changes in areal-mean aggregated population exposure to **(A)**, **(B)** 10-year, **(C)**, **(D)** 20-year and **(E)**, **(F)** 50-year RX1day and RX5day over China under the 1.5–4.0°C warmer climate as well as the carbon peak (2030) and neutrality periods (2060) under all the four SSPs. The data points and error bars represent the MMEs and interquartile model spreads, respectively. Units: %.

distinguished from SSP5-8.5 scenario, the decreases are reported to shrink and weaken with warming under SSP3-7.0 scenario, and also with a lower model agreement. Specifically, the decreases can still be observed over the Tibetan Plateau at the 1.5°C warming level, but are confined to a smaller region and weaker as opposed to the same levels under SSP5-8.5. In the 2–4.0°C warmer climates, pronounced increases for population exposure were predominant almost everywhere across China and the decreases are estimated to nearly vanish under SSP3-7.0 scenario. This suggests the important role of societal decisions in future changes in population exposure to the dangerous precipitation extremes (Jones and O'Neill, 2016).

Figure 7 comprehensively summarizes the areal mean exposure changes to dangerous precipitation extremes with return periods ranging from 10 to 50 years for RX1day and RX5day at the four warming levels from different scenarios. We prioritize illustrating the results from SSP5-8.5 scenario. Given the similar results from RX1day and RX5day, our following analysis is mainly based on RX1day. Overall, future warming heightens the aggregated population exposure to precipitation extremes. Considering the 20-year events first, the exposure changes increase with the global mean temperature increasing. The warming against the current state to 1.5–4.0°C warmer climate leads to about 34.0% (25.8–74.9%), 60.1% (49.7–101.2%), 113.0% (80.0–129.2%), and 150.3% (95.5–168.4%) increases in the population exposure on average, respectively. Similar tendencies can be observed in exposure for the 10-year events, whereas the increasing magnitudes are smaller than those of the 20-year events at the same warming levels, with respective increases of approximately 29.9% (23.8–62.7%), 47.8% (36.8–79.8%), 72.9% (49.3–93.3%), and 84.3% (58.8–99.9%). In contrast, changes in the 50-year events outpace changes in more moderate events such as the 20-year events under the continued global warming, with the evidently larger increasing magnitudes at the same warming levels. Correspondingly, similar to changes in occurring probability of the dangerous precipitation extremes, the relative population changes exposed to precipitation extremes are also larger for the rarer and more extreme events. In addition, the interquartile model uncertainties are larger for the rarer events.

Differing from the changes in occurring probability, the areal weighted average exposure changes are somewhat sensitive to the selected forcing scenarios, embodying the role of demographic change in the exposure. For SSP1-2.6 and SSP2-4.5 scenarios, the exposure also increases consistently with the future warming, but the differences from changes under SSP5-8.5 scenario are not very clear owning to the limited models reaching the high warming thresholds. However, it is evident that compared to SSP5-8.5 scenario, the areal mean population exposure presents a larger proportional increase at the same warming levels under SSP3-7.0 scenario, particularly for the high warming targets, regardless of the return periods of precipitation extremes. For instance, the 4.0°C warming with respect to the current climate

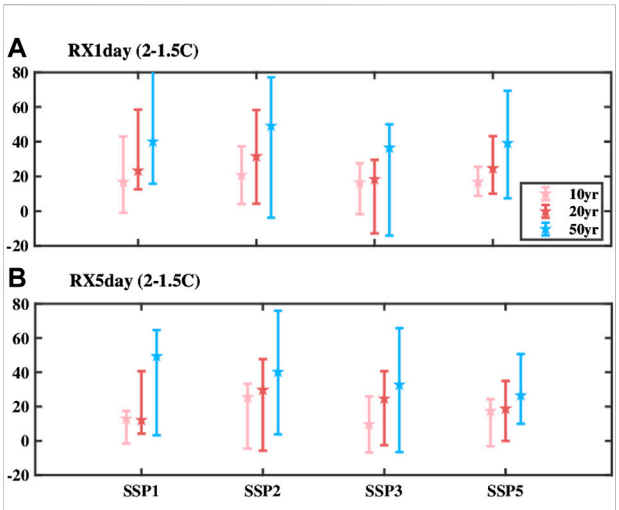

FIGURE 8
The regional mean reduced population exposure to 10-year, 20-year and 50-year **(A)** RX1day and **(B)** RX5day under the 1.5°C warmer climate instead of the 2.0°C warmer climate. The star points and error bars represent the MMEs and interquartile model spreads, respectively. Units: %.

will drive an increase of over 300% in the exposure to the 50-year RX1day on average under SSP3-7.0 scenario, about 80% more than the changes under SSP5-8.5 scenario. As a consequence, population exposure changes are subject to the chosen emission scenarios, implying the importance of societal decisions. Briefly, the spatial patterns of exposure changes are in good agreement with the areal averages of exposure changes, confirming the robustness of our findings in this study.

We further estimate the avoided impacts in terms of the population exposure if the global mean temperature increases to 1.5°C instead of 2.0°C (Figure 8). The aggregated mean indicates that a 0.5°C reduced warming is projected to trigger more decreases of about 16.7, 20.8, 16.5, and 16.9% for exposure to the 10-year RX1day events under SSP1-2.6, SSP2-4.5, SSP3-7.0, and SSP5-8.5 scenarios, respectively. For more intense events, including the 20-year and 50-year RX1day events, the population exposure decreases more remarkably in response to the 0.5°C reduced warming under all the emission scenarios. The cases are also true for RX5day. Notably, the rarer events also bear the larger model uncertainty for the avoided changes.

Roles of climate and population changes in exposure

To assess the role of the factors to the changes in population exposure to the dangerous precipitation extremes over China, we further decompose the aggregate exposure change into three elements, i.e., the population change component, the climate change component, and their interaction effect. Figure 9 illustrates the contributions of the three components to the exposure changes for the 10-year events under the future warming climate from the four SSP scenarios. RX1day and RX5day also yield similar outcomes, thus choosing RX1day for analyzing. Under SSP5-8.5 scenario, increases in population exposure are mainly sourced from the climate change, followed by the relatively minor contribution from the population change and their interaction effect. If the global mean temperature increases by 1.5°C, pronounced increases are expected in exposure for the 10-year events with about 2.1 million person-days. Herein, the climate driver contributes most to the increase of 1.4 million person-days, accounting for 67% of the total exposure increase, whereas the minor attributable increases to population change and their effects only account for 28 and 5%, respectively (Figure 9 and Supplementary Figure S8). With the warming level increasing, the contribution from climate change shows a dramatic increase, while the effects of population change and their interaction decreases, making an increasingly negative contribution to the exposure increases. At the 4.0°C warming levels, the climate change exerts a more pronounced effect on the increased exposure compared to the lower warming levels, adding 12.1 million person-days, but counteracted by the negative effect of population change and the interaction component of 6.1 million person-days totally. Consequently, the exposure increases by about 6.0 million person-days, just approximately 1.1 million person-days larger than those at the 3.0°C warming levels owning to the important offsetting role of the population change and interaction components.

Concerning the contribution rate of the three components, under the 1.5°C warmer climate under SSP5-8.5 scenario, the climate change dominates the exposure change, but the population contribution is also clear due to the relatively small risk of precipitation extremes at the limited warming target (Supplementary Figure S8). From 2.0 to 4.0°C warming, the contribution rate of the climate change component exhibits a progressive decrease, declining from a key dominance of 91–67%. Simultaneously, the contribution portions of the combined negative effects from population and interaction components are estimated to increase from 9 to 33%, but they still take a back seat to the climate driver.

Briefly, at the low warming level, the combined positive effects from the three factors drive the increased exposure, dominated by the climate change. Meanwhile, at the high warming level, the increased population exposed to precipitation extremes can be also largely attributed to the climate change factor but partially offset by the negative contribution from the population and interaction components. Additionally, under other scenarios, the change in population exposure is also heavily influenced by climate change, followed by the demographic change and their interaction effects (Figure 9). Particularly, compared to

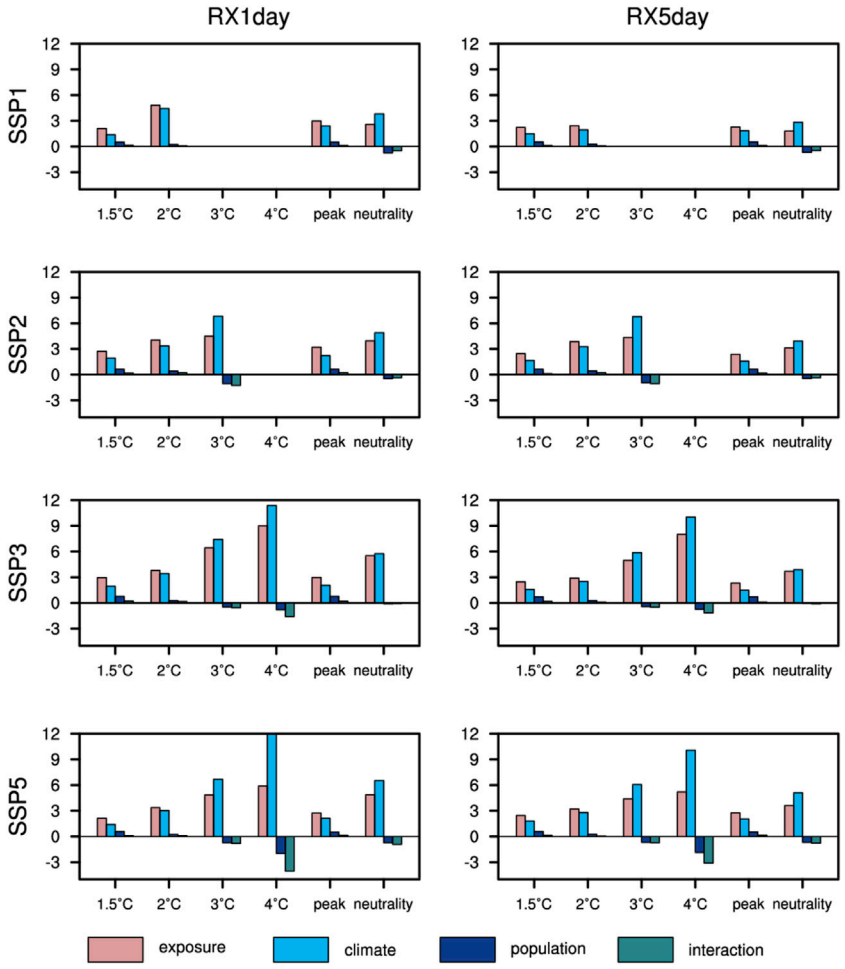

FIGURE 9
Contribution from climate change, population change, and their interaction effect on the exposure change in response to the 1.5–4.0°C warming as well as the carbon peak (2030) and neutrality periods (2060) under all the four SSPs. Units: 10^6 person-days.

SSP5-8.5 scenario, the demographic change plays a more minor negative role in the increased exposure owing to the slow population decline under SSP3-7.0 scenario. Overall, the similar features between emission scenarios enhance the credibility of the outcomes.

Changes in exposure during carbon peak and neutrality periods

As part of the Paris Agreement, China aims to peak its carbon emissions by 2030 and reach carbon neutrality by 2060 to combat climate change (Guan et al., 2018; Liu Z. et al., 2021). The population changes exposed to the dangerous precipitation extremes over China during the two periods under different emission scenarios are thus of specific concern. By 2030, a similar pattern of the exposure changes can be reported with the changes at the 1.5°C warming levels, with the increases prevailing over eastern China and decreases over some parts of western China, especially over the Tibetan Plateau (Supplementary Figure S9). The areal means for all the scenarios show similar overall increases (Figure 7). Under the further warming induced by the continued emissions of the greenhouse gases, dangerous precipitation extremes are more influential on the population over China by 2060, with the exposure increases enlarging over most of the regions with a high model agreement, except for the Tibetan Plateau. The areal-mean increased exposure by 2060 is comparable to the increases induced by 2.0–3.0°C global warming, especially pronounced under the high emission scenarios of SSP3-7.0 and SSP5-8.5 (Figure 7). Such findings emphasize the crucial role that continued emissions of greenhouse gases play in contributing to the precipitation-related risks over China, and highlight the necessity of conducting the regulation policies to reduce the carbon emissions.

Conclusion and discussion

This study projects the future changes in dangerous precipitation extremes and the population exposure to these hazards over China at 1.5–4.0°C warming levels under different SSPs with respect to the current climate, paying particular attention to the relative roles of climate and population effect in the exposure. As global mean temperature increases, the CMIP6 simulations project more frequent dangerous precipitation extremes with return periods ranging from 10 to 50 years across China, with more remarkable increases in the occurrence probability at the high warming levels. This is in accordance with the results of previous CMIP models (Li et al., 2018). For instance, the areal mean occurring probability of 20-year RX1day is reported to significantly increase by approximately 40, 80, 150, and 250% at the 1.5, 2.0, 3.0, and 4.0°C warming climate under SSP5-8.5 scenario with respect to the current climate of 1995–2014, respectively. Notably, the magnitudes of the increases rely on the rarity of precipitation extremes, and the increases are more intense for rarer events. Other scenarios yield the similar features with SSP5-8.5, implying the independence of the outcomes to emission scenarios. RX5day also shares the similar results with RX1day. Briefly, global warming will exacerbate the increases in the occurrence of dangerous precipitation extremes with different return periods across China regardless of the chosen scenarios.

As a consequence of the increased occurrence, population exposure to dangerous precipitation extremes over China presents persistent increases with continued future warming. The 1.5–4.0°C warming relative to present-day results in approximately 29.9, 47.8, 72.9, and 84.3% increases in the aggregated population exposure to the 10-year RX1day under SSP5-8.5 scenario on average, respectively. A similar tendency can be expected in exposure for events with other return periods, but the increasing magnitudes for the population exposed to precipitation extremes are also larger for more extreme events. Spatially, the increases dominate in most regions of China, particularly for regions of eastern and southern China, with more widespread and intense increases for the higher warmer climate. Conversely, some parts of northwestern China and the Tibetan Plateau experience decreasing exposure with future warming. In addition, different from the occurrence changes, the areal weighted average exposure changes are somewhat sensitive to the selected forcing scenarios. Despite the consistent increases in exposure with future warming under other scenarios, the aggregated population exposure presents the larger proportional increases at the same warming levels from the regional-rivalry scenario of SSP3-7.0 compared to the fossil-fueled development scenario of SSP5-8.5. This indicates population exposure changes are subject to emission scenarios, embodying the importance of societal decisions.

Previous literature has documented that limiting global warming from 2.0 to 1.5°C can reduce the population exposure to the 20-year events over the global land monsoon region by 36% (Zhang et al., 2018). In this study, the 0.5°C less warming is estimated to trigger remarkable decreases of 16.5–20.5% for exposure to the 10-year events over China. Our results are also in line with Zhang et al. (2018) that the avoided impacts are more significant for rarer events.

Climate and population changes both drive the exposure changes. Analysis of their relative role shows that the climate change effect is the key determinant of the increased exposure to precipitation extremes, which is partly counteracted by the negative effects of the population change and their interaction components. The offsetting effect of the population is sourced from the population decline over China, while the negative contribution of their interaction component is mainly attributed to the asynchronous changes in climate and population (Jones et al., 2015). Majority of the regions over China undergoing increased precipitation present the decreased population, which may be the primary cause of the negative effect of the interaction component. This highlights the importance of mitigation strategies for precipitation extremes to decrease population exposure, particularly for vulnerable and populous regions such as eastern China.

The projection of precipitation extremes still bears large uncertainties, especially for the rarer events, which is generally consistent with the outcomes of previous CMIP outputs (Kharin et al., 2018). The global models have difficulty in simulating the precipitation extremes in some local regions with complex topography due to their coarse resolutions (Zhou et al., 2019; Xie et al., 2021). More different models for climate or population should be adopted in further exploration. Nevertheless, the analysis from multiple emission scenarios and precipitation indices leads to generally consistent qualitative results, verifying the robust estimation for exposure over China in this study. In addition, recently, investigations are emerging about the exposure to the compound events, such as the co-occurrence of drought and heatwaves (Liu W. et al., 2021), which may trigger more amplified consequences as opposed to the individual events. This encourages us to assess the risks arising from the compound events in the future work.

Data availability statement

The original contributions presented in the study are included in the article/Supplementary Material, further inquiries can be directed to the corresponding author.

Author contributions

HX: formal analysis; investigation; writing original draft; writing—review and editing. HC: conceptualization; methodology; supervision; writing original draft; writing—review and editing. HW: resources; supervision.

Funding

This research was jointly supported by the Strategic Priority Research Program of the Chinese Academy of Sciences (Grant No: XDA23090102) and the National Natural Science Foundation of China (Grant No: 41922034, 42075021).

Conflict of interest

The authors declare that the research was conducted in the absence of any commercial or financial relationships that could be construed as a potential conflict of interest.

Publisher's note

All claims expressed in this article are solely those of the authors and do not necessarily represent those of their affiliated organizations, or those of the publisher, the editors and the reviewers. Any product that may be evaluated in this article, or claim that may be made by its manufacturer, is not guaranteed or endorsed by the publisher.

Supplementary material

The Supplementary Material for this article can be found online at: https://www.frontiersin.org/articles/10.3389/feart.2022.963042/full#supplementary-material

References

Barriopedro, D., Fischer, E. M., Luterbacher, J., Trigo, R. M., and Garcia-Herrera, R. (2011). The hot summer of 2010: redrawing the temperature record map of europe. *Science* 332, 220–224. doi:10.1126/science.1201224

Chen, H., and Sun, J. (2019). Increased population exposure to extreme droughts in China due to 0.5 °C of additional warming. *Environ. Res. Lett.* 14, 064011. doi:10.1088/1748-9326/ab072e

Chen, H., and Sun, J. (2018). Projected changes in climate extremes in China in a 1.5°C warmer world. *Int. J. Climatol.* 38, 3607–3617. doi:10.1002/joc.5521

Chen, H., and Sun, J. (2021). Significant increase of the global population exposure to increased precipitation extremes in the future. *Earth's. Future* 9, 2020EF001941. doi:10.1029/2020ef001941

Dong, S., and Sun, Y. (2018). Comparisons of observational data sets for evaluating the CMIP5 precipitation extreme simulations over Asia. *Clim. Res.* 76, 161–176. doi:10.3354/cr01534

Guan, D., Meng, J., Reiner, D. M., Zhang, N., Shan, Y., Mi, Z., et al. (2018). Structural decline in China's CO2 emissions through transitions in industry and energy systems. *Nat. Geosci.* 11, 551–555. doi:10.1038/s41561-018-0161-1

Harrington, L. J., and Otto, F. E. L. (2018). Changing population dynamics and uneven temperature emergence combine to exacerbate regional exposure to heat extremes under 1.5°C and 2°C of warming. *Environ. Res. Lett.* 13, 034011. doi:10.1088/1748-9326/aaaa99

Hu, D., Jiang, D., Tian, Z., and Lang, X. (2022). How skillful was the projected temperature over China during 2002–2018? *Sci. Bull.* 67, 1077–1085. doi:10.1016/j.scib.2022.02.004

Huang, J., Yu, H., Dai, A., Wei, Y., and Kang, L. (2017). Drylands face potential threat under 2 °C global warming target. *Nat. Clim. Chang.* 7, 417–422. doi:10.1038/nclimate3275

Ionita, M., Tallaksen, L. M., Kingston, D. G., Stagge, J. H., Laaha, G., Van Lanen, H. A. J., et al. (2017). The European 2015 drought from a climatological perspective. *Hydrol. Earth Syst. Sci.* 21, 1397–1419. doi:10.5194/hess-21-1397-2017

IPCC (2021). *Climate change 2021: The physical science basis. Contribution of working group I to the sixth assessment Report of the intergovernmental panel on climate change*. Cambridge: Cambridge University Press.

Iyakaremye, V., Zeng, G., Yang, X., Zhang, G., Ullah, I., Gahigi, A., et al. (2021). Increased high-temperature extremes and associated population exposure in Africa by the mid-21st century. *Sci. Total Environ.* 790, 148162. doi:10.1016/j.scitotenv.2021.148162

Jiang, D. B., Hu, D., Tian, Z. P., and Lang, X. M. (2020). Differences between CMIP6 and CMIP5 models in simulating climate over China and the East Asian monsoon. *Adv. Atmos. Sci.* 37, 1102–1118. doi:10.1007/s00376-020-2034-y

Jones, B., O'Neill, B. C., McDaniel, L., McGinnis, S., Mearns, L. O., and Tebaldi, C. (2015). Future population exposure to US heat extremes. *Nat. Clim. Chang.* 5, 652–655. doi:10.1038/nclimate2631

Jones, B., and O'Neill, B. C. (2016). Spatially explicit global population scenarios consistent with the Shared Socioeconomic Pathways. *Environ. Res. Lett.* 11, 084003. doi:10.1088/1748-9326/11/8/084003

Jones, B., Tebaldi, C., O'Neill, B. C., Oleson, K., and Gao, J. (2018). Avoiding population exposure to heat-related extremes: demographic change vs climate change. *Clim. Change* 146, 423–437. doi:10.1007/s10584-017-2133-7

Kharin, V. V., Flato, G. M., Zhang, X., Gillett, N. P., Zwiers, F., and Anderson, K. J. (2018). Risks from climate extremes change differently from 1.5°C to 2.0°C depending on rarity. *Earth's. Future* 6, 704–715. doi:10.1002/2018ef000813

Kharin, V. V., Zwiers, F. W., Zhang, X., and Hegerl, G. C. (2007). Changes in temperature and precipitation extremes in the IPCC ensemble of global coupled model simulations. *J. Clim.* 20, 1419–1444. doi:10.1175/jcli4066.1

Kim, Y. H., Min, S. K., Zhang, X., Sillmann, J., and Sandstad, M. (2020). Evaluation of the CMIP6 multi-model ensemble for climate extreme indices. *Weather Clim. Extrem.* 29, 100269. doi:10.1016/j.wace.2020.100269

Leonard, M., Westra, S., Phatak, A., Lambert, M., van den Hurk, B., McInnes, K., et al. (2013). A compound event framework for understanding extreme impacts. *WIREs Clim. Change* 5, 113–128. doi:10.1002/wcc.252

Li, C., Zwiers, F., Zhang, X., Chen, G., Lu, J., Li, G., et al. (2019). Larger increases in more extreme local precipitation events as climate warms. *Geophys. Res. Lett.* 46, 6885–6891. doi:10.1029/2019gl082908

Li, C., Zwiers, F., Zhang, X., Li, G., Sun, Y., and Wehner, M. (2021). Changes in annual extremes of daily temperature and precipitation in CMIP6 models. *J. Clim.* 34, 3441–3460. doi:10.1175/jcli-d-19-1013.1

Li, W., Jiang, Z., Zhang, X., Li, L., and Sun, Y. (2018). Additional risk in extreme precipitation in China from 1.5 °C to 2.0 °C global warming levels. *Sci. Bull.* 63, 228–234. doi:10.1016/j.scib.2017.12.021

Liu, W., Sun, F., Feng, Y., Li, C., Chen, J., Sang, Y. F., et al. (2021a). Increasing population exposure to global warm-season concurrent dry and hot extremes under different warming levels. *Environ. Res. Lett.* 16, 094002. doi:10.1088/1748-9326/ac188f

Liu, Z., Deng, Z., He, G., Wang, H., Zhang, X., Lin, J., et al. (2021b). Challenges and opportunities for carbon neutrality in China. *Nat. Rev. Earth Environ.* 3, 141–155. doi:10.1038/s43017-021-00244-x

Matthews, T. K., Wilby, R. L., and Murphy, C. (2017). Communicating the deadly consequences of global warming for human heat stress. *Proc. Natl. Acad. Sci. U. S. A.* 114, 3861–3866. doi:10.1073/pnas.1617526114

Michaelides, S. (2013). Vulnerability of transportation to extreme weather and climate change. *Nat. Hazards* 72, 1–4. doi:10.1007/s11069-013-0975-5

O'Neill, B. C., Tebaldi, C., van Vuuren, D. P., Eyring, V., Friedlingstein, P., Hurtt, G., et al. (2016). The scenario model Intercomparison project (ScenarioMIP) for CMIP6. *Geosci. Model Dev.* 9, 3461–3482. doi:10.5194/gmd-9-3461-2016

Riahi, K., van Vuuren, D. P., Kriegler, E., Edmonds, J., O'Neill, B. C., Fujimori, S., et al. (2017). The Shared Socioeconomic Pathways and their energy, land use, and greenhouse gas emissions implications: An overview. *Glob. Environ. Change* 42, 153–168. doi:10.1016/j.gloenvcha.2016.05.009

Risser, M. D., and Wehner, M. F. (2017). Attributable human-induced changes in the likelihood and magnitude of the observed extreme precipitation during Hurricane Harvey. *Geophys. Res. Lett.* 44, 12457–12464. doi:10.1002/2017gl075888

Rohat, G., Flacke, J., Dosio, A., Dao, H., and Maarseveen, M. (2019). Projections of human exposure to dangerous heat in african cities under multiple socioeconomic and climate scenarios. *Earth's. Future* 7, 528–546. doi:10.1029/2018ef001020

Selvey, L. A., Rutherford, S., Dodds, J., Dwyer, S., and Robinson, S. M. (2014). The impact of climate-related extreme events on public health workforce and infrastructure - how can we be better prepared? *Aust. N. Z. J. Public Health* 38, 208–210. doi:10.1111/1753-6405.12219

Sillmann, J., Kharin, V. V., Zwiers, F. W., Zhang, X., and Bronaugh, D. (2013). Climate extremes indices in the CMIP5 multimodel ensemble: Part 2. Future climate projections. *J. Geophys. Res. Atmos.* 118, 2473–2493. doi:10.1002/jgrd.50188

Van Oldenborgh, G. J., Van der Wiel, K., Sebastian, A., Singh, R., Arrighi, J., Otto, F., et al. (2017). Attribution of extreme rainfall from Hurricane Harvey, August 2017. *Environ. Res. Lett.* 12, 124009. doi:10.1088/1748-9326/aa9ef2

Wang, H., Sun, J., Chen, H., Zhu, Y., Zhang, Y., Jiang, D., et al. (2012). Extreme climate in China: Facts, simulation and projection. *Meteorol. Z.* 21, 279–304. doi:10.1127/0941-2948/2012/0330

Wang, J., Song, Y., and Xue, D. (2021). Spatio-temporal evolution of natural disasters and its social-economic effects in China. *J. Zhejiang Univ. Sci. Ed.* 48, 750–759.

Wang, W., Zhou, W., Li, X., Wang, X., and Wang, D. (2015). Synoptic-scale characteristics and atmospheric controls of summer heat waves in China. *Clim. Dyn.* 46, 2923–2941. doi:10.1007/s00382-015-2741-8

Wang, X. X., Jiang, D. B., and Lang, X. M. (2019). Extreme temperature and precipitation changes associated with four degree of global warming above pre-industrial levels. *Int. J. Climatol.* 39, 1822–1838. doi:10.1002/joc.5918

Wu, J., Han, Z., Xu, Y., Zhou, B., and Gao, X. (2020). Changes in extreme climate events in China under 1.5°C–4°C global warming targets: Projections using an ensemble of regional climate model simulations. *J. Geophys. Res. Atmos.* 125, e2019JD031057. doi:10.1029/2019jd031057

Xie, W., Zhou, B., Han, Z., and Xu, Y. (2021). Projected changes in heat waves over China: Ensemble result from RegCM4 downscaling simulations. *Int. J. Climatol.* 41, 3865–3880. doi:10.1002/joc.7047

Xie, W., Zhou, B., Han, Z., and Xu, Y. (2022). Substantial increase in daytime-nighttime compound heat waves and associated population exposure in China projected by the CMIP6 multimodel ensemble. *Environ. Res. Lett.* 17, 045007. doi:10.1088/1748-9326/ac592d

Xu, H., Chen, H., and Wang, H. (2021). Future changes in precipitation extremes across China based on CMIP6 models. *Int. J. Climatol.* 42, 635–651. doi:10.1002/joc.7264

Yu, H., Wu, D., Piao, X., Zhang, T., Yan, Y., Tian, Y., et al. (2020). Reduced impacts of heat extremes from limiting global warming to under 1.5°C or 2°C over Mediterranean regions. *Environ. Res. Lett.* 16, 014034. doi:10.1088/1748-9326/abd132

Zhai, P., Zhang, X., Wan, H., and Pan, X. (2005). Trends in total precipitation and frequency of daily precipitation extremes over China. *J. Clim.* 18, 1096–1108. doi:10.1175/jcli-3318.1

Zhang, G., Zeng, G., Yang, X., and Jiang, Z. (2021). Future changes in extreme high temperature over China at 1.5°C–5°C global warming based on CMIP6 simulations. *Adv. Atmos. Sci.* 38, 253–267. doi:10.1007/s00376-020-0182-8

Zhang, M., Yu, H., King, A. D., Wei, Y., Huang, J., and Ren, Y. (2020). Greater probability of extreme precipitation under 1.5 °C and 2 °C warming limits over East-Central Asia. *Clim. Change* 162, 603–619. doi:10.1007/s10584-020-02725-2

Zhang, W., Zhou, T., Zou, L., Zhang, L., and Chen, X. (2018). Reduced exposure to extreme precipitation from 0.5°C less warming in global land monsoon regions. *Nat. Commun.* 9, 3153. doi:10.1038/s41467-018-05633-3

Zhang, X., Zwiers, F. W., Li, G., Wan, H., and Cannon, A. J. (2017). Complexity in estimating past and future extreme short-duration rainfall. *Nat. Geosci.* 10, 255–259. doi:10.1038/ngeo2911

Zhou, B., Cheng, Y., Han, Z., Xu, Y., and Wang, X. (2020). Future changes of cluster high temperature events over China from RegCM4 ensemble under RCP4.5 scenario. *Adv. Clim. Change Res.* 11, 349–359. doi:10.1016/j.accre.2020.11.007

Zhou, B., Wu, J., Xu, Y., Han, Z., and Shi, Y. (2019). Projected changes in autumn rainfall over West China: Results from an ensemble of dynamical downscaling simulations. *Int. J. Climatol.* 39, 4869–4882. doi:10.1002/joc.6115

Zhu, H., Jiang, Z., and Li, L. (2021). Projection of climate extremes in China, an incremental exercise from CMIP5 to CMIP6. *Sci. Bull.* 66, 2528–2537. doi:10.1016/j.scib.2021.07.026

Zwiers, F. W., Zhang, X., and Feng, Y. (2011). Anthropogenic influence on long return period daily temperature extremes at regional scales. *J. Clim.* 24, 881–892. doi:10.1175/2010jcli3908.1

frontiers | Frontiers in Earth Science

TYPE Review
PUBLISHED 08 September 2022
DOI 10.3389/feart.2022.988710

OPEN ACCESS

EDITED BY
Huopo Chen,
Institute of Atmospheric Physics (CAS), China

REVIEWED BY
Liqiang Zhao,
Guangdong Ocean University, China
Guo Donglin,
Institute of Atmospheric Physics, (CAS), China

*CORRESPONDENCE
Faezah Pardi,
faezahpardi@uitm.edu.my
Mohd Iqbal Mohd Noor,
mohdiqbalmn@uitm.edu.my

SPECIALTY SECTION
This article was submitted to Interdisciplinary Climate Studies, a section of the journal Frontiers in Earth Science

RECEIVED 07 July 2022
ACCEPTED 01 August 2022
PUBLISHED 08 September 2022

CITATION
Nor Azra M, Mohd Noor MI, Pau Tan M, Dawood M, Amin M, Zekker I, Fuad Abdullah M, Abd Latif Z and Pardi F (2022), Zebrafish and Medaka as model organisms for climate change research: Global literature scientometric analysis. *Front. Earth Sci.* 10:988710. doi: 10.3389/feart.2022.988710

Zebrafish and Medaka as model organisms for climate change research: Global literature scientometric analysis

Mohamad Nor Azra[1,2], Mohd Iqbal Mohd Noor[3,4]*, Min Pau Tan[1,2], Mahmoud Dawood[5,6], Muhammad Amin[7], Ivar Zekker[8], Muhammad Fuad Abdullah[3,9], Zulkiflee Abd Latif[3,10] and Faezah Pardi[3,11]*

[1]Institute of Marine Biotechnology (IMB), Universiti Malaysia Terengganu (UMT), Kuala Terengganu, Terengganu, Malaysia, [2]Climate Change Adaptation Laboratory, Institute of Marine Biotechnology (IMB), Universiti Malaysia Terengganu (UMT), Terengganu, Malaysia, [3]Institute for Biodiversity and Sustainable Development, Universiti Teknologi MARA (UiTM), Shah Alam, Selangor, Malaysia, [4]Faculty of Business Management, Universiti Teknologi MARA (UiTM), Pahang, Malaysia, [5]The Center for Applied Research on the Environment and Sustainability, The American University in Cairo, Cairo, Egypt, [6]Animal Production Department, Faculty of Agriculture, Kafrelsheikh University, Kafr el-Sheikh, Egypt, [7]Department of Zoology, University of Karachi, Karachi, Pakistan, [8]Institute of Chemistry, University of Tartu, Tartu, Estonia, [9]Faculty of Business Management, Universiti Teknologi MARA (UiTM) Selangor, Bandar Puncak Alam, Selangor, Malaysia, [10]Faculty of Architecture, Planning and Surveying Universiti Teknologi MARA (UiTM) Shah Alam, Selangor, Malaysia, [11]Faculty of Applied Sciences, Universiti Teknologi MARA (UiTM) Shah Alam, Selangor, Malaysia

Determining how climate change affects aquatic organisms, such as fish is vital, since this could directly or indirectly impact food and protein sources that are important for human nutrition. Thus, identifying suitable organisms for studying the impacts of climate change on aquatic species is essential. It is most effective to select model organisms for climate change study and determine how each organism might adapt within the diversity of organisms present. This study aimed to review the current development and frontiers of climate change's model organism based on the literature. We conducted a scientometric analysis by differentiating between publications on different model species, the number and origin of authors and affiliations involved, the citation analysis, and the most common keywords used. Increased publication numbers for Zebrafish and Medaka were detected during the analysis of the networks. Our results showed that both species are among the most important aquatic model organisms for climate change related research. Furthermore, we found that these model organisms, especially the Zebrafish are becoming increasingly important towards climate change related studies, because of their simple anatomy and established biological studies. Our analysis could be on the forefront for disseminating and communicating scientific knowledge and impactful discoveries to researchers, academics, policymakers, and to the public worldwide for future contribution to the community resources preservation.

KEYWORDS

bibliometrics, Citespace, environmental sciences, global warming, hypoxia number of articles affiliations

1 Introduction

Fish are vital sources for human protein and are a basic necessity for a large percentage of the world, especially who lived in the coastal area (Braña et al., 2021; Mamun et al., 2021; Maulu et al., 2021). The future sustainability of aquatic products, such as seafood, is partly related to the human response to climate change. For example, sea surface temperature is changing the distribution of fish stock (Sunday et al., 2012), thus altering where fish can sustainably be caught (Free et al., 2022). Due to the diversity of aquatic organisms, it is more effective to select a few aquatic organisms as model species, and assess how they might adapt to climate change rather than trying to assess many species at once The concept of model organism research started in the early 1960s and 1970s due to the increasing number of techniques available in the molecular biological field (Dietrich et al., 2014). Research organisms or model organisms are also frequently used for laboratory research for specific characterization experiments. This type of research helps to inform on the fundamental mechanisms in other organisms and their behaviour. Some examples of classic model species in biology include mice and chickens (Müller and Grossniklaus, 2010; Tregaskes and Kaufman, 2021); Zebrafish and Medaka can also be considered as model organisms, especially among aquatic species.

There are a few traits which make a species a good candidate for being a model species, including: short generation times or short life cycle and rapid development (Silvertown et al., 2011), anatomically simple and clearly defined biological system, tolerance to various environmental conditions (Morgan et al., 2019), capability for breeding or inbreeding, established domestication (Joubert and Bijlsma, 2010) and complete reference genomic studies (Waldvogel et al., 2020). Zebrafish and Medaka are species living in freshwater and marine water environments (Hsu et al., 2014), thus making them suitable organisms for understanding organism function changes within climate change-related studies in either environment. Zebrafish and Medaka's ecology and evaluation are well established as natural model organisms, and knowledge of how they should best be managed is vital for various research (Marx, 2021; Chowdhury et al., 2022). In addition, Zebrafish and Medaka also share the same anatomy, genetic, and physiological elements (Hsu et al., 2014; Chowdhury et al., 2022).

Publication trends on model organisms have been assessed by previous authors, however, these authors only focused on a few species, mostly terrestrial (e.g., rat, mouse, common fruit flies, chicken, and frogs) rather than aquatic species (Dietrich et al., 2014). Therefore, comprehensive bibliographic analysis on aquatic model organisms, such as author and affiliation network or citation analysis is needed. Scientometrics is known as the idea of measuring the networks of scientists, institutions and ideas from a large database or number of sources. The fields of scientometrics and bibliometrics are growing, and there is an increased appreciation for their importance in many scientific fields. Previous scientometric analysis also has been done on the global mapping of zebrafish species (Kinth et al., 2013), however, their relationship with climate change was not assessed. There are no available scientometric-based studies for the Medaka species and this study is among the first to identify the different scientometrics for this species. Previous studies showed that various model organisms can be useful for researching climate change related studies, such as climate-induced water temperature changes (Morgan et al., 2019), acidification, and eutrophication (Altshuler et al., 2011) as well as pollution (Vilas-Boas et al., 2020). However, still missing is an analysis that broadly assesses how model organisms can improve our understanding of climate change.

Thus, the goal of this study was to examine the impact of climate change on two select aquatic model organisms. By employing bibliometric analyses and scientific techniques, we aimed to answer questions about the structure and dynamics of Zebrafish and Medaka as model organisms for climate change related studies. The questions were divided in two different categories, which were 1) the descriptive dataset and 2) the scientometrics-based analysis. The descriptive dataset includes the number of articles published, the citation counts of the articles, the distribution of the countries involved, and the active authors. Meanwhile, for the scientometrics data, the distribution of the cited authors and articles as well as the most abundant keywords used were generated from Citespace software.

The type of bibliometric based studies are also expected to increase the visibility of the field of research and future collaboration between authors and institutions involved. The study is also expected to contribute to the bioclimatology, policymakers, philanthropic and the public worldwide on how to invest limited resources in policies, programs, and research on the impacts of climate change on aquatic species.

2 Methods

2.1 Data sources

Methodological framework for the current study is shown in Figure 1. Web of Science (WOS) Core Collection (WOSCC) was the only database used for the study because it is the general standard for scientometric-based analysis for identifying and

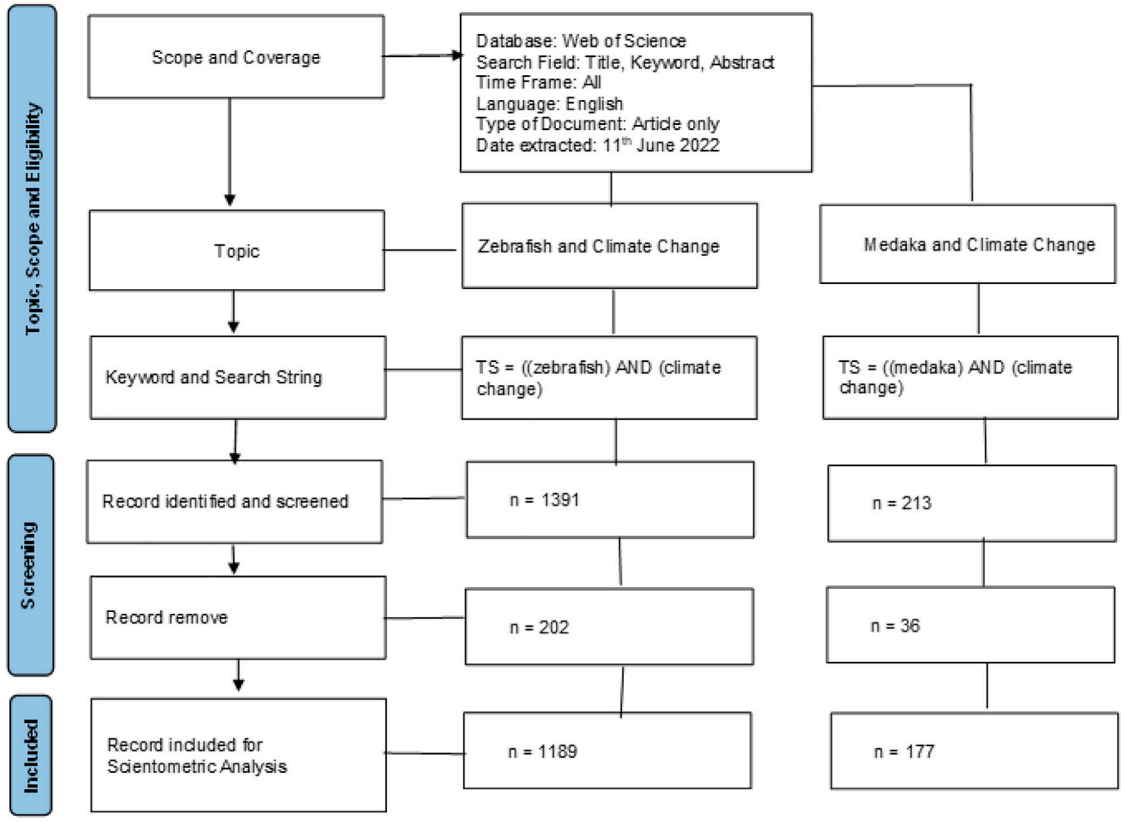

FIGURE 1
Flowchart indicating methodological framework where two separate searches were done focusing on: (i) Zebrafish and (ii) Medaka relation with climate change.

monitoring research trends and development. The WOSCC searching index and database includes the "topic" (TS) field (i.e., article titles, abstracts, keywords, KeyWords Plus). There are few steps applied in the review process of the data, including selection of the database, identification of the articles that relate to our study, screening and eligibility criteria, and included documents. The various qualifying and exclusion criteria were considered, the article type, the language used and the source type of the article. Figure 1 shows that there were various types of methods employed in the systematic review process such as scope and coverage (i.e., database, keywords, etc.), topic identification, screening eligibility, merging, duplicate removal and included documents for the scientometric analysis.

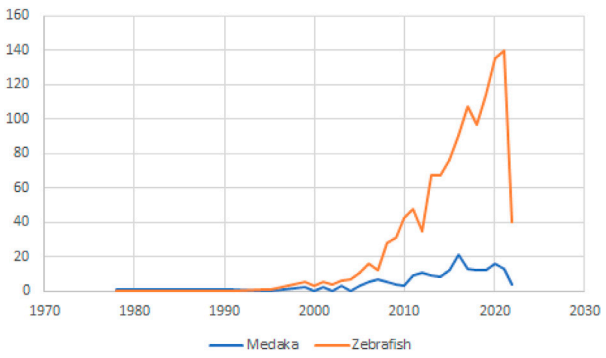

FIGURE 2
Number of research articles related to climate change effects on Medaka and/or Zebrafish published annually since 1978.

The common name as well as the scientific name for both fish species were collected from FishBase, where the current correct information on fishes is provided by various experts and with the support of the European Commission. The climate change related keywords were similar as in Azra et al. (2022). As such, our search strings included the following:

1st searches

Zebrafish:

TS = ((*zebrafish*) OR ("*Danio rerio*") OR ("*Girella* zebra") OR ("*Pterois russelii*") OR ("*Pterois volitans*") OR ("*D. rerio*") OR ("*G. zebra*") OR ("*P. russelii*") OR ("*P. volitans*"))

AND

Climate change:

TS= (("climat* chang*") OR ("global warm*") OR ("seasonal* variat*") OR ("extrem* event*") OR

("environment* variab*") OR ("anthropogenic effect*") OR ("greenhouse effect*") OR ("sea level ris*") OR (erosio*) OR ("agricult* runoff") OR ("weather* variab*") OR ("weather* extrem*") OR ("extreme* climat*") OR ("environment* impact*") OR ("environment* chang*") OR ("anthropogenic stres*") OR ("temperature ris*") OR ("temperature effect*") OR ("warm* ocean") OR ("sea surface* temperat*") OR (heatwav*) OR (acidific*) OR (hurrican*) OR ("el nino") OR ("el-nino") OR ("la nina") OR (la-nina) OR (drought*) OR (flood*) OR ("high precipit*") OR ("heavy rainfall*") OR ("CO_2 concentrat*") OR ("melt* of the glacier*") OR ("melt* ice*") OR ("therm* stress*") OR (drought) OR (hypoxia))

2nd searches

Medaka:

TS = [(medaka) OR ("Oryzias latipes") OR ("*Aphyocypris* kikuchii") OR ("*O. latipes*") OR ("A. kikuchii")]

AND

Climate change:

TS = ((climat* chang*) OR ("global warm*") OR ("seasonal* variat*") OR ("extrem* event*") OR ("environment* variab*") OR ("anthropogenic effect*") OR ("greenhouse effect*") OR ("sea level ris*") OR (erosio*) OR ("agricult* runoff") OR ("weather* variab*") OR ("weather* extrem*") OR ("extreme* climat*") OR ("environment* impact*") OR ("environment* chang*") OR ("anthropogenic stres*") OR ("temperature ris*") OR ("temperature effect*") OR ("warm* ocean") OR ("sea surface* temperat*") OR (heatwav*) OR (acidific*) OR (hurrican*) OR (el nino) OR ("el-nino") OR ("la nina") OR (la-nina) OR (drought*) OR (flood*) OR ("high precipit*") OR ("heavy rainfall*") OR ("CO_2 concentrat*") OR ("melt* of the glacier*") OR ("melt* ice*") OR ("therm* stress*") OR (drought) OR (hypoxia)).

2.2 Analysis tool

2.2.1 Software tool

Data from WOSCC were imported directly to the CiteSpace software as a text file (*.txt). The CiteSpace version 6.1.R2 on 64-bit was used for the analysis. CiteSpace is among one of the popular software to analyze scientometric based results (Noor et al., 2021; Feng et al., 2022; Shi et al., 2022). It also shows various types of interactive visualization (i.e., network analysis and visualization), such as most active areas, major related areas, key papers for a given area, critical transitions in the history of the development of the field and its turning points.

The data were divided into the number of authors, number of institutions, countries involved, terminologies used, consistent and most common keywords, cited authors as well as cited references in the field. The threshold setting for CiteSpace was set at "*Top 50 N*" *per* slice, which allows the selection of most cited items from each slice to form a network based on the input value and node types. "Pruning" parameter was chosen to prune the network. All term sources in Web of Science, including title, abstract, author keywords, and keywords plus, were chosen for text processing. Three types of scientometric analysis were used in this study, namely; 1) cluster analysis, 2) co-citation analysis and 3) burstness analysis. The explanation for each analysis is given below.

2.2.2 Cluster analysis

Cluster analysis was used to identify research clusters in focus areas. For this study, variable use for cluster analysis is based on the Articles Cluster. Log-likelihood ratio was used to provide the cluster label as it gives the best results in terms of uniqueness and coverage (Hiekkalinna et al., 2012). The "timeline view" and "cluster view" were used to visualize the articles cluster network's shape and form. The "timeline view" displayed a vertical range of chronological time periods from left to right, whereas the "cluster view" displayed a spatial network of colour-coded and automatically labeled representations in a landscape format (Chen 2004; Chen and Leydesdorff 2014).

The modularity Q index, average silhouette metric, and centrality metric were used to assess the quality and homogeneity of the document cluster analyses, as well as the detected clusters (Chen et al., 2009; Chen, 2020). The modularity Q index ranges between 0 and 1, where larger index values indicate higher reliability. The average silhouette metric has a value between −1 and 1, where values greater than 0 indicate greater homogeneity. Centrality is a measure of influence that shows the degree to which publications or journals stand between each other, where publications with high centrality would have higher influence on the network as they connect more publications or journals and therefore, more information and paths pass through them.

2.2.3 Co-citation analysis

Co-citation analyses generate a research network consisting of nodes and link and density values to show the main structure of selected variables. For this study, selected variables included 1) Cited Articles analysis and 2) Cited Author analysis. Co-citation analysis will allow us to obtain the cluster of co-citing variables, where a co-citation instance occurs when two articles/authors are cited together in one paper (Boyack and Klavans, 2010). The analysis quality was assessed using degree, betweenness, and sigma (Chen and Song, 2019). The degree value represents the number of citations an article/author receives from another article/author, with a higher degree indicating more citations. Betweenness is a measure of influence that shows the influence to which the same article/author has on others. High betweenness means the article/author has a greater influence on the research areas because it connects other articles/authors, and thus more information and paths pass through them. Centrality is the

TABLE 1 The articles with the highest citations for research on medaka and climate change.

No	Title	Source title	Publication year	Total citations	Average per year
1	Evaluation of the toxic impact of silver nanoparticles on Japanese medaka (oryzias latipes)	Aquatic Toxicology	2009	210	15
2	Evolutionary dynamics of olfactory receptor genes in fishes and tetrapods	Proceedings of the National Academy of Sciences of the United States of America	2005	200	11.11
3	Zinc oxide nanoparticles induce oxidative DNA damage and ROS-triggered mitochondria-mediated apoptosis in zebrafish embryos	Aquatic Toxicology	2016	137	19.57
4	2,3,7,8-Tetrachlorodibenzo-p-dioxin alters cardiovascular and craniofacial development and function in sac fry of rainbow trout (Oncorhynchus mykiss)	Toxicological Sciences	1999	104	4.33
5	Cumulative ecological impacts of two successive annual treatments of imidacloprid and fipronil on aquatic communities of paddy mesocosms	Ecotoxicology and Environmental Safety	2012	97	8.82
6	Development of a marine fish model for studying *in vivo* molecular responses in ecotoxicology	Aquatic Toxicology	2008	97	6.47
7	Leptins and leptin receptor expression in the goldfish (*Carassius auratus*). Regulation by food intake and fasting/overfeeding conditions	Peptides	2012	87	7.91
8	Hypoxia causes transgenerational impairments in reproduction of fish	Nature Communications	2016	80	11.43
9	Molecular cloning, characterization and expression profiles of multiple leptin genes and a leptin receptor gene in orange-spotted grouper (*Epinephelus coioides*)	General and Comparative Endocrinology	2013	75	7.5
10	Comprehensive Transcriptome Analysis Reveals Accelerated Genic Evolution in a Tibet Fish, *Gymnodiptychus pachycheilus*	Genome Biology and Evolution	2015	64	8

combination value based on betweenness and burstiness scores (described below), ranging from 0 to 1 where the highest value is associated with high value research articles (Aryadoust et al., 2019).

2.2.4 Burstiness analysis

Citation burstiness were used to determine top keywords related to research areas. Burst detection is defined as a sudden increase in the number of citations for a specific article, or "an abrupt elevation of the frequencies (of citations) over a specific time interval," as indicated by a red ring around the node (Hou et al., 2018).

3 Results

3.1 Trends in literature

This study focused on scientific publications related to climate change and its relationship with zebrafish and medaka species. Research on medaka and climate change started in 1978 (Figure 2), where a total of 177 original articles have been published since then, with an average of 10 publications per year since 2011. On the other hand, the first scientific publication on zebrafish and climate change was only published in Web of Science in 1994. However, zebrafish publications rapidly outnumbered medaka publications, with a total of 1189 papers published since 1994.

Article citation is an indicator that shows the impact of a study in its research field. Based on previous studies, the direction of a research field is associated with the articles that are most frequently cited (Chen et al., 2010; Chen, 2020). The top three articles with the highest number of total citations for medaka and climate changes were, 1) "Evaluation of the toxic impact of silver nanoparticles on Japanese medaka (Oryzias latipes)" (210 citations); 2) "Evolutionary dynamics of olfactory receptor genes in fishes and tetrapods" (200 citations); and 3) "Zinc oxide nanoparticles induce oxidative DNA damage and ROS-triggered mitochondria-mediated apoptosis in zebrafish embryos" (137 citations). Tables 1, 2 show the highest citations for climate change research associated with Medaka and Zebrafish, respectively.

For research focusing on Zebrafish and Climate Change, the top 3 most cited publications were: 1) "Toxicity of silver nanoparticles in zebrafish models" (681 citations); 2) "The Oxygen-Rich Postnatal Environment Induces Cardiomyocyte Cell-Cycle Arrest through DNA Damage Response" (437 citations) and 3) "The Serine Protease Matriptase-2 (TMPRSS6) Inhibits Hepcidin Activation by Cleaving Membrane Hemojuvelin" (405 citations).

TABLE 2 The top ten articles with the highest number of citations for research on Zebrafish and climate change.

No	Title	Source title	Publication year	Total citations	Average per year
1	Toxicity of silver nanoparticles in zebrafish models	Nanotechnology	2008	681	45.4
2	The Oxygen-Rich Postnatal Environment Induces Cardiomyocyte Cell-Cycle Arrest through DNA Damage Response	Cell	2014	437	48.56
3	The Serine Protease Matriptase-2 (TMPRSS6) Inhibits Hepcidin Activation by Cleaving Membrane Hemojuvelin	Cell Metabolism	2008	405	27
4	Live imaging of neuronal degradation by microglia reveals a role for v0-ATPase a1 in phagosomal fusion *in vivo*	Cell	2008	380	25.33
5	Hypoxia induces heart regeneration in adult mice	Nature	2017	347	57.83
6	Comparison of the toxicity of silver, gold and platinum nanoparticles in developing zebrafish embryos	Nanotoxicology	2011	315	26.25
7	The composition of the zebrafish intestinal microbial community varies across development	Isme Journal	2016	290	41.43
8	Assessing the toxicity of Pb- and Sn-based perovskite solar cells in model organism *Danio rerio*	Scientific Reports	2016	275	39.29
9	Acute toxicities of six manufactured nanomaterial suspensions to *Daphnia* magna	Journal of Nanoparticle Research	2009	263	18.79
10	A horizon scan of global conservation issues for 2010	Trends In Ecology Evolution	2010	249	19.15

3.2 Trends in countries

Research papers in the sample for medaka and climate change research came from 65 countries around the world. Figure 3 shows the distribution of countries working on the Medaka and Zebrafish as a model organism in climate change research and development. China was the most frequent publisher (56 publications), followed by the United States, Japan, Canada, France, Germany, Norway, South Korea, Taiwan and Australia as the top 10 countries that have published in this research area. In the research areas focusing on zebrafish and climate changes, a total of 74 countries contributed between 1994–2022. The United States of America contributed the highest number of articles (342 publications), followed by China, Canada, England, Germany, Australia, France, Italy, Brazil, and Taiwan.

3.3 Trends of authors

For the zebrafish subsample, there were 842 authors who published an article related to climate change and zebrafish, but only two authors published more than 10 articles (Figure 3). Rudolf S.S Wu from Education University of Hong Kong contributed the most with 12 articles, followed by Keng Po Lai (10 articles), and Doris Wai Ting Au/Ting Fung Chan (9 articles). Tables 3, 4 indicate the list of top ten most productive authors regarding research on medaka and zebrafish, respectively, and climate change. Within the zebrafish subsample, out of a total of 6015 authors, Steve F. Perry published the most articles (34 articles), followed by Michael G. Jonz (16 articles), and Bernd Pelster (15 articles).

3.4 Scientometric analysis

3.4.1 Author co-citation analysis

Figure 4 depicts authors in the zebrafish subsample that have a betweenness score greater than 0.05.

There were 886 nodes and 3010 connections in the author co-citation network for the zebrafish subsample. The co-citation network density value was 0.0077. Figure 4 depicts authors that have a centrality score greater than 0.1. Pamela A. Padilla from Fred Hutchinson *Cancer* Research Center was the most interconnected author, with a degree connection of 30, betweenness score of 0.07, and a sigma of 1.81. Andrew Y. Gracey was the second most influential author, with a degree connection of 56, betweenness score 0.11 and Sigma score of 1.65. Even though Andrew Y. Gracey's degree connection and betweenness score are higher than Pamela A. Padilla's, his sigma score is lower. This shows that Pamela A. Padilla is located more central in the network and is cited by authors with higher betweenness and degree than Andrew Y. Gracey, making him less influential. Christopher Ton was the third most influential author (Degree Connection: 30; Betweenness: 0.05, Sigma: 1.45). Table 5 shows the details for the top ten authors with the most influence in zebrafish and climate change research.

The author's co-citation network for medaka and climate changes had 679 nodes, 2200 connections, and a density of

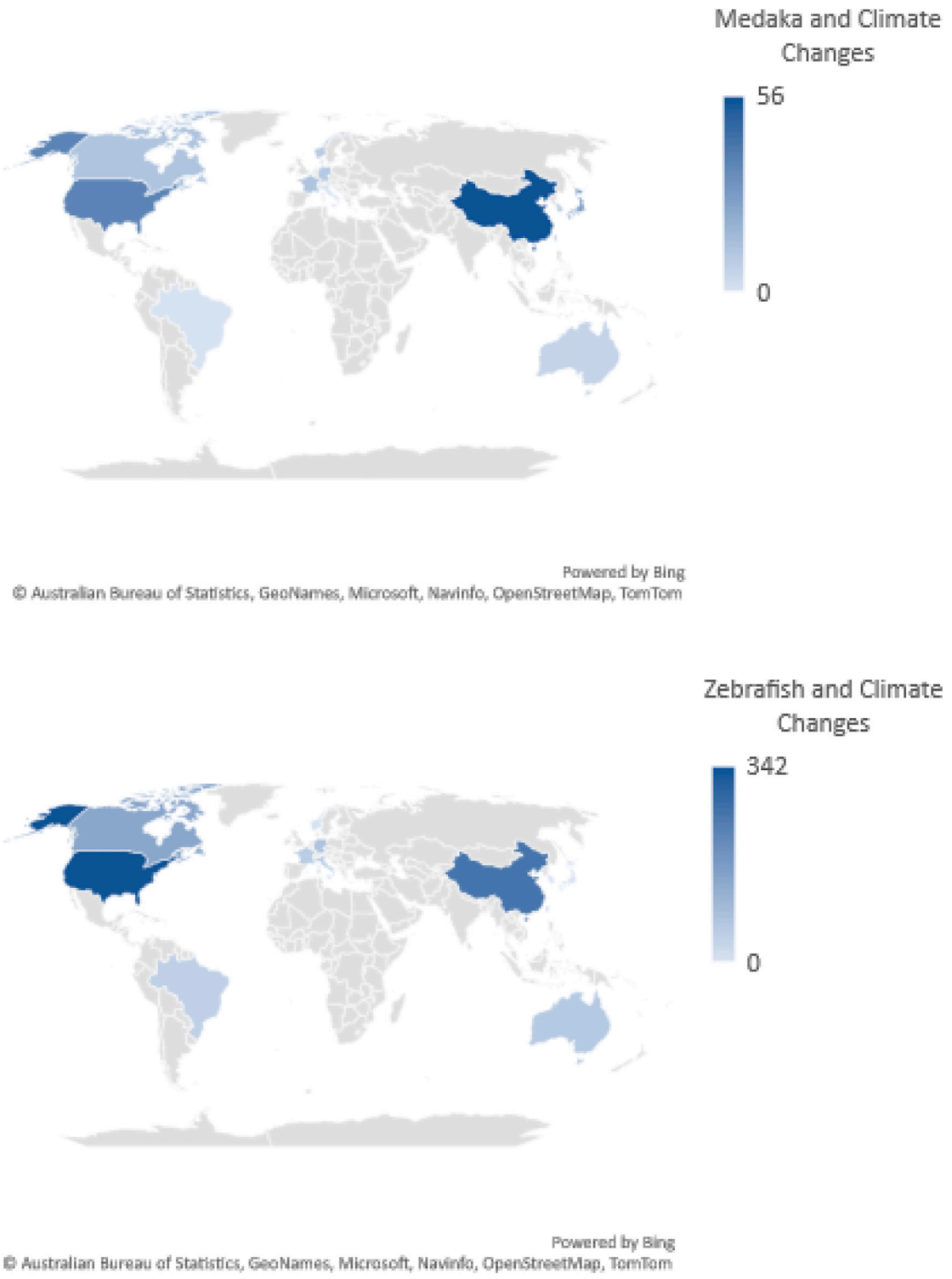

FIGURE 3
The distribution of countries that work on Medaka and Zebrafish as a model organism in climate change research and development.

TABLE 3 Top ten most productive authors regarding research on medaka and climate change.

Top authors for on medaka and climate changes	Number of articles	Affiliations
Rudolf S.S. Wu	12	Education university of Hong Kong
Keng Po Lai	10	Guilin Medical University
Doris Wai Ting Au	9	City University of Hong Kong
Ting Fung Chan	9	Chinese University of Hong Kong
Richard Yuen Chong Kong	8	City University of Hong Kong
Jing-Woei Li	8	Chinese University of Hong Kong
Anna Chung Kwan Tse	7	University of Hong Kong
Pei-Jen Chen	6	National Taiwan University
Daniel Schlenk	6	University of California Riverside
Simon Yuan Wang	5	Boston Children's Hospital

TABLE 4 Top ten most productive authors regarding research on zebrafish and climate change.

Top authors for on zebrafish and climate changes	Number of articles	Affiliations
Steve F. Perry	34	University of ottawa
Michael G. Jonz	16	University of Ottawa
Bernd Pelster	15	University of Innsbruck
Yuan Li	13	China Agricultural University
Warren W. Burggren	12	University of North Texas Denton
Cunming Duan	12	University of Michigan
Rudolf S.S. Wu	12	Education University of Hong Kong
Michael Lardelli	11	University of Adelaide
Thorsten Schwerte	11	University of Innsbruck
Yihai Cao	10	Karolinska Institutet

0.0096. Figure 5 illustrates the knowledge map for the author co-citation analysis, including only authors with betweenness scores greater than 0.05. Table 6 shows the details for the top ten authors involved in the Medaka subsample with the highest influence based on the authors degree, centrality, and sigma score.

Kinoshita Masato from Kyoto University was the most influential author with degree connection = 27, betweenness score = 0.15 and sigma score 1.72. The second and third most influential authors were Angel Amores (degree: 9, centrality: 0.05 and sigma: 1) and Philip L. Munday (degree: 6, centrality: 0.01 and sigma: 1).

3.4.2 Articles co-citation analysis

Figure 6 illustrates the articles' co-citation analysis for the zebrafish subsample. The network had 969 nodes and 2824 connections, with a density of 0.006. Only articles with a centrality score greater than 0.1 were listed.

Table 7 displays the top ten most influential scientific publications according to the degree, betweenness, and sigma score. "*Zebrafish mutants in the von Hippel-Lindau tumor suppressor display a hypoxic response and recapitulate key aspects of Chuvash polycythemia*" was the most influential article in zebrafish subsample, with a degree connection of 30, betweenness 0.19 and sigma score of 3.17. "*The zebrafish reference genome sequence and its relationship to the human genome*" was the second most influential article, with a degree connection of 12, betweenness 0.20 and sigma 2.14. The article "*Hypoxia-inducible factor-1 mediates adaptive developmental plasticity of hypoxia tolerance in zebrafish, Danio rerio*" was the third most influential article (degree = 21, centrality = 0.12 and sigma = 1.80).

Figure 7 shows the majority of highly influential articles based on the article co-citation analysis for the medaka subsample. The network contained 617 nodes and

TABLE 5 Top 10 authors co-citation score for Zebrafish and Climate Change Research Areas.

Author	Affiliation	Degree	Betweenness	Sigma
Pamela a. Padilla	Fred hutchinson cancer research center	30	0.07	1.81
Andrew Y. Gracey	Stanford University	56	0.11	1.65
Christopher Ton	University of Toronto	30	0.05	1.45
Shingo Kajimura	University of Michigan	29	0.05	1.44
Rudolf S.S. Wu	City University of Hong Kong	22	0.05	1.27
Ellen van Rooijen	University Medical Center Utrecht	19	0.03	1.26
Robert J Diaz	College of William and Mary	32	0.06	1.26
Douglas Bates	University of Wisconsin-Madison	11	0.07	1.25
Thorsten Schwerte	University of Innsbruck	22	0.02	1.17
Diego A. Rojas	Universidad de Chile	15	0.02	1.14

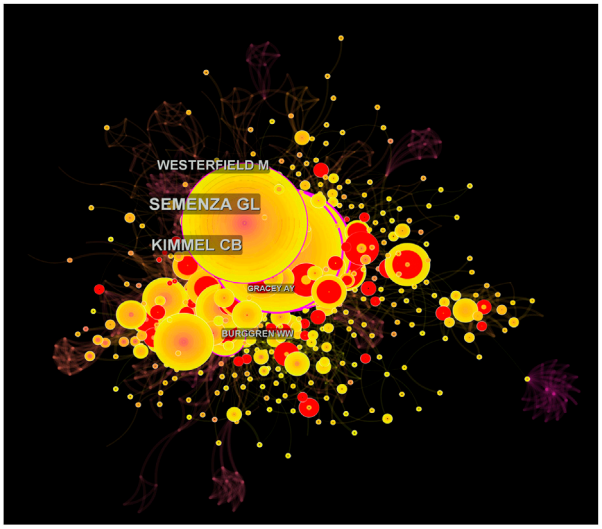

FIGURE 4
The distribution of cited authors for research on zebrafish and climate change. Node size and font size increase as centrality score increases.

1695 links. Each node represents an article with the first author's name and the publication year. The links between nodes represent co-citation relations between two articles. As there were no articles with a betweenness score >0.1, there are no names listed in the figure.

Table 8 shows the most influential publications (publications according to the degree, betweenness, and sigma score in the medaka subsample. The most influential article is "Epigenetics in teleost fish: From molecular mechanisms to physiological phenotypes" with degree connection of 109, betweenness score 0.04 and Sigma of 1. Interestingly, there are no articles with sigma more than 1, which might indicate there are no highly recognizable articles in this domain.

3.4.3 Articles cluster

The Modularity Q Index and the Mean Silhouette metric for the zebrafish subsample's article cluster analysis were 0.8963 and 0.9642 respectively, suggesting more than average reliability and homogeneity for the network. The analysis yielded a total of 17 co-citation clusters which are summarized in Table 9, where each cluster represents a different research topic. The cluster's size is equal to the number of publications it has. Each of the clusters has range between 4 and 80 publications, with Cluster #0 having the most (95 publications). Cluster silhouette score ranged from 0.927 to 1.000, indicating a high degree of homogeneity among publications in each cluster (silhouette score ranges from −1 to 1, with scores >0 seen as homogenous). This indicator measures the combined strength of structural and temporal properties of a node, namely, its betweeness centrality and citation burst. A composite metric sigma is defined in CiteSpace to measure the combined strength of structural and temporal properties of a node, namely, its betweenness centrality and citation burst. Sigma is computed as (centrality +1) burstness (50), with higher values indicating works with higher influential potential. (Chen et al., 2009).

Figure 8 depicts these 17 clusters summarized on a horizontal line, with the cluster label on the right side. The clusters were numbered and ranked in order of size, with #0 being the largest and #39 the smallest. The solid yellow line within each cluster represents the cluster's lifetime. Text mining and a keyword analysis algorithm in CiteSpace software were used to generate the cluster labels, then the log likelihood ratio was used to name these clusters (LLR).

The Modularity Q Index and the Mean Silhouette metric for the Medaka subsample's cluster analysis were 0.9645 and 0.9980 respectively, suggesting again more than average reliability and homogeneity for the network. The analysis yielded a total of 3 co-citation clusters which are summarized in Table 10. Each

TABLE 6 Top 10 Authors co-citation score for research on Medaka and Climate Change.

Author	Affiliation	Degree	Betweenness	Sigma
Kinoshita masato	Kyoto university	27	0.15	1.72
Angel Amores	University of Oregon	9	0.05	1
Philip L. Munday	James Cook University	6	0.01	1
Lianguo Chen	Chinese Academy of Sciences	16	0	1
Mark D. Robinson	The University of Melbourne	5	0.01	1
Serpil Aliriz	Yuzunzu Yil University	7	0	1
James C.W. Lam	City University of Hong Kong	16	0	1
Matthew M. Alloy	University of North Texas	2	0.01	1
Anneli Bohne-Kjersem	University of Bergen	12	0	1
Thaïs Aznar-Fernández	CICS	7	0	1

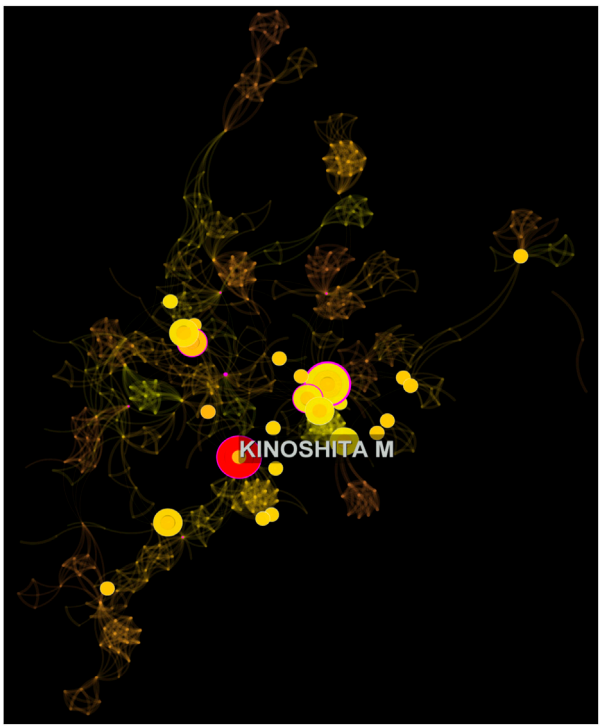

FIGURE 5
The distribution of cited authors for related to medaka and climate change.

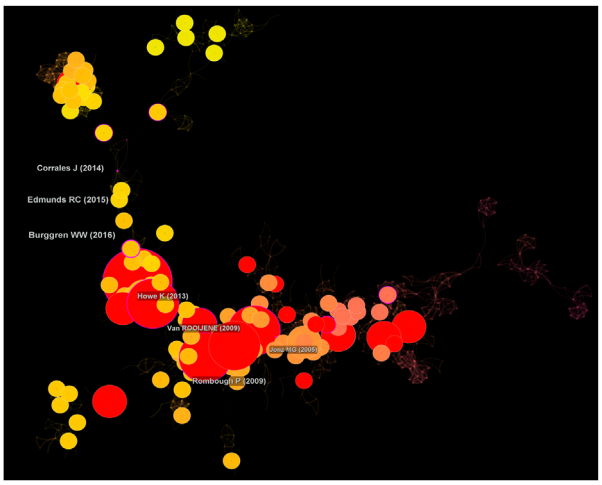

FIGURE 6
Network of Document Co-citation Analysis where articles with a centrality score greater than 0.1 are shown.

cluster ranged between 12 and 35 publications, with Cluster #0 having the most (35 publications). Cluster silhouette score ranged from 0.997 to 1.000, indicating a high degree of homogeneity among publications in each cluster.

Figure 9 depicts these 20 clusters summarized on a horizontal line, with the cluster label on the right side as well as with three major cluster summarized in Table 10. The clusters were numbered and ranked in order of size, with #0 being the largest and #16 the smallest. As before, text mining and keyword analysis algorithms in CiteSpace software was used to generate the cluster labels, and log likelihood ratio was used to name the clusters (LLR).

3.5 Keyword burst

Table 11 displays the keywords with the keyword citation burst for the zebrafish subsample. There were no burst keywords from the medaka subsample. Bursts reflect the emergence of a keyword within a subject area during a specific time period (the blue line), here from 1994 to 2022, while the red lines represent the burst period. Beginning in 2019 and ending in 2022, the word "temperature" had the highest burst strength (6.81). The following top keywords were "embryonic development"

TABLE 7 Top 10 (of 1189) most influential scientific publications related to research on zebrafish and climate change.

Title	Year	Degree	Betweenness	Sigma
Zebrafish mutants in the von hippel-lindau tumor suppressor display a hypoxic response and recapitulate key aspects of Chuvash polycythemia	2009	30	0.19	3.17
The zebrafish References genome sequence and its relationship to the human genome	2013	12	0.20	2.14
Hypoxia-inducible factor-1 mediates adaptive developmental plasticity of hypoxia tolerance in zebrafish, *Danio rerio*	2014	21	0.12	1.80
Development of oxygen sensing in the gills of zebrafish	2014	31	0.17	1.75
Gene expression profiling of the long-term adaptive response to hypoxia in the gills of adult zebrafish	2005	21	0.10	1.68
Serotonergic and cholinergic elements of the hypoxic ventilatory response in developing zebrafish	2005	12	0.10	1.51
Gene expression profile of zebrafish exposed to hypoxia during development	2013	33	0.07	1.50
HIF signaling and overall gene expression changes during hypoxia and prolonged exercise differ considerably	2003	27	0.07	1.50
Cloning of hif-1α and hif-2α and mRNA expression pattern during development in zebrafish	2011	26	0.08	1.43
Linking Oxygen to Time: The Bidirectional Interaction Between the Hypoxic Signaling Pathway and the Circadian Clock	2007	26	0.08	1.42

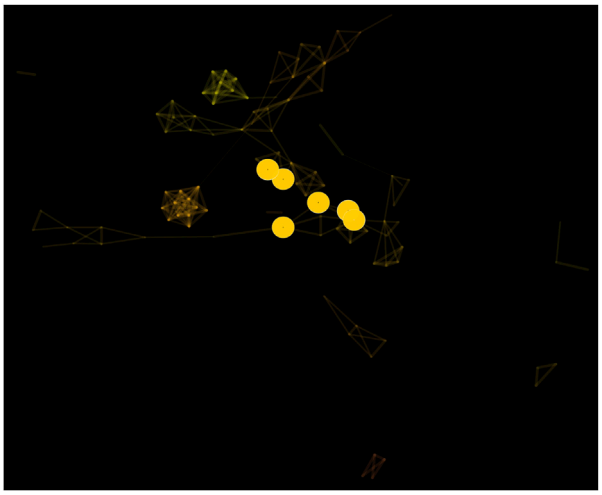

FIGURE 7
Medaka and Climate Change Network of Document Co-citation Analysis, where articles with a centrality score greater than 0.1 are shown.

(Strength = 5.5, 2016–2019) and "*in vivo*" (Strength = 4.78, 2009–2013).

4 Discussion

4.1 Descriptive analysis

Here, research related to climate change and either zebrafish or medaka was synthesized, revealing the research landscape in terms of the year, journals, authors, countries, keywords, and references. A descriptive analysis was performed on the number of publications, authors, and the countries/regions where authors were affiliated with when papers were published.

Both research domains saw the number of articles published increase annually, but the zebrafish subsample saw a higher increase in articles published, with a 10-years average of 92.9 publications per year; whereas medaka subsample only published a 10-years average of 12.7 articles per year. Consequently, the number of papers with high citation counts also differed, where zebrafish had 10 articles with >200 citations whereas medaka only had two articles with >200 citations. Both domains had China and the United States of America as the highest contributors for the number of papers published in the field. The top ten countries and authors varied in terms of region, but were dominated by developed countries and high-ranking institutions. As this result may be due to developed countries and high-ranking institutions having more resources to conduct scientific analyses, we strongly suggest that more international scientific research exchange and collaboration be conducted in the future. The difference in publication numbers and citations indicates that biology as a field has focused more on using zebrafish as a model species when it comes to climate change research, rather than medaka.

Tables 1, 2 showed that most of the top papers published were not related to climate change-related studies. Keywords related to environmental conditions, environmental change, and stress appeared to capture some articles that were not directly related to our objectives regarding climate change. Most of the articles on medaka discussed the ability and roles of the model organism towards various fields of study, such as nanotechnology (i.e., nanomaterials/nanoparticles) (Chae et al., 2009; Zhao et al., 2016) and genetics (Niimura and Nei, 2005). Similarly, articles on zebrafish discussed the species' ability and role in the fields of nanotechnology

TABLE 8 Top 10 (of 117) most influential publications related to research on medaka and climate change.

Title	Year	Degree	Betweenness	Sigma
Epigenetics in teleost fish: From molecular mechanisms to physiological phenotypes	2015	109	0.04	1
Hypoxia causes transgenerational impairments in reproduction of fish	2011	8	0.03	1
Early Dioxin Exposure Causes Toxic Effects in Adult Zebrafish	2007	40	0.02	1
Using Zebrafish as a Model System for Studying the Transgenerational Effects of Dioxin	2011	40	0.02	1
Hypoxia alters steroidogenesis in female marine medaka through miRNAs regulation	2016	9	0.02	1
Developmental exposure to a complex PAH mixture causes persistent behavioral effects in naive Fundulus heteroclitus (killifish) but not in a population of PAH-adapted killifish	2011	40	0.02	1
Sex in troubled waters: Widespread agricultural contaminant disrupts reproductive behaviour in fish	2009	25	0.02	1
Stress, novel sex genes, and epigenetic reprogramming orchestrate socially controlled sex change	2015	14	0.02	1
Genome Sequencing of the Perciform Fish Larimichthys crocea Provides Insights into Molecular and Genetic Mechanisms of Stress Adaptation	2009	107	0.02	1
Declining oxygen in the global ocean and coastal waters	2015	61	0.02	1

TABLE 9 Seventeen (17) major clusters from the article co-citation analysis for research on zebrafish and climate changes.

ClusterID	Size	Silhouette	Label (LLR)	Average year
0	95	0.924	Hypoxia-inducible transcription factor	2014
1	81	0.927	Respiratory developmental plasticity	2009
2	56	0.978	Gene expression profiling	2004
3	55	0.996	Invasive lionfish	2015
5	46	0.979	Respiratory gasses	2015
6	44	1.000	Zebrafish larvae	2020
7	31	1.000	Toxicity	2000
8	28	0.955	Maladaptive larval phenotype	2018
9	27	0.964	Complex response	2004
10	26	0.936	Oxygen deprivation	2002
11	26	0.954	Ventilatory control	2006
12	25	0.976	Pathological hypoxia-driven angiogenesis	2009
13	24	1.000	Hypoxic cell	2017
15	12	1.000	Accelerated gene evolution	2015
28	7	1.000	Rainbow trout	2012
29	7	0.997	Marine medaka	2016
39	4	0.996	Drug-resistant gene expression	2015

(Asharani et al., 2008) and cell metabolism (Silvestri et al., 2008; Puente et al., 2014).

However, there were a few articles on Medaka and Zebrafish that were directly related to climate change issues and elements, such as environmental stress caused by hypoxia (Kong et al., 2008; Wang et al., 2016) and agricultural runoff (Hayasaka et al., 2012) and pollution (Babayigit et al., 2016). Basically, global warming can induce coastal hypoxia by decreasing oxygen solubility and resulting in an increase in the oxygen demand of the aquatic species. Adult marine medaka was used as a model organism for the determination of environmental stress of hypoxia, and the results showed that there were significant alterations in levels of cell proliferation marker and protein in liver conditions of the species, *Oryzias melastigma* (Kong et al., 2008). Sexually matrure marine medaka, *O. melastigma* were also affected by hypoxia, causing retarded gonad development, decrease in sperm count and sperm motility of the fish (Wang et al., 2016). Hayasaka et al. (2012) showed the effects of toxic agro-chemicals on the abundance of benthic organisms, such as Medaka, in aquatic paddy communities. They found that adult and juvenile medaka body size were smaller in the treated insecticide pools compared to the controls over the 2 year experiment. In the Zebrafish experiment, environmental pollution caused by the lead and tin impacted the fish embryonic development (Babayigit

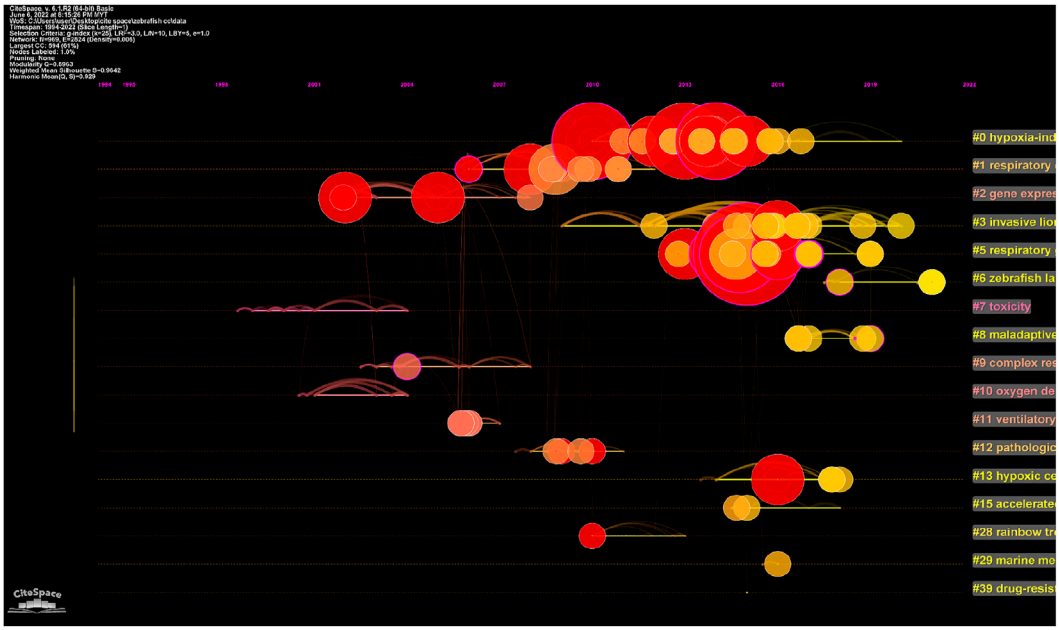

FIGURE 8
Summary of identified document cluster lifetimes (solid lines). Cluster labels were generated from CiteSpace.

TABLE 10 Three (3) major clusters that emerged from the article co-citation analysis for research on medaka and climate change.

ClusterID	Size	Silhouette	Label (LLR)	Average year
0	35	0.997	Transcriptomic responses	2014
5	20	1.000	Hypoxia alters steroidogenesis	2016
16	12	0.998	Multiple leptin gene	2012

et al., 2016). These results show that climate change research using medaka or zebrafish as models have largely focused on the effects of agriculture runoff and hypoxia. Specifically, research appears to have focused on how these effects change development and growth within these model species.

4.2 Scientometric based analysis

There is a huge difference between the most influential author analysis for the zebrafish subsample compared to the medaka subsample. The zebrafish subsample had >10 influential authors with a sigma score >1.0, while the medaka subsample only had one influential author. Even though the medaka subsample started earlier than the zebrafish subsample, the latter was more abundant and had higher influence in the scientific network than the former. From our results, the most influential authors in medaka research are clearly not active anymore as there is hardly any new research being published, indicating low scientific novelty for this domain. This demonstrates the need to change the current approach and introduce more disciplines in this domain. It is critical to start developing experts in these fields and build connections between sub-disciplines or the domain might cease to exist in the future. Our study also suggest that the domain (i.e., medaka and climate change) might not producing enough valuable research, and this could be shows less publication. This is also could be affected that the zebrafish are a better model organism for climate change related studies.

In bibliometrics, co-citation analysis is one way to assess similar articles. Document or article co-citation analysis is a unique method for tracking similar papers that are cited together in journals by many authors; it will lastly identify clusters of research (Boyack and Klavans, 2010). Here, we only found a few articles for both species that fell into categories related to the current objectives of the paper (which is the use of model organisms in climate change

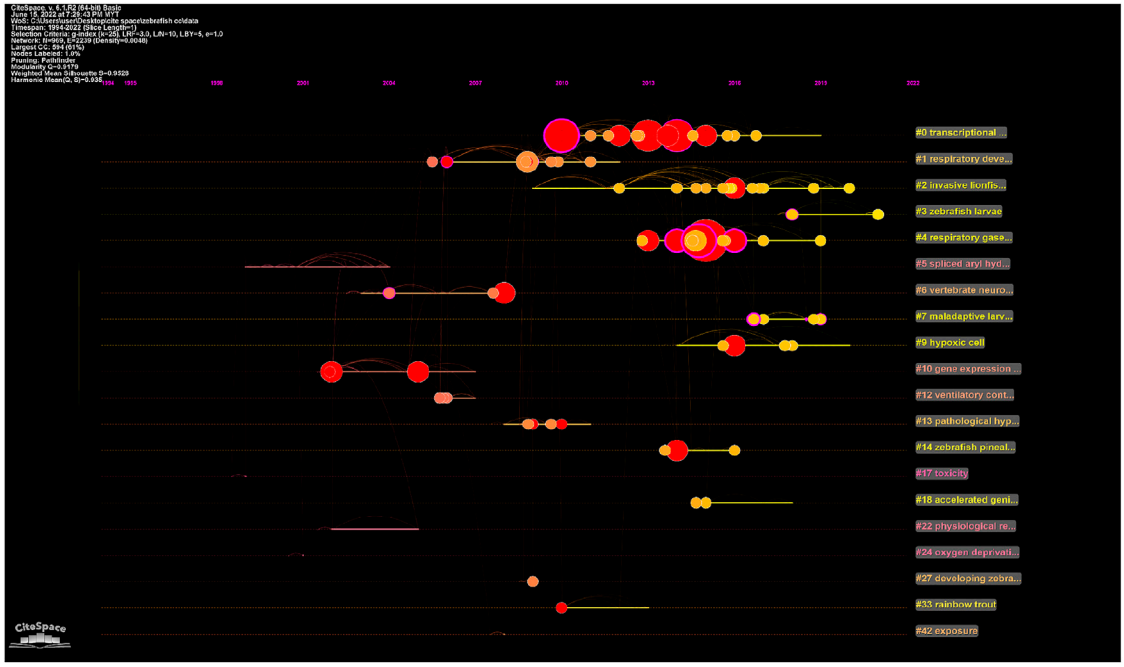

FIGURE 9
Summary of identified medaka and climate changes cluster lifetimes (solid lines). Cluster labels were generated from CiteSpace.

TABLE 11 Fifteen keywords with a citation burst for research on zebrafish and climate change.

Keywords	Year	Strength	Begin	End	1994–2022
Temperature	1994	**6.81**	2019	2022	
Embryonic development	1994	**5.5**	2016	2019	
In vivo	1994	**4.78**	2009	2013	
Danio rerio	1994	**4.74**	2002	2006	
Differentiation	1994	**4.61**	2013	2016	
Pharmaceutical	1994	**4.37**	2019	2020	
Neuroepithelial cell	1994	**4.02**	2014	2015	
Cancer	1994	**3.89**	2011	2012	
Nanoparticle	1994	**3.77**	2018	2020	
Angiogenesis	1994	**3.58**	2003	2011	
Aryl hydrocarbon receptor	1994	**3.49**	2000	2012	
Developmental toxicity	1994	**3.48**	2017	2022	
Messenger rna expression	1994	**3.43**	2011	2013	
Zebrafish embryo	1994	**3.43**	2018	2020	
Zebrafish danio rerio	1994	**3.42**	2015	2018	

The bold value refers to citation burst. The beginning of a blue line depicts when an article is published. The beginning of a red segment marks the beginning of a period of burst, whereas the end of the red segment marks the end of the burst period.

research). Instead most of the related studies were on hypoxia and agricultural runoff of chemical pollution (Robertson et al., 2014; Bertram et al., 2015; Lai et al., 2016; Wang et al., 2016). However, few articles have an impact in terms of documents co-citation analysis. For zebrafish species, there were only two articles with a sigma value higher than 2 (which indicates importance of the papers in the field), whereas no articles from the Medaka species reached a sigma value of 2. The studies by Rooijen et al. (2009) and Howe et al. (2013) had sigma values above 2.0. Rooijen et al. (2009) used zebrafish as a model organism to understand cellular response of tumors in humans by exposing fish to hypoxic conditions. Meanwhile, the study by Howe et al. (2013) showed the relationship between the zebrafish reference genome sequence with the human genome. This shows that the zebrafish was not only used for the climate change impacted the aquatic ecosystem or organism, it was also used for the human related studies. This could be impacted the number of researcher using this animals (i.e., zebrafish) rather than the Medaka species. Based on Table 11, there were a total of 15 top keywords generated from the scientometrics analysis. Surprisingly, the top keyword was temperature, in which it was the key driving force in climate change related studies, especially related to the aquatic organisms (Bozinovic and Pörtner, 2015). However, none of the papers or cluster was actually related to the temperature and climate change. This could be attributed to keywords used for researcher when conducted their related studies towards climate change, such as climate-induce water temperature changes or surface temperature (Borges et al., 2019; Azra et al., 2020). As mentioned above, the zebrafish subsample was the most related to climate change studies (Table 11), which indicates the importance of this species towards climate change related research.

Based on the previous scientometric results that was discussed in the present study, the authors found that the Zebrafish and Medaka have been widely used as one of the model species for ecotoxicological based studies. Agriculture runoff is categorized as one of the climate change elements (Azra et al., 2022), and this could directly or indirectly associated with many toxicological chemicals in the environment (Boxall et al., 2009). However, as both Zebrafish and Medaka can be found in the freshwater and seawater ecosystem, future insight into the potential of how these model species could be properly employed to improve our understanding of climate-driven changes are truly needed. For example, climate-induce water temperature changes could be one of the great example on how global warming could impacted the growth and development of both model species. Their results could be compared and future adaptation strategies could be proposed in the future.

5 Conclusions, strengths and limitations

Studying model organisms helps increase our understanding and knowledge on various types of systems as impacts can be applied to other species. The Zebrafish and Medaka are among one of the most popular aquatic model organisms for studies on climate change. However, our analysis has shown that zebrafish are the most versatile model organism compared to Medaka for climate change as well as in bioindication domain-related studies. Within climate change research, hypoxia and agriculture runoff were common examples for work using these species as models. While the number of publications on these species has increased rapidly, particularly for zebrafish, still missing are more specific studies related to climate change. To understand how other marine or freshwater species will be affected by climate change, particularly climate warming, zebrafish and medaka can be used in experimental studies as model species.

To our knowledge, this is the first study that systematically analyzes and differentiates the data of model-based organisms in climate change studies. However, this survey has some limitations. With respect to our search approach, we included only research articles that were published in English (excluding books, conference papers, abstract, notes, etc.). Additionally our keywords may have been too general, which may be why we saw a high percentage of research not directly related to climate change elements.

6 Recommendations

For future scientometric work, other databases such as Scopus, Directory of Open Access Journals etc. should be used for article searching and indexing in the future to include a wider array of articles. We also recommend including other alternative climate change species models, such as the *Artemia*. With respect to primary climate change research, our results indicate that work further investigating the effects of climate-induced hypoxia as well as chemical tolerance on model organisms would be beneficial. Further, we strongly suggest the use of model organisms in climate research to understand more climate induced effects, such as heatwaves, freshwater influx from flooding, or drought conditions that all may influence fish or other organism's development.

Author contributions

MN: Preliminary idea; First draft; Final draft MM: Preliminary idea; First draft; Final draft MP: Literature search; Critically revised; Software application; Final draft MD: Literature search; Critically revised; Second draft; Final draft MA: Literature search; Critically revised; Second draft; Final draft IZ: Literature search; Critically revised; Final draft MF: Literature search; Critically revised; Second draft; Final draft ZA: Literature

search; Critically revised; Supervision; Final draft FP: Preliminary idea; Critically revised; Funding Acquisition; Final draft.

Acknowledgments

The funding was received through PYPA Initiative managed by the Universiti Teknologi MARA (UiTM).

Conflict of interest

The authors declare that the research was conducted in the absence of any commercial or financial relationships that could be construed as a potential conflict of interest.

Publisher's note

Supplementary material

The Supplementary Material for this article can be found online at: https://www.frontiersin.org/articles/10.3389/feart.2022.988710/full#supplementary-material

References

Altshuler, I., Demiri, B., Xu, S., Constantin, A., Yan, N. D., and Cristescu, M. E. (2011). An integrated multi-disciplinary approach for studying multiple stressors in freshwater ecosystems: Daphnia as a model organism. *Integr. Comp. Biol.* 51, 623–633. doi:10.1093/icb/icr103

Aryadoust, V., Tan, H. A. H., and Ng, L. Y. (2019). A scientometric review of rasch measurement: The rise and progress of a specialty. *Front. Psychol.* 10, 2197. doi:10.3389/fpsyg.2019.02197

Asharani, P. V., Wu, Y. L., Gong, Z., and Valiyaveettil, S. (2008). Toxicity of silver nanoparticles in zebrafish models. *Nanotechnology* 19, 255102. doi:10.1088/0957-4484/19/25/255102

Azra, M. N., Aaqillah-Amr, M. A., Ikhwanuddin, M., Ma, H., Waiho, K., Ostrensky, A., et al. (2020). Effects of climate-induced water temperature changes on the life history of brachyuran crabs. *Rev. Aquac.* 12, 1211–1216. doi:10.1111/raq.12380

Azra, M. N., Noor, M. I. M., Sung, Y. Y., and Ghaffar, M. A. (2022). What evidence exists on the impact of climate change on some of the worst invasive fish and shellfish? A systematic map protocol. *Environ. Evid.* 11, 19. doi:10.1186/s13750-022-00273-z

Babayigit, A., Thanh, D. D., Ethirajan, A., Manca, J., Muller, M., Boyen, H. G., et al. (2016). Assessing the toxicity of Pb- and Sn-based perovskite solar cells in model organism *Danio rerio*. *Sci. Rep.* 6, 18721. doi:10.1038/srep18721

Bertram, M. G., Saaristo, M., Baumgartner, J. B., Johnstone, C. P., Allinson, M., Allinson, G., et al. (2015). Sex in troubled waters: Widespread agricultural contaminant disrupts reproductive behaviour in fish. *Hormones Behav.* 70, 85–91. doi:10.1016/j.yhbeh.2015.03.002

Borges, J. S., Grande, F. R. D., and Costa, T. M. (2019). Do lower air or water temperatures limit the southern distribution of the white mangrove Laguncularia racemosa in South America? *Estuar. Coast. Shelf Sci.* 230, 106449. doi:10.1016/j.ecss.2019.106449

Boxall, A. B. A., Hardy, A., Beulke, S., Boucard, T., Burgin, L., Falloon, P. D., et al. (2009). Impacts of climate change on indirect human exposure to pathogens and chemicals from agriculture. *Environ. Health Perspect.* 117, 508–514. doi:10.1289/ehp.0800084

Boyack, K. W., and Klavans, R. (2010). Co-citation analysis, bibliographic coupling, and direct citation: Which citation approach represents the research front most accurately? *J. Am. Soc. Inf. Sci. Technol.* 61, 2389–2404. doi:10.1002/asi.21419

Bozinovic, F., and Pörtner, H. O. (2015). Physiological ecology meets climate change. *Ecol. Evol.* 5, 1025–1030. doi:10.1002/ece3.1403

Braña, C. B. C., Cerbule, K., Senff, P., and Stolz, I. K. (2021). Towards environmental sustainability in marine finfish aquaculture. *Front. Mar. Sci.* 8, 666662. doi:10.3389/fmars.2021.666662

Chae, Y. J., Pham, C. H., Lee, J., Bae, E., Yi, J., and Gu, M. B. (2009). Evaluation of the toxic impact of silver nanoparticles on Japanese medaka (*Oryzias latipes*). *Aquat. Toxicol.* 94, 320–327. doi:10.1016/j.aquatox.2009.07.019

Chen, C., Chen, Y., Horowitz, M., Hou, H., Liu, Z., and Pellegrino, D. (2009). Towards an explanatory and computational theory of scientific discovery. *J. Inf.* 3, 191–209. doi:10.1016/j.joi.2009.03.004

Chen, C., Ibekwe-SanJuan, F., and Hou, J. (2010). The structure and dynamics of cocitation clusters: A multiple-perspective cocitation analysis. *J. Am. Soc. Inf. Sci. Technol.* 61, 1386–1409. doi:10.1002/asi.21309

Chen, C., and Leydesdorff, L. (2014). Patterns of connections and movements in dual-map overlays: A new method of publication portfolio analysis. *J. Assoc. Inf. Sci. Technol.* 65, 334–351. doi:10.1002/asi.22968

Chen, C., and Song, M. (2019). Visualizing a field of research: A methodology of systematic scientometric reviews. *Plos One* 14, e0223994. doi:10.1371/journal.pone.0223994

Chen, C. (2020). *How to use CiteSpace*. British Columbia, Canada: Lean Publishing, 246. Available at: https://citespace.podia.com/view/downloads/ebook-how-to-use-citespace.

Chen, C. (2004). Searching for intellectual turning points: Progressive knowledge domain visualization. *Proc. Natl. Acad. Sci. U. S. A.* 101, S5303–S5310. doi:10.1073/pnas.0307513100

Chowdhury, K., Lin, S., and Lai, S. L. (2022). Comparative study in Zebrafish and Medaka unravels the mechanisms of tissue regeneration. *Front. Ecol. Evol.* 10, 78381. doi:10.3389/fevo.2022.783818

Dietrich, M. R., Ankeny, R. A., and Chen, P. M. (2014). Publication trends in model organism research. *Genetics* 198, 787–794. doi:10.1534/genetics.114.169714

Feng, L., Shang, S., Feng, X., Kong, Y., and Bai, J. (2022). Evolution and trend analysis of research hotspots in the field of pollution-intensive industry transfer—based on literature quantitative empirical study of China as world factory. *Front. Environ. Sci.* 10, 732734. doi:10.3389/fenvs.2022.732734

Free, C. M., Cabral, R. B., Froehlich, H. E., Battista, W., Ojea, E., O'Reilly, E., et al. (2022). Expanding ocean food production under climate change. *Nature* 605, 490–496. doi:10.1038/s41586-022-04674-5

Hayasaka, D., Korenaga, T., Suzuki, K., Saito, F., Sánchez-Bayo, F., and Goka, K. (2012). Cumulative ecological impacts of two successive annual treatments of imidacloprid and fipronil on aquatic communities of paddy mesocosms. *Ecotoxicol. Environ. Saf.* 80, 355–362. doi:10.1016/j.ecoenv.2012.04.004

Hiekkalinna, T., Goring, H. H. H., and Terwilliger, J. D. (2012). On the validity of the likelihood ratio test and consistency of resulting parameter estimates in joint linkage and linkage disequilibrium analysis under improperly specified parametric models. *Ann. Hum. Genet.* 76, 63–73. doi:10.1111/j.1469-1809.2011.00683.x

Hou, J., Yang, X., and Chen, C. (2018). Emerging trends and new developments in information science: A document co-citation analysis (2009–2016). *Scientometrics* 115, 869–892. doi:10.1007/s11192-018-2695-9

Howe, K., Clark, M. D., Torroja, C. F., Torrance, J., Berthelot, C., Muffato, M., et al. (2013). The zebrafish reference genome sequence and its relationship to the human genome. *Nature* 496, 498–503. doi:10.1038/nature12111

Hsu, H. H., Lin, L. Y., Tseng, Y. C., Horng, J. L., and Hwang, P. P. (2014). A new model for fish ion regulation: Identification of ionocytes in freshwater- and seawater-acclimated medaka (*Oryzias latipes*). *Cell. Tissue Res.* 357, 225–243. doi:10.1007/s00441-014-1883-z

Joubert, D., and Bijlsma, R. (2010). Interplay between habitat fragmentation and climate change: Inbreeding affects the response to thermal stress in *Drosophila melanogaster*. *Clim. Res.* 43, 57–70. doi:10.3354/cr00883

Kinth, P., Mahesh, G., and Panwar, Y. (2013). Mapping of Zebrafish research. A global outlook. *Zebrafish* 10, 510–517. doi:10.1089/zeb.2012.0854

Kong, R. Y. C., Giesy, J. P., Wu, R. S. S., Chen, E. X. H., Chiang, M. Wl, Lim, P. L., et al. (2008). Development of a marine fish model for studying *in vivo* molecular responses in ecotoxicology. *Aquat. Toxicol.* 86, 131–141. doi:10.1016/j.aquatox.2007.10.011

Lai, K. P., Li, J. W., Tse, C. K., Chan, T. F., and Wu, R. S. S. (2016). Hypoxia alters steroidogenesis in female marine medaka through miRNAs regulation. *Aquat. Toxicol.* 172, 1–8. doi:10.1016/j.aquatox.2015.12.012

Mamun, A. A., Murray, F. J., Sprague, M., McAdam, B. J., Roos, N., de-Roos, B., et al. (2021). Pounds Am little DCExport-driven, extensive coastal aquaculture can benefit nutritionally vulnerable people. *Front. Sustain. Food Syst.* 5, 713140. doi:10.3389/fsufs.2021.713140

Marx, V. (2021). Model organisms on roads less traveled. *Nat. Methods* 18, 235–239. doi:10.1038/s41592-021-01086-7

Maulu, S., Nawanzi, K., Abdel-Tawwab, M., and Khalil, H. S. (2021). Fish nutritional value as an approach to children's nutrition. *Front. Nutr.* 8, 780844. doi:10.3389/fnut.2021.780844

Morgan, R., Sundin, J., Finnoen, M. H., Dresler, G., Vendrell, M. M., Dey, A., et al. (2019). Are model organisms representative for climate change research? Testing thermal tolerance in wild and laboratory zebrafish populations. *Conserv. Physiol.* 7, coz036. doi:10.1093/conphys/coz036

Müller, B., and Grossniklau, U. (2010). Model organisms — a historical perspective. *J. Proteomics* 73, 2054–2063. doi:10.1016/j.jprot.2010.08.002

Niimura, Y., and Nei, M. (2005). Evolutionary dynamics of olfactory receptorgenes in fishes and tetrapods. *Proc. Natl. Acad. Sci. U. S. A.* 102, 6039–6044. doi:10.1073/pnas.0501922102

Noor, M. I. M., Azra, M. N., Lim, V. C., Zaini, A. A., Dali, F., Hashim, I. M., et al. (2021). Aquaculture research in Southeast Asia - a scientometric analysis (1990-2019). *Int. Aquatic Res.* 13, 271–288. doi:10.22034/IAR.2021.1932503.1166

Puente, B. N., Kimura, W., Muralidhar, S. A., Moon, J., Amatruda, J. F., Phelps, K. L., et al. (2014). The oxygen-rich postnatal environment induces cardiomyocyte cell-cycle arrest through DNA damage response. *Cell.* 24, 565–579. doi:10.1016/j.cell.2014.03.032

Robertson, C. E., Wright, P. A., Koblitz, L., and Bernier, N. J. (2014). Hypoxia-inducible factor-1 mediates adaptive developmental plasticity of hypoxia tolerance in zebrafish, *Danio rerio*. *Proc. R. Soc. B* 281, 20140637. doi:10.1098/rspb.2014.0637

Rooijen, E. V., Voest, E. E., Logister, I., Korving, J., Schwerte, T., Schulte-Merker, S., et al. (2009). Zebrafish mutants in the von Hippel-Lindau tumor suppressor display a hypoxic response and recapitulate key aspects of Chuvash polycythemia. *Blood* 113, 6449–6460. doi:10.1182/blood-2008-07-167890

Shi, X., Zhang, J., Lu, S., Wang, T., and Zhang, X. (2022). China carbon neutralization research status and research frontier tracking. *Front. Environ. Sci.* 10, 896524. doi:10.3389/fenvs.2022.896524

Silvertown, J., Cook, L., Cameron, R., Dodd, M., McConway, K., Worthington, J., et al. (2011). Citizen science reveals unexpected continental-scale evolutionary change in a model organism. *PLoS ONE* 6, e18927. doi:10.1371/journal.pone.0018927

Silvestri, L., Pagani, A., Nai, A., Domenico, I. D., Kaplan, J., and Camaschella, C. (2008). The serine Protease matriptase-2 (TMPRSS6) Inhibits Hepcidin activation by cleaving Membrane Hemojuvelin. *Cell. Metab.* 8, 502–511. doi:10.1016/j.cmet.2008.09.012

Sunday, J. M., Bates, A. E., and Dulvy, N. K. (2012). Thermal tolerance and the global redistribution of animals. *Nat. Clim. Chang.* 2, 686–690. doi:10.1038/nclimate1539

Tregaskes, C. A., and Kaufman, J. (2021). Chickens as a simple system for scientific discovery: The example of the MHC. *Mol. Immunol.* 135, 12–20. doi:10.1016/j.molimm.2021.03.019

Vilas–Boas, J. A., Cardoso, S. J., Senra, M. V. X., Rico, A., and Dias, R. J. P. (2020). Ciliates as model organisms for the ecotoxicological risk assessment of heavy metals: A meta–analysis. *Ecotoxicol. Environ. Saf.* 199, 110669. doi:10.1016/j.ecoenv.2020.110669

Waldvogel, A. M., Schreiber, D., Pfenninger, M., and Feldmeyer, B. (2020). Climate change genomics calls for standardized data reporting. *Front. Ecol. Evol.* 8, 242. doi:10.3389/fevo.2020.00242

Wang, S. Y., Lau, K., Lai, K. P., Zhang, J. W., Tse, A. C. K., Li, J. W., et al. (2016). Hypoxia causes transgenerational impairments in reproduction of fish. *Nat. Commun.* 7, 12114. doi:10.1038/ncomms12114

Zhao, X., Ren, X., Zhu, R., Luo, Z., and Ren, B. (2016). Zinc oxide nanoparticles induce oxidative DNA damage and ROS-triggered mitochondria-mediated apoptosis in zebrafish embryos. *Aquat. Toxicol.* 180, 56–70. doi:10.1016/j.aquatox.2016.09.013

frontiers | Frontiers in Environmental Science

TYPE Mini Review
PUBLISHED 13 September 2022
DOI 10.3389/fenvs.2022.983637

OPEN ACCESS

EDITED BY
Qiang Zhang,
Beijing Normal University, China

REVIEWED BY
Li Wen,
Industry and Environment, Australia

*CORRESPONDENCE
Floris M. van Beest,
flbe@ecos.au.dk

SPECIALTY SECTION
This article was submitted to Interdisciplinary Climate Studies, a section of the journal Frontiers in Environmental Science

RECEIVED 01 July 2022
ACCEPTED 29 August 2022
PUBLISHED 13 September 2022

CITATION
van Beest FM, Barry T, Christensen T, Heiðmarsson S, McLennan D and Schmidt NM (2022), Extreme event impacts on terrestrial and freshwater biota in the arctic: A synthesis of knowledge and opportunities. *Front. Environ. Sci.* 10:983637. doi: 10.3389/fenvs.2022.983637

Extreme event impacts on terrestrial and freshwater biota in the arctic: A synthesis of knowledge and opportunities

Floris M. van Beest [1,2]*, Tom Barry [3], Tom Christensen [1,2], Starri Heiðmarsson [4], Donald McLennan[5] and Niels M. Schmidt [1,2]

[1]Department of Ecoscience, Aarhus University, Roskilde, Denmark, [2]Arctic Research Centre, Aarhus University, Aarhus, Denmark, [3]Conservation of Arctic Flora and Fauna (CAFF), Secretariat, Akureyri, Iceland, [4]Icelandic Institute of Natural History, Garðabær, Iceland, [5]Polar Knowledge Canada, Canadian High Arctic Research Station, Cambridge Bay, NU, Canada

Extreme weather events are increasing in frequency and intensity across the Arctic, one of the planet's most rapidly warming regions. Studies from southern latitudes have revealed that the ecological impacts of extreme events on living organisms can be severe and long-lasting, yet data and evidence from within the terrestrial Arctic biome appear underrepresented. By synthesizing a total of 48 research articles, published over the past 25 years, we highlight the occurrence of a wide variety of extreme events throughout the Arctic, with multiple and divergent impacts on local biota. Extreme event impacts were quantified using a myriad of approaches ranging from circumpolar modelling to fine-scale experimental studies. We also identified a research bias towards the quantification of impacts related to a few extreme event types in the same geographic location (e.g. rain-on-snow events in Svalbard). Moreover, research investigating extreme event impacts on the ecology of arthropods and especially freshwater biota were scant, highlighting important knowledge gaps. While current data allow for hypotheses development, many uncertainties about the long-term consequences of extreme events to Arctic ecosystems remain. To advance extreme event research in the terrestrial Arctic biome, we suggest that future studies i) objectively define what is extreme in terms of events and ecological impacts using long-term monitoring data, ii) move beyond single-impact studies and single spatial scales of observation by taking advantage of pan-Arctic science-based monitoring networks and iii) consider predictive and mechanistic modelling to estimate ecosystem-level impacts and recovery.

KEYWORDS

arctic environment, climate change, environmental monitoring, extreme event, terrestrial

Introduction

There is ample scientific evidence revealing the destructive impacts from long-term changes in mean climatic conditions on biodiversity and ecosystem functioning (Sintayehu, 2018; Turner et al., 2020; Weiskopf et al., 2020). However, in addition to gradual changes in global climate, there is also an increase in the intensity, frequency and duration of extreme events that are directly or indirectly related to weather and climate. Extreme events are considered rare within their statistical reference distributions at a particular time or place (IPCC, 2012); from here on: "extreme events". Some well-known examples are transient but severe precipitation events (Kirchmeier-Young and Zhang, 2020), heatwaves (Perkins-Kirkpatrick and Lewis, 2020) and wildfires (Boer et al., 2020). The impact of extreme events on ecosystems can be severe and long-lasting (Harris et al., 2018), with profound implications for species conservation and environmental management (Maxwell et al., 2019). Documenting, quantifying, and understanding the impacts of extreme events on species and their natural environment has become a prominent research focus, demonstrated by the sharp increase in the number of published research papers over the last 5 decades (Figure 1A) and numerous systematic reviews on the topic (Ummenhofer and Meehl, 2017; McPhillips et al., 2018; Aoki et al., 2022).

Nowhere else is climate change more apparent than in the Arctic (Post et al., 2019; IPCC, 2021). Because of the long-term and gradual increase in surface air temperatures, sea ice loss, and permafrost thaw associated with Arctic amplification (Previdi et al., 2021), the Arctic biophysical system is now experiencing unprecedented change, with implications for regions far beyond the Arctic (Box et al., 2019). Occurrences of extreme events across the region have also increased considerably over the past decades (Landrum and Holland, 2020; Walsh et al., 2020), specifically in terms of precipitation (Bintanja, 2018) and temperature (Dobricic et al., 2020) anomalies. In some areas,

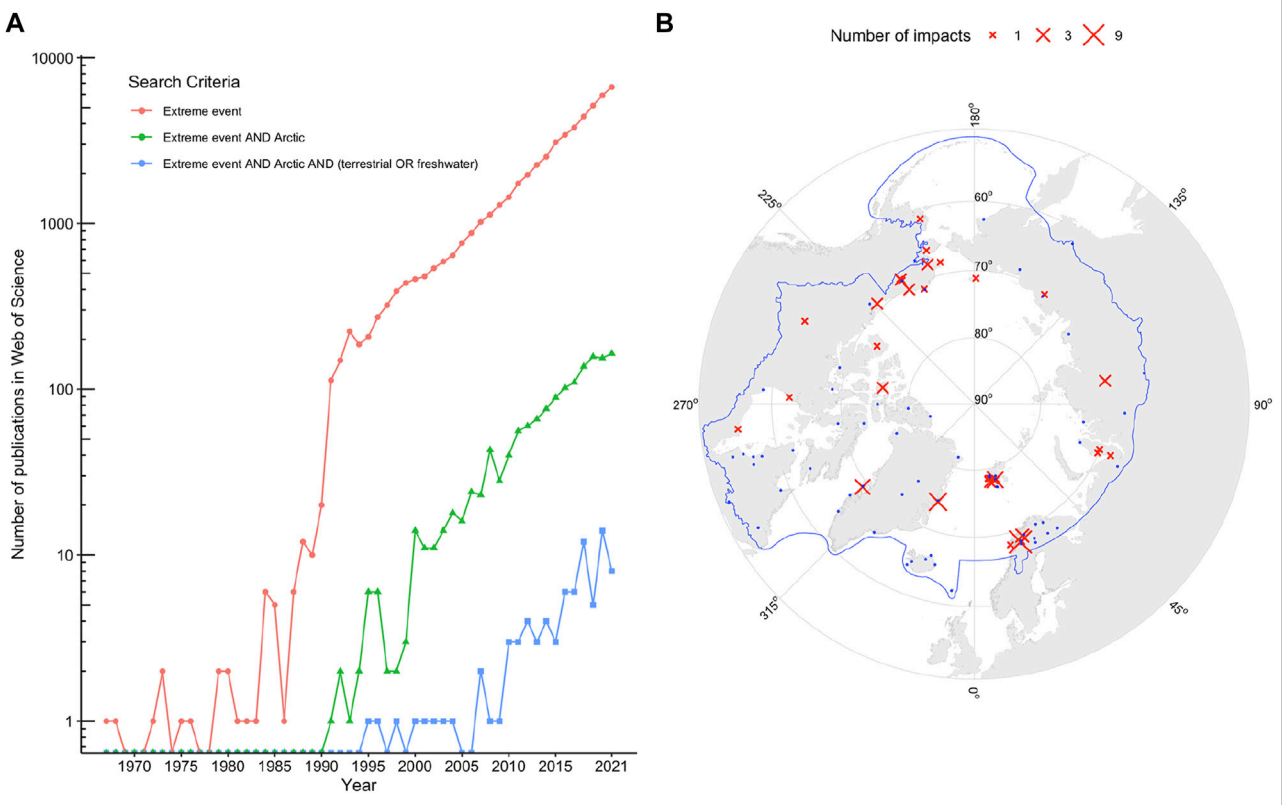

FIGURE 1
Panel a shows trends in annual number of published research articles dealing with extreme events across the entire globe (in SALMON), extreme event studies in the Arctic (in GREEN) and extreme event studies in the Arctic considering only terrestrial and freshwater studies (in BLUE). Trends are based on a literature search through the Institute for Scientific Information (ISI) Web of Science database (June 2022) using the search criteria provided in the figure legend. Note that the *y*-axis of the graph is on a logarithmic scale. Panel b shows the location (indicated with a red x) of the 48 published studies included in our mini-review that were concerned with impacts of extreme events on terrestrial and freshwater biota in the Arctic. The size of the study location indicator is scaled relative to the total number of impacts quantified (n = 69). The Arctic boundary as defined by the Conservation of Arctic Flora and Fauna (CAFF) group is shown as a blue line. Blue dots on the map show the location of research stations connected to the International Network for Terrestrial Research and Monitoring in the Arctic (INTERACT).

such extremes are leading to a marked increase in frequency of icing (Tyler, 2010) and rain-on-snow events during winter (Putkonen et al., 2009) with negative ecological and socioeconomic consequences (Hansen et al., 2014; Forbes et al., 2016). As elsewhere in the world, the intensity and duration of wildfires are also increasing and pose a serious risk to the carbon-storage capacity of the Arctic ecosystem (Hu et al., 2015).

The potential of extreme events to influence the Arctic and its biodiversity is substantial and documenting these impacts is a research priority (Post et al., 2009b; McCrystall et al., 2021). However, the number of published papers dealing with extreme event impacts in the Arctic biome represents only a small fraction of the entire research output on this topic and, moreover, the number of studies on terrestrial and freshwater biota appear especially limited (Figure 1A). To fill this knowledge gap, we synthesized the scientific literature dealing with extreme events in the Arctic and their ecological impacts on terrestrial and freshwater biota. We are particularly interested in providing an overview of the different types of extreme events studied, the ecological impacts detected, the focal species or taxonomic groups studied, the methods employed, and whether or not impact recovery was quantified. We finish the mini-review with a number of recommendations aimed to facilitate the detection, evaluation, and documentation of extreme event impacts on terrestrial and freshwater species within the Arctic biome.

Extreme event research in the terrestrial arctic: A mini-review

Based on a literature search through the Institute for Scientific Information (ISI) Web of Science database and using the search criteria “Extreme event” AND “Arctic” AND (“terrestrial” OR “freshwater”), we found 48 published studies that investigated ecological impacts of extreme events on terrestrial and freshwater biota in the Arctic (Figure 1B). An overview of the published articles and data extracted can be found in Supplementary Table S1.

Our literature search detected research from sites that were scattered across the Arctic region (Figure 1B), yet the majority of studies were conducted in mainland Scandinavia (n = 16), Svalbard (n = 14), Alaska (n = 13), and Greenland (n = 11) and relatively few extreme event impact studies took place in Russia (n = 7) and Canada (n = 7). No published studies were found from Iceland, Finland and the Faroe Islands. Geographic bias in research output is a known limitation within ecological literature originating from temperate and tropical systems (Culumber et al., 2019). Such bias may lead to important gaps in scientific knowledge with implications for environmental management, conservation and policy. While it has been argued that studies of extreme events in northern regions are somewhat opportunistic and uncoordinated (Walsh et al., 2020), geographic bias in extreme event research in the Arctic has never been formally tested. A likely explanation for the clustered research output identified here is that logistical constraints associated with working in remote and often inaccessible areas in the Arctic hinders the design and implementation of coordinated and geographically balanced research (Metcalfe et al., 2018).

Ten different types of extreme events in the Arctic were reported in the literature (Figure 2) with most of the effort dedicated to quantifying potential impacts of rain-on-snow events on terrestrial biota (n = 19). Extreme summer cooling and rain events, pest outbreaks and landslides were reported least (Figure 2). In addition, the vast majority of studies reported on ecological responses following a single extreme event (n = 44) and only four studies quantified impacts of multiple extreme events. Although extreme events are by definition rare and as such single-event studies should be most common, the occurrence of multiple extreme events as well as the documentation of their impacts on species and ecosystems elsewhere in the world are increasing (Bailey and van de Pol, 2016). While the current data and knowledge gained through single-event studies in the Arctic can contribute to future hypothesis development and more dedicated experimental designs, there seems to be a need for a greater focus on multi-event studies as these are expected to become more common under continuing global warming (Raymond et al., 2020).

To synthesize ecological impacts of extreme events on Arctic biota (Figure 2), we relied on five categories as used in the structure of the Circumpolar Biodiversity Monitoring Programme (CBMP), which was developed specifically to monitor and report on trends in Arctic biodiversity entities (Christensen et al., 2012; Culp et al., 2012). Potential ecological impacts of extreme events were most often quantified on vegetation (n = 33) followed by mammals (n = 19), birds (n = 9), arthropods (n = 6) and lastly on freshwater fish (n = 2). Hence, the total number of ecological impacts included in our mini-review (n = 69) was larger than the number of published studies (Figure 1 and Figure 2, Supplementary Table S1). Studying climate change effects on arthropods in the Arctic is a known research gap (Høye, 2020), but the reasons for the few published research articles of extreme event impacts on freshwater biota in the Arctic are unclear, especially given the large body of work done on extreme event impacts in aquatic systems elsewhere in the world (Aoki et al., 2022). It is possible that freshwater systems in the Arctic are generally studied less compared to terrestrial systems or that extreme events are less common in Arctic freshwater systems. Alternatively, studies on extreme events in freshwater systems may be reported using different definitions and terminology than those used in our literature search criteria. Whatever the reason, multiple and intimate linkages exist between terrestrial and aquatic ecosystems (Gratton et al., 2008; Wrona et al., 2016),

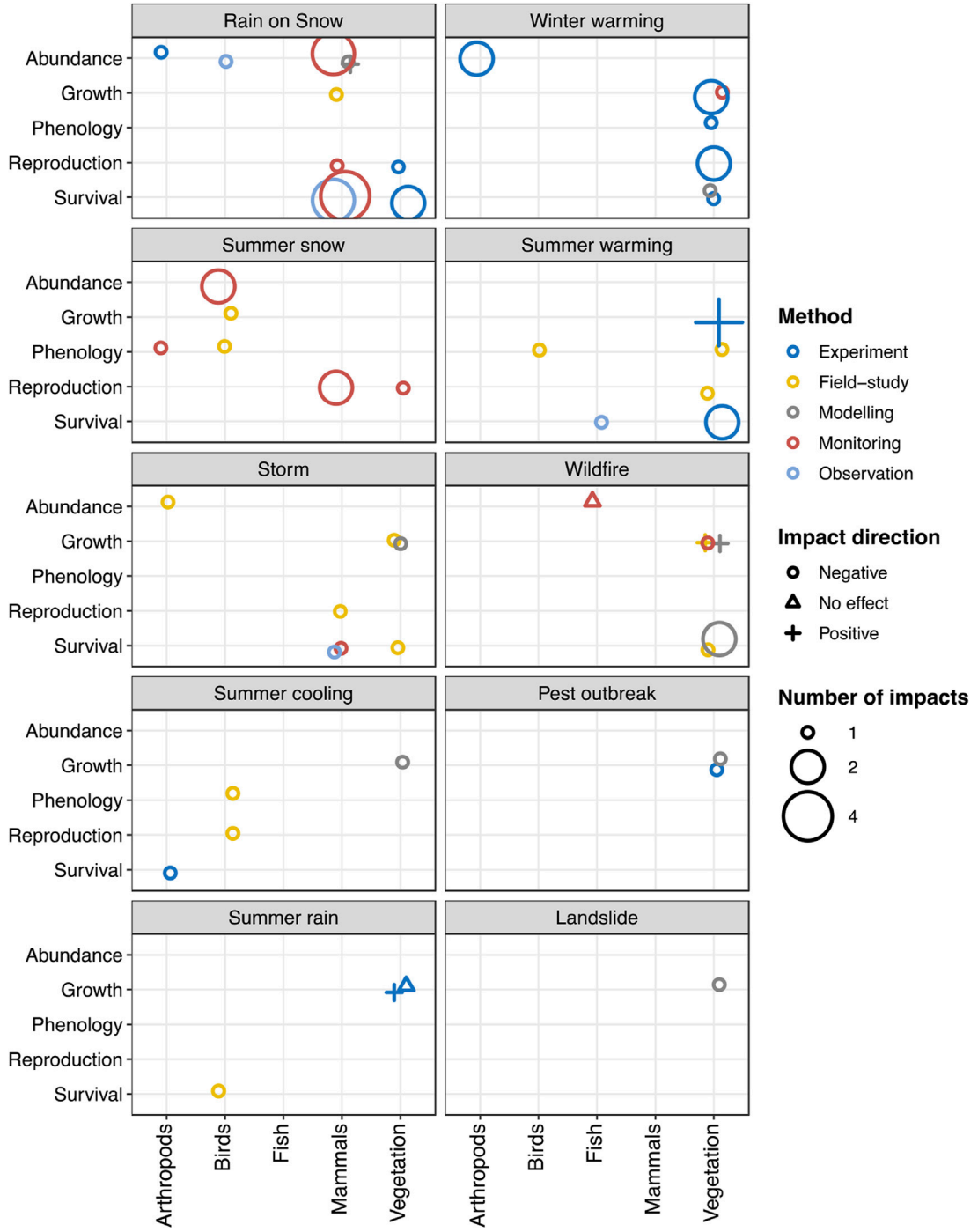

FIGURE 2
Categorization of the ecological impacts (n = 69) of extreme events on biota that were observed in terrestrial and freshwater Arctic ecosystems as documented in 48 studies published between 1995 and 2021. The shapes of the symbols indicate the direction of the ecological impact detected. The colours of the symbols reflect the method used to quantify the impact, and the size of the symbols are scaled relative to the number of studies that detected the impact.

and a more integrated approach to quantify extreme event effects on catchments in the future seems desirable, at least in the Arctic.

Ecological responses to extreme events by terrestrial and freshwater biota in the Arctic were predominantly negative (n = 61), with six of the ecological impacts being positive and

only two publications found no effect (Figure 2). Positive responses were mostly restricted to increased growth of Arctic vegetation following wildfires (Frost et al., 2020) or experimental summer warming (Marchand et al., 2005). Interestingly, simulating extreme rain events during summer also increased growth of the shrub vegetation in north east Siberia but the same experimental treatment in northern Sweden showed no effect on the same vegetation community (Keuper et al., 2012). It remains unclear why extreme events can have such divergent impacts on the same species or conversely why ecological impacts are often species- or group-specific (i.e. idiosyncratic) and what the involved mechanisms are. Such understanding is required to improve our predictive capacity on future change so as to determine whether extreme event-induced ecological impacts are important determinants of long-term population trends or ecosystem changes (van de Pol et al., 2017).

Quantification of extreme event impacts on Arctic biota were most often obtained through experimental studies (n = 20), followed by empirical monitoring (n = 18), field-studies (n = 15), modelling (n = 10) and opportunistic observation (n = 6). The size of the impacted area varied between the different methods employed (Supplementary Figure S1) with experiments covering smaller areas than dedicated field-studies, long-term monitoring, opportunistic observation data, and empirical-based modelling approaches. Impact recovery (i.e. post extreme event) on Arctic biota was assessed in 42% of the cases (n = 29) while in the remaining 58% this was not considered or done (n = 40). Impact recovery was most often quantified using experimental (14% of all cases) or long-term monitoring studies (10% of cases).

Overall, this mini-review highlights that a wide variety of extreme events do occur throughout the Arctic and dedicated effort has been undertaken over the past 25 years to document and quantify associated ecological impacts on local biota. It is certainly possible that this mini-review underestimates the work being done on extreme events in the Arctic as we did not, for example, consider "grey" literature. While this makes our synthesis necessarily myopic, the rationale was to provide a concise and transparent overview of extreme event impacts in the Arctic based on research that is easily accessible and interpretable by the entire scientific community. In doing so, we identified various knowledge gaps and outstanding questions related to extreme event effects. As climate change will continue to put pressure on Arctic biodiversity (Post et al., 2009a; Box et al., 2019), improved and coordinated efforts to study and monitor potential impacts and recoveries over extended temporal and geographic ranges are critical. Below we provide a number of recommendations that will hopefully benefit the design and effectiveness of future research and monitoring efforts on extreme event impacts in the Arctic biome.

Define what is considered extreme in terms of event and ecological impact

There is a general lack of coherence and scientific agreement in what constitutes and defines an extreme event and whether or not an ecological impact is even required (van de Pol et al., 2017; McPhillips et al., 2018; Latimer and Zuckerberg, 2019). In our mini-review, we considered both qualitative and quantitative definitions of extreme events as well as "no effect" studies, but many of the examined papers were opaque in their definition or qualification of the extremeness of the event and any associated impact. Lack of clear definitions of "extreme" makes it difficult to formally attribute ecological impacts or responses to anthropogenic climate change and, moreover, limits our ability to generalize ecological responses from site-specific events and comparison of findings through time and space (i.e. meta-analyses). Therefore, we support previous pleas that clear definitions of what constitutes extreme are needed (Smith, 2011; Aoki et al., 2022). Because extreme events and their impacts are research foci across disciplines (Broska et al., 2020) more precise definitions of extreme events will improve the application of ecological research within a multidisciplinary research context. We do acknowledge, however, that adopting a universal definition of extreme is difficult under contemporary climate and environmental change. This may be especially applicable to research taking place in the Arctic where climate change is occurring at such a pace that baseline estimates and values on weather and climatic conditions are rapidly changing. This means that what may be quantified as an anomaly or extreme event now, may no longer be so in the (near) future (Landrum and Holland, 2020). Fitting examples of this issue are rain-on-snow events and tundra wildfires. Although such events were rare and considered extreme in the past (and still are in some areas), they appear to become routine (e.g. annual) occurrence in some areas of the Arctic and could thus be considered the new normal. Nonetheless, consistent definitions, quantification and clear communication of extreme events can only enhance the understanding and management of potential impacts. We urge future studies in the Arctic to objectively and quantitatively define the extremeness of the event (i.e. conditions observed are at the *x*th percentile of their statistical reference distributions at a particular time or place) but also from the perspective of the response of the biota under investigation by comparing the impacts to baseline variability in the system. Clearly the formulation of such definitions relies on long-term data of environmental conditions as being collected in some science-based monitoring programs such as the International Tundra Experiment (ITEX: Henry and Molau, 1997), the Long Term Ecological Research Network (LTER: Knapp et al., 2012) and the Circumpolar Biodiversity Monitoring Program (CBMP: Christensen et al., 2020). Increased collaboration among such long-term and science-based monitoring programmes across the Arctic would greatly benefit our understanding of extreme event

impacts on the Arctic environment and biota as it facilitates collection of critical data on the spatiotemporal variation in the occurrences of extreme events and their ecological responses.

Go beyond single-event-impact studies and spatial scales of observation

As we move further into the Anthropocene with extreme climatic events impacting biodiversity and peoples livelihood (Hansen et al., 2014; Forbes et al., 2016), there is a strong scientific and socioeconomic need to go beyond single-event and single-impact studies. We found only three studies that quantified multiple impacts of an extreme event across local biota (Supplementary Table S1). However, given that food webs in the Arctic are highly interconnected (Schmidt et al., 2017), impacts on one trophic level may easily cascade onto others, with potential ecosystem-wide consequences. Drawing (statistical) inference on the ecological impacts of extreme climatic events, and identifying the mechanisms involved, relies on replication and control across a wide range and number of events and impacts (Altwegg et al., 2017). Again, long-term and science-based monitoring programmes provide the temporal resolution and data needed to start quantifying patterns and drivers of natural variability in biodiversity across scales. Such programmes will also increase chances of capturing effects of multiple extreme events in an area or multiple impacts of single events, and finally they allow for quantification of potential cascading consequences. Crucial in this respect is experimental replication over time and space so as to increase the likelihood of collecting data from areas that did experience the extreme events (impact) and sites that did not (control) but also before and after an extreme event (Elmendorf et al., 2012). We recommend that such experimental setups within a sound hypothesis testing framework are implemented more widely across the Arctic, which would be possible by taking advantage of an already existing network of research stations under the umbrella of the International Network for Terrestrial Research and Monitoring in the Arctic (INTERACT, 2015). One clear advantage of designing and implementing a coordinated research structure on extreme event impacts using INTERACT is that it will likely reduce geographic bias in research output identified in our mini-review as connected research stations are present in some of the areas that are currently understudied (Figure 1B). Moreover, a pan-Arctic, long-term monitoring and science-based network will facilitate the application of a myriad of data collection methods that can transcend difficulties with spatial and temporal upscaling of results (Ummenhofer and Meehl, 2017). We acknowledge that it is not always possible to design long-term experiments or use a combination of research methods that captures all possible impacts or extreme events, and most often study designs need to be tailored to specific research questions. However, to achieve a more holistic understanding of extreme event impacts the goal should be to use a combination of research methods as much as possible and where baseline data from long-term science-based monitoring programmes are complemented with insights from field studies, opportunistic observations, remote sensing, experimental data, and models. Long-term experiments or dedicated field studies are especially valuable as they can identify potential lag effects, feedbacks and interactions of extreme event impacts and to assess system recovery (Harris et al., 2020). Implementing multiple study designs into pan-Arctic research networks will offer great potential to further improve our understanding of extreme event impacts that can occur across multiple spatial and temporal scales.

Consider predictive modelling and ecosystem-level impacts

Empirical data and evidence on the impacts of extreme events on biota are often geographically and taxonomically idiosyncratic (Bailey and van de Pol, 2016; Metcalfe et al., 2018; Landrum and Holland, 2020). We also found that the direction of extreme event impacts in the Arctic sometimes differed within and between biota and across extreme events (Figure 2). Although this highlights that the predictability of local responses to extreme events is low, and more empirical data is clearly required to better understand the mechanisms and processes involved, we echo the view that predictive modelling efforts are a useful addition to the toolkit required to tackle some of the current knowledge gaps (Sillmann et al., 2017; Boult and Evans, 2021). Empirical data derived from long-term, science-based monitoring programmes combined with e.g., remote sensing products greatly facilitates the development of hindcasting and forecasting models to assess previous and future conditions over large geographic areas and temporal scales. While modelling entire ecosystems is a demanding task, statistical models that can incorporate multiple data streams derived from research-based long-term monitoring programmes to assess ecosystem dynamics and state changes are already available (McClintock et al., 2020). We see particular value for what are called next-generation Individual Based Models, which can be tailored specifically to study and assess how ecosystem function and services respond to changes in e.g. land use and climate (Grimm et al., 2017). Such process-based simulation models are constructed using pattern-oriented modelling approaches based on data that can be directly provided by long-term monitoring programmes and experimental work embedded within. Doing so makes these models structurally realistic and increases predictive power when applied under changing climatic conditions (Stillman et al., 2015). As we collect more empirical data and gain better

understanding of the processes and drivers underlying extreme events and their impacts on Arctic biota, these models can be used to iteratively evaluate and progress current evidence and knowledge.

Author contributions

FvB, TB, TC, and NS conceived the study. FvB coordinated the literature search and all authors contributed to the search and review of articles. FvB drafted the manuscript and all authors critically revised the manuscript, gave approval for publication, and agree to be accountable for all aspects of the work.

Acknowledgments

We thank the International Network for Terrestrial Research and Monitoring in the Arctic (INTERACT)-III for financial support (GA n. 871120). We also wish to thank Knud Falk and Willem Goedkoop for their constructive feedback on a previous version of this manuscript.

Conflict of interest

The authors declare that the research was conducted in the absence of any commercial or financial relationships that could be construed as a potential conflict of interest.

Publisher's note

Supplementary material

The Supplementary Material for this article can be found online at: https://www.frontiersin.org/articles/10.3389/fenvs.2022.983637/full#supplementary-material

References

Altwegg, R., Visser, V., Bailey, L. D., and Erni, B. (2017). Learning from single extreme events. *Phil. Trans. R. Soc. B* 372, 20160141. doi:10.1098/rstb.2016.0141

Aoki, L. R., Brisbin, M. M., Hounshell, A. G., Kincaid, D. W., Larson, E. I., Sansom, B. J., et al. (2022). Preparing aquatic research for an extreme future: Call for improved definitions and responsive, multidisciplinary approaches. *Bioscience* 72, 508–520. doi:10.1093/BIOSCI/BIAC020

Bailey, L. D., and van de Pol, M. (2016). Tackling extremes: Challenges for ecological and evolutionary research on extreme climatic events. *J. Anim. Ecol.* 85, 85–96. doi:10.1111/1365-2656.12451

Bintanja, R. (2018). The impact of Arctic warming on increased rainfall. *Sci. Rep.* 8, 16001–16006. doi:10.1038/s41598-018-34450-3

Boer, M. M., Resco de Dios, V., and Bradstock, R. A. (2020). Unprecedented burn area of Australian mega forest fires. *Nat. Clim. Chang.* 10, 171–172. doi:10.1038/s41558-020-0716-1

Boult, V. L., and Evans, L. C. (2021). Mechanisms matter: Predicting the ecological impacts of global change. *Glob. Chang. Biol.* 27, 1689–1691. doi:10.1111/GCB.15527

Box, J. E., Colgan, W. T., Christensen, T. R., Schmidt, N. M., Lund, M., Parmentier, F. J. W., et al. (2019). Key indicators of arctic climate change: 1971-2017. *Environ. Res. Lett.* 14, 045010. doi:10.1088/1748-9326/aafc1b

Broska, L. H., Poganietz, W. R., and Vögele, S. (2020). Extreme events defined—a conceptual discussion applying a complex systems approach. *Futures* 115, 102490. doi:10.1016/J.FUTURES.2019.102490

Christensen, T., Barry, T., Taylor, J. J., Doyle, M., Aronsson, M., Braa, J., et al. (2020). Developing a circumpolar programme for the monitoring of Arctic terrestrial biodiversity. *Ambio* 49, 655–665. doi:10.1007/s13280-019-01311-w

Christensen, T., Payne, J., Doyle, M., Ibarguchi, G., Taylor, J., Schmidt, N. M., et al. (2012). *The arctic terrestrial biodiversity monitoring plan*. Akureyri, Iceland: CAFF.

Culp, J., Goedkoop, W., Lento, J., Christoffersen, K., Frenzel, S., Guobergsson, G., et al. (2012). *Arctic freshwater biodiversity monitoring plan*. Akureyri, Iceland: Caff. Available at: https://www.caff.is/freshwater/freshwater-monitoring-publications/196-arctic-freshwater-biodiversity-monitoring-plan (Accessed March 25, 2021).

Culumber, Z. W., Anaya-Rojas, J. M., Booker, W. W., Hooks, A. P., Lange, E. C., Pluer, B., et al. (2019). Widespread biases in ecological and evolutionary studies. *Bioscience* 69, 631–640. doi:10.1093/BIOSCI/BIZ063

Dobricic, S., Russo, S., Pozzoli, L., Wilson, J., and Vignati, E. (2020). Increasing occurrence of heat waves in the terrestrial Arctic. *Environ. Res. Lett.* 15, 024022. doi:10.1088/1748-9326/ab6398

Elmendorf, S. C., Henry, G. H. R., Hollister, R. D., Björk, R. G., Bjorkman, A. D., Callaghan, T. V., et al. (2012). Global assessment of experimental climate warming on tundra vegetation: Heterogeneity over space and time. *Ecol. Lett.* 15, 164–175. doi:10.1111/j.1461-0248.2011.01716.x

Forbes, B. C., Kumpula, T., Meschtyb, N., Laptander, R., Macias-Fauria, M., Zetterberg, P., et al. (2016). Sea ice, rain-on-snow and tundra reindeer nomadism in Arctic Russia. *Biol. Lett.* 12, 20160466. doi:10.1098/rsbl.2016.0466

Frost, G. V., Loehman, R. A., Saperstein, L. B., Macander, M. J., Nelson, P. R., Paradis, D. P., et al. (2020). Multi-decadal patterns of vegetation succession after tundra fire on the Yukon-Kuskokwim Delta, Alaska. *Environ. Res. Lett.* 15, 025003. doi:10.1088/1748-9326/ab5f49

Gratton, C., Donaldson, J., and Zanden, M. J. V. (2008). Ecosystem linkages between lakes and the surrounding terrestrial landscape in northeast Iceland. *Ecosystems* 11, 764–774. doi:10.1007/s10021-008-9158-8

Grimm, V., Ayllón, D., and Railsback, S. F. (2017). Next-generation individual-based models integrate biodiversity and ecosystems: Yes we can, and yes we must. *Ecosystems* 20, 229–236. doi:10.1007/s10021-016-0071-2

Hansen, B. B., Isaksen, K., Benestad, R. E., Kohler, J., Pedersen, Å., Loe, L. E., et al. (2014). Warmer and wetter winters: Characteristics and implications of an extreme weather event in the High Arctic. *Environ. Res. Lett.* 9, 114021–114031. doi:10.1088/1748-9326/9/11/114021

Harris, R. M. B., Beaumont, L. J., Vance, T. R., Tozer, C. R., Remenyi, T. A., Perkins-Kirkpatrick, S. E., et al. (2018). Biological responses to the press and pulse of climate trends and extreme events. *Nat. Clim. Chang.* 8, 579–587. doi:10.1038/s41558-018-0187-9

Harris, R. M. B., Loeffler, F., Rumm, A., Fischer, C., Horchler, P., Scholz, M., et al. (2020). Biological responses to extreme weather events are detectable but difficult to formally attribute to anthropogenic climate change. *Sci. Rep.* 10, 14067. doi:10.1038/s41598-020-70901-6

Henry, G. H. R., and Molau, U. (1997). Tundra plants and climate change: The international tundra experiment (ITEX). *Glob. Chang. Biol.* 3, 1–9. doi:10.1111/J.1365-2486.1997.GCB132.X

Høye, T. T. (2020). Arthropods and climate change – arctic challenges and opportunities. *Curr. Opin. Insect Sci.* 41, 40–45. doi:10.1016/j.cois.2020.06.002

Hu, F. S., Higuera, P. E., Duffy, P., Chipman, M. L., Rocha, A. V., Young, A. M., et al. (2015). Arctic tundra fires: Natural variability and responses to climate change. *Front. Ecol. Environ.* 13, 369–377. doi:10.1890/150063

INTERACT (2015). *Research and monitoring international network for terrestrial research and monitoring in the arctic*. Brussels: European Commision.

IPCC (2021). *Climate change 2021: The physical science basis. Contribution of working group I to the sixth assessment report of the intergovernmental Panel on climate change*. Cambridge, UK: Cambridge University Press.

Keuper, F., Parmentier, F. J. W., Blok, D., Van Bodegom, P. M., Dorrepaal, E., Van Hal, J. R., et al. (2012). Tundra in the rain: Differential vegetation responses to three years of experimentally doubled summer precipitation in siberian shrub and Swedish bog tundra. *Ambio* 41, 269–280. doi:10.1007/s13280-012-0305-2

Kirchmeier-Young, M. C., and Zhang, X. (2020). Human influence has intensified extreme precipitation in North America. *Proc. Natl. Acad. Sci. U. S. A.* 117, 13308–13313. doi:10.1073/pnas.1921628117

Knapp, A. K., Smith, M. D., Hobbie, S. E., Collins, S. L., Fahey, T. J., Hansen, G. J. A., et al. (2012). Past, present, and future roles of long-term experiments in the LTER network. *Bioscience* 62, 377–389. doi:10.1525/BIO.2012.62.4.9

Landrum, L., and Holland, M. M. (2020). Extremes become routine in an emerging new Arctic. *Nat. Clim. Chang.* 10, 1108–1115. doi:10.1038/s41558-020-0892-z

Latimer, C. E., and Zuckerberg, B. (2019). How extreme is extreme? Demographic approaches inform the occurrence and ecological relevance of extreme events. *Ecol. Monogr.* 89, e01385. doi:10.1002/ecm.1385

Marchand, F., Mertens, S., Kockelbergh, F., Beyens, L., and Nijs, I. (2005). Performance of High Arctic tundra plants improved during but deteriorated after exposure to a simulated extreme temperature event. *Glob. Chang. Biol.* 11, 2078–2089. doi:10.1111/j.1365-2486.2005.01046.x

Maxwell, S. L., Butt, N., Maron, M., McAlpine, C. A., Chapman, S., Ullmann, A., et al. (2019). Conservation implications of ecological responses to extreme weather and climate events. *Divers. Distrib.* 25, 613–625. doi:10.1111/ddi.12878

McClintock, B. T., Langrock, R., Gimenez, O., Cam, E., Borchers, D. L., Glennie, R., et al. (2020). Uncovering ecological state dynamics with hidden Markov models. *Ecol. Lett.* 23, 1878–1903. doi:10.1111/ele.13610

McCrystall, M. R., Stroeve, J., Serreze, M., Forbes, B. C., and Screen, J. A. (2021). New climate models reveal faster and larger increases in Arctic precipitation than previously projected. *Nat. Commun.* 121 (12), 6765. doi:10.1038/s41467-021-27031-y

McPhillips, L. E., Chang, H., Chester, M. V., Depietri, Y., Friedman, E., Grimm, N. B., et al. (2018). Defining extreme events: A cross-disciplinary review. *Earth's. Future* 6, 441–455. doi:10.1002/2017EF000686

Metcalfe, D. B., G Hermans, T. D., Ahlstrand, J., Becker, M., Berggren, M., Björk, R. G., et al. (2018). Patchy field sampling biases understanding of climate change impacts across the Arctic. *Nat. Ecol. Evol.* 2, 1443–1448. doi:10.1038/s41559-018-0612-5

IPCC (2012). "Climate change: New dimensions in disaster risk, exposure, vulnerability, and resilience," in *Managing the risks of extreme events and disasters to advance climate change adaptation*. Editors P. M. M. C. B. Field, V. Barros, T. F. Stocker, D. Qin, D. J. Dokken, et al. (Cambridge, UK, and New York, NY, USA): Cambridge University Press), 22–64.

Perkins-Kirkpatrick, S. E., and Lewis, S. C. (2020). Increasing trends in regional heatwaves. *Nat. Commun.* 11, 3357–3358. doi:10.1038/s41467-020-16970-7

Post, E., Alley, R. B., Christensen, T. R., Macias-Fauria, M., Forbes, B. C., Gooseff, M. N., et al. (2019). The polar regions in a 2°C warmer world. *Sci. Adv.* 5, eaaw9883. doi:10.1126/sciadv.aaw9883

Post, E., Brodie, J., Hebblewhite, M., Anders, A. D., Maier, J. A. K., and Wilmers, C. C. (2009a). Global population dynamics and hot spots of response to climate change. *Bioscience* 59, 489–497. doi:10.1525/bio.2009.59.6.7

Post, E., Forchhammer, M. C., Bret-Harte, M. S., Callaghan, T. V., Christensen, T. R., Elberling, B., et al. (2009b). Ecological dynamics across the arctic associated with recent climate change. *Science* 325, 1355–1358. doi:10.1126/science.1173113

Previdi, M., Smith, K. L., and Polvani, L. M. (2021). Arctic amplification of climate change: A review of underlying mechanisms. *Environ. Res. Lett.* 16, 093003. doi:10.1088/1748-9326/AC1C29

Putkonen, J., Grenfell, T. C., Rennert, K., Bitz, C., Jacobson, P., and Russell, D. (2009). Rain on snow: Little understood killer in the north. *Eos Trans. AGU.* 90, 221–222. doi:10.1029/2009EO260002

Raymond, C., Horton, R. M., Zscheischler, J., Martius, O., AghaKouchak, A., Balch, J., et al. (2020). Understanding and managing connected extreme events. *Nat. Clim. Chang.* 107 (10), 611–621. doi:10.1038/s41558-020-0790-4

Schmidt, N. M., Hardwick, B., Gilg, O., Høye, T. T., Krogh, P. H., Meltofte, H., et al. (2017). Interaction webs in arctic ecosystems: Determinants of arctic change? *Ambio* 46, 12–25. doi:10.1007/s13280-016-0862-x

Sillmann, J., Thorarinsdottir, T., Keenlyside, N., Schaller, N., Alexander, L. V., Hegerl, G., et al. (2017). Understanding, modeling and predicting weather and climate extremes: Challenges and opportunities. *Weather Clim. Extrem.* 18, 65–74. doi:10.1016/j.wace.2017.10.003

Sintayehu, D. W. (2018). Impact of climate change on biodiversity and associated key ecosystem services in africa: A systematic review. *Ecosyst. Health Sustain.* 4, 225–239. doi:10.1080/20964129.2018.1530054

Smith, M. D. (2011). An ecological perspective on extreme climatic events: A synthetic definition and framework to guide future research. *J. Ecol.* 99, 656–663. doi:10.1111/j.1365-2745.2011.01798.x

Stillman, R. A., Railsback, S. F., Giske, J., Berger, U., and Grimm, V. (2015). Making predictions in a changing world: The benefits of individual-based ecology. *Bioscience* 65, 140–150. doi:10.1093/biosci/biu192

Turner, M. G., Calder, W. J., Cumming, G. S., Hughes, T. P., Jentsch, A., LaDeau, S. L., et al. (2020). Climate change, ecosystems and abrupt change: Science priorities. *Phil. Trans. R. Soc. B* 375, 20190105. doi:10.1098/rstb.2019.0105

Tyler, N. J. C. (2010). Climate, snow, ice, crashes, and declines in populations of reindeer and caribou (*Rangifer tarandus* L.). *Ecol. Monogr.* 80, 197–219. doi:10.1890/09-1070.1

Ummenhofer, C. C., and Meehl, G. A. (2017). Extreme weather and climate events with ecological relevance: A review. *Phil. Trans. R. Soc. B* 372, 20160135. doi:10.1098/rstb.2016.0135

van de Pol, M., Jenouvrier, S., Cornelissen, J. H. C., and Visser, M. E. (2017). Behavioural, ecological and evolutionary responses to extreme climatic events: Challenges and directions. *Phil. Trans. R. Soc. B* 372, 20160134. doi:10.1098/rstb.2016.0134

Walsh, J. E., Ballinger, T. J., Euskirchen, E. S., Hanna, E., Mård, J., Overland, J. E., et al. (2020). Extreme weather and climate events in northern areas: A review. *Earth. Sci. Rev.* 209, 103324. doi:10.1016/j.earscirev.2020.103324

Weiskopf, S. R., Rubenstein, M. A., Crozier, L. G., Gaichas, S., Griffis, R., Halofsky, J. E., et al. (2020). Climate change effects on biodiversity, ecosystems, ecosystem services, and natural resource management in the United States. *Sci. Total Environ.* 733, 137782. doi:10.1016/j.scitotenv.2020.137782

Wrona, F. J., Johansson, M., Culp, J. M., Jenkins, A., Mård, J., Myers-Smith, I. H., et al. (2016). Transitions in Arctic ecosystems: Ecological implications of a changing hydrological regime. *J. Geophys. Res. Biogeosci.* 121, 650–674. doi:10.1002/2015JG003133

frontiers | Frontiers in Earth Science

TYPE Original Research
PUBLISHED 23 September 2022
DOI 10.3389/feart.2022.953605

OPEN ACCESS

EDITED BY
Claudio Fabian Szlafsztein,
Federal University of Pará, Brazil

REVIEWED BY
Luigi Aldieri,
University of Salerno, Italy
Jian Tao,
Shandong Institute of Business and Technology, China

*CORRESPONDENCE
Jing Peng,
pengjing@tea.ac.cn

SPECIALTY SECTION
This article was submitted to Interdisciplinary Climate Studies, a section of the journal Frontiers in Earth Science

RECEIVED 26 May 2022
ACCEPTED 17 August 2022
PUBLISHED 23 September 2022

CITATION
Peng J, Dan L, Tang X and Yang F (2022), Impact of radiative forcing of spatially varying CO_2 concentrations on net primary production.
Front. Earth Sci. 10:953605.
doi: 10.3389/feart.2022.953605

Impact of radiative forcing of spatially varying CO_2 concentrations on net primary production

Jing Peng[1]*, Li Dan[1], Xiba Tang[2] and Fuqiang Yang[1]

[1]CAS Key Laboratory of Regional Climate-Environment for Temperate East Asia, Institute of Atmospheric Physics, Chinese Academy of Sciences, Beijing, China, [2]Laboratory of Cloud-Precipitation Physics and Severe Storms (LACS), Institute of Atmospheric Physics, Beijing, China

The radiative forcing of spatially varying carbon dioxide (CO_2) concentrations has modified the climate by altering surface energy, the water budget, and carbon cycling. Over the past several decades, due to anthropogenic emissions, atmospheric CO_2 concentrations in the whole terrestrial ecosystem have become greater than the global mean. The relationship between climatic variables and net primary production (NPP) can be regulated by the radiative forcing of this spatial variation. The present results show that owing to the radiative forcing of spatially varying CO_2 concentrations, NPP has reduced globally by −0.6 Pg C yr^{-1}. Region 2, with increased CO_2 and decreased NPP, shows the greatest reductions, by −0.7 Pg C yr^{-1}. Variations of both NPP and CO_2 concentrations are distributed asymmetrically. As human activities are mainly located in the Northern Hemisphere, increased CO_2 has mainly manifested in these regions. Especially in region 2, with increased CO_2 and decreased NPP, increasing downward longwave radiation has heated the ground surface by 2.2 W m^{-2} and raised surface temperatures by 0.23°C. At the same time, due to the radiative forcing of spatial variations in CO_2 concentrations, local dependence of NPP on soil moisture has increased due to enhanced temperature and evapotranspiration coupling, which may improve negative NPP anomalies locally, especially in region 2. With continued increasing CO_2 concentrations, its spatial variation due to radiative forcing is likely to amplify warming and have a negative impact on NPP in the terrestrial ecosystem.

KEYWORDS

spatial variations of CO_2 concentrations, temperature, downward longwave radiation, net primary production (NPP), radiative forcing of CO_2

Highlights

- Radiative forcing of non-uniform CO_2 concentrations after 1956 has decreased terrestrial NPP globally by −0.7 Pg C yr^{-1}

- Enhanced temperature and ET coupling due to radiative forcing of spatial variations in CO_2 concentrations have a negative impact on NPP, especially in region 2 with increased CO_2 concentrations and decreased NPP
- Enhanced downward longwave radiation is a main contributor to widely increased surface temperatures caused by radiative forcing of spatially varying CO_2 concentrations

1 Introduction

As the most important driving force behind current climate change, the radiative forcing of atmospheric carbon dioxide (CO_2) concentrations affects the trends, mean, and interannual variations of global carbon fluxes (Friedlingstein et al., 2013; Friedlingstein 2015; Schimel et al., 2015; Sitch et al., 2015; Friedlingstein et al., 2020). In the high latitudes of the Northern Hemisphere, temperatures have risen mainly in response to the increase in the radiative forcing of rising atmospheric CO_2 concentrations, which can promote the production of terrestrial ecosystems (Govindasamy and Caldeira, 2000; Peng and Dan, 2015; Etminan et al., 2016; Govindasamy and Caldeira, 2000; Peng and Dan, 2015; Yuan et al., 2019). Conversely, at low latitudes, higher temperatures do not promote vegetation production (Cox et al., 2013; Piao et al., 2020). Radiative forcing by higher CO_2 concentrations modifies vegetation production and respiration of the terrestrial ecosystem and ultimately regulates the concentration of CO_2 in the atmosphere (Cox et al., 2013; Ballantyne et al., 2017). Therefore, understanding how the radiative forcing of CO_2 concentrations affects the terrestrial carbon cycle could be beneficial for predictions regarding climate change (Friedlingstein et al., 2006; Ramaswamy et al., 2019; Friedlingstein et al., 2020).

The influence of atmospheric CO_2 concentrations on terrestrial carbon fluxes (i.e., the net primary production, NPP) is mainly expressed in two ways: one is a fertilization effect of CO_2 concentrations, and the other is the radiative effect. Increased atmospheric CO_2 concentrations affect the global carbon cycle not only through their effect on plant physiology but also through their radiative greenhouse effect. Increasing CO_2 concentrations tend to enhance downward longwave radiation, prompting changes in temperature and precipitation and, thus, generating changes in plant photosynthesis rates, carbon allocation, and soil respiration. This driver of climate change is referred to as "CO_2 radiative forcing," which is different from CO_2 physiological forcing. Due to the latter effect, increases in CO_2 concentration can enhance photosynthesis and, ultimately, NPP (Ainsworth and Long, 2005; Medlyn et al., 2015).

The non-uniformity of the concentration of CO_2 refers to its spatial variation. The terrestrial carbon cycle will be modified by the radiative forcing of spatially varying atmospheric CO_2 concentrations. For example, previous studies have shown that changes in CO_2 radiative forcing lead to changes in the spatial responses of terrestrial carbon flux (Friedlingstein 2015; Canadell et al., 2021), as atmospheric CO_2 radiative forcing can be regulated through changes in the average background states (e.g., RNET, atmospheric circulation patterns, surface temperature, and rainfall) (Cao et al., 2010; Peng et al., 2014). The radiative forcing of CO_2 is partly regulated by anthropogenic carbon emissions, which can lead to other spatial differences in CO_2 concentrations in addition to the effect of vegetation growth. Under climate change, therefore, there is an urgent need to quantitatively assess changes in carbon fluxes caused by the radiative forcing of spatially varying CO_2 concentrations.

Currently, there are still large uncertainties in the modeling of the intensity of the radiative forcing effect of CO_2 concentrations combined with feedback processes of cloud–aerosol interaction and poleward energy transports through radiative forcing (Myhre et al., 2013; Huang et al., 2017). There also is a lack of research on the influence of the radiative forcing of spatially varying CO_2 concentrations on NPP. Although results suggest that there are clear spatial differences in atmospheric CO_2 concentrations at regional scales (Nassar et al., 2013; Falahatkar et al., 2017), how and why the associated radiative forcing of spatial variations in CO_2 concentrations affects NPP remains unknown (Wang et al., 2019).

In this study, we carried out simulations of different forcing scenarios, including non-uniform and uniform CO_2 concentrations, and then studied the changes in the response of terrestrial carbon fluxes. The influence of the radiative forcing of spatially varying CO_2 concentrations on terrestrial carbon fluxes can be detected by changes in the climate state, including the surface energy budget, atmospheric circulation, surface temperature, and rainfall. However, there is a limited number of studies on the effects of the radiative forcing of spatially varying CO_2 concentrations on carbon fluxes in the terrestrial ecosystem. The overarching goal of this study was to assess the impacts of the radiative forcing of spatially varying CO_2 concentration on the NPP of terrestrial ecosystems. Thus, we focused on answering two main scientific questions: 1) How does the radiative forcing of spatially varying CO_2 concentrations alter the climate state? 2) What changes have occurred in the response of terrestrial carbon fluxes to the radiative forcing of spatial variations in CO_2 concentrations, and what are the reasons behind these changes?

2 Methods and simulations

2.1Methods

We simulated corresponding changes in climatic variables and NPP due to the radiative forcing of spatial variations in CO_2 concentrations from 1850 to 2005. We took the mean of the last

50 years to ensure the carbon cycle balance of our model. We explored the contribution of each component in the surface energy budget to temperature, which was regulated by the inhomogeneity of CO_2 radiative forcing.

A linear regression approach was used to quantify the sensitivity of the dependent variable (y) to the independent variable (x). This method was applied by Poulter et al. (2014) as follows:

$$y = \beta_i x + \varepsilon_i, \quad (1)$$

where β_i is the sensitivity of y to x, and ε_i is an error in which i refers to the ith independent variable (e.g., surface air temperature or precipitation).

According to the Stefan–Boltzmann law, the radiation emitted by the surface land determines the surface temperature. Such surface temperature is regulated by the balance of net shortwave radiation, net longwave radiation, sensible heat, latent heat, and ground heat flux:

$$\sigma \times Tas^4 = \mathrm{RSS} + \mathrm{RLDS} - (\mathrm{RG} + \mathrm{HFS} + \mathrm{HFL}), \quad (2)$$

where σ is the Stefan–Boltzmann constant. Therefore, according to Eq. 2, the surface temperature is determined by the net shortwave radiation (RSS), downward longwave radiation (RLDS), sensible heat flux (HFS), latent heat flux (HFL), and ground heat flux (RG). We focus on the contribution of these energy components to temperature changes caused by the radiative forcing of non-uniform CO_2.

2.2 Model

We used version 2.0 of the FGOALS–AVIM model at a resolution of 2.81 × 1.66. This version of FGOALS has previously been used to assess the effects of CO_2 radiative forcing on the total cloud fraction, temperature, and water vapor under different abruptly quadrupling CO_2 concentrations (Chen et al., 2014; Capistrano et al., 2020). Evaluations of the model performance have revealed that FGOALS can quite reasonably reproduce the mean annual GPP (gross primary production) and NPP (Wang et al., 2013), the mean summer evapotranspiration (ET), and mean annual runoff in the Lake Baikal basin (Törnqvist et al., 2014); and the major global-scale biogeochemical fluxes and pool sizes of carbon (Peng and Dan, 2014).

The model used in this study, i.e., FGOALS-s2 (Bao et al., 2013), was one of the models that participated in CMIP5 (phase 5 of the Coupled Model Intercomparison Project) and was also used as an assessment tool in the fifth Assessment Report of the Intergovernmental Panel on Climate Change. It is a fully coupled Earth system model consisting of four independent components that simultaneously simulate Earth's atmosphere (SAMIL2), ocean (LICOM2), surface (AVIM), and sea ice (CSIM) and includes a central coupler component (CPL6). It has an interactive carbon cycle model in the land component and an ecosystem–biogeochemical module in the ocean component.

Although carbon release resulting from permafrost thawing would potentially impact climate change because large amounts of carbon previously locked in frozen organic matter will decompose into CO_2 and methane (Ballantyne et al., 2017), FGOALS–AVIM has only a simple carbon permafrost model at present, and no marine methane release is included. Supplementary Figure S1 shows the spatial distribution of plant functional type (PFT). The land component of the model, i.e., FGOALS–AVIM, only simulates the different responses of fixed PFTs, not PFT dynamics, therefore, we could not simulate the NPP responses to changes in land cover or land use.

2.3 Data and simulations

The time series of atmospheric CO_2 concentration was provided by CMIP6 (i.e., fossil fuel combustion, cement manufacturing, and oilfield natural gas combustion) with a monthly resolution from 1850 to 2014. However, because the atmospheric CO_2 variations from CMIP6 only consider its latitudinal and not longitudinal spatial variation, to fully reflect the spatial non-uniformity of atmospheric CO_2 concentrations and describe the impact of anthropogenic carbon emissions due to their spatial distribution, we adopted the 1 × 1 resolution Open Data Inventory of Anthropogenic Carbon Dioxide (Oda et al., 2018) to establish the quantitative relationship between the emissions of individual grid boxes and latitude-averaged carbon emissions (Eqn. s1 in the supporting information). It was assumed that this quantitative relationship is also applicable to the relationship between the atmospheric CO_2 concentration of each pixel and the latitude-averaged CO_2 concentration from CMIP6 (Eq. 2 in the supporting information). The CO_2 concentration was then generated by fully considering the spatial non-uniformity, which can reflect the variations of anthropogenic carbon emissions, both latitudinally and longitudinally. The CO_2 datasets under the historical conditions of 1850–2005 were generated by redividing the 1 × 1 grid into a spatial resolution of 2.81 × 1.66. Based on this method, we then used the CO_2 datasets as input data in our simulations.

To quantify the impact of the radiative forcing of spatially varying CO_2 concentrations on carbon fluxes, we used FGOALS–AVIM to carry out two different simulation experiments to evaluate NPP. The period covered was from 1850 to 2005 (Table 1). To separate the impacts on NPP of CO_2 radiative and fertilization effects due to the spatial variations of CO_2 concentrations, we carried out two simulations (simulations U1 and N1) that for the radiative process used uniform CO_2 concentrations (in U1) or spatially varying CO_2 concentrations (in N1), but for the physiological process CO_2 concentrations were fixed at 347 ppm in both simulations. The

TABLE 1 CO_2 forcing data for simulations.

Simulation	CO_2 forcing	Components
N1	Spatially and temporally varying	Fully coupled atmosphere, land, ocean, and sea ice
U1	Only temporally varying (i.e., without spatial variation)	Fully coupled atmosphere, land, ocean, and sea ice

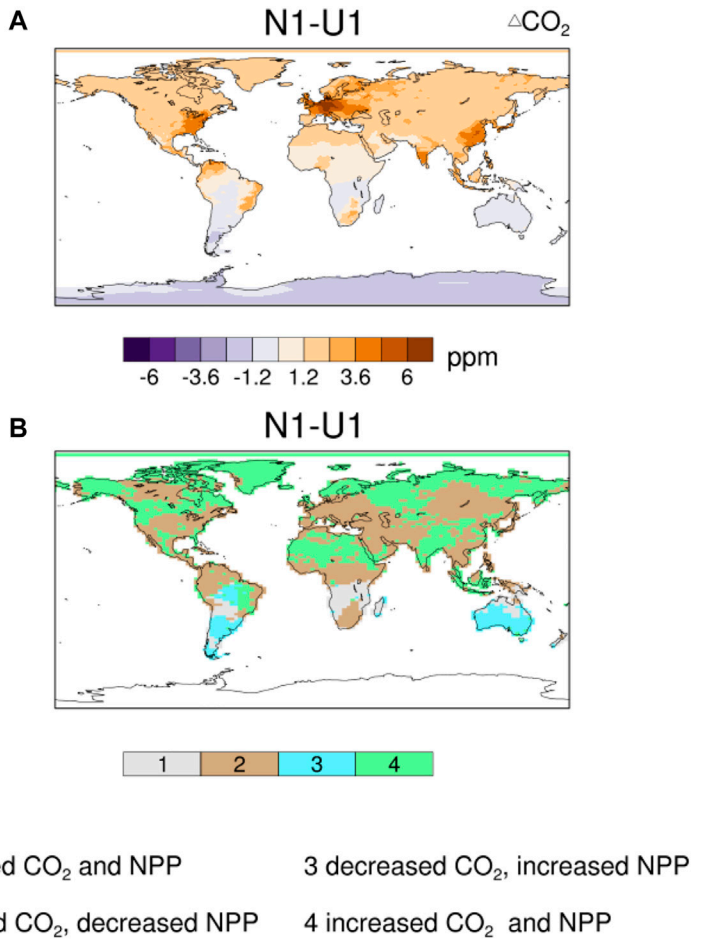

FIGURE 1
(A) Spatial variations of atmospheric CO_2 anomalies from simulation N1 minus U1 over the period 1956–2005. **(B)** Spatial distributions of the relationship between CO_2 anomalies and corresponding NPP anomalies caused by radiative forcing of CO_2 non-uniformity over the same period.

difference in NPP between simulations N1 and U1 represents the effects of CO_2 radiative forcing due to spatial variations of CO_2 concentrations. Simulation N1 included components based on an active atmosphere, land, ocean, and sea ice, which used atmospheric CO_2 concentrations, including temporal and spatial variations, as forcing data. Simulation U1 fixed the same atmospheric CO_2 level in individual grid boxes, that is, CO_2 concentrations without spatial variations. The differences between the N1 and U1 simulations represent the impacts of the spatially varying atmospheric CO_2 concentrations.

3 Results

3.1 Regional CO_2 concentrations and NPP over terrestrial ecosystems

The CO_2 concentrations in the Northern and Southern Hemispheres vary widely. Australia, most of Africa, and southern South America have lower CO_2 concentrations than globally. In Europe, the eastern United States, and eastern Asia, CO_2 is higher than the global level. Simulation N1 used the

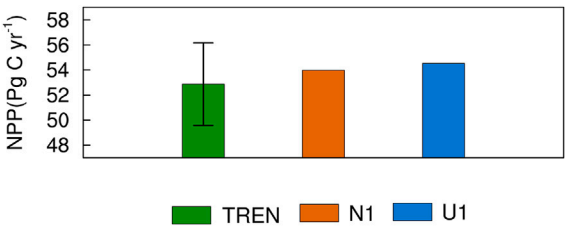

FIGURE 2
Comparison of different estimates of global NPP during the period 1956–2005: estimates based on TRENDY (TREN, green bar), simulation N1 using radiative forcing of spatial variations in CO_2 concentrations (N1, orange bar), and simulation U1 using radiative forcing of uniform CO_2 concentrations (U1, blue bar).

forcing data of CO_2 concentration with non-uniform spatial differences, which ranged from 339 to 351 ppm (Figure 1A). Simulation U1 used the same CO_2 data globally, without spatial variations.

Anthropogenic emissions can amplify the spatial difference in CO_2 concentrations between the Northern and Southern Hemispheres (Figure 1A), which may lead to corresponding changes in annual NPP anomalies (Figure 1B). We divided the land into four regions according to the changes of both CO_2 concentrations and NPP in response to the impact of radiative forcing due to spatial variations of CO_2 concentrations over the period 1956–2005: region 1, which includes decreased CO_2 concentrations and NPP; region 2, which features increased CO_2 concentrations and decreased NPP; region 3, which is defined by decreased CO_2 concentrations and increased NPP; and region 4, which includes increased CO_2 concentrations and increased NPP. Region 2 is mainly located in mid–low latitudes, while region 4 primarily occurs in high latitudes. These two regions contribute the largest fraction of the whole land surface, accounting for 51% and 31%, respectively.

3.2 Estimates of NPP simulated by FGOALS–AVIM

Figure 2 shows the estimation of terrestrial NPP from simulations N1 and U1 under present conditions from 1956 to 2005. The NPP from the TRENDY dataset, consisting of seven process-based terrestrial ecosystem model simulations CLM4C, CLM4CN, LPJ, LPJ-GUESS, OCN, SDGVM, and TRIFFID (Zhang et al., 2016), was selected to compare with our simulations in the same period. An ensemble of experiment S2 from the TRENDY project was used, in which only atmospheric CO_2 and climate change were included (land use changes were kept unchanged) (Piao et al., 2013), and the results show good agreement between the global NPP of both simulations (N1 and U1) and that of TRENDY.

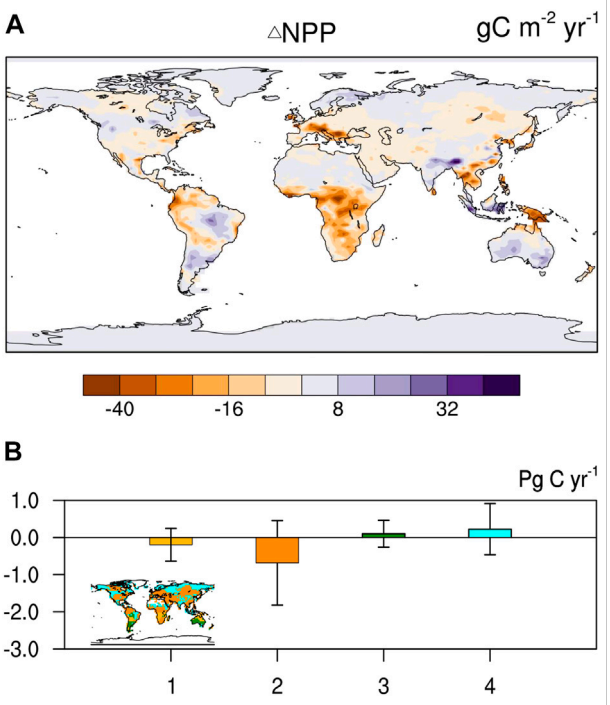

FIGURE 3
(A) Spatial distribution of NPP anomalies due to radiative forcing of spatial variations of CO_2 concentrations during 1956–2005. **(B)** Comparison of NPP anomalies in region 1 (yellow), region 2 (orange), region 3 (green), and region 4 (light blue) during 1956–2005. The vertical black lines represent the differences between the maximum and minimum NPP anomalies for each region over 1956–2005.

Comparing the NPP simulated by FGOALS–AVIM with that of TRENDY in spatial terms (Supplementary Figure S2), which has been used previously to assess the carbon budget of the terrestrial ecosystem (Piao et al., 2013; Friedlingstein et al., 2020), the estimated NPP produced with or without spatially varying CO_2 concentrations agrees well with the simulations from TRENDY for the period 1956–2005, i.e., for the tropical forest, NPP values are higher than other plant types, and for barren and tundra they are lower. During this period from 1956 to 2005, the U1 experiment simulates smaller NPP values in the high latitudes of the Northern Hemisphere than the mean values of the TRENDY ensemble. However, the NPP simulated by the N1 experiment shows close agreement with TRENDY in these regions. The underestimation of NPP is improved to some extent by the latter experiments considering spatially varying CO_2 concentrations.

Obvious negative annual NPP anomalies appear in the northern Amazon, central Africa, most of Europe, eastern Siberia, eastern Asia, and mid-latitude North America (see Figure 3A). The largest values of negative NPP anomalies in these regions reach as high as -50 g C m^{-2} yr^{-1} in central Africa and -40 g C m^{-2} yr^{-1} in the northwestern Amazon Basin. The maximum values reach -40 g C m^{-2} yr^{-1} along the northern coast

of the Mediterranean Sea. Positive NPP anomalies occur over northern Eurasia, mid-latitude North America, Alaska, India, and South Asian islands. The magnitudes of positive anomalies are much smaller than those of negative anomalies. The spatial inhomogeneity of anthropogenic emissions could cause spatially varying CO_2 concentrations, which in turn would alter the physical climate due to CO_2 radiative forcing and thus regulation of NPP. However, the anomalies vary among regions. To examine which regions contribute the most to NPP anomalies resulting from inhomogeneous CO_2 radiative forcing the terrestrial ecosystem was divided into four regions. Among these regions, region 2 includes tropical and temperate forests, which are major contributors to the NPP of terrestrial ecosystems (Cox et al., 2013; Poulter et al., 2014; Schimel et al., 2015). As can be seen, they contribute the largest fraction to the decreased NPP at 0.7 Pg C yr^{-1} (Figure 3B), accounting for ~57% of the changes in global NPP. The negative contribution of the region to NPP anomalies seems to be proportional to their current contribution. Therefore, the annual anomalies of NPP in region 2, which is located in low–mid latitudes, can dominate the global carbon cycle response to heterogeneous CO_2 radiative forcing.

CO_2 concentrations at the PFT scale vary accordingly among the four seasons between simulations N1 and U1 (Supplementary Figure S3). From 1956 to 2005, larger CO_2 concentrations are used in simulation N1 than U1 in spring for all PFTs, especially evergreen needle leaf forest (ENF), tundra, and crop. In contrast, the CO_2 concentration in summer decreases from 0.5 ppm for evergreen broadleaf forest (EBF) to 4.2 ppm for ENF in simulation N1, in contrast with simulation U1. In autumn, the CO_2 concentration used in simulation N1 increases from 0.5 ppm for EBF to 2.5 ppm for ENF. Greater CO_2 concentrations in winter are used by simulation N1 than simulation U1, ranging from 2.1 ppm for EBF to 5.9 ppm for ENF.

At the PFT level, the simulated changes in NPP from 1956 to 2005 in spring, summer, and autumn are similar for DNF (deciduous needleleaf forest), C3 grass, and C4 grass (Supplementary Figure S4). In spring, there are larger decreases in NPP for deciduous broadleaf forest (DBF), but greater increases, by 0.38 Pg C yr^{-1}, in NPP for ENF and tundra in the high latitudes than in other seasons. In summer, greater decreases for ENF and BDF are simulated than for other plant types. For EBF, the simulated decrease in NPP in autumn is similar to that for DBF, C3 grass, and C4 grass. In this season, changes in NPP for ENF and tundra are faint. In winter, excluding C3 grass, the relative differences in the simulated changes in NPP are generally much smaller for other PFTs.

3.4 Responses of NPP to temperature, precipitation, and net surface radiation

Because NPP is greatly affected by the local temperature and rainfall (Schimel et al., 2015; Swann et al., 2016; Kim et al., 2017), the annual anomalies of NPP caused by the radiative forcing of spatially varying CO_2 concentrations are therefore mainly due to the contribution of annual anomalies of local temperature or rainfall. How temperature or rainfall changes is a key issue toward understanding the changes in the carbon cycle related to heterogeneous CO_2 radiative forcing under the influence of anthropogenic emissions. Figures 4A–F shows the correlation coefficients of NPP anomalies with anomalies of temperature, rainfall, or net surface radiation (RNET) considering the effect of heterogeneous CO_2 radiative forcing. In terms of spatial distribution, the annual anomalies of NPP are highly correlated and consistent with the annual anomalies of rainfall. In the low latitudes, the correlation coefficients between the annual anomalies of NPP and temperature are greater, showing significant negative correlations. The correlation coefficients between the annual anomalies of NPP and RNET are weak, displaying most regions as not passing the significance test at the 0.05 level.

Generally, NPP is an output of the land component. The changes in NPP could be regulated by the physical climate due to the radiative forcing of non-uniform CO_2 concentrations. The changes in NPP might be induced by changes in the surface temperature in most land areas, although, of course, changes in NPP could also respond to changes in precipitation over land. However, on the basis of Student's *t*-test at the 5% level, changes in precipitation are not statistically significant in most terrestrial ecosystems (Figure 4B). Thus, we hypothesize that the effects of changes in the physical climate on NPP due to radiative forcing of non-uniform CO_2 concentrations are mainly expressed in terms of the impact of changes in surface temperature on NPP (Figures 4A,C).

3.5 Radiative forcing drivers of near-surface temperature and precipitation

Figures 5A–D shows that RLDS might dominate the radiative forcing changes. According to Eq. 2, we show the influence of each radiation component on near-surface temperature. The positive temperature anomalies in the mid-latitude and high-latitude regions of the Northern Hemisphere are consistent with the contribution of RLDS and RSS. In temperate and boreal forests of Eurasia, increased RLDS ($+0.9 \pm 0.9$ W m^{-2}) is responsible for most of the warming, followed by increased RNET ($+0.24 \pm 0.3$ W m^{-2}). The warming in the west of North America shows consistent signs of RSS and RLDS. The positive temperature anomalies in central Siberia are caused by the same signs of RLDS ($+2.5 \pm 2.4$ W m^{-2}) and RSS ($+0.01 \pm 0.1$W m^{-2}), which are located in the maximum warming.

Annual anomalies of RLDS dominate the temperature anomalies in region 2 (Figure 5A). The positive temperature anomalies in region 2 are mainly driven by increased RLDS ($+2.2 \pm 1.6$ W m^{-2}), which is partly offset by the decrease in RSS

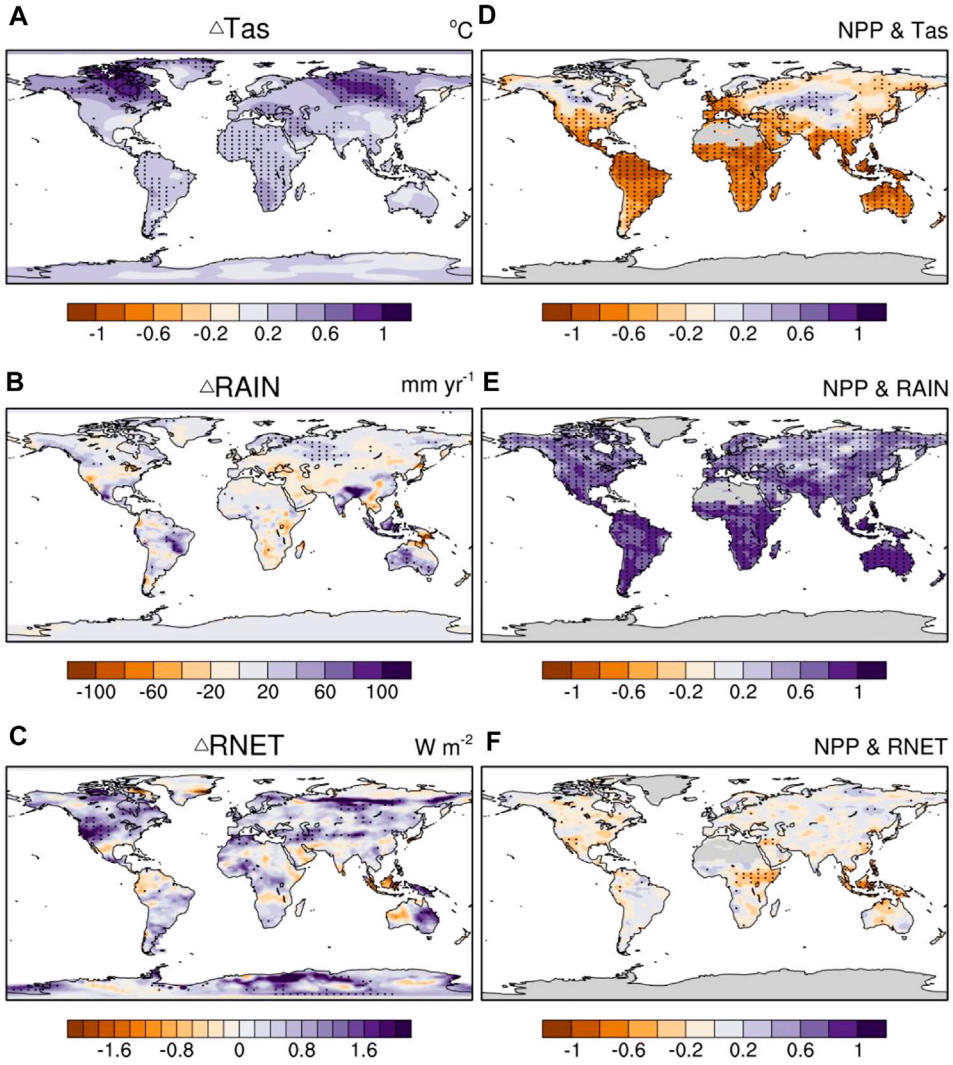

FIGURE 4
(A–C) Spatial distribution of anomalies of surface temperature (Tas), rainfall (RAIN), and surface net radiation (RNET), respectively, caused by radiative forcing of spatial variations of CO_2 concentrations over the period 1956–2005. **(D–F)** Correlation coefficients of NPP and local Tas, RAIN or RNET, respectively. Dotted areas in **(A–F)** are areas with statistically significant changes at the 5% level using Student's *t*-test.

(-0.2 ± 0.9 W m^{-2}). The positive temperature anomalies in region 4 are mainly caused by radiation components with opposite signs: RLDS increases ($+2.0 \pm 1.5$ W m^{-2}) and RSS decreases (-0.2 ± 0.9 W m^{-2}). Noticeably, as compared to region 2 or 4, the reduction of RSS in region 1, by -0.3 ± 2.0 W m^{-2}, is greater.

To explore how near-surface temperature anomalies are affected by radiative forcing due to spatial variations of CO_2 concentrations, we also analyzed the annual anomalies of temperature in different regions and how clouds drive temperature anomalies (Figure 6). There are obvious differences in the influence of cloud fraction on the near-surface temperature in individual regions. Mid clouds ($\beta = -0.4$, $p = 0.00$) have greater impacts on temperature anomalies than low clouds in region 2. In this region, increases of mid clouds are about four times the changes in low clouds (see Supplementary Figure S5). Increased mid clouds tend to reduce solar radiation reaching the surface. Therefore, in this region, the largest increases in CO_2 concentrations do not accompany the largest increases in temperature. In region 4, the relationship between the anomalies of clouds and the temperature is not significant.

A previous study showed that anomalies of atmospheric CO_2 concentration can modify the energy balance through radiative forcing, which correspondingly affects rainfall (Allen and Ingram, 2002). Results in the present study show that rainfall

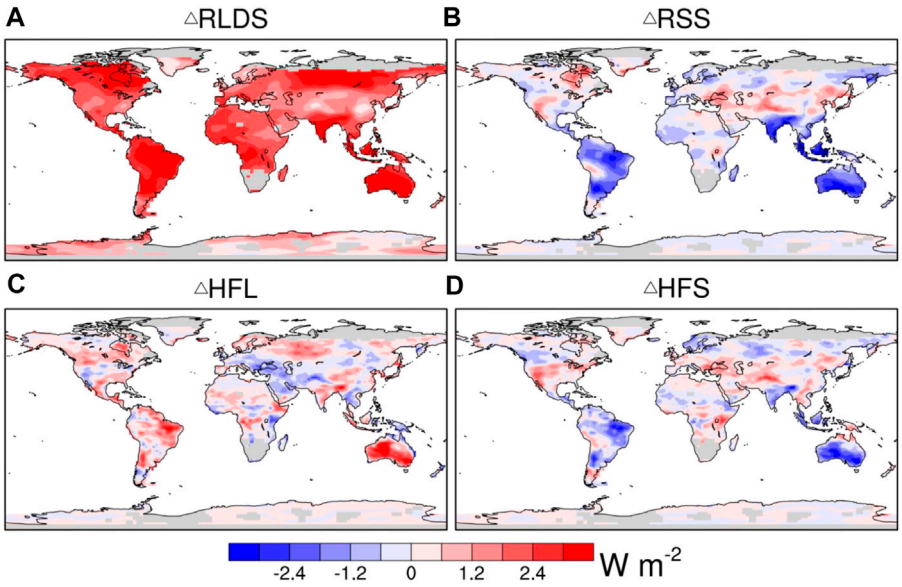

FIGURE 5
Spatial distribution of anomalies of **(A)** downward longwave radiation (RLDS), **(B)** shortwave radiation (RSS), **(C)** latent heat flux (HFL), and **(D)** sensible heat flux (HFS), caused by radiative forcing of spatial variations of CO_2 concentrations over the period 1956–2005.

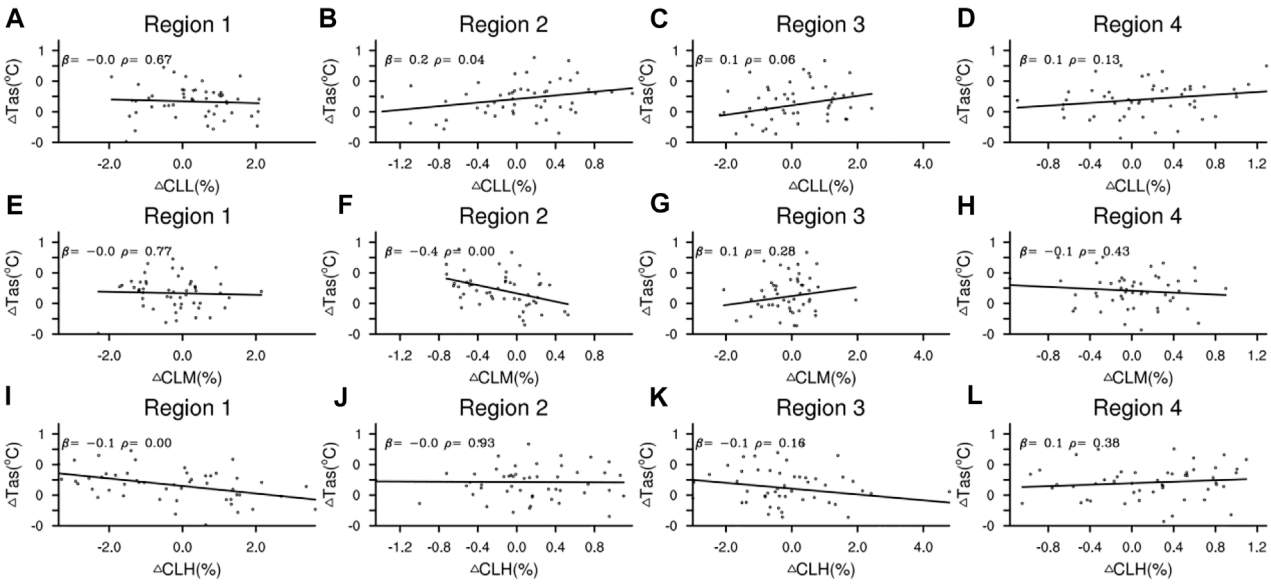

FIGURE 6
Annual anomalies of **(A–D)** low-cloud fraction (CLL), **(E–H)** mid-cloud fraction (CLM), and **(I–L)** high-cloud fraction (CLH) against anomalies of surface temperature (Tas) as estimated by FGOALS–AVIM2 for regions 1, 2, 3, and 4, where β represents the sensitivity of surface temperature to CLL, CLM, or CLH over the period 1956–2005, and ρ denotes the p value.

anomalies are significantly negatively correlated with anomalies of sensible heat flux over 80% of the land area ($p < 0.01$) (see Figure 7). Previous studies have shown that annual sensible heat flux anomalies play an important role in the occurrence of opposite-sign annual rainfall anomalies (Myhre et al., 2018). In northern North America, northern Europe, and southern

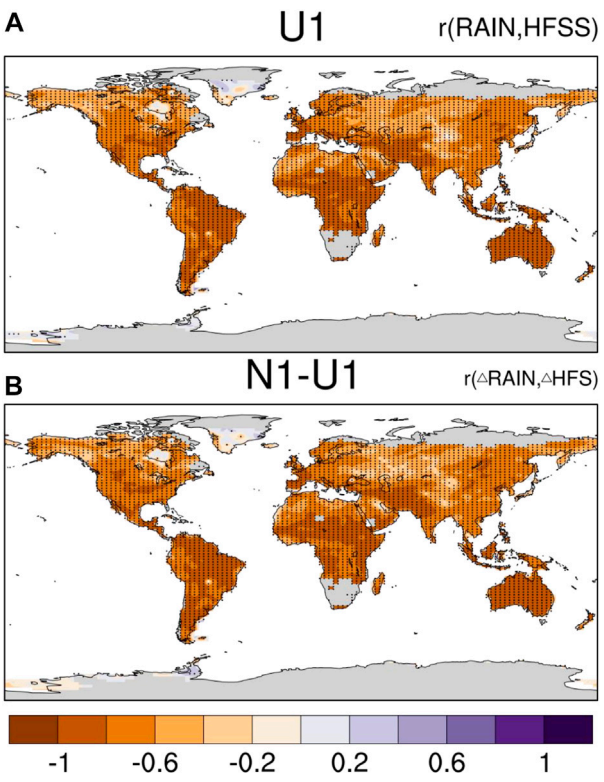

FIGURE 7
Correlation coefficients of annual anomalies of sensible heat flux (HFS) with local anomalies of rainfall estimated by FGOALS–AVIM during 1956–2005 from simulation U1 in A and simulation N1 minus U1 in B. Dotted areas are areas with statistically significant changes at the 5% level using Student's *t*-test.

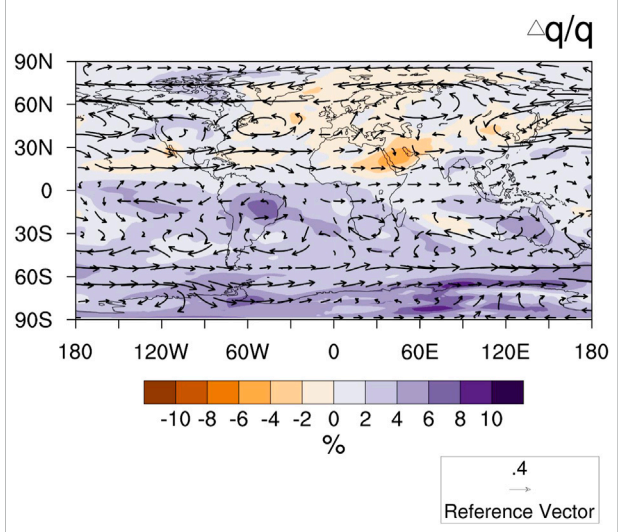

FIGURE 8
Spatial percentage of changes of specific humidity (units: %) relative to simulation U1 integrated between the surface pressure level and 300 hPa, and 850 hPa wind (vectors; units: m s^{-1}), over the period 1956–2005, as estimated using FGOALS–AVIM, due to radiative forcing of spatially varying of CO_2 concentrations.

China, the obvious negative anomalies of sensible heat flux strengthen the positive anomalies of local rainfall. Conversely, in the low-latitudes of North America, central Africa, and the Mediterranean, negative anomalies of rainfall respond to the obvious positive anomalies of sensible heat flux.

Radiative forcing of spatially varying CO_2 concentrations plays an important role in the change in NPP associated with climatic change. On the one hand, radiative forcing of spatially varying CO_2 concentrations revises the surface energy budget (Figure 5) and then continues to regulate the surface climate locally. On the other hand, the radiative forcing of heterogeneous CO_2 may influence the atmospheric circulation (Figure 8), which further affects the large-scale terrestrial water cycle. Therefore, non-uniform CO_2 triggers anomalies of specific humidity in each region and subsequently anomalies of rainfall and thus terrestrial NPP.

On a global scale, an increase in relative humidity does not necessarily mean an increase in rainfall. In contrast, in Figure 8, based on the results of FGOALS–AVIM, the westerly winds weaken, thereby suppressing humid airflow from the Atlantic Ocean to western Europe, causing negative anomalies of rainfall and a decrease in soil moisture. In addition, dry air is strengthened from the northeastern to the southeastern United States. This type of circulation is not conducive to the transportation of the eastern ocean flow to the eastern continental United States. In eastern China, dry air from inland is also strengthened. Consequently, it will suppress the monsoon from the eastern Pacific Ocean, thereby reducing rainfall and causing a decrease in NPP (Figure 4E).

There is a close relationship among soil moisture, temperature, and ET (Seneviratne et al., 2006; Jung et al., 2010; Seneviratne et al., 2010). Figure 9C shows the correlation between ET and surface temperature, where the coupling of ET and temperature could reflect the evaporative demand of the air (Figure 9A). In tropical regions including the Amazon Basin, Australia, Central Africa, and southern Asia, and low- and mid-latitude regions in Europe–Asia and North America, FGOALS–AVIM presents a strong and negative correlation between ET and surface temperature (Figure 9C). Such negative coupling of ET and surface temperature could imitate the intensity of water limitation due to the high evaporative demand of air under warmer conditions. Such a negative coupling between ET and temperature is heightened due to the radiative forcing of spatial variations in CO_2 concentrations (Figure 9D), which is accompanied by an enhanced NPP dependence on soil moisture (Figure 9B).

4 Discussion

In regions 2 and 4, positive anomalies of surface temperature and changes in rainfall have comprehensively affected the level of

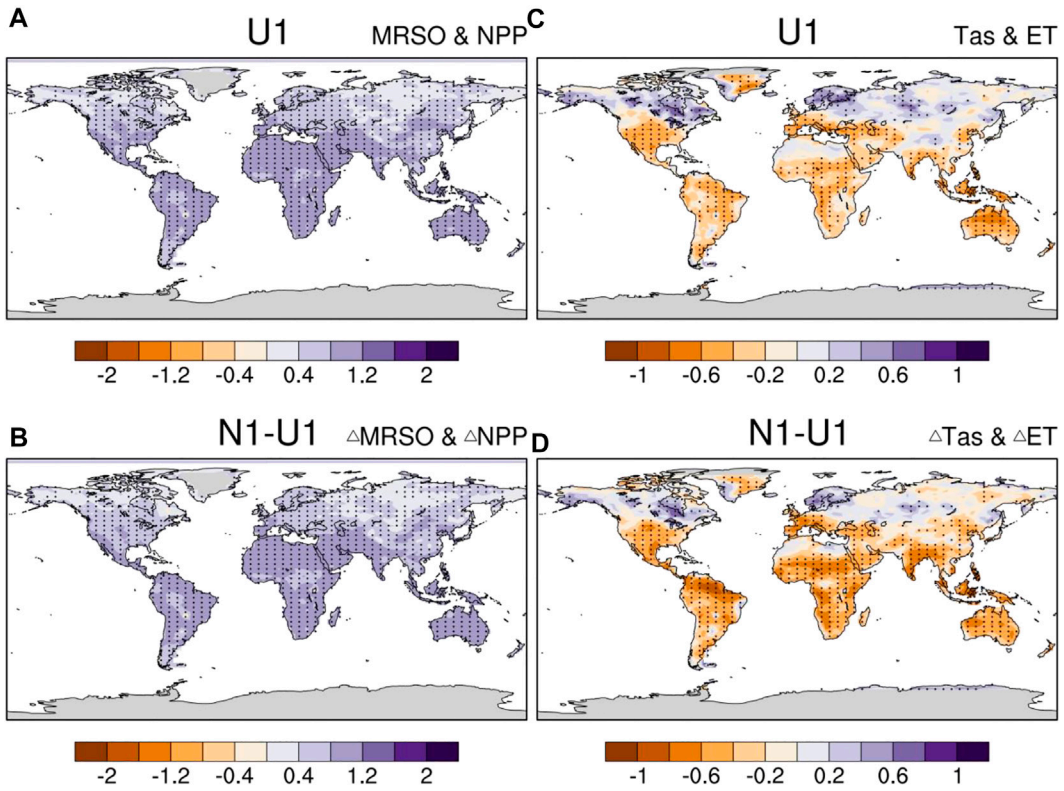

FIGURE 9
Spatial distribution of **(A)** sensitivity of NPP to soil moisture (MRSO; units: gC yr^{-1} kg^{-1}) from simulation U1 and **(B)** anomalies of MRSO resulting from the effect of radiative forcing of spatially varying CO_2 concentrations. Correlation coefficients of **(C)** surface temperature and soil evaporation from simulation U1 and **(D)** anomalies of surface temperature and soil evaporation due to the radiative forcing of spatial variations of CO_2 concentrations. Dotted areas in **(C,D)** are areas with statistically significant changes at the 5% level using Student's *t*-test.

soil moisture depletion on land and reduced NPP. In the high latitudes of region 4, positive anomalies of surface temperature have had the opposite influence. As a result, such responses of terrestrial ecosystems indicate that the radiative forcing of spatially varying CO_2 concentrations might modify vegetation production substantially. Consequently, the responses will eventually adjust the atmospheric CO_2 concentration. Therefore, understanding the relationship between the radiative forcing of spatially varying CO_2 concentrations and the terrestrial carbon cycle might provide an excellent way to predict changes in the global carbon cycle.

Positive anomalies of atmospheric CO_2 account for more than two-thirds of the global land area. The maximum positive anomalies are mainly located in region 2. Our results show that the higher radiative forcing of CO_2 non-uniformity can induce warming in these regions. Circulation might promote the transport of warmer air from these regions to higher latitudes. Warmer air flows from the eastern United States, western Europe, and eastern Asia to the higher latitudes of the Northern Hemisphere (Figure 8), causing more positive anomalies of surface temperature to the north of 50°N (Figure 4A). Such a change at high latitudes is conducive to an increase in surface temperature and enhanced NPP in boreal forests and tundra.

The atmospheric CO_2 concentration significantly modifies the surface energy budget through radiative forcing, especially the RLDS of the atmosphere, which in turn affects the surface temperature (Vargas Zeppetello et al., 2019) and greatly influences the interannual changes in NPP. According to the simulation of FGOLS–AVIM, the global specific humidity increases, which reflects the increase in atmospheric water vapor. These increases may amend the surface energy balance and surface temperature, mainly through the RLDS, which our results show possesses a good positive specific humidity sensitivity (β = 8.8 W m^{-2}/(g kg^{-1}); p value < 0.01) (Figure 10). Therefore, to a certain extent, the changes in specific humidity reliably describe the changes in RLDS (Stanhill 2011; Liu et al., 2019). Increased specific humidity and water vapor would help prevent longwave radiation from moving from the surface into space, and also cause increases in downward longwave radiation (Figure 5). Consequently, in part, this will result in increased RLDS to heat the atmosphere and

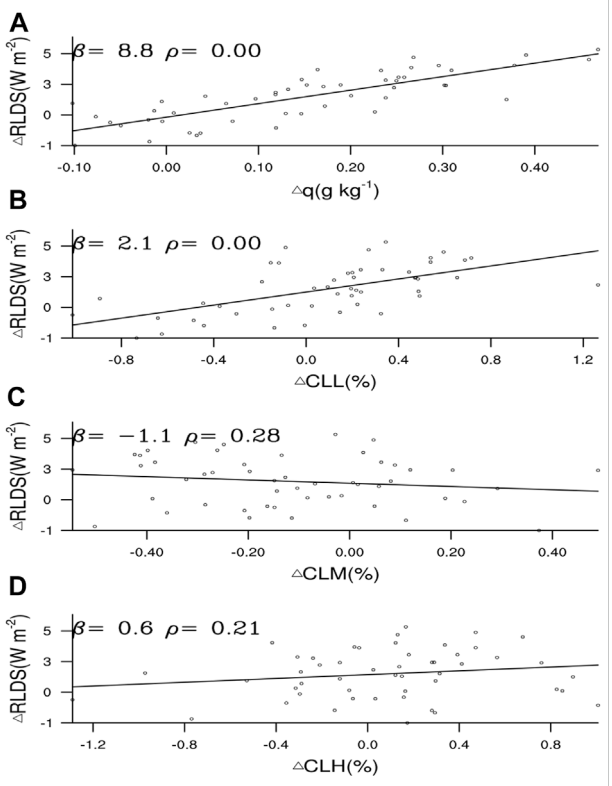

FIGURE 10
Annual anomalies of **(A)** specific humidity (q), **(B)** low-cloud fraction (CLL), **(C)** mid-cloud fraction (CLM), and **(D)** high-cloud fraction (CLH), against anomalies of downward longwave radiation (RLDS), as estimated by FGOALS–AVIM2, for the globe, where β represents the sensitivity of RLDS to CLL, CLM, and CLH over the period 1956–2005, and ρ denotes the p-value.

surface [see Eq. 2]. In addition, in regions without water limitation, especially in the ocean, warmer surfaces might increase evaporation, resulting in higher water content in the atmosphere, which would cause more RLDS. Therefore, the radiative forcing of increased specific humidity may lead to positive anomalies of surface temperature in low-latitudes and Southern Hemisphere regions, although CO_2 in most of these regions has not increased.

To explore how each radiative component is modified by spatially varying CO_2 concentrations, we present their spatial distribution patterns (Figure 5) and analyze how their drivers respond (Figures 10A–D). The results suggest that, in the Amazon Basin, Australia, Central Africa, and Southeast Asia, significant asymmetrical RLDS associated with the non-uniformity of CO_2 concentrations might be caused by another factor. The enhanced low-cloud fraction in these regions (Supplementary Figure S5B) might prevent longwave radiation from being emitted from the surface into space (Figure 10B). This can also lead to asymmetrical temperature anomalies associated with increased RLDS. For example, in these regions, the increases of RLDS at low latitudes and in the Southern Hemisphere are associated with positive anomalies in water vapor and low clouds ($p < 0.01$) (Figure 10).

The linear relationships between changes in global soil moisture and NPP and changes in the sea surface temperature (SST) are shown in Supplementary Figure S6. Changes in SST could regulate the local hydrological conditions of soil moisture and thus NPP (Kim et al., 2016; Schine et al., 2016; Frederiksen et al., 2018). Particularly, the changes in global mean soil moisture show a significant negative relation with SST in the eastern tropical Pacific Ocean. In contrast, in the northwestern Pacific around Japan, southwestern Pacific around Oceania, and North Atlantic Ocean, positive changes in soil moisture respond to positive changes in SST. In spatial distribution terms, the responses of the simulated changes in NPP from 1956 to 2005 due to the radiative forcing of the non-uniform CO_2 concentrations to SST are similar to the soil moisture. However, a greater negative relationship between the changes in global NPP and SST is shown in the eastern tropical Pacific Ocean, compared with the relationship between global mean soil moisture and SST. This is likely because the tropics are the main contributor to global NPP, which might be related to El Niño–Southern Oscillation (ENSO) (Kim et al., 2017; Park et al., 2020; Kim et al., 2021). Correspondingly, how ENSO, the Pacific Decadal Oscillation, and the Arctic Oscillation influence NPP through ocean–atmosphere teleconnections should be further investigated.

Spatially varying CO_2 concentrations could increase the coupling between temperature and ET in terrestrial ecosystems. Accordingly, due to the warmer conditions (Figure 4A) transpiration might be reduced in the northwest Amazon Basin, central and southern Africa, eastern Asia, and northern Mediterranean (Supplementary Figure S7). When the temperature increases (Figure 4A), an enhanced negative relation between surface temperature and ET decreases could result in reduced leaf stomata conductance, which would limit the absorption of CO_2 at the canopy level (Oren et al., 1999; Wever et al., 2002; Yuan et al., 2016). Such inhibition could lead to a reduction in canopy development, thereby reducing NPP (Figure 3). Therefore, the enhanced negative ET–temperature coupling can characterize the increased moisture deficit (Yuan et al., 2016; Yuan et al., 2019). In other words, due to the enhancement in the negative coupling of ET and temperature, the limitation strength of local water availability for plants due to the radiative forcing of spatially varying CO_2 concentrations could cause local enhanced sensitivity of NPP to soil moisture (Yuan et al., 2016).

In addition, climate forcing caused by spatial variations in CO_2 concentration can also alter atmospheric circulation, which in turn affects precipitation. The combination of these changes will cause changes in NPP. However, a more detailed understanding of the physical processes and reasons behind the NPP response to CO_2 radiative forcing would be needed. The results are mainly based on the correlation between climate

variables and NPP, which makes it difficult to recognize the cause/effect because each climate variable is interrelated. Some physical explanations may need to be included to really identify the cause/consequence. In future work, sensitivity runs are necessary to detect causes/consequences, as suggested by Liu et al. (2019).

We used FGOALS–AVIM to estimate the impacts of changes in climate state due to the radiative forcing of non-uniform CO_2 concentrations. It should be noted that these simulations based solely on FGOALS–AVIM are not ensembles. Thus, uncertainty in the simulations might result from the internal variability of this model, meaning the addition of more models for the non-uniform CO_2 concentration-driven runs are needed in the future. Finally, it is well known that stronger spatially varying anthropogenic carbon emissions in the future will lead to greater spatially varying CO_2 concentrations. Changes in the radiative forcing of non-uniform CO_2 concentrations under future conditions were not included in our simulations. Elucidating the future impact on NPP of such greater spatial variations would help towards better understanding its impact in the real world. This too requires further investigation.

5 Conclusion

Fossil fuel-based anthropogenic emissions could induce the spatial variation in atmospheric CO_2 concentrations. This study shows that the CO_2 radiative forcing of spatial variations in CO_2 concentrations has resulted in an additional decrease in NPP in region 2 by 0.7 Pg C yr^{-1}, or a 57% additional decrease in NPP for the whole terrestrial ecosystem, over the period 1956–2005. Such reductions in NPP mainly relate to increases in surface temperature, by 0.4°C. Jointly driven by the strengthened coupling between evaporation and temperature, the dependence of NPP on soil moisture in region 2 has decreased. Consequently, reduced soil moisture under warmer conditions due to the radiative forcing of spatial variations in CO_2 concentrations has significantly decreased NPP. In addition, the increase in downward longwave radiation can be attributed to such an increase in surface temperature. To a certain extent, this increase in downward longwave radiation results from low-level cloud. We argue that regional changes in NPP due to the radiative forcing of spatial variations in CO_2 concentrations should be an integral part of future studies on the responses of carbon fluxes to climate change.

Data availability statement

The raw data supporting the conclusion of this article will be made available by the authors, without undue reservation.

Author contributions

JP wrote the manuscript. LD, XT, and FY led data analysis with a considerable comment, contribution, and interpretation from all authors.

Acknowledgments

The authors thank the National Natural Science Foundation of China (Grant Nos. 42141017, 41975112, 42175142, and 42175013) and the National Key Research and Development Program of China (Grant No. 2016YFA0602501) for supporting this study. They thank Prof. Yongkang Xue from the University of California, Los Angeles (UCLA), CA, United States, for the great suggestions.

Conflict of interest

The authors declare that the research was conducted in the absence of any commercial or financial relationships that could be construed as a potential conflict of interest.

Publisher's note

Supplementary material

The Supplementary Material for this article can be found online at: https://www.frontiersin.org/articles/10.3389/feart.2022.953605/full#supplementary-material

References

Ainsworth, E. A., and Long, S. P. (2005). What have we learned from 15 years of free-air CO2 enrichment (face)? A meta-analytic review of the responses of photosynthesis, canopy properties and plant production to rising CO2. *New Phytol.* 165, 351–372. doi:10.1111/j.1469-8137.2004.01224.x

Allen, M. R., and Ingram, W. J. (2002). Constraints on future changes in climate and the hydrologic cycle. *Nature* 419, 228–232. doi:10.1038/nature01092

Ballantyne, A., Smith, W., Anderegg, W., Kauppi, P., Sarmiento, J., Tans, P., et al. (2017). Accelerating net terrestrial carbon uptake during the warming hiatus due to reduced respiration. *Nat. Clim. Chang.* 7, 148–152. doi:10.1038/nclimate3204

Bao, Q., Lin, P., Zhou, T., Liu, Y., Yu, Y., Wu, G., et al. (2013). The flexible global ocean-atmosphere-land system model, spectral version 2: FGOALS-s2. *Adv. Atmos. Sci.* 30, 561–576. doi:10.1007/s00376-012-2113-9

Canadell, J. G., Monteiro, P. M. S, Costa, M. H., Cotrim da Cunha, L., Cox, P. M., Eliseev, A. V., et al. (2021). "Global Carbon and other Biogeochemical Cycles and Feedbacks," in *Climate Change 2021: The Physical Science Basis. Contribution of Working Group I to the Sixth Assessment Report of the Intergovernmental Panel on Climate Change*. Editors V. Masson-Delmotte, P. Zhai, A. Pirani, S. L. Connors, C. Péan, S. Berger, et al. (Cambridge, United Kingdom and New York, NY: Cambridge University Press), 673–816. doi:10.1017/9781009157896.007

Cao, L., Bala, G., Caldeira, K., Nemani, R., and Ban-Weiss, G. (2010). Importance of carbon dioxide physiological forcing to future climate change. *Proc. Natl. Acad. Sci. U. S. A.* 107, 9513–9518. doi:10.1073/pnas.0913000107

Capistrano, V. B., Nobre, P., Veiga, S. F., Tedeschi, R., Silva, J., Bottino, M., et al. (2020). Assessing the performance of climate change simulation results from BESM-OA2.5 compared with a CMIP5 model ensemble. *Geosci. Model Dev.* 13, 2277–2296. doi:10.5194/gmd-13-2277-2020

Chen, X., Zhou, T., and Guo, Z. (2014). Climate sensitivities of two versions of FGOALS model to idealized radiative forcing. *Sci. China Earth Sci.* 57, 1363–1373. doi:10.1007/s11430-013-4692-4

Cox, P., Pearson, D., Booth, B., Friedlingstein, P., Huntingford, C., Jones, C., et al. (2013). Sensitivity of tropical carbon to climate change constrained by carbon dioxide variability. *Nature* 494, 341–344. doi:10.1038/nature11882

Etminan, M., Myhre, G., Highwood, E. J., and Shine, K. P. (2016). Radiative forcing of carbon dioxide, methane, and nitrous oxide: A significant revision of the methane radiative forcing. *Geophys. Res. Lett.* 43 (12), 614–612. doi:10.1002/2016gl071930

Falahatkar, S., Mousavi, S. M., and Farajzadeh, M. (2017). Spatial and temporal distribution of carbon dioxide gas using GOSAT data over Iran. *Environ. Monit. Assess.* 189, 627. doi:10.1007/s10661-017-6285-8

Frederiksen, C. S., Ying, K., Grainger, S., and Zheng, X. (2018). Modes of interannual variability in northern hemisphere winter atmospheric circulation in CMIP5 models: Evaluation, projection and role of external forcing. *Clim. Dyn.* 50, 2845–2865. doi:10.1007/s00382-017-3776-9

Friedlingstein, P. (2015). Carbon cycle feedbacks and future climate change. *Phil. Trans. R. Soc. A* 373, 20140421. doi:10.1098/rsta.2014.0421

Friedlingstein, P., Cox, P., Betts, R., Bopp, L., von Bloh, W., Brovkin, V., et al. (2006). Climate–carbon cycle feedback analysis: Results from the C4MIP model Intercomparison. *J. Clim.* 19, 3337–3353. doi:10.1175/jcli3800.1

Friedlingstein, P., Meinshausen, M., Arora, V. K., Jones, C. D., Anav, A., Liddicoat, S. K., et al. (2013). Uncertainties in CMIP5 climate projections due to carbon cycle feedbacks. *J. Clim.* 27, 511–526. doi:10.1175/jcli-d-12-00579.1

Friedlingstein, P., O'Sullivan, M., Jones, M. W., Andrew, R. M., Hauck, J., and Olsen, A. (2020). Global carbon budget 2020. *Earth Syst. Sci. Data* 12, 3269–3340.

Govindasamy, B., and Caldeira, K. (2000). Geoengineering Earth's radiation balance to mitigate CO2-induced climate change. *Geophys. Res. Lett.* 27, 2141–2144. doi:10.1029/1999gl006086

Huang, Y., Xia, Y., and Tan, X. (2017). On the pattern of CO2 radiative forcing and poleward energy transport. *J. Geophys. Res. Atmos.* 122, 10578–10593. doi:10.1002/2017jd027221

Jung, M., Reichstein, M., Ciais, P., Seneviratne, S. I., Sheffield, J., Goulden, M. L., et al. (2010). Recent decline in the global land evapotranspiration trend due to limited moisture supply. *Nature* 467, 951–954. doi:10.1038/nature09396

Kim, I.-W., Stuecker, M. F., Timmermann, A., Zeller, E., Kug, J.-S., Park, S.-W., et al. (2021). Tropical Indo-Pacific SST influences on vegetation variability in eastern Africa. *Sci. Rep.* 11, 10462. doi:10.1038/s41598-021-89824-x

Kim, J.-S., Kug, J.-S., and Jeong, S.-J. (2017). Intensification of terrestrial carbon cycle related to El Niño–Southern Oscillation under greenhouse warming. *Nat. Commun.* 8, 1674. doi:10.1038/s41467-017-01831-7

Kim, J.-S., Kug, J.-S., Yoon, J.-H., and Jeong, S.-J. (2016). Increased atmospheric CO2 growth rate during El Niño driven by reduced terrestrial productivity in the CMIP5 ESMs. *J. Clim.* 29, 8783–8805. doi:10.1175/jcli-d-14-00672.1

Liu, Y., Xue, Y., MacDonald, G., Cox, P., and Zhang, Z. (2019). Global vegetation variability and its response to elevated CO₂, global warming, and climate variability – A study using the offline SSiB4/TRIFFID model and satellite data. *Earth Syst. Dynam.* 10, 9–29. doi:10.5194/esd-10-9-2019

Medlyn, B. E., Zaehle, S., De Kauwe, M. G., Walker, A. P., Dietze, M. C., Hanson, P. J., et al. (2015). Using ecosystem experiments to improve vegetation models. *Nat. Clim. Chang.* 5, 528–534. doi:10.1038/nclimate2621

Muller, C. J., and O'Gorman, P. A. (2011). An energetic perspective on the regional response of precipitation to climate change. *Nat. Clim. Chang.* 1, 266–271. doi:10.1038/nclimate1169

Myhre, G., Samset, B. H., Hodnebrog, O., Andrews, T., Boucher, O., Faluvegi, G., et al. (2018). Sensible heat has significantly affected the global hydrological cycle over the historical period. *Nat. Commun.* 9, 1922. doi:10.1038/s41467-018-04307-4

Myhre, G., Samset, B. H., Schulz, M., Balkanski, Y., Bauer, S., Berntsen, T. K., et al. (2013). Radiative forcing of the direct aerosol effect from AeroCom Phase II simulations. *Atmos. Chem. Phys.* 13, 1853–1877. doi:10.5194/acp-13-1853-2013

Nassar, R., Napier-Linton, L., Gurney, K. R., Andres, R. J., Oda, T., Vogel, F. R., et al. (2013). Improving the temporal and spatial distribution of CO2 emissions from global fossil fuel emission data sets. *J. Geophys. Res. Atmos.* 118, 917–933. doi:10.1029/2012jd018196

Oda, T., Maksyutov, S., and Andres, R. J. (2018). The open-source data inventory for anthropogenic CO₂, version 2016 (ODIAC2016): A global monthly fossil fuel CO₂ gridded emissions data product for tracer transport simulations and surface flux inversions. *Earth Syst. Sci. Data* 10, 87–107. doi:10.5194/essd-10-87-2018

Oren, R., Sperry, J. S., Katul, G. G., Pataki, D. E., Ewers, B. E., Phillips, N., et al. (1999). Survey and synthesis of intra- and interspecific variation in stomatal sensitivity to vapour pressure deficit. *Plant Cell Environ.* 22, 1515–1526. doi:10.1046/j.1365-3040.1999.00513.x

Park, S.-W., Kim, J.-S., Kug, J.-S., Stuecker, M. F., Kim, I.-W., and Williams, M. (2020). Two aspects of decadal ENSO variability modulating the long-term global carbon cycle. *Geophys. Res. Lett.* 47, e2019GL086390. doi:10.1029/2019gl086390

Peng, J., Dan, L., and Dong, W. (2014). Are there interactive effects of physiological and radiative forcing produced by increased CO2 concentration on changes of land hydrological cycle? *Glob. Planet. Change* 112, 64–78. doi:10.1016/j.gloplacha.2013.11.007

Peng, J., and Dan, L. (2015). Impacts of CO2 concentration and climate change on the terrestrial carbon flux using six global climate-carbon coupled models. *Ecol. Modell.* 304, 69–83. doi:10.1016/j.ecolmodel.2015.02.016

Peng, J., and Dan, L. (2014). "The response of the terrestrial carbon cycle simulated by FGOALS-AVIM to rising CO 2," in *Flexible global ocean-atmosphere-land system model* (Berlin, Germany: Springer), 393–403.

Piao, S., Sitch, S., Ciais, P., Friedlingstein, P., Peylin, P., Wang, X., et al. (2013). Evaluation of terrestrial carbon cycle models for their response to climate variability and to CO2 trends. *Glob. Chang. Biol.* 19, 2117–2132. doi:10.1111/gcb.12187

Piao, S., Wang, X., Park, T., Chen, C., Lian, X., He, Y., et al. (2020). Characteristics, drivers and feedbacks of global greening. *Nat. Rev. Earth Environ.* 1, 14–27. doi:10.1038/s43017-019-0001-x

Poulter, B., Frank, D., Ciais, P., Myneni, R. B., Andela, N., Bi, J., et al. (2014). Contribution of semi-arid ecosystems to interannual variability of the global carbon cycle. *Nature* 509, 600–603. doi:10.1038/nature13376

Ramaswamy, V., Collins, W., Haywood, J., Lean, J., Mahowald, N., Myhre, G., et al. (2019). Radiative forcing of climate: The historical evolution of the radiative forcing concept, the forcing agents and their quantification, and applications. *Meteorol. Monogr.* 59, 14.1–14.101. doi:10.1175/amsmonographs-d-19-0001.1

Schimel, D., Stephens, B. B., and Fisher, J. B. (2015). Effect of increasing CO_2 on the terrestrial carbon cycle. *Proc. Natl. Acad. Sci. U. S. A.* 112, 436–441. doi:10.1073/pnas.1407302112

Schine, C. M. S., van Dijken, G., and Arrigo, K. R. (2016). Spatial analysis of trends in primary production and relationship with large-scale climate variability in the Ross Sea, Antarctica (1997–2013). *J. Geophys. Res. Oceans* 121, 368–386. doi:10.1002/2015jc011014

Seneviratne, S. I., Corti, T., Davin, E. L., Hirschi, M., Jaeger, E. B., Lehner, I., et al. (2010). Investigating soil moisture–climate interactions in a changing climate: A review. *Earth. Sci. Rev.* 99, 125–161. doi:10.1016/j.earscirev.2010.02.004

Seneviratne, S. I., Lüthi, D., Litschi, M., and Schär, C. (2006). Land–atmosphere coupling and climate change in Europe. *Nature* 443, 205–209. doi:10.1038/nature05095

Sitch, S., Friedlingstein, P., Gruber, N., Jones, S. D., Murray-Tortarolo, G., Ahlstrom, A., et al. (2015). Recent trends and drivers of regional sources and sinks of carbon dioxide. *Biogeosciences* 12, 653–679. doi:10.5194/bg-12-653-2015

Stanhill, G. (2011). The role of water vapor and solar radiation in determining temperature changes and trends measured at Armagh, 1881–2000. *J. Geophys. Res.* 116, D03105. doi:10.1029/2010jd014044

Swann, A. L. S., Hoffman, F. M., Koven, C. D., and Randerson, J. T. (2016). Plant responses to increasing CO2 reduce estimates of climate impacts on drought severity. *Proc. Natl. Acad. Sci. U. S. A.* 113, 10019–10024. doi:10.1073/pnas.1604581113

Törnqvist, R., Jarsjö, J., Pietroń, J., Bring, A., Rogberg, P., Asokan, S. M., et al. (2014). Evolution of the hydro-climate system in the Lake Baikal basin. *J. Hydrology* 519, 1953–1962. doi:10.1016/j.jhydrol.2014.09.074

Vargas Zeppetello, L. R., Donohoe, A., and Battisti, D. S. (2019). Does surface temperature respond to or determine downwelling longwave radiation? *Geophys. Res. Lett.* 46, 2781–2789. doi:10.1029/2019gl082220

Wang, J., Bao, Q., Zeng, N., Liu, Y., Wu, G., and Ji, D. J. A. i. A. S. (2013). Earth System Model FGOALS-s2: Coupling a dynamic global vegetation and terrestrial carbon model with the physical climate system model. *Adv. Atmos. Sci.* 30, 1549–1559. doi:10.1007/s00376-013-2169-1

Wang, Y., Feng, J., Dan, L., Lin, S., and Tian, J. (2019). The impact of uniform and nonuniform CO2 concentrations on global climatic change. *Theor. Appl. Climatol.* 139, 45–55. doi:10.1007/s00704-019-02924-7

Wever, L. A., Flanagan, L. B., and Carlson, P. J. (2002). Seasonal and interannual variation in evapotranspiration, energy balance and surface conductance in a northern temperate grassland. *Agric. For. Meteorology* 112, 31–49. doi:10.1016/s0168-1923(02)00041-2

Yuan, W., Cai, W., Chen, Y., Liu, S., Dong, W., Zhang, H., et al. (2016). Severe summer heatwave and drought strongly reduced carbon uptake in Southern China. *Sci. Rep.* 6, 18813. doi:10.1038/srep18813

Yuan, W., Zheng, Y., Piao, S., Ciais, P., Lombardozzi, D., Wang, Y., et al. (2019). Increased atmospheric vapor pressure deficit reduces global vegetation growth. *Sci. Adv.* 5, eaax1396. doi:10.1126/sciadv.aax1396

Zhang, X., Rayner, P. J., Wang, Y.-P., Silver, J. D., Lu, X., Pak, B., et al. (2016). Linear and nonlinear effects of dominant drivers on the trends in global and regional land carbon uptake: 1959 to 2013. *Geophys. Res. Lett.* 43, 1607–1614. doi:10.1002/2015gl067162

frontiers | Frontiers in Environmental Science

TYPE Original Research
PUBLISHED 19 October 2022
DOI 10.3389/fenvs.2022.1008886

OPEN ACCESS

EDITED BY
Claudio Fabian Szlafsztein,
Federal University of Pará, Brazil

REVIEWED BY
Junqiang Yao,
China Meteorological Administration, China
Xiuping Li,
Institute of Tibetan Plateau Research(CAS), China

*CORRESPONDENCE
Yuqing Feng,
fengyq@email.cugb.edu.cn
Sihai Liang,
liangsh@cugb.edu.cn

SPECIALTY SECTION
This article was submitted to Interdisciplinary Climate Studies, a section of the journal Frontiers in Environmental Science

RECEIVED 01 August 2022
ACCEPTED 04 October 2022
PUBLISHED 19 October 2022

CITATION
Yuan N, Feng Y, Liang S, Wang G, Yin T, Yan D, Wu P, Kuang X and Wan L (2022), Spatial gathering characteristics of drought in the Qinghai-Tibet Plateau. *Front. Environ. Sci.* 10:1008886. doi: 10.3389/fenvs.2022.1008886

Spatial gathering characteristics of drought in the Qinghai-Tibet Plateau

Ning Yuan[1], Yuqing Feng[2,3,4]*, Sihai Liang[1]*, Guangjun Wang[5], Tao Yin[1], Dezhao Yan[6], Pan Wu[7], Xingxing Kuang[2] and Li Wan[1]

[1]School of Water Resources and Environment, China University of Geosciences (Beijing), Beijing, China, [2]School of Environmental Science and Engineering, Southern University of Science and Technology, Shenzhen, China, [3]Hebei Province Collaborative Innovation Center for Sustainable Utilization of Water Resources and Optimization of Industrial Structure, School of Water Resources and Environment, Hebei GEO University, Shijiazhuang, China, [4]Hebei Province Key Laboratory of Sustained Utilization and Development of Water Resources, School of Water Resources and Environment, Hebei GEO University, Shijiazhuang, China, [5]School of Land Science and Technology, China University of Geosciences (Beijing), Beijing, China, [6]Institute of Tibetan Plateau Research, Chinese Academy of Sciences, Beijing, China, [7]Wuhan Center of China Geological Survey, Wuhan, China

Due to climate change, drought has caused serious impacts on the eco-environment, hydrology and agriculture, and drought events in the Qinghai-Tibet Plateau (QTP) have become more severer and frequent; therefore, understanding the characteristics and variations of drought is crucial to reduce its eco-environmental and socio-economic impacts. This study used the Standardized Precipitation Evapotranspiration Index (SPEI) to identify drought and assessed its interannual changes from 1980 to 2020. Then, the Hurst exponent and intensity analysis were used to identify future drought trend and the characteristics of drought intensity. Moreover, Empirical Orthogonal Function (EOF) analysis was performed to examine the main spatial gathering characteristics. The results indicate that: 1) the QTP was becoming wetter in general, and drying places were mainly distributed in the southeast and northeast of the QTP, as well as the Qaidam Basin accounting for 27% areas of QTP. 2) The trend of wet and dry in the future in most regions would be the same as the present, only 10% of the regions would have the reverse trend. 3) The rate of wet/drought changes was faster in the 1980s and 2000s. 4) The EOF mode1 revealed a gathering distribution structure with negative values in the southeast and east of the QTP and positive values in the center and west. The west was more sensitive to the variation of dry and wet, and most areas will continue to be wet in the future. EOF mode2 and mode3 mainly indicated opposite gathering patterns of southwest-northeast and south-north. The results provide favorable evidence for policymakers to better understand and prevent drought.

KEYWORDS

climate change, drought, gathering characteristics, empirical orthogonal function, Qinghai-Tibet Plateau

1 Introduction

Few extreme events can lead to more tremendous damage than drought (Dai, 2011). Drought can lead to serious negative impacts on water resources, agricultural production, environments, and ecosystems (Potop et al., 2014). Though the number of drought disasters amounts to only 5% of the total disasters, the loss can reach 30% of the loss resulting from all natural disasters (Wang et al., 2014). Drought brings the world about 221 billion dollars loss annually for the past 60 years (Tong et al., 2018). The number and duration of drought events would increase in the future (Blunden et al., 2011), and dryland will occupy 50% of the world's land area before the end of the 21st century (Huang et al., 2016). So it is essential to accurately understand and identify the characteristics and variations of drought to provide an early warning for decision-making groups (Hayes et al., 2011).

Generally, there are four categories of drought: meteorological drought, hydrological drought, agricultural drought, and socio-economic drought (Mishra and Singh, 2010). Many indices have been developed to characterize different categories of drought, such as the Palmer Drought Severity Index (PDSI) (Palmer, 1965), Standardized Precipitation Evapotranspiration Index (SPEI) (Vicente-Serrano et al., 2010), Standardized Precipitation Index (SPI) (McKee et al., 1993), Surface Water Supply Index (SWSI) (Mishra and Singh, 2010), and Standardized Runoff Index (SRI) (Shukla and Wood, 2008). Meteorological drought is usually the first step in drought occurrence and also contributes to the occurrence of the other three drought categories (Eslamian et al., 2017). After considering the applicability of the meteorological drought index, SPEI is chosen to identify drought in this paper. It combines the advantages of PDSI sensitivity to potential evapotranspiration (PET) as well as takes into account the advantages of the SPI multi-time scale (Yu et al., 2014).

The Qinghai-Tibet Plateau (QTP), known as the primary water source for Asia, provides more than two billion people with water directly and indirectly (Rangwala and Miller, 2012). The QTP is sensitive and vulnerable to climate change, which will have a significant influence on the surrounding regions and the worldwide climate (Kang et al., 2010). Due to climate warming (You et al., 2021), drought is particularly prevalent in the QTP, affecting vegetation carbon uptake (Ye et al., 2020), growth (Liu et al., 2019a), and further aggravating water stress (Li et al., 2019). At the same time, the drought had a serious impact on some basins, approximately 29 drought events occurred in the Yangtze River Basin from 1979 to 2012 (Zhang et al., 2016), and the long-term average drought in the Yellow River Basin lasted nearly 5.8 months from 1953 to 2012 (Huang et al., 2015). Moreover, the discharge of rivers that originate in the QTP shrunk drastically due to drought (Wang et al., 2011). Since 1960, the Yellow River discharge has dropped to zero 3 times, and the longest duration recorded is 226 days (Liang et al., 2010). The Yangtze River Basin experienced the severest drought in the spring of 2011, and the rainfall is at the lowest level since 1961 (Lu et al., 2014). Therefore, studying the long-term drought development in the QTP is important to understand the causes and characteristics of drought better, guide the decision-making departments to monitor and analyze drought, and prevent local agriculture and animal husbandry from drought disasters.

In recent decades, drought indices are beginning to be used to identify and analyze the drought characteristics in the QTP. A study based on the SPEI found that drought intensity occurred more seriously before the 1990s in the QTP, then the

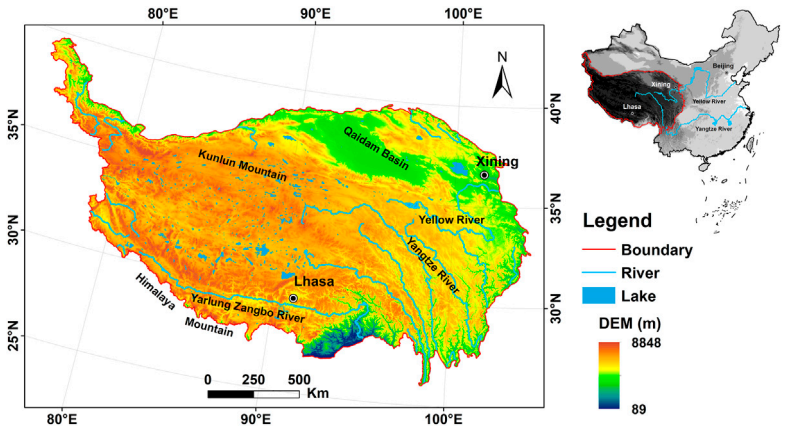

FIGURE 1
Location and elevation of Qinghai-Tibet Plateau.

degree of drought trended to ease, and the evolution of drought had noticeable interdecadal differences after 1997 (Liang et al., 2018). During the growth season, though the northeastern and southern parts experienced a significant wetting trend, the eastern fringe of the QTP tended to be dry, and this trend will continue (Zhang et al., 2019). The altitude dependence of drought characteristics was investigated based on SPEI and 4,000 m a. s. l was determined as the dividing line, the higher the altitude, the greater the changing trend (Feng et al., 2020). However, the spatial gathering characteristics of drought resulting from climate change are still unclear in the QTP, particularly in the conditions of the complex topography, environments, and lack of observational meteorological data.

In this study, the 12-month-scale SPEI over 41 years from 1980 to 2020 was used to identify the specific spatial gathering characteristics of the QTP. The objectives of this paper are: 1) to depict the changing trend of drought; 2) to predict the future change trend of drought; 3) to analyze the rate and intensity of drought transformation in each time interval and 4) to detect the spatial gathering characteristics of drought.

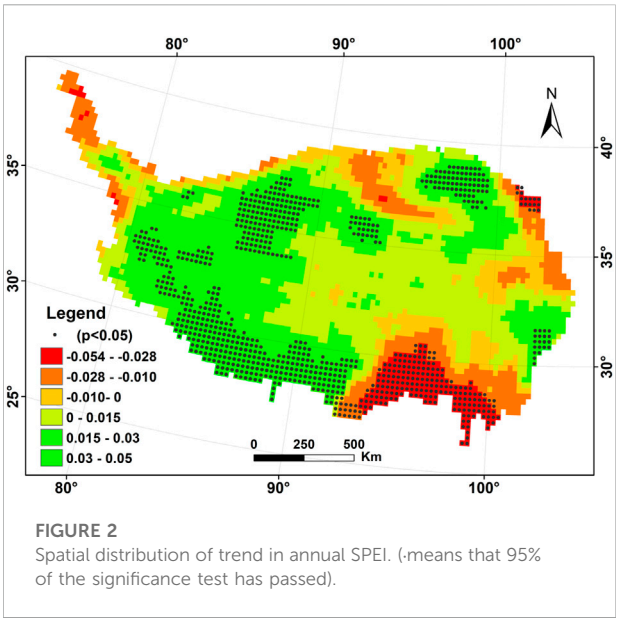

FIGURE 2
Spatial distribution of trend in annual SPEI. (·means that 95% of the significance test has passed).

2 Materials and methods

2.1 Study area and data

The QTP, referred to as the "Asian water tower" and "The Third Pole," is located in western China and covers an area of 2.5 million square kilometers (Immerzeel et al., 2010). The QTP is from 300 km to 1,500 km wide from 24°37′27″N to 41°09′13″N, and 2,800 km long from 73°18′52″E to 106°19′30″E, with an average altitude of above 4,000 m a. s. l. The plateau suffers from strong solar radiation, low temperature, and air pressure, as well as distinct seasonal and spatial precipitation heterogeneity due to its unique geographic location and large-scale terrain (Yao et al., 2012). The annual mean temperature varies between −2.2 and 0°C, and the annual mean precipitation ranges from over 1,000 mm in the southeast to less than 50 mm in the northwest. Precipitation between June and September contributes to more than 60%–90% of total yearly precipitation (Kuang and Jiao, 2016), and the mean annual potential evapotranspiration and evapotranspiration are approximately 940 mm and 380 mm, respectively (Chen et al., 2013; Feng et al., 2021). The QTP is the headwaters of many prominent rivers in Asia (Sun et al., 2021) (Figure 1). Glaciers and permafrost are widely distributed on the plateau, as well as alpine meadow and alpine grassland (Feng et al., 2019).

This study focuses on the meteorological drought in the QTP. In order to fully understand the spatial and temporal characteristics of drought, long-term datasets related to precipitation and potential evapotranspiration are fundamental. However, there are insufficient meteorological stations covering QTP characterized by complex topography and harsh climate, so the grid datasets of potential evapotranspiration (PET), precipitation, and temperature derived from the European Centre for Medium-Range Weather Forecasts (ECMWF) were served as substitutes of station observations (Zhou et al., 2021). ERA5 is the fifth generation of the ECMWF reanalysis for the global climate and weather (https://cds.climate.copernicus.eu/cdsapp#!/home). The datasets cover the period from 1980 to 2020, and the temporal coverage is 1 month, while the spatial resolution is 0.25°× 0.25° for each pixel. We used the boundary of the QTP to extract the raster of potential evapotranspiration, temperature, and precipitation and then conduct the following post-processing.

2.2 Methods

2.2.1 SPEI calculation

SPEI is an ideal indicator to monitor drought, its principle is that the drought in a region can be aggregated by the deviation of the difference between precipitation and PET from the average state (Lu et al., 2019; Hu et al., 2021). The calculation process please refer to Vicente-Serrano et al. (2010) for details. In this study, 12 months scale of SPEI was computed as the SPEI-annual, and the drought classification based on the SPEI value is shown in Supplementary Table S1.

2.2.2 Trend analysis

Sen's slope and Mann-Kendall trend test are employed to examine the trend of drought. Sen. slope estimation is a non-

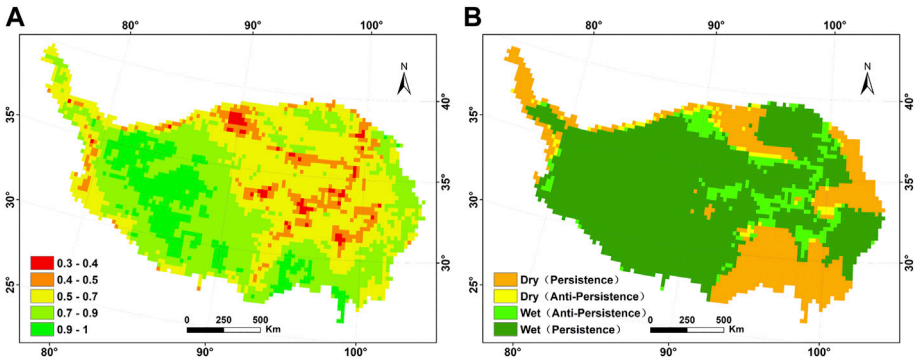

FIGURE 3
Spatial distribution of Hurst index **(A)** and persistence analysis **(B)**.

parametric trend slope calculation method, which is not affected by the singular values of a series and can well reflect the degree of change trend of the time series. Mann-Kendall trend test is a nonparametric test to assess the trend of climate and hydrological factors of a time series, using the statistic Z to check the significance of the changing trend (Gocic and Trajkovic, 2013).

2.2.3 Hurst exponent

The Hurst exponent serves as a practical statistical tool to predict the time series persistence. The rescaled range (R/S) analysis has been used by many studies to calculate the Hurst exponent, and the calculation steps are as follows (Tong et al., 2018):

Firstly, the time series of SPEI $\{X_i\}$ (i = 1, 2, 3, . . . , n) is grouped into a number of sub-series and then calculate the average value.

$$M = \frac{1}{n}\sum_{i=1}^{n} X_i \tag{1}$$

The cumulative deviation is calculated by

$$Z_t = \sum_{t=1}^{n}(X_t - M) \quad 1 \le t \le n \tag{2}$$

The range of each sub-series is computed by

$$R(n) = \max(Z_1, Z_2, \ldots\ldots\ldots, Z_n) - \min(Z_1, Z_2, \ldots\ldots\ldots, Z_n) \tag{3}$$

The standard deviation series is given as

$$S(n) = \sqrt{\frac{1}{n}\sum_{i=1}^{n}(X_i - M)^2} \tag{4}$$

Finally, we calculate the rescaled range R/S

$$\hat{H} = \frac{\log R/S}{\log n} \tag{5}$$

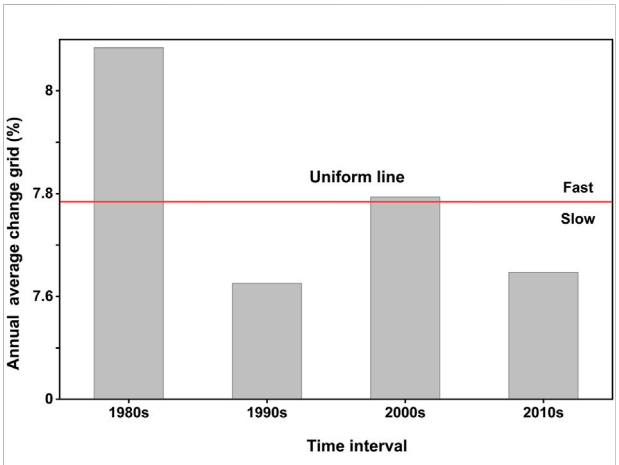

FIGURE 4
The interval intensity analysis for the 1980s, 1990s, 2000s, and 2010s.

The value of H is in the range of 0–1. The value in the range of 0–0.5 means that there is anti-persistence in the time series, 0.5-1 indicates long-term memory, and H = 0.5 is an independent process (García and Requena, 2019).

2.2.4 Intensity analysis

The intensity analysis was initially applied to the analysis of land use and land cover change (Huang et al., 2012), then it was used as an effective method to analyze drought characteristics (Wang et al., 2019a). Intensity analysis can account for the change in interval, category, and conversion level. Interval intensity is used to analyze the change rate and identify whether the change rate is fast or not at a certain time interval, and category intensity can determine the state of category change, namely relatively active or dormant, while transition intensity is to determine which one is in the dominant position in the transition during the time interval (Abdullah and Nakagoshi, 2006;

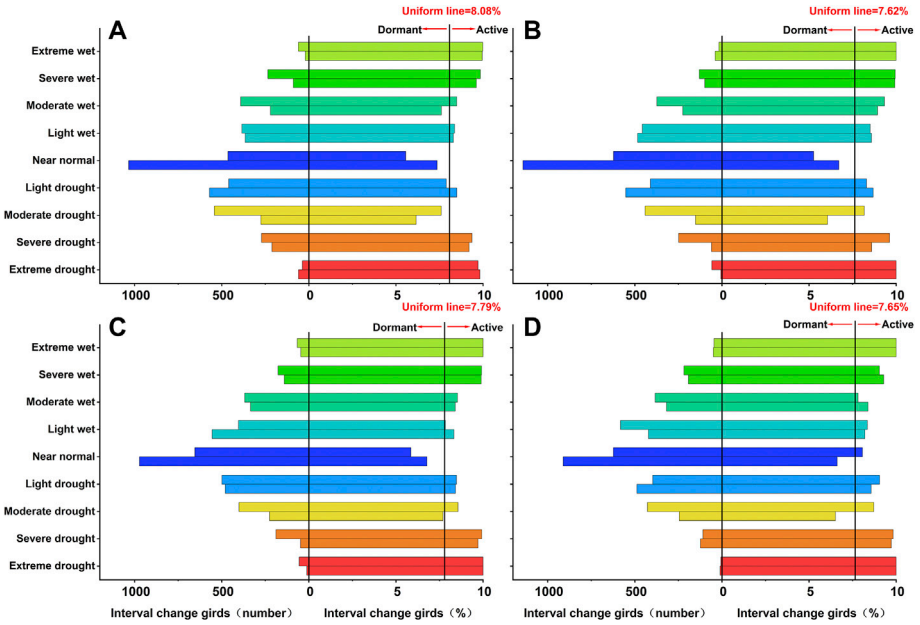

FIGURE 5
Intensity analysis of change for each category for the **(A)** 1980s **(B)** 1990s **(C)** 2000s and **(D)** 2010s.

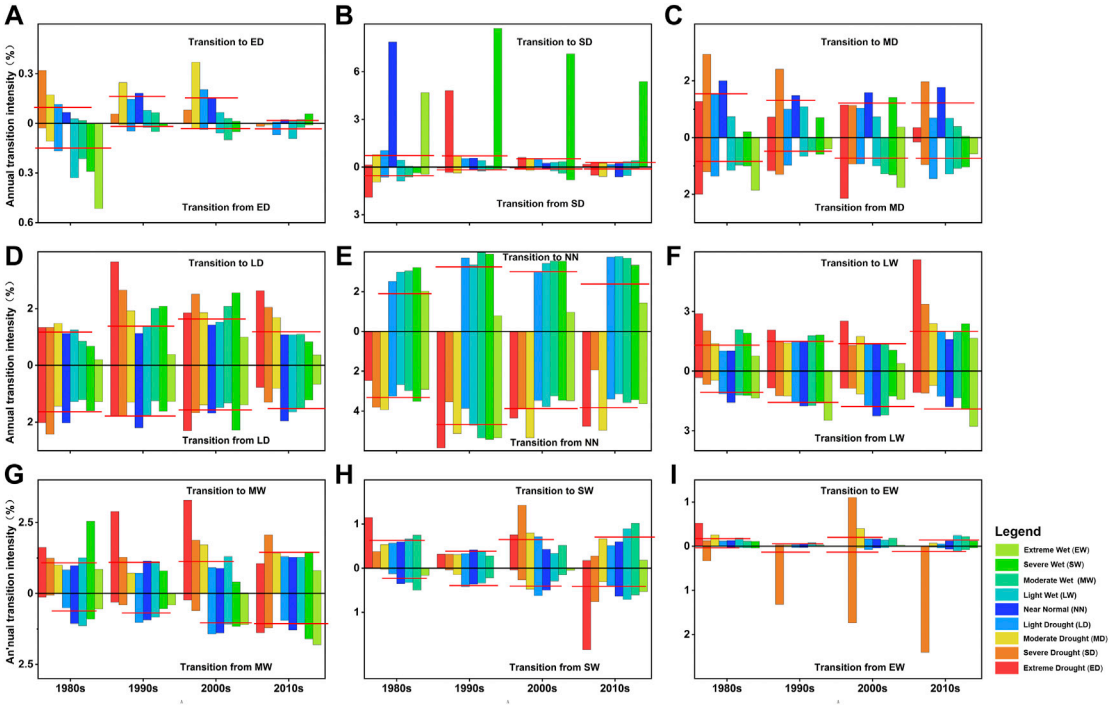

FIGURE 6
Intensity analysis of transition category in each interval.

Aldwaik and Pontius, 2012). The equations related to intensity analysis are shown in Supplementary Table S2.

2.2.5 Empirical Orthogonal Function

EOF is one of the most widely used tools in meteorological research (Dai et al., 2004), and it aims to convey as much information provided by raw data as possible with fewer independent variables. EOF reduces the dimensionality of a large amount of raw data to obtain the dominant spatial pattern and temporal coefficients (Wang et al., 2019b). The significant test was conducted to determine whether the decomposed eigenvectors are physically meaningful (North et al., 1982).

3 Results

3.1 Spatial and temporal changes in drought

Figure 2 shows the annual spatial change trend of drought distribution characterized by SPEI from 1980 to 2020. About 73% of the areas showed an increasing trend, suggesting that a majority of the areas were becoming wetter, especially in the western and southwest regions. Only 27% of the areas were prone to drying, and it was mainly distributed in the southeast and northeast of the QTP, as well as the Qaidam Basin. The areas with the significant trend all passed the 95% significance test.

3.2 Persistence analysis of drought

Figure 3 shows the Hurst exponent from 1980 to 2020. In general, 90% areas of the QTP had the value of Hurst exponent between 0.5 and 1.0, indicating that the current state would have a persistent trend in the future, and was primarily distributed in the west and the south of the QTP (Figure 3A). In the remaining 10% of the area with the Hurst exponent less than 0.5, the current state would be reversed. Combining the trend analysis of SPEI (Figure 2) and Hurst exponent, 65% areas of the QTP would continue to be wet in the future. The wetting trend would be distributed in the western regions and some of the eastern QTP. Areas with persistent drying trend accounted for around 24% of the QTP and were primarily found in the southeast and northeast of the QTP, as well as the Qaidam Basin. The remaining 10% of the QTP would be transformed from dry to wet or from wet to dry (Figure 3B).

3.3 Changes in drought intensity characteristics

We divided the drought into nine categories for the 1980s, 1990s, 2000s, and 2010s. The number of grids for each drought category was calculated from one-time interval to the next, as shown in Supplementary Table S3. Figure 4 shows the overall rate of change in the drought during each time interval. The horizontal axis shows the time interval, and the vertical axis displays the percentage variation in the number of pixels per year, with the horizontal solid line indicating the uniform annual change. If the bar does not exceed the uniform annual change line, it means that the interval changes slowly. On the contrary, the interval changed quickly if the bar is above the uniform annual change line. The rate of change was relatively quick for the 1980s and 2000s, and slow for the 1990s and 2010s. The 1980s was the fastest rate of change.

Figure 5 shows whether the change rate of the nine drought categories in each interval was an active or dormant state. Each category has two horizontal bars, the lower bar shows the number of loss grids and the annual intensity of change, while the upper bar represents the gain. The solid line is the uniform line, if the bar finishes on the right side of the uniform line, the variation in the interval is relatively active, and if the bar ends on the left side of the uniform line, the variation in the interval is dormant.

In the 1980s interval, all wet categories gained more grids than lose grids. The intensity of both extreme wet and drought exceeded the uniform line in the interval, close to 10%, indicating that they were relatively active. The near normal was negative incomes and relatively dormant, with the largest grid changes of more than 1 k (Figure 5A). In the 1990s interval, except for near-normal and moderate drought (loss) in a dormant state, the rest were relatively active. Moderate wet and below moderate drought were positive incomes, but the light drought was negative, and the largest number of grid changes was near normal (Figure 5B). In the 2000s interval, the grids changes of each wet category were the same basically, but light wet and near-normal were negative incomes, and all drought types were positive gains (Figure 5C). In the last interval, the average intensity was relatively small, all types were above the uniform line and were in an active state, the gross gain of wet was positive, and the gross gain of the moderate drought was large, which could indicate that the number of grids transferred to moderate drought was large, and the rest were the same in general (Figure 5D).

Figure 6 demonstrates the intensity analysis of the transition level. The upper vertical bar is the transition intensity from category i to category m (gain), and the lower vertical bar is the transition intensity from category m to category i (loss, $m \neq i$). The solid red line indicates the uniform transition intensity. If the vertical bar exceeds the uniform line, it shows that the transition intensity of this drought category is dominant.

Combining Supplementary Table S3 with Figure 6, the results indicated that the 1980s were primarily dominated by moderate drought and slight wet transition. The gross grids transformed between drying and wetting were the same, indicating there was no obvious transformation of the drying and wetting area during this interval. But in the 1990s, the drying areas were more than the wetting areas in general, light drought, near normal, and light wet

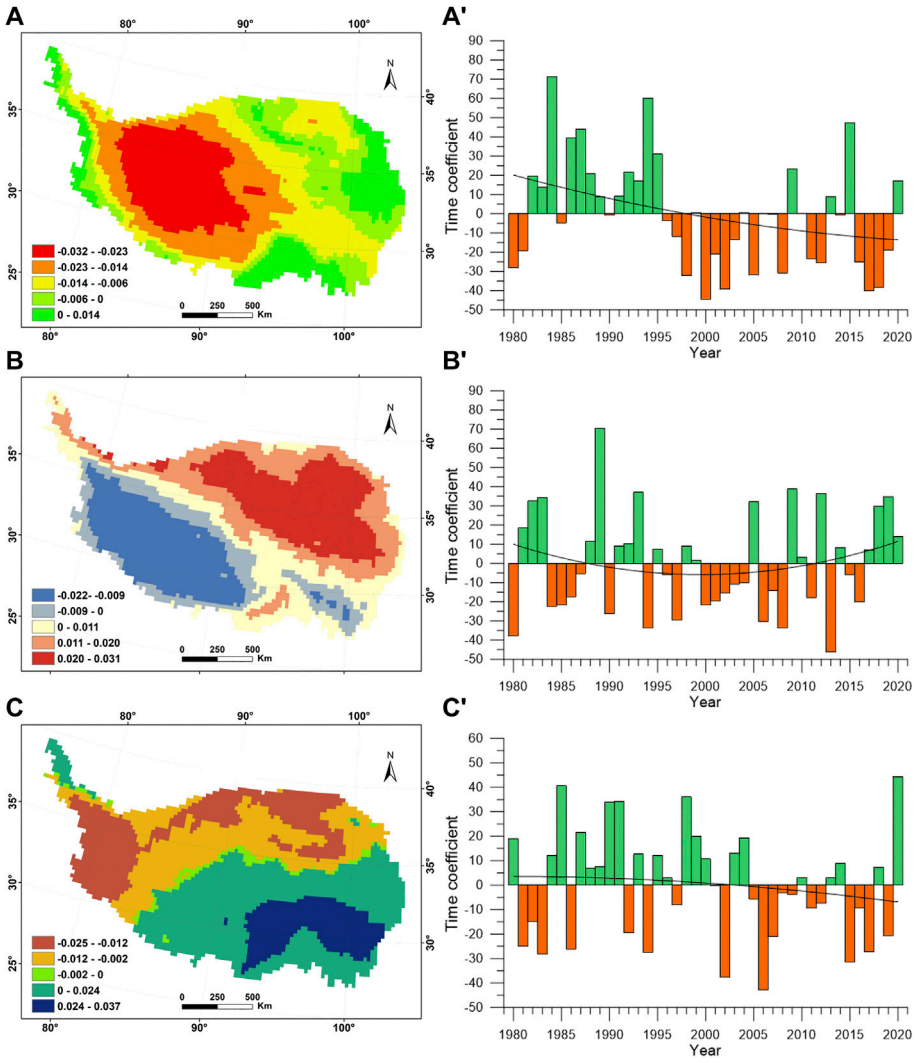

FIGURE 7
Spatial gathering distribution and time coefficients. **(A,A')** EOF mode1, **(B,B')** EOF mode2, **(C,C')** EOF mode3.

were dominant, and the number of interconverted grids among near normal, severe and light drought, moderate and light wet were high. In the 2000s, it was obvious that all of them were transformed to the lower level of drought, near-normal and light wet were the dominant transition, and the drying area was increasing. It was dominated by light wet and moderate drought in the 2010s, the number of wetting grids was significantly greater than the drying grids, and the area of wetting was expanding.

3.4 Main spatial gathering patterns of drought

The 12-month-scale SPEI was used to perform EOF analysis to obtain the main spatial gathering characteristics of drought in the QTP, and the significance test was performed using the North significance test. The spatial distribution characteristics of the first few eigenvectors having passed the significance test could maximize the distribution gathering characteristics of drought. If each component of the eigenvector has the same sign, the variation of this region shows the same, while if the components of an eigenvector are distributed in a positive and negative pattern, they represent two different types of distributions. The larger absolute value is the center, and the value of the eigenvector multiplies by the value of the time coefficient represents the actual value. As shown in Supplementary Table S4, the cumulative variance contribution rate of the first five eigenvectors accounts for 70.8%. The eigenvectors with a variance contribution rate of less than 10% are not strong enough to explain, while the cumulative

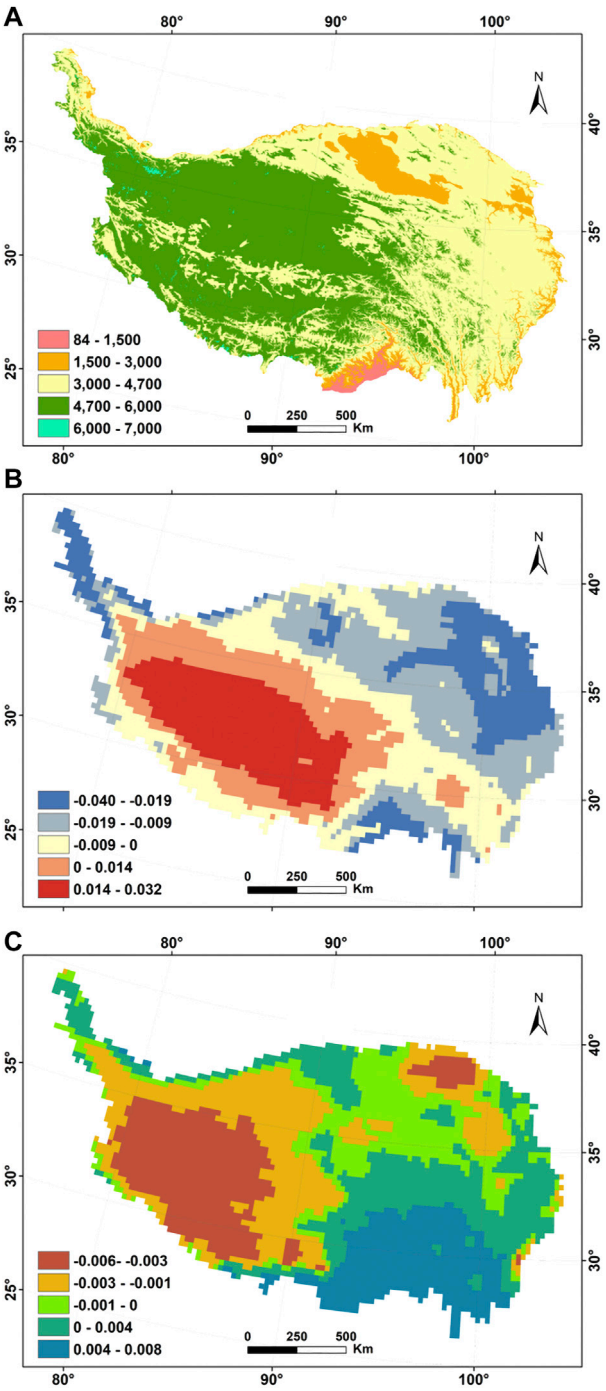

FIGURE 8
Spatial distribution of altitude**(A)** and the spatial gathering distribution of the second mode of PET**(B)**, the first mode of P**(C)**.

variance contribution rate of the first three eigenvectors close to 60%. Therefore, the first three eigenvectors are used to characterize the main spatial gathering characteristics of SPEI in the QTP.

The variance contribution rate of the EOF mode1 was the largest with 23%, which was the principal spatial gathering distribution of drought, and exhibited a gathering distribution structure with negative values in the southeast and east of the QTP and positive values in the center and west (Figure 7A). The low-value center was in the west, indicating that the variation of dry and wet was more obvious there, and the regional changes were consistent. Combined with the time coefficients, the turning point of dry and wet occurred about 1998, indicating that the west was dry before 1998 and wet afterward. Extreme drought years occurred in 1985, 1995, and 2015, respectively, and extreme wet years occur in 1998, 2000, 2002, 2017, and 2018, respectively. From the trend line of the time coefficients, we could also determine that wetting trend would continue in most areas in the future.

The spatial gathering distribution of the EOF mode2 was shown in Figure 7B. The variance contribution rate reached 20%, close to the first mode, reflecting the eigenvector field of the southwest and northeast inversions with the low-value center in the southeast and the high-value center in the northeast. The time coefficients before 1987 and after 2012 were positive, indicating that the southwest was dry while the northeast was wet. The extreme drought years in the southwest were 1989, 1993, 2009, and 2012, and the extreme wet years were 1980, 1994, 1997, and 2013 respectively.

The EOF mode3 showed an opposite trend between the north and south with a 13% variance contribution rate (Figure 7C). The high-value centers were mainly located in the east and south, while the low-value centers were mainly found in the west and parts of the north. The 2004 year was a turning point. The south was in a wet situation before that, and it had been in a dry state after that. The years of extreme drought in the south occurred in 1981, 1983, 1986, 1994, 2002, 2006, and 2015, respectively, and the extremely wet ones were in 1985, 1990, 1991, 1998, and 2020, respectively.

In order to analyze the causes of the three distinct spatial gathering characteristics, we also investigated the gathering characteristics of precipitation, temperature, and potential evapotranspiration, taking into account all spatial characteristics with contribution rates of more than 5%, as shown in Supplementary Table S5. It indicates that the principal spatial gathering distribution of the EOF mode one might correspond to the altitude and temperature (Figure 8A); The southwest-northeast mode might be closely connected to potential evapotranspiration, and potential evapotranspiration changes have a greater impact on the trend of the dry and wet change (Figure 8B); Precipitation and potential evapotranspiration might be related to the south-north mode (Figure 8C), the superposition of the precipitation decreasing and potential evapotranspiration increasing might be the main reason for the north-south difference.

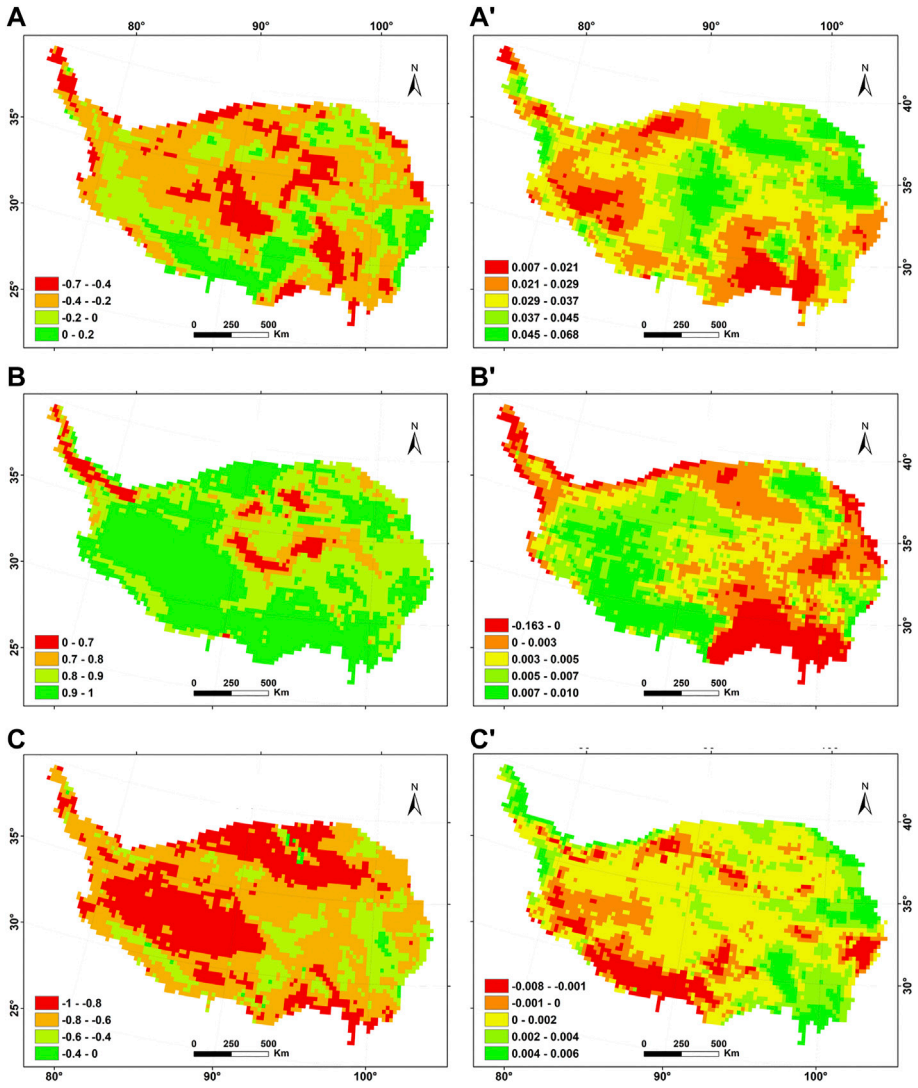

FIGURE 9
Correlation analysis of T, P and PET with SPEI **(A–C)** and their trend analysis **(A′–C′)**.

We also analyzed the correlation of precipitation, temperature, and potential evaporation with SPEI, as well as its trend analysis. The result showed that SPEI was strongly positively connected to precipitation but negatively associated with potential evapotranspiration. The positive correlation with the temperature only occurred in a few areas (Figure 9). Wetting regions had a significant increase in precipitation and a significant decrease in potential evapotranspiration, whereas precipitation in dry areas decreased and potential evaporation increased. The reasons of drought in these regions might be associated with the static wind and central plateau convection, which caused the unequal distribution of rainfall, while warming led land evapotranspiration to increase. The superposition caused runoff decrease and the occurrence of drought (Yang et al., 2014; Yang et al., 2011).

4 Discussion

The QTP was wetter in general, and only 27% of the areas tended to be dry from 1980 to 2020. Several recent studies also concluded that the QTP became wetter in recent years (Li et al., 2010; Chen and Sun, 2015; Gao et al., 2015; Liu et al., 2015; Wang et al., 2015; Liu et al., 2019b). However, some studies pointed out that the southern regions were becoming wetter (Yu et al., 2014; Wang et al., 2017). To understand the differences with other studies, we also compared some studies with different drought indices and data in the QTP, and their findings were listed in Table 1. Furthermore, The PET of SPEI calculated by the Thornthwaite method would exhibit significantly greater differences than SPEI_PM (Chen and Sun, 2015). The unequal period covering the study and

TABLE 1 Previous studies on drought in the QTP.

Reference	Study area	Data	Period	Index	Conclusion
Yu et al. (2014)	China	Meteorological data	1951–2009	SPEI_TH	The eastern and southern parts of the Tibetan Plateau get wetter
Wang et al. (2017)	China	Remote sensing data	1961–2009	SC-PDSI	Significant wetting in the southern QTP
Gao et al. (2015)	QTP	Meteorological data	1979–2011	P/PET	Significantly wetter in the west and significantly drier in the east-central and southernmost parts
Chen and Sun, (2015)	China	Meteorological data	1961–2012	SPEI_PM, SPEI_TH, SC-PDSI_PM	1. SPEI-PM calculates that the overall becomes wetter and the south and east-central may become drier; 2. SPEI-TH calculates that the whole QTP becomes dry. 3. SC-PDSI-PM also indicates that the QTP becomes wetter overall and drier in parts of the southern and western parts
Chen et al. (2017)	China	Remote sensing data	1961–2012	SPEI, PDSI_PM, SC-PDSI_PM, PDSI_TH, SC-PDSI_TH	All indices indicate QTP is overall getting wetter, and the western and southern parts are becoming drier
Wang et al. (2021)	QTP	Remote sensing data	2000–2015	SPI, SPEI	Both SPI and SPEI showed that the northeast became wetter and the west and southeast became drier during April to September
This study	QTP	Remote sensing data	1980–2020	SPEI-PM	The QTP is becoming wetter in general, drying places are mainly in the southeast and northeast of the QTP

usage of the different datasets as well as different methods might affect the results.

Apparently, the causes of drought are extremely complex. Human activities, such as land use/cover change (LUCC) and urbanization, change the exchange of water and energy between the atmosphere and the soil by modifying the Earth's surface, further aggravating drought (Meshesha et al., 2012; Yang et al., 2017). The interaction of dust-cloud, atmosphere-land, atmosphere-ocean has a significant impact on regional climate change and hydrological cycle, leading to the variations of precipitation, temperature, PET and soil moisture, which can affect drought (Huang et al., 2017). The drought might also be related to geographical environmental characteristics and elevation (Feng et al., 2020). Therefore, in order to better understand the drought, more detailed investigations in drought mechanisms are needed in future studies.

Though in this study we analyze the drought characteristics in the QTP from 1980 to 2020 using grid datasets and have made some findings, there are still some limitations. Firstly, the dataset is not as accurate as traditional meteorological data and contains some anomalies. Besides, the causes of drought are complicated, we did not accurately distinguish whether natural factors or human activities influenced the drought, e.g., the government's afforestation project, returning farmland to forests, and protection of pastures, which may be responsible for the regional wetness (Li et al., 2013). Furthermore, the causes of the inversion of dry to wet and wet to dry are not addressed in this study. In the future, high-resolution grid data could be used to analyze different drought indices, and to compare their similarities and differences. The influence mechanism and propagation time of different climate variables on drought are also very interesting topics and need to be further explored.

5 Conclusion

Based on the trend analysis, Hurst exponent analysis, intensity analysis, and EOF analysis methods, we analyzed the dry and wet changes, future persistent changes of drought, drought intensity, and transfer, as well as spatial structure characteristics of drought from 1980 to 2020 in the QTP. The following are the main conclusions:

1) In the past 41 years, there was an overall wetting trend in the QTP, with about 27% of the southeast and some of the northeast of the QTP experiencing regional drying. In the 1980s and 2000s, the drought intensity was relatively fast, while it was slow in the 1990s and 2010s.
2) The future trend of wet and dry in most areas would be the same as the current trend, only 10% of the areas had the reverse transformation trend.
3) EOF mode1 revealed a gathering distribution structure with negative values in the southeast and east of the QTP and positive values in the center and west. The west was more sensitive to climate change, and the wet/dry changeover occurred about in 1998. Most areas will continue to be wet in most areas in the future. A contrast gathering pattern between southwest and northeast was found by analysis of EOF mode2. The southwest was dry while the northeast was wet before 1987 and after 2012, the reverse occurred between 1987 and 2012; EOF mode3 showed the opposite phases between the south

and north regions, and the southern regions were prone to be dry with a high amplitude, and the year of transition was in 2004.

Data availability statement

Publicly available datasets were analyzed in this study. This data can be found here: https://cds.climate.copernicus.eu/cdsapp#!/home.

Author contributions

NY: Writing—original draft, writing—review and editing, visualization; YF: Conceptualization, data curation, writing—review and editing, formal analysis; SL: Writing—review and editing, validation; GW: writing—review and editing, validation; TY: Validation; DY: Validation; PW: Validation; XK: Validation; LW: Validation.

Funding

This research was supported by the Strategic Priority Research Program of the Chinese Academy of Sciences (Grant No. XDA2010010306), the National Natural Science Foundation of China (92047202, 41330634, 41072191, 91125011), the China Geological Survey since 2000, and the Fundamental Research Funds for Central Universities are gratefully acknowledged.

Acknowledgments

The authors greatly appreciate the valuable comments and suggestions of the editors and reviewers using their time and effort to improve this manuscript.

Conflict of interest

The authors declare that the research was conducted in the absence of any commercial or financial relationships that could be construed as a potential conflict of interest.

Publisher's note

All claims expressed in this article are solely those of the authors and do not necessarily represent those of their affiliated organizations, or those of the publisher, the editors and the reviewers. Any product that may be evaluated in this article, or claim that may be made by its manufacturer, is not guaranteed or endorsed by the publisher.

Supplementary material

The Supplementary Material for this article can be found online at: https://www.frontiersin.org/articles/10.3389/fenvs.2022.1008886/full#supplementary-material

References

Abdullah, S. A., and Nakagoshi, N. (2006). Changes in landscape spatial pattern in the highly developing state of Selangor, peninsular Malaysia. *Landsc. Urban Plan.* 77 (3), 263–275. doi:10.1016/j.landurbplan.2005.03.003

Aldwaik, S. Z., and Pontius, R. G., Jr (2012). Intensity analysis to unify measurements of size and stationarity of land changes by interval, category, and transition. *Landsc. Urban Plan.* 106 (1), 103–114. doi:10.1016/j.landurbplan.2012.02.010

Blunden, J., Arndt, D. S., and Baringer, M. O. (2011). State of the climate in 2010. *Bull. Am. Meteorol. Soc.* 92 (6), S1–S236. doi:10.1175/1520-0477-92.6.s1

Chen, H., and Sun, J. (2015). Changes in drought characteristics over China using the standardized precipitation evapotranspiration index. *J. Clim.* 28 (13), 5430–5447. doi:10.1175/jcli-d-14-00707.1

Chen, H., Zhu, Q., Peng, C., Wu, N., Wang, Y., Fang, X., et al. (2013). The impacts of climate change and human activities on biogeochemical cycles on the Qinghai-Tibetan Plateau. *Glob. Chang. Biol.* 19 (10), 2940–2955. doi:10.1111/gcb.12277

Chen, T., Zhang, H., Chen, X., Hagan, D. F., Wang, G., Gao, Z., et al. (2017). Robust drying and wetting trends found in regions over China based on Köppen climate classifications. *J. Geophys. Res. Atmos.* 122 (8), 4228–4237. doi:10.1002/2016jd026168

Dai, A. (2011). Drought under global warming: A review. *WIREs Clim. Change* 2 (1), 45–65. doi:10.1002/wcc.81

Dai, A., Trenberth, K. E., and Qian, T. (2004). A global dataset of Palmer Drought Severity Index for 1870–2002: Relationship with soil moisture and effects of surface warming. *J. Hydrometeorol.* 5 (6), 1117–1130. doi:10.1175/jhm-386.1

Eslamian, S., Ostad-Ali-Askari, K., Singh, V. P., Dalezios, N. R., Ghane, M., Yihdego, Y., et al. (2017). A review of drought indices. *Int. J. Constr. Res. Civ. Eng.* 3, 48–66.

Feng, W., Lu, H., Yao, T., and Yu, Q. (2020). Drought characteristics and its elevation dependence in the Qinghai–Tibet plateau during the last half-century. *Sci. Rep.* 10 (1), 1–11. doi:10.1038/s41598-020-71295-1

Feng, Y., Kuang, X., Liang, S., Liu, S., Yao, Y., Xie, Y., et al. (2021). A simple and efficient method for correction of basin-scale evapotranspiration on the Tibetan plateau. *Remote Sens. (Basel).* 13 (19), 3958. doi:10.3390/rs13193958

Feng, Y., Liang, S., Kuang, X., Wang, G., Wang, X.-S., Wu, P., et al. (2019). Effect of climate and thaw depth on alpine vegetation variations at different permafrost degrading stages in the Tibetan Plateau, China. *Arct. Antarct. Alp. Res.* 51 (1), 155–172. doi:10.1080/15230430.2019.1605798

Gao, Y., Li, X., Leung, L. R., Chen, D., and Xu, J. (2015). Aridity changes in the Tibetan Plateau in a warming climate. *Environ. Res. Lett.* 10 (3), 034013. doi:10.1088/1748-9326/10/3/034013

García, M. d. l. N. L., and Requena, J. P. R. (2019). Different methodologies and uses of the Hurst exponent in econophysics. *Estud. Econ. Appl.* 37 (2), 96–108. doi:10.25115/eea.v37i2.2603

Gocic, M., and Trajkovic, S. (2013). Analysis of changes in meteorological variables using Mann-Kendall and Sen's slope estimator statistical tests in Serbia. *Glob. Planet. Change* 100, 172–182. doi:10.1016/j.gloplacha.2012.10.014

Hayes, M., Svoboda, M., Wall, N., and Widhalm, M. (2011). The lincoln declaration on drought indices: Universal meteorological drought index recommended. *Bull. Am. Meteorol. Soc.* 92 (4), 485–488. doi:10.1175/2010bams3103.1

Hu, W., She, D., Xia, J., He, B., and Hu, C. (2021). Dominant patterns of dryness/wetness variability in the Huang-Huai-Hai River Basin and its relationship with multiscale climate oscillations. *Atmos. Res.* 247, 105148. doi:10.1016/j.atmosres.2020.105148

Huang, J., Li, Y., Fu, C., Chen, F., Fu, Q., Dai, A., et al. (2017). Dryland climate change: Recent progress and challenges. *Rev. Geophys.* 55 (3), 719–778. doi:10.1002/2016rg000550

Huang, J., Pontius, R. G., Jr, Li, Q., and Zhang, Y. (2012). Use of intensity analysis to link patterns with processes of land change from 1986 to 2007 in a coastal watershed of southeast China. *Appl. Geogr.* 34, 371–384. doi:10.1016/j.apgeog.2012.01.001

Huang, J., Yu, H., Guan, X., Wang, G., and Guo, R. (2016). Accelerated dryland expansion under climate change. *Nat. Clim. Chang.* 6 (2), 166–171. doi:10.1038/nclimate2837

Huang, S., Qiang, H., Chang, J., Zhu, Y., Li, X., and Xing, L. (2015). Drought structure based on a nonparametric multivariate standardized drought index across the Yellow River basin, China. *J. Hydrol. X.* 530, 127–136. doi:10.1016/j.jhydrol.2015.09.042

Immerzeel, W. W., van Beek, L. P. H., and Bierkens, M. F. P. (2010). Climate change will affect the asian water towers. *Science* 328 (5984), 1382–1385. doi:10.1126/science.1183188

Kang, S., Xu, Y., You, Q., Flügel, W.-A., Pepin, N., and Yao, T. (2010). Review of climate and cryospheric change in the Tibetan Plateau. *Environ. Res. Lett.* 5 (1), 015101. doi:10.1088/1748-9326/5/1/015101

Kuang, X., and Jiao, J. J. (2016). Review on climate change on the Tibetan Plateau during the last half century. *J. Geophys. Res. Atmos.* 121 (8), 3979–4007. doi:10.1002/2015jd024728

Li, B., Chen, Y., Chen, Z., Li, W., and Zhang, B. (2013). Variations of temperature and precipitation of snowmelt period and its effect on runoff in the mountainous areas of Northwest China. *J. Geogr. Sci.* 23 (1), 17–30. doi:10.1007/s11442-013-0990-1

Li, L., Yang, S., Wang, Z., Zhu, X., and Tang, H. (2010). Evidence of warming and wetting climate over the Qinghai-Tibet Plateau. *Arct. Antarct. Alp. Res.* 42 (4), 449–457. doi:10.1657/1938-4246-42.4.449

Li, S., Yao, Z., Liu, Z., Wang, R., Liu, M., and Adam, J. C. (2019). The spatio-temporal characteristics of drought across tibet, China: Derived from meteorological and agricultural drought indexes. *Theor. Appl. Climatol.* 137 (3), 2409–2424. doi:10.1007/s00704-018-2733-9

Liang, J., Zhang, B., Ma, B., and Wei, H. (2018). Drought evolution characteristics on the Tibetan Plateau based on daily standardized precipitation evapotranspiration index. *J. Glaciol. Geocryol.* 40, 1100–1109.

Liang, S., Ge, S., Wan, L., and Zhang, J. (2010). Can climate change cause the Yellow River to dry up? *Water Resour. Res.* 46 (2), W02505. doi:10.1029/2009wr007971

Liu, L., Niu, Q., Heng, J., Li, H., and Xu, Z. (2019a). Transition characteristics of the dry-wet regime and vegetation dynamic responses over the yarlung zangbo River Basin, southeast Qinghai-Tibet Plateau. *Remote Sens. (Basel).* 11 (10), 1254. doi:10.3390/rs11101254

Liu, L., Wang, Y., You, N., Liang, Z., Qin, D., and Li, S. (2019b). Changes in aridity and its driving factors in China during 1961–2016. *Int. J. Climatol.* 39 (1), 50–60. doi:10.1002/joc.5781

Liu, X., Wang, S., Zhou, Y., Wang, F., Li, W., and Liu, W. (2015). Regionalization and spatiotemporal variation of drought in China based on standardized precipitation evapotranspiration index (1961–2013). *Adv. Meteorol.*, 1–18. doi:10.1155/2015/950262

Lu, E., Liu, S., Luo, Y., Zhao, W., Li, H., Chen, H., et al. (2014). The atmospheric anomalies associated with the drought over the Yangtze River basin during spring 2011. *J. Geophys. Res. Atmos.* 119 (10), 5881–5894. doi:10.1002/2014jd021558

Lu, Y., Cai, H., Jiang, T., Sun, S., Wang, Y., Zhao, J., et al. (2019). Assessment of global drought propensity and its impacts on agricultural water use in future climate scenarios. *Agric. For. Meteorol.* 278, 107623. doi:10.1016/j.agrformet.2019.107623

McKee, T. B., Doesken, N. J., and Kleist, J. (1993). "The relationship of drought frequency and duration to time scales," in Proceedings of the 8th Conference on Applied Climatology (California, 179–183.17).

Meshesha, D. T., Tsunekawa, A., and Tsubo, M. (2012). Continuing land degradation: Cause–effect in Ethiopia's central rift valley. *Land Degrad. Dev.* 23 (2), 130–143. doi:10.1002/ldr.1061

Mishra, A. K., and Singh, V. P. (2010). A review of drought concepts. *J. Hydrol. X.* 391 (1-2), 202–216. doi:10.1016/j.jhydrol.2010.07.012

North, G. R., Bell, T. L., Cahalan, R. F., and Moeng, F. J. (1982). Sampling errors in the estimation of empirical orthogonal functions. *Mon. Weather Rev.* 110 (7), 699–706. doi:10.1175/1520-0493(1982)110<0699:seiteo>2.0.co;2

Palmer, W. C. (1965). *Meteorological drought*. Washington, DC: U.S. Department of Commerce Weather Bureau, 58. Research Paper No. 45.

Potop, V., Boroneanț, C., Možný, M., Štěpánek, P., and Skalák, P. (2014). Observed spatiotemporal characteristics of drought on various time scales over the Czech Republic. *Theor. Appl. Climatol.* 115 (3), 563–581. doi:10.1007/s00704-013-0908-y

Rangwala, I., and Miller, J. R. (2012). Climate change in mountains: A review of elevation-dependent warming and its possible causes. *Clim. Change* 114 (3-4), 527–547. doi:10.1007/s10584-012-0419-3

Shukla, S., and Wood, A. W. (2008). Use of a standardized runoff index for characterizing hydrologic drought. *Geophys. Res. Lett.* 35 (2), L02405. doi:10.1029/2007gl032487

Sun, Y., Liu, S., Liu, Y., Dong, Y., Li, M., An, Y., et al. (2021). Effects of the interaction among climate, terrain and human activities on biodiversity on the Qinghai-Tibet Plateau. *Sci. Total Environ.* 794, 148497. doi:10.1016/j.scitotenv.2021.148497

Tong, S., Lai, Q., Zhang, J., Bao, Y., Lusi, A., Ma, Q., et al. (2018). Spatiotemporal drought variability on the Mongolian Plateau from 1980–2014 based on the SPEI-PM, intensity analysis and Hurst exponent. *Sci. Total Environ.* 615, 1557–1565. doi:10.1016/j.scitotenv.2017.09.121

Vicente-Serrano, S. M., Beguería, S., and López-Moreno, J. I. (2010). A multiscalar drought index sensitive to global warming: The standardized precipitation evapotranspiration index. *J. Clim.* 23 (7), 1696–1718. doi:10.1175/2009jcli2909.1

Wang, A., Lettenmaier, D. P., and Sheffield, J. (2011). Soil moisture drought in China, 1950–2006. *J. Clim.* 24 (13), 3257–3271. doi:10.1175/2011jcli3733.1

Wang, Q., Wu, J., Lei, T., He, B., Wu, Z., Liu, M., et al. (2014). Temporal-spatial characteristics of severe drought events and their impact on agriculture on a global scale. *Quat. Int.* 349, 10–21. doi:10.1016/j.quaint.2014.06.021

Wang, W., Zhu, Y., Xu, R., and Liu, J. (2015). Drought severity change in China during 1961–2012 indicated by SPI and SPEI. *Nat. Hazards* 75 (3), 2437–2451. doi:10.1007/s11069-014-1436-5

Wang, Y., Fu, B., Liu, Y., Li, Y., Feng, X., and Wang, S. (2021). Response of vegetation to drought in the Tibetan Plateau: Elevation differentiation and the dominant factors. *Agric. For. Meteorol.* 306, 108468. doi:10.1016/j.agrformet.2021.108468

Wang, Y., Liu, G., and Guo, E. (2019a). Spatial distribution and temporal variation of drought in inner Mongolia during 1901–2014 using standardized precipitation evapotranspiration index. *Sci. Total Environ.* 654, 850–862. doi:10.1016/j.scitotenv.2018.10.425

Wang, Y., Liu, X., Ren, G., Yang, G., and Feng, Y. (2019b). Analysis of the spatiotemporal variability of droughts and the effects of drought on potato production in northern China. *Agric. For. Meteorol.* 264, 334–342. doi:10.1016/j.agrformet.2018.10.019

Wang, Z., Li, J., Lai, C., Zeng, Z., Zhong, R., Chen, X., et al. (2017). Does drought in China show a significant decreasing trend from 1961 to 2009? *Sci. Total Environ.* 579, 314–324. doi:10.1016/j.scitotenv.2016.11.098

Yang, Y., McVicar, T. R., Donohue, R. J., Zhang, Y., Roderick, M. L., Chiew, F. H., et al. (2017). Lags in hydrologic recovery following an extreme drought: Assessing the roles of climate and catchment characteristics. *Water Resour. Res.* 53 (6), 4821–4837. doi:10.1002/2017wr020683

Yao, T., Thompson, L. G., Mosbrugger, V., Zhang, F., Ma, Y., Luo, T., et al. (2012). Third pole environment (TPE). *Environ. Dev.* 3, 52–64. doi:10.1016/j.envdev.2012.04.002

Ye, C., Sun, J., Liu, M., Xiong, J., Zong, N., Hu, J., et al. (2020). Concurrent and lagged effects of extreme drought induce net reduction in vegetation carbon uptake on Tibetan Plateau. *Remote Sens. (Basel).* 12 (15), 2347. doi:10.3390/rs12152347

You, Q., Cai, Z., Pepin, N., Chen, D., Ahrens, B., Jiang, Z., et al. (2021). Warming amplification over the arctic Pole and Third Pole: Trends, mechanisms and consequences. *Earth-Science Rev.* 217, 103625. doi:10.1016/j.earscirev.2021.103625

Yu, M., Li, Q., Hayes, M. J., Svoboda, M. D., and Heim, R. R. (2014). Are droughts becoming more frequent or severe in China based on the standardized precipitation evapotranspiration index: 1951–2010? *Int. J. Climatol.* 34 (3), 545–558. doi:10.1002/joc.3701

Zhang, D., Zhang, Q., Werner, A. D., and Liu, X. (2016). GRACE-based hydrological drought evaluation of the Yangtze River Basin, China. *J. Hydrometeorol.* 17 (3), 811–828. doi:10.1175/jhm-d-15-0084.1

Zhang, H., Ding, M., Li, L., and Liu, L. (2019). Continuous wetting on the Tibetan plateau during 1970–2017. *Water* 11 (12), 2605. doi:10.3390/w11122605

Zhou, Z., Shi, H., Fu, Q., Ding, Y., Li, T., Wang, Y., et al. (2021). Characteristics of propagation from meteorological drought to hydrological drought in the Pearl River Basin. *JGR. Atmos.* 126 (4), e2020JD033959. doi:10.1029/2020jd033959

frontiers | Frontiers in Environmental Science

TYPE Original Research
PUBLISHED 22 November 2022
DOI 10.3389/fenvs.2022.917469

OPEN ACCESS

EDITED BY
Qiang Zhang,
Beijing Normal University, China

REVIEWED BY
Andrea L. Pierce,
University of Delaware, United States
Mohamad N. Azra,
Institute of Marine Biotechnology,
Universiti Malaysia Terengganu,
Malaysia

*CORRESPONDENCE
Gang Liu,
lglhm@tju.edu.cn

SPECIALTY SECTION
This article was submitted to Interdisciplinary Climate Studies, a section of the journal Frontiers in Environmental Science

RECEIVED 11 April 2022
ACCEPTED 04 November 2022
PUBLISHED 22 November 2022

CITATION
Fan J, Liu G, Xia Z and Cai S (2022), A bibliometric analysis of climate change risk perception: Hot spots, trends and improvements.
Front. Environ. Sci. 10:917469.
doi: 10.3389/fenvs.2022.917469

A bibliometric analysis of climate change risk perception: Hot spots, trends and improvements

Jitong Fan[1,2], Gang Liu[3]*, Ziqian Xia[2] and Sanfa Cai[2]

[1]School of Civil Engineering, Tianjin University, Tianjin, China, [2]School of Economics and Management, Tongji University, Shanghai, China, [3]College of Management and Economics, Tianjin University, Tianjin, China

Climate change is a global problem, and it is receiving increasing scientific attention due to its significant impact. To provide valuable insights for understanding and summarizing the research trends and prospects on climate change risk perception, this study takes a qualitative and quantitative analysis by using bibliometric tools. This analysis presents information related to authors, countries, institutions, journals, top cited publications, research hot spots, trends, and prospects. The analysis involved 4429 articles after rigorous screening and evaluated them on the risk perception of climate change in countries and the public. The majority of publications were published during the period of 2016–2022 (70.92%), with *Climatic Change* being the dominant journal and most research originating from the USA, England and Australia. The research content of this topic is primarily divided into several categories, including environmental sciences, atmospheric sciences, water resources and public health. The results showed that adaptation and vulnerability attract much attention. Finally, this paper identifies and discusses five research themes that should be further studied: determinants of perception, human behavior, human mental health risk, agriculture and adaptive strategy.

KEYWORDS

Climate Change, Risk Perception, Bibliometric, impact, adaptive strategy

1 Introduction

Recently, the Sixth Assessment Report of IPCC (Intergovernmental Panel on Climate Change), the authority on global climate change, warns that global action to mitigate climate change and adaptation is urgent and that any delay will make people's futures unlivable and sustainable. At the same time, scientists, politicians, and economists have all centered their attention on climate change in recent decades. It is one of the main causes of adverse impacts and key risks to natural and human social systems. Denying climate change, especially by governments and policymakers, is a serious problem because it hinders the process of risk mitigation and strategy adaptation. There is a broad scientific conclusion that global climate change is taking place. Research on the impact of climate change mainly focuses on environmental and economic aspects, including food security (Parvin and Ahsan, 2013), water resources (Yang et al., 2018), health (Madeira et al.,

2018), biodiversity (Fei et al., 2017), energy (Wang et al., 2018) and some other aspects. Scientists' research on climate change has been quite comprehensive.

Climate change has been a widespread concern, but less attention has been given to climate change risk perception. Climate change is a human-reduced, serious risk, but the public's perception of climate change and support for climate change policies are still ambiguous in many parts of the world (Brechin and Bhandari, 2011), which depends on their environment and world outlook (Becerra et al., 2020). Many scholars from various countries have conducted much research on the risk perception of climate change. For instance, Leiserowitz studied the perception of the American people on the local climate and found that most people pay high attention to the global climate change problem, but they believe that the risk of climate change is medium, and the public perception of climate change also affects their perception of relevant government policies (Leiserowitz, 2005). Recent research on the public perception of climate change has improved our understanding of the changing public response (Brulle et al., 2012). These climate change risk perception studies are important to inform and support local people, technical experts and decision makers (Funatsu et al., 2019). Understanding and encouraging the potential drivers of local people to adapt to climate change can help develop plans and strategies, which has a greater possibility of achieving positive results.

Climate change risk perception is a complex problem with subjectivity based on environmental and cultural characteristics. However, it is important for scientists and politicians to develop adaptation and mitigation strategies and policies (Armah et al., 2017). Strengthening the research on the risk perception of climate change and judging whether public perception is accurate by comparing with the actual climate change trend. These results can provide a reference for government decision-making behavior. Although many articles cover different perspectives of climate change risk perception, it is necessary to conduct a comprehensive bibliometric analysis to help scholars evaluate current research progress and determine future research directions. Since these publications are geographically and spatially distributed, our analysis will show the relationship between them and how much they are related to each other.

The application of big data and bibliometric analysis makes it more convenient to collect and process scientific climate change research. This helps to understand the relationship between previous research and the current literature (Callaghan et al., 2020). Bibliometric research has been proven to be very useful for natural science, urban research and other research directions (Wu et al., 2018) and has become one of the most prominent methods to evaluate and predict the research trends of specific topics (Zhao et al., 2018). At the same time, this research method is helpful for revealing the research trends and the characteristics of academic publishing, as well as the relationship among different documents, authors and publishing regions (Lee, 2017). In bibliometric analysis, big data is defined as "big literature", which is characterized by high velocity, volume, and variability (Nunez Mir et al., 2016). The objective of this study is to analyze the 4429 pieces of literature collected (from 2000 to 2022) and thus derive a research analysis of climate change risk perception.

We identified hot spots, trends and improvements in climate change risk perception in recent years through bibliometric analysis. Moreover, we analyzed the core topic, future research hotspots and practical research methods to provide an overview of references for theoretical research and practical work on climate change risk perception. The dataset has been made publicly available on figshare (https://figshare.com/articles/dataset/data_zip/21314085).

2 Materials and methods

2.1 Data collection

We comprehensively searched the Web of Science Core Collection (WoSCC) database to search publications, and the selected time span ranged from 2000 to 2022. The reason for only including 22 years of studies is that only 16 papers were found before 2000 by searching WoSCC using our preidentified keywords (see below). Additionally, papers published before 2000 are not very relevant to the current study due to the long distance between them. Therefore, we selected papers from 2000-2022 for analysis. The retrieval time was March 13th, 2022. The search statement is "TS= (("climat* chang*" or "climat* var*" or "environment* chang*" or "climat* warm*") and risk and (aware* or percept* or sense* or feel* or cogni*)) AND PY= (2000-2022)". The WoSCC is currently one of the primary sources for most bibliometric analyses (Mongeon and Paul-Hus, 2015). We restricted the language of our results to English. We choose the related categories, including environmental sciences, environmental studies, meteorology atmospheric sciences, water resources, public environmental occupational health, geosciences multidisciplinary, geography or ecology, economics, development studies, energy fuels, social sciences interdisciplinary, multidisciplinary sciences, biodiversity conservation, regional urban planning, mathematics interdisciplinary applications, psychology multidisciplinary and communication. We finally selected original research and review articles, filtering publications to 4429 records. Remove papers that are not related to the research topic, including ethics, limnology, toxicology, pediatrics, etc. The timeframe spanned more than 20 years, which made the analysis of the structure and trends of knowledge domains more typical. To ensure an accurate search, our theoretical approaches consider what is now understood as climate change risk perception research. Three independent variables, climate change, risk and perception, were defined as the search keywords.

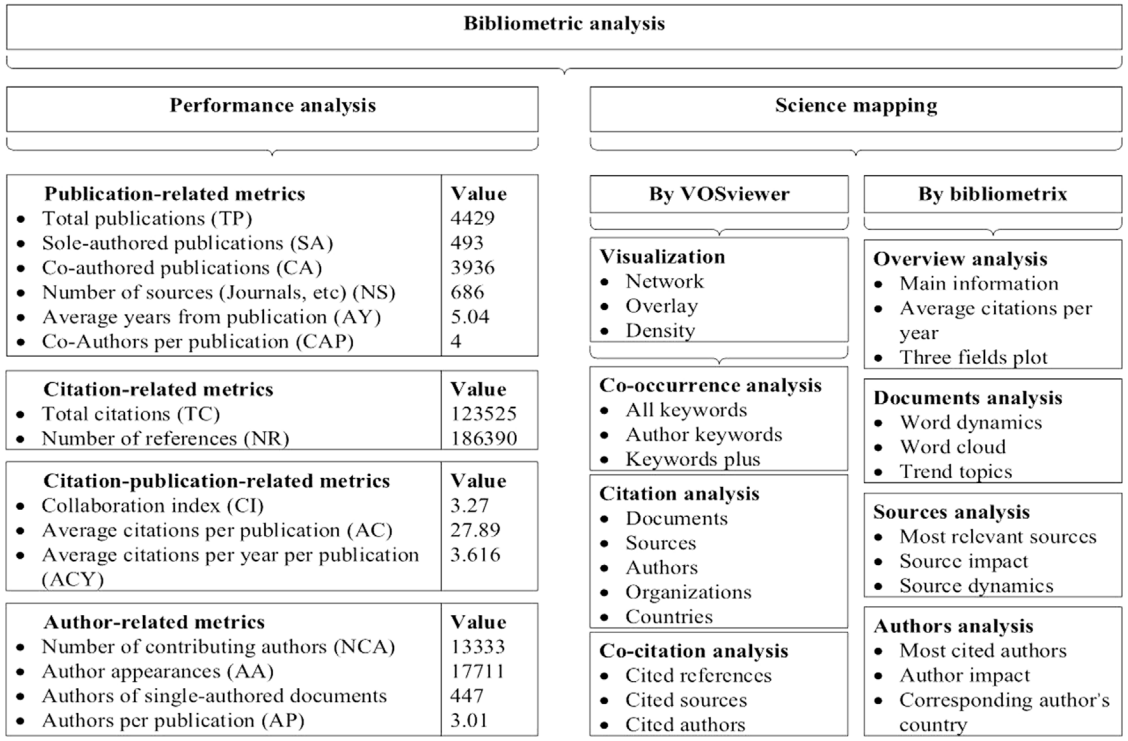

FIGURE 1
Overview of the bibliometric analysis in this paper

2.2 Topic explanation

The theme of this paper is "climate change risk perception," which means people's perception of climate change risk. Compared with (Howe et al., 2015), our paper pays more attention to climate change risk perception globally; our paper focuses on the many aspects of climate change risk perception, rather than just the climate change risk perception about environment (Bradley et al., 2020); compared with (Tam and McsDaniels, 2013), our research focuses on relevant policies; also, our paper is more concentrated on the people of all classes than (Parvin and Ahsan, 2013) and (Wu et al., 2018).

2.3 Bibliometric Analysis

Bibliometrics provides an important method for analyzing academic documents. It can visually show the statistical results of academic documents by using bibliometric tools such as VOSviewer and Bibliometrix (Li et al., 2017). Bibliometrix, an important R-tool for comprehensive bibliometric analysis designed in R language (Aria and Cuccurullo, 2017). With a complete process of data import, data transformation, data analysis, and scientific visualization, Bibliometrix basically meets the requirements of bibliometric analysis (Chen et al., 2022). We used it to make diagrams and tables, including thematic map, thematic evolution, network map, co-citation network, co-authorship network and co-occurrence network. VOSviewer is a program developed for constructing and viewing bibliometric maps. The program is freely available to the bibliometric research community (van Eck and Waltman, 2010). Therefore, we use VOSviewer, which also has three types of visualization: network, overlay and density. It is color-coded depending on the popularity and similarity of the studies. The line used in the interconnection of words also changes in contrast. As the word is commonly used in different studies, the color becomes vibrant (Tamala et al., 2022). The viewing capabilities of VOSviewer are particularly useful for analyses that contain at least a moderate number of items (at least 100 items) (van Eck and Waltman, 2010).

3 Results

3.1 Overview of result data and map

As shown in Figure 1. First, we summarize the data and network diagram obtained by analyzing the collected documents with bibliometric tools. In the performance analysis, we study the following aspects: publication-related, citation-related, citation-publication-related and author-related metrics. Combining these

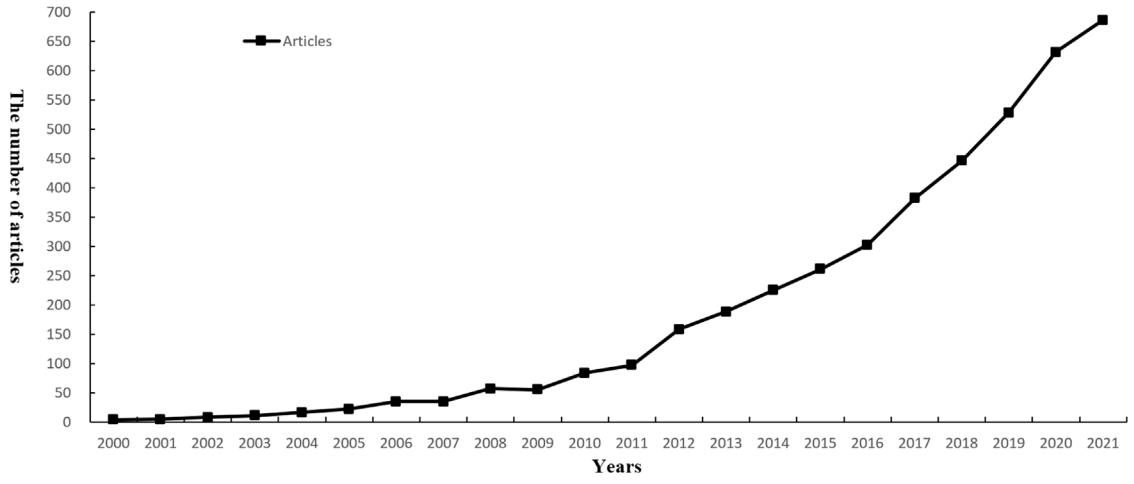

FIGURE 2
Number of articles per year from 2000 to 2021.

TABLE 1 The Top 10 articles according to the number of total citations and total citations per year and local citation score

Rank	Cited publications	Citations	Cited per year publications	Citations	Local citation score publications	LCS	GCS
1	Adger, (2006), Global Environ Chang	2,895	Adger, (2006), Global Environ Chang	170.2941	Leiserowitz, (2006), Climatic Change	428	1,078
2	Dryhurst et al. (2020), J Risk Res	482	Dryhurst et al. (2020), J Risk Res	160.6667	Grothmann and Patt, 2005, Global Environ Chang	316	960
3	Gatto et al. (2020), P Natl Acad Sci Usa	404	Gatto et al. (2020), P Natl Acad Sci Usa	134.6667	Weber. (2006), Climatic Change	226	603
4	Adger. (2009), Climatic Change	1,267	Adger et al. (2009), Climatic Change	90.5	Leiserowitz. (2005), Risk Anal	220	502
5	Khanna et al. (2021), Nat Clim Change	993	Khanna et al. (2012), Nat Clim Change	90.2727	Whitmarsh, 2008, J Risk Res	205	359
6	Estrada et al., 2017, Sci Adv	467	Estrada et al., 2017, Sci Adv	77.8333	Adger et al. (2009), Climatic Change	197	1,267
7	Kahan et al., 2011, J Risk Res	824	Kahan et al., 2011, J Risk Res	68.6667	Lorenzoni et al., 2007, Global Environ Chang	193	972
8	Gifford, 2011, Am Psychol	781	Gifford, 2011, Am Psychol	65.0833	Spence et al. (2011), Risk Anal	193	544
9	Leiserowitz, (2006), Climatic Change	1,078	Leiserowitz. (2006), Climatic Change	63.4118	Lorenzoni and Pidgeon, 2006, Climatic Change	186	579
10	Lorenzoni et al., 2007, Global Environ Chang	972	Lorenzoni et al., 2007, Global Environ Chang	60.75	Weber. (2006), Wires Clim Change	161	395

data, we can see the current situation of climate change risk perception research, the degree of citation of relevant literatures and the overall level of the authors. We use two bibliometric tools to map science mapping. Through VOSviewer, we can obtain three main types of graphs: network, overlay and density visualization maps. Co-occurrence, citation and co-citation analyses are represented by these three kinds of diagrams. Furthermore, we used the Bibliometrix package in R language for visual analysis. Using it, we can obtain a visual map of overview, documents, sources and authors.

3.2 Analysis of articles

The annual growth rate of related publications is 15.76%. The number of related publications increased slowly from 2000 to 2015, accounting for just 29.08% of the total. The number of publications has increased substantially since 2015. The number of related papers has grown rapidly, with 26.49% during 2016-2017. The majority of publications (70.92%) were published from 2016 to 2022, which is shown in Figure 2. This may be because these years had the greatest impact from climate change. A

TABLE 2 The Primary performance of the top 10 most productive journals.

Journals	Country	Amount	*h*-index	Impact factor	Total citation
1.*Climatic Change*	Netherlands	190	40	4.743	8,812
2. *Sustainability*	Switzerland	176	15	3.251	120
3. *International Journal of Environmental Research and Public Health*	Switzerland	131	20	3.39	1,422
4. *Global Environmental Change-Human and Policy Dimensions*	England	124	53	9.523	14,036
5. *Risk Analysis*	England	120	40	4.0	19
6. *International Journal of Disaster Risk Reduction*	Netherlands	118	21	4.32	1,527
7.*Journal of Risk Research*	England	98	24	2.583	3,441
8. *Natural Hazards*	Netherlands	93	28	3.102	2,202
9.*Regional Environmental Change*	Germany	84	28	3.678	2,113
10. *Energy Policy*	England	79	31	6.142	3,552

World Meteorological Organization survey showed that 2015 was the hottest year on record, and during this period, concentrations of the major greenhouse gases continued to rise and reached record levels for the instrumental period (World Meteorological Organization, 2019). In addition, *the Paris Agreement* was adopted by the United Nations Climate Change Conference in 2015 (United Nations, 2015). All these factors have led to the upsurge in climate change research since 2015.

3.2.1 Citations of articles

Table 1 shows the top 10 articles according to the number of total citations and total citations per year and local citation scores. (Adger, 2006), published in the *Global Environmental Change* in 2006, is cited the most 2895 times, which reviews research traditions of vulnerability to environmental change and the challenges for present vulnerability research in integrating with the domains of resilience and adaptation (Adger, 2006). The other three articles are also cited more than 1000 times (Adger et al., 2009) (1267 times), (Leiserowitz, 2006) (1078 times) and (Parry et al., 2004) (1023 times). Meanwhile, (Adger, 2006) is also the most cited article per year (170.29), followed by (Dryhurst et al., 2020) (160.67) and (Gatto et al., 2020) (134.67). The most cited articles can provide helpful insights to researchers interested in this field. Moreover, two important indicators, the local citation score (LCS) and global citation score (GCS), were used to identify hot publications with citation analysis (Huang et al., 2022). GCS refers to the total number of citations in the Web of Science database. LCS represents the number of times a document has been cited in the current sample literature (Huang et al., 2022). The article with the highest local citation score in the current research field is (Leiserowitz, 2006), with an LCS of 428 and GCS of 1078, which means that its local citations are more than others. However, there are some articles, for example, (Adger et al., 2009) with high GCS (1267) but low LCS (197), which shows that their study content is mostly interdisciplinary research.

3.2.2 Co-Citation Network Analysis

Co-citation is a bibliographic analysis method that indicates a connection between two documents that are both cited by an identical third document (Nadelhoffer and Raich, 1992). The co-citation analysis of VOSviewer software includes cited references, cited sources, and cited authors, which can find close relationship between articles, journals and authors in that field. In the co-citation network, a cluster can be defined as a group of well-connected articles in a research field, and the connection with articles in other clusters or research fields is limited (Huang et al., 2022).

Among the 196313 cited references, according to the calculated total strength of links with other cited references. There is a co-citation network composed of the top 50 influential articles (each has more than 97 cited references) is displayed in Figure 3A, which has a small table about the information of the top 3. The reason for choosing the top 50 articles for the network diagram is that 50 items can display the main content of the graph in a reasonable way when drawing, without cluttering the graph because of too many items. At the same time, the graph does not contain too little information due to the small number of items. Moreover, most of the bibliometric literature also selects approximately 50 items for network diagramming (e.g., (Rana, 2020)). (Leiserowitz, 2006) has the highest total link strength. This study found that American risk perceptions and policy support are strongly influenced by experiential factors, which is 2268, followed by (Spence et al., 2011) (1487) and (Weber, 2006) (1425), and they are all the top influence co-citation articles. Figure 3A also shows 3 clusters in these articles, and each cluster has a different color. The red cluster with 22 articles focuses on public perception (Weber, 2006; Spence et al., 2011); the green cluster with 15 items focuses on risk perception (Slovic, 2020); and the blue cluster with 13 publications focuses on perception and policy support (Leiserowitz, 2006).

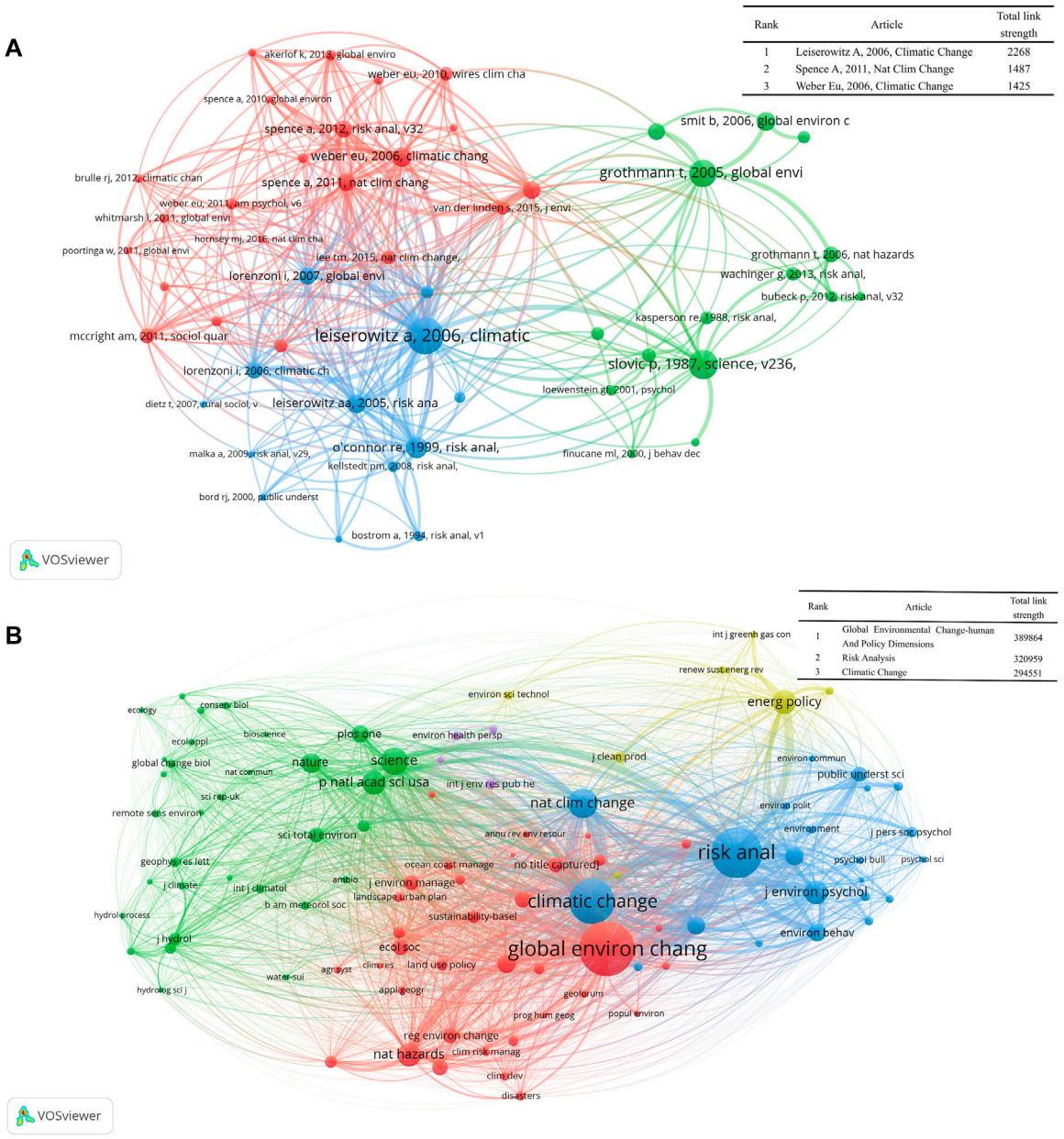

FIGURE 3
Cocitation map of articles **(A)** (top 50 articles with more than 97 cited references) and journals **(B)** ((top 50 journals with more than 488 cited references)

3.3 Analysis of journals

3.3.1 Distribution of journals

The results show that the 4429 selected studies are published in 686 types of journals. Table 2 shows the primary performance of the top 10 most productive journals. The results find that *Climatic Change* (Climatic Change is dedicated to the totality of the problem of climatic variability and change, including its descriptions, causes, implications and interactions among these) is the most productive journal publishing 190 papers, followed by *Sustainability* (176 papers) and *International Journal of Environmental Research and Public Health* (131 papers). *Global Environmental Change-human And Policy Dimensions* has the highest *h*-index (53), followed by *Climatic Change* (40) and *Risk Analysis* (40). *Global Environmental Change-human And Policy Dimensions* also has the highest total citations

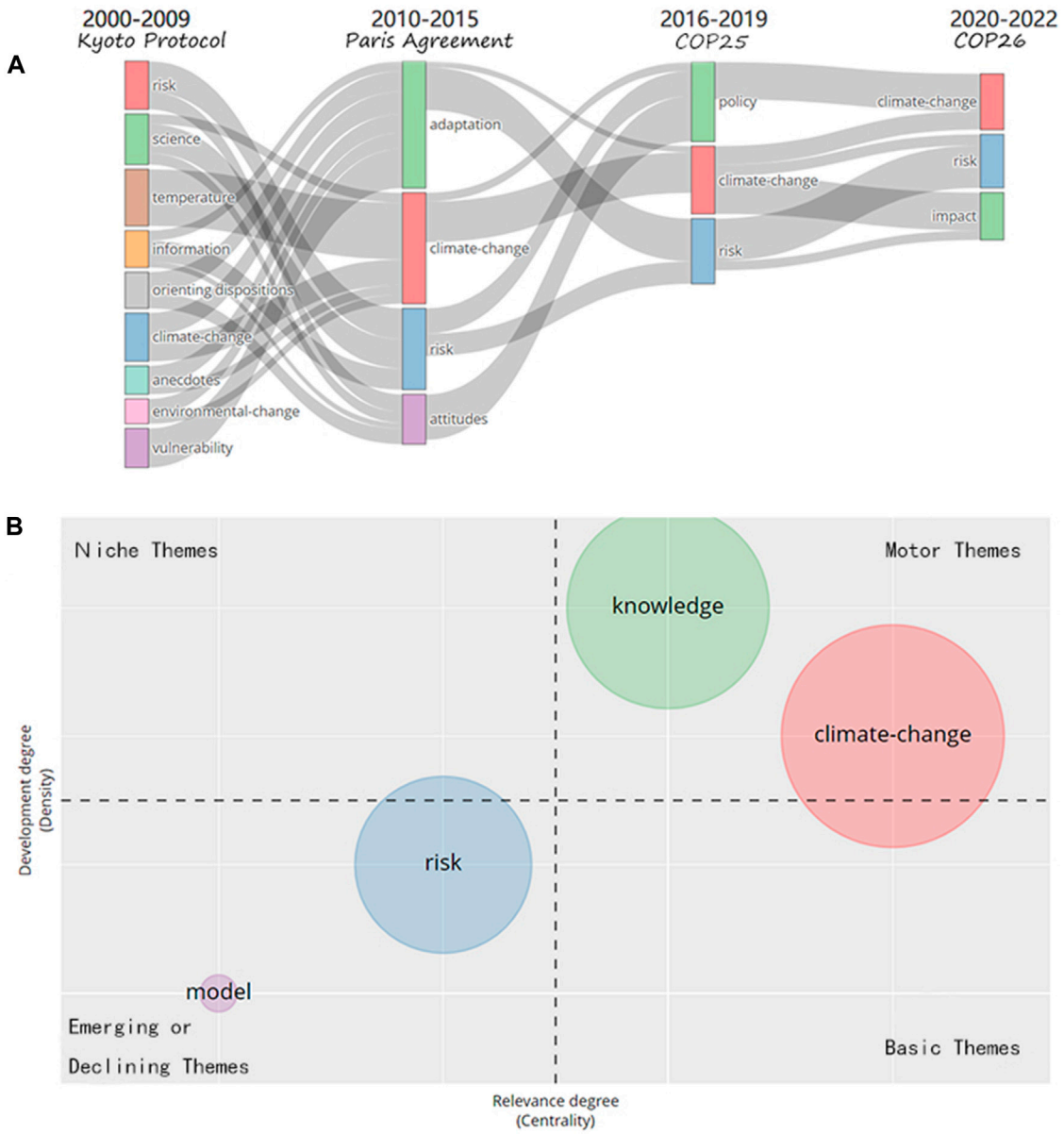

FIGURE 4
The change in the themes at different times during the period 2000-2022 **(A)**; status and development trend of different themes during the period 2016-2022 **(B)**.

(14036). These all indicate that *Global Environmental Change-human And Policy Dimensions, Climatic Change*, *Risk Analysis, Sustainability* and *International Journal of Environmental Research and Public Health* have significant contributions in this field, while the rest of journals have additional contributions. Among these ten journals, 4 were in England, 3 were in the Netherlands and 2 were in Switzerland, and they all had high impact factors.

3.3.2 Co-Citation of journals

In the visualization of journal co-citation, the distance between the two journals reflects the correlation between different journals and disciplines. Generally, the closer the distance between the two journals, the stronger the correlation between them. We can easily find that VOSviewer divides journals into five clusters in Figure 3B: environmental and global in the red cluster (*Global Environmental Change-Human And Policy*

TABLE 3 The top 10 authors regarding the number of papers, total citations and h-index.

Rank	Author	Papers	Author	TC	Author	*h*-index
1	Leiserowitz A	32	Adger Wn	5,621	Leiserowitz A	18
2	Pidgeon N	28	Lorenzoni I	4,317	Pidgeon N	18
3	Siegrist M	26	Leiserowitz A	3,190	Siegrist M	17
4	Botzen Wjw	22	Poortinga W	2,698	Lorenzoni I	16
5	Poortinga W	21	Whitmarsh L	2,557	Poortinga W	16
6	Bostrom A	18	Pidgeon Nf	2,554	Botzen Wjw	14
7	Vedlitz A	18	Kahan et al., 2011	2,454	Pidgeon Nf	13
8	Howe Pd	17	Dessai S	2,292	Dessai S	12
9	Lorenzoni I	17	Wolf J	2087	Howe Pd	12
10	Bohm G	16	Weber Eu	1942	Visschers Vhm	12

Dimensions, Natural Hazards and *Environmental Science & Policy*); risk and climate change in the blue cluster (*Climatic Change, Risk Analysis* and *Nature Climate Change*); nature and biology in green cluster (*Nature*, *Science* and *Plos One*); energy and technology (*Energy Policy*, *Energy Research & Social Science* and *Environmental Science & Technology*); public health in purple (*International Journal Of Environmental Research And Public Health* and *Environmental Health Perspectives*). Among the 67859 sources, Global Environmental Change-Human and Policy Dimensions, which advance knowledge about the human and policy dimensions of global environmental change, have the highest total link strength, which is 389864.

3.4 Subject categories analysis

The top 10 subject categories included environmental sciences (1933 articles, accounting for 43.64% of the total), environmental studies (1399 articles, 31.59%), meteorology atmospheric sciences (809 articles, 18.27%), water resources (563 articles, 12.71%), public environmental occupational health (488 articles, 11.01%), geosciences multidisciplinary (414 articles, 9.35%), geography (292 articles, 6.60%), ecology (243 articles, 5.49%), economics (213 articles, 4.81%), and development studies (163 articles, 3.68%). The number of various publications reflects the trend of climate change risk perception research in different fields. Between 2000 and 2022, the number of publications in environmental sciences, environmental studies and meteorology atmospheric sciences increased significantly, while the number of publications in other categories increased gradually.

3.5 Changes and trends of themes

In Figure 4A, the time periods analyzed are divided according to important time points (e.g., the enactment of important agreements). The themes are generated automatically by the analysis of Bibliometrix. The different themes were weighted by using a modified version of the inclusion index, taking into account the occurrences per period of each keyword appearing in a theme (Aria et al., 2020). In Figure 4B, motor theme means a theme that is currently being researched and is likely to become a hot topic for future research. The basic theme means that it is more basic and from which most other research is developed. A declining theme means that it is fading and will likely not be researched in the future. The niche theme means a theme of a small group that deviates from the main direction of research.

3.5.1 Change of the themes

In Figure 4A, we can find the change in the themes at different times, the influence of different events, and the future development trends. With the implementation of the *Kyoto Protocol* during the period 2000-2009, countries began to perceive climate change and gradually recognize the risks it poses. Therefore, during this period, the main themes were risk, science, temperature and information. In addition, the basic themes are science and climate change. After 2009, the themes were changed, when 129 countries discussed follow-up plans after the expiration of phase I commitments of the *Kyoto Protocol*. Between 2010 and 2015, they became adaptation, change and climate change, and it was determined that the motor theme was adaptation. The active participation of countries led to the signing of the Paris Agreement, which will cause a change in research direction. Moreover, countries' awareness of climate change risk perception is deepening. Therefore, COP25 was held in Madrid in 2019, and COP26 was held in Glasgow in 2021. The global perception of climate change is becoming stronger.

In fact, the keywords that shift from one period to another are also relevant. The shift from 9 keywords in the 2000-2009 period of research to 4 keywords in the 2010-2015 period of research indicates that scientists' research on climate change risk perception tends to be rational and targeted. The shift from temperature and environmental change in the first period (2000-2009) to climate change in the second period (200-2015) shows that scientists' research on climate change is gradually becoming systematic. From "adoption" in the

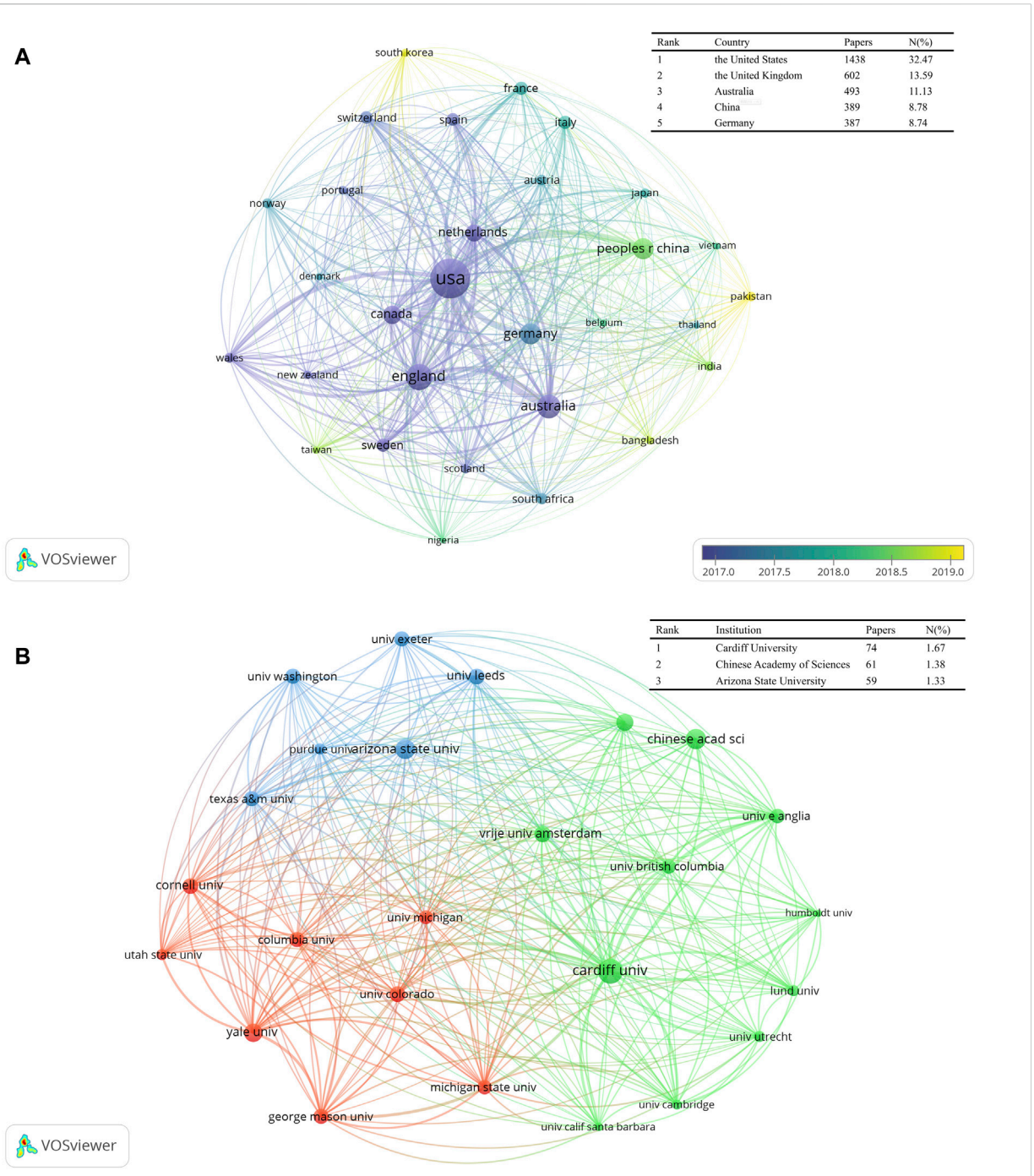

Rank	Country	Papers	N(%)
1	the United States	1438	32.47
2	the United Kingdom	602	13.59
3	Australia	493	11.13
4	China	389	8.78
5	Germany	387	8.74

Rank	Institution	Papers	N(%)
1	Cardiff University	74	1.67
2	Chinese Academy of Sciences	61	1.38
3	Arizona State University	59	1.33

FIGURE 5
The Network map of **(A)** the top 30 productive countries (top 30 countries with more than 45 documents) and **(B)** the top 25 institutions for research on climate change risk perception (top 25 institutions with more than 950 cited references).

second period and "policy" in the third period, we can see that people are increasingly trying to find solutions to the problems caused by climate change. In the fourth period (2020-2022), "impact" becomes one of the key words, indicating that scientists are looking for the far-reaching effects of climate change.

3.5.2 Trend of different themes during the period 2016-2022

Figure 4B depicts the status and development trend of different themes during the period 2016-2022. The main themes turned into policy, climate change and risk during 2015-2019 (Figure 4B).

TABLE 4 The Top 10 frequencies of author keywords and keywords used during 2000–2022.

Rank	Author keywords	Occurrence	Keywords plus	Occurrence
1	Climate change	1,256	Climate-change	1,559
2	Risk perception	407	Risk	909
3	Adaptation	381	Perceptions	644
4	Vulnerability	183	Adaptation	634
5	Climate change adaptation	146	Vulnerability	528
6	Resilience	134	Management	426
7	Risk	121	Policy	330
8	Perception	117	Impacts	326
9	Risk communication	100	Attitudes	314
10	Adaptive capacity	93	Knowledge	312

Meanwhile, the basic theme is risk, and the niche theme is policy. The motor theme is knowledge, and the declining theme is the model. More importantly, from this figure, we can see that the themes of "climat-change" and "risk" are becoming increasingly important. After this period, countries actively cooperated and took action to deal with climate change.

3.6 Active authors, countries and institutions

A total of 13333 authors were involved in the study of climate change risk perception. Table 3 illustrates the top 10 authors in the number of papers, total citations and *h*-index. In this topic, Leiserowitz A (School of the Environment Yale University) published the largest number of 32 papers, followed by Pidgeon N (28) and Siegrist M (26). Adger Wn has the highest total citations (5621), followed by Lorenzoni I (4317) and Leiserowitz A (3190). Meanwhile, Leiserowitz A has the highest *h*-index. Therefore, Leiserowitz A made a great contribution to this topic.

All of the papers were from 145 countries, among which the United States published the highest number of 1438 papers, accounting for 32.47%, followed by the United Kingdom (602 papers, 13.59%), Australia (493 papers, 11.13%), China (389 papers, 8.78%) and Germany (387 papers, 8.74%). Figure 5A shows the number of papers and collaborations among the 30 most productive countries. The table of the data of the top 5 countries is in the upper right corner. The size of the node in the figure indicates the number of papers. The larger the node is, the more papers there are (Li et al., 2019). Moreover, the thickness of the line between two points indicates the degree of contact between the two countries. It is obvious that China has the closest cooperative relationship with the United States and Australia. The color of the node in the figure from dark to light indicates the time sequence when the country began to study. We can see that the United States began research earlier, while China began research in recent years. This may be because the Obama administration (beginning in 2009) has established the action policy of building a green economy and developing new energy and explored new economic growth models to achieve America's economic recovery. However, starting from the construction of "The Belt and Road" (since 2015), China began to clearly implement the new concept of global governance, which is to build a community of human destiny to achieve win–win cooperation and common development.

Network maps can provide information about influential research institutions and potential collaborators and can help researchers establish collaborations (Shi et al., 2020). A total of 4063 institutions worldwide contribute to research on climate change risk perception. Figure 5B shows the top 25 institutions with the most contributions; in addition, the table about the information of the top 3 institutions is in the upper right corner. Cardiff University is ranked first, contributing 74 papers, accounting for 1.67%. Then, the Chinese Academy of Sciences published 61 papers (1.38%), followed by Arizona State University (59 papers, 1.33%). The graph also shows frequent exchanges between Cardiff University, Yale University, Chinese Academy of Sciences, the University of Queensland and Michigan State University.

3.7 Keyword analysis

3.7.1 Hotspots of keywords

The frequency analysis of keywords is key to investigating hot topics and developments associated with a given field (Wang, 2018). We use author keywords and keywords plus to explore hot issues and identify the research trends in this topic. Author keywords can provide important information about the core content and research trends (Ma and Zhang, 2020), while keywords plus are generated by an ISI algorithm from words or expressions of the article's reference titles (Huang et al., 2022).

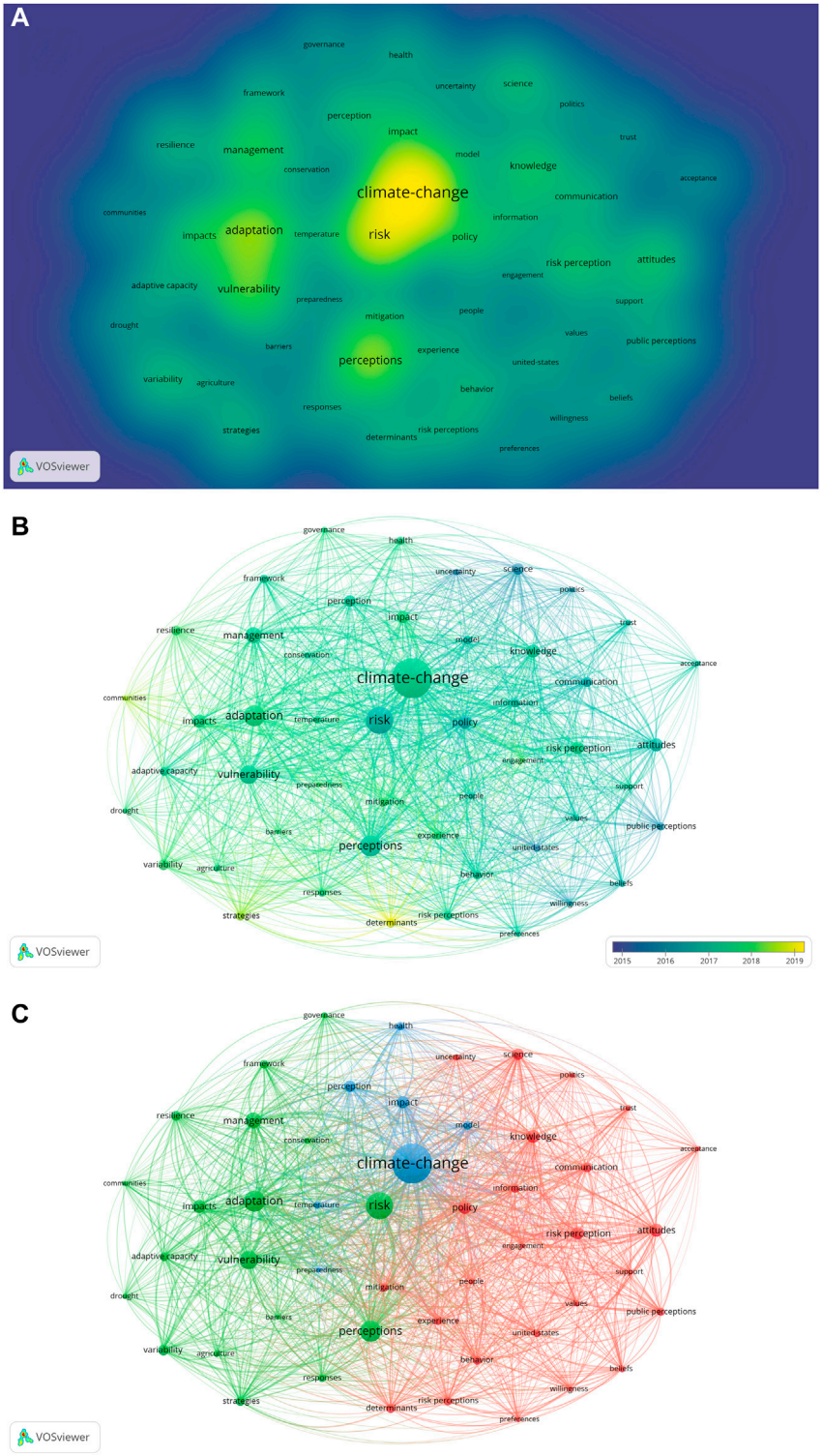

FIGURE 6
The Density **(A)**, overlay **(B)** and network **(C)** visualization map of keywords plus.

Except for the search terms in this study, the two most commonly used author keywords and keywords plus are all "adaptation" and "vulnerability" (Table 4). Meanwhile, “climate change adaptation” and “resilience” are also common keywords, and “management” and “policy” are common keywords plus. Figure 6A shows the density visualization (a function of VOSviewer) based on the keywords plus and the intensity of hot spots with the color spectrum, with warm red colors representing hot areas and cool blue colors representing cool areas (Zhang et al., 2020). In addition, the distance between them means the extent of their relationship, such as “climate-change”, “risk” and “policy”, are closer than other words.

3.7.2 Co-occurrence keyword analysis

Figure 6B is an overlay visualization map illustrating the keywords plus from 2015 to 2019. The yellower the color of the node in the figure is, the newer the keywords. The keywords in the blue region almost appeared before 2015. Obviously, most keywords have appeared in the past five years. This may reflect that climate change risk perception is a new field. In addition, Figure 6C shows network visualization, which consists of different nodes and wires. All these keywords are divided into 3 clusters, and the size of the node in the figure indicates the frequency of the keywords. The color of the nodes represents the cluster to which it belongs, and different clusters are represented by different colors. The red cluster focuses on policy, people and information about risk perception. The keywords with the highest frequency in the blue cluster are health and climate change. The green one concerns the influence of climate change risk perception in different fields: adaptation, strategy, vulnerability, management and agriculture.

4 Discussion

By summarizing the collected literature with a high number of citations in recent years and analyzing Figure 6C, we discuss the following topics. They largely reflect the hot spots of research in recent years and future trends.

4.1 Determinants of risk perception

The determinants affecting climate change risk perception are an important research topic (Figure 6C red cluster). At present, the relationship between education level and climate change risk perception has been basically confirmed (Lee et al., 2015). Research shows that the higher the level of education is, the sharper the risk perception of climate change. We argue that this is because higher educators have a better understanding of the phenomenon and connotations of climate change, and they are more likely to worry about the world. Moreover, experience is also an important factor affecting climate change risk perception. Usually, the elderly have more experience (Rufat and Botzen, 2022), especially compared the current climate with the climate of their youth, since they experience climate change longer than young people. At the same time, we found that beliefs and values also play an important role in perception ("beliefs” and “values” are all the keywords in the red cluster). Different beliefs pay different attention to climate, which leads to differences in perception. Some religions encourage believers to raise awareness of climate change and participate in environmental protection (Hornsey et al., 2016).

4.2 Human behavior

On the other hand, we can see that the red cluster also contains another core view of "behavior" (Figure 6C red cluster). First, human behavior is the main cause of global climate change (Ayal et al., 2021). At the same time, behavior is also bidirectional, which means that climate change will affect people’s behavior. Because of the drastic change in climate, people choose adaptive behavior and support for government policies to reduce personal losses (Xue et al., 2021). Research has shown that adaptation is essential to reduce or avoid the negative effects of climate change (Valkengoed and Steg, 2019). The majority of people actively or passively take actions conducive to the environment. At present, the government’s intervention policies are mainly divided into monetary intervention and nonmonetary intervention. Monetary intervention is often more able to motivate the public and achieve better results (Khanna et al., 2021). People preferably take action when they return from the government. However, when people take environmentally friendly actions for the first time, they are more likely to continue. In the future, we should continue to study what kind of intervention can improve people’s enthusiasm to take action to protect the environment.

4.3 Human mental health risk

Climate change will not only have an influence on human behavior but also have an important impact on public health, especially on mental health (Figure 6C blue cluster). Climate change can affect mental health through a variety of risk pathways (Cunsolo and Ellis, 2018), including the extinction of wild animals and the deterioration of the surrounding environmental landscape. People’s emotions are largely related to their environment. However, clinical medicine has not revealed the specific relationship between climate change and mental health (Brown et al., 2021). Grief is a normal response to the

deterioration of the environment, and this psychology will become more common with the aggravation of climate change, ultimately affecting the overall mental health of the public. In addition, this emotion may encourage them to take measures to protect the environment. While climate change will affect all people, some groups bear greater risks than others (Manning and Clayton, 2018). Generally, this emotion, grief, increases with the improvement of perception level. At the same time, women and children are easily affected, perhaps because of their relative psychological vulnerability. Researchers should further explore the specific relationship between climate change and mental health and strengthen counseling for the mental health of vulnerable people.

4.4 Impact on Agriculture

Climate change has an impact on almost all human production and life, especially on agricultural production (keyword "agriculture" in Figure 6C green cluster). Climate change has been shown to increase temperature and reduce precipitation, resulting in lower soil water content, which in turn affects agricultural production (Grusson et al., 2021). In fact, the agricultural production system is very fragile, and climate change will hinder the development of agriculture. Because they themselves heavily rely on the climate, it is difficult to make self-regulation in the short term. Therefore, farmers are required to actively adopt adaptive plans to adjust agricultural production. A study in Sri Lanka shows that farmers' adaptation measures can increase rice production (Suresh et al., 2021). However, farmers generally have limited capacity and are especially unable to cope with extreme weather and long-term climate risks caused by climate change. Relevant researchers should search for appropriate and targeted adaptive measures, guiding agricultural producers to implement.

4.5 Adaptive strategy

The continuous change in climate led to the attention of adaptive strategies (Figure 6C green cluster). However, based on existing traditional concepts, most people only accept adaptation strategies similar to the current situation (Tam and McDaniels, 2013). Nevertheless, these strategies often do not play a substantive role, and the adaptive effect is very small. This is closely related to people's conservative ideas. Some people even sacrifice their livelihood to maintain their original way of life. For example, some shrimp fishermen in Bangladesh tend to maintain their customs, resulting in a decline in production, which has also had a great impact on the development of the country. Therefore, governments should introduce adaptive policies. At the same time, natural and social scientists also need to contact and work with decision makers (Seddon et al., 2020). Moreover, in Figure 6B, we found that the word "adaptation" has only been studied in the last five years, which is also the key content of the Paris Agreement, signed in 2015 and implemented in 2016. Obviously, the signing of the Paris Agreement has promoted the emergence and development of adaptive policies. We suggest that climate change research should be guided by the international situation in the future.

4.6 Summary of discussion

This paper also reveals some characteristics and directions of current climate change risk perception. At present, research in this direction is relatively sufficient, but there are still some deficiencies. In the future, we should strengthen the research in the following aspects. First, it is important to explore the determinants that affect the public's risk perception of climate change. We should continue to reveal them, which will help to purposefully improve the perception level of the public. Then, governments should increase investment in research and intervention policies to encourage people to carry out adaptive behavior. Moreover, the research proves that climate change will lead to mental health diseases, but it does not reveal the specific relationship between them. Psychologists and environmentalists should cooperate in this research. On the other hand, climate change also causes an imbalance in the agricultural system. Farmers use adaptive methods, which is an effective way to solve the problem, but farmers' capability is limited, and they need further guidance from researchers. In addition, we find that moderate adaptation policies have little effect. Finally, the analysis shows that more cooperation between different research institutions is needed to maximize success (Chen et al., 2022).

Conclusion

The great impact of climate change on human society and global ecosystems has attracted the attention of the whole world. Although the importance of climate change is obvious, climate change risk perception still needs further research. This paper conducts a bibliometric analysis of the global research overview of climate change risk perception and provides relevant information, including countries, institutions, journals, articles, authors, hot topics and research trends. From 2000 to 2022, the publication of relevant articles gradually increased with increasingly serious climate change. Among them, articles published by the United States, the United Kingdom and Australia account for 57.19%. Cardiff University, the Chinese Academy of Sciences and Arizona State University are the top productivity institutions. *Climatic Change* and *Global Environmental Change-Human and Policy Dimensions* are the most productive and influential journals, respectively. Keywords co-occurrence analysis reveals three key research

topics: policy of risk perception, health and adaptation strategy. Determinations and strategies are recent research directions. At the same time, it reveals that the current climate change research has been interdisciplinary research involving the environment, politics, medicine, agriculture and other disciplines.

Data availability statement

The original contributions presented in the study are included in the article/supplementary material, further inquiries can be directed to the corresponding author/s.

Author contributions

JF: Methodology, Formal analysis, and Writing—Original Draft; GL: Conceptualization, Resources, Writing—Review & Editing and Funding acquisition; ZX: Methodology and Writing—Review & Editing; SC: Methodology and Writing—Review & Editing.

Funding

This work was supported by the International Cooperation and Exchange of the National Key Research and Development Program of China (2021YFC3201204).

Conflict of interest

The authors declare that the research was conducted in the absence of any commercial or financial relationships that could be construed as a potential conflict of interest.

Publisher's note

All claims expressed in this article are solely those of the authors and do not necessarily represent those of their affiliated organizations, or those of the publisher, the editors and the reviewers. Any product that may be evaluated in this article, or claim that may be made by its manufacturer, is not guaranteed or endorsed by the publisher.

References

Adger, W. N., Dessai, S., Goulden, M., Hulme, M., Lorenzoni, I., Nelson, D. R., et al. (2009). Are there social limits to adaptation to climate change? *Clim. Change* 93 (3), 335–354. doi:10.1007/s10584-008-9520-z

Adger, W. N. (2006). Vulnerability. *Glob. Environ. Change* 16 (3), 268–281. doi:10.1016/j.gloenvcha.2006.02.006

Aria, M., and Cuccurullo, C. (2017). bibliometrix: An R-tool for comprehensive science mapping analysis. *J. Informetr.* 11, 959–975. doi:10.1016/j.joi.2017.08.007

Aria, M., Misuraca, M., and Spano, M. (2020). Mapping the evolution of social research and data science on 30 Years of social indicators research. *Soc. Indic. Res.* 149 (3), 803–831. doi:10.1007/s11205-020-02281-3

Armah, F. A., Yengoh, G. T., Ung, M., Luginaah, I., Chuenpagdee, R., and Campbell, G. (2017). The unusual suspects? Perception of underlying causes of anthropogenic climate change in coastal communities in Cambodia and Tanzania. *J. Environ. Plan. Manag.* 60, 2150–2173. doi:10.1080/09640568.2017.1281797

Ayal, D. Y., Tilahun, K., Ture, K., and Terefe Zeleke, T. (2021). Psychological dimensions of climate change: Perceptions, collective efficacy, and responses in berehet district, north shoa, Ethiopia. *Clim. Change* 165 (1–2), 32. doi:10.1007/s10584-021-03033-z

Becerra, M. J., Pimentel, M. A., De Souza, E. B., and Tovar, G. I. (2020). Geospatiality of climate change perceptions on coastal regions: A systematic bibliometric analysis. *Geogr. Sustain.* 1 (3), 209–219. doi:10.1016/j.geosus.2020.09.002

Bradley, G. L., Babutsidze, Z., Chai, A., and Reser, J. P. (2020). The role of climate change risk perception, response efficacy, and psychological adaptation in pro-environmental behavior: A two nation study. *J. Environ. Psychol.* 68, 101410. doi:10.1016/j.jenvp.2020.101410

Brechin, S. R., and Bhandari, M. P. (2011). Perceptions of climate change worldwide. *Wiley Interdiscip. Rev. Clim. Change* 2, 871–885. doi:10.1002/wcc.146

Brown, M. J., White, B. P., and Nicholas, P. K. (2021). Mental health impacts of climate change: Considerations for nurse practitioners. *J. Nurse Pract.* 18, 359–363. doi:10.1016/j.nurpra.2021.07.013

Brulle, R. J., Carmichael, J., and Jenkins, J. C. (2012). Shifting public opinion on climate change: An empirical assessment of factors influencing concern over climate change in the U.S., 2002–2010. *Clim. Change* 114, 169–188. doi:10.1007/s10584-012-0403-y

Callaghan, M. W., Minx, J. C., and Forster, P. M. (2020). A topography of climate change research. *Nat. Clim. Chang.* 10, 118–123. doi:10.1038/s41558-019-0684-5

Chen, Y., Lin, M., and Zhuang, D. (2022). Wastewater treatment and emerging contaminants: Bibliometric analysis. *Chemosphere* 297, 133932. doi:10.1016/j.chemosphere.2022.133932

Cunsolo, A., and Ellis, N. R. (2018). Ecological grief as a mental health response to climate change-related loss. *Nat. Clim. Chang.* 8, 275–281. doi:10.1038/s41558-018-0092-2

Dryhurst, S., Schneider, C. R., Kerr, J., Freeman, A. L. J., Recchia, G., van der Bles, A. M., et al. (2020). Risk perceptions of COVID-19 around the world. *J. Risk Res.* 23 (7–8), 994–1006. doi:10.1080/13669877.2020.1758193

Estrada, A., Garber, P. A., Rylands, A. B., Roos, C., Fernandez-Duque, E., Di Fiore, A., et al. (2017). Impending extinction crisis of the world's primates: Why primates matter. *Sci Adv.* 3 (1), e1600946. Published January 18, 2017. doi:10.1126/sciadv.1600946

Fei, S., Desprez, J. M., Potter, K. M., Jo, I., Knott, J. A., and Oswalt, C. M. (2017). Divergence of species responses to climate change. *Sci. Adv.* 3, e1603055. doi:10.1126/sciadv.1603055

Funatsu, B. M. (2019). Perceptions of climate and climate change by Amazonian communities. *Glob. Environ. Change* 57, 101923. doi:10.1016/j.gloenvcha.2019.05.007

Gatto, M., Bertuzzo, E., Mari, L., Miccoli, S., Carraro, L., Casagrandi, R., et al. (2020). Spread and dynamics of the COVID-19 epidemic in Italy: Effects of emergency containment measures. *Proc. Natl. Acad. Sci. U. S. A.* 117 (19), 10484–10491. doi:10.1073/pnas.2004978117

Gifford, R. (2011). The dragons of inaction: psychological barriers that limit climate change mitigation and adaptation. *Am. Psychol.* 66 (4), 290–302.

Grothmann, T., and Patt, A. (2005). Adaptive capacity and human cognition: The process of individual adaptation to climate change. *Glob. Environ. Change-Human and Pol. Dimensions* 15, 199–213.

Grusson, Y., Wesström, I., and Joel, A. (2021). Impact of climate change on Swedish agriculture: Growing season rain deficit and irrigation need. *Agric. Water Manag.* 251, 106858. doi:10.1016/j.agwat.2021.106858

Hornsey, M. J., Harris, E. A., Bain, P. G., and Fielding, K. S. (2016). Meta-analyses of the determinants and outcomes of belief in climate change. *Nat. Clim. Chang.* 6 (6), 622–626. doi:10.1038/nclimate2943

Howe, P. D., Mildenberger, M., Marlon, J. R., and Leiserowitz, A. (2015). Geographic variation in opinions on climate change at state and local scales in the USA. *Nat. Clim. Chang.* 5 (6), 596–603. doi:10.1038/nclimate2583

Huang, L., Xia, Z., and Cao, Y. (2022). A bibliometric analysis of global fine roots research in forest ecosystems during 1992–2020. *Forests* 13 (1), 93–16. doi:10.3390/f13010093

Kahan, D., Jenkins-Smith, H. C., and Braman, D. (2011). Cultural cognition of scientific consensus. *J. Risk Res.* 14, 147–174.

Khanna, T. M., Baiocchi, G., Callaghan, M., Creutzig, F., Guias, H., Haddaway, N. R., et al. (2021). A multi-country meta-analysis on the role of behavioural change in reducing energy consumption and CO2 emissions in residential buildings. *Nat. Energy* 6 (9), 925–932. doi:10.1038/s41560-021-00866-x

Lee, I. (2017). Big data: Dimensions, evolution, impacts, and challenges. *Bus. Horizons* 60, 293–303. doi:10.1016/j.bushor.2017.01.004

Lee, T. M., Markowitz, E. M., Howe, P. D., Ko, C. Y., and Leiserowitz, A. A. (2015). Predictors of public climate change awareness and risk perception around the world. *Nat. Clim. Chang.* 5 (11), 1014–1020. doi:10.1038/nclimate2728

Leiserowitz, A. (2005). American risk perceptions: Is climate change dangerous? *Risk Anal.* 25, 1433–1442. doi:10.1111/j.1540-6261.2005.00690.x

Leiserowitz, A. (2006). Climate change risk perception and policy preferences: The role of affect, imagery, and values. *Clim. Change* 77 (1), 45–72. doi:10.1007/s10584-006-9059-9

Li, C., Wu, K., and Wu, J. (2017). A bibliometric analysis of research on haze during 2000–2016. *Environ. Sci. Pollut. Res.* 24, 24733–24742. doi:10.1007/s11356-017-0440-1

Li, H. (2019). An analysis of research hotspots and modeling techniques on carbon capture and storage. *Sci. Total Environ.* 687, 687–701. doi:10.1016/j.scitotenv.2019.06.013

Lorenzoni, I., and Pidgeon, N. F. (2006). Public views on climate change: European and USA perspectives. *Clim. Change* 77, 73–95.

Lorenzoni, I., Nicholson-Cole, S. A., and Whitmarsh, L. (2007). Barriers perceived to engaging with climate change among the UK public and their policy implications. *Glob. Environ. Change-Human and Pol. Dimensions* 17, 445–459.

Ma, Q., and Zhang, Y. (2020). Global research trends and hotspots on submarine groundwater discharge (sgd): A bibliometric analysis. *Int. J. Environ. Res. Public Health* 17, 830. doi:10.3390/ijerph17030830

Madeira, C., Mendonca, V., Leal, M. C., Flores, A. A., Cabral, H. N., Diniz, M. S., et al. (2018). Environmental health assessment of warming coastal ecosystems in the tropics - application of integrative physiological indices. *Sci. Total Environ.* 643, 28–39. doi:10.1016/j.scitotenv.2018.06.152

Manning, C., and Clayton, S. (2018). "9 - threats to mental health and wellbeing associated with climate change," in *Psychology and climate change*. Editors S. Clayton and C. Manning (New York: Academic Press), 217–244. doi:10.1016/B978-0-12-813130-5.00009-6

Mongeon, P., and Paul-Hus, A. (2015). The journal coverage of Web of science and scopus: A comparative analysis. *Scientometrics* 106, 213–228. doi:10.1007/s11192-015-1765-5

Nadelhoffer, K. J., and Raich, J. W. (1992). Fine root production estimates and belowground carbon allocation in forest ecosystems. *Ecology* 73, 1139–1147. doi:10.2307/1940664

Nunez Mir, G. C., Iannone, B. V., Pijanowski, B. C., Kong, N., and Fei, S. (2016). Automated content analysis: Addressing the big literature challenge in ecology and evolution. *Methods Ecol. Evol.* 7, 1262–1272. doi:10.1111/2041-210x.12602

Parry, M. L., Rosenzweig, C., Iglesias, A., Livermore, M., and Fischer, G. (2004). Effects of climate change on global food production under SRES emissions and socio-economic scenarios. *Glob. Environ. Change* 14 (1), 53–67. doi:10.1016/j.gloenvcha.2003.10.008

Parvin, G. A., and Ahsan, M. S. (2013). Impacts of climate change on food security of rural poor women in Bangladesh. *Manag. Environ. Qual. Int. J.* 24, 802–814. doi:10.1108/meq-04-2013-0033

Rana, I. A. (2020). Disaster and climate change resilience: A bibliometric analysis. *Int. J. Disaster Risk Reduct.* 50, 101839. doi:10.1016/j.ijdrr.2020.101839

Rufat, S., and Botzen, W. J. W. (2022). Drivers and dimensions of flood risk perceptions: Revealing an implicit selection bias and lessons for communication policies. *Glob. Environ. Change* 73, 102465. doi:10.1016/j.gloenvcha.2022.102465

Seddon, N. (2020). Understanding the value and limits of nature-based solutions to climate change and other global challenges. *Philosophical Trans. R. Soc. B Biol. Sci.* 375, 1794. doi:10.1098/rstb.2019.0120

Shi, J., Shi, S., Shi, S., Jia, Q., Yuan, G., Chu, Y., et al. (2020). Bibliometric analysis of potassium channel research. *Channels* 14 (1), 18–27. doi:10.1080/19336950.2019.1705055

Slovic, P. (2020). Risk perception and risk analysis in a hyperpartisan and virtuously violent world. *Risk Anal.* 40, 2231–2239. doi:10.1111/risa.13606

Spence, A., Poortinga, W., Butler, C., and Pidgeon, N. F. (2011). Perceptions of climate change and willingness to save energy related to flood experience. *Nat. Clim. Chang.* 1 (1), 46–49. doi:10.1038/nclimate1059

Suresh, K. (2021). An economic analysis of agricultural adaptation to climate change impacts in Sri Lanka: An endogenous switching regression analysis. *Land Use Policy* 109, 105601. doi:10.1016/j.landusepol.2021.105601

Tam, J., and McDaniels, T. L. (2013). Understanding individual risk perceptions and preferences for climate change adaptations in biological conservation. *Environ. Sci. Policy* 27, 114–123. doi:10.1016/j.envsci.2012.12.004

Tamala, J. K., Maramag, E. I., Simeon, K. A., and Ignacio, J. J. (2022). A bibliometric analysis of sustainable oil and gas production research using VOSviewer. *Clean. Eng. Technol.* 7, 100437. doi:10.1016/j.clet.2022.100437

United Nations (2015). "'Adoption of the Paris agreement, proposal by the president, Draft decision'," in *Conference of the parties* (FCCC), 32. Available at: http://unfccc.int/resource/docs/2015/cop21/eng/l09r01.pdf.

Valkengoed, A. M. V., and Steg, L. (2019). Meta-analyses of factors motivating climate change adaptation behaviour. *Nat. Clim. Chang.* 9, 158–163. doi:10.1038/s41558-018-0371-y

van Eck, N. J., and Waltman, L. (2010). Software survey: VOSviewer, a computer program for bibliometric mapping. *Scientometrics* 84 (2), 523–538. doi:10.1007/s11192-009-0146-3

Wang, B. (2018). Role of renewable energy in Chins energy security and climate change mitigation: An index decomposition analysis. *Renew. Sustain. Energy Rev.* 90, 187–194. doi:10.1016/j.rser.2018.03.012

Wang, Z., Zhao, Y., and Wang, B. (2018). A bibliometric analysis of climate change adaptation based on massive research literature data. *J. Clean. Prod.* 199, 1072–1082. doi:10.1016/j.jclepro.2018.06.183

Whitmarsh, L. (2008). Are flood victims more concerned about climate change than other people? The role of direct experience in risk perception and behavioural response. *J. Risk Res.* 11, 351–374.

Weber, E. U. (2006). Experience-based and description-based perceptions of long-term risk: Why global warming does not scare us (yet). *Clim. Change* 77 (1), 103–120. doi:10.1007/s10584-006-9060-3

World Meteorological Organization (2019). The global climate in 2015 - 2019. *Centre Res. Epidemiol. Disasters Natl. Inst. Space Res.* 1179, 32. Available at: https://library.wmo.int/doc_num.php?explnum_id=10251.

Wu, F., Geng, Y., Tian, X., Zhong, S., Wu, W., Yu, S., et al. (2018). Responding climate change: A bibliometric review on urban environmental governance. *J. Clean. Prod.* 204, 344–354. doi:10.1016/j.jclepro.2018.09.067

Xue, M., Zhao, Y., Wang, Z., and Zhang, B. (2021). Behavioural determinants of an individual's intention to adapt to climate change: Both internal and external perspectives. *Environ. Impact Assess. Rev.* 91, 106672. doi:10.1016/j.eiar.2021.106672

Yang, L. E., Chan, F. K. S., and Scheffran, J. (2018). Climate change, water management and stakeholder analysis in the Dongjiang River basin in South China. *Int. J. Water Resour. Dev.* 34, 166–191. doi:10.1080/07900627.2016.1264294

Zhang, Y., Pu, S., Lv, X., Gao, Y., and Ge, L. (2020). Global trends and prospects in microplastics research: A bibliometric analysis. *J. Hazard. Mater.* 400, 123110. doi:10.1016/j.jhazmat.2020.123110

Zhao, L., Deng, J., Sun, P., Liu, J., Ji, Y., Nakada, N., et al. (2018). Nanomaterials for treating emerging contaminants in water by adsorption and photocatalysis: Systematic review and bibliometric analysis. *Sci. Total Environ.* 627, 1253–1263. doi:10.1016/j.scitotenv.2018.02.006

frontiers | Frontiers in Environmental Science

TYPE Original Research
PUBLISHED 05 December 2022
DOI 10.3389/fenvs.2022.1025760

OPEN ACCESS

EDITED BY
Dabang Jiang,
Institute of Atmospheric Physics (CAS), China

REVIEWED BY
Mojisola Oluwayemisi Adeniyi,
University of Ibadan, Nigeria
Mohammad Zakwan,
Maulana Azad National Urdu University, India
Rajneesh Singh,
University of Minnesota Twin Cities, United States
Santosh S. Palmate,
Texas A&M AgriLife Research and Extension Center at El Paso, United States

*CORRESPONDENCE
Jahangeer Jahangeer,
jahangeer.tomar@gmail.com
Vikram Kumar,
25.vikram@gmail.com

†These authors have contributed equally to this work

SPECIALTY SECTION
This article was submitted to Interdisciplinary Climate Studies, a section of the journal Frontiers in Environmental Science

RECEIVED 23 August 2022
ACCEPTED 17 November 2022
PUBLISHED 05 December 2022

CITATION
Nyembo LO, Mwabumba M, Jahangeer J and Kumar V (2022), Historical and projected spatial and temporal rainfall status of Dar es Salaam, Tanzania, from 1982 to 2050. *Front. Environ. Sci.* 10:1025760. doi: 10.3389/fenvs.2022.1025760

Historical and projected spatial and temporal rainfall status of Dar es Salaam, Tanzania, from 1982 to 2050

Latifa O. Nyembo[1†], Mohamed Mwabumba[2†], Jahangeer Jahangeer[3*†] and Vikram Kumar[4*]

[1]Petroleum Upstream Regulatory Authority, Dar es Salaam, Tanzania, [2]Tanzania Meteorological Authority (TMA), Dar es Salaam, Tanzania, [3]Department of Environmental Science, Jamia Millia Islamia, New Delhi, India, [4]Bihar Mausam Seva Kendra, Patna, India

Dar es Salaam, like other cities in Africa, experiences flash floods during the rainfall season that destroy infrastructure due to the overflow of rivers and blocked sewage. This study investigates the historical and future variability and changes in spatial and temporal rainfall over Dar es Salaam. Station data and Climate Hazards Group Infrared Precipitation with Stations (CHIRPS) gridded data crossing 38 years (1982–2019) were used as a baseline and the Coordinated Regional Climate Downscaling Experiment (CORDEX) dataset from 2021 to 2050 was used for projection under Representative Concentration Pathway (RCP 4.5) forcing scenarios. A trend analysis of historical data was conducted at monthly, seasonal, and annual timescales. Mann–Kendall statistical tests and Sen's slope estimator were applied to identify the current trend direction and magnitude of changes in rainfall patterns over time. A standardized anomaly index (SAI) was also employed to detect the region's trends in wetness and dryness. The spatial distribution of rainfall in the city was investigated using an inverse distance weighted (IDW) interpolation technique. The statistical results reveal that a non-significant trend in rainfall was observed on monthly, seasonal, and annual timescales. Generally, in the future (2021–2050), the annual cycle of rainfall shows a slight decrease in monthly rainfall, especially from January to August, and an increase from September to December compared to historical (1982–2019) rainfall, for most of studied locations. Spatially, the distribution of projected rainfall shows that the southern part of the city will experience higher rainfall than other parts. The most significant findings were a decrease in annual projected rainfall by 20%, the MAM projected rainfall season increased by 42%, and an increase of 38% of the OND-projected rainfall season. The findings of this study will be useful for the improved management and planning of the city.

KEYWORDS

rainfall, historical, projection, spatial and temporal distribution, statistical analysis

1 Introduction

Globally, climate change challenge is the latest challenge facing humanity, and nations must unite to address it in their communities (Nyatichi, 2015; Mwabumba et al., 2022a). Climate change and variability are believed to be a catastrophic phenomenon, which have potential implications for almost every global goal for sustainable development. Changes and variability have already been observed and associated with extreme weather events like floods, drought, and heat waves. These extreme events are becoming increasingly unpredictable and result in worsening climatic impact on socioeconomic activities (Pachauri and Meyer, 2014; JahangeerGupta and Yadav, 2017; Kumar, 2017). Furthermore, the uneven distribution of climate change and variability impacts are a specific feature in some parts of the world with significant reductions in precipitation or major alterations in the timing of future wet and dry seasons (Kumar, 2017; Kumar et al., 2022). In Sub-Saharan Africa, climate change and variability pose a very serious challenge to the social, economic, and ecological system (Kotir, 2011). Several researchers in Africa observed that the current changes in climate conditions have resulted in changes in the rainfall patterns of different regions (Meshram et al., 2018; Sipayung et al., 2018).

These major patterns include increased rainfall trends in wet areas and decreases in dry areas (Luhunga et al., 2018; Borhara et al., 2020). In recent decades, East Africa has been affected by increased extreme rainfall events, which often translate into hazards (Odulami et al., 2018). The socio-climatic impacts of such climate-related extremes include the alteration of ecosystems (Palmate et al., 2021), disruption of food production (Palmate et al., 2022) and water supply (Kumar and Sen, 2020), and damage to infrastructure (JahangeerGupta and Yadav, 2018; Zakwan et al., 2018) and settlements (Maskrey et al., 2007). Unfortunately, these social and economic impacts, which threaten some sectors, such as food security, tourism, and hydropower plants, directly affect economic development around the country (Irish, 2016; Umar et al., 2022; Kumar et al., 2021). These effects are most consistently experienced during rainfall seasons with a significant lack of preparedness for current climate variability in many sectors (Tschakert et al., 2010; Ddamulira, 2016).

In Tanzania, the impact of climate change has already been felt in various parts of the country, and studies (Luhunga et al., 2018; Borhara et al., 2020) indicate that rainfall will be significantly impacted in future scenarios. For instance, Luhunga et al. (2018) predicted an increased intensity of extreme rainfall events in the northeastern highlands and coastal parts of the country. However, due to the complexity of the geographical patterns of the country, the future variability of weather and climate and occurrence of extreme events differ from place to place.

Therefore, localized studies to capture climate variability and the associated extremes and impacts are vital for planning climate change adaptation measures. Studies have been conducted to explore the spatial and temporal climate change and climate variability around the country (Luhunga et al., 2018; Borhara et al., 2020), but few studies (Mzava et al., 2020; Nyembo et al., 2021; Mwabumba et al., 2022b) have analyzed the climate variability at local scales. However, little has been carried out to determine climate variability and its associated extremes and impacts in the cities and towns with large populations and major economic activities. For example, Anande and Park (2021) examined the local climatic impacts associated with projected urban growth by simulating rainfall and temperature over the rapidly growing cities of the middle-eastern region in Tanzania. However, this study was only conducted for 10 days during the rainfall season in April 2018 and suggests further research to understand the effects of urbanization on the future climate in large cities. Therefore, this study investigates the historical and future variability and changes in spatial and temporal rainfall over Dar es Salaam city in planning for adaptation measures.

Dar es Salaam plays an important role as a major city and has a large port and harbor that provides services and goods for the neighboring countries. The city has experienced rapid urbanization, population growth, climate change, and variability with the increase in frequency and intensity of flood occurrence. However, the combination of the challenges in the region lead to flash floods during the rainfall season that lead to the destruction of infrastructure due to the overflow of rivers and blockage of sewage. Considering the high vulnerability of Dar es Salaam to climate extremes, an in-depth local-scale climatic assessment is required. Therefore, the focus of the present study was to analyze the future changes in precipitation under Representative Concentration Pathway (RCP 4.5) forcing scenarios. The study considered RCP 4.5 to accommodate stabilized radiative forces around 2050 and influenced by the current effort to reduce greenhouse gas emissions (San José et al., 2016). The study applied station data and Climate Hazards Group Infrared Precipitation with Stations (CHIRPS) data spanning 38 years (1982–2019) as a baseline and the CORDEX dataset from 2021–2050 for projection under RCP 4.5 forcing scenarios. These findings will provide a better understanding of the future changes in precipitation that may have critical impacts on the development of Dar es Salaam. The findings will further help meet the Sustainable Development Goal (SDG) 11 in building sustainable cities and communities in the 2030s.

2 Methods

2.1 Study area

This study was conducted in Dar es Salaam, located on the northern coast of Tanzania, between latitudes 6.36°S and 7°S and longitude 33.33°S and 39°E with an elevation of 53 m above the

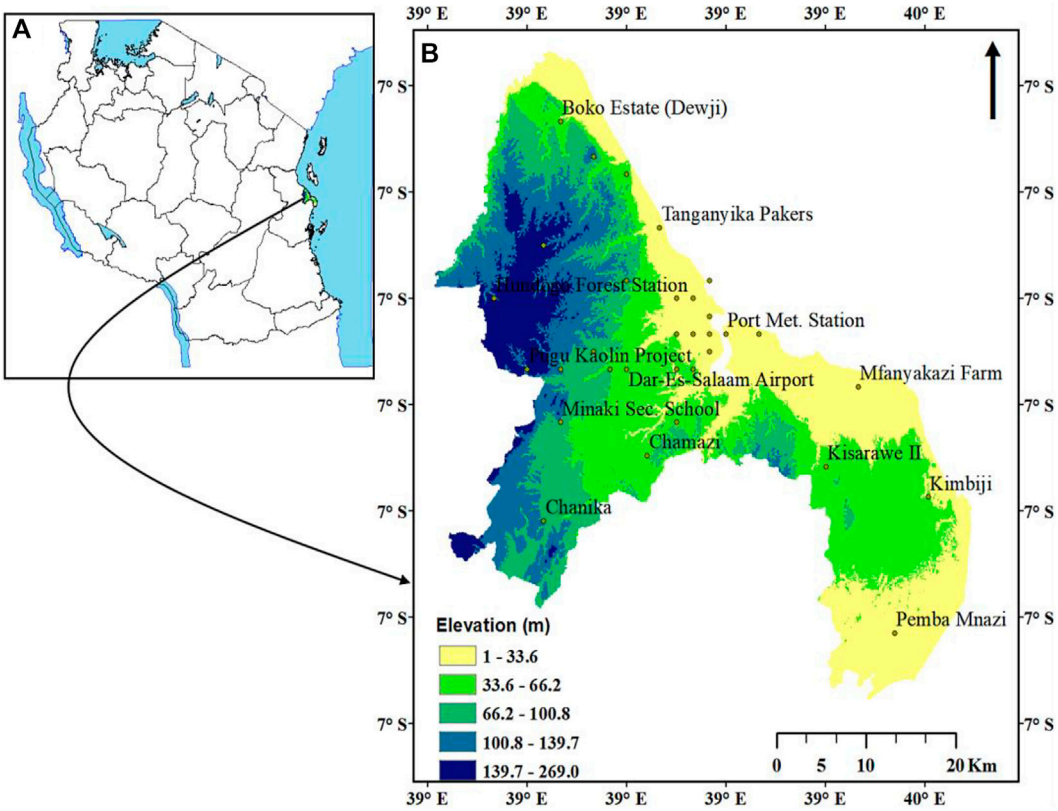

FIGURE 1
The study area map, showing Tanzania **(A)** and Dar es Salaam region with the location of meteorological stations **(B)**.

mean sea level (Figure 1). The area is also characterized by the variation of the elevation level in which the western part experiences the highest elevation and the southern part experiences the lowest elevation. The climate is a tropical type characterized by the warm Indian Ocean. Climatologically, the city experiences two different rainfall seasons: the long rainfall seasons and the short rainfall seasons. The long seasons (Masika) start in March, April, and May (MAM), while the shortest rainfall seasons start in October, November, and December. These rainfall seasons are mainly attributed to the Inter-Tropical Convergence zone (ITCZ) movement, which moves southward in October, reaches the southern part of the country in January or February, and reverses northward in March, April, and May. The average annual rainfall at Dar es Salaam is approximately 1146 mm. The main economic activities of the study area are business and industrial development. The area also has a large population compared to the other regions of the country.

TABLE 1 Stations used in the study.

No.	Station name	Longitude	Latitude
1	Chanika	39.1	−7.0
2	Chamazi	39.2	−6.9
3	Kisarawe II	39.4	−7.0
4	Kimbiji	39.5	−7.0
5	Pemba Mnazi	39.5	−7.1
6	Hundogo forest station	39.1	−6.8
7	Pugu kaolin project	39.1	−6.9
8	Minaki Sec. School	39.1	−6.9
9	Malindi Institution	39.3	−6.9
10	Tanganyika Packers	39.2	−6.7
11	Boko estate (Dewji)	39.1	−6.6
12	Mfanyakazi Farm	39.4	−6.9
13	Port Met	39.3	−6.8
14	Julius Nyerere Int. Airport	39.2	−6.9

2.2 Climate data

Monthly observed rainfall data from 1982 to 2019 were collected from the Tanzania Meteorological Authority (TMA). The study used rainfall data only for the Julius Nyerere International Airport (JNIA) and Port Meteorological stations due to poor observation networks and the unavailability of

station data for an extended period (more than 30 years). The city has more than 30 stations but only two have adequate climatic data; therefore, the study applied daily precipitation data from the Climate Hazards Group Infrared Precipitation with Station (CHIRPS) at 0.05° resolution (Funk et al., 2015) for analysis. The study used fourteen (14) station points (Table1), including two stations (Julius Nyerere International Airport and Port Met) with observed data, to analyze the climate of the study area.

2.3 Data quality control

A data quality control was performed by validation of the CHIRPS data using two TMAs observed stations' data for the period 1990–2000 and using the Pearson correlation coefficient (r), the Nash–Sutcliffe efficiency (NSE) and the percentage bias (PBIAS) described in Larbi et al. (2018) and Mwabumba et al. (2022b). Furthermore, CHIRPS data were applied in the gape and filled in for the missing values in observed rainfall data.

2.4 Trend and magnitude detection of the historical period

Using the Mann–Kendall (MK) statistical test, the monthly and annual trend analysis for twelve chosen stations was investigated. The World Meteorological Organization (WMO) recommended the Mann–Kendall statistical test as the most effective method for evaluating trends in the environmental data time series (Huret and Legras, 2014). The test to determine whether specific climate parameters, such as rainfall, were statistically significant was performed using the R software version 4.1.1. Trend analysis of climatic parameters is very sensitive to various factors, and the selection of appropriate statistical techniques is important among the available tests to reach reliable trend results (Abolverdi et al., 2016). Therefore, in the present study, the following methodology was followed for rainfall trend analysis:

1. Descriptive statistics of monthly and seasonal rainfall for the study location were calculated and used for the period 1982–2019.
2. MK and linear regression techniques were used to extract months and seasons and showed a significant trend at a 90% level. Only those periods, which commonly fall into the 90% level of significance of MK and the linear regression test, were extracted and used in the analysis. The results and therefore the extracted data obtained using linear regression and MK in this study were not supplementary but complementary to each other.

The significant period obtained using linear regression was used to obtain the MMKT trend. The annual rainfall trends in the current study were computed with a 95% confidence level (Yavuz and Erdoan, 2012). The MK tests (Eqs 1–5) were used to calculate the slope of the line formed by plotting the variable of interest against time but only considers the sign and not the magnitude of the slope. The MK statistic S was computed as follows:

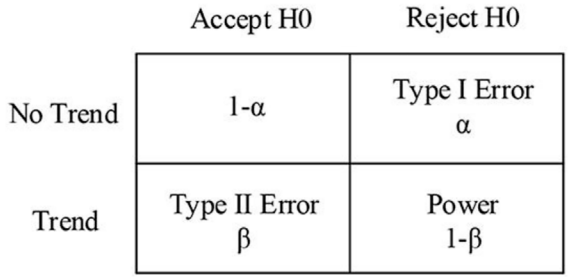

FIGURE 2
Probability matrix for the MK test.

$$S = \sum_{k=1}^{n-1} \sum_{j=k+1}^{n} \operatorname{sgn}\left(x_j - x_k\right), \tag{1}$$

where x_j and x_k are sequential data values for the time series data of length n. The sgn series is defined as:

$$\operatorname{sgn}(x) = \begin{cases} +1 \ldots\ldots if \ldots\ldots\ldots (x_j - x_k) > 0, \\ 0 \ldots\ldots\ldots if \ldots\ldots\ldots (x_j - x_k) = 0, \\ -1 \ldots\ldots if \ldots\ldots\ldots (x_j - x_k) < 0. \end{cases} \tag{2}$$

Whenever there is an identical and independent dataset distribution, the mean of S is zero, whereas the variance of S is given by Eq. 3.

$$Var(S) = \frac{n(n-1)(2n+5) - \sum_{i=1}^{m} t_i (t_i - 1)(2t_i + 5)}{18}, \tag{3}$$

where t_i is the extent of any given tie. Σt_i denotes the summation over all ties and is only used if the data series contains tied values. The standard normal variate Z is calculated as indicated in Eq. 4:

$$Z = \begin{cases} \frac{S+1}{\sqrt{Var(S)}} if \rightarrow S > 0, \\ 0 \ldots\ldots\ldots if \rightarrow S = 0, \\ \frac{S-1}{\sqrt{Var(S)}} if \rightarrow S < 0. \end{cases} \tag{4}$$

The trend decreases if Z is negative and increases if Z is positive. H_0, the null hypothesis of no trend, is rejected if the absolute value of Z is greater than $Z1$- α/2, where Z1- α/2 is obtained from the standard normal cumulative distribution tables.

2.4.1 Significance of the MK test

For the statistical hypothesis test, the significance level α is the probability of rejecting the null hypothesis when there is no

trend. The power of the MK test is the probability of rejecting the null hypothesis, 1−β, when there is a trend contained in the data sample as shown in Figure 2.

While applying the hypothesis test, the Type I error can be controlled by the significance level α, but the Type II error depends on the sample length in addition to α. In specific cases, the Type II error should also be controlled in addition to reducing the Type I error, especially when the MK test is associated with hydropower station design, flood risk assessment, and water quality evaluation.

2.4.2 Sen's slope estimator

Sen's slope estimation technique is a typical non-parametric method of estimating the slope of the regression line, which fits a pair of elements in the vector of (x, y) based on the least square method. The median of all Sen's slope values for different years is the final slope indicating the magnitude of the whole vector of data. Eqs 5, 6 are other nonparametric methods for trend analysis of the rainfall dataset. They are used to detect the magnitude of the trend from the direction trend of the Mann–Kendall statistical test (Sen, 1968). The methods use a linear model to calculate the change of the slope, and the variance of the residuals should be constant in time

$$Q_i = \frac{\left(X_j - X_k\right)}{\left(j - k\right)} \, for \, all \quad k < j \, and \, i = 1, ..N, \tag{5}$$

$$Q_{med} = \begin{cases} Q\left[\frac{(n+1)}{2}\right], & \text{where } N \text{ is odd,} \\ Q\left(\frac{N}{2}\right) + Q\left[\frac{N+2}{2}\right], & \text{where } N \text{ is even,} \end{cases} \tag{6}$$

where Q_i is the slope between data points X_j and X_k and Q_{med} is the median slope estimator, which reflects the direction of the trend in the data.

2.5 Standardized anomaly index

A standard anomaly index of rainfall was calculated to examine the nature of trends. It enables the determination of dry and wet years in the record and is used to assess the frequency and severity of drought; it is computed as Eq. 7.

$$SAI_i = \frac{x_i - \bar{x}}{\sigma}, \tag{7}$$

where Xi is the annual rainfall of the particular year, X is the long-term mean annual rainfall throughout the observation period, and σ is the standard deviation of annual rainfall throughout the observation. Negative values indicate a drought period compared to the chosen reference period, while the positive values indicate a wet situation. SAI is also computed for the seasonal scale, and the SAI value classification is presented in Table 2.

TABLE 2 SAI value classification (McKee et al., 1993).

SAI value	Category
Above 2	Extremely wet
1.5 to 1.99	Very wet
1.0 to 1.49	Moderately wet
−0.99 to 1.49	Near normal
−1.0 to −1.49	Moderately dry
−1.5 to −1.99	Severely dry
−2 or less	Extremely dry

2.6 Future projection data 2021–2050

The ensemble model can be downloaded from http://www.cordexesg.dmi.dk/esgf-web-fe/. Africa datasets provided the future climate information used in this investigation. Furthermore, future climatic data over the city of Dar es Salaam were obtained using the Coordinated Regional Climate Downscaling Experiment (CORDEX) Africa simulation data from four regional climate models (Table 3). For the typical concentration pathway (RCP 4.5) scenario of climate change, the simulated data were from the historical period (1971–2005) and then for the near future (2021–2050). To observe regional and temporal variability, the climatic data for Dar es Salaam were evaluated per historical data.

2.7 Spatial distribution analysis of rainfall

The study applied an inverse distance weighted (IDW) interpolation technique in Arc GIS to analyze the spatial distribution of rainfall in the study area for the historical (1982–2019) and future (2021–2050) periods. The IDW interpolation method averages the points while giving the closest neighbors' points greater weight (Shepard, 1968).

Eq. 8 provides the IDW approach as follows:

$$w\left(d\right) = \frac{1}{d^p}, \quad p > 0 \tag{8}$$

where p is the number of points, d is the distance between points, and w is the weighting function.

3 Results and discussion

3.1 Validation of CHIRPS data

The statistical results of CHIRPS rainfall data showed r = 0.96, NSE = 0.82, PBIAS = −8.2, and r = 0.97, NSE = 0.85, and PBIAS = −12.7 for the Nyerere International Airport and Port Met stations, respectively, on a monthly timescale. Therefore,

TABLE 3 Characteristics of the CORDEX-Africa models used (Luhunga et al., 2018).

RCM	Model center	Short name of RCM	GCM
CLM com COSMO-CLM (CCLM4)	Climate Limited- Area Modelling (CLM) Community	CCLM4	MPI-ICHEC CNRM
DMI HIRHAMS	Darmarks Meteorologiske Instut (DMI) Danmark	HIRHAMS	ICHEC
SMHI Rossby Atmospheric Climate Model (RCA4)	Sveriges Meteorologiske Och Hydrologisks Instut (SMHI) Sweden	RCA 4	MPI-ICHEC CNRM
KNMI Atmospheric Climate Models, version 2.2 (RACMO2.2T)	Konkinklijk Nederland Instituut (KNMI) Netherlands	RACMO 2.2T	ICHEC

TABLE 4 Mann–Kendall statistical results of (a) Julius Nyerere International Airport (b), Port Met station, and (c) Chanika.

Season	Month	Z	Sen's slope	P	tau	n	s	α	
MAM	March	2.04	2.39	0.04	0.22	38	189.0	0.05	(a)
	April	0.82	1.16	0.41	0.09	38	77.0	0.05	
	May	−1.13	−2.14	0.26	>0	38	>0	0.05	
OND	October	−1.41	−0.84	0.16	−0.15	38	−131.0	0.05	
	November	−1.11	−1.29	0.27	−0.12	38	−103.0	0.05	
	December	−1.12	−1.03	0.26	−0.12	38	−104.0	0.05	
Annual		0.61	−2.41	0.54	0.05	38	132.0	0.05	
MAM	March	−0.10	0.07	0.92	−0.01	38	−9.0	0.05	(b)
	April	0.50	0.11	0.96	0.01	38	5.0	0.05	
	May	−1.46	0.85	0.14	−0.17	38	−29.0	0.05	
OND	October	−1.46	−0.68	0.14	−0.17	38	−117.0	0.05	
	November	−0.30	0.20	0.76	−0.04	38	−25.0	0.05	
	December	−1.65	−2.09	0.10	−0.19	38	−132.0	0.05	
Annual		−0.08	−0.22	0.94	−0.01	38	−7.0	0.05	
MAM	March	1.43	0.98	0.15	0.16	38	119.0	0.05	(c)
	April	1.06	1.49	0.29	0.12	38	89.0	0.05	
	May	−0.07	−0.15	0.94	−9.45	38	−7.0	0.05	
OND	October	0.75	0.55	0.45	0.09	38	63.0	0.05	
	November	1.55	1.47	0.12	0.17	38	129.0	0.05	
	December	−0.05	0.10	0.96	−6.75	38	−5.0	0.05	
Annual		1.02	3.24	0.31	0.11	38	85.0	0.05	

CHIRPS rainfall data compare very well with observed data at monthly timescales.

3.2 Rainfall trend and magnitude of the historical period

The trend and magnitude direction of historical (1982–2019) rainfall were performed by the statistical test as indicated in Table 4. The results indicate annual and seasonal rainfall variability and change in most of the analyzed stations. However, Table 4 highlights the results of the seasonal (MAM and OND) and annual statistical trend test of rainfall for Dar es Salaam, Chanika, and Port Met stations. Seasonally, the MAM showed a slight increase in rainfall amount while the OND season indicated a decrease in seasonal rainfall. The annual trend showed increased rainfall, except for the Port Met station, which indicates a decreasing trend.

During the MAM season, the results indicated a falling trend in the month of May with significance at the 0.05 level, whereas significant rising trends were determined in March and April at the 0.05 level of significance. The annual precipitation in Dar es

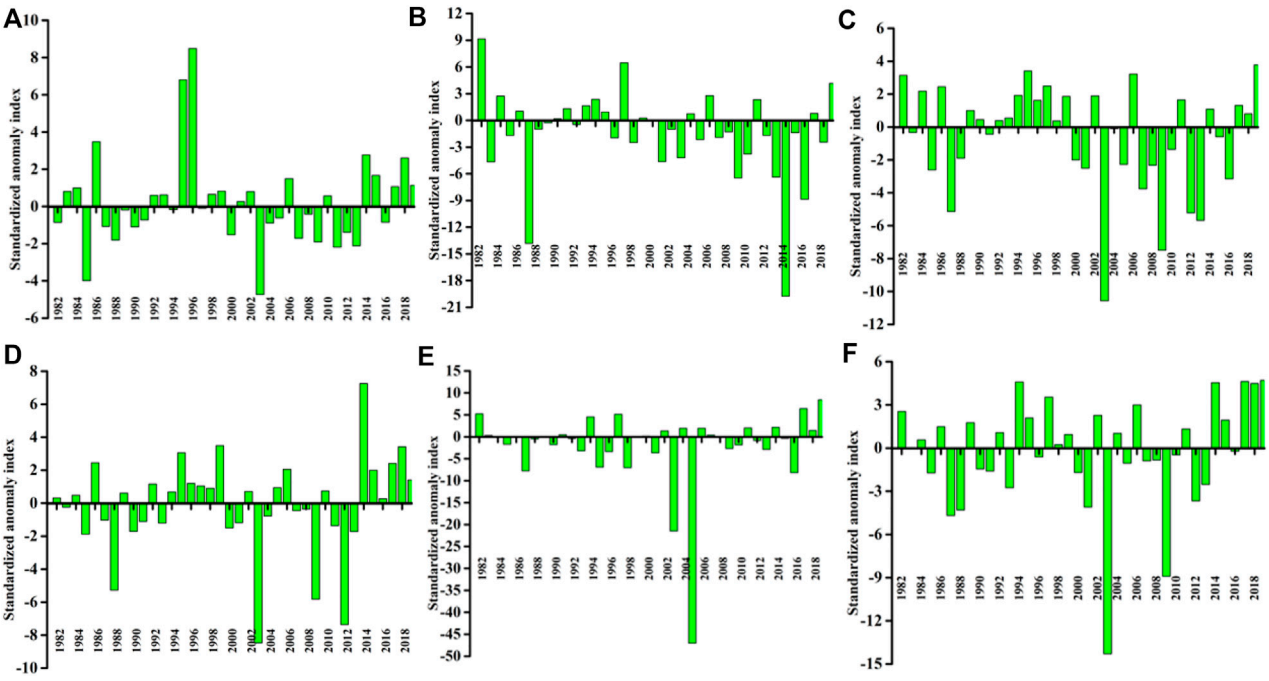

FIGURE 3
Observed historical (1982–2019) Standardized Anomaly Index (SAI) of JNIA meteorological stations for MAM **(A)**, OND **(B)**, and annual rainfall **(C)**, and Boko stations for MAM **(D)**, OND **(E)**, and annual rainfall **(F)**.

Salaam showed an increasing trend (Z value ranging from 0.61 to +1.70). An increasing trend in the annual and seasonal rainfall trends will agree well with the total water availability in Dar es Salaam. An increasing rainfall amount in Dar es Salaam has been associated with an increase in flood frequency, which poses a significant impact on the economy and communities' livelihoods.

The results indicate that for most areas on the high ground of Dar es Salaam, rainfall is higher compared to the lower ground; for example, when we compare the results of Chanika station (high ground) and Port Met station (low ground) in Table 4. The presence of the forest around the Pugu area accelerates the availability of more rainfall compared to the other areas in the city. The stations around the area at high elevation showed an increase in annual rainfall, including Chanika and Hundogo forest, while the area around JNIA and Port Met showed a decrease in rainfall. These results were supported by Sen's slope estimator as indicated in Table 4. Several studies detected similar results for the heterogeneity of the station due to the different geographical locations during rainfall formation (Mzava et al., 2020; Nyembo et al., 2021). These results indicate that the amount of rainfall in the region is extremely variable. Generally, the variability was very high in the region due to highly variable year-to-year rainfall as indicated in the study results in Table 4. Variability in rainfall is of great importance for policymakers in their decision regarding the use of water availability in the region. An underdeveloped area like this, in particular, is highly susceptible to significant influences of climate variability in rainfall, which is the main driver of agricultural growth in the studied region, and hence its extreme occurrence during monsoon and also during post and pre-monsoon months is very crucial to growth.

3.3 Standardized anomaly index

The SAI was analyzed to detect the drought in the study area, and the results, as indicated in Figure 3, showed high variability of rainfall in seasons and annual time steps. MAM showed the highly positive and OND negative percentage of the SAI over the study area, indicating wetness and dryness of the area in the seasons. Generally, a large positive percentage in the region was observed in MAM at 55% and OND at 43% and 49% in the annual rainfall. That means more wetness is experienced in the MAM season compared to the OND rainfall season in Dar es Salaam.

3.4 Comparison between future projection and historical rainfall

3.4.1 Future projection monthly cycle

The results in Figure 4 show the monthly cycle for the historical and future projected rainfall around Dar es Salaam.

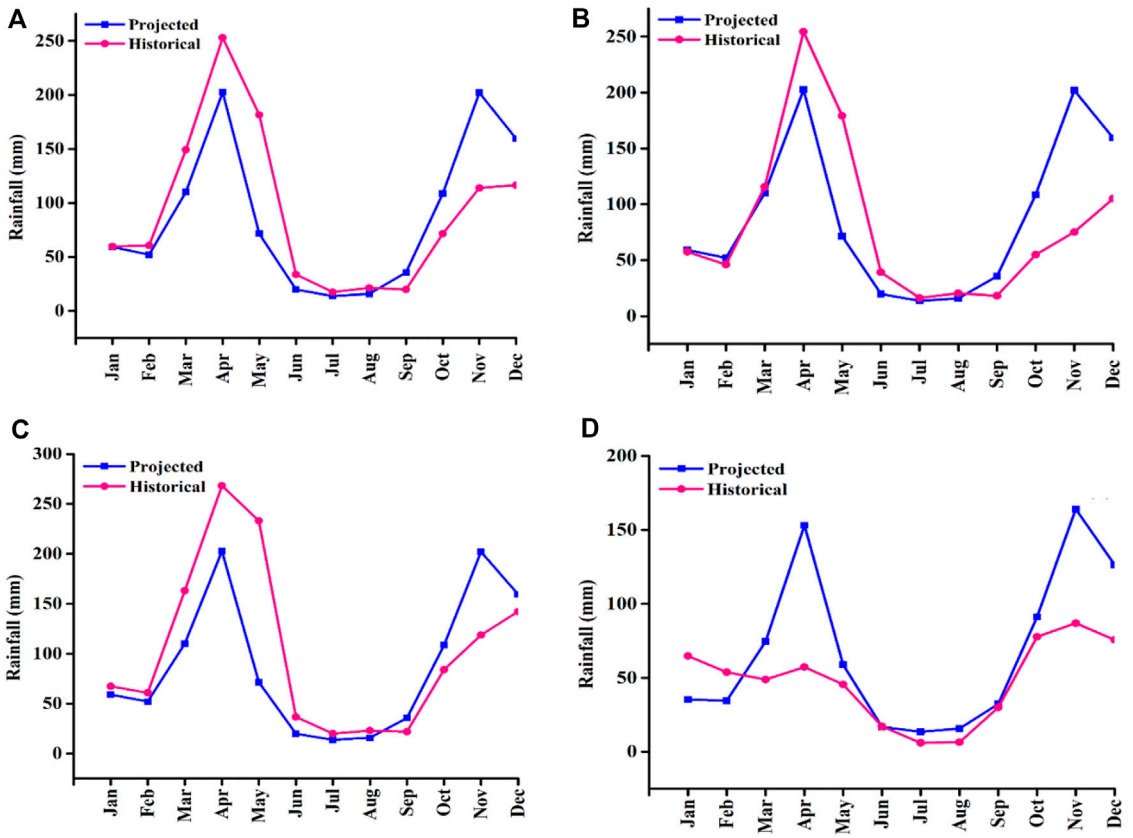

FIGURE 4
Projected monthly mean rainfall (2021–2050) compared to historical (1983–2019) rainfall of Dar es Salaam for JNIA **(A)**, Port Met **(B)**, Chanika **(C)**, and Boko estate **(D)** meteorological stations.

The results for most of the stations indicate that the highest rainfall month will be in April for 2021–2050, and this is similar for the historical rainfall; however, the future projection results indicate a decrease in the amount of rainfall for all months except August to December for JNIA, Chanika, and Port Met. In contrast, the results for Boko station indicate an increasing trend except for January and February. Furthermore, the season's trends show a decrease in amounts of rainfall during MAM, while the OND showed an increase in rainfall in most areas around the city. The decrease in the amount of rainfall, especially during the MAM season, which normally contributes more to the annual rainfall, would result in a water shortage around the city in the future. This water shortage may lead to limited access to water for household purposes, such as drinking, cooking, and cleaning, and would also raise water prices, force rationing, and even devastate vital water sources like wells during dry conditions. The results on the increase in rainfall during the OND season coincide with previous studies (Gulacha and Mulungu, 2017; Luhunga et al., 2018), which also projected an increase in rainfall over some parts of Tanzania including Dar es Salaam. Another study by Anande and Park (2021) reported a decrease in precipitation on wet days in urbanized areas including Dar es Salaam.

Increased precipitation in coastal urban regions was mainly due to the strong updraft motion as there were large spatial variations in precipitation. Additionally, large increases or decreases in precipitation occurred along the shorelines. Precipitation in some areas near the coastal region increased, while in other adjacent areas precipitation slightly decreased. Overall, the intensity of rainfall increased, and the occurrence of precipitation became more frequent due to urbanization. As urbanization progresses, daily mean, maximum, and minimum air temperatures in urbanized regions will increase. The minimum temperature increases will be higher than the maximum temperature increases.

3.4.2 Historical and projected spatial rainfall distribution

The results showed that the Dar es Salaam average MAM rainfall was 655.7 mm/y, OND was 324.8 mm/y, and the annual amount was 1235.7 mm/y. Moreover, the results of the spatial distribution of rainfall are presented in Figure 5 for both

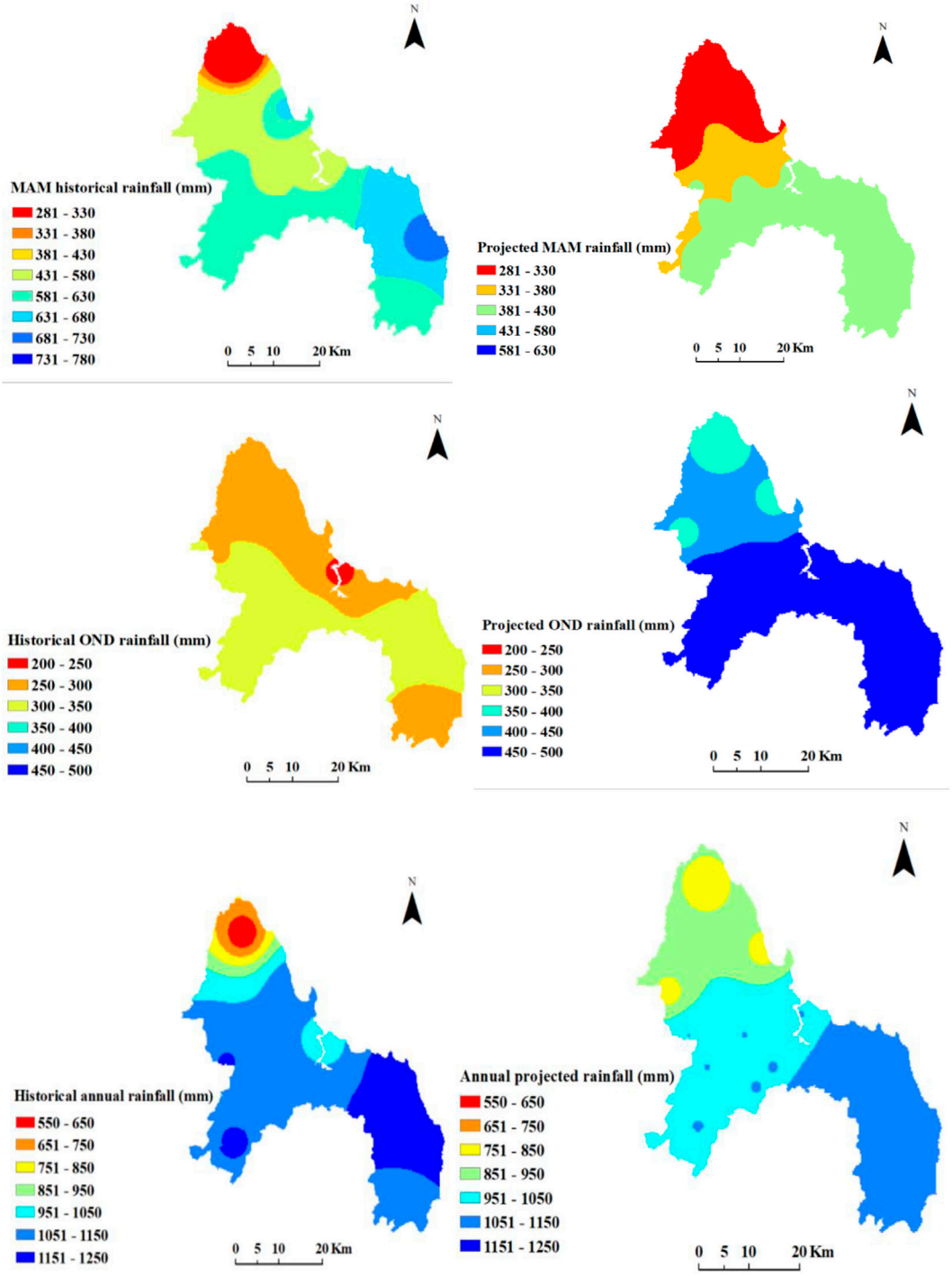

FIGURE 5
Spatial distribution of historical and projected rainfall at a season (MAM and OND) and annual timescale.

historical and projected rainfall. Results conclude that the highest amount of rainfall was obtained over the MAM season. The historical spatial distribution results indicate that variability was very high in the city, where a higher amount of rainfall was experienced in the area around Kimbiji and a lower amount in the port met station areas. Also, the results of the future projection of the spatial rainfall distribution are divided into three parts. The northern part will receive a lower amount of

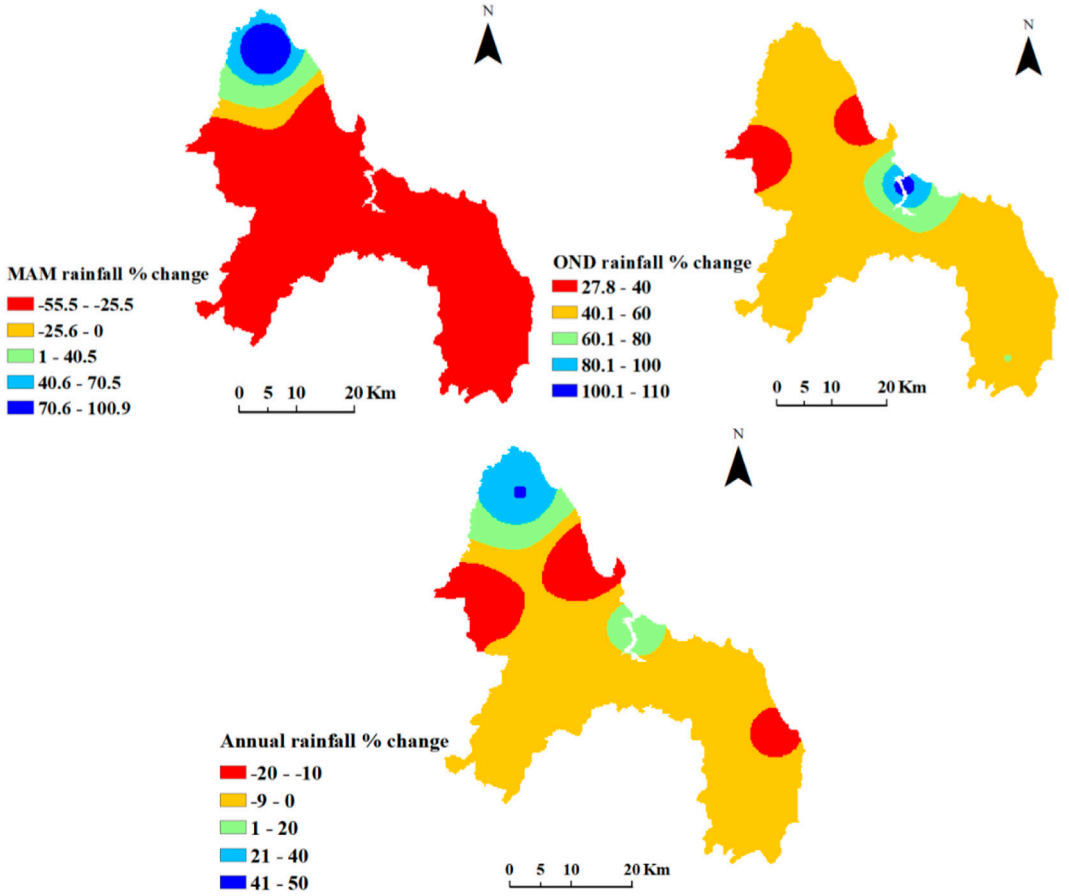

FIGURE 6
Spatial distribution of percentage change in rainfall at a season MAM, OND, and annual timescale.

rainfall, the middle region will experience a moderate amount of rainfall, and the lower (south) part will receive the highest amount of rainfall over the city.

The OND results indicate most of the areas received a high amount of rainfall of approximately 354.4 mm compared to the other seasons. The area around Kimbiji and the southern region received a high amount of rainfall, contrary to the Port Met station, which received a 225.5 mm lower amount of rainfall in the city. In the future, the northern part of the city will receive the highest amount of rainfall, averaging 470.1 mm, while the lowest amount will occur around the southern region at approximately 381.7 mm. The annual rainfall distribution results show that the variability was very high in the city, whereby very few regions received a high amount of rainfall such as 1681.3 mm around JNIA station and surrounding areas, while the area around the Port Met station received the lowest amount of rainfall of approximately 960.1 mm.

3.4.3 Rainfall variations and changes

The spatial historical and projected rainfall seasons at Dar es Salaam were analyzed and the results are shown in Figure 5. The MAM historical variability was highly apparent in the study area, where a small part of the northern side experienced less rainfall than other areas. In the future, the spatial distribution showed a decrease in rainfall over the study area with increased coverage of rainfall reduction over the northern part. However, during the OND rainfall season, the spatial distribution of rainfall is projected to increase in many parts of the city by more than half of the historical rainfall amount. The historical annual rainfall distribution showed that a small part of the northern area experienced a lower amount of rainfall. In contrast, the remaining study areas showed a good amount of rainfall distribution. In the future, rainfall distribution in the northern part showed that a lower amount is expected compared to the southern part where more rainfall is expected compared to the rest of the study area.

The spatial rainfall distribution percentage change was also analyzed as indicated in Figure 6. The results showed that MAM's future rainfall would experience a high decrease in rainfall in many parts of the city by −55%–25%; however, rainfall is expected to increase over a small area in the

north. Furthermore, the OND rainfall seasonal change in large part is expected to have a slight increase of rainfall of approximately 40%–60% regarding the region's average rainfall. The annual rainfall showed a normal to slight decrease in rainfall over a large area. However, small areas in the north will experience an increase in rainfall. The adaptation and execution of policies are highly dependent on climatic conditions, and therefore detection and understanding of rainfall patterns and future projections are of utmost important. According to an IPCC report, upcoming climate changes are likely to distress agriculture, which will amplify hunger and water paucity.

4 Conclusion

The overall aim of this study was to characterize the historical and projected patterns of trends and rainfall variability over Dar es Salaam. However, some studies attempted to portray the climate variability of the area in a different context. This study analyses variations in seasonal rain patterns by looking at the rainfall amount and distribution over Dar es Salaam. April is the highest rainfall month for both historical and future projections. However, there is a seasonal shift in rainfall as a more elevated amount will be observed during the OND season in the future (2021–2050) and in contrast to the historical (1982–2019) period, which showed higher rainfall during the MAM season. The seasonal shifts and high rainfall over the few areas in Northern Dar es Salaam, while a decrease will occur in a large part of the city from the central to the south, calls for the development of adaptation measures and a strategic plan for managing the impacts associated with these changes. The increase or decrease of rainfall in some areas of Dar es Salaam would result in different social and economic impacts associated with dry conditions and floods in some parts. These changes in rainfall patterns over Dar es Salaam call for optimized urban planning to minimize the adverse climate change impacts on communities. Further studies are required on climate change impacts in urbanized areas to build a climate-resilient community and maintain flexibility in adaptation to future uncertainty. This will help concerned stakeholders to consider rainfall variability in their climate change adaptation strategy and allow policymakers to develop a robust framework for overall development.

Data availability statement

The raw data supporting the conclusion of this article will be made available by the authors, without undue reservation.

Author contributions

LN: investigation, data analysis, and writing—original draft. MM: review and editing and data analysis. JJ: conceptualization, methodology, and writing—reviewing and editing. VK: writing—review and editing.

Acknowledgments

The authors are thankful to the Tanzania Meteorological Authority (TMA) for quality input datasets to facilitate this study.

Conflict of interest

The authors declare that the research was conducted in the absence of any commercial or financial relationships that could be construed as a potential conflict of interest.

Publisher's note

All claims expressed in this article are solely those of the authors and do not necessarily represent those of their affiliated organizations, or those of the publisher, the editors, and the reviewers. Any product that may be evaluated in this article, or claim that may be made by its manufacturer, is not guaranteed or endorsed by the publisher.

References

Abolverdi, J., Ferdosifar, G., Khalili, D., Kamgar-Haghighi, A. A., and Physics, A. (2016). Spatial and temporal changes of precipitation concentration in Fars province, southwestern Iran. *Meteorol. Atmos. Phys.* 128 (2), 181–196. doi:10.1007/s00703-015-0414-0

Anande, D. M., and Park, M. S. (2021). Impacts of projected urban expansion on rainfall and temperature during rainy season in the middle-eastern region in Tanzania. *Atmosphere* 12 (10), 1234. doi:10.3390/atmos12101234

Borhara, K., Pokharel, B., Bean, B., Deng, L., and Wang, S-Y. S. (2020). On Tanzania's precipitation climatology, variability, and future projection. *Climate* 8 (2), 34. doi:10.3390/cli8020034

Ddamulira, R. (2016). Climate change and energy in East Africa. *Development* 59, 257–262. doi:10.1057/s41301-017-0101-1

Funk, C., Peterson, P., Landsfeld, M., Pedreros, D., Verdin, J., Shukla, S., et al. (2015). The climate hazards infrared precipitation with stations—A new environmental record for monitoring extremes. *Sci. Data* 2 (1), 1–21. doi:10.1038/sdata.2015.66

Gulacha, M. M., and Mulungu, D. M. (2017). Generation of climate change scenarios for precipitation and temperature at local scales using SDSM in Wami-Ruvu River Basin Tanzania. *Phys. Chem. Earth Parts A/B/C* 100, 62–72.

Huret, N., and Legras, B. (2014). Climate change and variability in sub-saharan Africa: A review of current and future trends and impacts on agriculture and food security. *Environ. Dev. Sustain* 13 (3), 587–605. doi:10.1007/s10668-010-9278-0

JahangeerGupta, P. K., and Yadav, B. K. (2018). "Spatial and temporal nitrate transport in deep heterogeneous vadose zone of India's alluvial plain". *Groundwater. Water science and technology library*. Editors V. Singh, S. Yadav, and R. Yadava (Singapore: Springer), Vol. 76. doi:10.1007/978-981-10-5789-2_13

JahangeerGupta, P. K., and Yadav, B. K. (2017). Transient water flow and nitrate movement simulation in partially saturated zone. *J. Irrig. Drain. Eng.* 143 (12), 04017048. doi:10.1061/(asce)ir.1943-4774.0001238

Kotir, J. H. (2011). Climate change and variability in Sub-Saharan Africa: A review of current and future trends and impacts on agriculture and food security. *Environ. Dev. Sustain.* 13 (3), 587–605.

Kumar, R., Kumar, A., Shankhwar, A. K., Vishkarma, D. K., Sachan, A., Singh, P. V., et al. (2022). Modelling of meteorological drought in the foothills of central Himalayas: A case study in uttarakhand state, India. *Ain Shams Eng. J.* 13 (3), 101595. doi:10.1016/j.asej.2021.09.022

Kumar, V., Chaplot, B., Omar, P. J., Mishra, S., and Md. Azamathulla, H. (2021). Experimental study on infiltration pattern: Opportunities for sustainable management in the northern region of India. *Water Sci. Technol.* 84 (10-11), 2675–2685. doi:10.2166/wst.2021.171

Kumar, Vikram, and Sen, Sumit (2020). Assessment of spring potential for sustainable agriculture: A case study in lesser Himalayas. *Appl. Eng. Agric.* 36 (1), 11–24. doi:10.13031/aea.13520

Kumar, V., Shanu, and Jahangeer (2017). Statistical distribution of rainfall in Uttarakhand, India. *Appl. Water Sci.* 7 (8), 4765–4776. doi:10.1007/s13201-017-0586-5

Larbi, I., Hountondji, F. C., Annor, T., Agyare, W. A., Mwangi Gathenya, J., and Amuzu, J. (2018). Spatio-temporal trend analysis of rainfall and temperature extremes in the Vea Catchment, Ghana. *Climate* 6 (4), 87.

Luhunga, P. M., Kijazi, A. L., Chang'a, L., Kondowe, A., Ng'Ongolo, H., and Mtongori, H. (2018). Climate change projections for Tanzania based on high-resolution regional climate models from the coordinated regional climate downscaling experiment (CORDEX)-Africa. *Front. Environ. Sci.* 6, 122. doi:10.3389/fenvs.2018.00122

Maskrey, A., Buescher, G., Peduzzi, P., and Schaerpf, C. (2007). "Disaster risk reduction: 2007 global review," in Prepared for the Global Platform for Disaster Risk Reduction First Session, Geneva, Switzerland (Consultation Edition), 5–7.

McKee, T. B., Doesken, N. J., and Kleist, J. (1993). The relationship of drought frequency and duration to time scales. *Proc. 8th Conf. Appl. Climatol.* 17 (22), 179–183.

Meshram, S. G., Singh, S. K., Meshram, C., Deo, R. C., and Ambade, B. (2018). Statistical evaluation of rainfall time series in concurrence with agriculture and water resources of Ken River basin, Central India (1901–2010). *Theor. Appl. Climatol.* 134 (3), 1231–1243. doi:10.1007/s00704-017-2335-y

Mwabumba, M., Jahangeer, J., Beegum, S., Yadav, B. K., and Rwiza, M. J. (2022a). Assessment of groundwater quality under changing climate in ngorongoro conservation area, Tanzania. *J. Irrig. Drain. Eng.* 148 (10), 04022032. doi:10.1061/(asce)ir.1943-4774.0001702

Mwabumba, M., Yadav, B. K., Rwiza, M. J., Larbi, I., Dotse, S. Q., Limantol, A. M., et al. (2022b). Rainfall and temperature changes under different climate scenarios at the watersheds surrounding the Ngorongoro Conservation Area in Tanzania. *Environ. Challenges* 7, 100446. doi:10.1016/j.envc.2022.100446

Mzava, P., Valimba, P., and Nobert, J. (2020). Trends and frequencies of extreme rainfall events in the urban catchments of dar es salaam, Tanzania. *J. Geogr. Assoc. Tanzan.* 40 (1).

Nyatichi, J. M. (2015). Co-Operatives and employment creation: The kenyan case. *Int. Co-op. Alliance Seminar Antalya Turk. 8th 13th November 2015* 57, 743.

Nyembo, L. O., Larbi, I., and andd Rwiza, M. J. (2021). Analysis of spatio-temporal climate variability of a shallow lake catchment in Tanzania. *J. Water Clim. Change* 12 (2), 469–483. doi:10.2166/wcc.2020.197

Pachauri, R. K., and Meyer, L. A. (2014). Climate change 2014: Synthesis report. *Contribution Work. Groups I, II III Fifth Assess. Rep. Intergov. Panel Clim. Change* 743, 1876.

Palmate, Santosh S., Ashish Pandey, Rajendra P. Pandey, Mishra, Surendra K., and Mishra, S. K. (2021). Assessing the land degradation and greening response to changes in hydro-climatic variables using a conceptual framework: A case-study in central India. *Land Degrad. Dev.* 32 (14), 4132–4148. doi:10.1002/ldr.4014

Palmate, Santosh S., Kumar, Saurav, Poulose, Thomas, Ganjegunte, Girisha K., Chaganti, Vijayasatya N., and Sheng., Zhuping (2022). Comparing the effect of different irrigation water scenarios on arid region pecan orchard using a system dynamics approach. *Agric. Water Manag.* 265, 107547. doi:10.1016/j.agwat.2022.107547

San José, R., Pérez, J. L., González, R. M., Pecci, J., Garzón, A., and Palacios, M. (2016). Impacts of the 4.5 and 8.5 RCP global climate scenarios on urban meteorology and air quality: Application to Madrid, Antwerp, Milan, Helsinki and London. *J. Comput. Appl. Math.* 293, 192–207. doi:10.1016/j.cam.2015.04.024

Sen, P. K. (1968). Estimates of the regression coefficient based on kendall's tau. *J. Am. Stat. Assoc.* 63 (324), 1379–1389. doi:10.1080/01621459.1968.10480934

Shepard, D. (1968). "A two dimensional interpolation function for irregularly spaced data," in Proceedings 23rd National Conference of the Association for Computing Machinery, Princeton, NJ (ACM), 517–524.

Sipayung, S. B., Nurlatifah, A., Siswanto, B., and Slamet S, L. (2018). Analysis of climate change impact on rainfall pattern of sambas district, west kalimantan IOP conference series: Earth and environmental science. *IOP Conf. Ser. Earth Environ. Sci.* 149 (1), 012029. doi:10.1088/1755-1315/149/1/012029

Tschakert, P., Sagoe, R., Ofori-Darko, G., and Codjoe, S. N. (2010). Floods in the Sahel: An analysis of anomalies, memory, and anticipatory learning. *Clim. Change* 103 (3), 471–502.

Umar, S., Lone, M. A., Goel, N. K., and Zakwan, M. (2022). Trend analysis of hydro-meteorological parameters in the Jhelum River basin, north Western Himalayas. *Theor. Appl. Climatol.* 148 (3), 1417–1428. doi:10.1007/s00704-022-04014-7

Yavuz, H., and Erdoğan, S. (2012). Spatial analysis of monthly and annual precipitation trends in Turkey. *Water Resour. manage.* 26 (3), 609–621. doi:10.1007/s11269-011-9935-6

Zakwan, M., Ahmad, Z., and Sharief, S. M. V. (2018). Magnitude-frequency analysis for suspended sediment transport in the Ganga River. *J. Hydrol. Eng.* 23 (7), 05018013. doi:10.1061/(asce)he.1943-5584.0001671

frontiers | Frontiers in Environmental Science

TYPE Original Research
PUBLISHED 14 December 2022
DOI 10.3389/fenvs.2022.936216

OPEN ACCESS

EDITED BY
Claudio Fabian Szlafsztein,
Federal University of Pará, Brazil

REVIEWED BY
Faheem Ur Rehman,
Ural Federal University, Russia
Md Shabbir Alam,
University of Bahrain, Bahrain

*CORRESPONDENCE
Md. Qamruzzaman,
zaman_wut16@yahoo.com

SPECIALTY SECTION
This article was submitted to Interdisciplinary Climate Studies, a section of the journal Frontiers in Environmental Science

RECEIVED 05 May 2022
ACCEPTED 21 November 2022
PUBLISHED 14 December 2022

CITATION
JinRu L, Qamruzzaman M, Hangyu W and Kler R (2022), Do environmental quality, financial inclusion, and good governance ensure the FDI sustainably in Belt and Road countries? Evidence from an application of CS-ARDL and NARDL.
Front. Environ. Sci. 10:936216.
doi: 10.3389/fenvs.2022.936216

Do environmental quality, financial inclusion, and good governance ensure the FDI sustainably in Belt and Road countries? Evidence from an application of CS-ARDL and NARDL

Long JinRu[1], Md. Qamruzzaman[2]*, Wu Hangyu[3] and Rajnish Kler[4]

[1]City College, KunMing University of Science and Technology, KunMing, China, [2]School of Business and Economics, United International University, Dhaka, Bangladesh, [3]Business School Beijing International Studies University, Beijing, China, [4]Department of Commerce Motilal Nehru College (E), University of Delhi, New Delhi, India

Domestic capital adequacy and sustainable economic growth are heavily reliant on technological advancement, managerial know-how, and money supply in the economy. In this context, FDI has emerged and is placed at an apex position due to its unprecedented impact on achieving sustainability across the world. The motivation of this study is to scale the effects of good governance, financial inclusion, and environmental quality on inflows of FDI in BRI nations for the period from 1990 to 2020. Several panel econometrical tools have been applied, for example, CDS, CADF, CIPS, CS-ARDL, and NARDL, to investigate the association and explanatory variables elasticity on inflows of FDI in BRI nations. CDS results revealed that research units share common dynamism and second-generation panel unit root test-documented variables are stationary after the first difference. The results of the panel co-integration with an error-correction term confirmed the empirical equation's long-run association. According to the CS-ARDL assessment, positive and statistically significant impacts have been documented, from financial inclusion, good governance, and environmental quality to FDI inflows. Study findings suggest that governmental effectiveness, easy access to financial services and benefits, and a less-regulated environmental concern economy motivate capital transfer decisions. The asymmetric assessment documented a long-run asymmetric association between FI, GG, EQ, and FDI. Referring to asymmetric shock elasticity, the study disclosed a positive and statistically significant relation to FDI inflows, especially in the long run. The directional causality test documented bidirectional causality running between FI, EQ, GG, and FDI [FI←→FDI; GG←→FDI; and EQ←→FDI] in the short-run.

KEYWORDS

financial inclusion, environmental quality, good governance, FDI, NARDL, CS-ARDL, road–belt countries

1 Background

Globalization has had a profound effect on the global economy and has played a significant role in the increase of FDI and its influence on economic growth during the last few decades (Sokang, 2018). Consequently, FDI has gained prominence as a source of foreign money, especially for developing countries (Oke et al., 2007). While the effect of FDI varies in the economic sector, it has the potential to make a considerable overall contribution to a country's economy by encouraging investment in manufacturing facilities and the host country's manufacturing sector. FDI promotes capital creation, provides for cross-border technology and information exchanges, and strengthens the host country's skills (Boateng et al., 2015; Logun, 2020; Andriamahery and Qamruzzaman, 2022a; 2022b). Foreign direct investment also helps emerging nations increase their total productivity, employment, and income development. However, research on the influence of FDI on economic development in LDCs and developing economies provides inconclusive findings. FDI flows have expanded considerably over the world during the last 3 decades. This drew our attention to the effect of such a surge in FDI on the host country's economic development. The link between FDI and economic advancement has since been a source of debate among scholars (Rehman and Ding, 2020). The literature suggests that FDI promotes economic development by promoting cross-border technology and knowledge transfer, resulting in more employment and enhancing the host country's skill capacity. Taking account the existing literature, two lines of research findings focusing on FDI can be found : the first group of researchers investigated the role of FDI inflows in the economy and subsequently advocated its positive link to economic growth (Azman-Saini et al., 2010; Pegkas, 2015; Saibu et al., 2022), employment generation, financial development (Alfaro et al., 2009), trade liberalization (Liargovas and Skandalis, 2012; Rehman & Sohag, 2022), industrialization (Adom and Amuakwa-Mensah, 2016; Ma and Qamruzzaman, 2022; Xia et al., 2022; Zhuo and Qamruzzaman, 2022), poverty reduction (Klein et al., 2001; Magombeyi and Odhiambo, 2017), and technological development (Liu & Wang, 2003). At the same time, another group of researchers showed the adverse effects of FDI, especially in environmental degradation through carbon emission and energy consumption escalation, typically fossil fuels. Second, the line of empirical evidence concentrated on exploring the key determinants attracting foreign investments and subsequently advocated for both macro and micro fundamentals, which can play an important role in ensuring persistent inflows of FDI in the economy, such as institutional quality, economic growth, financial development, domestic capital formation, and financial inclusion (Vijayakumar et al., 2010; Barthel et al., 2011; Saini and Singhania, 2018; Chattopadhyay et al., 2022). For example, Samargandi et al. (2022) investigated the key factors responsible for encouraging FDI inflows in Saudi from 1981 to 2018 by implementing an ARDL-bound testing approach with a structural break. The study documented that domestic trade liberalization and institutional quality promise FDI inflow augmentation.

The study considered environmental quality (EQ), good governance (GG), and financial inclusion (FI) in the FDI inflow assessment. Nowadays, efficient markets and financial services with an appropriate attitude toward financial activity simplify the whole financial work, creating a mass area and the desire for improved cross-border capital flow or foreign direct investment (Nasreen et al., 2020; Jia et al., 2021). The financial efficiency that offers a clear picture of any firm's financial data and activities is why it significantly influences the foreign currency flow across borders (Alam and Shah, 2013; Qamruzzaman, 2015, 2021). This ease of entrance results in a wide positive acceleration for all international and domestic investors. Foreign investment is highly dependent on the success of the stock market and the quality of accounting data. A robust capital system contributes significantly to the economic activity by cutting transaction costs and effectively allocating resources (Greenwood and Jovanovic, 1990; Levine, 1997). Moreover, according to the literature, a robust financial sector is essential for developing commercial activities and the country's overall economic growth (Bourkhis and Nabi, 2013; Bilawal et al., 2014). Enhancing money flows across borders, promoting financial inclusion, and improving financial efficiency are critical (Abid and Goaied, 2017). The company's cash flow is built on financial efficiency since it attracts investors from both domestic and international markets. International capital flows may be optimistic if a country's financial market seems efficient (Kablan, 2009). The positive feedback shed more light on the link between financial inclusion and cross-border capital flows (Krause ad Rioja, 2006). Financial reform, effective financial intermediation, the adoption and distribution of financial technology, the transformation of financial aid, the efficient mobilization of economic resources, and the expansion of financial markets are all examples of policies that can be implemented. Another factor contributing to foreign investment is effective governmental practices (Aibai et al., 2019; Huynh and Hoang, 2019; Dorozynski et al., 2020; Cong Minh Huynh, 2022). The study of Narayanan et al. (2020), for example, explored the relationship of FDI and good governance for the ASEAN countries, as a sample, for the period from 2002 to

2015 using the PMG estimation method. The study concluded that FDI positively impacts the economic growth in good governance, so it should be encouraged to attain maximum benefit. In their study, Cong Minh Huynh (2022) concluded that at the beginning, FDI inflows aid in improving institutional quality, but in the presence of an underground economy it has negative impacts, reducing the merits. Thus, it is suggested to ensure governmental effectiveness for efficient reallocation of FDI inflows in the economy. Recent literature studies have documented that environmental protection particularly carbon reduction, green energy inclusion, and energy efficient technology adaptation have become prominent and considerable factors in foreign capital flows (Assadzadeh and Pourqoly, 2013; Herrera-Echeverri et al., 2014a; Mengistu and Adhikary, 2011; Shah et al., 2015). The study of Bhujabal et al. (2021), for example, examined the impact of FDU on the environmental quality in the prime Asia-Pacific countries for time series of 1990–2018 using the PMG causality test. A study documented that as FDI increases, ICT infrastructure rises and it reduces the air pollution, making the environment better in the long run. In their study, Contractor et al. (2020) studied the connection of FDI in improving the environment and economy using proper regulations on 189 economies (World Bank 2016 data) applying random-effect, fixed-effect, and regression models. Studies prove a strong positive connection between business and the overall environment. As FDI is more inclined toward investment in less efficient entry and exit systems, government policies must be restructured (Alam, 2022; Rehman and Islam, 2022; Xia et al., 2022).

This study aims to evaluate the impact of environmental quality, good governance, and financial inclusion on inflows of forcing cash flows in BRI nations for 1990–2020.

As a case study, we considered a panel of 46 BRI countries. The BRI, which aspires to increase China's international collaboration with new partners, is a driving force behind China's long-term economic growth. BRI was the premier platform for national connectivity in 2013 through promoting regional and intra-regional integration. Because of the Chinese government's commitment to establishing a more open economy, this program emphasized the need to invest in a solid infrastructure that enables connections within China and with China on a global scale (Rehman and Noman, 2021). Infrastructure building is a key component of the Belt and Road Initiative, but the endeavor also involves policy discussions, access to infrastructure, unrestricted commerce, financial help, and human relationships (Dai et al., 2022; Muhammad et al., 2022; Shi and Qamruzzaman, 2022; Xia et al., 2022). Given China's track record of economic growth, infrastructure is projected to play a critical role, especially in the initiative's early stages. Several plans have been proposed to connect different areas, including building superhighways, installing oil and gas pipelines, and installing power and communication lines. In addition to the funds provided by the AIIB, the BRICS New Development Bank, and the World Bank and the Asian Development Bank, major investments are expected to be made by Chinese institutions such as the Silk Road Fund (SRF), the China Development Bank (CDB), and numerous Chinese firms. To reduce trade costs and increase foreign direct investment (FDI) into China and other Belt and Road nations, one of the primary objectives of BRI is to develop transportation networks linking countries of the Belt and Road Initiative (Hussain et al., 2022; Su et al., 2022).

Additionally, the Belt and Road Initiative (BRI) has the potential to significantly reduce policy uncertainty and policy risks posed by host countries for Chinese companies that invest in the Belt and Road countries. This further encourages China's foreign and internal FDIs within the belt–road countries through top-level international political cooperation, policy coordination, and government support. At this early point in the construction of the Belt and Road Initiative (BRI), some of these incentives for foreign direct investment (FDI) are already in place, while others are still mostly anticipated rather than fully realized. Because of the bright prospects for the BR program, Chinese companies, who have always played a significant role in ensuring the success of the program, will increase their trade and foreign direct investments more rapidly than their counterparts in other countries (Du & Zhang, 2022; Fuest et al., 2022). Empirical studies focusing on BRI countries have created intense interest among researchers, and a growing number of studies have been performed to explore fresh insights with diverse motivations. Foreign investors need extensive information on the market's financial stability, economic health, and level of financial inclusion. Almost every major industrialized country strives to boost the effectiveness of its courtiers' financial openness to attract foreign investments. If a market risk occurs due to the foreign company's activities, the foreign direct investor or corporation will want to be shown a varied market. To compile all of these data and analyze economic circumstances, the host country must provide sufficient financial inclusion to attract foreign direct investments. The only source of change is cross-border financial flows. On the other side, financial inclusion entails the widespread availability of all financial services and the prevalence of monetary transactions. Macroeconomic growth seems necessary because easy access to financial instruments enables smooth spending and asset building, boosting individual wellbeing and economic development potential. Domestic capital adequacy and sustainable economic growth immensely rely on technological advancement, managerial know-how, and money supply in the economy. In this context, FDI has emerged and is placed at an apex position due to its unprecedented impact on achieving sustainability across the world (Lingyan et al., 2021; Meng et al., 2021; Pu et al., 2021; Xu et al., 2021).

The motivation of the study is to scale the effects of good governance, financial inclusion, and environmental quality on

inflows of FDI in BRI nations for the period from 1990 to 2020. Several panel econometrical tools have been applied, for example, CDS, CADF, CIPS, CS-ARDL, and NARDL, in investigating the association and explanatory variable elasticity on the inflows of FDI in BRI nations. CDS results revealed that research units share common dynamism, and second-generation panel unit root test-documented variables are stationary after the first difference, and neither has been exposed after the first difference. The results of panel co-integration with the error correction term confirmed the empirical equation's long-run association. According to the CS-ARDL assessment, positive and statistically significant impacts have been documented, from financial inclusion, good governance, and environmental quality to FDI inflows. The study findings suggest that governmental effectiveness, easy access to financial services and benefits, and a less-regulated environmental concern economy motivate capital transfer decisions. The asymmetric assessment documented a long-run asymmetric association between FI, GG, EQ, and FDI. Referring to asymmetric shock elasticity, the study disclosed a positive and statistically significant tie to FDI inflows, especially in the long run. Directional causality test documented bidirectional casualty running between FI, EQ, GG, and FDI [FI←→FDI; GG←→FDI; EQ←→FDI] in the short-run.

The contribution of the present study to the existing literature is as follows: First, according to the existing literature, financial development in the financial system plays an important role in accelerating foreign participation in the economy. However, the effects of financial inclusion, that is, the accessibility to financial services and benefits in the financial institutions on the inflows of FDI, are yet to be investigated, focusing on the BRI initiatives extensively. The present study has included financial inclusion in the equation of FDI for exploring fresh insights and the new direction of FDI development in BRI nations. Second, the present study has implemented symmetric and asymmetric frameworks to establish the empirical nexus. It is mentioned here that the implementation of an asymmetric framework offers diverse information dealing with an appropriate explanation of positive and negative innovations in explanatory variables and their appropriate influence on explained variables. Thus, it is plausible to assist and support effective policy formulation for future development.

The remaining structure of the article is as follows. The literature survey of the study deals with Section 2. Section 3 reports the study's variables' definitions, model specifications, and econometrical methodology. The empirical model estimation and output are shown in Section 4. Discussion of the findings is available in Section 5. Finally, Section 6 deals with the conclusion and policy suggestions.

2 Literature review

2.1 Financial inclusion and foreign direct investment

The hand of international money flows is a vital component in driving any country's economic progress. Cross-border cash flow has become an important part of the global economy's financial sector development. Cross-border cash flow is crucial for improving the industry service and financial affectivity, supporting developing economies and ensuring sustained GDP and international trade growth. Financial inclusion and efficiency are linked to cross-border cash transfers. In the study by Toxopeus and Lensink (2008), financial inclusion positively impacts cross-border capital flows. According to the research, which analyzed 2008 data from 63 countries from the IFM, World Bank, and GLS, remittances are included in international or cross-border cash flows. Additionally, remittances may increase if financial inclusion is properly implemented. According to them, financial inclusion boosts economic activity, which supports remittance providers by making it easier to send money back home. Foreign currency reserves must be increased to increase financial inclusion. Qamruzzaman and Jianguo (2018) used the System GMM technique in 58 developing nations between 1993 and 2017 to show that foreign capital flow has significantly impacted a vital economic development function. A country's financial inclusion must be improved to promote cross-border cash mobility, demonstrating a positive association.

G. A. Zwedu (2014) used the BDY financial stability and inclusive development model to assess 593 banks from 2010 to 2013. In other words, increasing access to financial services may help a country's commercial and economic standing. What makes a foreign investor want to invest money into a nation with more financial users? The lack of financial inclusion and foreign capital inflows that do not improve the growth rates are emphasized. Sarma and Pais (2011) showed that improving financial inclusion boosted the daily financial activity and the number of financial employees, which enhanced the effectiveness of foreign capital flows in the nation, according to an empirical analysis done on 88 countries in 2010. This is proof of a favorable relationship. According to Ramasamy and Yeung (2010), financial inclusion incentives increased the number of financial users from 1988 to 2010. The number of transactions from this rise was directly proportional to the FDI attracted. This demonstrates a favorable relationship between FDI and foreign cash flow. Based on an analysis of a panel of 16 EU countries from 1988 to 2004, Bevan et al. (2004) concluded that the financial inclusion rate of developed countries is higher in those countries that implement financial inclusion than those countries that do not. Therefore, it has a lower growth rate in foreign cash flows, which does not practice or promote financial inclusion.

Morgan and Pontines (2018) discovered mutually reinforcing financial inclusion and financial market stability. The short period and restricted availability of foreign capital exacerbated the connection between foreign capital flow and foreign financial inclusion. This was discovered in another study by Singh and Zammit (2000), who used the financial stability and inclusive growth model with 63 developing countries in the 1990s and 2000s and discovered that rural poverty and gender inequality could affect financial inclusion, implying that the relationship between foreign cash flow and foreign cash flow appears to be negative. Other studies have indicated that expanding financial inclusion does not influence foreign capital flows, but the country's overall financial status may impact FDI, making the statement neutral. Barrell et al. (2003) used a panel of nine European Union countries to study system dynamics between 1991 and 1997. According to the findings, technology transfer is linked to financial inclusion risk, affecting cross-border cash flow. There is a risk that the liquid cash problem may develop differently with maximum financial inclusion applications if the monetary transaction assessment is reduced considerably. According to a study conducted by Barajas et al. (2000), financial inclusion has a general financial development in the cross-border cash flow sector, implying a positive relationship between financial inclusion and cross-border cash flows. Bailliu (2000) created an economic growth model for 1975–2000 using panel data from 40 developing countries gathered between 1975 and 2000. Financial data show the financial effectiveness of an organization. Due to increased financial efficiency, FDI transparency improves, which benefits foreign cash flows.

The empirical analytic technique, FDI-growth, was used by Adeniyi et al. (2015) to evaluate the financial efficiency of different financial resistances throughout the country that may affect cross-border cash flow between 1990 and 2015. Remittances and cross-border cash flow may suffer as a result of increased efficiency. The study found that foreign capital has been important to the sustained high investment and output rate in three countries from 1990 through 1996, using a dynamic model and a panel from Korea, Malaysia, and Indonesia. Only Korea was unwilling to accept any foreign investment, no matter how mature it was. All three East Asian countries were prepared to accept foreign funding strongly dependent on financial efficiency. Economic and financial developments rely on a country's level of financial affectivity, which has been positively related to foreign capital flows in a separate study.

According to Taylor and Sarno (1997), as a counteraction plan between the United States and Latin American and Asian nations from 1988 to 1997 in developed countries, FDI was difficult to identify as an effective financial instrument, causing difficulty in foreign investor linkage and foreign cash flow. Another study by Katarzyna Anna and Adam (2012) found a positive association between financial efficiency and cross-border cash flow. Sturm and Williams (2008) used the system dynamic approach on a panel of foreign banks in Australia between 1998 and 2008 to investigate how different financial barriers impact cross-border cash flow. The efficiency of cross-border money transfers may have a detrimental influence on remittances.

2.2 Good governance/institutional quality and foreign direct investment

Existing literature has suggested that researchers and academicians have extensively assessed the key determinants of foreign capital flows and documented several macros and micro agents such as exchange rates, domestic capital formation, and trade liberalization. However, many studies have established good governance, referred to as institutions and traditions, by which power exercised by the authority significantly influences foreign capital flows (Kaufmann and Wei, 1999; Rehman et al., 2021). Even though good governance has been extensively investigated, focusing on FDI, the conclusive direction has yet to be established (Herrera-Echeverri et al., 2014b; Shah et al., 2015; Hamid et al., 2022a). The study of Ross (2019), for example, investigated the current, holistic governance of FDI in 122 developing countries from 2002 to 2017 using World Bank's "good governance index" and econometrics method. The results say good governance is an undeniable indicator of a host country's FDI, as weak institutional capacity can adversely impact those economies. Furthermore, Cong Minh Huynh (2022) established the FDI inflows on institutional quality in 43 developing countries worldwide during 2002–2009 using FGLS and SGMM estimations. The findings concluded that at the beginning, FDI inflows aided in improving institutional quality, but in the presence of an underground economy, it had negative impacts, reducing the merits. Thus, this is indifferent to conclude, and it suggests controlling the underground economy to minimize the demerits. However, considering the present literature on good governance-led FDI, we can be segregated it into two lines positive association linkage and neutral effects.

The first line of literature has suggested a positive and statistically significant association between good governance and inflows of FDI (Assadzadeh et al., 2013; Aziz, 2018; Younsi et al., 2019; Bouchoucha and Benammou, 2020; Mengistu and Adhikary, 2011; Shittu et al., 2020). The study of Dorozynski et al. (2020), for example, verified the institutional quality on FDI for 17 countries of Central and Eastern Europe from 2007–2017, exercising hierarchical cluster analysis; panel models. The study documented a positive association of FDI with GDP with efficient institutional systems and quality. Furthermore, Narayanan et al. (2020) explored the relationship between FDI and good governance using the ASEAN countries as samples from 2002 to 2015 using the PMG estimation method. The study concludes that FDI

positively impacts economic growth in the presence of good governance, so it should be encouraged to attain maximum benefit from it. The article of Omri and Mabrouk (2020) established that political and good governance positively relates to the FDI improving the economy and environment but could have some minor adverse impacts on human flourishing. This could be reduced by improving both political and institutional governance. Huynh and Hoang (2019) postulated that proper policies should be implemented, and better governance ensures that FDI can positively help reduce the shadow economy while improving institutional quality. Moreover, in a study, Khan et al. (2019) analyzed the relationship between good governance and FDI in India from 1996 to 2012 through multiple regression models. A study proves that India could attract more FDI due to its good governance system, which helps them attain employment and expand economic growth and income through the investment of more outside investors.

In their research, Raza et al. (2021b) investigated the relationship between FDI and economic expansion with good governance of OECD countries for the period of 1996 to 2013, exercising the fixed-effect model and GMM estimators. The study documented a positive association of the variables, but it is necessary to modify the laws to reduce corruption. Aibai, Huang, Luo, Peng, et al. (2019) explored the role of FDI on financial expansion and institutional quality in a sample of 50 countries from 1989 to 2011 that joined the Belt and Road Initiative by conducting the GMM method. From the result of the study, it is concluded that there is a stronger and more positive relationship which says FDI can easily thrive in financial enhancement by improving institutional quality and financial function. Biro et al. (2019) examined the effect of good governance on FDI in Latin American countries from 2001 to 2012 using the gravity model, OLS, and PPML measures. The study established a positive association stating good governance can attract FDI for developing the target economies. Sabir et al. (2019) documented a positive relationship between FDI and institutional quality in all the assigned countries, but developed countries have more significance in institutional quality than developing countries.

In their study, Kasasbeh et al. (2018) showed the FDI and institutional quality and good governance relationship using developing economies, i.e., Jordan, from 1980 to 2016, applying multivariate VAR analysis. The study says FDI significantly reduces corruption while effectively improving governance and institutional quality, assuring a positive relationship. Peres et al. (2018) investigated the importance of FDI on the productivity of technology, employment, and many more economic factors using 110 developed and developing countries for the period of 2002–2012, exercising panel data set and econometrics models including OLS. The findings concluded that good governance can significantly affect FDI, though, for some developing countries, it is not that significant. But, it is inferred from the study that proper governance can attract more FDI inflows. The study of Kayalvizhi and Thenmozhi (2018) explored the technology, culture, and corporate governance relationship with inward FDI in 22 emerging economies from 1996 to 2014 using panel models with fixed effects. The study's findings prove a positive proportional relationship between corporate governance and FDI, improving economy, technology, and culture. The research article of Hayat and Development (2019) investigated whether institutional quality plays a crucial role in enhancing economic flourish through FDI, considering a sample of 104 countries from the years 1996–2015 applying the GMM method. The study concludes a positive association between FDI and institutional quality in low- and middle-income economies but a slowed association in high-income nations.

The second direction line explains the neutral effects of good governance on FDI inflows. The study of Cong Minh Huynh (2022), for example, established the FDI inflows on institutional quality in 43 developing countries throughout the world during 2002–2009 using FGLS and SGMM estimations. The findings concluded that at the beginning, FDI inflows aid in improving institutional quality, but in the presence of an underground economy, it has negative impacts, reducing the merits. Thus, this is indifferent to conclude, and it suggests controlling the underground economy to minimize the demerits. Thus, it is postulated that FDI inflows improve institutional quality and ensure efficient mobilization in the economy. Similar evidence is available in the study of Miao et al. (2020). The study established contingent impacts from country to country, based on the efficiency of policy to control intuitional quality.

2.3 Environmental quality and foreign direct investment

FDI inflow in the economy ensures technological advancement, knowledge sharing, and industrial development with capital support. On the other hand, the excessive application of conventional energy, that is, fossil fuel integration, causes environmental degradation (Abdouli and Hammami, 2017; Zomorrodi and Zhou, 2017; Hao et al., 2020). Foreign direct investment has an environmental impact, whether it improves or degrades the quality of natural resources or living organisms. Environmental degradation may be triggered by several circumstances, including resource depletion, the risk to living creatures, and human activity contributing to environmental degradation. Degradation of the environment is an essential prerequisite for the growth of these factors, which ultimately results in rising costs and capital depletion. The growing cost of conducting business in terms of capital loss emphasizes the critical importance of environmental quality. Additionally, since the environment significantly impacts clean drinking water and air availability, it is critical to resolve this problem. As a result, environmental quality is crucial for human and

business health alike. Given that FDI inflows account for a significant portion of economically developed enterprises and institutions, it is critical to keep a check on them *via* environmental regulations. Three major elements affect the environmental quality of FDI inflows: environmental legislation, pollutant levels, and industry-specific FDI. Three lines of evidence have been found in the empirical literature focusing on the nexus between environmental quality and foreign direct investment (Alam et al., 2022). The first positive linkage was done by Opoku and Boachie, 2020; Bao et al., 2011; Kirkulak et al., 2011; and An et al., 2021. Bhujabal et al. (2021), for example, examined the impact of FDU on the environmental quality in the prime Asia-Pacific countries for the time series from 1990–2018 using the PMG causality test. The study documented that as FDI increases, ICT infrastructure rises, reducing air pollution and making the environment better in the long run. Contractor et al. (2020) disclosed a strong positive connection between business and the overall environment. As FDI is more attracted to investing in less efficient entry and exit systems, government policies must be restructured. In their study, Ssali et al. (2019) explored the nexus between environmental quality on FDI using six selected sub-Saharan African nations from 1980 to 2014 using ARDL and other methods. The study established a positive causality of FDI on the environment by properly using eco-technology to maintain a green environment. The research of Saini and Sighania (2019) reviewed the economic expansion and environmental quality of FDI inflows using developed and developing countries from 1990 to 2017 using the GMM technique. The study documented the existence of the Kuznets curve saying cleaner environment can eradicate the bad impacts of economic growth on the environment.

In their study, Wang et al. (2019) examined the relationship between FDI on environmental regulation and pollution using eastern, central, and western regions of China from 2000 to 2014, applying the PCSE method. The results showed that FDI can substantially reduce environmental pollution more in the eastern and central regions than in the western regions, providing a stricter environmental regulatory system. Sapkota and Bastola (2017) analyzed the impact of FDI and income on pollution in 14 Latin-American countries for the time series of 1980–2010, applying PHH and EKC hypotheses. The results conveyed that policies concentrating on clean and energy-effective industries through FDI would be sustainable and flourish economically. The research of Zomorrodi et al. (2017) suggested that better environmental regulation with modern technology from FDI can help reduce problems regarding pollution, making FDI beneficial. A similar line of findings is available in the study of Seker et al. (2015).

The second line of association documented a negative association between them (Hitam et al., 2012; Arif et al., 2021). The study of Bulus et al. (2021), see, for example, analyzed the impact of FDI and government spending on the environmental quality in Korea from 1970 to 2018 using ARDL. The results of the study say that as FDI increases, pollution increases, limiting and degrading environmental quality. Thus, it recommends implementing holistic green-growth measures. The study by Khan et al. (2020) examined the connection between environmental pollution by carbon dioxide emission through FDI in 17 countries in Asia for the phase from 1980 to 2014. Through panel co-integration and other tests, the results conveyed that FDI increases environmental pollution, so more government initiatives should be implemented to reduce such pollution from FDI. Rafindadi et al. (2018) examined the impact of FDI and energy consumption on the environment of GCC economies from 1990–2014, applying the PMG methodology. The study results show a negative association with the environment as FDI inflows, suggesting promoting green energy to assure the reduction of carbon dioxide emission. The study of Doytch and Uctum (2016) analyzed the correlation of environment on FDI inflows in low and lower-middle income countries for the period of 1984–2011 using the system GMM method. The results showed a negative association as FDI inflows degrades the environment which is proved in three levels of studies and for the reliability of the conclusion it used all sectors' data but not just the firm level. The article of Hakimi et al. (2016) investigated the economic impact of FDI on environmental quality in Tunisia and Morocco (1971–2013) using VECM and co-integration techniques. The results concluded that trade liberation has a negative impact on the environment though it may benefit economies. The research investigated whether environmental pollution is a concerning issue of FDI in Malaysia for the phase 1965–2010, applying a non-linear model. The study documented the existence of the Kuznets curve and as FDI increases, the environment degrades badly.

The third line of evidence suggests a neutral association between environmental quality and FDI inflows in the economy (Kurtishi-Kastrati, 2013; Adeel-Farooq et al., 2021; Neequaye and Oladi, 2015). The study of Demena and Afesorgbor (2020), for example, investigated the impact of FDI on environment quality using mixed-income countries for 2017 and 2018 using meta-analysis. Contrary to the literature, which conveys the negative impact of these two variables, the study shows the likelihood of a positive association between them. Thus, theoretically, there could be positive and negative associations of FDI and a cleaner environment (Manigandan et al., 2022). Different pollutants represent controversial outcomes following a neutral outcome of the study. Pazienza (2019) investigated the relationship and magnitude of the FDI impact on the environment in 30 OECD countries from 1989-to 2016 using the panel data technique. The study's findings mostly supported the positive coalition of FDI on the environment through some adverse impacts on some alternative specifications, making the study reconsider.

TABLE 1 Variable proxies and data sources.

Variable	Definition	Unit	Data sources
Foreign direct investment	Net inflows of FDI as a % of GDP	%	WDI
Financial inclusion	No. of branches per 100,000 people	Index	
Environmental quality	Carbon emission		WDI
Good governance	Governmental effectiveness		WGI
Trade openness	Sum of import and export as a % of GDP	%	WDI
Gross capital formation	Gross capital formation as a % of GDP	%	WDI

TABLE 2 Results of the cross-sectional dependency test and heterogeneity test.

	LM_{BP}	LM_{PS}	LM_{ADJ}	CD_{PS}	Δ	Adj.Δ
FDI	441.604***	18.05***	113.931***	31.89***	34.76***	42.974***
EQ	152.958***	33.988***	183.79***	16.134***	14.619***	34.55***
GG	162.324***	42.36***	178.833***	51.438***	22.865***	51.949***
FI	395.765***	32.593***	126.278***	32.271***	45.425***	31.26***
TO	279.815***	17.766***	244.677***	26.758***	17.537***	44.178***
GCF	402.36***	36.963***	209.303***	13.35***	5.318***	35.329***

Note: the superscript *** denotes a 1% level of significance.

The research of Shahbaz et al. (2015) aimed to examine the non-linear correlation of FDI and environmental degradation for all 99 income-based economies from 1975 to 2012 using the FMLOS and causality test. The study documented that different levels have different impacts of FDO on their respective environment, so sound policies should be implemented to improve the environmental quality and economic situation using FDI (Rehman and Noman, 2022).

3 Data and methodology

3.1 Model specification

The present study intended to investigate the impact of environmental quality, good governance, and financial inclusion on FDI inflows in the BRI counties (a panel of 59 nations) from 1990 to 2020. The study considered a panel of six BRI nations and selected target countries purely relying on data availability. The pertinent data for the study have been extracted from world development indicators published by the World Bank and international financial statistics published by the International Monetary Fund (IMF). All the data were transformed into a natural logarithm prior to empirical estimation to reduce internal data inconsistencies (Qamruzzaman and Karim, 2020). The generalized empirical model is as follows:

$$FDI^{*} = \alpha_0 + \beta_1 EQ_{it} + \beta_2 FI_{it} + \beta_3 GG_i^{*} + \beta_3 X_i^{*} \omega_{it} \qquad (1)$$

FDI stands for foreign direct investment in the economy, FI denotes financial inclusion, EQ specifies environmental quality, GG stands for good governance, and X* for the equation's list of control variables. Table 1 displays the research variables, proxies, and data sources.

3.2 Variables' definitions

As an explained variable, FDI is proxied by net inflows of FDI as a % GDP. For explanatory variables, the study has accounted for financial accessibility, financial inclusion, the stats of environmental protection measured by carbon emission, and a strong governmental initiative in the economy Table 2.

Apart from the explained and explanatory variables, following the existing literature dealing with the determinants of FDI, the present study has considered trade openness (TO) which is measured by the total trades as a % of the GDP and gross capital formation (GCF), which is proxied by total gross capital formation as a % of GDP. It is

anticipated that economic openness and capital adequacy in the economy positively accelerate the inflows of FDI by enticing foreign investors to channel their capital in the form of FDI (Hamid et al., 2022b).

3.3 Estimation strategy

3.3.1 Cross-sectional dependency test and test of heterogeneity.

Globalization established interconnection across the world; therefore, every economy is prone to react due to economic shocks in other economies (Jia et al., 2021; Qamruzzaman, 2022b; Zhuo and Qamruzzaman, 2022). As a result, empirical research employing panel data will almost certainly be necessary to ascertain the existence of cross-sectional dependence. The literature has suggested several ways to detect the possible presence of cross-sectional dependency by employing the CD_{lm} test offered by Breusch and Pagan (1980), the CD_{lm} test with a scaled version following Pesaran (2021), the CD test following Pesaran (2006), and the bias-adjusted LM test proposed by Pesaran et al. (2008).

The LM test statistics can be computed with the following equation:

$$LM = T\sum_{i=1}^{N-1}\sum_{j=i+1}^{N}\hat{\rho}_{IJ\to d}X^2N(N+1)2, \tag{2}$$

where $\hat{\rho}_{ij}$ represents the pairwise correlation of the residuals.

The scaled version of the Lagrange multiplier (CD_{lm}) can be implemented in the following manner

$$CD_{lm} = \sqrt{\frac{N}{N(N-1)}}\sum_{I=1}^{N-1}\sum_{J=i+1}^{N}\left(T\hat{\rho}_{ij}-1\right) \tag{3}$$

The proposed cross-sectional test established by Pesaran (2006), commonly known as the CD test, can be executed with the following equation.

$$CD_{lm} = \sqrt{\frac{2T}{N(N-1)}}\sum_{I=1}^{N-1}\sum_{J=i+1}^{N}\left(\hat{\rho}_{ij}\right) \tag{4}$$

Finally, the CD test following Pesaran et al. (2008), known as bias-adjusted LM statistics, can be computed with the following equation:

$$CD_{lm} = \sqrt{\frac{2}{N(N-1)}}\sum_{I=1}^{N-1}\sum_{J=i+1}^{N}\left(\frac{(T-K)\hat{\rho}_{ij}^2-u_{Tij}}{v_{Tij}^2}\right)\vec{d}(N,0) \tag{5}$$

3.4 Panel unit root test

The framework for the unit root test with CADE following Pesaran (2007) is as follows:

$$\Delta Y_{it} = \mu_i + \theta_i y_{i,t-1} + \gamma_i\bar{y}_{t-1} + \vartheta_i\bar{y}_t + \tau_{it} \tag{6}$$

Putting long-term in Eq. 7 results in the subsequent Eq. 8:

$$\Delta Y_{it} = \mu_i + \theta_i y_{i,t-1} + \gamma_i\bar{y}_{t-1} + \sum_{k=1}^{p}\gamma_{ik}\Delta y_{i,k-1} + \sum_{k=0}^{p}\gamma_{ik}\overline{\Delta y}_{i,k-0} + \tau_{it} \tag{7}$$

where $Y_{it}-1$ and $\bar{y}_{t-1}$ stand as the lagged level average and the first difference operator for each cross-section, respecitvely;the CIPS unit root test is displayed in Eq. 9.

$$CIPS = N^{-1}\sum_{i-1}^{N}\partial_i(N,T) \tag{8}$$

where the parameter $\partial_i(N,T)$ explain the test statistics of CADF, which can be replaced in the following manner:

$$CIPS = N^{-1}\sum_{i-1}^{N}CADF \tag{9}$$

3.5 Westerlund co-integration test

The error-correction techniques for long-run co-integration assessment following Westerlund (2007) are as follows:

$$\Delta Z_{it} = \partial_i^{'}d_i + \varnothing_i\left(Z_{i,t-1}-\delta_i^{'}W_{i,t-1}\right) + \sum_{r=1}^{p}\varnothing_{i,r}\Delta Z_{i,t-r} + \sum_{r=0}^{p}\gamma_{i,j}\Delta W_{i,t-r} + \epsilon_{i,t} \tag{10}$$

The results of the group test statistics can be derived with Eqs 12, 13.

$$G_T = \frac{1}{N}\sum_{i-1}^{N}\frac{\varphi_i}{SE\varphi_i} \tag{11}$$

$$G_a = \frac{1}{N}\sum_{i-1}^{N}\frac{T\varphi_i}{\varphi_i(1)} \tag{12}$$

The test statistics for panel co-integration can be extracted by implementing Eqs 14, 15:

$$P_T = \frac{\varphi_i}{SE\varphi_i} \tag{13}$$

$$P_a = T\varphi_i \tag{14}$$

3.6 Cross-sectional ARDL

Nonetheless, the defects in panel ARDL are cross-sectional. However, if the unobserved common components of the regressors are connected, such apparent conceptions may result in erroneous estimates and adversely biased estimations in certain cases. Chudik and Pesaran (2015) proposed the common correlated effects (CCE) approach to panel ARDL models. Pesaran (2006) explains how the equation's average values represent unobserved common components as proxy variables for dependent and independent variables. As a consequence, when Eqs 2, 3 are averaged across time, the result is that we obtain:

$$\overline{FDI}_{it} = \bar{\alpha}_{it} + \sum_{j=1}^{p}\bar{\beta}_{ij}\overline{FDI}_{i,t-j} + \sum_{j=0}^{q}\bar{\gamma}_{ij}\overline{GLO}_{i,t-j} + \sum_{j=0}^{q}\bar{\gamma}_{ij}\overline{EQ}_{i,t-j} + \sum_{j=0}^{q}\bar{\gamma}_{ij}\overline{FI}_{i,t-j} + \bar{\omega}_t^{'}Q_t + \bar{\epsilon}_{it} \tag{15}$$

where $\bar{\alpha}_{it} = \frac{\sum_{i=1}^{N}\alpha_i}{N}$

$\overline{FDI}_{t-j} = \frac{\sum_{i}^{N}FDI_{i,,t-j}}{N}, \overline{GLO}_j = \frac{\sum_{i}^{N}GLO_{i,j}}{N}\ j = 0, 1, 2p$

$\overline{EQ}_{t-j} = \frac{\sum_{i}^{N}EQ_{i,,t-j}}{N}, \overline{FI}_j = \frac{\sum_{i}^{N}FI_{i,j}}{N}, J = 0, 1, 2q\ \bar{\omega}_j = \frac{\sum_{i=1}^{N}\omega_i}{N}, \bar{\varepsilon}_t = \frac{\sum_{i}^{N}\epsilon_{i,t}}{N}$

It is further extended as follows:

$$\begin{aligned}\overline{FDI}_{it} &= \bar{\alpha}_{it} + \sum_{j=1}^{p}\bar{\beta}_{ij}\overline{FDI}_{i,t-j} + \sum_{j=0}^{q}\bar{\gamma}_{ij}\overline{GLO}_{i,t-j} + \sum_{j=0}^{q}\bar{\gamma}_{ij}\overline{EQ}_{i,t-j} + \sum_{j=0}^{q}\bar{\gamma}_{ij}\overline{FI}_{i,t-j} + \bar{\omega}_t^{'}Q_t\downarrow\\ \bar{\omega}_t^{'}Q_t &= \overline{FDI}_{it} - \bar{\alpha}_{it} + \sum_{j=1}^{p}\bar{E}_{ij}\overline{FDI}_{i,t-j} + \sum_{j=0}^{q}\bar{\gamma}_{ij}\overline{GLO}_{i,t-j} + \sum_{j=0}^{q}\bar{\gamma}_{ij}\overline{EQ}_{i,t-j} + \sum_{j=0}^{q}\bar{\gamma}_{ij}\overline{FI}_{i,t-j}\\ G_t &= \overline{FDI}_{it} - \bar{\alpha}_{it} + \sum_{j=1}^{p}\bar{E}_{ij}\overline{FDI}_{i,t-j} + \sum_{j=0}^{q}\bar{\gamma}_{ij}\overline{GLO}_{i,t-j} + \sum_{j=0}^{q}\bar{\gamma}_{ij}\overline{EQ}_{i,t-j} + \sum_{j=0}^{q}\bar{\gamma}_{ij}\overline{FI}_{i,t-j}\Big/\bar{\omega}_t^{'}\end{aligned} \tag{16}$$

Thus, the panel CS-ARDL specification of Eq. 17 is

$$FDI_{it} = \epsilon_{it} + \sum_{j=1}^{p}\bar{E}_{ij}\overline{FDI}_{i,t-j} + \sum_{j=0}^{q}\bar{\gamma}_{ij}\overline{GLO}_{i,t-j} + \sum_{j=0}^{q}\bar{\gamma}_{ij}\overline{EQ}_{i,t-j} + \sum_{j=0}^{q}\bar{\gamma}_{ij}\overline{FI}_{i,t-j} + \sum_{j=0}^{p}\bar{\partial}_t^{'}\bar{Q}_{i,t-j} + \epsilon_{it} \tag{17}$$

where $\bar{Q} = (\overline{FDI}, \bar{X})$ and $S_{\bar{Z}}$ are the number of lagged cross-sectional averages. Furthermore, Eq. 8 can be re-parameterized to the effects of ECM presentation of panel CS-ARDL as follows:

$$\begin{aligned}\Delta FDI_{it} &= \alpha_i + \xi_i\left(FDI_{it-1} - \omega_t^{'}X_{it-1}\right) + \sum_{J=1}^{M-1}\gamma_{ij}\Delta FDI_{it-J} + \sum_{J=0}^{N-1}\beta_{ij}\Delta X_{it-J} + \sum_{j=1}^{p}\lambda_j\overline{\Delta FDI}_{i,t-j}\\ &+ \sum_{j=0}^{q}\delta_j\overline{\Delta X}_{i,t-j} + \sum_{j=0}^{S_{\bar{Z}}}\bar{\partial}_{tj}^{'}\bar{Q}_{i,t-j} + \mu_{it}\end{aligned} \tag{18}$$

where $\overline{\Delta FDI}_{t-j} = \frac{\sum_{i}^{N}\Delta FCF_{i,,t-j}}{N}$ and $\overline{\Delta X}_{t-j} = \frac{\sum_{i}^{N}\Delta R_{i,,t-j}}{N}$

3.7 Asymmetric ARDL estimation

In the recent literature, the application of a non-linear framework has extensively considered addressing the asymmetric effects of explanatory variables on target variables (Anwar et al., 2021; Liu and Qamruzzaman, 2021; Yang et al., 2021; Adebayo et al., 2022; Qamruzzaman, 2022a; Xia et al., 2022). The following non-linear equation has been developed following the initial non-linear framework familiarized by Shin et al. (2014).

$$\begin{aligned}\Delta FDI_{it} &= \beta_{0i} + \beta_{1i}FDI_{it-1} + \beta_{2i}^{+}FI_{t-1}^{+} + \beta_{2i}^{-}FI_{t-1}^{-} + \beta_{3t}^{+}EQ_{t-1}^{+} + \beta_{3t}^{-}EQ_{t-1}^{-} + \beta_{4t}^{+}GG_{t-1}^{+} + \beta_{4t}^{-}GG_{t-1}^{-}\\ &+ \sum_{J=1}^{M-1}\gamma_{ij}\Delta FDI_{i,t-J} + \sum_{J=0}^{N-1}\left(\gamma_{ij}^{+}\Delta FI_{i,t-j}^{+} + \gamma_{ij}^{-}\Delta FI_{i,t-j}^{-}\right)\\ &+ \sum_{J=0}^{O-1}\left(\left(\delta_{ij}^{+}\Delta EQ_{i,t-j}^{+} + \delta_{ij}^{-}\Delta EQ_{i,t-j}^{-}\right)\right)\\ &+ \sum_{J=0}^{P-1}\left(\mu_{ij}^{+}\Delta GG_{i,t-j}^{+} + \mu_{ij}^{-}\Delta GG_{i,t-j}^{-}\right) + \varepsilon it\end{aligned} \tag{19}$$

The asymmetric shocks of financial inclusion (FI^{+}/ FI^{-}), good governance (GG^{+}/ GG^{-}), and environmental quality (EQ^{+}/ EQ^{-}) can be derived by executing the following equations.

$$\begin{cases}FI_i^{+} = \sum_{k=1}^{t}\Delta FI_{ik}^{+} = \sum_{K=1}^{T}MAX\left(\Delta FI_{ik}, 0\right)\\ FI_i^{-} = \sum_{k=1}^{t}\Delta FI_{ik}^{-} = \sum_{K=1}^{T}MIN\left(\Delta FI_{ik}, 0\right)\end{cases} \tag{20}$$

$$\begin{cases}EQ_i^{+} = \sum_{k=1}^{t}\Delta EQ_{ik}^{+} = \sum_{K=1}^{T}MAX\left(\Delta EQ_{ik}, 0\right)\\ EQ_i^{-} = \sum_{k=1}^{t}\Delta EQ_{ik}^{-} = \sum_{K=1}^{T}MIN\left(\Delta EQ_{ik}, 0\right)\end{cases} \tag{21}$$

$$\begin{cases}GG_t^{+} = \sum_{k=1}^{t}\Delta GG_{ik}^{+} = \sum_{K=1}^{T}MAX\left(\Delta GG_{ik}, 0\right)\\ GG_t^{-} = \sum_{k=1}^{t}\Delta GG_{ik}^{-} = \sum_{K=1}^{T}MIN\left(\Delta GG_{ik}, 0\right)\end{cases} \tag{22}$$

The error correction version of Eq. 19 is as follows:

TABLE 3 First-generation panel unit root test.

	Levin, Lin, and Chu t		Im, Pesaran, and Shin W-stat		ADF–Fisher chi-square	
	t	t&c	t	t&c	T	t&c
Panel –A: At a level						
FDI	−3.071	−0.677	−3.994	−3.881	59.001	40.281
EQ	−3.268	−3.467	−3.592	−2.093	47.749	56.297
GG	−0.302	−1.555	−0.03	−3.946	45.164	46.11
FI	−0.664	−0.279	−1.057	−1.073	37.585	35.792
TO	−1.482	−2.704	−1.876	−2.178	53.706	54.593
GCF	−2.663	−2.004	−1.128	−2.453	45.418	56.137
Panel –B: after the First difference						
FDI	−8.276***	−20.401***	−14.056***	−5.93***	199.245***	150.151***
EQ	−12.864***	−19.765***	−7.414***	−6.912***	204.401***	88.035***
GG	−5.649***	−15.104***	−19.304***	−5.235***	140.385***	96.859***
FI	−5.872***	−6.966***	−7.928***	−5.735***	292.066***	206.338***
TO	−6.796***	−22.47***	−7.195***	−7.182***	201.12***	185.119***
GCF	−9.423***	−6.69***	−16.448***	−7.685***	295.895***	104.256***

Note: */**/*** denotes the level of significant at a 10%/5/1%, respectively. Δ specify the first difference operation.

TABLE 4 Results of second-generation unit root test.

	CIPS		CADF	
	At level	First difference	At level	First difference
FDI	−2.494	−4.911***	−1.185	−3.496***
EQ	−2.126	−6.932***	−1.52	−4.233***
GG	−1.162	−5.113***	−2.76	−5.218***
FI	−2.823	−3.091***	−2.286	−2.237***
TO	−1.509	−5.087***	−1.433	−4.764***
GCF	−1.504	−3.028***	−2.971	−7.701***

Note: */**/***, denotes the level of significant at a 10%/5/1%, respectively. Δ specify the first difference operation.

$$\Delta FDI_{it} = \tau_{1i}\xi_{it-1} + \sum_{J=1}^{M-1}\gamma_{ij}\Delta FDI_{i,t-J} + \sum_{J=0}^{N-1}\left(\gamma_{ij}^{+}\Delta FI_{i,t-j}^{+} + \gamma_{ij}^{-}\Delta FI_{i,t-j}^{-}\right) + \sum_{J=0}^{O-1}\left(\left(\delta_{ij}^{+}\Delta EQ_{i,t-j}^{+} + \delta_{ij}^{-}\Delta EQ_{i,t-j}^{-}\right)\right) + \sum_{J=0}^{P-1}\left(\mu_{ij}^{+}\Delta GG_{i,t-j}^{+} + \mu_{ij}^{-}\Delta GG_{i,t-j}^{-}\right) + \varepsilon it \tag{23}$$

4 Model estimation and interpretation

4.1 Unit root test, homogeneity test, and cross-sectional dependency test

In the cross-sectional dependency test, we evaluated all four tests. All test variable values were statistically significant in the Breusch–Pagan LM (Breusch and Pagan, 1980), Pesaran-scaled LM, Pesaran bias-corrected scaled LM, and Pesaran CD. The four cross-sectional dependency tests have a cross-sectional relationship between all variables. Each variable influences or contributes to the outcome of another value. Each of the six variables is dependent on the others. They do not have to be mutually exclusive; one influences the other. Each variable seems significant, implying that the data and variables we use to describe teats are cross-sectionally dependent and influence one another. Along with CDS, the following section will look into heterogeneity using the Pesaran and Yamagata (2008) framework. The estimate's findings Table 2. Comprising two coefficients, adj., and by rejecting the null hypothesis of homogeneity at a 1% significance level, the study's findings show that heterogeneous traits are present in the sampled dataset.

Next, the study employed first-generation and second-generation unit root tests to document the variable's order of integration. The panel unit root test result is displayed in

TABLE 5 Panel co-integration test.

Panel A: Pedroni panel co-integration test				
Panel $_{\text{v-Statistic}}$	2.005		Panel $_{\text{v-Statistic}}$	−1.437
Panel $_{\text{rho-Statistic}}$	−6.407***		Panel $_{\text{rho-Statistic}}$	−11.635***
Panel $_{\text{PP-Statistic}}$	−10.444***		Panel $_{\text{PP-Statistic}}$	−10.844***
Panel $_{\text{ADF-Statistic}}$	−5.726***		Panel $_{\text{ADF-Statistic}}$	−9.859***
Group $_{\text{rho-Statistic}}$	−8.295***			
Group $_{\text{PP-Statistic}}$	−10.775***			
Group $_{\text{ADF-Statistic}}$	−2.884			
Panel B: Westerlund (2007) panel co-integration test				
Model	Gt	Ga	Pt	Pa
FDI|GLO, EQ, FI, X	−12.579***	−10.351***	−15.714***	−12.118***

Note: */**/***, denotes the level of significant at a 10%/5/1%, respectively.

TABLE 6 Baseline estimation: financial inclusion, financial efficiency, and foreign capital inflows.

Variable	OLS	Random effect	Fixed effects
EQ	0.11 (0.0259)[4.237]	0.486 (0.0513)[9.465]	0.201 (0.0441)[4.551]
GG	0.141 (0.0283)[4.968]	0.321 (0.0794)[4.042]	0.32 (0.0282)[11.347]
FI	0.309 (0.0305)[10.12]	0.099 (0.0099)[9.989]	0.407 (0.0364)[11.162]
TO	0.521 (0.1128)[4.617]	0.208 (0.0339)[6.126]	0.111 (0.0094)[11.766]
GCF	0.269 (0.0216)[12.421]	0.168 (0.0301)[5.579]	0.603 (0.0988)[6.102]
C	−0.042 (0.0065)[−6.365]	−0.198 (0.0156)[-12.671]	0.574 (0.1214)[4.726]
H-test (p-value		0.151	

Note: the superscript of *** denotes the significance level at a 1% level.

Tables 3, 4. According to the first-generation unit root test statistics, all the variables are exposed to stationary after the first difference but neither revealed stationary after the second difference.

The second-generation unit root test has been implemented following the framework proposed by Pesaran (2007), which is widely known as CIPS and CADF. Referring to the test statistics seen in Table 3, the null hypothesis of non-stationary has been rejected after the first difference assessment. The study established that all the research units are stationary after the first difference, and none are exposed to the second difference. Study findings from Unit root test has suggested the inclusion and implementation of robust econometric techniques for empirical assessment.

The study has executed a panel co-integration test following Pedroni (2001) and further developed by Pedroni (2004) and Westerlund (2007) in assessing the long-run association between FDI and explanatory variables. The results of the panel co-integration test are displayed in Table 5. The Pedroni co-integration test results are displayed in Panel–A of Table 5. The study documented that the majority of the test statistics revealed statistical significance at a 1% level, explaining the rejection of the null hypothesis, that is, no co-integration. Alternatively, the study unveiled the long-run association between FDI, environmental quality, financial inclusion, good governance, trade openness, and gross capital formation in BRI nations. The study further moves in assessing the long-run association by using the co-integration test based on the error-correction term. According to the test output, panel-B in Table 5, all the statistics are statistically significant at a 1% level, suggesting the long-term relationship between FDI inflows and explanatory variables.

4.2 Baseline estimation with OLS, RE, and FE

Prior to executing the target model, the study assessed the empirical equation by implementing OLS, random-effect, and fixed-effects regression to get the intended association

TABLE 7 Results of CS-ARDL estimation.

Variable	Coefficient	Std. Error	t-Statistic	Variable	Coefficient	Std. error	t-Statistic
Panel–A: Long run equation				Panel–B: Short run equation			
FI	0.0960***	0.0099	9.6412	ΔFI	0.0347***	0.0068	5.0956
EQ	0.0597**	0.0436	1.3695	ΔEQ	0.0438**	0.0261	1.6730
IQ	0.1041***	0.0451	2.3119	ΔIQ	0.0318**	0.0167	−1.9021
TO	0.0592**	0.0429	1.3795	ΔTO	0.0561***	0.0208	2.6977
GCF	0.0711**	0.0454	1.5665	ΔGCF	0.0791***	0.0128	6.1697
				ECT (−1)	−0.2557***	0.0488	−5.2301
				C	2.7213***	0.2054	13.2456
				CD test	17.311		

Note: the superscript ***/**/* denotes the level of significant at a 1%/5%/10% level.

between environmental quality, good governance, and financial inclusion on FDI inflows in BRI nations. According to the Hausman test statistic and associated *p*-value, the fixed-effects model estimation revealed efficiency in explaining the empirical association between FDI and explanatory variables. The results of baseline estimation are displayed in Table 6. The studies documented that environmental quality measured by carbon emission is positively connected with FDI inflows, suggesting that less-regulated environmental policies act as inducing factors and motivate the foreign investor to channel funds to the host economy. Furthermore, good governance and institutional quality revealed a positive relation with FDI inflows, implying that the protection of invested capital, stability of law and order, and governmental effectiveness in ensuring a congenial environment indulge the foreign investors in transferring knowledge and technology in those economies. The role of financial inclusion has been disclosed as positive and statistically significant to FDI, implying that financial institutions' access to financial services and benefits ensure efficient financial intermediation and efficient reallocation of economic resources in the economy. Referring to the control variable's impact on FDI inflows, it is apparent that a positive effect running from trade openness and gross capital formation in the economy accelerates the present trend in FDI inflows in the economy.

4.3 CS-ARDL estimation

Next, the study investigates the impact of financial inclusion, environmental quality, and good governance on FDI inflows in BRI nations using Equation 16. The results of CS-ARDL are displayed in Table 7.

Financial inclusion on FDI inflows in BRI countries has been positive and statistically significant in the long run (short-run) with a coefficient of 0.096 (0.0347). It suggests that access to financial services and benefits in the financial system allows investors to get pertinent information and efficient financial intermediation, which motivates foreign investors to select an economy for their capital investment destination. In particular, study coefficients advocated that a 10% development in access to financial services will increase the present trend of FDI inflows in the economy by 0.96% in the long run and 0.347% in the short run. The existing literature supports our study findings, for instance, Bevan et al. (2004), Toxopeus and Lensink (2008), Qamruzzaman and Wei (2019), and Zwedu (2014), but conflicts with the study findings of Morgan and Pontines (2014), Singh and Zammit (2000), and Morgan and Pontines (2018).

The study documented the positive effects of environmental quality on FDI inflows in the long run (a coefficient of 0.0597) and the short run (a coefficient of 0.0438). This suggests a 10% increase in carbon emission will augment FDI inflows in the economy by 0.597% in the long run and 0.438% in the short run. The positive association between carbon emission and FDI indicates the "pollution haven" hypothesis that foreign investors prefer an environmentally less-regulated economy for their capital flows because clean energy integration in the production process incurs additional investment costs. The study's findings are in line with the existing literature, for instance, Pingfang et al. (2011), Shao et al. (2022), but contradict the study findings of Yüksel et al. (2020) for G7 countries and those of Shao et al. (2022) in China.

The impact of good governance on FDI inflows in BRI was established to be positive and statistically significant both in the long run (a coefficient of 0.1041) and in the short run (a coefficient of 0.0318). In particular, a 1% institutional

TABLE 8 Results of the asymmetric effect assessment.

Variable	Coefficient	Std. error	t-Statistic		Coefficient	Std. error	t-Statistic
Panel-A: Long-run equation				*Panel-B: Short-run equation*			
FI^{+}	0.13583***	0.055665	2.440133	ΔFI^{+}	0.0642***	0.013029	4.931499
FI^{-}	0.0916**	0.055454	1.652613	ΔFI^{-}	0.0605***	0.017873	3.345203
EQ^{+}	0.0243***	0.009465	2.570523	ΔEQ^{+}	−0.075***	0.020981	−3.60326
EQ^{-}	0.1223***	0.011959	10.23246	ΔEQ^{-}	−0.0603**	0.030862	−1.95444
GG^{+}	0.0923***	0.031341	2.947736	ΔIQ^{+}	0.0664***	0.023574	2.817723
GG^{-}	0.1401***	0.034142	4.106174	ΔIQ^{-}	−0.0681*	0.06357	−1.07236
TO	0.1372***	0.013558	10.12288	ΔTO	−0.0543**	0.020411	−2.66116
GCF	0.0542***	0.018443	2.941767	ΔGCF	0.0355**	0.015494	2.295727
				ECT (−1)	−0.1821***	0.036693	−4.96463
				C	−0.7604***	0.019185	-39.6356
Symmetry test for long run and short run							
W_{LR}^{FI}	12.6415***			W_{SR}^{FI}	9.845***		
W_{LR}^{GG}	11.511***			W_{SR}^{GG}	1.642		
W_{LR}^{EQ}	21.512***			W_{SR}^{EQ}	2.341		
Hausman test	3.641 (0.8574)						
No of obs	810						
likelihood	2030.143						

Note: the superscript ***/**/* denotes the level of significant at a 1%/5%/10% level.

development can accelerate the economy's FDI inflow by 0.1041% in the long run and 0.0318% in the short run. Study findings postulate that governmental effectiveness ensures investment protection and amicable ambiance for investment, which induces foreign investors to transfer capital to an economy with a strong governmental presence. The existing literature supports our study findings such as Mengistu and Adhikary (2011) in Asian countries, Fazio and Chiara Talamo (2008), (Shah et al., 2015) in SAARC nations, Niarachma et al. (2021) in ASEAN countries, and Kayani and Ganic (2021) in China.

Referring to controlling variables' effects on foreign direct investment, the study documented that trade openness (TO) and gross capital formation (gcf) are positively associated in the long run and short run. More precisely, 10% domestic trade openness (gross capital formation) increases the foreign direct investment by 0.592% (0.911%) in the long run and by 0.561% (0.791%) in the short run. The study findings postulated that domestic trade internationalization creates an open market for additional demand that offers investment opportunities in the economy. Furthermore, capital adequacy ensures investment capitalization and aggregate output expansion, which is the opportunity for further investment, eventually motivating foreign investors to maximize economic resource reallocation.

4.4 Non-ARDL estimation

The study has implemented the non-linear framework for assessing the asymmetric effects of financial inclusion, environmental quality, and good governance on inflows of FDI in BRI nations. The result of asymmetric estimation is displayed in Table 8. The long-run asymmetric coefficients and symmetry tests are displayed in Panel-A, and the short-run coefficient and symmetry test results are available in Panel-B.

Reforest to asymmetric effects of financial inclusion on FDI inflows in a long-run study documented positive and statistically significant links between asymmetric shocks that are positive (a coefficient of 0.1358) and negative (a coefficient of 0.0916) and FDI inflows in the BRI. The study findings postulated that access to financial services and benefits increases FDI inflow and *vice versa*. In particular, a 10% positive (negative) innovation in financial inclusion in the financial system can accelerate (decrease) the inflows of FDI by 1.1358% (0.9165). A similar

TABLE 9 Results of the panel Granger causality test under the error-correction term.

Causality assessment							
	Short-run causalities						Long-run
	FDI	FI	EQ	IQ	TO	GCF	ECT (-1)
FDI	-	12.1438***	5.8334***	10.462***	1.5378	9.1511***	−0.1562***
FI	6.852***	-	2.106	11.7124***	6.5361***	1.8267	0.6104
EQ	19.8439***	23.4799***	-	19.3778***	2.7017	5.2079***	0.5263
IQ	51.4986***	16.2003***	21.317***	-	0.9403	60.9416***	−0.2705***
TO	1.8661	3.9365	11.6105	5.8755****	-	11.442***	−1.4853***
GCF	45.0086***	1.8226	4.7104	5.0565***	0.8972	-	0.4641

Note: the superscript ***/**/* denotes the level of significant at a 1%/5%/10% level.

line of evidence can be found that is a positive and statistically significant relation between the asymmetric shock of financial inclusion and FDI in the short run. More precisely, a 10% development in financial inclusion will increase FDI inflows by 0.642%. The disadvantageous outcome can be derived from a 10% negative innovation in financial accessibility with an elasticity of 0.605%. The study documented that environmental quality positively influences FDI inflows. A 1% increase in carbon emission will boost the trend of FDI in the economy by 0.234%. The similar rate of carbon contraction results in a downward trend in receiving FDI in the BRI nations by 1.223%. In terms of a short-run assessment, the study documented asymmetric shocks of environmental quality that are positive (a coefficient of −0.0756) and negative (a coefficient of −0.06032), exposing a negative and statistically significant link with FDI inflows. Accounting for the asymmetric environmental quality assessment on FDI, it is apparent that relaxed and less-regulated environmental regulations motivate foreign investment. It indicates that foreign investors prefer to mobilize their capital to those economies where they can capitalize on the benefits of conventional energy application at the cost of ecological degradation. Furthermore, the inclusion of clean energy becomes costly in the initial stage; therefore, an environmentally strict and strongly regulated economy is the least preferred among foreign investors.

The asymmetric effects of good governance on FDI inflows have been positively and statistically significant, suggesting that storing governmental activities and investment protection induce foreign capital flow in the economy. In particular, a 10% positive (negative) shock in good governance can increase (decrease) FDI inflows in the BRI by 0.923% (1.401%). A study suggests that governmental quality determination significantly impacts FDI, and its elasticity has a greater impact than a positive development in governmental practices. For the short run, the asymmetric short of good governance has established that positive (negative) shocks are positive (negative) and statistically significant. More precisely, 10% positive (negative) innovation causes inflows of FDI by 0.664% (−0.681%).

The standard Wald test has been implemented to assess the possible asymmetric association between financial inclusion, good governance, environmental quality, and FDI in the long and short runs with a null symmetry hypothesis. The results of the Wald test suggested that rejecting the null hypothesis alternatively established asymmetric association, especially in the long run.

4.5 Panel Granger causality test under VECM

The study implements the Granger causality test under the error correction term to assess the directional association between environmental qualities, good governance, financial inclusion, trade openness, gross capital formation, and FDI. The causality test results are displayed in Table 9. The coefficient of long-run causalities can be derived from ECT (−1), which must be negative and statistically significant. According to an ECT (−1) study which documented long-run causalities in the empirical equation with FDI, IQ too is a dependent variable. In the short run, the study documented several causalities. The bidirectional causality has been established between financial inclusion, environmental quality, good governance, and gross capital formation with foreign direct investment [FI←→FDI; EQ←→FDI; IQ←→FDI; and GCF←→FDI].

5 Discussion of the study findings

Financial inclusion has revealed a catalyst for augmenting FDI inflows in BRI nations, suggesting a 1% growth of easy accessibility to financial services and benefits in the financial system which can accelerate the FDI inflows by 0.097% in the

long run to 0.0346% in the short run. The study postulated that opening the financial services and benefits with a reasonable cost and process will boost foreign investors and support investment decisions, eventually transferring capital and technology to those economies in the form of investments. Due to its potential to accelerate an economy's growth and sustainability, financial inclusion has focused worldwide interest in development finance and economics for years. Because millions of individuals throughout the world are banned from formal financial institutions, there is a risk of losing deposits or savings and investable money, and hence the global economy's ability to build wealth. The potential of financial services to facilitate credit creation and capital accumulation, hence promoting investment and economic activity, is well-recognized. Martinez (2011) advocated that governments and politicians should use financial access to support economic progress. Economic activity and production are increased by improving economic actors' access to and the availability of money. Financial inclusion helps people of all income levels to participate in the financial system and contribute to inclusive development. The study of Al-Zubaidi and Khudair (2021) established that the host's economy financial accessibility and easy access to essential financial supports motivate foreign investors to transfer their expertise, technological know-how, and competencies in the form of capital. Furthermore, the study suggested that financial inclusion helps the country's economic and social development by maintaining a continuous contact between clients and banks and providing them with simple and quick access to money, all of which are necessary for growth and development.

FDI inflows in the economy accelerated capital formation and aggregated output with the potential effect of poverty reduction and trade liberalization. The study documented the positive relation between good governance and FDI inflows in BRI nations, suggesting that good governance is an effective tool for attracting foreign investors; moreover, the practices of good governance increase investors' confidence in its economic performance in the light of their investment protection (Fertő and Sass, 2020; Raza et al., 2021a). For the inflow of FDI into China, Kayani and Ganic (2021) documented that political stability, accountability, and law rules motivate foreign investors to transfer their capital and technological know-how to China. The existence of private capital defines international economic openness flows in the form of foreign direct investment (FDI), which is one of the most important sources of funding for development and productivity growth (Sahoo, 2012; Zhuo and Qamruzzaman, 2021). Foreign direct investment (FDI) is advantageous to most countries because it creates employment, increases market competition, and offers a way of transferring foreign-acquired technology and skills (Borensztein et al., 1998; Qamruzzaman, 2015; Iamsiraroj, 2016). In their respective studies, Cuervo-Cazurra (2008) and Jensen (2003) explained that the capacity of a government to maintain stable governance circumstances results in predictable and trustworthy market conditions. The government may issue this assurance to potential investors and enterprises to boost productivity and reduce manufacturing costs. Furthermore, the existing literature suggests that good governance has augmented the economic performance in terms of aggregated level and firms' level, indicating that a higher return is ensured from investment with a lower degree of risk (Billett et al., 2011; Shank et al., 2013; Qamruzzaman, 2022b; 2022c; Li and Qamruzzaman, 2022; Zhuo and Qamruzzaman, 2022). The study of Albaity et al. (2021), for example, disclosed that risk-assuming behavior had been indulged by the governmental quality that is good governance substantially reduces investment risk exposure in MENA countries. Corporate governance structures and processes become critical components in this context for maximizing returns on investment and minimizing risk. Increased interest in corporate governance laws and standards may also represent a growing realization among international and domestic investors that they assess the quality of corporate governance, financial performance, and other factors. Corporate governance mechanisms help companies demonstrate their accountability to society and investors and help domestic firms gain a competitive edge over foreign competitors, resulting in increased productivity and long-term benefits for industrialization, growth, and overall corporate performance.

Environmental development and ecological protection have been placed at the top of every discussion, indicating that economic processes at the cost of environmental degradation should not be appreciated. Therefore, controlled environment guidelines and effective implementation have been initiated worldwide. Moreover, the inclusion of clean energy and energy-efficient technology has acted differently, implying that the economic structure and status have different motivations in controlling the environment. With the increasingly serious environmental pollution, the environmental policies introduced by governments to reduce environmental pollution may lead to a decrease in foreign investment. Furthermore, relaxed and less-regulated environmental regulations act as a motivating factor for foreign investment. It indicates that foreign investors prefer to mobilize their capital to those economies where they can capitalize on the benefits of conventional energy application at the cost of ecological degradation. Furthermore, the inclusion of clean energy becomes costly in the initial stage; therefore, an environmentally strict and strongly regulated economy is the least-preferred among foreign investors (Saini and Sighania, 2019; Ssali et al., 2019; Guang-Wen et al., 2022). The positive association between carbon emission and FDI indicates the "pollution haven" hypothesis where foreign investors prefer an environmentally less-regulated economy for their capital flows because clean energy

integration in the production process incurs additional investment costs. The study findings are in line with the existing literature, for instance, Pingfang et al. (2011) and Shao et al. (2022), but contradict the study findings of Yüksel et al. (2020) for G7 countries and those of Shao et al. (2022) in China.

6 Conclusion

Receipts of foreign capital have become the key pillar for sustainable development, especially in developing nations. Moreover, the role of FDI is widely appreciated and acknowledged in capital accumulation, increase of production capacity, transfer and sharing of knowledge, and economic competitiveness (Borensztein et al., 1998). Domestic capital adequacy and sustainable economic growth immensely rely on technological advancement, managerial know-how, and money supply in the economy. In this context, FDI has emerged and is placed at an apex position due to its unprecedented impact on achieving sustainability across the world. The motivation of the study is to scale the effects of good governance, financial inclusion, and environmental quality on inflows of FDI in BRI nations for the period 1990 to 2020. Several panel econometrical tools have been applied, for example, CDS, CADF, CIPS, CS-ARDL, and NARDL, in investigating the association and explanatory variables elasticity on inflows of FDI in BRI nations. CDS results revealed that research units share common dynamism, and second-generation panel unit root test-documented variables are stationary after the first difference, and neither has been exposed after the first difference. The results of panel co-integration with the error correction term confirmed the empirical equation's long-run association. According to the CS-ARDL assessment, positive and statistically significant impacts have been documented from financial inclusion, good governance, and environmental quality to FDI inflows. The study findings suggest that governmental effectiveness, easy access to financial services and benefits, and a less-regulated environmental concern economy motivate capital transfer decisions. The asymmetric assessment documented a long-run asymmetric association between FI, GG, EQ, and FDI. Referring to asymmetric shock elasticity, the study disclosed a positive and statistically significant tie to FDI inflows, especially in the long run. Directional causality test documented bidirectional casualty running between FI, EQ, GG, and FDI [FI←→FDI; GG←→FDI; EQ←→FDI] in the short run.

Data availability statement

Publicly available datasets were analyzed in this study. These data can be found here: WDI and WGI public data base.

Author contributions

LJ: introduction, empirical estimation, and final version; MQ: literature survey, empirical estimation, first draft, and final version; WH: literature survey, data curation, and the final draft; and RK: literature survey, methodology, and the final version of the manuscript.

Funding

The study has received financial support from the Institutions for Advanced Research (IAR) under project financing—IAR/2022/PUB/15.

Conflict of interest

The authors declare that the research was conducted in the absence of any commercial or financial relationships that could be construed as a potential conflict of interest.

Publisher's note

All claims expressed in this article are solely those of the authors and do not necessarily represent those of their affiliated organizations, or those of the publisher, the editors, and the reviewers. Any product that may be evaluated in this article, or claim that may be made by its manufacturer, is not guaranteed or endorsed by the publisher.

References

Abdouli, M., and Hammami, S. (2017). The impact of FDI inflows and environmental quality on economic growth: An empirical study for the MENA countries. *J. Knowl. Econ.* 8 (1), 254–278. doi:10.1007/s13132-015-0323-y

Abid, I., and Goaied, M. (2017). A meta-frontier assessment of bank efficiency in Middle East and North Africa countries. *Int. J. Prod. Perform. Manag.* 66, 266–296. doi:10.1108/ijppm-01-2016-0020

Adebayo, T. S., Oladipupo, S. D., Kirikkaleli, D., and Adeshola, I. (2022). Asymmetric nexus between technological innovation and environmental degradation in Sweden: An aggregated and disaggregated analysis. *Environ. Sci. Pollut. Res.* 29, 36547–36564. doi:10.1007/s11356-021-17982-6

Adeel-Farooq, R. M., Riaz, M. F., and Ali, T. J. E. (2021). *Improving the environment begins at home: Revisiting the links between FDI and environment*, 215.119150

Adeniyi, O., Oyinlola, A., Omisakin, O., and Egwaikhide, F. O. (2015). Financial development and economic growth in Nigeria: Evidence from threshold modelling. *Econ. Analysis Policy* 47, 11–21. doi:10.1016/j.eap.2015.06.003

Adom, P. K., and Amuakwa-Mensah, F. (2016). What drives the energy saving role of FDI and industrialization in East Africa? *Renew. Sustain. Energy Rev.*, 65, 925–942. doi:10.1016/j.rser.2016.07.039

Aibai, A., Huang, X., Luo, Y., and Peng, Y. (2019). Foreign direct investment, institutional quality, and financial development along the belt and road: An empirical investigation. *Emerg. Mark. Finance Trade* 55 (14), 3275–3294. doi:10.1080/1540496x.2018.1559139

Al-Zubaidi, M. N., and Khudair, J. M. (2021). Financial inclusion and foreign direct investments/obstacles and solutions. *Warith Sci. J.* 3 (7).

Alam, A., and Shah, S. Z. A. (2013). Determinants of foreign direct investment in OECD member countries. *J. Econ. Stud.* 40, 515–527. doi:10.1108/jes-10-2011-0132

Alam, M. S., Alam, M. N., Murshed, M., Mahmood, H., and Alam, R. (2022). Pathways to securing environmentally sustainable economic growth through efficient use of energy: A bootstrapped ARDL analysis. *Environ. Sci. Pollut. Res.* 29 (33), 50025–50039. doi:10.1007/s11356-022-19410-9

Alam, M. S. (2022). Is trade, energy consumption and economic growth threat to environmental quality in Bahrain–evidence from VECM and ARDL bound test approach. *Int. J. Emerg. Serv.* 11 (3), 396–408. doi:10.1108/IJES-12-2021-0084

Albaity, M., Md Noman, A. H., and Mallek, R. S. (2021). Trustworthiness, good governance and risk taking in MENA countries. *Borsa Istanb. Rev.*, 21(4), 359–374. doi:10.1016/j.bir.2020.12.002

Alfaro, L., Kalemli-Ozcan, S., and Sayek, S. (2009). FDI, productivity and financial development. *World Econ.* 32 (1), 111–135. doi:10.1111/j.1467-9701.2009.01159.x

An, T., Xu, C., Liao, X. J. E. S., and Research, P. (2021). The impact of FDI on environmental pollution in China: Evidence from spatial panel data. *Environ. Sci. Pollut. Res.* 28 (32), 44085–44097. doi:10.1007/s11356-021-13903-9

Andriamahery, A., and Qamruzzaman, M. (2022b). A symmetry and asymmetry investigation of the nexus between environmental sustainability, renewable energy, energy innovation, and trade: Evidence from environmental Kuznets curve hypothesis in selected MENA countries. *Front. Energy Res.* 9. doi:10.3389/fenrg.2021.778202

Andriamahery, A., and Qamruzzaman, M. (2022a). Do access to finance, technical know-how, and financial literacy offer women empowerment through women's entrepreneurial development? [Original research]. *Front. Psychol.* 12 (5889), 776844. doi:10.3389/fpsyg.2021.776844

Anwar, A., Sharif, A., Fatima, S., Ahmad, P., Sinha, A., Rehman Khan, S. A., et al. (2021). The asymmetric effect of public private partnership investment on transport CO2 emission in China: Evidence from quantile ARDL approach. *J. Clean. Prod.*, 288, 125282. doi:10.1016/j.jclepro.2020.125282

Arif, U., Arif, A., and Khan, F. N. (2021). Environmental impacts of FDI: evidence from heterogeneous panel methods. *Environ. Sci. Pollut. Res. Int.* 29 (16), 23639–23649. doi:10.1007/s11356-021-17629-6

Assadzadeh, A., Pourqoly, J. J. J. o. E., Businessand Management (2013). The relationship between foreign direct investment, institutional quality and poverty: Case of MENA countries. *Case MENA Ctries.* 1 (2), 161–165. doi:10.7763/joebm.2013.v1.35

Assadzadeh, A., and Pourqoly, J. (2013). The relationship between foreign direct investment, institutional quality and poverty: Case of MENA countries. *J. Econ. Bus. Manag.* 1 (2), 161–165. doi:10.7763/joebm.2013.v1.35

Aziz, O. G. J. F. R. L. (2018). Institutional quality and FDI inflows in Arab economies. *Financ. Res. Lett.* 25, 111–123. doi:10.1016/j.frl.2017.10.026

Azman-Saini, W. N. W., Law, S. H., and Ahmad, A. H. (2010). FDI and economic growth: New evidence on the role of financial markets. *Econ. Lett.*, 107(2), 211–213. doi:10.1016/j.econlet.2010.01.027

Bailliu, J. (2000). "Private capital flows, financial development, and economic growth in developing countries," in Staff Working Papers 00-15, (Bank of Canada).

Bao, Q., Chen, Y., Song, L. J. E., and Economics, D. (2011). Foreign direct investment and environmental pollution in China: A simultaneous equations estimation. *Environ. Dev. Econ.* 16 (1), 71–92. doi:10.1017/s1355770x10000380

Barajas, A., Steiner, R., and Salazar, N. J. J. o. d. e. (2000). The impact of liberalization and foreign investment in Colombia's financial sector. *J. Dev. Econ.* 63 (1), 157–196. doi:10.1016/s0304-3878(00)00104-8

Barrell, R., Gottschalk, S., and Hall, S. G. (2003). *Foreign direct investment and exchange rate uncertainty in imperfectly competitive industries*. Discussion Papers-National Institute Of Economic And Social Research.

Barthel, F., Busse, M., and Osei, R. (2011). The characteristics and determinants of FDI in Ghana. *Eur. J. Dev. Res.* 23 (3), 389–408. doi:10.1057/ejdr.2011.4

Bevan, A., Estrin, S., and Meyer, K. J. I. b. r. (2004). Foreign investment location and institutional development in transition economies. *Int. Bus. Rev.* 13 (1), 43–64. doi:10.1016/j.ibusrev.2003.05.005

Bhujabal, P., Sethi, N., and Padhan, P. C. (2021). ICT, foreign direct investment and environmental pollution in major Asia Pacific countries. *Environ. Sci. Pollut. Res.* 28 (31), 42649–42669. doi:10.1007/s11356-021-13619-w

Bilawal, M., Ibrahim, M., Abbas, A., Shuaib, M., Ahmed, M., Hussain, I., et al. (2014). Impact of exchange rate on foreign direct investment in Pakistan. *Adv. Econ. Bus.* 2 (6), 223–231. doi:10.13189/aeb.2014.020602

Billett, M. T., Garfinkel, J. A., and Jiang, Y. (2011). The influence of governance on investment: Evidence from a hazard model. *J. Financial Econ.*, 102(3), 643–670. doi:10.1016/j.jfineco.2011.07.004

Biro, F. P., Erdey, L., Gall, J., and Markus, A. J. G. E. J. (2019). The effect of governance on foreign direct investment in Latin America—Issues of model selection. *Glob. Econ. J.* 19 (01), 1950006. doi:10.1142/s2194565919500064

Boateng, A., Hua, X., Nisar, S., and Wu, J. (2015). Examining the determinants of inward FDI: Evidence from Norway. *Econ. Model.* 47, 118–127. doi:10.1016/j.econmod.2015.02.018

Borensztein, E., De Gregorio, J., and Lee, J.-W. (1998). How does foreign direct investment affect economic growth? *J. Int. Econ.* 45 (1), 115–135. doi:10.1016/s0022-1996(97)00033-0

Bouchoucha, N., and Benammou, S. J. J. o. t. K. E. (2020). Does institutional quality matter foreign direct investment? *J. Knowl. Econ.* 11 (1), 390–404. doi:10.1007/s13132-018-0552-y

Bourkhis, K., and Nabi, M. S. (2013). Islamic and conventional banks' soundness during the 2007–2008 financial crisis. *Rev. Financ. Econ.* 22 (2), 68–77. doi:10.1016/j.rfe.2013.01.001

Breusch, T. S., and Pagan, A. R. (1980). The Lagrange multiplier test and its applications to model specification in econometrics. *Rev. Econ. Stud.* 47 (1), 239–253. doi:10.2307/2297111

Bulus, G. C., Koc, S. J. E. S., and Research, P. (2021). The effects of FDI and government expenditures on environmental pollution in Korea: The pollution haven hypothesis revisited. *Environ. Sci. Pollut. Res.* 28 (28), 38238–38253. doi:10.1007/s11356-021-13462-z

Chattopadhyay, A. K., Rakshit, D., Chatterjee, P., and Paul, A. (2022). Trends and determinants of FDI with implications of COVID-19 in BRICS. *Glob. J. Emerg. Mark. Econ.* 14, 43–59. doi:10.1177/09749101211067091

Chudik, A., and Pesaran, M. H. (2015). Common correlated effects estimation of heterogeneous dynamic panel data models with weakly exogenous regressors. *J. Econ.* 188 (2), 393–420. doi:10.1016/j.jeconom.2015.03.007

Cong Minh Huynh (2022). How does the impact of foreign direct investment on institutional quality depend on the underground economy? *J. Sustain. Finance Invest.* 12 (2), 554–569. doi:10.1080/20430795.2020.1788851

Contractor, F. J., Dangol, R., Nuruzzaman, N., and Raghunath, S. J. I. B. R. (2020). How do country regulations and business environment impact foreign direct investment (FDI) inflows? *Int. Bus. Rev.* 29 (2), 101640. doi:10.1016/j.ibusrev.2019.101640

Cuervo-Cazurra, A. (2008). Better the devil you don't know: Types of corruption and FDI in transition economies. *J. Int. Manag.*, 14(1), 12–27. doi:10.1016/j.intman.2007.02.003

Dai, M., Qamruzzaman, M., and Hamadelneel Adow, A. (2022). An assessment of the impact of natural resource price and global economic policy uncertainty on financial asset performance: Evidence from bitcoin. *Front. Environ. Sci.* 10. doi:10.3389/fenvs.2022.897496

Demena, B. A., and Afesorgbor, S. K. J. E. P. (2020). The effect of FDI on environmental emissions: Evidence from a meta-analysis. *Energy Policy* 138, 111192. doi:10.1016/j.enpol.2019.111192

Dorozynski, T., Dobrowolska, B., Kuna-Marszalek, A. J. E. B., and Review, E. (2020). Institutional quality in central and East European countries and its impact on. *FDI Inflow* 8 (1), 91–110.

Doytch, N., and Uctum, M. J. E. S. (2016). Globalization and the environmental impact of sectoral FDI. *Econ. Syst.* 40 (4), 582–594. doi:10.1016/j.ecosys.2016.02.005

Du, J., and Zhang, Y. (2022). "In fear of trojan horse? China's cross-border acquisitions in Europe amid the one belt one road initiative," in *China and the belt and road initiative: Trade relationships, business opportunities and political impacts*. Editor Y.-C. Kim (Springer International Publishing), 75–109. doi:10.1007/978-3-030-86122-3_5

Fazio, G., and Chiara Talamo, G. M. (2008). "How "attractive" is good governance for FDI?,". Editors J. J. Choi and S. Dow (Emerald Group Publishing Limited), 9, 33–54. doi:10.1016/S1569-3767(08)09002-X*Institutional Approach Glob. Corp. Gov. Bus. Syst. Beyond*

Fertő, I., and Sass, M. (2020). FDI according to ultimate versus immediate investor countries: Which dataset performs better? *Appl. Econ. Lett.* 27 (13), 1067–1070. doi:10.1080/13504851.2019.1659925

Fuest, C., Hugger, F., Sultan, S., and Xing, J. (2022). What drives Chinese overseas M&A investment? Evidence from micro data. *Rev. Int. Econ.*, 30(1), 306–344. doi:10.1111/roie.12566

Greenwood, J., and Jovanovic, B. (1990). Financial development, growth, and the distribution of income. *J. Political Econ.* 98 (5), 10761076–10761107. doi:10.1086/261720https://EconPapers.repec.org/RePEc:ucp:jpolec:v:98:y

Guang-Wen, Z., Murshed, M., Siddik, A. B., Alam, M. S., Balsalobre-Lorente, D., and Mahmood, H. (2022). *Achieving the objectives of the 2030 sustainable development goals agenda: Causalities between economic growth, environmental sustainability, financial development, and renewable energy consumption*. Sustainable Development.

Hakimi, A., Hamdi, H. J. R., and Reviews, S. E. (2016). Trade liberalization, FDI inflows, environmental quality and economic growth: A comparative analysis between Tunisia and Morocco. *Renew. Sustain. Energy Rev.* 58, 1445–1456. doi:10.1016/j.rser.2015.12.280

Hamid, I., Alam, M. S., Kanwal, A., Jena, P. K., Murshed, M., and Alam, R. (2022a). Decarbonization pathways: The roles of foreign direct investments, governance, democracy, economic growth, and renewable energy transition. *Environ. Sci. Pollut. Res.* 29 (33), 49816–49831. doi:10.1007/s11356-022-18935-3

Hamid, I., Alam, M. S., Murshed, M., Jena, P. K., Sha, N., and Alam, M. N. (2022b). The roles of foreign direct investments, economic growth, and capital investments in decarbonizing the economy of Oman. *Environ. Sci. Pollut. Res.* 29 (15), 22122–22138. doi:10.1007/s11356-021-17246-3

Hao, Y., Wu, Y., Wu, H., and Ren, S. (2020). How do FDI and technical innovation affect environmental quality? Evidence from China. *Environ. Sci. Pollut. Res.* 27 (8), 7835–7850. doi:10.1007/s11356-019-07411-0

Hayat, A. J. T. J. o. I. T., and Development, E. (2019). Foreign direct investments, institutional quality, and economic growth. *J. Int. Trade Econ. Dev.* 28 (5), 561–579. doi:10.1080/09638199.2018.1564064

Herrera-Echeverri, H., Haar, J., and Estévez-Bretón, J. B. (2014a). Foreign direct investment, institutional quality, economic freedom and entrepreneurship in emerging markets. *J. Bus. Res.* 67 (9), 1921–1932. doi:10.1016/j.jbusres.2013.11.020

Herrera-Echeverri, H., Haar, J., and Estévez-Bretón, J. B. J. J. o. B. R. (2014b). Foreign direct investment, institutional quality. *Econ. freedom Entrepreneursh. Emerg. Mark.* 67 (9), 1921

Hitam, M. B., Borhan, H. B. J. P.-S., and Sciences, B. (2012). FDI, growth and the environment: Impact on quality of life in Malaysia. *Procedia - Soc. Behav. Sci.* 50, 333–342. doi:10.1016/j.sbspro.2012.08.038

Hussain, M. N., Li, Z., Sattar, A., and Ilyas, M. (2022). Evaluating the impact of energy and environment on economic growth in BRI countries. *Energy & Environ.* 0 (0), 0958305X2110738. doi:10.1177/0958305x211073805

Huynh, C. M., and Hoang, H. H. (2019). Foreign direct investment and air pollution in asian countries: Does institutional quality matter? *Appl. Econ. Lett.* 26 (17), 1388–1392. doi:10.1080/13504851.2018.1563668

Iamsiraroj, S. (2016). The foreign direct investment–economic growth nexus. *Int. Rev. Econ. Finance* 42, 116–133. doi:10.1016/j.iref.2015.10.044

Jensen, N. M. (2003). Democratic governance and multinational corporations: Political regimes and inflows of foreign direct investment. *Int. Organ.* 57 (3), 587–616. doi:10.1017/S0020818303573040

Jia, Z., Mehta, A. M., Qamruzzaman, M., and Ali, M. (2021). Economic Policy uncertainty and financial innovation: Is there any affiliation? *Front. Psychol.* 12, 631834. doi:10.3389/fpsyg.2021.631834

Kablan, S. (2009). Banking efficiency and financial development in sub-Saharan Africa (SSA). *Afr. Finance J.* 11 (2), 28–50.

Kasasbeh, H. A., Mdanat, M. F., Khasawneh, R. J. A. E., and Review, F. (2018). Corruption and FDI inflows: Evidence from a small developing economy. *Asian Econ. Financial Rev.* 8 (8), 1075–1085. doi:10.18488/journal.aefr.2018.88.1075.1085

Katarzyna Anna, C., and Adam, W. (2012). "Foreign exchange market efficiency: Empirical results for the USD/EUR market," in *e-Finanse: Financial Internet Quarterly*. ISSN 1734-039X (Rzeszów: University of Information Technology and Management), 8 (3), 1–9.

Kaufmann, D., and Wei, S.-J. (1999). *Does" grease money" speed up the wheels of commerce?* USA: National bureau of economic research Cambridge, Mass.

Kayalvizhi, P., and Thenmozhi, M. J. E. M. R. (2018). Does quality of innovation, culture and governance drive FDI? *Emerg. Mark. Rev.* 34, 175–191. doi:10.1016/j.ememar.2017.11.007

Kayani, F. N., and Ganic, M. (2021). The impact of governance on Chinese inward FDI: The generalized method of moments technique. *Humanit. Soc. Sci. Lett.* 9 (2), 175–184. doi:10.18488/journal.73.2021.92.175.184

Khan, H., Khan, I., Jan, M. S., Jandan, A. H., and Khan, S. J. M. E. (2019). Does good governance matter fdi inflow? *Evid. india* 10 (6), 1526–1538. doi:10.4236/me.2019.106101

Khan, M. A., Ozturk, I. J. E. S., and Research, P. (2020). Examining foreign direct investment and environmental pollution linkage in Asia. *Environ. Sci. Pollut. Res.* 27 (7), 7244–7255. doi:10.1007/s11356-019-07387-x

Kirkulak, B., Qiu, B., and Yin, W. (2011). *The impact of FDI on air quality: Evidence from China*.

Klein, M. U., Aaron, C., and Hadjimichael, B. (2001). *Foreign direct investment and poverty reduction*. World Bank Policy Research Working Paper.

Krause, S., and Rioja, F. (2006). Financial development and monetary policy efficiency. *Emory Econ.* 613 (158), 100

Kurtishi-Kastrati, S. J. E. S. J. (2013). Impact of FDI on economic growth: An overview of the main theories of FDI and empirical research. 9(7).

Levine, R. (1997). Financial development and economic growth: Views and agenda. *J. Econ. Literature* 35 (1), 688

Li, J., and Qamruzzaman, M. (2022). Dose tourism induce Sustainable Human capital development in BRICS through the channel of capital formation and financial development: Evidence from Augmented ARDL with structural Break and Fourier TY causality. *Front. Psychol.* 13, 804349. doi:10.3389/fpsyg.2022.804349

Liargovas, P. G., and Skandalis, K. S. (2012). Foreign direct investment and trade openness: The case of developing economies. *Soc. Indic. Res.* 106 (2), 323–331. doi:10.1007/s11205-011-9806-9

Lingyan, M., Qamruzzaman, M., and Adow, A. H. E. (2021). Technological adaption and open innovation in SMEs: An strategic assessment for women-owned SMEs sustainability in Bangladesh. *Sustainability* 13 (5), 2942. doi:10.3390/su13052942

Liu, J., and Qamruzzaman, M. (2021). An asymmetric investigation of remittance, trade openness impact on inequality: Evidence from selected south asian countries. *Front. Psychol.*, 4022.

Liu, X., and Wang, C. (2003). Does foreign direct investment facilitate technological progress?: Evidence from Chinese industries. *Res. Policy*, 32(6), 945. doi:10.1016/S0048-7333(02)00094-X

Logun, A. (2020). Foreign direct investments, exports and economic growth: Panel ARDL and causality analysis for E7 countries. *J. Acad. Res. Econ. (JARE)* 12 (1), 7

Ma, R., and Qamruzzaman, M. (2022). Nexus between government debt, economic policy uncertainty, government spending, and governmental effectiveness in BRIC nations: Evidence for linear and nonlinear assessments. *Front. Environ. Sci.* 10, 952452. doi:10.3389/fenvs.2022.952452

Magombeyi, M. T., and Odhiambo, N. M. (2017). Foreign direct investment and poverty reduction. *Comp. Econ. Res.* 20 (2), 73–89. doi:10.1515/cer-2017-0013

Manigandan, P., Alam, M. S., Alagirisamy, K., Pachiyappan, D., Murshed, M., and Mahmood, H. (2022). Realizing the sustainable development goals through technological innovation: Juxtaposing the economic and environmental effects of financial development and energy use. *Environ. Sci. Pollut. Res. Int.* doi:10.1007/s11356-022-22692-8

Martinez, M. V. (2011). *The political economy of increased financial access*. Georgetown University.

Meng, L., Qamruzzaman, M., and Adow, A. H. E. (2021). Technological adaption and open innovation in SMEs: An strategic assessment for women-owned SMEs sustainability in Bangladesh. *Sustainability* 13 (5), 2942. doi:10.3390/su13052942

Mengistu, A. A., and Adhikary, B. K. (2011). Does good governance matter for FDI inflows? Evidence from asian economies. *Asia Pac. Bus. Rev.* 17 (3), 281–299. doi:10.1080/13602381003755765

Miao, M., Lang, Q., Borojo, D. G., Yushi, J., and Zhang, X. J. E. (2020). The impacts of Chinese FDI and China–Africa trade on economic growth of African countries: The role of institutional quality. *Economies* 8 (3), 53. doi:10.3390/economies8030053

Morgan, P. J., and Pontines, V. J. T. S. E. R. (2018). Financial stability and financial inclusion. *Singap. Econ. Rev.* 63 (01), 111–124. doi:10.1142/s0217590818410035

Morgan, P., and Pontines, V. (2014). "Financial stability and financial inclusion," in ADBI Working Paper 488 (Tokyo: Asian Development Bank Institute). Available at: http://www.adbi.org/working-paper/2014/07/07/6353.financial.stability.inclusion/.

Muhammad, S., Pan, Y., Agha, M. H., Umar, M., and Chen, S. (2022). Industrial structure, energy intensity and environmental efficiency across developed and developing economies: The intermediary role of primary, secondary and tertiary industry. *Energy*, 247, 123576. doi:10.1016/j.energy.2022.123576

Narayanan, S., Choong, C. K., and Lau, L. S. J. E. B. (2020). An investigation on the role of good governance as a mediating factor in the FDI-Growth nexus. *ASEAN Perspective* 40 (4), 2769–2779.

Nasreen, S., Mahalik, M. K., Shahbaz, M., and Abbas, Q. (2020). How do financial globalization, institutions and economic growth impact financial sector development in European countries? *Res. Int. Bus. Finance* 54, 101247. doi:10.1016/j.ribaf.2020.101247

Neequaye, N. A., and Oladi, R. J. I. R. o. E. (2015). Environment, growth, and FDI revisited. *Int. Rev. Econ. Finance* 39, 47–56. doi:10.1016/j.iref.2015.06.002

Niarachma, R., Effendi, N., and Ervani, E. (2021). The effect of governance on FDI inflows in ASEAN. *Optim. J. Ekon. Dan. Pembang.*, 11, 44. doi:10.12928/optimum.v11i1.3620

Oke, S., Ayanwale, T., and Isola, O. (2007). Soil seedbank in four contrasting plantations in Ile-Ife area of Southwestern Nigeria. *Res. J. Bot.* 2 (1), 13–22. doi:10.3923/rjb.2007.13.22

Omri, A., and Mabrouk, N. B. J. E. I. A. R. (2020). Good governance for sustainable development goals: Getting ahead of the pack or falling behind? *Environ. Impact Assess. Rev.* 83, 106388. doi:10.1016/j.eiar.2020.106388

Opoku, E. E. O., and Boachie, M. K. J. E. P. (2020). The environmental impact of industrialization and foreign direct investment. *Energy Policy* 137, 111178. doi:10.1016/j.enpol.2019.111178

Pazienza, P. J. E. I. A. R. (2019). The impact of FDI in the OECD manufacturing sector on CO2 emission: Evidence and policy issues. *Environ. Impact Assess. Rev.* 77, 60–68. doi:10.1016/j.eiar.2019.04.002

Pedroni, P. (2004). Panel cointegration: Asymptotic and finite sample properties of pooled time series tests with an application to the PPP hypothesis. *Econ. Theory* 20 (3), 597–625. doi:10.1017/s0266466604203073

Pedroni, P. (2001). Purchasing power parity tests in cointegrated panels. *Rev. Econ. Statistics* 83 (4), 727–731. doi:10.1162/003465301753237803

Pegkas, P. (2015). The impact of FDI on economic growth in Eurozone countries. *J. Econ. Asymmetries*, 12(2), 124–132. doi:10.1016/j.jeca.2015.05.001

Peres, M., Ameer, W., and Xu, H. J. E. r.-E. i. (2018). The impact of institutional quality on foreign direct investment inflows: Evidence for developed and developing countries. *Econ. Research-Ekonomska Istraz.* 31 (1), 626–644. doi:10.1080/1331677x.2018.1438906

Pesaran, M. H. (2007). A simple panel unit root test in the presence of cross-section dependence. *J. Appl. Econ.* 22 (2), 265–312. doi:10.1002/jae.951

Pesaran, M. H. (2006). Estimation and inference in large heterogeneous panels with a multifactor error structure. *Econometrica* 74 (4), 967–1012. doi:10.1111/j.1468-0262.2006.00692.x

Pesaran, M. H. (2021). General diagnostic tests for cross-sectional dependence in panels. *Empir. Econ.* 60, 13–50. doi:10.1007/s00181-020-01875-7

Pesaran, M. H., Ullah, A., and Yamagata, T. (2008). A bias-adjusted LM test of error cross-section independence. *Econom. J.* 11 (1), 105–127. doi:10.1111/j.1368-423x.2007.00227.x

Pesaran, M. H., and Yamagata, T. (2008). Testing slope homogeneity in large panels. *J. Econ.* 142 (1), 50–93. doi:10.1016/j.jeconom.2007.05.010

Pingfang, Z., Zhengyu, Z., and Guolin, J. (2011). Empirical study of the relationship between FDI and environmental regulation: An intergovernmental competition perspective. *Econ. Res. J.* 6, 133

Pu, G., Qamruzzaman, M., Mehta, A. M., Naqvi, F. N., and Karim, S. (2021). Innovative finance, technological adaptation and SMEs sustainability: The mediating role of government support during COVID-19 pandemic. *Sustainability* 13 (16), 9218. doi:10.3390/su13169218

Qamruzzaman, M. (2022c). A symmetry and asymmetry investigation of the nexus between environmental sustainability, renewable energy, energy innovation, and trade: Evidence from environmental Kuznets curve hypothesis in selected MENA countries. *Front. Energy Res.* 873, 8202. doi:10.3389/fenrg.2021.778202

Qamruzzaman, M. (2022a). An asymmetric investigation of the nexus between economic policy uncertainty, knowledge spillover, climate change and green economy: Evidence from BRIC nations. *Front. Environ. Sci.* 9, 682. doi:10.3389/fenvs.2021.807424

Qamruzzaman, M. (2015). Determinants of foreign direct investment (FDI): Evidence from Bangladesh. *Pac. Bus. Rev. Int.* 7 (10), 97.

Qamruzzaman, M., and Jianguo, W. (2018). Does foreign direct investment, financial innovation, and trade openness coexist in the development process: Evidence from selected Asian and African countries. *Br. J. Econ. Finance Manag. Sci.* 16 (1), 73.

Qamruzzaman, M., and Karim, S. (2020). Nexus between economic volatility, trade openness and FDI: An application of ARDL, NARDL and asymmetric causality. *Asian Econ. Financial Rev.* 10 (7), 790–807. doi:10.18488/journal.aefr.2020.107.790.807

Qamruzzaman, M. (2022b). Nexus between economic policy uncertainty and institutional quality: Evidence from Indian and Pakistan." in *Macroeconomics and finance in emerging market economies*, 1–20. doi:10.1080/17520843.2022.2026035

Qamruzzaman, M. (2021). Nexus between environmental quality, institutional quality and trade openness through the channel of FDI: An application of common correlated effects estimation (CCEE), NARDL, and asymmetry causality. *Environ. Sci. Pollut. Res.* 28, 52475–52498. doi:10.1007/s11356-021-14269-8

Qamruzzaman, M., and Wei, J. J. Q. F. E. (2019). Do financial inclusion, stock market development attract foreign capital flows in developing economy: A panel data investigation. *Quantitative Finance Econ.* 3, 88–108. doi:10.3934/qfe.2019.1.88

Rafindadi, A. A., Muye, I. M., Kaita, R. A. J. S. E. T., and Assessments (2018). The effects of FDI and energy consumption on environmental pollution in predominantly resource-based economies of the GCC. *Sustain. Energy Technol. Assessments* 25, 126–137. doi:10.1016/j.seta.2017.12.008

Ramasamy, B., and Yeung, M. J. W. E. (2010). The determinants of foreign direct investment in services. *World Econ.* 33 (4), 573–596. doi:10.1111/j.1467-9701.2009.01256.x

Raza, S. A., Shah, N., and Arif, I. J. G. B. R. (2021b). Relationship between FDI and economic growth in the presence of good governance system: Evidence from OECD Countries. *Glob. Bus. Rev.* 22 (6), 1471–1489. doi:10.1177/0972150919833484

Raza, S. A., Shah, N., and Arif, I. (2021a). Relationship between FDI and economic growth in the presence of good governance system: Evidence from OECD countries. *Glob. Bus. Rev.* 22 (6), 1471–1489. doi:10.1177/0972150919833484

Rehman, F. U., and Ding, Y. (2020). The nexus between outward foreign direct investment and export sophistication: New evidence from China. *Appl. Econ. Lett.* 27 (5), 357–365. doi:10.1080/13504851.2019.1616056

Rehman, F. U., and Islam, M. M. (2022). Financial infrastructure—Total factor productivity (TFP) nexus within the purview of FDI outflow, trade openness, innovation, human capital and institutional quality: Evidence from BRICS economies. *Appl. Econ.*, 1–19. doi:10.1080/00036846.2022.2094333

Rehman, F. U., and Noman, A. A. (2022). China's outward foreign direct investment and bilateral export sophistication: A cross countries panel data analysis. *China Finance Rev. Int.* 12 (1), 180–197. doi:10.1108/CFRI-04-2020-0040

Rehman, F. U., and Noman, A. A. (2021). Trade related sectorial infrastructure and exports of belt and road countries: Does belt and road initiatives make this relation structurally instable? *China Econ. J.* 14 (3), 350–374. doi:10.1080/17538963.2020.1840014

Rehman, F. U., Popp, J., Ahmad, E., Khan, M. A., and Lakner, Z. (2021). Asymmetric and symmetric link between quality of institutions and sectorial foreign direct investment inflow in India: A fresh insight using simulated dynamic ARDL approach. *Sustainability* 13 (24), 13760. doi:10.3390/su132413760

Rehman, F. U., and Sohag, K. (2022). Does transport infrastructure spur export diversification and sophistication in the G-20 economies? An application of CS-ARDL. *Appl. Econ. Lett.*, 1–5. doi:10.1080/13504851.2022.2083554

Ross, A. G. J. T. C. R. (2019). Governance infrastructure and FDI flows in developing countries. *Transnatl. Corp. Rev.* 11 (2), 109–119. doi:10.1080/19186444.2019.1640572

Sabir, S., Rafique, A., and Abbas, K. J. F. I. (2019). Institutions and FDI: Evidence from developed and developing countries. *Financ. Innov.* 5 (1), 8–20. doi:10.1186/s40854-019-0123-7

Sahoo, P. (2012). Determinants of FDI in south Asia: Role of infrastructure, trade openness and reforms. *J. World Invest. Trade* 13 (2), 256–278. doi:10.1163/221190012x627638

Saibu, O. M., Ikechukwu, O. M., and Nwosa, P. I. (2022). Dynamic effects of foreign aid, trade openness and fdi on economic growth for west african countries. *J. Dev. Areas* 56 (2), 49–63. doi:10.1353/jda.2022.0034

Saini, N., and Sighania, M. (2019). "Environmental impact of economic growth, emission and FDI: systematic review of reviews," in *Qualitative Research in Financial Markets* (Emerald Group Publishing), 11 (1), 81–134.

Saini, N., and Singhania, M. (2018). Determinants of FDI in developed and developing countries: A quantitative analysis using GMM. *J. Econ. Stud.* 45 (2), 348–382. doi:10.1108/JES-07-2016-0138

Samargandi, N., Alghfais, A., and AlHuthail, H. M. (2022). Factors in Saudi FDI inflow. *SAGE Open* 12 (1), 215824402110672. doi:10.1177/21582440211067242

Sapkota, P., and Bastola, U. J. E. E. (2017). Foreign direct investment, income, and environmental pollution in developing countries: Panel data analysis of Latin America. *Energy Econ.* 64, 206–212. doi:10.1016/j.eneco.2017.04.001

Sarma, M., and Pais, J. (2011). Financial inclusion and development. *J. Int. Dev.* 23 (5), 613–628. doi:10.1002/jid.1698

Seker, F., Ertugrul, H. M., Cetin, M. J. R., and Reviews, S. E. (2015). The impact of foreign direct investment on environmental quality: A bounds testing and causality analysis for Turkey. *Renew. Sustain. Energy Rev.* 52, 347–356. doi:10.1016/j.rser.2015.07.118

Shah, M. H., Afridi, A. G., Shah, M. H., and Afridi, A. G. (2015). Significance of good governance for FDI inflows in SAARC countries. *Bus. Econ. Rev.* 7 (2), 31–52. doi:10.22547/ber/7.2.2

Shahbaz, M., Nasreen, S., Abbas, F., and Anis, O. J. E. E. (2015). Does foreign direct investment impede environmental quality in high-middle-and low-income countries? *Energy Econ.* 51, 275–287. doi:10.1016/j.eneco.2015.06.014

Shank, T., Paul Hill, R., and Stang, J. (2013). Do investors benefit from good corporate governance? *Corp. Gov. Int. J. Bus. Soc.* 13 (4), 384–396. doi:10.1108/CG-03-2010-0027

Shao, W., Yu, X., and Chen, Z. (2022). Does the carbon emission trading policy promote foreign direct investment?: A quasi-experiment from China [systematic review]. *Front. Environ. Sci.* 9, 438. doi:10.3389/fenvs.2021.798438

Shi, Z., and Qamruzzaman, M. (2022). Re-visiting the role of education on poverty through the channel of financial inclusion: Evidence from lower-income and lower-middle-income countries. *Front. Environ. Sci.* 10, 873652. doi:10.3389/fenvs.2022.873652

Shin, Y., Yu, B., and Greenwood-Nimmo, M. (2014). "Modelling asymmetric cointegration and dynamic multipliers in a nonlinear ARDL framework," in *Festschrift in honor of peter schmidt* (Springer), 281

Shittu, W. O., Yusuf, H., Houssein, A. E. M. E., and Hassan, S. (2020). The impacts of foreign direct investment and globalisation on economic growth in west africa: Examining the role of political governance. *J. Econ. Stud.* 47 (7), 1733–1755.

Singh, A., and Zammit, A. J. W. d. (2000). International capital flows: Identifying the gender dimension. *World Dev.* 28 (7), 1249–1268. doi:10.1016/s0305-750x(00)00026-7

Sokang, K. (2018). The impact of foreign direct investment on the economic growth in Cambodia: Empirical evidence. *Int. J. Innovation Econ. Dev.* 4 (5), 31–38. doi:10.18775/ijied.1849-7551-7020.2015.45.2003

Ssali, M. W., Du, J., Mensah, I. A., Hongo, D. O. J. E. S., and Research, P. (2019). Investigating the nexus among environmental pollution, economic growth, energy use, and foreign direct investment in 6 selected sub-Saharan African countries. *Environ. Sci. Pollut. Res.* 26 (11), 11245–11260. doi:10.1007/s11356-019-04455-0

Sturm, J.-E., and Williams, B. J. J. o. B. (2008). Characteristics determining the efficiency of foreign banks in Australia. *J. Bank. Finance* 32 (11), 2346–2360. doi:10.1016/j.jbankfin.2007.12.029

Su, X., Li, Y., Fang, K., and Long, Y. (2022). Does China's direct investment in "Belt and Road Initiative" countries decrease their carbon dioxide emissions? *J. Clean. Prod.*, 339, 130543. doi:10.1016/j.jclepro.2022.130543

Taylor, M. P., and Sarno, L. J. T. W. B. E. R. (1997). Capital flows to developing countries: Long-and short-term determinants. *World Bank. Econ. Rev.* 11 (3), 451–470. doi:10.1093/wber/11.3.451

Toxopeus, H. S., and Lensink, R. (2008). "Remittances and financial inclusion in development," in *Development finance in the global economy*. Editors T. Addison and G. Mavrotas (London: Palgrave Macmillan). doi:10.1057/9780230594074_10

Vijayakumar, N., Sridharan, P., and Rao, K. C. S. (2010). Determinants of FDI in BRICS countries: A panel analysis. *Int. J. Bus. Sci. Appl. Manag. (IJBSAM)* 5 (3), 1

Wang, H., Liu, H. J. E. S., and Research, P. (2019). Foreign direct investment, environmental regulation, and environmental pollution: An empirical study based on threshold effects for different Chinese regions. *Environ. Sci. Pollut. Res.* 26 (6), 5394–5409. doi:10.1007/s11356-018-3969-8

Westerlund, J. (2007). Testing for error correction in panel data. *Oxf. Bull. Econ. Stat.* 69 (6), 709–748. doi:10.1111/j.1468-0084.2007.00477.x

Xia, C., Qamruzzaman, M., and Adow, A. H. (2022). An asymmetric nexus: Remittance-led human capital development in the top 10 remittance-receiving countries: Are FDI and gross capital formation critical for a road to sustainability? *Sustainability* 14 (6), 3703. doi:10.3390/su14063703

Xu, S., Qamruzzaman, M., and Adow, A. (2021). Is financial innovation bestowed or a curse for economic sustainably: The mediating role of economic policy uncertaintys note: MDPI stays neutral with regard to jurisdictional claims in published. *Sustainability* 2021 (13), 2391. doi:10.3390/su13042391

Yang, Y., Qamruzzaman, M., Rehman, M. Z., and Karim, S. (2021). Do tourism and institutional quality asymmetrically effects on FDI sustainability in BIMSTEC countries: An application of ARDL, CS-ARDL, NARDL, and asymmetric causality test. *Sustainability* 13 (17), 9989. doi:10.3390/su13179989

Younsi, M., Bechtini, M. J. E. o. T., and Change, I. (2019). Does good governance matter for FDI? New evidence from emerging countries using a static and dynamic panel gravity model approach. *Econ. Transit.* 27 (3), 841–860. doi:10.1111/ecot.12224

Yüksel, S., Dinçer, H., Karakuş, H., and Ubay, G. G. (2020). "The negative effects of carbon emission on FDI: A comparative analysis between E7 and G7 countries," in *Handbook of research on sustainable supply chain management for the global economy* (IGI Global), 20

Zhuo, J., and Qamruzzaman, M. (2021). Do financial development, FDI, and globalization intensify environmental degradation through the channel of energy consumption: Evidence from belt and road countries. *Environ. Sci. Pollut. Res.* 29, 2753–2772. doi:10.1007/s11356-021-15796-0

Zhuo, J., and Qamruzzaman, M. (2022). Do financial development, FDI, and globalization intensify environmental degradation through the channel of energy consumption: Evidence from belt and road countries. *Environ. Sci. Pollut. Res.* 29 (2), 2753–2772. doi:10.1007/s11356-021-15796-0

Zomorrodi, A., and Zhou, X. (2017). Impact of FDI on environmental quality of China. *Int. J. Bus. Econ. Manag.* 4 (1), 1–15. doi:10.18488/journal.62/2017.4.1/62.1.1.15

Zomorrodi, A., Zhou, X. J. I. J. o. B., Economicsand Management (2017). Impact of FDI on environmental quality of China. *Int. J. Bus. Econ. Manag.* 4 (1), 1–15. doi:10.18488/journal.62/2017.4.1/62.1.1.15

Zwedu, G. A. (2014). *Financial inclusion, regulation and inclusive growth in Ethiopia*. ODI.

frontiers | Frontiers in Earth Science

TYPE Original Research
PUBLISHED 04 January 2023
DOI 10.3389/feart.2022.1024037

OPEN ACCESS

EDITED BY
Dabang Jiang,
Institute of Atmospheric Physics (CAS), China

REVIEWED BY
Mohamad N. Azra,
Universiti Malaysia Terengganu, Malaysia
Haiyun Shi,
Southern University of Science and Technology, China

*CORRESPONDENCE
Zhonggen Wang,
wangzg@igsnrr.ac.cn

SPECIALTY SECTION
This article was submitted to Hydrosphere, a section of the journal Frontiers in Earth Science

RECEIVED 20 August 2022
ACCEPTED 05 December 2022
PUBLISHED 04 January 2023

CITATION
Li R, Huang HQ, Wang Z and Zhao R (2023), Quantitative assessment of the impacts of climate and human activities on streamflow of the Lancang-Mekong river over the recent decades.
Front. Earth Sci. 10:1024037.
doi: 10.3389/feart.2022.1024037

Quantitative assessment of the impacts of climate and human activities on streamflow of the Lancang-Mekong river over the recent decades

Renzhi Li[1,2], He Qing Huang[3,4], Zhonggen Wang[1,2]* and Ruxin Zhao[1]

[1]National Institute of Natural Hazards, Ministry of Emergency Management of the People's Republic of China, Beijing, China, [2]Key Laboratory of Compound and Chained Natural Hazards Dynamics, Ministry of Emergency Management of China, Beijing, China, [3]Institute of Geographic Sciences and Natural Resources Research, Chinese Academy of Sciences, Beijing, China, [4]University of Chinese Academy of Sciences, Beijing, China

The impacts of climate and human activities exerted on streamflow over the recent decades in the Lancang-Mekong River Basin (LMRB) have been examined in separate forms and this study performed an integrated quantitative evaluation. Using the meteorological and hydrological data measured in LMRB during 1961–2015, we analyzed the varying trend and abrupt change characteristics of streamflow along the river course, and constructed a SWAT hydrological model to quantitatively evaluate the contributions of climate and human activities by taking into account their spatial heterogeneity. At the yearly timescale, the results show that for significant complex changes in streamflow along the Lancang-Mekong River, the ratios of the contributions of the impacts of human activity (η_h) before 2000 to those after 2000 are under 15.2%, 17.5% and 32.4% respectively in the source area above Jiuzou (China), the upper area between Jiuzhou and Yunjinghong (China), and the middle area between Jiuzhou and Vientiane (Laos). In the lower area between Vientiane and Stung Treng (Cambodia), η_h was only 22.6% before 2000 and yet dramatically increased to 59.1% after 2000. While the same situation happened at the seasonal time scale, η_h has relatively larger values during dry seasons than in wet seasons. In contrast to the gradually increased impacts of human activities, the impacts of climate on streamflow gradually decreased from the upper to the lower areas. Furthermore, the impacts of the changes in land use types account for about 1/3 in the Lancang River Basin and yet reaches more than 1/2 in the Mekong River Basin.

KEYWORDS

Lancang-Mekong river basin, climate change, human activities, streamflow, SWAT model

1 Introduction

Over the last several decades, streamflow regimes have experienced significant alterations around the world (Zhao et al., 2015). Due to the combined impacts of climate and human activities on streamflow process in large river basins, streamflow regime shifts often in complex cascading forms (Best 2019; Hughes et al., 2013). Understanding physical mechanisms by which the two drivers of changes take effect and their relative contributions on streamflow regime shift have been a hot topic for research for bolstering the management of river basin systems (Hu et al., 2021; Ali et al., 2022).

Changes in climate and land use types have long been regarded as the major factors influencing the water resources in the Lancang-Mekong River Basin (LMRB) (e.g., Wang et al., 2017). The increasing human activity stress in LMRB has caused streamflow discharge to increase from a pristine level to a much higher one by the early 2010s then to decline following a decrease in the human activity stress (Song et al., 2020). To quantitatively assess the impacts of climatic variation and human activities on streamflow in the LMRB, numerous methods such as empirical statistical analysis, multi-parameter vulnerability assessment, and hydrological modeling have been employed (Wu et al., 2016; Wang et al., 2019). Li et al. (2020) used the Mann-Kendall test and double cumulative curve method to determine the varying trend in the annual streamflow of the Mun River into the Mekong River from 1980 to 2018. Their results showed that the significant reduction in forest area and slight reductions in evaporation and farmland area since 1999 helped increase the streamflow of the Mun River. Gui et al. (2021) used the multi-parameter vulnerability assessment method to quantitatively assess the impacts of natural and anthropogenic interferences on water resources in the Lancang River Basin (LRB) from 1998 to 2014 and identified that the southeast region of LRB especially Dali area was mainly influenced by human activities. Although the method used by Gui et al. (2021) is able to directly quantify the contributions of climatic and human activities factors, the spatial differences of these factors in the very large LMRB may lead to inaccurate results. The hydrological simulation methods, typically the Soil & Water Assessment Tool (SWAT), Variable Infiltration Capacity (VIC), Simple Hydrological Model (SIMHYD), and Geomorphology-Based Hydrological Modelling (GBHM), all provide a more detailed illustration of hydrological cycle for river basins with diverse spatial patterns (Wang et al., 2017; Yun et al., 2020). Using a SWAT model, Li et al. (2021) quantitatively assessed the effects of climate change on streamflow in the Mun River under the RCP 2.6, 4.5, and 8.5 scenarios. Tatsumi et al. (2015) adopted VIC model to study the influence of agricultural irrigation water use on streamflow of the Mekong River. Wang et al. (2017) combined the large scale distributed hydrological GBHM with a simple reservoir regulation model to study the influence of dam construction and climate change on floods in the LMRB. While those modelling studies greatly facilitated quantitative evaluation of the factors affecting streamflow variation in LMRB, the Lancang and Mekong River Basins have not been treated as an integrated one large basin, and the temporal and spatial connections between the parts and the whole LMRB have been ignored in most cases. Furthermore, previous studies mainly focused on a certain aspect of the impact of human activities, such as reservoirs and irrigation, generally covered relatively short periods of variation and used insufficient model calibration data.

Aiming at quantitatively evaluating the impact of climate change and human activities on streamflow over a much long period and in a form well integrating the different parts of the entire LMRB, this study fused multi-source data, including long series of meteorological site and grid, land use types, and soil data and more, and then built a meteorological-soil-hydrological database. Importantly, a SWAT hydrological model was constructed by taking into account of the spatial heterogeneity in climatic and human activities factors across the entire LMRB and consequently the contributions of climatic and human activities factors in the streamflow changes over different parts of LMRB were quantified.

2 Research area and methods

2.1 Research area

As the seventh largest river in the world, the Lancang-Mekong River (LMR) is shared by six nations in Southeast Asia (Figure 1, Liu et al., 2021). It originates from the Tibetan Plateau in China, flows through Myanmar, Lao People's Democratic Republic, Thailand, and Cambodia, and draining into the South China Sea from the Mekong Delta in Vietnam (Gupta, 2022). The LMRB is generally divided into the upper (Lancang River Basin in China, LRB) and lower parts (Mekong River Basin, MRB). The entire length of the LMR is 4,880 km with a total area of 795,000 km^2 (Dong et al., 2022). The main stream of the Lancang River is 2,161 km long and covers a drainage area of 165,000 km^2, accounting for 20.7% of the total area of the LMRB. The main stream of the Mekong River is 2,668 km long and covers a drainage area of approximately 630,000 km^2, accounting for 79.3% of the whole LMRB.

The LMRB comprises high mountains (4,500 m elevation) and deep gullies in the upstream area, relatively flat terrain with medium-sized mountains in the midstream, and wide valleys and large tributary river systems in the downstream area, and is characterized by unique and complex hydrologic, climatic, and physiographic features (Fan and Luo, 2019). The distribution of mean annual precipitation over the whole basin follows a distinct north-to-south and west-to-east gradient. Annual precipitation can be as little as 600 mm in the north of the Jiuzhou area in the

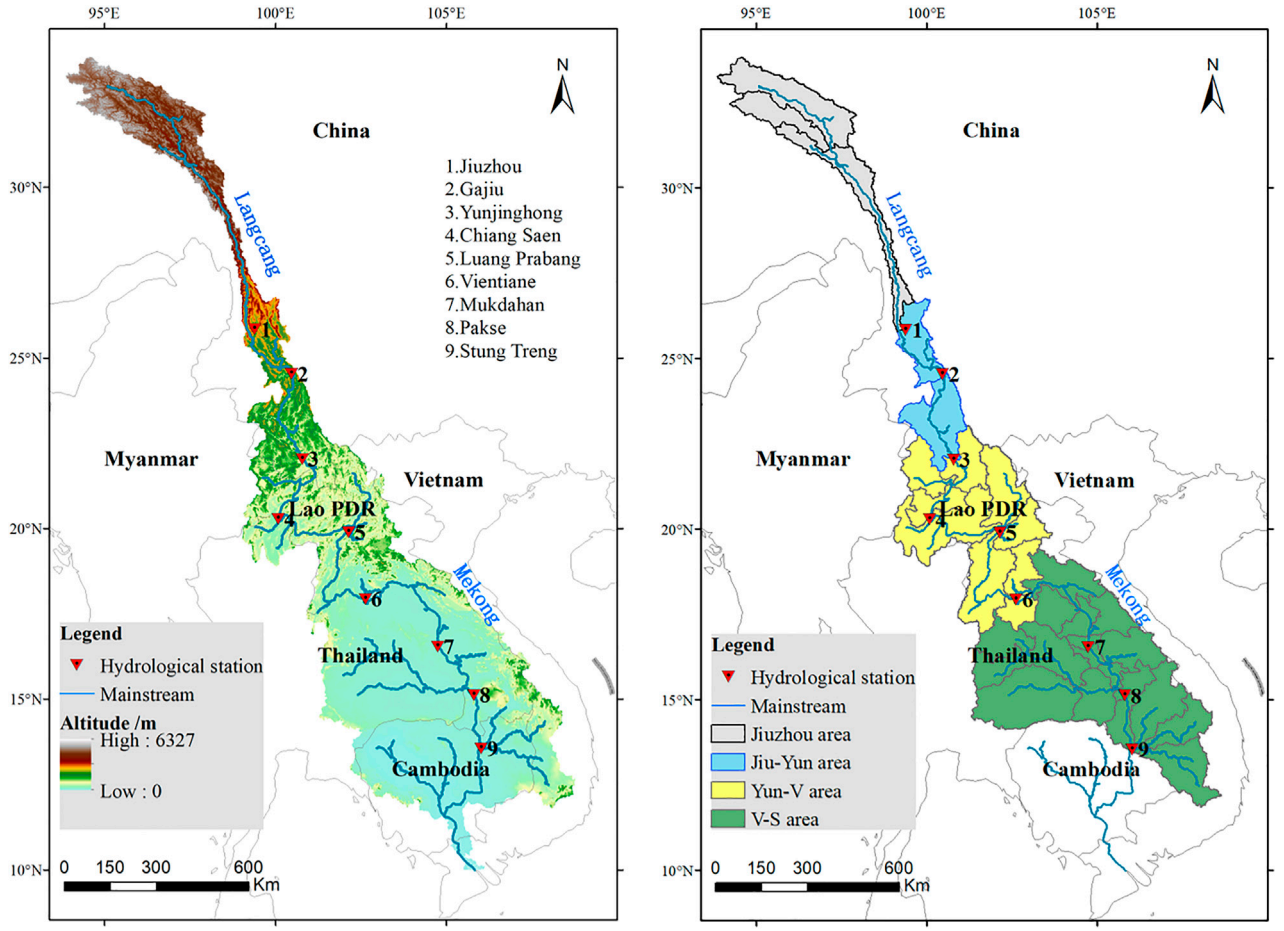

FIGURE 1
The Lancang-Mekong River Basin and the distribution of hydrological stations.

Tibetan Plateau, and as much as 1,700 mm in the southern mountains of the Jiu-Yun area. Regulated by the global monsoon system, the rain-soaked uplands in the V-S area receive the most precipitation (3,000 mm) and the semi-arid Khorat Plateau in the west receives the least (1,000 to 1,600 mm). The LMRB has two distinct seasons: a wet (May–October) and a dry season (November–April). Although interannual variation of monsoon precipitation is high, the wet season can contribute more than 80% of the annual regional precipitation. During the dry season, the basin is influenced mostly by dry air from the northeastern land (Räsänen and Kummu, 2013). The annual temperature in the LMRB is mainly influenced by latitude. The average temperatures in Jiuzhou, Jiu-Yun, Yun-V, and V-S are 2.5°C, 15.5°C, 26°C, and 30°C, respectively. Population density also increases with latitude from north to south.

In this study, the Mekong Estuary Delta region was not given a detailed investigation due to the lack of detailed hydrological data. According to the locations of Jiuzhou, Yunjinghong, Vientiane and Stung Treng hydrological stations (Figure 1), four parts of areas were zoned as Jiuzhou and above (Jiuzhou) area, Jiuzhou-Yunjinghong (Jiu-Yun) area, Yunjinghong-Vientiane (Yun-V) area and Vientiane-Stung Treng (V-S) area.

2.2 Data collection

The number of observation stations and data series in the LMRB, especially in the MRB, are insufficient, and the data sources and scales are inconsistent, which causes great difficulties for systematic and subsequent modeling analyses. To solve this problem, this study adopted the data input format as site in LRB + grid in MRB, with each observation and grid station containing one group of data, including precipitation, temperature, evapotranspiration, DEM, soil and land cover data. Specific data sources are as follows:

1) Meteorological data

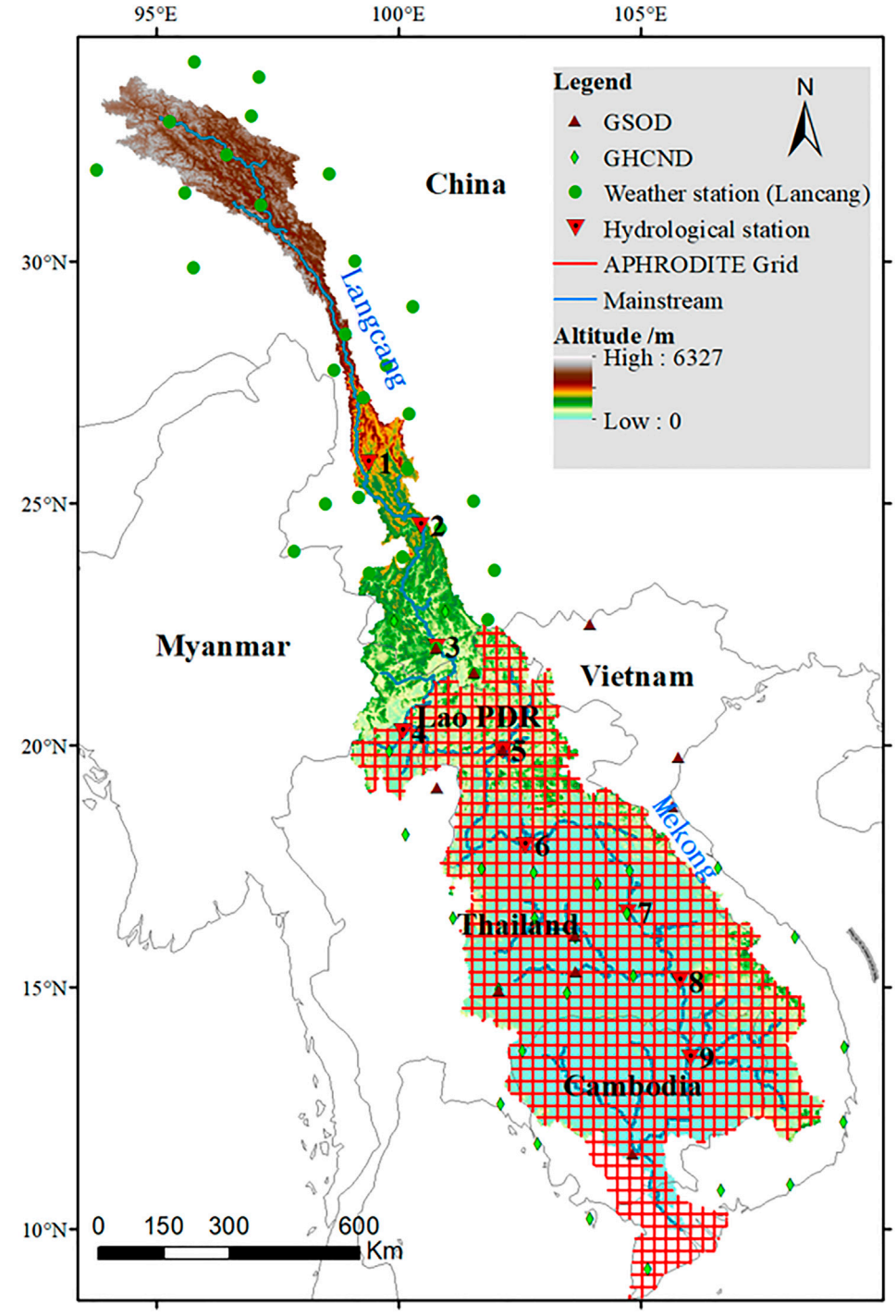

FIGURE 2
Distribution of meteorological stations in the Lancang-Mekong River Basin.

Daily observed meteorological data such as precipitation, temperature, wind and solar radiation data of the LRB (Figure 2) were collected from the Chinese meteorological data sharing service system (http://data.cma.cn/). Daily grid meteorological data of the MRB were collected from Mekong River Commission (MRC, https://www.mrcmekong.org/) and the Asian

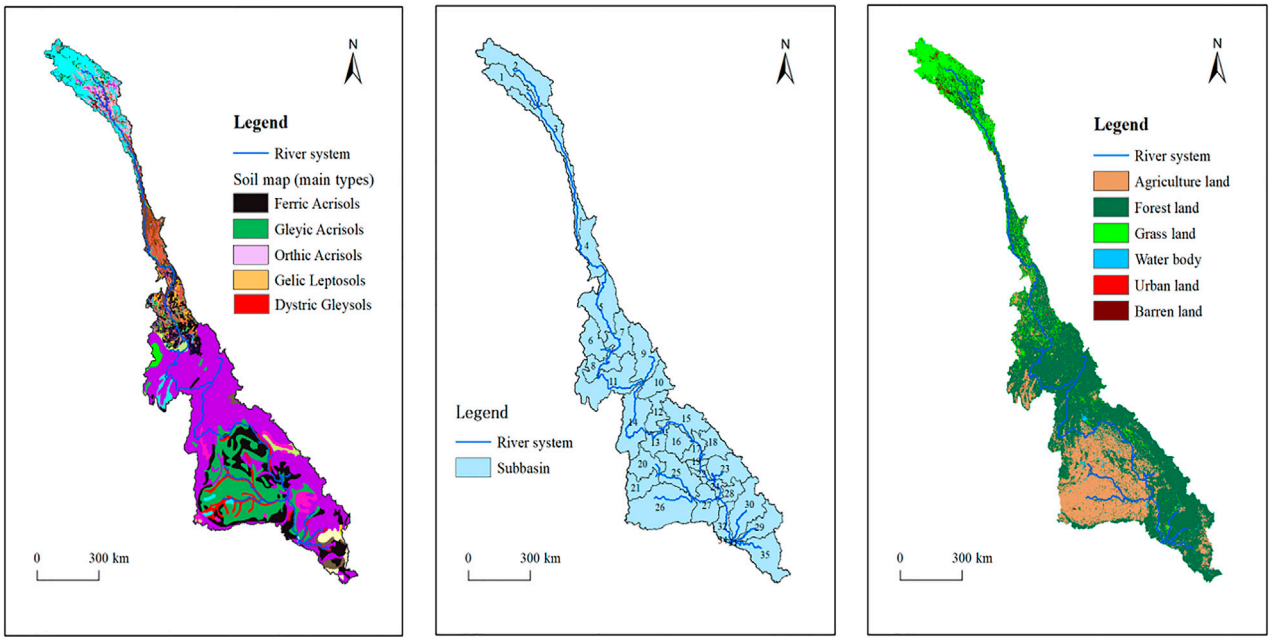

FIGURE 3
Sub-basin division by SWAT hydrological model in Lancang-Mekong River Basin **(A)** Watershed soil types map. **(B)** HRUs division map of sub-basins. **(C)** Watershed land use types map.

Precipitation-Highly-Resolved Observational Data Integration Towards Evaluation (APHRODITE, 0.25° x 0.25°, http://aphrodite.st.hirosaki-u.ac.jp/download/), respectively. To compensate for the lack of APHRODITE data at the maximum and minimum temperature, this study used the Global Surface Summary of the Day (GSOD, https://data.noaa.gov/dataset/dataset/global-surface-summary-of-the-day-gsod) data and Global Historical Climatology Network data (GHCND, https://www.ncei.noaa.gov/products/land-based-station/global-historical-climatology-network-daily) from NOAA (National Oceanic Atmospheric Adminstration). Evapotranspiration was calculated using the Penman-Monteith equation based on weather generator in SWAT model with default parameters setting.

2) Hydrological and topographic data

The streamflow data were provided by Yunnan University and the Mekong River Commission (MRC). The data series duration of Jiuzhou, Yunjinghong, Vientiane and Stung Treng station are 1961–2010, 1961–2014, 1961–2006 and 1961–2015, respectively. The geographical data, such as the 1 km × 1 km raster data, was extracted and resampled from 90 m resolution digital elevation model (DEM) data provided by the USGS (available from http://www.usgs.gov).

3) Land cover and soil data

The land use and land cover data of the LRB (1980–2015, per 5 years) were produced by the Institute of Geographical Sciences and Resources, Chinese Academy of Sciences, and the similar data of the MRB were downloaded and resampled from the Servir-Mekong dataset from 1987 to 2015 (available from https://servir.adpc.net). Soil data in LMRB was obtained from the Harmonized World Soil Database (HWSD).

2.3 Materials and methods

2.3.1 Construction of SWAT model in the study area

SWAT (Soil and Water Assessment Tool) model is a semi-distributed watershed hydrological model developed by Blackland Research and Extension Center of USDA in the early 1990s, which is mainly used to simulate the process of land and water surface cycle (Gassman et al., 2007). The land surface part can be divided into the process of streamflow generation and slope confluence, while the water surface part is the river network confluence (Paiva et al., 2011; Tan et al., 2022.).

Database including the spatial and attribute data is necessary to be bulit first. Spatial data such as DEM, the location of meteorological stations, land cover types, and soil distribution map, and attribute data such as meteorological data series and soil attribute data were edited and input into

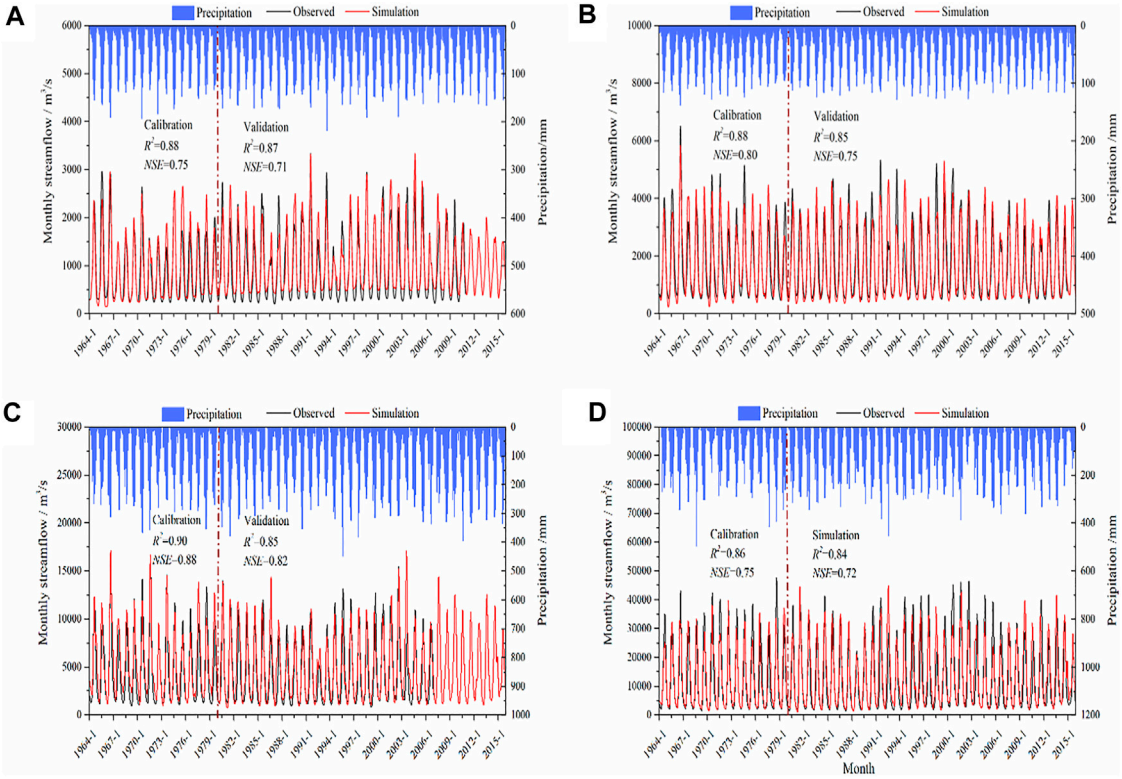

FIGURE 4
Calibration and validation results of the SWAT model for the monthly average streamflow at Jiuzhou **(A)**, Yunjinghong **(B)**, Vientiane **(C)**, and Stung Treng **(D)** stations based on the flow data measured during 1961–2015 in line with the monthly average precipitation (the blue column with the right vertical axis).

the SWAT model, respectively. Based on the established LMRB database, the LMRB system network was generated by extracting DEM data from the database. Combined with soil, land cover types, and slope values, the LMRB was divided into 35 sub-basins. Considering the calculation accuracy and processing speed, 35 sub-basins are further divided into 311 HRUs (hydrological response units) with an average area of 2,000 km^2, as shown in Figure 3.

2.3.2 Calibration and validation of SWAT model

The calibration and validation periods of the SWAT model were from 1961 (3 years warm-up period) to 1980, and 1981 to 2015, respectively. For validation, 35 years of data was considered sufficiently long (Liu et al., 2010; Zhang et al., 2012), when compared with other studies that used 2–3 years of data. The land cover data of 1990, which was less affected by human activities, was input to the model as the underlying surface data for the restoration of natural streamflow. This study adopted the step-by-step calibration principle to validate the streamflow data from upstream to downstream and LH-OAT (Latin-Hypercube & One Factor-At-a-Time) method to analyze the sensitivity of the main parameters. Method LH-OAT assumes that there are p parameters to be analyzed in the model, which are divided into N layers in space according to the LH (Latin-Hypercube) sampling idea, and then taking a sampling in each layer. After that, parameters of each LH sampling parameter group are changed according to the OAT (one Factor-at-a-time) method, and each small change is recorded as GS_i (global sensitivity). The sensitivity classification and the the detailed calibration process of the GS_i are given in Table 1 and Formula 1, respectively.

$$GS_i = \frac{\frac{M\left(e_{1,k},\ldots,e_{i,k}+\Delta e_{i,k},\ldots,e_{p,k}\right)-M\left(e_{1,k},\ldots,e_{i,k},\ldots,e_{p,k}\right)}{M\left(e_{1,k},\ldots,e_{i,k}+\Delta e_{i,k},\ldots,e_{p,k}\right)+M\left(e_{1,k},\ldots,e_{i,k},\ldots,e_{p,k}\right)/2}}{\Delta e_{i,k}/e_{i,k}} \quad (1)$$

$M(*)$ is the indicator function of the kth LH sampling set; $e_{i,k}$ is the value of the ith parameter in the kth LH sampling layer; and $\Delta e_{i,k}$ is some disturbance of parameter $e_{i,k}$.

Before applying the SWAT model to reconstruct natural streamflow in the LMR, the simulation capability of the model needs to be evaluated in the study area. The coefficient of determination (R^2) and the Nash–Sutcliffe efficiency (NSE) were used to evaluate the merits of the SWAT model. R^2

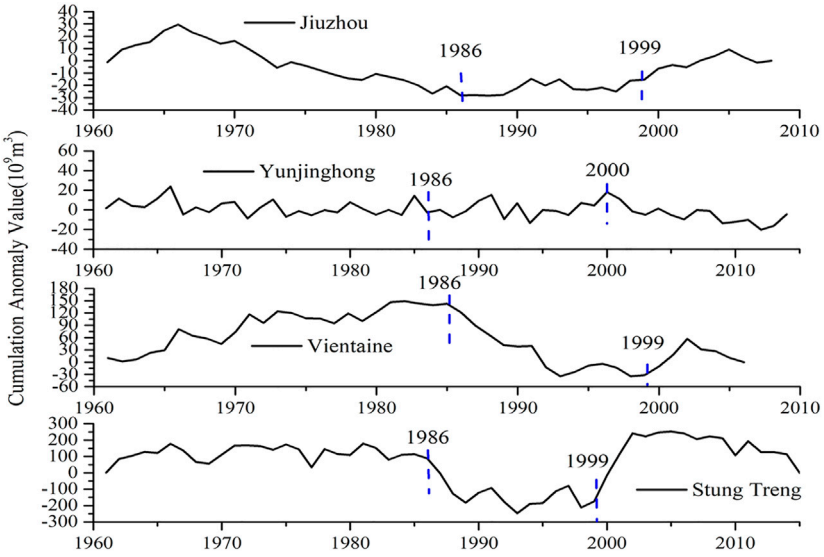

FIGURE 5
The cumulative anomaly variation of annual streamflow at Jiuzhou **(A)**, Yunjinghong **(B)**, Vientiane **(C)**, and Stung Treng **(D)** station.

TABLE 1 Sensitivity classification.

Class	Sensitivity range	Sensitive degree
1	0.00≤ $\|GS_i\|$<0.05	Insensitivity
2	0.05≤ $\|GS_i\|$<0.20	General sensitive
3	0.20≤ $\|GS_i\|$<1.00	Sensitive
4	1.00≤ $\|GS_i\|$	Supersensitive

calculates the linear correlations between observed and modelled data from SWAT. *NSE* evaluates the SWAT model's goodness of fit. R^2 and *NSE* are defined as follows:

$$NSE = 1 - \frac{\sum_{i=1}^{n}(Q_0 - Q_S)^2}{\sum_{i=1}^{n}(Q_0 - Q_{0,ave})^2} \quad (2)$$

$$R^2 = \frac{\sum_{d=1}^{n}\left[(Q_{0,d} - Q_{0,ave})(Q_{0,d} - Q_{0,ave})\right]^2}{\sum_{d=1}^{n}(Q_{0,d} - Q_{0,ave})^2 \sum_{i=1}^{n}(Q_{s,d} - Q_{s,ave})^2} \quad (3)$$

Where Q_0 and Q_s are the measured and simulated flow (m^3/s) of time step d, respectively. $Q_{0,ave}$ and $Q_{s,ave}$ are the measured and simulated average flow (m^3/s) during simulation, respectively.

Figure 4 shows the observed and simulated monthly streamflow of Jiuzhou, Yunjinghong, Vientiane, and Stung Treng stations during the calibration and validation periods. The NSE values of the calibration period of the four stations were 0.75, 0.80, 0.88, and 0.75, respectively. During the validation period, the NSE values were 0.71,0.75, 0.82, and 0.72, respectively. The R^2 values were all >0.84. Based on the recommendations of previous research, a hydrological simulation is satisfactory when NSE>0.50 and R^2 >0.6.

2.3.3 Assessment of the contributions of climatic variations and human activities to streamflow changes

According to the calculation principle of the hydrological model, the difference in observed streamflow between the reference and change period is ΔQ. This parameter represents a combination of climate change and human activity. The difference in natural streamflow (simulated streamflow) between the two periods, ΔQ_c, reflects the impact of climate change. Therefore, the contributions of both climatic variations and human activities to streamflow changes were quantified by using the following formulas:

$$\Delta Q = Q_{obs} - Q_{base} = \Delta Q_c + \Delta Q_h \quad (4)$$

$$\Delta Q = \Delta Q_c + \Delta Q_{lucc} + \Delta Q_w \quad (5)$$

$$\Delta Q_c = Q_{sim*} - Q_{base} \quad (6)$$

$$\Delta Q_w = Q_{obs} - Q_{base} \quad (7)$$

$$\Delta Q_{lucc} = Q_{sim} - Q_{sim^*} \quad (8)$$

$$\eta_c = \frac{\Delta Q_c}{|\Delta Q_h| + |\Delta Q_c|} \times 100\% \quad (9)$$

$$\eta_h = 1 - \eta_c \quad (10)$$

$$\eta_{lucc} = \frac{(1 - \eta_c) \times |\Delta Q_{lucc}|}{|\Delta Q_{lucc}| + |\Delta Q_w|} \times 100\% \quad (11)$$

where $\Delta Q(m^3)$ represents the change amount of observed streamflow in the variation period relative to the reference

TABLE 2 The results of Mann-Kendall trend tests for the hydro-climatic data in Lancang-Mekong River.

Station	Timescale	Precipitation (mm/10a)						Streamflow (10^9m^3/10a)					
		Basis period		Change period A		Change period B		Basis period		Change period A		Change period B	
		Z value	Trend	Z value	Trend	Z value	Trend	Z value	Trend	Z value	Trend	Z value	Trend
Jiuzhou area	Annual	−0.22	−8.00	0.12	3.47	−2.26**	−91.39	−1.07	−3.30	0.37	1.57	−1.66*	−6.96
	Dry season	1.91	14.40	0.70	8.41	0.18	7.80	−0.55	−0.81	1.36	0.48	−1.40	−0.67
	Wet season	−0.29	−21.15	0.04	-4.94	−2.87	−99.19	−0.81	−3.34	0.37	1.11	−1.65*	−6.41
Jiu-Yun area	Annual	−1.20	−35.88	1.98**	78.27	−2.41	−133.81	−1.46	−4.64	0.99	5.73	−2.52**	−13.56
	Dry season	−0.29	−7.29	0.00	3.74	−0.88	−19.33	−0.98	−0.50	0.69	0.93	−0.99	−1.35
	Wet season	−0.94	−28.59	1.68*	74.53	−2.08**	−114.48	−1.20	−4.17	0.89	4.90	−0.88	−3.27
Yun-V area	Annual	0.55	50.45	0.99	143.61	−0.30	−92.65	−0.49	−3.23	1.64	20.95	−0.90	−80.51
	Dry season	0.36	1.93	0.33	26.09	0.00	38.57	−1.65*	−2.87	0.66	1.73	−1.80*	−14.87
	Wet season	0.49	48.55	0.99	117.52	−0.60	−131.22	−0.42	−0.36	1.86*	19.22	−1.20	−65.64
V-S area	Annual	1.01	18.60	1.31	130.97	−0.77	−108.89	−1.72*	−31.87	1.09	54.66	−0.86	−32.95
	Dry season	0.03	4.11	2.19**	117.17	0.50	10.07	−1.33	−4.69	1.65*	17.18	−0.41	−2.04
	Wet season	0.23	14.49	0.00	13.80	−1.13	−118.95	−1.52	−27.19	0.66	37.48	−0.99	−30.91

Note: *, ** indicated that the data series passed significance test at α=0.10 and 0.05 levels, respectively.

10.3389/feart.2022.1024037

TABLE 3 Scenarios for quantitative analysis the contributions of human activities and climate change in Lancang-Mekong River Basin.

Station	Group	Land use	Station	Group	Land use	Objectiive
Jiuzhou	$Base_1$:1961–1980	L1990	Jiu-Yun	$Base_2$:1961–1980	L1990	η_c and η_h
	A_1:1986–1999	L2000		A_2:1986–2000	L2000	
	B_1:2000–2010	L2010		B_2:2001–2014	L2010	η_c and η_h
	A_1^a:1986–1999	L1990		A_2^a:1986–2000	L1990	η_c
	B_1^a:2000–2010	L1990		B_2^a:2001–2014	L1990	η_c
Yun-V	$Base_3$:1961–1980	L1990	V-S	$Base_4$:1961–1980	L1990	
	A_3:1986–1999	L2000		A_4:1986–1999	L2000	η_c and η_h
	B_3:2000–2006	L2005		B_4:2000–2015	L2010	η_c and η_h
	A_3^a:1986–1999	L1990		A_4^a:1986–1999	L1990	η_c
	B_3^a:2000–2006	L1990		B_4^a:2000–2015	L1990	η_c

[a]Base, A, B, A[a].
And B[a]represent the period of different scenarios.

period. Q_{obs} and Q_{base} (m^3) represent the observed mean streamflow during variation and the reference period, respectively. ΔQ_h and ΔQ_c represent the impact amount from human activities and climate change on streamflow changes, respectively. ΔQ_{lucc} represents the impact amount from land use change, ΔQ_w represents the impact amount from other forms of human activities except land use, such as reservoir regulation, inter-basin water diversion, *etc.* η_c, η_h, and η_{lucc} are the contributions of climatic variations, human activities, and land use to streamflow changes, respectively.

3 Results and discussion

3.1 Reference and change periods judgement

The cumulative anomalies of streamflow series at Jiuzhou, Yunjinghong, Vientiane, and Stung Treng hydrological stations are shown in Figure 5, and an obvious decrease in the annual streamflow can be noticed from 1966 to 1980 at Jiuzhou (Figure 5A), from 1986 to 2000 at Yunjinghong (Figure 5B), and from 1986 to 1999 at Vientiane and Stung Treng stations (Figures 5C,D). Hence, the impact of human activities on streamflow from 1961 to 1980 can be regarded as at a low level and so the period is taken as the reference period in this study, while 1986 can be regarded as the sudden changing year in the annual streamflow series at these four stations. This division is consistent with the findings of other studies (e.g., Tang et al., 2014; Wang et al., 2017). Therefore, we divided the change periods of annual streamflow at four stations into two periods: at Jiuzhou, periods A_1 (1986–1997) and B_1 (1998–2010); at Yunjinghong, periods A_2 (1986–2000) and B_2 (2001–2014); at Vientiane, periods A_3 (1986–1999) and B_3 (2000–2006); and at Stung Treng, periods A_4 (1986–1999) and B_4 (2000–2015). Correspondingly, the reference periods were named $Base_1$, $Base_2$, $Base_3$, and $Base_4$, respectively.

3.2 Trends of hydro-climatic factors during 1961–2015

The yearly and seasonal average streamflow at Jiuzhou, Yunjinghong, Vientiane, and Stung Treng stations in different periods are listed in Table 2. At the annual timescale, the streamflow volume at the four stations showed an obvious increase from upstream to downstream. By comparison with the volume of the streamflow in base periods, the volume of the streamflow increased in the changing period B_1 at Jiuzhou station, B_3 at Vientiane station, and B_4 at Stung Treng station, and yet an obvious decrease in the changing period B_2 at Yunjinghong station, A_3 at Vientiane station, and A_4 at Stung Treng station. At the seasonal timescale, the streamflow volume at the four stations showed little change in the dry season, but a much more dramatic change in the wet season.

The Mann-Kendall (M-K) non-parametric trend test method was used to conduct trend detection of streamflow at these four stations and precipitation in Jiuzhou, Jiu-Yun, Yun-V, and V-S areas on yearly and seasonal time scales from 1961 to 2015 (Kendall, 1975; Yanming et al., 2012; Noszczyk et al., 2017; Ning et al., 2021). The Z value, which is the result of M-K test, obeyed the standard normal distribution. A positive Z value indicates an increasing trend, while a negative Z value indicates a decreasing trend. The bilateral significance level test was used to test the monotonic trend of increase or decrease. If $|Z| > 1.645$, 1.96, and 2.576, it shows that the time series have passed the confidence test of α=0.01, 0.05, and 0.1 respectively. At the yearly time scale, the

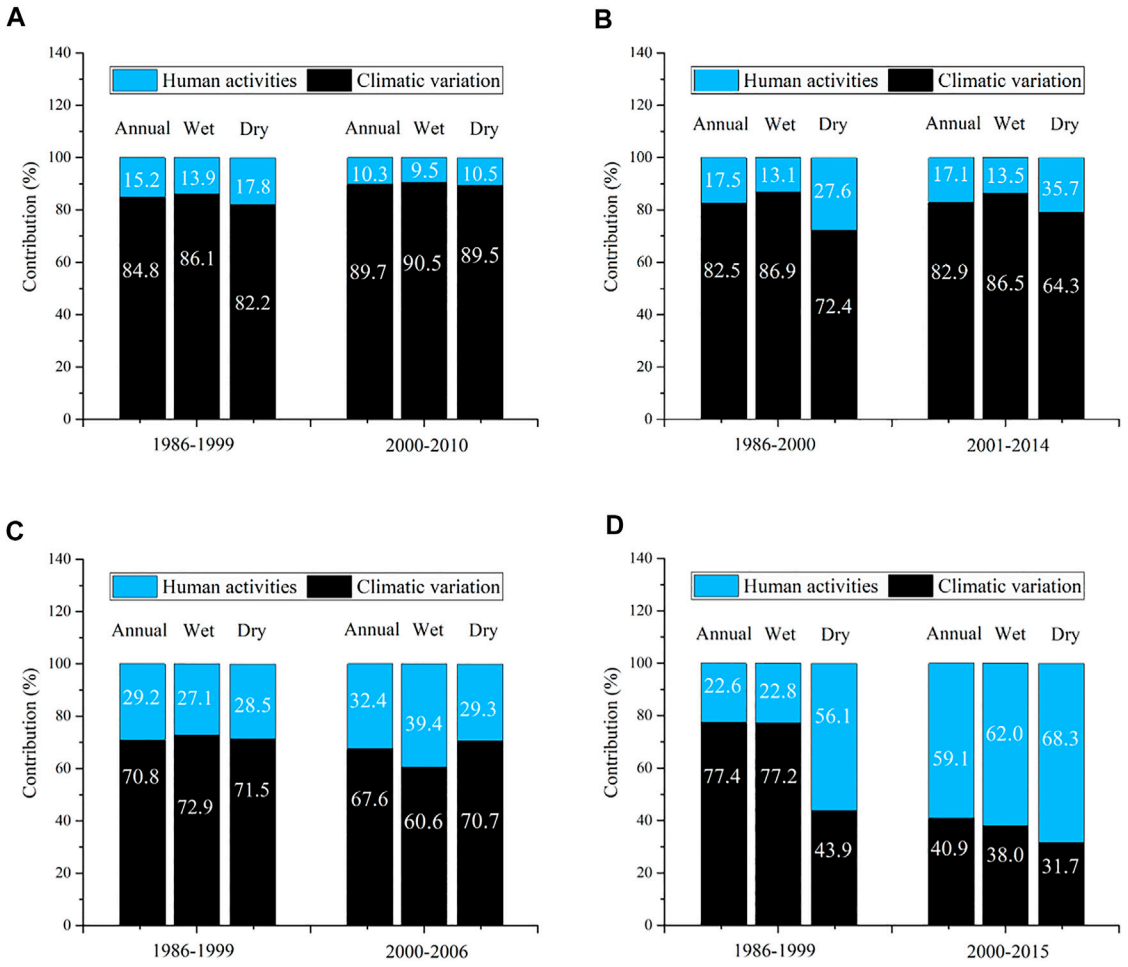

FIGURE 6
Contributions of climatic variations and human activities to annual and seasonal streamflow changes in Jiuzhou **(A)**, Jiu-Yun **(B)**, Yun-V **(C)**, and V-S **(D)** area.

streamflow at Jiuzhou station and that in the basis period and A_2 of Yunjinghong station did not show any obvious trends. However, the streamflow in change period B_2 showed a significant decreasing trend (0.05 significance level). The total streamflow at Vientiane and Stung Treng stations showed decreasing and increasing trends, respectively. However, both showed an increasing trend first and then decreased in the changing periods. At the seasonal time scale, the variation trends of streamflow in the dry and wet seasons were basically consistent with that at the yearly time scale in each area. However, the streamflow had a significant downward trend at Vientiane station and a significant upward trend at Stung Treng station in the dry season, and a significant downward trend at Jiuzhou station and a significant upward trend at Vientiane station in the wet season, while other stations had little change.

According to the correlation calculation results, the correlated degree of annual average precipitation and streamflow reached 0.91 in Jiuzhou, 0.74 in Jiu-Yun, 0.65 in Yun-V, but only 0.17 in V-S. The streamflow trends were consistent with precipitation in the dry season (Nov-next Apr) throughout the four areas with more than 0.5 correlation values and less precipitation and streamflow variation than in the wet season. The streamflow trends were consistent with the annual precipitation variation in the wet season of the four areas and the correlation degree between regional average precipitation and streamflow gradually weakened from upstream to downstream.

3.3 Contributions of climate and human activities to streamflow changes

In terms of Formulas (4–9) and the different scenarios setting for quantitative contribution analysis of the human activities and climate change in LMRB (Table 3), the contributions of climate change and human activities to streamflow change were quantified by comparing the observed and simulated

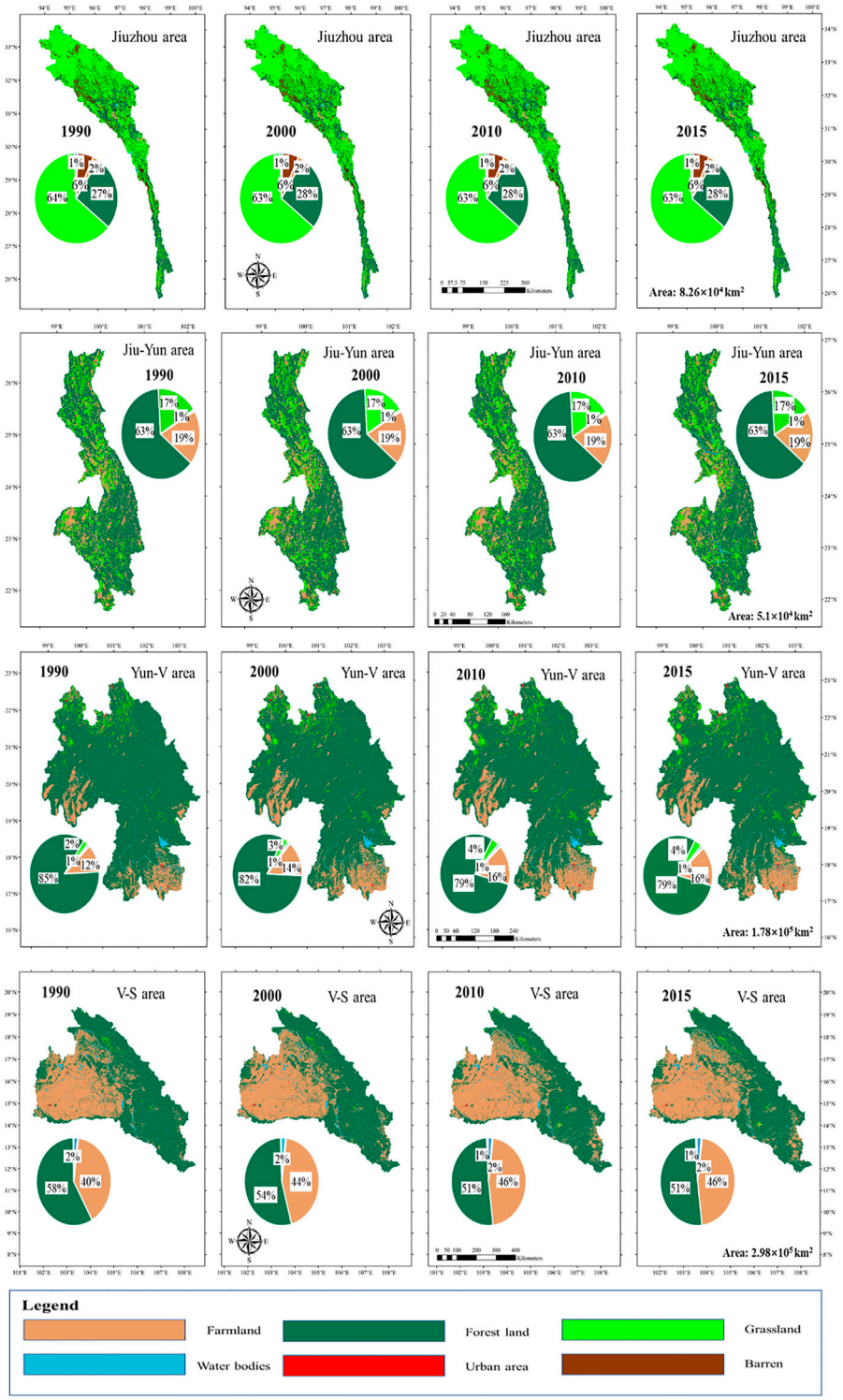

FIGURE 7
The situation of Land use types change in Lancang-Mekong River Basin.

TABLE 4 The contributions of land use types change to annual and seasonal streamflow changes in Lancang-Mekong River Basin.

Station	Period	η_{lucc}	Station	Period	η_{lucc}	Station	Period	η_{lucc}	Station	Period	η_{lucc}
Jiuzhou	A_1	5.88%	Jiu-Yun	A_2	9.68%	Yun-V	A_3	20.67%	V-S	A_4	14.99%
	B_1	4.79%		B_2	7.48%		B_3	22.21%		B_4	30.12%
	A_1-dry	8.95%		A_2-dry	17.67%		A_3-dry	16.63%		A_4-dry	30.67%
	B_1-dry	4.68%		B_2-dry	10.29%		B_3-dry	20.70%		B_4-dry	36.66%
	A_1-wet	7.74%		A_2-wet	2.75%		A_3-wet	14.48%		A_4-wet	11.57%
	B_1-wet	4.87%		B_2-wet	6.87%		B_3-wet	27.46%		B_4-wet	22.68%

[a]A-dry and A-wet are short for the period of dry and wet seasons, respectively.

streamflow during basic and change periods. The contributions of the two factors were analyzed at the yearly and seasonal time scales, respectively. The results are illustrated in Figure 6.

At the yearly time scale, the contributions of human activities (η_h) to the streamflow changes, which maintained a low percentage, were 15.2% (1986–1999) and 10.3% (2000–2010), respectively, in Jiuzou area (Figure 6A). More farmland and water conservancy projects were found in Jiu-Yun area, so the contributions of human activity accounted for 17.5% in 1986–2000 and 17.1% in 2001–2014 (Figure 6B), which was slightly more than that in Jiuzhou area. The contributions of human activity in Yun-V (Figure 6C) and V-S (Figure 6D) areas were much greater after 1999 (32.4%, 59.1%) than in 1986–1999 (29.2%, 22.6%).

At the seasonal time scale, human activities had a relatively larger contribution to streamflow changes during dry seasons than in wet seasons, such as the value of Jiu-Yun area between 1986 and 2000, where the η_h accounted for 27.6% during the dry season but 13.1% in the wet season. Additionally, in the V-S area between 1986 and 1999, human activity accounted for 68.3% during the dry season but 62.0% during the wet season.

3.4 Impact of land use type change on streamflow in different areas

In terms of Formulas (10) and 11and the control scenarios in Table 3, further quantitative assessment of the impact from land use type changes (η_{lucc}) in Jiuzhou, Jiu-Yun, Yun-V, and V-S areas on the annual and seasonal streamflow could be analyzed. The detailed analysis and contributions of land use type changes during 1990–2015 are shown in Figure 7 and Table 4. Land use change is often caused by climate change and human activities; however, according to previous studies (Tang et al., 2021; Ep et al., 2021), human activities played a major role in the LMRB. Therefore, we did not take the impact of climate on land use types into consideration here.

In Jiuzhou, each area of land use types remained stable except from a small proportion reduce of the grassland from 1990 to 2000, so the η_{lucc} on long-term streamflow is under 6%. In Jiu-Yun area, because of there were more farmland and urban area than in Jiuzhou, but small land use types change, the η_{lucc} accounts for 9.68% and 7.48% in A_2 and B_2, respectively. In Yun-V area, the areas of forest land decreased by 6% and farmland increased by 4% from 1990 to 2010. Therefore, the contribution from land use type changes showed a relatively high proportion (20.67%) in A_3 and 22.21% in B_3 at the yearly time scale. The same situation occurred in V-S area, where the area of forest land decreased by 7% and farmland increased by 6% from 1990 to 2010. Correspondingly, the yearly contribution from land use type changes remained at a high level, at 14.99% and 30.12% in A_4 and B_4, respectively. Furthermore, the dry seasons were easier to be affected in the most area of LMRB than in wet seasons.

3.5 Discussion

3.5.1 Uncertainties in the simulation

Although this study provides a quantitative evaluation of the impacts of climatic variation and human activities on streamflow changes in the integrated form in LMRB and the SWAT model could well simulate the natural streamflow, there are still some uncertainties in the model simulations (Sangam et al., 2022). The uncertainty mainly comes from the reference and change periods judgement, the model structure setting, input data and parameter calibration (Han and Zheng, 2016; Chen et al., 2022). First, this study judged the mutation year by cumulative anomalies of streamflow series, but different assumptions and methods may lead to different changing points, further affecting the follow-up analysis. Second, SWAT model assumes that each HRU has the same slope, which may affect the flow production and confluence simulation of different land types. Third, multi-source meteorological data such as reanalysis data and interpolated data were used as the input data in the simulation process, which may cause bias to some extent (Li et al., 2022; Sudesan et al., 2022). Finally, our model was calibrated and validated based on only observed streamflow data, and thus, the simulation of evaporation and infiltration need to be further validated after the calculation of observed data (Gowda et al., 2022).

3.5.2 Limitations of this research

Due to the large span of time-space and great differences in geographical conditions in the LMRB, the observed data was difficult to be obtained. The limitation was related to three aspects. The first limitation is that the streamflow data in the most of the stations in LMRB were absent and inconsecutive, which lead to the streamflow simulation of estuary area was not been achieved. The second limitation is that the human activities such as the reservoir discharge and irrigation water were not considered in this study. Reservoirs, such as the Xiao wan and Nuozhadu hydropower stations in LRB may affect the simulation result in certain years (Wang et al., 2017). The third limitation is that this study used muti-source data in the format like site in LRB + grid in MRB instead of all grid data (Han et al., 2012; Tang et al., 2019). Through comparing the correlation between these two data forms and the observed streamflow series, using the site data in LRB could ensure the accuracy of streamflow simulation and the process of calibration and validation to the maximum extent (Swain et al., 2018; Tang et al., 2021).

4 Conclusion

As the largest transboundary river in Asia, the Lancang-Mekong River (LMR) not only connects six countries with significant geographical, economic, and cultural differences, but also spans the alpine, temperate, and tropical climatic zones, making the Lancang-Mekong River Basin (LMRB) suffer significant influences from climate change and human activities. This study performed a detailed analysis of the impacts of climate and human activities across the entire LMRB on streamflow process over the recent decades in an integrated form using a large number of multi-source data, trend analysis and cumulative anomaly methods and SWAT model. The main results obtained in this study are:

1) At the yearly timescale, there is no significantly increasing or decreasing trend showing in the streamflow process at Jiuzhou station, but a significant decrease at Yunjinghong station, an insignificant decreasing trend at Vientiane station and an increasing trend at Stung Treng station. At the seasonal timescale, the varying trend of streamflow at each hydrological station was consistent essentially with that at the yearly timescale.
2) At the yearly timescale, the ratios of the contributions of human activities (η_h) to the streamflow changes before 2000 to the counterparts after 2000 are 15.2% and 10.3%, 17.5% and 17.1%, 29.2% and 32.4%, 22.6% and 59.1% in Jiuzou, Jiu-Yun, Yun-V and V-S areas, respectively. At the seasonal timescale, η_h in the dry season before to after 2000 is 17.8% and 10.5%, 27.6% and 35.7%, 28.5% and 29.3%, 56.1% and 68.3%, respectively. In the wet season, η_h is 13.9% and 9.5%, 13.1% and 13.5%, 27.1% and 39.4%, 22.8% and 62%, respectively.
3) The impacts of climate change on streamflow in the LMRB gradually decreased from the upper to the lower reaches, while the impacts of human activities gradually increased. Furthermore, the impacts of climate change on streamflow in the dry season were more significant than in the wet season. The contributions of Land use types change (η_{lucc}) account for about 1/3 of η_h in LRB but more than 1/2 of η_h in MRB.

Although this study provides a quantitative evaluation of the impacts of climatic variation and human activities on streamflow changes in the integrated form in LMRB, some shortcomings remain. While this study took the effects of climate, topography, soil, vegetation, and other spatial-temporal variability on streamflow into consideration, the parameter values, sensitivity, and scale effects of those factors on streamflow process were not systematically investigated and further detailed studied are required (Ahn and Merwade, 2014; Gao et al., 2020; Andaryani et al., 2021; Wang et al., 2021).

Data availability statement

Publicly available datasets were analyzed in this study. This data can be found here: 1) Meteorological data. Daily precipitation and temperature data of the LMRB were collected from the Chinese meteorological data sharing service system (available from http://data.cma.cn/data/detail/dataCode/A.0012.0001.html) and the Asian Precipitation-Highly-Resolved Observational Data Integration Towards Evaluation (APHRODITE, 0.25° x 0.25°, available from http://aphrodite.st.hirosaki-u.ac.jp/download/), respectively. To compensate for the lack of APHRODITE data at the maximum and minimum temperature, this study used the Global Surface Summary of the Day (GSOD, available from https://data.noaa.gov/dataset/dataset/global-surface-summary-of-the-133 day-gsod) data from NOAA and Global Historical Climatology Network (GHCND, available from https://www.ncei.noaa.gov/products/land-based-station/global-historical-climatology-network-daily) data. Evapotranspiration was calculated using the Penman-Monteith equation. 2) Hydrological and topographic data. The streamflow data were provided by Yunnan University and the Mekong River Commission (MRC). The geographical data, such as the 1 km × 1 km raster data, was extracted and resampled from 90 m resolution digital elevation model (DEM) data provided by the USGS (available from http://www.usgs.gov). 3) Land cover and soil data. The land use and land cover data of the LRB (1980–2015, per 5 years) were produced by the Institute of Geographical Sciences and Resources, Chinese Academy of Sciences, and the similar data of the MRB were downloaded and resampled from the Servir-Mekong dataset from 1987 to 2015 (available from https://rlcms-servir.adpc.net/en/landcover).

Soil data in LMRB was obtained from the Harmonized World Soil Database (HWSD).

Author contributions

Conceptualization, RL and HH; methodology, RL and RZ; software, RL and ZW; validation, RL and HH; formal analysis, RL and HH; investigation, RL, HH, and ZW; resources, HH and RZ; data curation, RL; writing—original draft preparation, RL; writing—review and editing, RL and HH; visualization, RL and HH; supervision, HH and ZW; project administration, HH and ZW; funding acquisition, ZW and HH.

Funding

This research was financially supported by the Strategic Priority Research Program of the Chinese Academy of Sciences (XDA19030204) and National Natural Science Foundation of China (Grant No. 41,561,144,012).

Conflict of interest

The authors declare that the research was conducted in the absence of any commercial or financial relationships that could be construed as a potential conflict of interest.

Publisher's note

All claims expressed in this article are solely those of the authors and do not necessarily represent those of their affiliated organizations, or those of the publisher, the editors and the reviewers. Any product that may be evaluated in this article, or claim that may be made by its manufacturer, is not guaranteed or endorsed by the publisher.

References

Ahn, K. H., and Merwade, V. (2014). Quantifying the relative impact of climate and human activities on streamflow. *J. Hydrology* 515, 257–266. doi:10.1016/j.jhydrol.2014.04.062

Ali, S., Wang, Q., Liu, D., Fu, Q., Mafuzur Rahaman, M., Abrar Faiz, M., et al. (2022). Estimation of spatio-temporal groundwater storage variations in the Lower Transboundary Indus Basin using GRACE satellite. *J. Hydrology* 605, 127315. doi:10.1016/j.jhydrol.2021.127315

Andaryani, S., Nourani, V., Ball, J., Jahanbakhsh Asl, S., Keshtkar, H., and Trolle, D. (2021). A comparison of frameworks for separating the impacts of human activities and climate change on river flow in existing records and different near-future scenarios. *Hydrol. Process.* 35 (7), e14301. doi:10.1002/hyp.14301

Chen, Changzheng, Gan, Rong, Feng, Dongmei, Yang, F., and Zuo, Q. (2022). Quantifying the contribution of SWAT modeling and CMIP6 inputting to streamflow prediction uncertainty under climate change. *J. Clean. Prod.* 364, 132675. doi:10.1016/j.jclepro.2022.132675

Dong, Z., Liu, H., Hu, H., Khan, M. Y. A., Wen, J., Chen, L., et al. (2022). Future projection of seasonal drought characteristics using CMIP6 in the Lancang-Mekong River Basin. *J. Hydrology* 610, 127815. doi:10.1016/j.jhydrol.2022.127815

Ep, A., Hlh, B., Dvbc, D., Kantoush, S., Poh, D., Alcantara, E., et al. (2021). Impacts of agricultural expansion on floodplain water and sediment budgets in the Mekong River. *J. Hydrology* 605, 127296. doi:10.1016/j.jhydrol.2021.127296

Fan, X., and Luo, X. (2019). Precipitation and flow variations in the Lancang-Mekong river basin and the implications of monsoon fluctuation and regional topography. *Water* 11 (10), 2086. doi:10.3390/W11102086Gowda

Gao, X., Yan, C., Wang, Y., Zhao, X., Zhao, Y., Sun, M., et al. (2020). Attribution analysis of climatic and multiple anthropogenic causes of runoff change in the loess plateau-A case-study of the jing River Basin. *Land Degrad. Dev.* 31 (13), 1622–1640. doi:10.1002/ldr.3557

Gassman, P. W., Reyes, M. R., Green, C. H., and J. G. Arnold (2007). The soil and water assessment tool: Historical development, applications, and future research directions. *Trans. ASABE* 50 (4), 1211–1250. doi:10.13031/2013.23637

Gowda, A. N. B., Patil, N. S., and Natarajan, M. (2022). "Multisite calibration of the ghataprabha sub-basin using soil and water assessment tool,". Editors R. Jha, V. P. Singh, V. Singh, L. B. Roy, and R. Thendiyath (Cham: Springer), Vol. 109. doi:10.1007/978-3-030-81358-1_12*Hydrol. Model.*

Gupta, A. (2022). *Large rivers: Geomorphology and management*. Second Edition, 661–686. doi:10.1002/9781119412632.ch22The M ekong river: Morphology, evolution, and management

Han, F., and Zheng, Y. (2016). Multiple-response bayesian calibration of watershed water quality models with significant input and model structure errors. *Adv. Water Resour.* 88, 109–123. doi:10.1016/j.advwatres.2015.12.007

Han, Z., and Zhou, T. (2012). Assessing the quality of aphrodite high-resolution daily precipitation dataset over contiguous China. *Chin. J. Atmos. Sci.* doi:10.3878/j.issn.1006-9895.2011.11043

Hu, K. X., Awange, J. L., Kuhn, M., Nanteza, J., et al. (2021). Inference of the spatio-temporal variability and storage potential of groundwater in data-deficient regions through groundwater models and inversion of impact factors on groundwater, as exemplified by the Lake Victoria Basin. *Sci. Total Environ.* 800, 149355. doi:10.1016/j.scitotenv.2021.149355

Kendall, M. G. (1975). Rank correlation methods. 2nd impression. In *Charles Griffin and Company Ltd. London and High*. Wycombe; Griffin, London, UK.

Li, C. Y., and Fang, H. Y. (2021). Assessment of climate change impacts on the streamflow for the Mun River in the Mekong basin, southeast Asia: Using SWAT model. *Catena* 201, 105199. doi:10.1016/j.catena.2021.105199

Li, Q., Zeng, T., Chen, Q., Han, X., Weng, X., He, P., et al. (2022). Spatio-temporal changes in daily extreme precipitation for the lancang–mekong River Basin. *Nat. Hazards (Dordr).* doi:10.1007/s11069-022-05569-4

Li, R., Huang, H., Yu, G., Bridhikitti, A., and Su, T. (2020). Trends of runoff variation and effects of main causal factors in Mun River, Thailand during 1980–2018. *Water* 12 (3), 831. doi:10.3390/w12030831

Liu, D. D., Chen, X. H., Lian, Y. Q., and Lou, Z. (2010). Impacts of climate change and human activities on surface runoff in the Dongjiang River Basin of China. *Hydrol. Process.* 24, 1487–1495. doi:10.1002/hyp.7609

Liu, J., Chen, D., Mao, G., Irannezhad, M., and Pokhrel, Y. (2021). Past and future changes in climate and water resources in the lancang–mekong River Basin: Current understanding and future research directions. *Engineering* 13, 144-152. doi:10.1016/j.eng.2021.06.026

MRC (2022). *Mekong low flow and drought*. Vientiane, Laos, Asia: MRC Secretariat. doi:10.52107/mrc.qx5yo7

Ning, Y. N., Yang, X. N., Sun, W. Y., Mu, X. m., Gao, P., Zhao, G. j., et al. (2021). The trend of runoff change and its attribution in the middle reaches of the Yellow River. *J. Nat. Resour.* 36 (1), 256–269. http://www.jnr.ac.cn/EN/Y2021/V36/I1/256. doi:10.31497/zrzyxb.20210117

Noszczyk, T., Rutkowska, A., and Hernik, J. (2017). Determining changes in land use structure in Małopolska using statistical methods. *Pol. J. Environ. Stud.* 26, 211–220. doi:10.15244/pjoes/64913

Paiva, R. C. D., Collischonn, W., and Tucci, C. E. M. (2011). Large scale hydrologic and hydrodynamic modeling using limited data and a GIS based

approach. *J. Hydrology* 406 (3-4), 170–181. doi:10.1016/j.jhydrol.2011.06.007

Räsänen, T. A., and Kummu, M. (2013). Spatiotemporal influences of ENSO on precipitation and flood pulse in the Mekong River Basin. *J. Hydrology* 476, 154–168. doi:10.1016/j.jhydrol.2012.10.028

Song, S., Wang, S., Fu, B., Liu, Y., Wang, K., Li, Y., et al. (2020). Sediment transport under increasing anthropogenic stress: Regime shifts within the Yellow River, China. *Ambio* 49, 2015–2025. doi:10.1007/s13280-020-01350-8

Ssa, B., Bba, D., Rt, C., and Virdis, S. G. P. (2022). Integrated assessment of the landuse change and climate change impacts on the sediment yield in the Songkhram River Basin, Thailand. *Catena (Amst).* 209, 105859. doi:10.1016/j.catena.2021.105859

Sudesan, S., Remesan, R., and Sen, D. (2022). "Hydrologic modeling with SWAT in an eastern Indian River Basin using different gridded data sets,". Editors R. Jha, V. P. Singh, V. Singh, L. B. Roy, and R. Thendiyath (Cham, Switzerland: Springer), 109. doi:10.1007/978-3-030-81358-1_34*Hydrol. Model.*

Swain, S., Verma, M. K., and Verma, M. K. (2018). "Streamflow estimation using SWAT model over seonath River Basin, Chhattisgarh, India,". Editors V. Singh, S. Yadav, and R. Yadava (Singapore: Springer), 81. doi:10.1007/978-981-10-5801-1_45*Hydrol. Model.*

Tan, Xueling, Liu, Suning, Tian, Yong, Zhou, Z., Wang, Y., Jiang, J., et al. (2022). Impacts of climate change and land use/cover change on regional hydrological processes: Case of the guangdong-Hong Kong-Macao greater bay area. *Front. Environ. Sci.* 9, 783324. doi:10.3389/fenvs.2021.783324

Tang, J., Yin, X. A., Yang, P., and Yang, Z. (2014). Assessment of contributions of climatic variation and human activities to streamflow changes in the Lancang River, China. *Water Resour. manage.* 28 (10), 2953–2966. doi:10.1007/s11269-014-0648-5

Tang, X., Woodcock, C. E., Olofsson, P., and Hutyra, L. R. (2021a). Spatiotemporal assessment of land use/land cover change and associated carbon emissions and uptake in the Mekong River Basin. *Remote Sens. Environ.* 256, 112336. doi:10.1016/j.rse.2021.112336

Tang, X., Zhang, J., Gao, C., Ruben, G., and Wang, G. (2019). Assessing the uncertainties of four precipitation products for swat modeling in Mekong river basin. *Remote Sens. (Basel).* 11, 304. doi:10.3390/rs11030304

Tang, X., Zhang, J., Wang, G., Ruben, G. B., Bao, Z., Liu, Y., et al. (2021b). Error Correction of multi-source weighted-ensemble precipitation (MSWEP) over the Lancang–Mekong river basin. *Remote Sens. (Basel).* 13, 312. doi:10.3390/rs13020312

Tatsumi, K., and Yamashiki, Y. (2015). Effect of irrigation water withdrawals on water and energy balance in the Mekong River Basin using an improved VIC land surface model with fewer calibration parameters. *Agric. Water Manag.* 159, 92–106. doi:10.1016/j.agwat.2015.05.011

Wang, C., Xu, J., Chen, Y., and Li, W. (2019). An approach to simulate the climate-driven streamflow in the data-scarce mountain basins of Northwest China. *J. Earth Syst. Sci.* 128 (4), 95–15. doi:10.1007/s12040-019-1117-6

Wang, J., Yun, X., Pokhrel, Y., Yamazaki, D., Zhao, Q., Chen, A., et al. (2021). Modeling daily floods in the lancang-mekong River Basin using an improved hydrological-hydrodynamic model. *Water Resour. Res.* 57 (8), e2021WR029734. doi:10.1029/2021WR029734

Wang, W., Lu, H., Ruby Leung, L., Li, H. Y., Zhao, J., Tian, F., et al. (2017). Dam construction in Lancang-Mekong River Basin could mitigate future flood risk from warming- induced intensified rainfall. *Geophys. Res. Lett.* 44, 10378–410386. doi:10.1002/2017GL075037

Wu, J., Chen, Y. F., and Hang, Q. (2016). Analysis of inconsistent hydrological frequency based on TFPW-MK-pettitt and EEMD, [C]. Proceedings of the Environmental Science and Sustainable Development: International Conference on Environmental Science and Sustainable Development (ICESSD 2015). 198–207. Bangkok, Thailand, doi:10.1142/9789814723039_0027

Yanming, Z., Jun, W., and Xinhua, W. (2012). in *Future computer, communication, control and automation* (Heidelberg, Germany: Springer), 505–513. doi:10.1007/978-3-642-25538-0_71*Study on the change trend of precipitation and temperature in Kunming city based on Mann-Kendall analysis.*

Yun, X., Tang, Q., Wang, J., Liu, X., Zhang, Y., Lu, H., et al. (2020). Impacts of climate change and reservoir operation on streamflow and flood characteristics in the Lancang-Mekong River Basin. *J. Hydrology* 590, 125472. doi:10.1016/j.jhydrol.2020.125472

Zhang, A. J., Zhang, C., Fu, G. B., Wang, B., Bao, Z., and Zheng, H. (2012). Assessments of impacts of climate change and human activities on runoff with SWAT for the Huifa River Basin, northeast China. *Water Resour. manage.* 26 (8), 2199–2217. doi:10.1007/s11269-012-0010-8

Zhao, G., Li, E., Mu, X., Wen, Z., Rayburg, S., and Tian, P. (2015). Changing trends and regime shift of streamflow in the Yellow River basin. *Stoch. Environ. Res. Risk Assess.* 29 (5), 1331–1343. doi:10.1007/s00477-015-1058-9

Frontiers in Earth Science

Investigates the processes operating within the major spheres of our planet

Advances our understanding across the earth sciences, providing a theoretical background for better use of our planet's resources and equipping us to face major environmental challenges.

Discover the latest Research Topics

See more →

Frontiers

Avenue du Tribunal-Fédéral 34
1005 Lausanne, Switzerland
frontiersin.org

Contact us

+41 (0)21 510 17 00
frontiersin.org/about/contact